A Mineralogical Investigation into the Beneficiation of a Rare-Earth Mineral Deposit Using Physical Separations

Christopher Marion

Department of Mining and Materials Engineering
McGill University
Montreal, Canada

A thesis submitted to McGill University in partial fulfillment of the
requirements of the degree of Doctor of Philosophy

April 2020

ABSTRACT

The rare-earth elements (REE), which comprise the fifteen elements of the lanthanoid series of the periodic table, as well as yttrium, have gained enormous public, economic and scientific attention in recent years. Their growing economic and strategic importance, coupled with uncertainty in the global supply of REE from China, have led to concerns about their future availability. As such, many new REE deposits have been identified and developed around the world. However, these deposits are often complex and contain various rare-earth minerals (REM) for which there is limited processing knowledge. This thesis examines the application of physical separations to the Nechalacho deposit in the Northwest Territories of Canada. It is specifically focused on relating the deposits mineralogical characteristics to quantify mineral separation behaviour in various processes; and ultimately proposing an industrially applicable beneficiation process for the ore. The valuable REE-bearing minerals in this ore are allanite, bastnäsite, columbite (Fe), fergusonite, monazite, synchysite and zircon; and the primary gangue minerals are quartz, feldspars and iron oxides.

Quantitative Evaluation of Minerals by Scanning Electron Microscopy (QEMSCAN) results indicate the grain size distributions and association behaviour of valuable minerals in the deposit cause them to be concentrated in high specific gravity (SG) particles, at particle sizes well above their liberation size. To take advantage of this property, a Knelson Concentrator and spiral are examined as methods to preconcentrate the ore at a relatively coarse particle size; with the goal of rejecting low SG silicate gangue minerals (quartz and feldspars) early in the beneficiation process. Both techniques are determined to be effective. However, due to its simplicity, the spiral is recommended as the more applicable process in an industrial setting. The optimization and application of such a process could have profound effects on any downstream processing, as well as in the overall economics, as it would minimize the energy required for comminution.

Following the preconcentration test work, a Knelson Concentrator, Multi-Gravity Separator (MGS) and Mozley Laboratory Shaking Table are studied to assess their ability to produce a bulk heavy mineral (REM, zircon and iron oxides) concentrate, at particle sizes much closer to the liberation size of the valuable minerals. All three techniques are effective at upgrading zircon and REM. But, the MGS is recommended as the superior process. The MGS is particularly effective

at recovering and concentrating zircon. Although REM are effectively upgraded, their recovery was relatively low. Mineralogical analysis indicates that with optimization of the comminution process and the MGS operating conditions, satisfactory recovery targets are likely to be achieved. However, it is noted that allanite recovery may remain depressed due to its relatively low SG compared to the other valuable minerals in the Nechalacho deposit.

Gravity concentrates from the MGS and Mozley Laboratory Shaking Table are then processed using a low-intensity magnetic separator, to remove iron oxide gangue, and a wet high intensity magnetic separator (WHIMS), to produce separate REM and zircon concentrates. Iron oxide gangue is effectively removed. But, its association with REM and zircon indicates that some losses of valuable material in this step may be unavoidable. The WHIMS is capable of producing a high-grade REM concentrate; with the relative magnetic response of REM following allanite > fergusonite > columbite (Fe) > monazite > bastnäsite > synchysite. However, a significant portion of REM remain in the non-magnetic fraction with zircon. Concluding that a magnetic separation step which can induce a high magnetic force on REM through high magnetic field gradients should be examined.

These metallurgical tests coupled with the use of automated mineralogy, along with other characterization techniques, led to the eventual proposal of a flowsheet to beneficiate the Nechalacho deposit. The proposed process involves early gangue rejection using a spiral, the production of a heavy mineral concentrate using a MGS, and the removal of iron oxides with a low-intensity magnetic separator. The bulk valuable mineral concentrate could be further separated into separate zircon and REM concentrates, using magnetic separation. However, separators which produce high magnetic field gradients are likely required. It is also suggested that allanite losses by the MGS, could be recovered by processing the MGS tails with a WHIMS. It is important to note that this proposed process is not representative of the currently selected process design for the Nechalacho deposit. Any application this process to this deposit would require optimization to ensure appropriate grade and recovery targets are met.

RÉSUMÉ

Les éléments de terre rare (REE), qui constituent les quinze éléments de la série lanthanoid de la table périodique, en plus du yttrium, ont acquis beaucoup d'attention publique, économique et scientifique au cours des dernières années. Leur importance économique et stratégique, couplée avec une incertitude sur la fourniture globale des REE provenant de la Chine, démontre une inquiétude par rapport à leur disponibilité future. Par conséquence, plusieurs nouveaux gisements ont été identifiés et développés autour du monde. Cependant, ces gisements sont souvent complexes et contiennent des minéraux de terre rare (REM) dont les connaissances de procédé sont limitées. Cette thèse examine l'application de méthodes de séparations physique sur le gisement Nechalacho situé dans les Territoires du Nord-Ouest, au Canada. La concentration est surtout sur l'utilisation des propriétés minéralogiques des gisements pour quantifier le comportement séparatoire des minéraux à travers une variété de procédés. Le but ultime est de proposer un procédé d'enrichissement du minerai pertinent pour l'industrie. Les minéraux contenant des REE de valeur sont l'allanite, le bastnäsite, le colombite (Fe), le fergusonite, la monazite, le synchysite et le zircon, et les minéraux de gangue primaire sont le quartz, le feldspath et les oxides de fer.

Les résultats de l'analyse quantitative des minéraux par la microscopie en balayage (QEMSCAN) indiquent que les distributions des tailles de grains et le comportement d'association des minéraux de valeur dans le gisement causent une concentration de ces minéraux dans des particules ayant une gravité spécifique (GS) haute et à des tailles de particule au-dessus de leur taille de libération. Pour prendre avantage de cette propriété, un concentrateur Knelson et un spiral sont examinés comme possibilités de méthode pour préconcentrer le minerai à des tailles de particule corses, avec le but de rejeter les minéraux de gangue à GS basse (le quartz et le feldspath) tôt dans le processus d'enrichissement. Les deux techniques ont prouvé être efficaces. Or, le spiral est recommandé d'autant plus comme procédé applicable à l'industrie dû à sa simplicité. Optimiser et appliquer un tel procédé peut avoir des effets profonds sur tous procédés postérieurs; et autant plus dans l'économie globale parce que l'énergie requise pour la comminution serait minimisée.

Après un travail d'investigation de la préconcentration, un concentrateur Knelson, un séparateur multi-gravitationnel (MGS) et une table vibratoire du laboratoire Mozley ont été étudiés pour

évaluer leur habileté à produire un concentré en frac de minéraux lourds (REM, zircon et oxides de fer) à des tailles de particules beaucoup plus proche de la taille de libération des minéraux de valeur. Les trois techniques sont efficaces pour valoriser le zircon et les REM. Par ailleurs, le MGS est recommandé comme procédé supérieure. Le MGS est particulièrement efficace pour le recouvrement et le concentrement du zircon. Outre, même si les REM sont effectivement valorisés, leur récupération était plutôt base. Une analyse minéralogique indique que, avec une optimisation du procédé de comminution et des conditions d'opération du MGS, des cibles de récupération satisfaisantes peuvent être atteintes. Cependant, ce fut noté que la récupération de l'allanite peut rester réduit dû à une GS relativement base comparer aux autres minéraux de valeur dans le gisement Nechalacho.

Par après, les concentrés obtenus par séparation gravitationnelle provenant du MGS et de la table vibratoire du laboratoire Mozley sont procédés en utilisant un séparateur magnétique à bas intensité, pour enlever la gangue d'oxides de fer, et un séparateur magnétique mouillé à haute intensité (WHIMS), pour produire des concentrés distincts de REM et de zircon. La gangue d'oxide de fer est effectivement enlevée. Or, son association avec les REM et le zircon indique qu'une quantité minime de perte de matériel de valeur est inévitable. Le WHIMS peut produire un concentré de REM de haute qualité avec une réponse magnétique relative suivante : allanite > Fergusonite > colombite (Fe) > monazite > bastänite > synchysite. Par ailleurs, une quantité significative de REM reste dans la fraction non-magnétique du zircon. Par conséquence, une étape de séparation magnétique qui peut induire une grande force magnétique sure les REM à travers des gradients de haut champ magnétique doit être examinée.

Ces analyses métallurgiques couplé avec la minéralogie automatisé et d'autres méthodes de caractérisations, ont éventuellement amené vers une proposition d'un schéma d'enrichissement pour le gisement Nechalacho. Le procédé proposé implique un rejet tôt de gangue à l'aide d'un spiral, la production d'un concentré de minéraux lourds en utilisant un MGS et l'enlèvement des oxides de fer avec un séparateur magnétique à bas intensité. Le concentré minéral de valeur en vrac peut être encore séparé dans des concentrés de zircon et REM avec la séparation magnétique. Cependant, des séparateurs qui produisent des gradients de haut champ magnétique sont possiblement requis. Ce fut aussi suggéré que les pertes d'allanite dues au MGS peuvent être récupérées en traitant les queues du MGS avec un WHIMS. C'est important de noter que ce procédé proposé n'est pas représentatif du procédé sélectionné à l'instant même pour le gisement Nechalacho. Toutes applications de ce procédé à ce gisement nécessiteraient de l'optimisation pour assurer que les cibles de qualité et de récupération sont atteintes.

ACKNOWLEDGEMENTS

First and foremost, I would like to thank my supervisor, Professor Kristian E. Waters, for his invaluable guidance and support. It has been a pleasure to have spent my graduate studies under his supervision. I very much appreciate the time he spent reviewing this thesis and the articles we have written. And will be forever grateful for the opportunities, both through research and travel, he has provided me. Moreover, I would like to express gratitude for his support and encouragement when applying for scholarships and awards throughout my graduate studies.

I am extremely grateful to have worked with Dr. Adam Jordens early in my graduate studies. He was an excellent mentor and his encouragement, instruction and guidance were invaluable. The impact he had on my professional growth cannot be understated.

I would like to acknowledge all the collaborators outside of McGill, who have been exceedingly generous with their equipment, expertise and time. Dr. Tassos Grammatikopoulos (QEMSCAN), Professor Neil Rowson (magnetic separation), Dr. Robert Fitzpatrick (MGS) and Treve Mildren (MGS) have all been vital to this project. I am especially thankful for the collaboration with Dr. Grammatikopoulos. Without his generosity and fruitful discussion this thesis could not have been completed. I look forward to a continued collaboration as I move forward in the next stage of my life.

Thanks are due to the numerous individuals, both past and present, of the McGill mineral processing group. I would like to specifically thank Professor Jim Finch, Dr. Joshua Sovechles, Dr. Pengbo Chu, Dr. Darryel Boucher, Dr. Ravinder Multani, Dr. Yue Hua Tan and Frank Rosenblum. Ray Langlois, Ronghao Li, Hillary Williams and Justin Paris are deserving of a special acknowledgement for their significant assistance in planning and running experiments. I would also like to thank Dr. Ozan Kokkilic and Luis Vinnett for all the fruitful conversations we have had over the years and to Mark Lepage for keeping me sane over the last few years of this journey.

There are many other individuals within the McGill community, who have influenced me and this project. Professor Raynald Gauvin and Hendrix Demers are acknowledged for their assistance with Scanning Electron Microscopy. Additionally, I am extremely grateful for Barbara Hanley and the

great assistance she provides to the department and all graduate students. She makes everyone's life significantly easier.

I would like to thank the numerous funding sources over the course of my graduate studies: The McGill Engineering Doctoral Award (MEDA); Vadasz Doctoral Fellowship; Natural Sciences and Engineering Research Council of Canada (NSERC) - for both masters and doctoral level awards; Post-Graduate Student SAG Award; Horrace Young Fellowship; William S Rugh Fellowship; Graduate Excellence Fellowship; Graduate Research Mobility Award (GRMA); and Graduate Research Enhancement and Travel Award (GREAT). NSERC and Avalon Advanced Materials Inc. are also acknowledged for providing the bulk of the funding for this research program through the Collaborative Research and Development (CRD) Program (CRDPJ 44537-12).

I would like to give a special shout-out to all those who have made Montreal my home. Adrian Battiston, Jay Hennessy, Ali Virji and Rob Hill were the best roommates. Jay and Adrian, you have made my time in Montreal an unforgettable one and your relaxed demeanor rubbed off on me, ensuring I was never too stressed. I would also like to thank Joey Rufo, Ray Rufo, Alex Taciuk, Nick Veenhoven, Trevor Drummond, Amy Harrington, Will Lepry, Amy Nommeots-Nomm and Roberto Cola (my irreplaceable gym buddy). Without you guys I probably would have finished my thesis much earlier – but my life outside of McGill would have been much less enjoyable.

A deep appreciation is expressed towards Sam Rudinsky. I could not have asked for a better person to enjoy this experience with. Not only was she a great help with all the Scanning Electron Microscopy work in this thesis; but also, a great travel buddy, support system and as she put it "worthy adversary". Her intelligence, dedication and drive will continue to inspire me. I cannot wait to see what adventures lie ahead for us!

Lastly, I would like to thank my family; my brother Steve, sister Nigel and ½, Mom and Dad. They have taught me to be disciplined, inquisitive and creative. All my successes are, in part, due to their guiding influence and love throughout my life. My sister is also deserving of a special thank you for being my own personal editor early in my graduate studies and ultimately teaching me how to write.

TABLE OF CONTENTS

LIST OF FIGURES

LIST OF TABLES

NOMENCLATURE

AHA		Acetrohydroxamic acid
AAS		Atomic adsorption spectroscopy
BHA		Benzohydroxamic acid
BSE		Backscatter-electrons
CVD		Continuous Variable Discharge
$\frac{dB}{dx}$	T m^{-1}	Magnetic field gradient
d_u / d_y	s^{-1}	Rate of shear
D, D_1, D_2	m	Particle diameter
DMS		Dense Medium Separation
EDS		Energy dispersive X-ray spectrometry
F_B	N	Bagnold force
F_w	N	Force from a particles apparent weight
F_x	N	Magnetic force felt by a particle in x-direction
g	m s^{-2}	Acceleration due to Earth’s gravity
G		Ratio of centrifugal force to the force due to Earth’s gravity

H	A m^{-1}	Applied magnetic field strength
HREE		Heavy rare-earth elements
IEP		Isoelectric point
ICP		Inductively coupled plasma
ICP-MS		Inductively coupled plasma mass spectrometry
k		Constant in Bagnold force equation
KBH		Potassium butyl hydroxamate
LIMS		Low-intensity magnetic separator
LREE		Light rare-earth elements
MGS		Multi-Gravity Separator
MREE		Medium rare-earth elements
n		Exponent in the free-settling ratio
OHA		Octylhydroxamic acid
PMA		Particle Mineral Analysis
POH		Potassium octyl hydroxamate
QEMSCAN		Quantitative evaluation of minerals by scanning electron microscopy

REE		Rare-earth elements
REM		Rare-earth minerals
REO		Rare-earth oxide
SEM		Scanning electron microscopy
SG		Specific gravity
SHA		Salicylhydroxamic acid
THA		Tetradecylhydroxamic acid
TREO		Total rare-earth oxide
V	m^3	Particle volume
VSM		Vibrating sample magnetometer
WHIMS		Wet high-intensity magnetic separator
XRD		X-ray diffraction
XRF		X-ray fluorescence
v_t	$m\ s^{-2}$	Terminal velocity
η_f	Pa s (=kg m^{-1} s^{-1})	Viscosity of fluid
ρ_f	kg m^{-3}	Density of fluid

ρ_s	kg m^{-3}	Density of particle
χ_f		Magnetic susceptibility of the fluid medium
χ_p		Magnetic susceptibility of the particle

KEY MINERALS OF NECHALACHO DEPOSIT

Allanite	$(REE,Ca)_2(Al,Fe^{2+},Fe^{3+})_3(SiO_4)_3(OH)$
Bastnäsite	$(REE)CO_3F$
Columbite	$FeNb_2O_6$
Fergusonite	$(REE)NbO_4$
Hematite	Fe_2O_3
K-Feldspar	$KAlSi_3O_8$
Magnetite	Fe_3O_4
Monazite	$(REE,Th)PO_4$
Plagioclase	$(Na,Ca)AlSi_3O_8$
Quartz	SiO_2
Synchysite	$Ca(REE)(CO_3)_2F$
Zircon	$(Zr,REE)SiO_4$

Chapter 1

Introduction

1.1 Introduction

The rare-earth elements (REE) have gained enormous public, economic and scientific attention in recent years. They are strategic metals which are indispensable to the development of modern defense systems, electronic applications and green technologies. The growing economic and strategic importance of these sectors, coupled with uncertainty in the global supply of REE from China, have led to concerns about the future availability of many of these metals. Due to these supply concerns and the increasing demand of REE, they have been designated as a critical resource by several countries, including the USA (United States Department of Energy, 2011), the EU (European Commission, 2017) and Canada (Fekete, 2014). Although significant and accelerating advancements continue in REE resource development, processing and applications, the rare-earth supply chain remains complex and continues to face challenges. It is therefore critically important to conduct research in all stages of the supply chain, from geology, beneficiation, separation and refining, to final product design, lifecycle management and recycling; with the focus of this thesis being on the beneficiation of REE deposits.

The REE supply disruption in 2010, as a result of China (the worlds primary supplier) implementing export quotas, prompted many companies and governments to explore REE resources and, consequently, many new deposits have been identified and developed around the world. As of 2015, there were 53 advanced REE projects outside of China (Hatch, 2015). These deposits are generally complex and contain multiple rare-earth element-bearing minerals (REM) for which there is limited processing knowledge. Among the advanced projects, many are in Canada, including the Nechalacho Deposit (owned by Avalon Advanced Materials Inc.) located in the Northwest Territories of Canada.

The supply of REE continues to be an increasingly important worldwide concern. During the second half of 2018, China reduced REE exports by 36 %, likely looking to crimp international exports and increase REE prices (Lewis and Scheyder, 2018). Compounding this is the trade war rhetoric between the USA and China, which has escalated with threats to cut off REE exports (Rogers *et al.*, 2019). Although the 2010 quotas resulted in increased research into new means of supply, including from both primary (Anderson, 2015; Cui, 2015; Espiritu, 2018; Jordens, 2016; Schriner, 2016; Xiong *et al.*, 2018; Yang *et al.*, 2015; Zhang, 2016) and secondary (recycling) resources (Abaka-Wood *et al.*, 2019a; Binnemans *et al.*, 2013; Hu *et al.*, 2017; Jowitt *et al.*, 2018; Lorenz and Bertau, 2019; Yin *et al.*, 2018), Chinese control of the industry remains strong, providing more than 80 % of the 130,000 t of documented rare-earth oxide (REO) supplied to the market in 2017 (Gambogi, 2018). These numbers become even worse when undocumented (illegal) production is accounted for, as it has been estimated that an additional ~40,000 t of illegally produced REO are supplied from China annually (Kingsnorth, 2018; Packey and Kingsnorth, 2016). Kennedy (2019) of ThREE (a consulting firm which provides services to the financial, mining and nuclear energy industry on strategic issues related to REE and thorium) wrote in a recent article that an embargo on REE could shut down nearly every automobile, computer, smartphone and aircraft assembly line outside of China. This further reiterates the criticality of timely research to fill the knowledge gaps surrounding REM projects.

1.2 Thesis Objectives

The goal of this thesis was to design an effective process for concentrating REM from the Nechalacho deposit. Most of the minerals in this deposit have limited established knowledge base in mineral processing. As such the main objectives of this research program were to:

- Quantify mineral separation behaviour in various separation processes
- Propose an industrially applicable beneficiation process which could be applied to the Nechalacho deposit

Although this thesis presents a possible processing route for the Nechalacho deposit, it is important to acknowledge its limits in scope. The thesis has limited discussion of its impact on downstream REE separation operations. All test work was performed purely on a bench scale and any application of the proposed process would require scale-up and optimization to ensure appropriate grade and recovery targets are met.

1.3 Thesis Structure

This thesis is presented as a traditional monograph thesis comprised of nine chapters and two appendices. The chapters summarize the current state of the rare-earth industry; mineral processing techniques; the application of physical separation methods to REE-bearing deposits; the methods employed in the experimental test work; the findings from ore beneficiation studies; and global conclusions, contributions and suggestions for future studies. Information outside the primary scope of this thesis, particularly with regards to REM flotation, is provided in the appendices. More specifically, the individual chapter and appendix details are as follows:

Chapter 1: Introduction provides a general introduction of REE along with an overview of the thesis objectives and structure;

Chapter 2: The Rare-Earth Elements details important background information on REE and REM. This includes important definitions, insight into the current global economic supply and demand of REE, and discusses the challenges associated with the supply of REE;

Chapter 3: Mineral Processing summarizes important background information on mineral processing, including the theories of different separation techniques and their operating principles;

Chapter 4: The Physical Beneficiation of Rare-Earth Minerals includes a thorough review of literature detailing the current knowledge base surrounding REM beneficiation using gravity and magnetic separation;

Chapter 5: Experimental Methods provides a detailed description of the experimental procedures employed throughout this research;

Chapter 6: Ore Characterization details the results of characterization experiments used to determine the properties of selected constituent minerals of the Nechalacho deposit. The implications of these results to the beneficiation of this deposit are discussed;

Chapter 7: Gravity Separation details the use of gravity separation techniques for the beneficiation of the Nechalacho deposit. The use of gravity separation for both preconcentration and primary separation stages are described. The results are characterised using a range of analytical tools to develop an in-depth understanding into their application to the Nechalacho deposit. An optimal process is selected for both preconcentration and primary separation. The optimal product produced from the primary separation stage is selected for downstream magnetic separation experiments;

Chapter 8: Magnetic Separation presents the findings of magnetic separation experiments performed on gravity concentrates. The results are similarly characterized by various analytical techniques and a physical separations-based flowsheet is proposed for processing the deposit;

Chapter 9: Conclusions, Contributions and Future Work presents the major conclusions derived from this research, highlights the contributions to original knowledge and suggests future studies to address areas in need of further research;

Appendix A: Preliminary Experimental Work provides two published manuscripts which are removed from the body of the thesis to improve its overall readability; and

Appendix B: Rare-Earth Mineral Flotation includes a thorough literature review of REM flotation and one published and one unpublished manuscript detailing work which was accomplished during this research and has importance to REM beneficiation, but was outside the general scope of this thesis.

Chapter 2

The Rare-Earth Elements and Minerals

2.1 Introduction

The REE comprise the fifteen metallic elements of the lanthanoid series of the periodic table, as well as chemically similar yttrium, and occasionally scandium (Krishnamurthy and Gupta, 2016). These elements are usually classified into two different sub-groups, the cerium sub-group of "light" rare-earth elements (LREE) and the yttrium sub group of "heavy" rare-earth elements (HREE) (Gambogi, 2015; Krishnamurthy and Gupta, 2016). A third sub-group, "medium" rare-earth elements (MREE), is also sometimes used (Kingsnorth, 2010; Krishnamurthy and Gupta, 2016; Zepf, 2013). The grouping of REE in these sub groups is not consistent among different authors, however, the most logical grouping is based on electron configuration (Gambogi, 2015; Zepf, 2013). Using this distinction, the LREE consist of cerium (atomic number 58) to gadolinium (atomic number 64), which have unpaired electrons in the 4f electron shell, and the HREE include terbium (atomic number 65) to lutetium (atomic number 71), which have paired electrons in the 4f electron shell (Gambogi, 2015; Zepf, 2013). Lanthanum (atomic number 57) does not have electrons in f-orbitals, however, it is generally grouped with the LREE (Gambogi, 2015; Zepf, 2013). Yttrium is generally classed as a HREE, as its ionic radius and chemical behaviour is similar to holmium (Zepf, 2013). Scandium, when classified as a REE, is not included in either the LREE or HREE classifications (Krishnamurthy and Gupta, 2016). While this sub-grouping is at present sufficient for REM exploitation and is what will be used here, it is important to note that the use of three groups may become more common, because, Chinese resource tax rates use this distinction (Argus Media Ltd., 2015; Zepf, 2016).

The name "rare-earths" is a historical misnomer, as these elements are quite abundant in the Earth's crust (with exception of promethium, which does not exist naturally in stable form). The 16 naturally occurring REE fall into the 50th percentile of elemental abundances (Cobb, 2012), and are significantly more abundant than other commonly exploited elements. The abundance of the individual REE in the upper continental crust is shown in Figure 2.1. Cerium (63 ppm), the most abundant REE, is more plentiful than copper (28 ppm), and even the least abundant REE, thulium (300 ppb) and lutetium (310 ppb), are more plentiful than elements such as silver (53 ppb) and gold (1.5 ppb) (Rudnick and Gao, 2003). The "zig-zag" pattern shown in Figure 2.1, is known as the Oddo-Harkin's rule, which states that elements with even atomic numbers are significantly more prevalent in the earths crust than their odd number neighbours in the periodic table (Parak, 1973; Trifonov, 1963). These abundances are, however, only average concentrations and do not reflect the nature and extent of their concentration in mineral deposits. REE are generally not found in high concentrations and they do not occur in nature as pure metals, like gold. They are concentrated in minerals such as carbonates, halides, oxides, phosphates and silicates (Krishnamurthy and Gupta, 2016; Vijayan *et al.*, 1989).

As of 2019, there are more than 250 REM that have been discovered; however, not all of them are of economic value (Bulatovic, 2010; Ferron *et al.*, 1991; Jordens *et al.*, 2013; Krishnamurthy and Gupta, 2016). These minerals can be considered as complex (containing all the REE), or selective (containing either predominately LREE or HREE) (Ferron *et al.*, 1991). Selective REM which contain mainly LREE are grouped as cerium type minerals or light rare-earth minerals (LREM), whereas those containing HREE are called yttrium type minerals or heavy rare-earth minerals (HREM). A list of some REM, along with their chemical formula, specific gravity (SG), magnetic characteristic, and content of REO, uranium and thorium, are shown in Table 2.1 to Table 2.5. The chemical and physical properties of these minerals will have implications in downstream beneficiation and separation processes. To date, only three of these minerals (bastnäsite, monazite and xenotime) have been exploited commercially on a large scale (Jordens *et al.*, 2013).

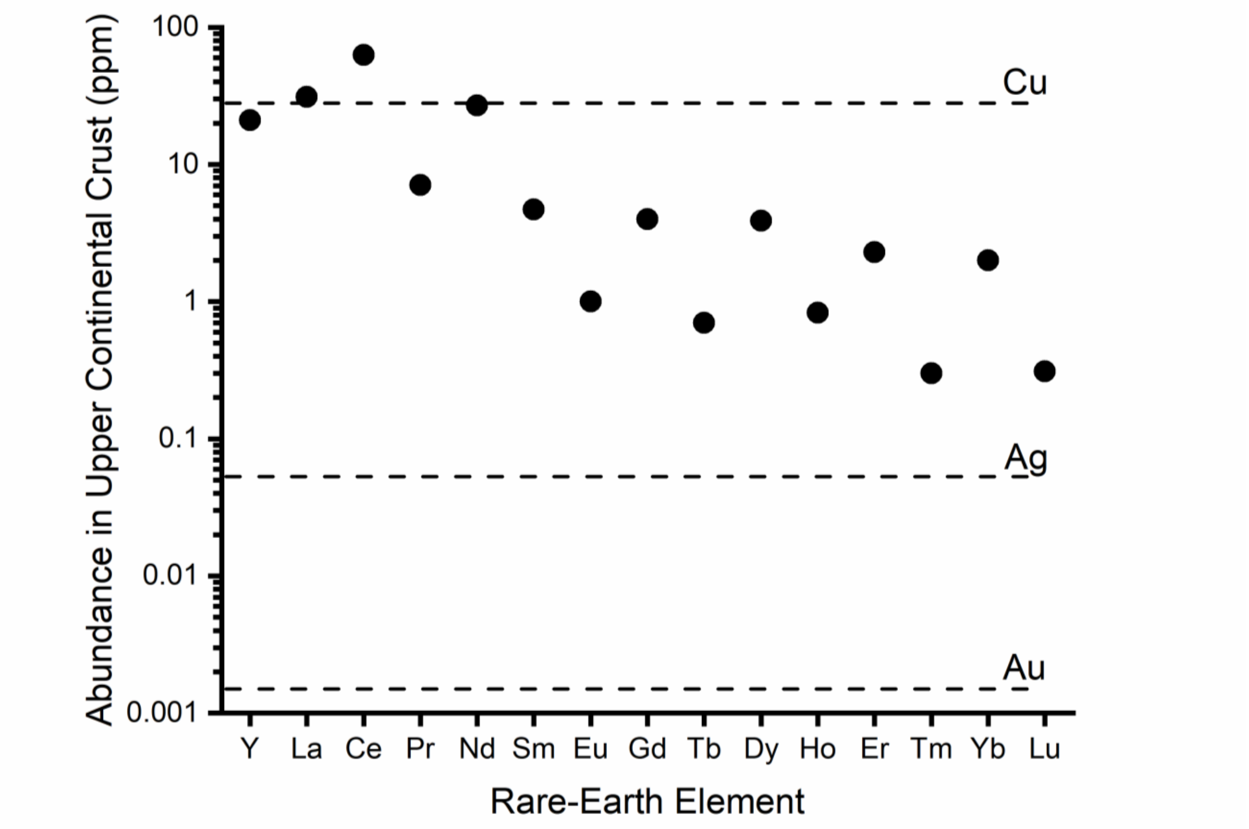

Figure 2.1 – Abundance of REE in upper continental crust. Adapted from Rudnick and Gao (2003)

Table 2.1 – Carbonate REM. Adapted from (Al-Ali *et al.*, 2019; Anthony *et al.*, 2001; Jordens *et al.*, 2013; Long *et al.*, 2012; Rosenblum and Brownfield, 2000)

Mineral Name	Chemical Formula	Specific Gravity	Magnetic Properties	Elemental Content (%)		
				REO	ThO_2	UO_2
Ancylite (Ce)	$Sr(Ce,La)(CO_3)_2OH \cdot H_2O$	3.82 – 4.30	N/A	46 – 53	0 – 0.4	0.1
Ancylite (La)	$Sr(La,Ce)(CO_3)_2OH \cdot H_2O$	3.69	N/A	46 – 53	0 – 0.4	0.1
Bastnäsite (Ce)	$(Ce,La)(CO_3)F$	4.90 – 5.20	Paramagnetic	70 – 74	0 – 0.3	0.09
Bastnäsite (La)	$(La,Ce)(CO_3)F$	N/A	Paramagnetic	70 – 74	0 – 0.3	0.09
Bastnäsite (Y)	$Y(CO_3)F$	3.90 – 4.00	Paramagnetic	70 – 74	0 – 0.3	0.09
Calcio-ancylite (Ce)	$(Ca,Sr)Ce_3(CO_3)_4(OH)_3 \cdot H_2O$	3.95	N/A	60	-	-
Calcio-ancylite (Nd)	$Ca(Nd,Ce,Gd,Y)_3(CO_3)_4(OH)_3 \cdot H_2O$	4.02	N/A	60	-	-
Doverite	$YCaF(CO_3)_2$	3.90	N/A	-	-	-
Parisite (Ce)	$Ca(Ce,La)_2(CO_3)_3F_2$	4.33	Paramagnetic	59	0 – 0.5	0 – 0.3
Parisite (Nd)	$Ca(Nd,Ce)_2(CO_3)_3F_2$	4.20 – 4.50	Paramagnetic	-	-	-
Röntgenite (Ce)	$Ca_2(Ce,La)_3(CO_3)_5F_3$	4.19	Paramagnetic	57	-	-
Synchysite (Ce)	$Ca(Ce,La)(CO_3)_2F$	3.90	Diamagnetic	49 – 52	1.6	-
Synchysite (Nd)	$Ca(Nd,La)(CO_3)_2F$	4.14 (calc)	N/A	-	-	-
Synchysite (Y) (doverite)	$Ca(Y,Ce)(CO_3)_2F$	3.90	N/A	-	-	-

Table 2.2 – Halide REM. Adapted from (Anthony *et al.*, 2001; Jordens *et al.*, 2013; Long *et al.*, 2012; Rosenblum and Brownfield, 2000)

Mineral Name	Chemical Formula	Specific Gravity	Magnetic Properties	Elemental Content (%)		
				REO	ThO_2	UO_2
Fluocerite (Ce)	$(Ce,La)F_3$	5.93	Paramagnetic	-	-	-
Fluocerite (La)	$(La,Ce)F_3$	5.93	Paramagnetic	-	-	-
Fluorite	$(Ca,REE)F_2$	3.18 – 3.56	Diamagnetic	-	-	-
Gagarinite (Y)	$NaCaY(F,Cl)_6$	4.11 – 4.29	N/A	-	-	-
Pyrochlore	$(Ca,Na,REE)_2Nb_2O_6(OH,F)$	4.45 – 4.90	Paramagnetic	-	-	-
Yttrofluorite	$(Ca,Y)F_2$	N/A	N/A	-	-	-

Table 2.3 – Oxide REM. Adapted from (Anthony *et al.*, 2001; Jordens *et al.*, 2013; Long *et al.*, 2012; Rosenblum and Brownfield, 2000)

Mineral Name	Chemical Formula	Specific Gravity	Magnetic Properties	Elemental Content (%)		
				REO	ThO_2	UO_2
Anatase	$(Ti,REE)O_2$	3.79 – 3.97	Diamagnetic	-	-	-
Brannerite	$(U,Ca,Y,Ce)(Ti,Fe)_2O_6$	4.20 – 5.43	Paramagnetic	-	-	-
Cerianite (Ce)	$(Ce^{4+},Th)O_2$	7.20 (syn)	N/A	-	-	-
Euxenite (Y)	$(Y,Ca,Ce,U,Th)(Nb,Ta,Ti)_2O_6$	5.30 – 5.90	Paramagnetic	-	-	-
Fergusonite (Ce)	$(Ce,La,Y)NbO_4$	5.45 – 5.48	Paramagnetic	-	-	-
Fergusonite (Nd)	$(Nd,Ce)(Nb,Ti)O_4$	N/A	Paramagnetic	-	-	-
Fergusonite (Y)	$YNbO_4$	5.60 – 5.80	Paramagnetic	-	-	-
Loparite (Ce)	$(Ce,Na,Ca)(Ti,Nb)O_3$	4.60 – 4.89	N/A	-	-	-
Perovskite	$(Ca, REE)TiO_3$	3.98 – 4.26	Diamagnetic	< 37	0 – 2	0 – 0.05
Samarskite	$(REE,Fe^{2+},Fe^{3+},U,Th,Ca)(Nb,Ta,Ti)O_4$	5.00 – 5.69	Paramagnetic	-	-	-
Uraninite	$(U,Th,Ce)O_2$	10.63 – 10.95	Paramagnetic	-	-	-

Table 2.4 – Phosphate REM. Adapted from (Anthony *et al.*, 2001; Jordens *et al.*, 2013; Long *et al.*, 2012; Rosenblum and Brownfield, 2000)

Mineral Name	Chemical Formula	Specific Gravity	Magnetic Properties	Elemental Content (%)		
				REO	ThO_2	UO_2
Britholite (Ce)	$(Ce,Ca)_5(SiO_4,PO_4)_3(OH,F)$	4.20 – 4.69	Paramagnetic	56	1.5	-
Britholite (Y)	$(Y,Ca)_5(SiO_4,PO_4)_3(OH,F)$	4.35	Paramagnetic	56	1.5	-
Brockite	$(Ca,Th,Ce)(PO_4)\cdot H_2O$	3.90	N/A	-	-	-
Chevkinite (Ce)	$(Ca,Ce,Th)_4(Fe^{2+},Mg)_2(Ti,Fe^{3+})_3Si_4O_{22}$	4.53 – 4.67	Paramagnetic	-	-	-
Churchite (Y)	$YPO_4\cdot H_2O$	3.26	N/A	-	-	-
Crandallite	$CaAl_3(PO_4)_2(OH)_5\cdot H_2O$	2.78 – 3.04	N/A	-	-	-
Florencite (Ce)	$CeAl_3(PO_4)_2(OH)_6$	3.45 – 3.54	N/A	-	1.4	-
Florencite (La)	$(La,Ce)Al_3(PO_4)_2(OH)_6$	3.52	N/A	-	1.4	-
Florencite (Nd)	$(Nd,Ce)Al_3(PO_4)_2(OH)_6$	3.70 (calc)	N/A	-	1.4	-
Fluorapatite	$(Ca,Ce)_5(PO_4)_3F$	3.10 – 3.25	N/A	-	-	-
Gorceixite	$(Ba,REE)Al_3[(PO_4)_2(OH)_5]\cdot H_2O$	3.04 – 3.19	Diamagnetic	-	-	-
Goyazite	$SrAl_3(PO_4)_2(OH)_5\cdot H_2O$	3.26	Diamagnetic	-	-	-
Monazite (Ce)	$(Ce,La,Nd,Th)PO_4$	4.98 – 5.43	Paramagnetic	35 – 71	0 – 20	0 – 16
Monazite (La)	$(La,Ce,Nd,Th)PO_4$	5.17 – 5.27	Paramagnetic	35 – 71	0 – 20	0 – 16
Monazite (Nd)	$(Nd,Ce,La,Th)PO_4$	5.43 (calc)	Paramagnetic	35 – 71	0 – 20	0 – 16
Rhabdophane (Ce)	$(Ce,La)PO_4\cdot H_2O$	3.77 – 4.01	N/A	-	-	-
Rhabdophane (La)	$(La,Ce)PO_4\cdot H_2O$	4.4	N/A	-	-	-
Rhabdophane (Nd)	$(Nd,Ce,La)PO_4\cdot H_2O$	4.79 (calc)	N/A	-	-	-
Vitusite (Ce)	$Na_3(Ce,La,Nd)(PO_4)_2$	3.60 – 3.70	N/A	-	-	-
Xenotime (Y)	YPO_4	4.40 – 5.10	Paramagnetic	52 – 67	-	0 – 5

Table 2.5 – Silicate REM. Adapted from (Anthony *et al.*, 2001; Jordens *et al.*, 2013; Long *et al.*, 2012; Rosenblum and Brownfield, 2000)

Mineral Name	Chemical Formula	Specific Gravity	Magnetic Properties	Elemental Content (%)		
				REO	ThO_2	UO_2
Allanite (Ce)	$(Ce,Ca,Y)_2(Al,Fe^{2+},Fe^{3+})_3(SiO_4)_3(OH)$	3.50 – 4.20	Paramagnetic	3 – 51	0 – 3	-
Allanite (Y)	$(Y,Ce,Ca)_2(Al,Fe^{3+})_3(SiO_4)_3(OH)$	N/A	Paramagnetic	3 – 51	0 – 3	-
Cerite (Ce)	$Ce_9Fe^{3+}(SiO_2)_6[(SiO_3)(OH)](OH)_3$	4.75	Paramagnetic	-	-	-
Cheralite (Ce)	$(Ca,Ce,Th)(P,Si)O_4$	5.28	Paramagnetic	-	< 30	-
Eudialyte	$Na_4(Ca,Ce)_2(Fe^{2+},Mn^{2+},Y)ZrSi_8O_{22}(OH,Cl)_2$	2.74 – 3.10	N/A	1 - 10	-	-
Gadolinite (Ce)	$(Ce,La,Nd,Y)_2Fe^{2+}Be_2Si_2O_{10}$	4.2	N/A	-	-	-
Gadolinite (Y)	$Y_2Fe^{2+}Be_2Si_2O_{10}$	4.36 – 4.77	Paramagnetic	-	-	-
Gerenite (Y)	$(Ca,Na)_2(Y,REE)_3Si_6O_{18}\cdot 2H_2O$	N/A	Paramagnetic	-	-	-
Hingganite (Ce)	$(Ce,Y)_2Be_2Si_2O_8(OH)_2$	4.82 (calc)	N/A	-	-	-
Hingganite (Y)	$(Y,Yb,Er)_2Be_2Si_2O_8(OH)_2$	4.42 – 4.57	N/A	-	-	-
Hingganite (Yb)	$(Yb,Y)_2Be_2Si_2O_8(OH)_2$	4.83 (calc)	N/A	-	-	-
Iimoriite (Y)	$Y_2(SiO_4)(CO_3)$	4.47	N/A	-	-	-
Kainosite (Y)	$Ca_2(Y,Ce)_2Si_4O_{12}(CO_3)\cdot H_2O$	3.52	N/A	-	-	-
Rinkite (rinkolite)	$(Ca,Ce)_4Na(Na,Ca)_2Ti(Si_2O_7)_2F_2(O,F)_2$	3.18 – 3.44	N/A	-	-	-
Sphene (titanite)	$(Ca,REE)TiSiO_5$	3.48 – 3.60	Paramagnetic	< 3	-	-
Steenstrupine (Ce)	$Na_{14}Ce_6Mn_2Fe_2(Zr,Th)(Si_6O_{18})_2(PO_4)_7\cdot 3H_2O$	3.38 – 3.47	N/A	-	-	-
Thalenite (Y)	$Y_3Si_3O_{10}(F,OH)$	4.16 – 4.41	N/A	-	-	-
Thorite	$(Th,U)SiO_4$	6.63 – 7.20	Paramagnetic	< 3	-	10 - 16
Zircon	$(Zr,REE)SiO_4$	4.60 – 4.70	Diamagnetic	-	0.1	-

2.2 Resources

The majority of the world's REE are derived from primary (natural) resources. These deposits can be divided into various categories based on their formation and major mineral types. They can be broadly classified, primarily, into four geologic environments: carbonatites, alkaline/peralkaline igneous rocks, placers (mineral sands), and ion adsorption clays (Castor, 2008; Goodenough *et al.*, 2018).

For more than 50 years, the majority of REE have been derived from carbonatite deposits; these are defined as an igneous rock deposit containing > 50 % carbonate minerals. These deposits tend to be large, high-grade, and generally contain a high proportion of LREE. There are currently several operating REE-bearing carbonatite deposits, as well as many others under investigation (Verplanck *et al.*, 2016). The world's largest REE mine, the Bayan Obo mine in China, along with the newly operating Mount Weld mine, in Australia, and the Mountain Pass mine (the world's primary producer from 1965 – 1995), in the USA, are all carbonatite deposits (Castor, 2008; Verplanck *et al.*, 2016). These deposits are large, high-grade, deposits which contain predominately LREE. Carbonatite deposits can contain a variety of REE-rich mineral phases, including bastnäsite, parisite, synchysite, ancylite, monazite and apatite; with bastnäsite being the primary mineral mined (Castor, 2008; Verplanck *et al.*, 2016).

The other group of "hard-rock" REE deposits are classified as alkaline/peralkaline igneous rock deposits. These deposits tend to have a much "flatter" REE distribution than carbonatite deposits, making them one of the most economically important resources of HREE (Dostal, 2016; Goodenough *et al.*, 2018). They are, however, often much more complex than carbonatite deposits, with highly variable mineralogy, both within individual deposits and particularly among the various deposits (Dostal, 2016). The only active REE deposits of this type are in the Kola Peninsula in Russia, where the main REE bearing mineral is loparite (Dostal, 2016; Goodenough *et al.*, 2018; Hedrick *et al.*, 1997). However, there are many alkaline/peralkaline igneous rock deposits which are currently being investigated, including the Nechalacho deposit. The Nechalacho deposit is one of the largest resources of this type, with an inferred resource of 160 million tons at a grade of 1.38

% total rare-earth oxide (TREO) (Avalon Rare Metals Inc., 2013; Castor, 2008). This deposit contains complex mineralogy with the REE hosted in various minerals including zircon, bastnäsite, synchysite, allanite, monazite, fergusonite and columbite (Fe).

Placers, or mineral sands, are sedimentary deposits formed by the natural physical concentration of minerals from weathering processes. Although placer deposits are most commonly processed for other commodities such as gold, tin (in cassiterite), titanium (in ilmenite and rutile) and zirconium (in zircon), many have potential to produce REE as a co-product (Goodenough *et al.*, 2018; Sengupta and Gosen, 2016). In fact, before full scale production began at the Mountain Pass mine, in 1965, placer mines were the world's chief REE supplier (Sengupta and Gosen, 2016). The REM found in these deposits are primarily monazite and, sometimes, xenotime. As they are generally more enriched in monazite, they contain more LREE than HREE, however, xenotime offers potential for HREE production (Goodenough *et al.*, 2018; Sengupta and Gosen, 2016). Although, placers deposits are, generally, smaller and have lower REE grades than carbonatite ores, they have very simple and well-established processing routes (with little to no comminution required) and can produce multiple salable products to offset mining costs (Goodenough *et al.*, 2018; Jordens *et al.*, 2013; Sengupta and Gosen, 2016).

The final major deposit type for REE are ion adsorption clays. Ion adsorption clays are currently the second major producer of REE and the world's chief source of HREE, with a large proportion coming from illegal Chinese producers (Brown and Eggert, 2018; Goodenough *et al.*, 2018; Sanematsu and Watanabe, 2016). These deposits are primarily located in China, with a few specific locations else where in the world (Goodenough *et al.*, 2018; Sanematsu and Watanabe, 2016). In ion adsorption clay deposits, REE are not held within minerals but adsorbed onto clay surfaces (Goodenough *et al.*, 2018; Sanematsu and Watanabe, 2016). Therefore, REE from these deposits can be easily extracted by ion-exchange using a dilute electrolyte solution, such as ammonium sulfate, and do not require any comminution or mineral processing steps (Goodenough *et al.*, 2018; Sanematsu and Watanabe, 2016).

2.3 Global Economic Supply and Demand

The first industrial application of REE dates to the 1890's, when Austrian scientist, inventor and entrepreneur, Carl Auer von Welsbach (who also discovered neodymium and praseodymium), developed the Auer incandescent mantle which composed of 99 % thorium oxide and 1 % cerium oxide (Greinacher, 1981). While the role of cerium was minor, the low cost and superior lighting properties of the Auer incandescent mantle resulted in widespread adoption and by the 1930's over 5 billion units had been sold. Auer von Welsbach's first invention developed two new problems: the gas mantles were difficult to ignite, and large quantities of unseparated REE from the production of incandescent mantles (thorium came from the mineral monazite which contains up to 20 % thorium and 35 - 71 % REO) had accumulated in large waste piles. He ameliorated this situation in the early 1900's by blending a mixture of unseparated REE (termed "Mischmetall") with iron to develop the pyrophoric metal alloy "flintstone", that sparked when struck. This became the first large scale application of REE, which continues to be used today.

From these first beginnings, several new applications for mixed or simply separated REE were developed over the next fifty years (some of which are listed in Table 2.6), however, they resulted in relatively small consumption of the REE which continually became available from the use of thorium (Greinacher, 1981; Spencer, 1919). This was particularly the case in the 1950's, when major programs for atomic energy were carried out. The stockpiling of thorium for these programs left behind large quantities of REE by-products. This abundant production of REE lead to intensive scientific examination into their separation and properties; by the early 1960's there was a stable scientific foundation, and several new applications using individual REE (Table 2.6).

From this point on, the number of applications which use REE has grown exponentially, and today it is difficult to find a piece of modern technology which does not use them. In 2017, more than 130,000 t of REO were produced (compared to just 2,270 tons in 1960) (Gambogi, 2018; Kelly and Matos, 2015), finding uses in numerous industrial and high technology applications. The major sectors which consume REE can be broadly classified as magnets, catalysts, metal alloys, polishing, glass, ceramics and phosphors. The division of total REE consumption by each application and the proportion of specific REE which are required for each of these classifications is shown in Table 2.7. Table 2.8 provides an estimate of total demand for each REE. The most important and fastest growing industrial application is in permanent magnets, used in vehicle electrification, wind power generation and robotics (Binnemans *et al.*, 2018; Mancheri *et al.*, 2019). Making the supply of REE required in this application, specifically neodymium, praseodymium and dysprosium, of utmost importance. The European Commission's Joint Research Centre (JRC) has classified these three elements along with europium, terbium and yttrium (for lighting applications) as critical due to their supply risk and economic importance to low-carbon energy technologies (Moss *et al.*, 2013). More recently, the European Commission (2017) has suggested all REE (with the exception of erbium), should be considered critical. A similar study, by the United States Department of Energy, found neodymium, europium, dysprosium, terbium and yttrium to be critical (United States Department of Energy, 2011). Although various governments have defined all or many of the REE as critical materials, it does not reflect mining project economics. Analysis comparing the distribution of REE by weight and revenue for concentrates produced from legal Chinese producers, illegal Chinese producers and Mount Weld (the world's three major suppliers) (Table 2.9) suggests only neodymium, praseodymium and dysprosium are of significant value to current REE producers (Brown and Eggert, 2018).

Table 2.6 - Selected early applications of REE. Adapted from (Greinacher, 1981; Krishnamurthy and Gupta, 2016; Spencer, 1919)

In Use by	Application	REE Used
1920	Auer Incandescent Mantles	Cerium
	Pyrophoric Alloys	Unseparated REE
	Electric Arc Lighting	Unseparated REE
	Colourants/Decolourants in Glass	Cerium, Didymium[1], Unseparated REE
	UV Adsorbing Glass	Unseparated REE, Didymium[1]
	Medical Uses	Unseparated REE, Cerium, Didymium[1]
	Catalysts	Unseparated REE, Cerium
1950	Glass Polishing	Cerium, Unseparated REE
	Ferrous Metallurgy	Cerium, Unseparated REE
	Non-Ferrous Metallurgy	Unseparated REE, Didymium[1],
1970	Phosphors	Europium, Yttrium
	Fluid Catalytic Cracking Catalysts	Unseparated REE
	Other Catalysts	Lanthanum, Cerium, Neodymium
	Permanent Magnets	Samarium

[1] Didymium is a mixture of praseodymium and neodymium

Table 2.7 – Major Uses of REE and estimates of their specific elemental requirements (based off 2010 values). Adapted from (Kingsnorth, 2018; Long *et al.*, 2012; Zepf, 2016)

Application	2017 Demand Estimate (%)	REE Required (%)										
		La	Ce	Pr	Nd	Sm	Eu	Gd	Tb	Dy	Y	Other
Magnets	30	-	-	23	69	-	-	2	1	5	-	-
Catalysts	18	64	34	1	1	-	-	-	-	-	-	-
Metal Alloys	18	40	42	4	13	1	-	-	-	-	-	-
Polishing	14	31	65	4	-	-	-	-	-	-	-	-
Glass	6	24	66	1	3	-	-	-	-	-	2	4
Ceramics	5	17	12	6	12	-	-	-	-	-	53	-
Phosphors	3	8	10	-	-	-	5	2	5	-	69	-
Other	6	19	39	4	15	2	-	1	-	-	19	-

Table 2.8 – Estimated total demand by REE in 2017. Adapted from Table 2.7

REE	Demand Estimate (%)	Demand Estimate (t) [Based off Gambogi (2018) estimate of total REO production[1]]	Demand Estimate (t) [Based off Kingsnorth (2018) estimate of total REO production[2]]
La	26.8	34,749	44,773
Ce	30.0	39,091	50,367
Pr	9.0	11,648	15,008
Nd	24.9	32,370	41,708
Sm	0.3	390	503
Eu	0.2	195	251
Gd	0.7	936	1,206
Tb	0.5	585	745
Dy	1.5	1,950	2,513
Y	6.0	7,774	10,017
Other	0.2	312	402
Total	100	130,000	167,500

[1] Gambogi (2018) production estimate does not include undocumented production

[2] Kingsnorth (2018) production estimate includes undocumented production

Table 2.9 Distribution of REE by weight and revenue for concentrates produced from legal Chinese producers, illegal Chinese producers and Mount Weld. Adapted from (Brown and Eggert, 2018)

	By Weight (%)			By Value (%)		
REE	Legal Chinese Producers	Illegal Chinese Producers	Mount Weld	Legal Chinese Producers	Illegal Chinese Producers	Mount Weld
La	25.4	13.9	45.7	2.6	0.9	5.1
Ce	40.5	18.7	25.6	6.8	2.0	4.7
Nd	16.7	14.0	18.6	46.4	24.6	56.8
Y	7.5	35.8	0.4	2.9	8.7	0.2
Pr	5.5	4.0	5.4	15.8	7.4	17.1
Sm	1.5	3.3	2.4	0.2	0.2	0.3
Gd	1.4	5.0	1.0	2.3	5.1	1.8
Dy	1.0	4.1	0.2	14.0	35.8	2.9
Eu	0.3	0.4	0.6	3.8	3.5	8.6
Tb	0.2	0.8	0.1	5.2	11.8	2.5

2.4 Supply Challenges

2.4.1 Geographic Concentration of Supply

Since the early 1990's, China has dominated the supply of REE. In 2017, China controlled an estimated 80 % of documented production (Gambogi, 2018), after accounting for more than 93 % of the worlds production from 2003 – 2011 (Cordier, 2011, 2012; Gambogi, 2013; Hendrick, 2005, 2006, 2007, 2008, 2009, 2010). If undocumented production is accounted for, estimates of Chinese production in 2017 are as high as 85 % of the total REE supply (Kingsnorth, 2018). The World's only other major producer is the Mount Weld Mine in Australia, which accounted for approximately 14 % of the total REE supplied to the market in 2017 (Brown and Eggert, 2018; Gambogi, 2018). This geographic concentration of production results in significant concerns for downstream users of REE and any developing REE deposits, as China has significant control over the supply chain. This is best exemplified by China's implementation of export quotas in 2010.

2.4.2 The Balance Problem

REE are concentrated in the same minerals, however, in different distributions. Therefore, if the demand of a lesser abundant element increases without an increase in demand for a more common one, a misbalance in demand is created. This "balance problem" has been a challenge for the rare-earth industry since their first application. In the early days, the high demand for thorium resulted in large quantities of unseparated REE for which there was limited demand (Greinacher, 1981). As individual REE found uses in specific applications, balancing their demand with the ratio which they are produced became, and continues to be, a challenge. In the 1960's, the most important application for REE was for red phosphors, which required europium. At the time the chief europium (and REE) supplier was the bastnäsite ore of the Mountain Pass deposit. The low concentrations of europium in bastnäsite led to large surpluses and stockpiling of LREE (the ratio of europium oxide to cerium oxide, for example, in the Mountain Pass ore is 1:450) (Binnemans and Jones, 2015; Binnemans *et al.*, 2018).

Today, the most important application of REE is in magnets (Table 2.7). This results in a high demand for neodymium, praseodymium and dysprosium relative to their distribution in mineral deposits (Table 2.9), which results in significant over production of the majority of other REE. The balance between demand and the abundances of the REE in ores is a major challenge for both producers of REE and downstream users of rare-earth magnets. Industries which require these magnets are forced to pay an elevated price as production costs for neodymium, praseodymium and dysprosium cannot be spread over all the REE (Binnemans *et al.*, 2018). In addition, producers are forced to stockpile certain REE for which there is not sufficient demand (Binnemans *et al.*, 2018). Different options to mitigate the balance problem include recycling, substitution, and new high-volume applications for REE that are produced in excess (Binnemans *et al.*, 2018).

2.4.3 Environmental Concerns

The history of pollution from REE mines has resulted in growing social and environmental concerns pertaining to the mining and processing of these ores. In China, the impact of large-scale mining and processing operations on local environments and people has been well documented (Li *et al.*, 2013; Pan and Li, 2016; Tong *et al.*, 2004; Yang *et al.*, 2013b). In the USA, a federal investigation of the Mountain Pass mine found that the operation had released over 2 million liters of radioactive toxic waste to the environment, from 60 different wastewater pipe spills (some of which were unreported) which occurred between 1984 and 1998 (Ali, 2014). These spills eventually led to the suspension of its separation plant in 1998 (Hedrick, 1999). The associated environmental compliance and cost challenges coupled with competition from Chinese suppliers eventually led to the mines closure in 2002 (Hedrick, 2003). This history of pollution coupled with the social and environmental issues associated with radioactive wastes are significant challenges for nearly all developing REE projects. This is best exemplified by the Mount Weld deposit, in Australia, and its processing plant [Lynas Advanced Materials Plant (LAMP)], in Malaysia, which have been operating under a cloud of uncertainty, due to concerns surrounding the storage and disposal of radioactive waste at the processing plant (Ali, 2014; Kaur, 2015; Tengku Ismail et al., 2016).

2.4.4 Other Supply Challenges

Other significant challenges which exist for potential REE producers are (Goodenough *et al.*, 2018; Jordens *et al.*, 2013):

- a lack of technical expertise outside of China
- high capital outlay associated with new plants
- a lack of predictable and readily available market prices (REE are sold on contract)
- new mines must start-up in short time to ensure enough demand for its products

While potential new REE projects are likely affected by all these challenges, the degree to which they must be addressed varies by deposit type. For example, the technical knowledge required to recover REE from alkaline/peralkaline igneous rock deposits is significantly lacking compared to the other three major REE deposit types. However, even for carbonatites, which are currently mined, the mineralogy varies for each REE project. Apart from bastnäsite, and to a certain extent, monazite, there is limited technical knowhow to beneficiate other REM found in these deposits. While processing routes for placers and ion-adsorption clay deposits are much simpler, placers typically contain high levels of radioactive thorium, leading to environmental concerns, and ion adsorption clays have never been commercially processed outside of China, where ground clearance and the use of ammonium sulfate have caused significant environmental damage (Goodenough *et al.*, 2018; Yang *et al.*, 2013b).

2.5 Conclusions

This chapter detailed important definitions related to REE, current and potential REE resources, the current status of REE supply and demand, and current challenges associated with the supply of REE. The findings from this chapter demonstrate the urgent need for research in all stages of the supply chain, particularly, to find efficient and environmentally friendly processing methods for REM and deposit types which have not been mined before.

Chapter 3

Mineral Processing

3.1 Introduction

In mineral processing, ores, which consist of valuable minerals and gangue, are subject to a series of liberation (size reduction), classification (sizing), and separation steps to produce a valuable mineral or metal concentrate. The processing route depends on the ore deposit being processed and can rely on multiple separation techniques which exploit differences in the physical and chemical properties of minerals. This chapter provides important background information on mineral processing. The theoretical aspects of various beneficiation and characterization techniques discussed here are only an overview to ensure readers who may be unfamiliar with certain facets of mineral processing can follow the proceeding sections of this thesis. For readers interested in a more in-depth discussion of mineral processing concepts, there is a large body of literature available, with Wills and Finch (2016a) being a good starting point.

3.2 Liberation

To separate valuable minerals (or metals) from gangue, a liberation stage is first required. Liberation is achieved by size reduction (comminution), which involves crushing and grinding rocks until valuable minerals are freed from the interlocked rock matrix (Figure 3.1). If a high-grade product is desired from a downstream separation process, a high degree of liberation is essential. However, comminution is often the greatest energy consumer in a mineral processing plant, and separation techniques are also heavily influenced by particle size (Figure 3.2). Fine grinding increases energy costs and can lead to the production of very fine particles which are difficult to process. Therefore, a compromise between liberation and particle size is often required.

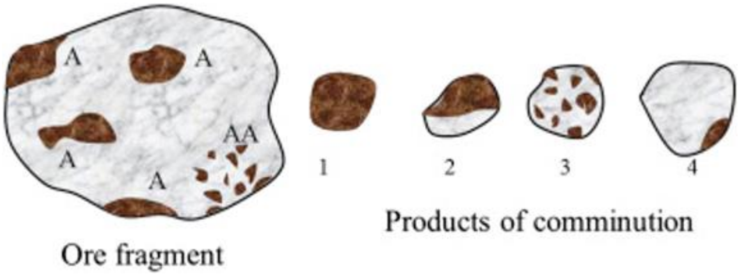

Figure 3.1 – Products of comminution. Adapted from Wills and Finch (2016b)

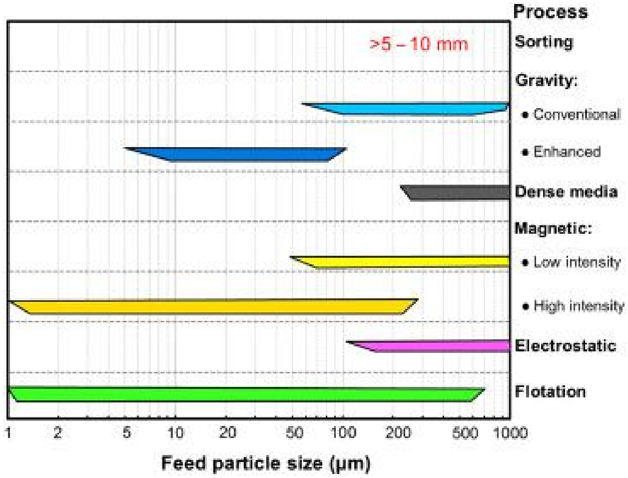

Figure 3.2 – Effective range of application for selected mineral separation techniques. Reproduced with permission from Wills and Finch (2016b)

Generally, the goal of the comminution process is to liberate valuable minerals at the coarsest possible particle size. However, a high degree of liberation is not always required, and in some cases, it is possible to concentrate or preconcentrate valuable minerals prior to complete liberation. Preconcentration is a processing step aimed at rejecting waste early in the concentration process. Earlier rejection of gangue can have significant benefits, including increased feed grades to downstream processes, and lower ore throughputs and operating costs. Ores amenable to preconcentration at coarser particle sizes would also benefit from lower energy requirements in the comminution stage. The method of separation used to reject gangue material during preconcentration is dependent on the physical properties of the ore and often rely on differences in SG, color, particle size, radioactivity, conductivity, or magnetic properties between valuable mineral-bearing particles and liberated gangue. The preconcentrate can then be reground to produce a more liberated feed for a downstream concentration process. A simplified example of such a flowsheet can be seen in Figure 3.3.

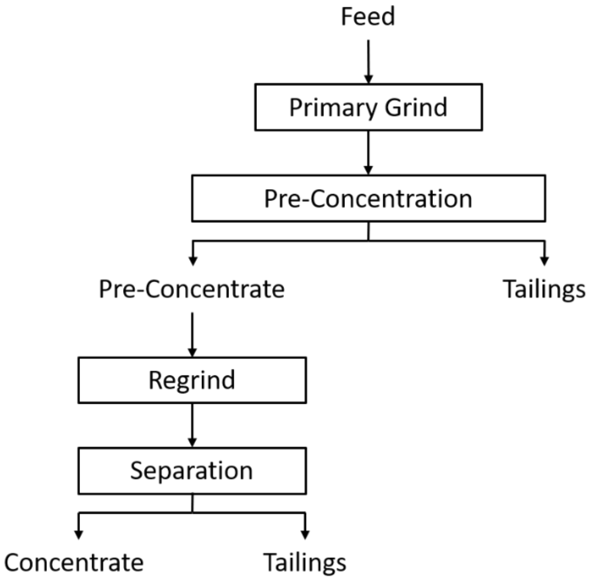

Figure 3.3 – Simplified flowsheet for a process utilizing a preconcentration stage

3.3 Froth Flotation

Although froth flotation is presently the primary method of REM beneficiation, the focus of this thesis is on physical separations. As such this topic will not be covered here, however, the focus of Appendix B is the flotation of REM, which contains a detailed description of the flotation principle.

3.3 Gravity Separation

Gravity separation exploits differences in SG to facilitate mineral separation. Although it becomes less effective at fine particle sizes (Figure 3.2), it offers multiple advantages over other separation techniques, such as flotation. Gravity separation techniques generally have low capital and operational costs (no reagent costs), comparatively little environmental impact and are relatively simple processes. These advantages are extremely important in today's mineral processing industry, especially for REM. While REM deposits are generally fine-grained, making gravity separation difficult, due to the relatively low price of the more common REE and general environmental concerns associated with new projects, only simple low-cost projects with a limited environmental footprint are likely to be successful.

There are a variety of different gravity separation methods. However, they can be generalized as devices which cause particles to flow with different velocities and trajectories, within a fluid, in response to a gravitational force and the resistance to motion imparted on particles by a viscous fluid. Therefore, the motion of a particle is often dependant upon its size and shape, in addition to its SG. Differentiation in the balance of these forces acting on particles is achieved through different mechanisms including, differential settling, interstitial trickling, flowing films, and Bagnold forces.

Settling refers to the sinking of particles in a fluid. If the volume of the fluid is large with respect to the total volume of particles (*i.e.* in well-dispersed pulps with a solids percentage of less than about 15 %), they can be said to be in a free settling regime, where particle-particle interactions are negligible. Under these conditions the forces acting on a particle are a downward acting gravitational force, and upward acting buoyancy and drag forces. The equilibrium of these three forces can be resolved, under different flow regimes, and the terminal velocity of the particles can be determined by Stokes' law (Equation 3.1) at particle Reynolds numbers less than 1 (particle sizes below 60 μm) or Newton's law (Equation 3.2) at particle Reynolds numbers greater than 1000 (particle sizes above 500 μm).

$$v_t = \frac{gD^2(\rho_s - \rho_f)}{18\eta_f} \tag{3.1}$$

$$v_t = \left[\frac{3gD(\rho_s - \rho_f)}{\rho_f}\right]^{1/2} \tag{3.2}$$

Where v_t is the particle terminal velocity (m s^{-1}), g the gravitational acceleration (m s^{-2}), D the diameter of the particle, ρ_s the density of the particle (g m^{-3}), ρ_f the density of the fluid (g m^{-3})

and η_f the viscosity of the fluid (Pa s). For intermediate Reynolds numbers (and particle sizes) there are various empirical models which can be used to estimate terminal velocities (Heiskanen, 1993). From the above expressions, the terminal velocity of a particle in a fluid is a function of its size and density, with larger, more dense particles settling at higher rates.

As the solids concentration in the pulp increases above 15 %, particle-particle interactions can no longer be ignored, and the system is said to be in a hindered settling regime. The system begins to behave as a heavy liquid whose density is that of the pulp rather than that of the carrier. The high density and viscosity of the pulp results in an increased drag on the particles causing them to settle at a slower rate. Under these conditions a modified form of Newton's law can be used to determine the approximate terminal velocity of particles, by replacing the density of the fluid with the density of the pulp in Equation 3.2. The reduction in effective density $(\rho_s - \rho_f)$ will be greater for particles of lower SG and will, therefore, have a greater reduction in their falling velocity. This increases the effect density differences have on separation, reducing the impact of particle size.

To compare settling rates of different minerals the free-settling ratio (Equation 3.3) can be used to indicate the ratio of particle size at which two particles of differing specific gravities will have the same settling velocity.

$$\frac{D_1}{D_2} = \left(\frac{\rho_{s_1} - \rho_f}{\rho_{s_2} - \rho_f}\right)^n \tag{3.3}$$

Where n is 0.5 for fine particles obeying Stokes' law and 1 for large particles obeying Newton's law. For intermediate particles n lies between 0.5 and 1. Therefore, as particle size becomes finer the free-setting ratio decreases and SG based separations become more difficult. To counteract this effect a centrifugal acceleration can be applied to significantly increase the apparent gravitational field felt by particles. Modern gravity separators, which impart additional centrifugal acceleration to particles, can produce an acceleration of up to 300 times that of Earth's gravity, which dramatically increases the settling velocities of small particles. This also increases the difference in settling velocity for near density minerals allowing for an improved separation.

From terminal velocities alone the rate at which particles settle is only a function of particle size and density, with increasing either resulting in more rapid settling. However, after some hindered settling has occurred to create a particle bed, separation occurs through two other distinct mechanisms. Heavy coarse particles with enough force can displace a path through the mobile particle bed and fine particles can trickle through the interstices of the coarse particles forming the bed. As a bed compacts, larger particles interlock and their movement is interrupted, but fine particles can still move in the interstices of the larger particles. As fine dense particles will have more rapid settling rates than those with a lower SG they will be preferentially recovered through interstitial trickling.

Many gravity concentrators rely on flowing films to impart separation. When a fluid is flowing on a solid surface, it can be said to have different layers with velocities ranging from zero at the solid-pulp interface to a maximum at the free surface. Particles in the fluid are thus subject to different magnitudes of fluid drag based on the fluid layer in which they are. Particles which settle faster (*i.e* high SG particles) will remain in the high velocity flow layers for less time and will therefore be less impacted by the flow of the fluid, and move more slowly down the surface, resulting in a lateral displacement of the material.

In concentrated flowing pulps, Bagnold forces also play a role in the preferential recovery of fines. As particles in a faster flowing layer flow over those in a slower layer or the stationary solid surface, they are subject to a continuous shear and a dispersive pressure is exerted between the particles. This dispersive pressure, known as the Bagnold force, is normal to the direction of shear and proportional to the square of the particle's diameter, the particle's density, the solids concentration in the pulp and the shear rate (Bagnold, 1954). If this dispersive pressure is greater than the apparent weight of a particle there will be a net force away from the solid surface. The ratio of the Bagnold force to the force caused by the apparent weight of a particle can be calculated by Equation 3.4 (Sivamohan and Forssberg, 1985).

$$\frac{F_B}{F_w} = \frac{kD\left({}^{du}/_{dy}\right)^2}{1-{}^{\rho_f}/_{\rho_s}} \tag{3.4}$$

Where F_B is the Bagnold force (N), F_w is the force from the particles apparent weight (N), *du/dy* is the rate of shear (s^{-1}) and k is a constant. From Equation 3.4, if two particles of different diameter are considered the particle with the larger diameter should tend to drift away from the solid surface, and smaller particles towards it. Similarly, a particle of lower SG should also drift away from the solid surface and higher SG particles towards it. In a mobile particle bed, the action of Bagnold forces causes it to dilate, which further promotes the recovery of fines through interstitial trickling. Bagnold forces coupled with interstitial trickling leads to vertical stratification of particles with coarse low SG particles on top, followed by fine low SG particles, then coarse high SG particles and fine high SG particles on the bottom.

3.3.1 Gravity Separation Techniques

Many different techniques have been designed and built to separate minerals based on SG differences. They can be classified as either conventional or enhanced gravity separators. Enhanced gravity separators are those which impart additional centrifugal acceleration to particles, making them much more effective at processing fine or relatively low SG minerals when compared to conventional gravity separators. Although conventional gravity separators are limited to processing relatively coarse (> 53 µm) material, they offer advantages in increased throughputs, greater simplicity, and they are better suited for higher grade (> 1% heavy material) deposits due to the semi-continuous nature of most enhanced gravity separators. An overview of gravity separation techniques used in this work are provided here, however, a more in-depth discussion of them or details on other gravity separation techniques can be found in Wills and Finch (2016c) and Falconer (2003); with an overview of dense medium separation (DMS) being found in Wills and Finch (2016d) and Napier-Munn *et al.* (2014).

3.3.1.1 Dense Medium Separation

DMS is a process which utilises a liquid (lab scale) or an aqueous suspension of fine particles (industrial scale) with predetermined density for which particles less dense than the liquid will float, while those heavier will sink. A simple schematic of its principle is shown in Figure 3.5. In the case of suspensions, the suspended particles that make up the dense media are always significantly finer than the particles to be separated. The process can be controlled with a high degree of precision over a wide range of separating densities and is commonly applied as a preconcentration step for minerals (such as cassiterite) and in the separation of coal from contaminants. However, the process is expensive, due to the cost of the medium and ancillary equipment needed to clean and recycle the medium; and is not effective for processing fine particle sizes at an industrial scale. Traditionally, DMS is performed using static bath separators, for which separation is only practical at coarse particle sizes (> 4 mm) as the slow settling rates of fine particles result in a poor separation efficiency. To improve the separation efficiency of finer particles, centrifugal separators have been employed to aid in their migration through the dense medium. Industrially, centrifugal DMS is considered practical for particle sizes down to 0.5 mm in diameter, however, several initiatives to beneficiate fine coal have shown that good separation can be achieved for particle sizes down to 25 µm (Aktaş *et al.*, 1998; Klima *et al.*, 1995), and more recently, work by Hirajima *et al.* (2005), investigating centrifugal DMS for the recycling of rare earth-activated phosphors from waste fluorescent lamps, demonstrated effective separation of particles with a size of 3–13 µm. At the lab scale, particle size is not a factor and sharp separations remain possible at very fine particle sizes (Browning, 1961).

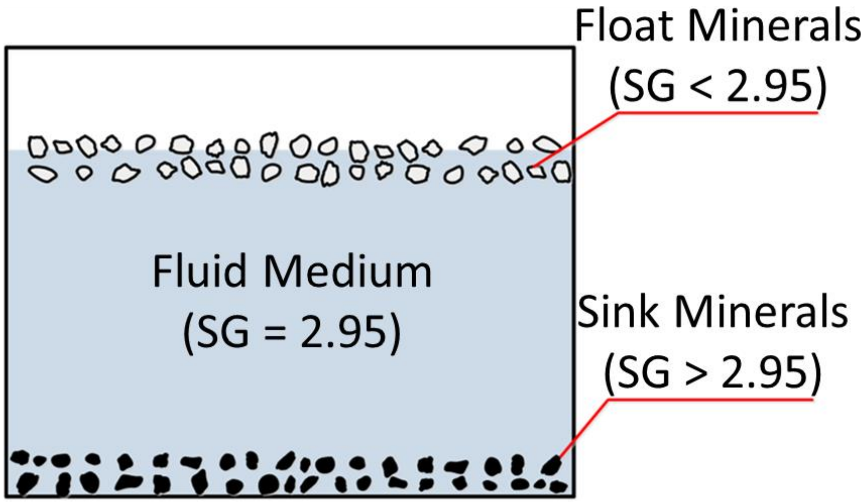

Figure 3.5 – Principle of DMS. Adapted from Wills and Finch (2016d)

3.3.1.2 Shaking Table

Mineral particles on a shaking-table are subject to two primary forces: the flowing film and the force caused by an oscillating motion applied to the solid surface. The flow of water carries light particles which remain suspended in the fast-moving layers down the table, where heavy particles are carried to the concentrate zone from the motion of the table. Using a slow forward stroke and a rapid return, particles at the surface of the of the table move slowly in the forward direction of the oscillating motion.

The Mozley Laboratory Shaking Table or "Superpanner" is a laboratory-scale shaking table. It is well-suited for early scoping studies on ores which appear to be amenable to gravity separation. The Mozley table can produce very precise SG separations and its low mass requirements make it a useful technique when insufficient material is available for larger scale tests such as spiral, shaking table or enhanced gravity separator testing.

3.3.1.3 Spiral Concentrator

A spiral concentrator is a conventional gravity separator composed of a slanted trough that spirals vertically downwards in helix configuration about a central axis. A feed pulp, between 15 $\%_{w/w}$ and 45 $\%_{w/w}$ solids, is introduced at the top of the spiral. As the pulp flows downwards, hindered settling, a flowing film action, interstitial trickling and Bagnold forces act to concentrate heavy particles near the surface of the trough, while light particles remain in the high-velocity layers travelling in a curved path (Sivamohan and Forssberg, 1985). Due to the spirals geometry, different pulp layers will not only travel with different velocities, but also centrifugal accelerations; from zero at the solid-pulp interface to a maximum at the free surface. This forces light particles (and water) to convey radially outwards accumulating in the outer portion of the trough and gives rise to a radial pressure gradient, as the hydrostatic pressure at the outer portion of the spiral will be greater than that at the inner portion. At a certain depth, the inward force resulting from the pressure gradient will exceed the force due to centrifugal acceleration. The lower layer of the pulp will flow inward as a result of this force imbalance, creating a secondary flow pattern (Holtham, 1990). These combined effects cause particles to stratify horizontally across the trough, with the heavier material concentrating in the inner part of the spiral and the lighter material flowing outward. A schematic demonstrating the primary and secondary flow patterns in a spiral and mineral stratification is shown in Figure 3.6.

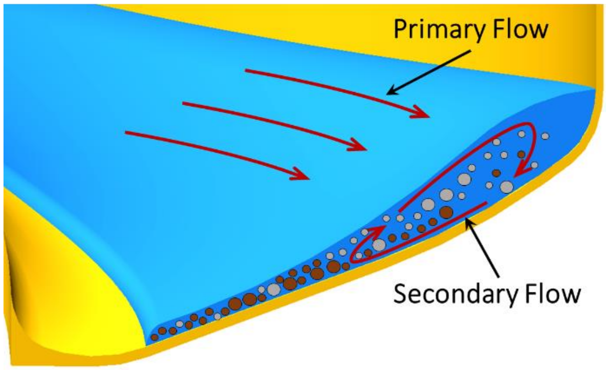

Figure 3.6 – Flow patterns present in a spiral. Adapted from Wills and Finch (2016c)

3.3.1.4 Knelson Concentrator

The Knelson Concentrator (Figure 3.7) is a compact enhanced gravity separator which employs a rotating inclined bowl, lined with fluidized grooves to collect high specific gravity particles. The feed is introduced at the bottom of the bowl, through a downcomer, where centrifugal acceleration forces particles to travel radial outward. Through hindered settling, enhanced by centrifugal acceleration, heavy particles are trapped in the grooves of the bowl and light particles are carried by water to the top of the unit and ejected. To prevent compaction of particles in the grooves, a pressurized water jacked forces water through perforations in the grooves, fluidizing the bed of heavy particles. This allows for the constant substitution of light particles (which may have reported to the concentrate) with heavy SG particles.

The Knelson Concentrator was originally developed for gold processing, employing semi-continuous units which stop to flush out the concentrate after a certain interval (when the bowl is filled with high SG material). While these units work well for mineral deposits which contain very low concentrations (< 1%) of high SG material, they run into operational difficulties when processing ores with higher concentrations. However, due to its relatively low cost, small environmental impact when compared to other separation techniques (such as froth flotation), and the development of the Continuous Variable Discharge (CVD) concentrator, the Knelson has become an active area of research for the processing of many low-SG deposits. A summary of the various low-SG minerals for which the Knelson Concentrator has been applied is shown in Appendix A (Table A.5). The Knelson Concentrator is typically operated to produce a gravitational field of 60 G, however, the newest models can produce up to 200 G for semi-continous units and 90 G for continuous units. It is important to note that most REM deposits contain relatively high concentrations of high SG material and would require the use of a continuous system. No such device exists at the lab-scale, however, work by Sakuhuni *et al.* (2016), has demonstrated a batch lab-scale Knelson Concentrator can be used for predicting CVD performance.

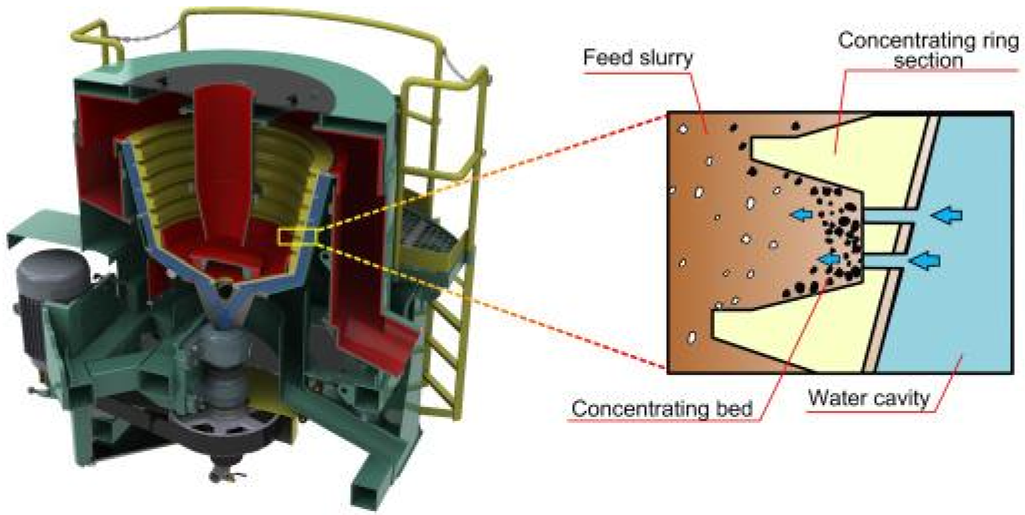

Figure 3.7 – Knelson Concentrator cutaway and schematic detailing the action in a concentrating groove. Reproduced with permission from Wills and Finch (2016c)

3.3.1.5 Multi-Gravity Separator

The Multi-Gravity Separator (MGS) is an enhanced gravity concentrator which utilizes the combined effects of centrifugal acceleration and the forces acting on a traditional shaking table to impart separation. The device can be visualized as rolling a conventional shaking table into a drum with a conical profile, then rotating it so that an elevated gravitational pull can be exerted on the mineral particles as they flow in the water layer across the surface. Because of the centrifugal acceleration and sinusoidal shaking, dense particles migrate through the water layer to form a bed of high SG particles against the drum wall. This high SG layer is conveyed by scrapers (which rotate in the same direction as the drum, but, at a slightly faster speed) towards the open end of the drum and low SG minerals are carried by the flow of wash water to the rear of the drum. Figure 3.8 depicts a pilot scale MGS, its main operating and design variables and the principle forces acting on a particle. While a good deal of work has reported on the effects of operating conditions (rotational velocity of the drum has been identified as the most important factor on separation) (Aslan, 2007a, b, 2008a, b; Chaurasia and Nikkam, 2017b; Özgen, 2012; Traore *et al.*, 1995; Turner and Hallewell, 1993), little work has gone into the influence of changes to design variables on MGS performance (Fitzpatrick et al., 2017). Design variables, such as the cone angle, shape or profile of the scraping blades and the relative velocity between the drum and the scraping blades would all be expected to have an influence on performance.

To improve the capacity of the MGS, a new scraping blade design has been developed by Gravity Mining Ltd (UK). A schematic of the blades can be seen in Figure 3.9. The scraper blades are low-profile in comparison to the conventional blades allowing for material to flow over the top of the blades. Initial test work using the new scraper design to recover tungsten from a magnetic waste stream, demonstrated significant improvements over the conventional scrapper system (Fitzpatrick *et al.*, 2018). Specifically, greater tungsten recovery (33 % *vs.* 20 – 25 %) was observed at the required minimum product grade (43 % WO_3).

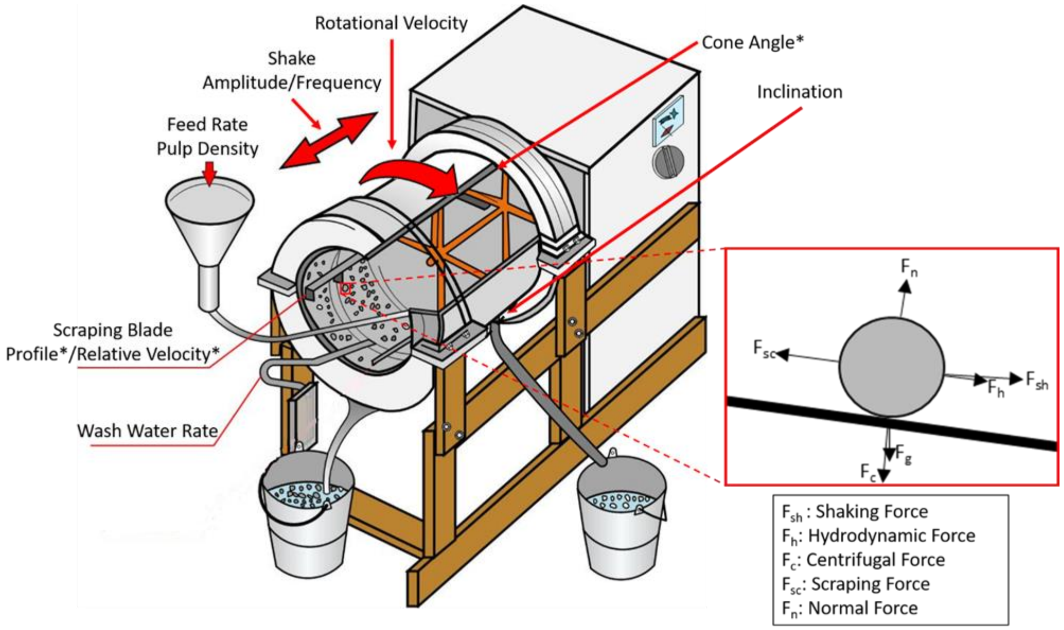

Figure 3.8 – Schematic of a pilot scale MGS, showing the main operating and design (denoted with *) variables, and the principle forces acting on a particle. Adapted from Wills and Finch (2016c) and Fitzpatrick *et al.* (2018)

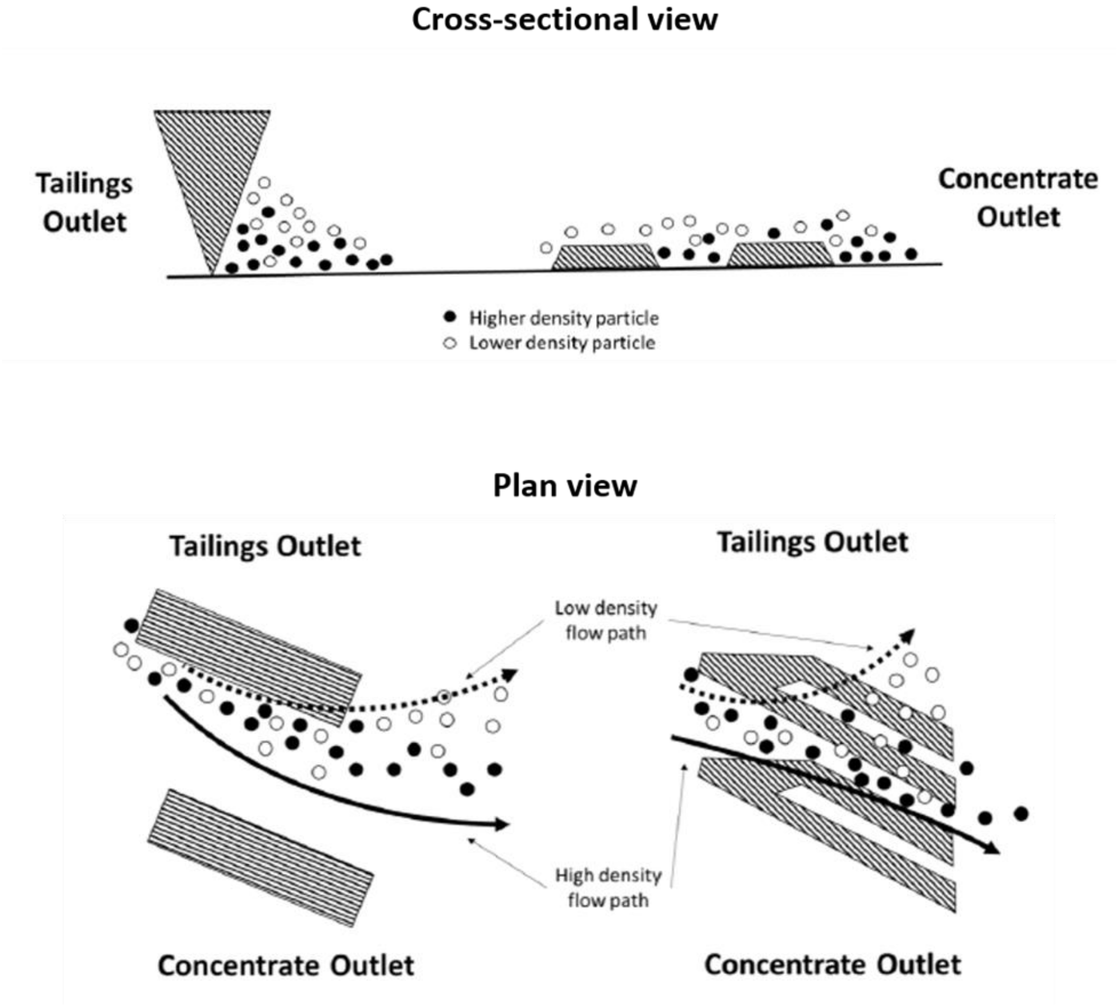

Figure 3.9 – Schematic of conventional scraping blades (left) and low-profile blades (right). Adapted from Fitzpatrick *et al.* (2018)

3.4 Magnetic Separation

The magnetic separation of minerals exploits differences in how a mineral particle will behave when exposed to a non-homogeneous applied magnetic field. The magnetic behaviour of a material depends, primarily, on its atoms' orbiting electrons. Under ordinary conditions (*i.e.* with no applied magnetic field), electrons in a material preferentially arrange themselves into pairs, to cancel out the opposite intrinsic magnetic moment of another electron, and fill subshells with zero net orbital magnetic moment. When a material has an electron configuration with unpaired electrons they will generally remain “non-magnetic”, as the electrons will contribute magnetic moments that point in different, random directions, thus cancelling. However, when placed in a magnetic field, paired electrons remain with their intrinsic magnetic moments pointing in opposite directions, while unpaired electrons, will tend to align themselves in the same direction as the applied field; thus, becoming attracted along the applied magnetic field lines. Therefore, depending on their electron configuration, a material can be considered diamagnetic (no unpaired electrons) or paramagnetic (with unpaired electrons). When a diamagnetic material is placed in a magnetic field, orbital magnetic moments will tend to align in such a way to oppose the applied field. A diamagnetic material will, therefore, be weakly repelled along the magnetic field lines. While all materials will undergo this orbital response to an applied magnetic field, in paramagnetic materials the effect caused by unpaired electrons is much more significant. Certain highly magnetic materials can be considered as being ferromagnetic. Ferromagnetism can be regarded as a special case of paramagnetism, where along with the tendency of unpaired electrons to align their intrinsic magnetic moments with an applied magnetic field, they also have the tendency to orient these magnetic moments parallel to each other even when there is no applied field. This spontaneous alignment of intrinsic magnetic moments allows a ferromagnetic material to be able to more rapidly align its magnetic moments along the applied magnetic field lines, resulting in much higher magnetisation at lower applied magnetic field strengths. This description is only meant to provide a simplified view into the magnetism of materials, a complete understanding requires a quantum-mechanical description which can be found in Jiles (2015).

Examples of diamagnetic, paramagnetic and ferromagnetic behaviour can be seen in Figure 3.10, represented as magnetization versus applied magnetic field strength. The slope of these curves represents the magnetic susceptibility of a material. Ferromagnetic materials will have a very high initial magnetic susceptibility, until all magnetic moments have aligned with the applied magnetic field, after which a further increase in the strength of the applied magnetic field will not be accompanied by an increase in magnetization. It should be noted that Figure 3.10 only shows the initial magnetisation curve of a ferromagnetic material and does not show its remnant magnetisation after an external magnetic field is removed.

To directly measure the magnetic properties of a mineral various techniques exist, including the vibrating sample magnetometer (VSM) (Foner, 1959; Svoboda, 2004). This technique suspends a small quantity of material from an oscillating rod, which is vibrated at small amplitude with a known frequency and phase. It is subjected to a series of uniform magnetic fields of varying strength. The field distortion produced by the sample is measured by a series of detection coils. The magnetic moment can be converted to magnetisation by dividing the volume of the sample and plotted against the applied magnetic field (as shown in Figure 3.10), to determine its magnetic properties.

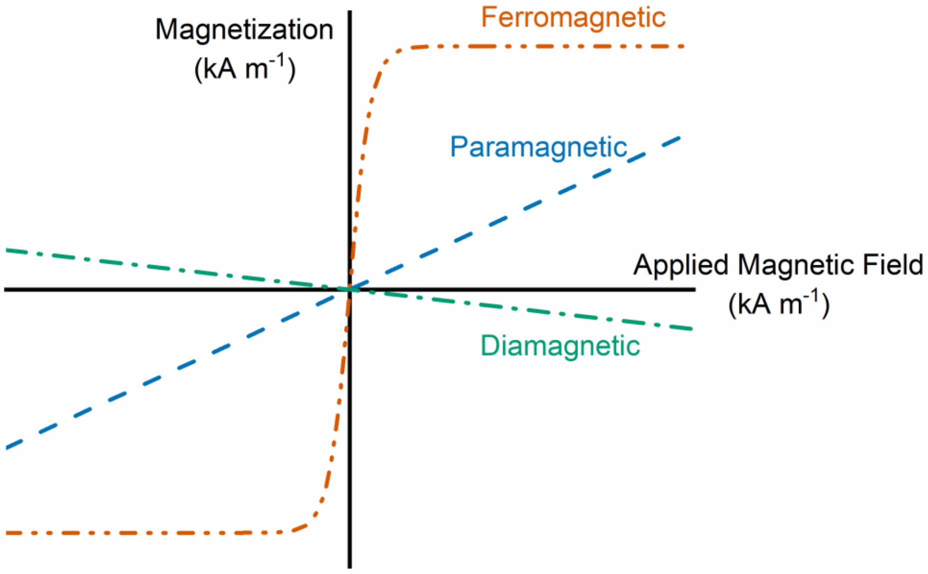

Figure 3.10 – Typical magnetization versus applied magnetic field strength trends for diamagnetic, paramagnetic and ferromagnetic materials

3.4.1 Magnetic Separation Techniques

Magnetic separators rely on the competition between magnetic force and competing forces. For fine particle sizes fluid drag forces are generally the dominate competing force, whereas at coarser sizes it is the force due to gravity. The magnetic force in a magnetic separator is dependant on the applied magnetic field strength, the magnetic field gradient, the particle size and the magnetic susceptibility of the particle and fluid medium. When considered only in the x-direction, it can be expressed by Equation 3.4:

$$F_x = V\left(\chi_p - \chi_f\right) H \frac{dB}{dx} \tag{3.4}$$

Where F_x is the magnetic force on the particle (N), V is the particle volume (m^3), H is the applied magnetic field strength ($A\ m^{-1}$), χ_p is the magnetic susceptibility of the particle, χ_f is the magnetic susceptibility of the fluid and $\frac{dB}{dx}$ is the magnetic field gradient ($T\ m^{-1}$). It must be noted, that while Equation 3.4 suggests an increase in magnetic field strength will result in an increased magnetic force, it can have a negative impact on particles which exhibit some degree of magnetic ordering, as it will decrease their magnetic susceptibility (Svoboda, 1994). Excess applied field strength may also decrease the field gradient in a given separator (Svoboda, 1994). Therefore, it is important that the appropriate magnetic field is applied for a given separation, as an increase in the intensity of the magnetic field may decrease the magnetic force acting on a particle.

The magnetic force will only be larger than the competing forces (fluid drag or gravity) over a specific size range, depending on the mineral's magnetic susceptibility. Minerals with high magnetic susceptibility will be able to be recovered over a wider range of particle sizes. The effective range of magnetic separation has been suggested as between approximately 5 μm to 1000 μm (Oberteuffer, 1974), however, there are initiatives to recover magnetic material at finer sizes (Arol and Aydogan, 2004; Ebner *et al.*, 1997; Menzel *et al.*, 2012; Roy, 2012). Various magnetic separation devices exist and while those used in this work are briefly explained here, a more in-depth discussion of them or details on other magnetic separation techniques can be found in Wills and Finch (2016e), Oberteuffer (1974), Svoboda and Fujita (2003) and Svoboda (2004).

3.4.1.1 Wet Magnetic Test Chute

A wet magnetic test chute (Figure 3.11) is a simple laboratory scale device for magnetic separation testing. Mineral slurry is fed down an include surface which is placed over a permanent magnet.

Mineral particles with high magnetic susceptibility will be attracted by the low-intensity magnetic field and be pinned to the surface. Mineral particles which are not attracted to the inclined surface report with the slurry water as non-magnetics at the bottom of the chute. To increase the magnetic force acting on particles (to recover minerals of lower magnetic susceptibility, or to overcome the influence fluid drag or gravity have on recovering fine and coarse particles, respectively) the permanent magnet can be replaced with a magnet of higher field strength (i.e replacing an iron-based magnet with a RE magnet).

Figure 3.11 – Laboratory wet magnetic test chute

3.4.1.2 Wet High-Intensity Magnetic Separator

To treat paramagnetic minerals of low magnetic susceptibility and/or fine size, high field strengths and gradients are required to induce a sufficiently high magnetic force on the particles to recover them. As high-intensity fields can negatively impact separation (Section 3.4.2), increases in field gradients are generally favoured. To achieve high magnetic field gradient, techniques such as a wet high intensity magnetic separator (WHIMS) (Figure 3.12), place a matrix constructed from a ferromagnetic material, such as steel, in a high-intensity magnetic field (generated by an electromagnet). This produces many sites of high field gradient for which particles with low magnetization can be captured.

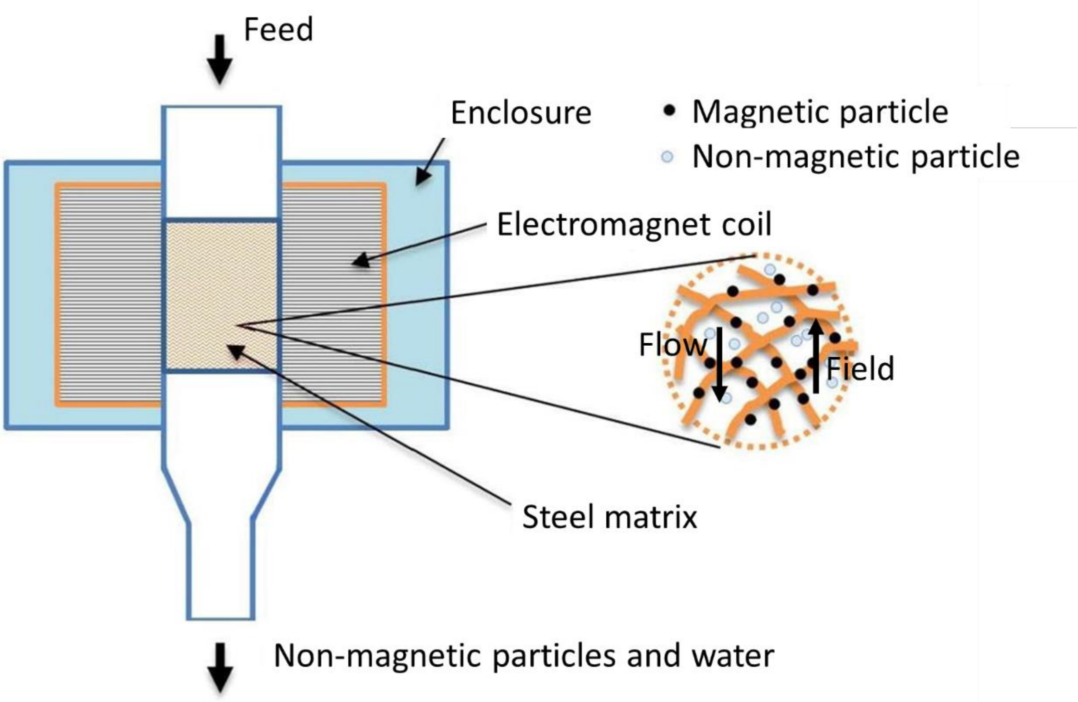

Figure 3.12 – Schematic of a wet high-intensity magnetic separator. Adapted from Ge *et al.* (2017)

3.5 Electrostatic Separation

Electrostatic separation of minerals exploits differences in how a mineral particle, which has been pre-charged, will behave under the influence of an electric field (electrophoresis). Mineral particles are charged through three main mechanisms: ion-bombardment (corona charging), conductive induction and contact charging (triboelectric charging). The most common electrostatic separator, the high-tension roll separator (Figure 3.13), uses corona charging. Mineral particles are fed onto a grounded metal roll, where they are charged by a corona-producing electrode, placed above the roll's surface. As mineral particles move past the field of ion bombardment, they will either remain pinned to the surface of the drum or thrown from it, depending on the particle's conductivity.

Strongly conductive minerals will lose their charge to the earthed roll rapidly and be thrown from its surface. Minerals with a low conductivity do not lose their charge and remain pinned to the grounded roll, until they are removed by a brush. This technique has limited uses in mineral processing, as it has difficult to achieve processing conditions (the feed must be perfectly dry) and is not effective at treating fine particle sizes (Figure 3.2). It is primarily used for placer deposits (as they do not require grinding, rending dry processing more economical), and due to the fine-grained nature of most REM deposits which are not placers, this is likely the only REE resource for which electrostatic separation can be applied. As such it will not be discussed further in this thesis.

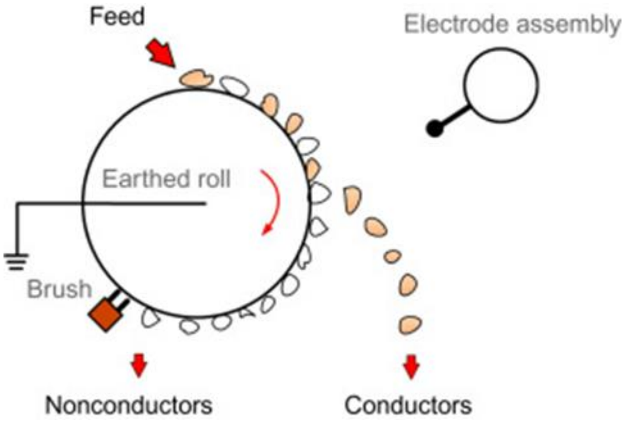

Figure 3.13 – Schematic of a high-tension roll separator. From Wills and Finch (2016e)

3.6 Process Mineralogy

Although mineral processing steps are focused on the concentration of minerals, typically, mineralogy is only considered and commissioned during exploration, feasibility and start-up stages of a mine (Butcher, 2010). Metallurgists tend to characterize mineral separations using elemental grade and recovery values, determined by chemical assays, obtained from techniques such as inductively coupled plasma (ICP), atomic absorption spectroscopy (AAS) or X-ray fluorescence (XRF). This is because, in most cases (except for industrial minerals), it is the valuable elements (and penalty elements) which define the economics of a process. In some very specific cases, such as for very simple ores, where metals are present in a single mineral phase (*i.e.* mineral balance is equal to the metal balance), this analysis is sufficient. However, to truly characterize the response of an ore to a beneficiation process, it is necessary to couple this chemical analysis with a mineralogical one. The application of mineralogical information to mineral processing (and other downstream processes) to improve understanding, solve problems and improve efficiency is commonly referred to as process mineralogy.

In the past, process mineralogy was generally only used when trying to diagnose a problem in a processing plant (*i.e.* decrease in concentrate grade or recovery occurred). However, as mining operations are now faced with processing much more complex resources, while dealing with volatile metal prices, heightened expectations from shareholders and much more stringent safety and environmental standards, effective use of process mineralogy in the development and optimization of a beneficiation process is of utmost importance (Butcher, 2010; Henley, 1983; Hiemstra, 1985; Petruk, 1985, 2000). This is particularly the case with REM deposits, which are often highly complex; containing multiple elements of interest, present in multiple different minerals, which are finely disseminated and have limited processing knowledge.

Historically, obtaining accurate and quantitative mineralogical information was a challenging and labour-intensive task (Henley, 1983), which is another reason as to why mineral beneficiation is typically characterized by elemental distributions. Today, however, there exists various fully automated and quantitative methods for this purpose. The most popular and widely used techniques are all based on scanning electron microscopes (SEM) equipped with energy dispersive X-ray spectrometers (EDS) and software for automatic data and image processing. The first widely adopted technology of this nature was Quantitative Evaluation of Minerals by Scanning Electron Microscopy (QEMSCAN). QEMSCAN acquires EDS and backscatter-electron (BSE) signals from each measurement point in a sample and identifies the minerals using the chemical composition from X-ray information preferentially over BSE intensity (Gottlieb *et al.*, 2000). If the constituent phases in a sample are chemically distinct, QEMSCAN is capable of reliably discriminating and quantifying minerals. Species which are chemically similar can be differentiated by element ratios or by BSE intensity, however, in complex samples, with multiple minerals and fine grain sizes, chemically similar minerals are often grouped. For example, while magnetite and hematite can be differentiated by their BSE signal they are commonly grouped as iron oxides. Other similar automated mineralogical techniques have been developed, such as the Mineral Liberation Analyser (MLA), Tescan Integrated Mineral Analyser (TIMA), Ziess Mineralogic and the Advanced Mineral Identification and Characterization System (AMICS). All these techniques are operationally different but are similar in the sense that they utilize BSE and EDS signals (in some new technologies other signals are also used) to identify and quantify minerals of a polished 2D section. Many questions arise as to the accuracy of these measurements as they are analysing sectioned particles, which may cause overestimation of the degree of liberation in composite particles. As such, work has been done to provide stereological corrections to the data (Lin *et al.*, 1999), but this is seldom used as it has been suggested that for multiphase natural ore systems stereological biases are minimal (Lätti and Adair, 2001).

3.7 Conclusions

This chapter detailed the fundamentals of mineral processing techniques which are pertinent to REM beneficiation. It covered the various separation techniques as well as the properties which govern them. The field of process mineralogy was also introduced, as it is important to REM beneficiation, due to the complex nature of many deposits and the limited fundamental understanding of their response to beneficiation processes.

Chapter 4

The Physical Beneficiation of Rare-Earth Minerals

4.1 Introduction

This chapter provides a summary of the current literature on REM beneficiation using gravity and magnetic separation. Although flotation is the most widely applied and studied beneficiation method, it is not a focus of this thesis. A detailed review of REM flotation can be found in Appendix B.

4.2 Gravity Separation

The specific gravity difference of REM (typical SG > 4) and the gangue minerals which they are commonly associated with, such as carbonates (typical SG < 3) and silicates (typical SG < 3), make them amenable to gravity separation. The application of gravity separation to REM beneficiation has been most commonly used for placer deposits (Chi *et al.*, 2001; Ferron *et al.*, 1991; Jordens *et al.*, 2013; Krishnamurthy and Gupta, 2016). These operations typically use a series of gravity, magnetic, electrostatic separation and flotation, depending on the mineralogy of the deposit, to create multiple valuable products.

In some cases, heavy minerals are found in very highly concentrated (> 70 %) placer deposits, however, most require an initial gravity separation stage to produce a bulk heavy mineral concentrate (Krishnamurthy and Gupta, 2016). One example strategy is to first upgrade the deposit (containing 2 – 5 % heavy minerals) using a cone concentrator, producing a concentrate consisting of 20 – 30 % heavy minerals. This concentrate is then further upgraded to > 80 % heavy minerals using spirals. Slight differences in specific gravity, magnetic susceptibility and surface ionization potential can then be exploited to separate the various heavy minerals. Along with cone concentrators and spirals, other commonly used gravity separation techniques employed in the beneficiation of placer deposits are jigs and tables (Chi *et al.*, 2001; Ferron *et al.*, 1991; Krishnamurthy and Gupta, 2016). Placer deposits which produce a REM stream are typically concentrating monazite and/or xenotime (Ferron *et al.*, 1991; Jordens *et al.*, 2013). However, there are some unique deposits where other REM may be concentrated, such as in the Central Eastern Desert of Egypt, where a heavy mineral occurrence with significant concentrations (approximately 1.5 %) of samarskite (Y) exists (Raslan, 2009). This deposit has been studied at the laboratory scale, using gravity and magnetic separation to produce a concentrate of 73.8 % samarskite (Y) (Raslan, 2009).

Along with their application to placer deposits, gravity separation techniques, particularly tables, have been employed at some of the largest REE deposits in China (and in the World): the Bayan Obo deposit, the Maoniuping deposit and the Weishan deposit (Chi *et al.*, 2001; Jordens *et al.*, 2013; Krishnamurthy and Gupta, 2016; Ling and Yang, 2014). While it seems as though the flowsheet at Bayan Obo may now strictly use flotation in its REM beneficiation circuit (feed of the REM beneficiation circuit is the non-magnetic tailings of an iron oxide circuit), the flowsheet which was employed in the mid 70's used a table between rougher and cleaner flotation stages (Chi *et al.*, 2001; Houot *et al.*, 1991; Krishnamurthy and Gupta, 2016; Ling and Yang, 2014; Luo and Chen, 1987). Gravity separation was likely abandoned due to unsatisfactory separation efficiency, particularly for fine particle sizes (Jordens *et al.*, 2013; Luo and Chen, 1987). At the Maoniuping and Weishan deposits, various bastnäsite beneficiation schemes have been developed for both ores, many of which utilize gravity separation. These include:

- direct tabling of the Maoniuping ore; producing three products with REO grades of 60 %, 50 % and 30 % with a recovery of 75 % (Chi *et al.*, 2001; Ling and Yang, 2014);
- preconcentrating the Maoniuping ore using a table to produce a 35 % REO product, which is then reground and floated; producing a 50 % - 60 % REO product with a recovery of 50 % – 60 % (Chi *et al.*, 2001; Ling and Yang, 2014);

- preconcentrating the Maoniuping ore using magnetic separation, followed by tabling; producing a 52 % REO product with a recovery over 55 % (Chi *et al.*, 2001; Ling and Yang, 2014);
- flotation of the Weishan ore followed by tabling; producing two products with grades of ≥ 68 % and ≥ 30 % with a recovery of 77 % – 84 % (Chi *et al.*, 2001); and
- processing of the Weishan ore using a complex gravity separation process to remove clays followed by flotation (Ling and Yang, 2014).

Outside of China, gravity separation is used to recover the REM loparite from the Kola Peninsula's Lovozero Alkali Massif, in Russia (Hedrick *et al.*, 1997). A combination of gravity and magnetic separation is used to produce a concentrate of 95 % loparite (Hedrick *et al.*, 1997). To the author's knowledge, this is the only other industrial application of gravity separation to REM. However, there may be other locations where it is employed but not reported in literature.

At the laboratory scale, many other the deposits, around the world, have examined the use of gravity separation. Guy *et al.* (2000) suggested a flowsheet for the Mount Weld deposit which employed gravity concentration of a + 300 μm crushed feed to produce a high-grade concentrate (52 % REO). The gravity tails would then be reground and processed by flotation. However, it was eventually decided to proceed with a flowsheet which relied solely on flotation for pilot testing (Guy *et al.*, 2000). The exact flowsheet employed at Mount Weld does not appear to be publicly available.

For finer particle sizes, various researchers have studied the use of centrifugal gravity concentrators (Abaka-Wood *et al.*, 2019a; Dehaine and Filippov, 2015; Filippov *et al.*, 2016; Jordens *et al.*, 2016b; Jordens *et al.*, 2016c; Jordens *et al.*, 2014; Özbayoğlu and Ümit Atalay, 1995, 2000; Schriner, 2016). Özbayoğlu and Ümit Atalay (1995) and Özbayoğlu and Ümit Atalay (2000) demonstrated the effectiveness of a MGS (Section 3.3.1.3) when processing a bastnäsite ore from a deposit in Eskişehir-Beylikahir, Turkey. The authors found bastnäsite was concentrated in particle sizes < 5 μm and produced a preconcentrate, using attrition scrubbing and hydrocyclones, with a grade of 28 % REO and recovery of 72.6 %. This preconcentrate was then processed using an MGS, which increased the grade to 35.5 % REO with 48 % recovery. The authors employed factorial design as an attempt to optimize the MGS, however, they only varied the shake frequency, wash water flow rate and shake amplitude. They found minimal effect on concentrate grade or recovery. This lack of significant impact is expected, as these are not the most important variables when trying the optimize an MGS, and the ranges the authors chose for each variable were likely too small to observe any statistically significant differences. It has been demonstrated by several authors that rotational speed of the drum is the most important variable for optimization of the MGS (Aslan, 2007a, b, 2008a, b; Chaurasia and Nikkam, 2017a; Fitzpatrick *et al.*, 2018; Özgen, 2012; Traore *et al.*, 1995; Turner and Hallewell, 1993), which was not varied here. Therefore, proper optimization may offer improved results.

Other authors have employed Knelson and Falcon concentrators as centrifugal gravity techniques (Abaka-Wood *et al.*, 2019a; Dehaine and Filippov, 2015; Filippov *et al.*, 2016; Jordens *et al.*, 2016b; Jordens *et al.*, 2016c; Jordens *et al.*, 2014; Schriner, 2016; Williams, 2018). The potential application of both techniques, to a REM deposit, was first demonstrated in literature by Jordens *et al.* (2014) in a study on the Nechalacho ore. Two different feeds were produced: one for concentration using a Knelson, with a P_{80} of 53 μm; and one for concentration using a Falcon, with a P_{80} of 44 μm. Products from both techniques were then subjected to magnetic separation. While this study was more focused on the magnetic behaviour of the ore and provided only a semi-quantitative analysis of separation using X-ray diffraction (XRD), it did indicate that both techniques could produce a heavy mineral preconcentrate. The authors suggested that the combination of Falcon and WHIMS was more effective compared to when the Knelson was employed. However, this was attributed to the fact that the finer particle size fed to the Falcon Concentrator allowed for more effective separation due to increased liberation.

Following this study, a much more extensive investigation was conducted on the same Nechalacho ore (Jordens *et al.*, 2016b; Jordens *et al.*, 2016c). The flowsheet which was followed is shown in Figure 4.1. The ore was ground to a P_{80} of 40 μm and processed by a Knelson and Falcon in series, with the tails of the Knelson Concentrator feeding the Falcon. The concentrates from each technique were then subjected to a series of low, medium and high-intensity magnetic separation steps. A thorough mineralogical analysis of the products suggested that the Knelson Concentrator exhibited greater selectivity for particle size and SG compared to the Falcon Concentrator. The Knelson Concentrator upgraded zircon [one of the most important minerals in the deposit (Ciuculescu et al*., 2*013; Grammatikopoulos et al., 2011)] 3.3 times, REM 1.8 times and iron oxides 3.4 times. Although recoveries remained low (zircon = 22 %, REM = 12.5 % and iron oxides = 23 %), this was attributed to a lack of recirculation in the tested flowsheet (Jordens *et al.*, 2016b). Along with recirculation of the feed, optimization of the Knelson's operating parameters may also offer significant benefits.

In addition to demonstrating the effectiveness of centrifugal gravity concentration, Jordens *et al.* (2016b) found that following grinding, coarse particle sizes (> 20 μm) were enriched in zircon. These coarse zircon particles were generally of elevated SG, even at sizes > 300 μm, where liberation was limited. While the mass in this size range was limited, the Knelson Concentrator was capable of upgrading zircon 1.75 times. The authors proposed a flowsheet which involved a much coarser grind (~300 μm) followed by a centrifugal gravity concentration step, followed by further grinding of the gravity concentrate and further separation. It was mentioned that this flowsheet would not be suitable for processing the entire deposit but might provide significant savings in grinding costs while producing an initial high-grade concentrate.

Schriner (2016) suggested using a Falcon Concentrator ahead of the flotation circuit at Mountain Pass. This process offered improvements in the flotation circuit, achieving the same REE grade (30 %) with higher recovery (82 % *vs*. 77 %), and a reduced calcium content in concentrate (5 % *vs*. 8 %). It is noted that in this study the overall REE recovery was low (41 %), as the recovery of three stages of a Falcon Concentrator is only 50 %. But the authors suggested a 6-stage Falcon process would increase REE recoveries above 80 %. Under this assumption the authors provided an economic analysis of this gravity-flotation process in comparison to a flotation only one. Although more capital intensive, they suggested it would yield a higher annual profit and a better 10-year net present value.

Williams (2018) also tested a Falcon Concentrator for the beneficiation of the Mountain Pass ore, but, as a final cleaning stage following flotation. In this study flotation produced a 44 % REO product with 81 % recovery. This concentrate was further upgraded using a Falcon to a grade of 47 %, maintaining a recovery of ~ 73 %. While these results demonstrate its effectiveness at producing a cleaner concentrate, an economic analysis suggested the addition of a gravity cleaning stage is not economically favourable without a significant rise in the price of the hydrochloric acid used downstream.

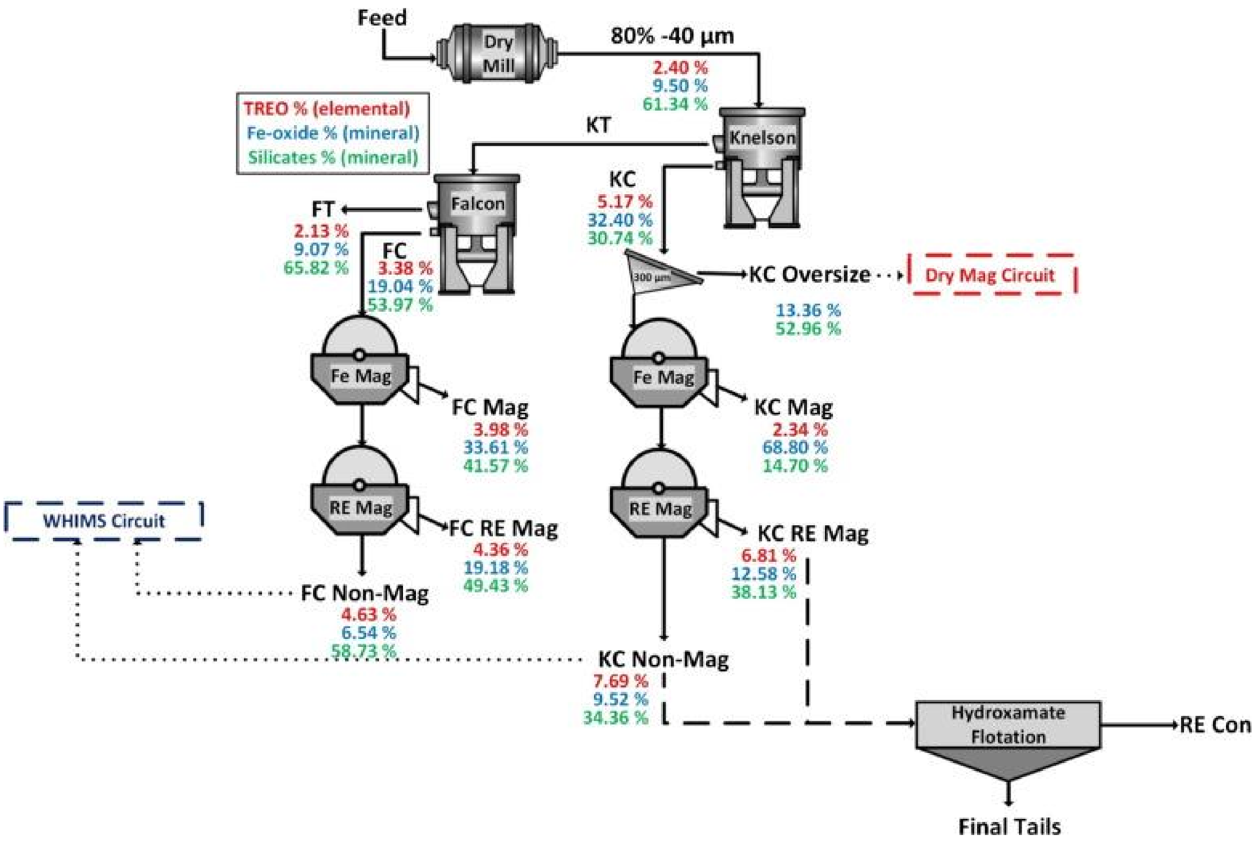

Figure 4.1 – Flowsheet detailing gravity and magnetic separation experiments carried out by Jordens *et al.* (2016b).

Abaka-Wood *et al.* (2019a) took a similar approach to Jordens *et al.* (2016b) and Schriner (2016), with the idea of producing a preconcentrate of REM from Australian iron oxide – silicate rich tailings, using gravity separation. The methods tested were a Knelson Concentrator and a Wilfley shaking table. The tested sample had a particle size distribution with a d_{50} of 13 μm and a d_{90} of 158 μm. In this case the authors found the shaking table outperformed the Knelson Concentrator, which was deemed ineffective with minimal upgrading. However, there are significant inconsistencies with the results which are presented. For instance, the ICP analysis found the shaking table and Knelson produced REO upgrade ratios of 1.2 and 0.9, respectively; whereas, QEMSCAN data found REM upgrade ratios of 3.3 and 1.6, respectively. The authors simply state that there are limitations when using ICP and that the QEMSCAN data is more reliable. However, typical practice is to compare QEMSCAN calculated assays to measured chemical assays, from a technique such as ICP (Becker *et al.*, 2009; Coetzee *et al.*, 2011; Grammatikopoulos *et al.*, 2011; Pooler and Dold, 2017; Smythe *et al.*, 2013). This is used as a validation and quality control mechanism for automated mineralogical analysis, to avoid any potential bias. One common concern is differential settling and density segregation of particles during the preparation of polished sections, which can result in overestimations of high SG minerals (Coetzee *et al.*, 2011; Kwitko-Ribeiro, 2012; Speirs *et al.*, 2008).

A final example of gravity separation being used as a preconcentration step is with regards to a REE-bearing micaceous residue from a kaolin plant in England (Dehaine and Filippov, 2015; Dehaine *et al.*, 2017; Filippov *et al.*, 2016). The initial study used a Falcon Semi-Batch (SB) Concentrator and a shaking table in series to produce concentrates for mineralogical characterization (Dehaine and Filippov, 2015). The feed had a particle size distribution with a d_{80} of ~80 μm; with 61 % of the LREE in particle sizes < 40 μm (compared to just 12.3 % of the feed mass). The grade of the micaceous residue was very low, with a LREE content of 0.011 %. Following separation grades remained low (maximum grade of ~0.6 % LREE was achieved), however, the gravity separation stages could recover 75 - 85 % of the LREE in 8 - 15 % of the mass.

Two subsequent papers were later published, expanding on this work (Dehaine *et al.*, 2017; Filippov *et al.*, 2016). A similar micaceous feed from the same plant was obtained and split at 53 μm. The over-sized fraction was processed using a two-stage gravity separation process consisting of a spiral followed by a shaking table (Dehaine *et al.*, 2017). The under-sized fraction was deslimed and split, and a comparative study of flotation and concentration using a Falcon Ultra-Fine (UF) Concentrator was performed (Filippov *et al.*, 2016). A single pass of the spiral concentrator recovered 70 % of LREE and 30 % heavy minerals in ~10 % of the mass (Dehaine *et al.*, 2017). Shaking table testing on the spiral concentrate resulted in concentrates of 98.5 % heavy minerals (Dehaine *et al.*, 2017). In this study LREE grades reached 1.6 % (Dehaine *et al.*, 2017); greater than those achieved in Dehaine and Filippov (2015), however, this is likely to be still too low to be directly considered a marketable REE product. For the finer (-53 μm) fraction, flotation was determined to be more efficient than the Falcon UF or Falcon SB, producing a product with a LREE grade of ~0.5 % and recovery of 80 % (Filippov *et al.*, 2016). The Falcon UF produced high recoveries but little enrichment (upgrade ratio = 1.3 – 1.4), whereas the Falcon SB produced higher grades (upgrade ratio = 56) but low recoveries (17 – 22 %) (Dehaine and Filippov, 2015; Filippov *et al.*, 2016).

4.3 Magnetic Separation

4.3.1 Magnetic Properties of REM

The most extensive study to date detailing the magnetic properties of REM is that by Rosenblum and Brownfield (2000). Although this study did not directly measure the magnetic susceptibility of minerals, it used a Frantz Isodynamic Separator to rank over 350 different minerals based on their magnetic response at different operating currents (lower current = higher magnetic susceptibility). The REM which were studied, their best extraction range in the Frantz, their magnetic properties and the number of different samples tested are listed in Table 4.1. In some cases, the reported recovery range was highly variable, which the authors reported to be due to varying chemistries between mineral samples. Ito *et al.* (1991) predicted REM magnetic susceptibilities using calculated magnetic susceptibilities of individual REE (M^{3+} ions), indicating that the magnetic susceptibilities of elements from gadolinium to erbium were the highest of all the lanthanides. The authors used this to explain the higher magnetic susceptibly of xenotime [$(HREE)PO_4$] (contains more gadolinium, dysprosium and erbium) compared with monazite

[(LREE)PO_4]. As such, it is reasonable to conclude that the magnetic behaviour of an individual REM may vary between deposits, or even within a deposit, depending on its chemical composition.

The magnetic properties and best Frantz recovery range for common gangue minerals found in REM deposits are provided in Table 4.2 (Rosenblum and Brownfield, 2000). Comparing the minerals of this table to the REM in Table 4.1, most REM are paramagnetic, while many of the commonly associated gangue minerals are diamagnetic. Deposits containing paramagnetic REM and diamagnetic gangue should be amenable to magnetic separation. The removal of highly magnetic gangue, such as magnetite, from REM should also be possible through a low-intensity magnetic separation (LIMS) step.

Some authors have measured and reported actual magnetic susceptibility values for various REM (Al-Ali *et al.*, 2019; Haapala *et al.*, 1969; Jordens *et al.*, 2014; Svoboda, 2004; Yang *et al.*, 2013a). These values are provided in Tables 4.3 – 4.5. Jordens *et al.* (2014) used a VSM to measure the magnetic susceptibilities of allanite, fergusonite, bastnäsite and two different samples of zircon (all of which are important minerals in the Nechalacho deposit) (Table 4.3). Their results correspond well to those of Rosenblum and Brownfield (2000) (Table 4.2), finding that allanite and fergusonite had the highest magnetic susceptibilities, followed by bastnäsite and then zircon. The zircon samples tested by Jordens *et al.* (2014) were slightly paramagnetic, which is in disagreement with the generally reported diamagnetic behaviour of zircon (Moustafa and Abdelfattah, 2010; Rosenblum and Brownfield, 2000). However, zircon's magnetic properties are dependent on its chemical composition and in some cases has been shown to exhibit paramagnetic behaviour (Jordens *et al.*, 2014; Raslan, 2009).

The magnetic susceptibilities of the polysomatic series of fluorocarbonate minerals consisting of bastnäsite, parasite, röntgenite and synchysite were measured by Al-Ali *et al.* (2019). The authors employed VSM (Table 4.3) and a superconducting quantum interference device (SQUID) (Table 4.4) for their measurments. Bastnäsite, parasite and röntgenite were measured using both techniques, whereas synchysite was only measured using SQUID due to sample limitation. The grain size of synchysite in ore deposits is typically very low, therefore obtaining enough pure crystals for fundamental studies is difficult, which was the case here. The minerals showed a successive decrease in magnetic susceptibility as the calcium content increased and the REE content decreased between the four minerals. Bastnäsite, which is calcium depleted, was the most paramagnetic, followed by parasite (11 % calcium). Röntgenite (13 % calcium) was slightly paramagnetic to diamagnetic (two different röntgenite samples originating from the same source were tested, exhibiting different magnetitic properties). And sychysite (16 % calcium) was diamagnetic.

Along with the REM studied by Jordens *et al.* (2014) and Al-Ali *et al.* (2019), the magnetic susceptibility of monazite (Table 4.5) has been reported (Haapala *et al.*, 1969; Svoboda, 2004; Yang *et al.*, 2013a). The magnetic susceptibility measurements suggest that monazite is paramagnetic, which corresponds well to its behaviour in literature (Rosenblum and Brownfield, 2000).

Table 4.1 – REM minerals in order of magnetic susceptibility. Adapted from Rosenblum and Brownfield (2000)

Mineral	Best Recovery Range (A)	Magnetic Properties	Samples Tested
Gadolinite	0.2 – 0.4	Paramagnetic	4
Samarskite	0.3 – 0.6	Paramagnetic	5
Allanite	0.4 – 0.5	Paramagnetic	7
Britholite (Y)	0.4	Paramagnetic	1
Chevkinite	0.4 – 0.5	Paramagnetic	1
Columbite (Fe,Mn)	0.4 – 0.5	Paramagnetic	13
Fergusonite	0.4 – 0.6	Paramagnetic	4
Xenotime	0.4 – 0.5	Paramagnetic	3
Euxernite	0.5 – 0.6	Paramagnetic	4
Monazite	0.5 – 0.8	Paramagnetic	8
Uraninite	0.5 - >1.7 dc[1]	Para/Diamagnetic	4
Cerite	0.6 – 0.7	Paramagnetic	5
Fluocerite (La)	0.6 – 0.7	Paramagnetic	1
Bastnäsite	0.7 – 0.9	Paramagnetic	4
Parisite	0.7	Paramagnetic	1
Thorite	0.7 – 1.0	Paramagnetic	2
Brannerite	0.8 – 1.0	Paramagnetic	1
Sphene (titanite)	0.8 - >1.7 dc[1]	Para/Diamagnetic	4
Pyrochlore	0.9 – >1.7 dc[1]	Para/Diamagnetic	2
Anatase	>1.7	Diamagnetic	1
Fluorite	>1.7	Diamagnetic	3
Gorceixite / Goyazite	>1.7	Diamagnetic	1
Perovskite	>1.7	Diamagnetic	3
Zircon	>1.7	Diamagnetic	5

[1] dc = depends on mineral chemistry

Table 4.2 – Common gangue minerals found in REM deposits in order of magnetic susceptibility. Adapted from Rosenblum and Brownfield (2000)

Mineral	Best Recovery Range (A)	Magnetic Properties	Samples tested
Magnetite	0.01	Ferrimagnetic	6
Hematite	0.1 – 0.3	Para/Ferromagnetic	11
Ilmenite	0.2 – 0.3	Paramagnetic	8
Albite	>1.7	Diamagnetic	1
Apatite	>1.7	Diamagnetic	8
Barite	>1.7	Diamagnetic	6
Calcite	>1.7	Diamagnetic	8
Dolomite	>1.7	Diamagnetic	4
Microcline	>1.7	Diamagnetic	4
Orthoclase	>1.7	Diamagnetic	2
Quartz	>1.7	Diamagnetic	10
Rutile	>1.7	Diamagnetic	10

Table 4.3 – Reported magnetic susceptibilities of REM measured using a VSM

Mineral	Magnetic Susceptibility	Magnetic Properties	Reference
Fergusonite	6.01×10^{-4}	Paramagnetic	(Jordens *et al.*, 2014)
Allanite	4.63×10^{-4}	Paramagnetic	(Jordens *et al.*, 2014)
Bastnäsite	3.0×10^{-4}	Paramagnetic	(Al-Ali *et al.*, 2019)
Bastnäsite	2.1×10^{-4}	Paramagnetic	(Jordens *et al.*, 2014)
Parisite	6.0×10^{-5}	Paramagnetic	(Al-Ali *et al.*, 2019)
Zircon	2.50×10^{-6}	Paramagnetic	(Jordens *et al.*, 2014)
Zircon	2.77×10^{-6}	Paramagnetic	(Jordens *et al.*, 2014)
Röntgenite	2.0×10^{-6}	Paramagnetic	(Al-Ali *et al.*, 2019)
Röntgenite	-1.0×10^{-5}	Diamagnetic	(Al-Ali *et al.*, 2019)

Table 4.4 – Reported magnetic susceptibilities of REM measured using a SQUID

Mineral	Magnetic Susceptibility	Magnetic Properties	Reference
Bastnäsite	8.0×10^{-4}	Paramagnetic	(Al-Ali *et al.*, 2019)
Parisite	5.0×10^{-4}	Paramagnetic	(Al-Ali *et al.*, 2019)
Röntgenite	3.0×10^{-4}	Paramagnetic	(Al-Ali *et al.*, 2019)
Synchysite	-4.0×10^{-4}	Diamagnetic	(Al-Ali *et al.*, 2019)

Table 4.5 – Reported magnetic susceptibility of monazite

`Mineral	Measurement Technique	Magnetic Susceptibility[1]	Magnetic Properties	Reference
Monazite	Not Reported	9.8×10^{-4}	Paramagnetic	(Svoboda, 2004)
	Magnetic susceptibility bridge	2.0×10^{-4}	Paramagnetic	(Haapala *et al.*, 1969)
	Not Reported	6.6×10^{-5}	Paramagnetic	(Yang *et al.*, 2013a)

[1]Magnetic susceptibilities were converted from mass magnetic susceptibilities using a monazite SG of 5.15

4.3.1 Application to REM

In addition to gravity separation (Section 4.2), magnetic separation is an important process for the beneficiation of REM bearing placer deposits (Jordens *et al.*, 2013). It is most commonly employed to remove highly magnetic gangue (such as magnetite or ilmenite) or to separate paramagnetic monazite and/or xenotime from diamagnetic heavy minerals (such as zircon and rutile) (Jordens *et al.*, 2013; Krishnamurthy and Gupta, 2016). As xenotime is more paramagnetic than monazite (Table 4.1), it may be isolated using magnetic separation (Jordens *et al.*, 2013). However, fine grained xenotime (< 100 μm) is generally recovered by flotation (Jordens *et al.*, 2013; Zhang and Edwards, 2012). For the unique samarskite (Y) occurrence discussed in Section 4.2, two stages of magnetic separation were used to produce a non-magnetic samarskite concentrate (Raslan, 2009). Although samarskite (Y) was determined to be moderately paramagnetic, with the exception of zircon, its magnetic susceptibility was significantly lower than the associated minerals (ilmenite, garnet, hematite, goethite, mica and columbite) (Raslan, 2009).

As was briefly described in Section 4.2, magnetic separation has been successfully applied to many REM deposits in China, including the Bayan Obo and Maoniuping deposits, the country's two largest. At Bayan Obo, the feed to its REM beneficiation circuit is the non-magnetic tailings of its iron oxide circuit (Chi *et al.*, 2001; Houot *et al.*, 1991; Krishnamurthy and Gupta, 2016; Ling and Yang, 2014; Luo and Chen, 1987). Yang *et al.* (2013a) demonstrated the ability to recover more iron from the flotation tailings of the REM circuit, using a magnetizing (reductive) roast on the tails prior to a LIMS step to produce an iron concentrate with a grade of 45 % and a recovery of 68 % (Yang *et al.*, 2013a). For the Maoniuping ore, magnetic separation has been successfully applied to reject non-magnetic gangue prior to production of a bastnäsite concentrate using gravity separation (REO grade = 52 %, recovery = 55%) (Chi *et al.*, 2001; Ling and Yang, 2014). The magnetic separation step resulted in a REO recovery of 74 %, increasing the grade from 3.2 % to 5.6 % (Chi *et al.*, 2001; Ling and Yang, 2014).

Outside of China, magnetic separation has been industrially applied in Russia for the beneficiation of loparite (Hedrick *et al.*, 1997). It has also been tested for other deposits at the laboratory scale (Abaka-Wood *et al.*, 2019b; Chan, 1992; Jordens *et al.*, 2016b; Jordens *et al.*, 2016c; Jordens *et al.*, 2014; Katzmarzyk *et al.*, 2018; Stark *et al.*, 2017). Chan (1992) explored the application of an Eriez high gradient magnetic separator (HGMS) to the Mount Weld deposit; evaluating the effect of particle size, magnetic field strength and roasting. The results obtained indicated that upgrading REM or the removal of iron bearing minerals was not possible (Chan, 1992).

Stark *et al.* (2017) demonstrated the use of a WHIMS as a preconcentration step prior to flotation to beneficiate the Norra Kärr (Sweden) eudialyte ore. A coarse (<250 μm) and fine (<100 μm) feed were tested. Preconcentration of the coarse feed resulted in a REE recovery of 81 % with a mass yield of 52 %. Lower REE recoveries were achieved with the fine particle feed (64 %), but the mass yield was also lower (35 %).

The use of magnetic separation steps for the beneficiation of the Nechalacho deposit has been detailed by Jordens *et al.* (2014), Jordens *et al.* (2016b) and Jordens *et al.* (2016c). In the initial study, Jordens *et al.* (2014) employed a WHIMS at varying magnetic field strengths following gravity preconcentration steps designed to remove low SG gangue (Section 3.2). The authors found that low SG non-magnetic gangue minerals such as feldspars, which were not rejected by the gravity separation step, reported to the non-magnetic fraction of the WHIMS. The results for the lowest magnetic field strength tested (0.1 T), indicated iron oxides (magnetite and hematite) were preferentially recovered. It was also found that zircon was being concentrated in this fraction. This suggests that some zircon in the Nechalacho deposit may possess a high degree of para/ferromagnetism, or it remains locked with another highly magnetic phase such as magnetite.

This led to the more extensive study (Jordens *et al.*, 2016b; Jordens *et al.*, 2016c), detailed in Figure 4.1, which employed a series of low-, medium- and high-intensity magnetic separation steps following gravity preconcentration. Using different chemical and mineralogical analyses, the authors found that the low intensity magnetic separator was able to selectively remove strongly ferromagnetic iron-bearing gangue. However, even after medium-intensity drum magnetic separation, iron oxide minerals at levels as high as the initial feed grade remained in the non-magnetic fraction. The products of WHIMS tests, following the wet drum magnetic separation steps, were only analysed semi-quantitatively using XRD, and found similar results to those of Jordens *et al.* (2014). Use of a WHIMS may allow the concentration of paramagnetic REM at more elevated magnetic intensities; whilst rejecting iron oxide gangue, not rejected by the wet magnetic drum separator, at lower magnetic intensities and silicate gangue into the non-magnetic fraction.

Following a similar approach, Abaka-Wood *et al.* (2019b) tested a WHIMS for the beneficiation of REM (primarily bastnäsite) from iron oxide/silicate rich tailings from Australia. The authors found iron oxide gangue could be rejected at low intensities (0.11 T), with minimal REM losses. However, found minimal upgrading of REM at higher magnetic strengths.

An interesting study was recently undertaken by Katzmarzyk *et al.* (2018) investigating dry magnetic separation as a preconcentration step for the Khalzan-Buregtei deposit in Mongolia. The deposit has similar mineralogy to the Nechalacho ore, with primary REM being zircon, bastnäsite, parisite, synchysite and pyrochlore. The primary gangue minerals are quartz, feldspars and iron oxides. Similar to Jordens *et al.* (2016b), selective comminution was identified. Following grinding (to a particle size < 250 μm), zircon, iron oxides, quartz and K-feldspar were concentrated in coarse sizes (> 63 μm), and pyrochlore and albite were concentrated in fine sizes (<63 μm). The authors also identified that although REM grain sizes were low (ranging from a P_{80} of 30 µm to 50 µm, depending on the mineral), at coarse grind sizes (< 250 µm) REM were primarily associated in magnetic mineral clusters, which would favor magnetic separation. Using dry magnetic separation, 45 % of the mass was rejected, while recovering > 97 % of the lanthanum and cerium, and > 88 % of the yttrium, niobium (primarily associated with pyrochlore) and zirconium (primarily associated with zircon).

4.4 Conclusions

This chapter detailed the available literature on the application of gravity and magnetic separation to REM deposits. These techniques are instrumental to the beneficiation of placer deposits. They are also commonly used as preconcentration steps prior to flotation of “hard-rock” deposits, and in some cases flowsheets utilising only gravity-magnetic separation have been successfully applied. While this thesis is focused on the use of gravity and magnetic separation, the importance of flotation to REM beneficiation is acknowledged. A detailed literature review of REM flotation along with relevant flotation studies which were undertaken during this research program are provided in Appendix B.

The Nechalacho deposit is unlike most of the currently operating REM deposits, which are primarily focused on the recovery of one or two minerals (bastnäsite, monazite or bastnäsite and monazite). In this case, there are a host of valuable minerals of different mineral types, namely bastnäsite (carbonate), synchysite (carbonate), monazite (phosphate), fergusonite (niobate), columbite (Fe) (niobate), allanite (silicate) and zircon (silicate). As such, it was hypothesised that a flowsheet based on physical separations would be more advantageous to a complex flotation process. Due to its complex mineralogy, the direct flotation of this ore is likely going to involve a highly complex reagent scheme with at least two different streams; one to recover valuable silicate minerals and another to recover the other REM (allanite and zircon to not respond to the same flotation collectors as the other REM) (Jordens *et al.*, 2016a). The complexity of this process and the typically high reagent consumption (>1 kg/ton collector) coupled with the relatively low cost of REE, may render the process uneconomical. Environmental and social concerns further challenge the application of flotation to the Nechalacho deposit (or any other new deposit looking to actively supply REE) (Section 2.4.3). Although nearly all REM mines are likely to suffer to some extent from social scrutiny due to their production of radioactive waste, limiting a mine's environmental footprint through the use of reagent free techniques such as gravity and magnetic separation may allow for a more seamless transition to gain the right to operate. For example, one concern with flotation could be the use of lead ions as an activating agent when using hydroxamic acid-based collectors (the primary collector for REM flotation), which is becoming a common area of research (Feng *et al.*, 2017; Jordens *et al.*, 2016a; Meng *et al.*, 2018; Ren *et al.*, 2017; Tian *et al.*, 2018; Xia *et al.*, 2015; Xu *et al.*, 2017). Although it has been shown to be an effective activating ion for the flotation of the Nechalacho deposit (specifically for the recovery of zircon and allanite) the potential environmental and social implications of using lead might result in various complications (Jordens *et al.*, 2016a; Xia *et al.*, 2015).

Chapter 5

Experimental Methods

5.1 Introduction

This chapter details the experimental methodologies used throughout the experimental program on which this thesis is based. The theoretical basis of each technique used is detailed in Chapter 3.

5.2 Materials

The ore used in this work originated from the Nechalacho deposit (Avalon Advanced Materials Inc., Canada) located in the Northwest Territories, Canada. The deposit has an inferred resource of 160 million tonnes at a grade of 1.38 % TREO (Avalon Rare Metals Inc., 2013). It has complex mineralogy with very fine-grained RE mineralization (approximately 10 – 20 μm). The REE are hosted in various minerals including zircon, bastnäsite, synchysite, allanite, monazite, fergusonite and columbite (Fe).

5.3 Ore Preparation

The as received ore sample, with an initial top size of 3.36 μm, was representatively split into four batches for different separation test work. The first (Feed 1), a 50 kg sample, was riffled to produce 1 kg representative samples for grinding. These samples were ground wet at 50 $\%_{w/w}$ solids using a laboratory ball mill for 40 min to produce a d_{80} and d_{50} particle size distribution of 66 μm and 31 μm, respectively. The ball mill used in this thesis had an inner diameter of 145 mm and length of 145 mm and was operated at 71 % of the critical mill speed. The ball charge weighed 4515 g, with balls varying in diameter from 16 – 25 mm. The mill products were subsequently combined and sieved wet at 38 and 53 μm to completely remove the - 38 μm material and the majority of - 53 μm particles (sieving at this size was performed inefficiently and there remained some - 53 + 38 μm material in the coarse particle feed), and at 800 μm to remove very coarse material from the feed. This resulted in a relatively coarse feed with a narrow size distribution ($d_{80} = 97$ μm,

d_{50} = 72 μm) and a fine (- 53 μm) feed. The coarse feed was then representatively split, by riffling, into two streams for comparative test work using a spiral and Knelson Concentrator. The fine particle feed was used for preliminary MGS test work. A simplified flowsheet detailing the operations carried out on this feed is provided in Figure 5.1. A representative 45 g sample was also taken from the coarse particle stream for DMS.

The second batch of feed (Feed 2), weighing 15 kg, was riffled to produce 1 kg representative samples for grinding. These samples were ground wet at 50 %w/w solids for 50 min using a laboratory rod mill. The rod mill used in this thesis had an inner diameter of 180 mm and length of 230 mm and was operated at 61 % of the critical mill speed. The rod charge consisted of 22 steel rods with a length of 190 mm, weighing 10 724 g and varying in diameter from 16 – 34 mm. The mill products were then combined to produce a feed with a d_{80} and d_{50} size distribution of 55 μm and 20 μm, respectively. This was then processed using a Knelson Concentrator. A simplified flowsheet detailing the operations carried out on this feed is provided in Figure 5.2.

The third batch of feed (Feed 3), weighing 15 kg, was processed in the same manner as Feed 2, however, a MGS was used in place of the Knelson Concentrator. The MGS concentrates were then subjected to a series of magnetic separation steps. A simplified flowsheet demonstrating the operations carried out can be seen in Figure 5.3.

The fourth batch of feed (Feed 4), weighing 15 kg, was riffled to produce 1 kg representative samples. Samples were then stage ground wet at 50 $\%_{w/w}$ solids using a laboratory rod mill for 5 min intervals, to avoid over production of fines, removing all the -150 μm material through sieving between each interval and refilling the mill to ensure a 1 kg charge. Following this initial grinding stage which produced a product with a d_{80} and d_{50} size distribution of 120 μm and 66 μm, respectively, the material was sieved at 53 μm to split it into a fine particle and course particle stream. The coarse particle stream was processed using a spiral concentrator. The spiral concentrate was then reground following a similar stage grinding procedure as the initial feed, however, in this case it was ground to - 53 μm. The ground concentrate was then combined with to the initial fine particle stream and processed using a shaking table followed by magnetic separation. The simplified flowsheet detailing the operations carried out on Feed 4 is provided in Figure 5.4.

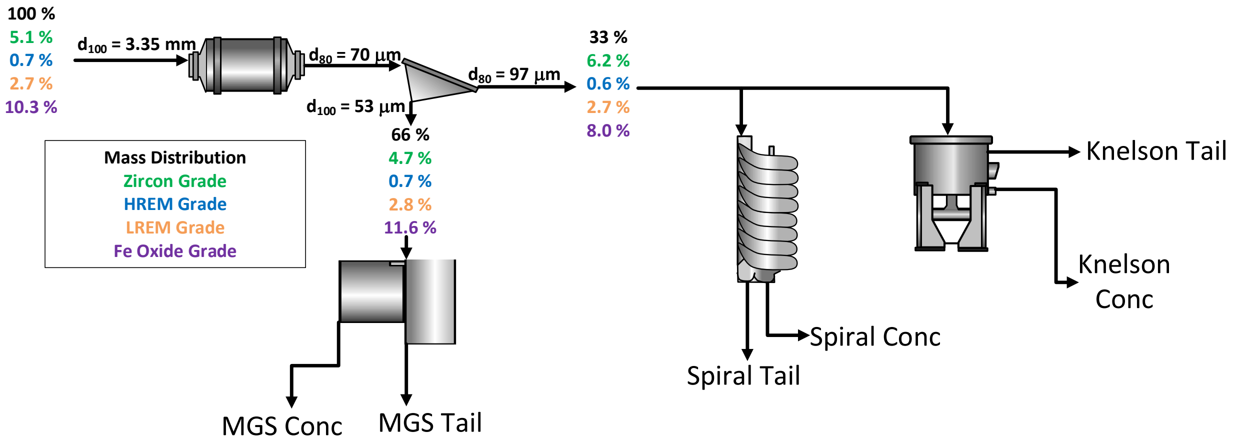

Figure 5.1 – Flowsheet detailing gravity separation experiments carried out on Feed 1. Mineral grades were determined by QEMSCAN analysis

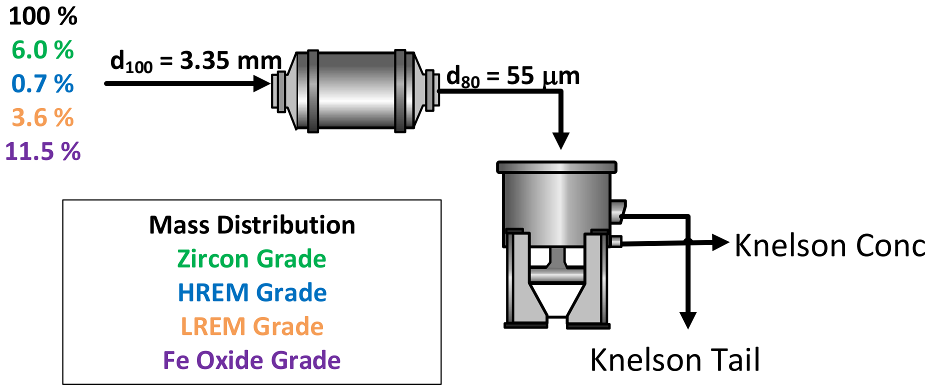

Figure 5.2 – Flowsheet detailing Knelson and magnetic separation experiments carried out on Feed 2. Mineral grades were determined by QEMSCAN analysis

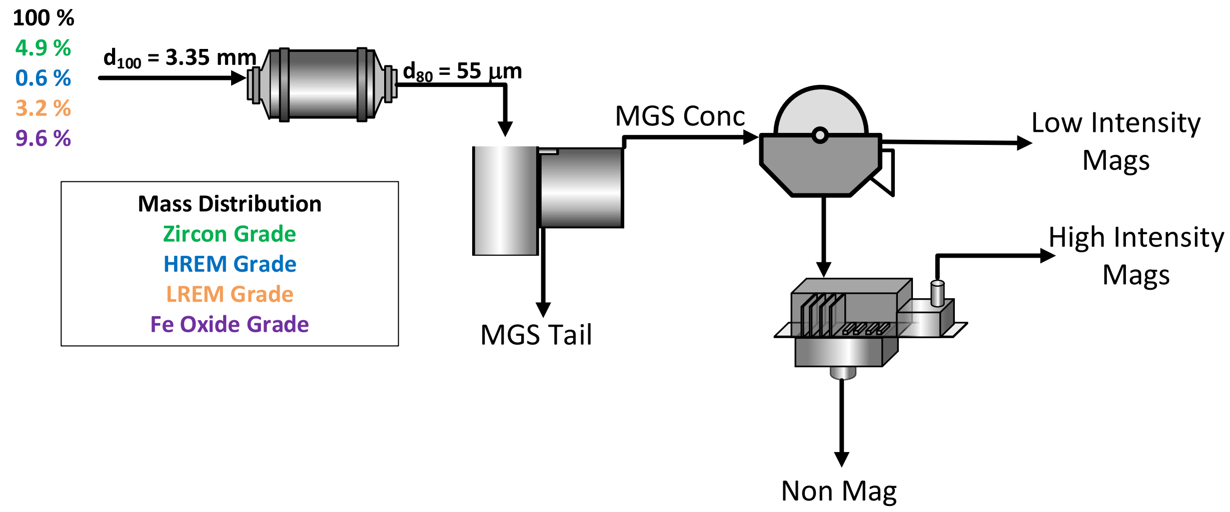

Figure 5.3 – Flowsheet detailing MGS and magnetic separation experiments carried out on Feed 3. Mineral grades were determined by QEMSCAN analysis

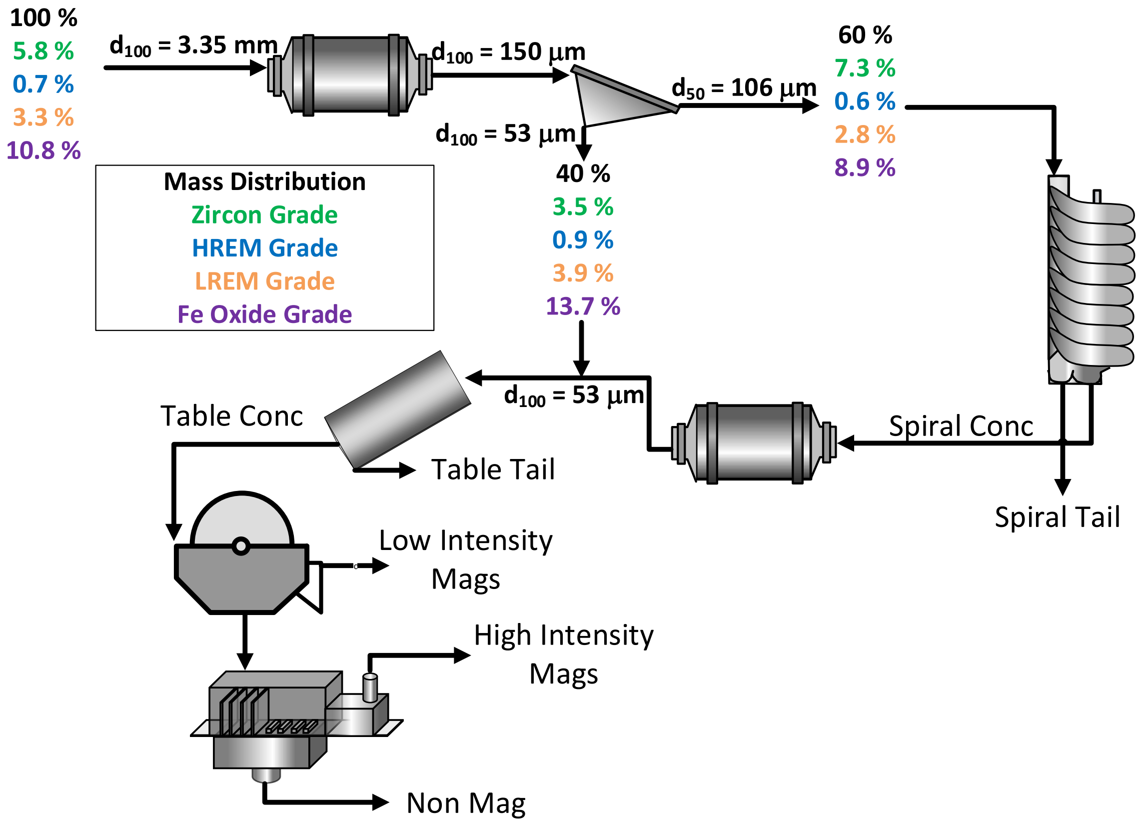

Figure 5.4 – Flowsheet detailing gravity and magnetic separation experiments carried out on Feed 4. Mineral grades were determined by QEMSCAN analysis

5.4 Characterisation Techniques

5.4.1 X-ray Diffraction

All XRD in this work was carried out with a Bruker (USA) D8 Discovery Diffractometer equipped with a cobalt X-ray source (wavelength = 1.789 Å). Diffraction patters were analyzed using Xpert High Score software (PANanalytical, Netherlands) to identify the main mineral phases which are present.

5.4.2 Inductively Coupled Plasma Mass Spectrometry

Inductively coupled plasma mass spectrometry (ICP-MS) was used to determine the REE content of the coarse fraction of Feed 1 and products of gravity separation experiments performed on this fraction. To digest samples, a homogenous melt was formed by mixing 0.1 g of sample with sodium peroxide which was then heated. The melt was then digested in hydrochloric acid. All digestions and ICP-MS in this work were conducted by SGS Canada (Lakefield, Canada). Assays are primarily used as validation of QEMSCAN.

5.4.2 X-ray Fluorescence

XRF was used in this work to determine ZrO_2, Fe_2O_3 and Ce_2O_3 content of Feed 1, Feed 2, Feed 3 and Feed 4; as well as any separation products produced on these samples. Prior to analysis mineral samples were pulverized and a homogenous glass disk was prepared by the fusion of the sample and a lithium tetraborate/lithium metaborate mixture. The prepared disks were analyzed by wavelength dispersion XRF (WD-XRF). The loss on ignition (LOI) was determined separately and gravimetrically at 1000 °C and included in the matrix corrections, which are performed by the XRF software. All XRF was conducted by SGS Canada (Lakefield, Canada). Assays are primarily used as validation of QEMSCAN.

5.4.4 Quantitative Evaluation of Minerals by Scanning Electron Microscopy

All samples in this study were analyzed using QEMSCAN to determine mineralogical information related to each sample. Prior to analysis samples were sieved into different size classes and representative samples were taken and prepared as polished sections; these were analyzed using QEMSCAN at the Advanced Mineralogy Facility at SGS Canada (Lakefield, Canada). QEMSCAN is an EVO 430 automated scanning electron microscope equipped with four light-element energy-dispersive X-ray spectrometers (EDS) detectors and iDiscover software capable of processing the data and images. QEMSCAN operates with a 25 kV accelerating voltage and a 5 nA beam current. The QEMSCAN measures, and the iDiscover software processes, data from every pixel across a sample with a pixel size defined based on the scope of the analysis. The software assigns each pixel a mineral name based on 1000 counts of energy dispersive X-ray spectral data and backscatter electron intensities.

If the minerals or constituent phases comprising the sample are chemically distinct, QEMSCAN is capable of reliably discriminating and quantifying minerals. Magnetite and hematite are grouped and referred to as Fe-oxides. Distinction between the two minerals when needed was conducted by optical mineralogy and X-ray diffraction (XRD) analysis. The mineral definitions were validated and refined to fit the particular samples. A reference mineral list was developed using XRD (primarily to define the major minerals), a scanning electron microscope (SEM) equipped with an energy dispersive spectrometer, and electron probe micro analysis (EPMA). REMs were identified based on their major REE composition.

The samples were analyzed with the Particle Mineral Analysis (PMA) method. PMA is a two-dimensional mapping analysis aimed at resolving liberation and locking characteristics of a set of particles. A pre-defined number of particles were mapped at a pixel size of 3.4–7 µm. The typical diameter of a polished section was 30 mm.

5.4.5 Scanning Electron microscopy

Representative samples from DMS experiments performed on the coarse particle fraction of Feed 1 were prepared as polished sections and analyzed with a Hitachi SU8000 cold field emission SEM (Hitachi High-Technologies, Canada) equipped with an 80 mm^2 X-MaxN Silicon Drift energy dispersive spectrometer (EDS) detector (Oxford Instruments, UK). X-ray maps were acquired at an accelerating voltage of 15 kV and beam current of 5 µA for one hour. The count rate and dead time were approximately 12 kcps and 20 % respectively. The qualitative phase maps were obtained using AZtec software (Oxford Instruments, UK).

The polished sections of products from magnetic separation experiments, created for QEMSCAN analysis, were analyzed with a Hitachi SU3500 tungsten filament SEM (Hitachi High-Technologies, Canada). The SEM is equipped with the same EDS detector and a similar procedure and analysis was followed as is detailed for the SU8000.

5.5 Gravity Separation

5.5.1 Dense Medium Separation

For DMS (Chapter 3, Section 3.3.1.1) experiments, which were performed on the coarse particle stream of Feed 1, the 45 g sample was split into three representative 15 g samples. These were added to 50 mL centrifuge tubes along with 30 mL of heavy liquid solution [lithium metatungstate (LMT), purchased from LMT Liquid, LLC (USA)] with an SG of 2.95. The suspensions were then mixed by hand shaking and centrifuged for 30 min at 4400 rpm using a IEC Centra CL2 centrifuge (Thermo Electron Corporation, USA). After centrifuging, the float fraction on the liquid surface was poured off along with the heavy liquid solution leaving the sink fraction behind. The float and sink fractions were then filtered, thoroughly washed, dried and weighed. The float fraction was then subsequently reprocessed following the same steps, but, using a heavy liquid solution with SG 2.75. Float and sink fractions were then analyzed by ICP-MS and SEM.

5.5.2 Knelson Concentrator

The Knelson Concentrator (Chapter 3, Section 3.3.1.4) used in this work was a lab scale KC MD3 model manufactured by FLSmidth Knelson (Canada).

5.5.2.1 Feed 1

The coarse particle stream of Feed 1 was processed operating the Knelson Concentrator with a bowl speed of 1250 rpm and fluidizing water rate of 2 L/min. The material was fed with a flow rate of 250 g/min, stopping every 4 min to remove the accumulated concentrate from the bowl. The particle size distribution, SG (calculated from pyncnometer measurements), mass recovery and major mineral phases (determined by XRD) were compared to ensure there were no major differences between concentrates. These results are provided in Figure 5.5, Table 5.1 and Figure 5.6, respectively. The five concentrates were then combined and, along with the tailings fraction, analyzed by ICP-MS, XRD and QEMSCAN.

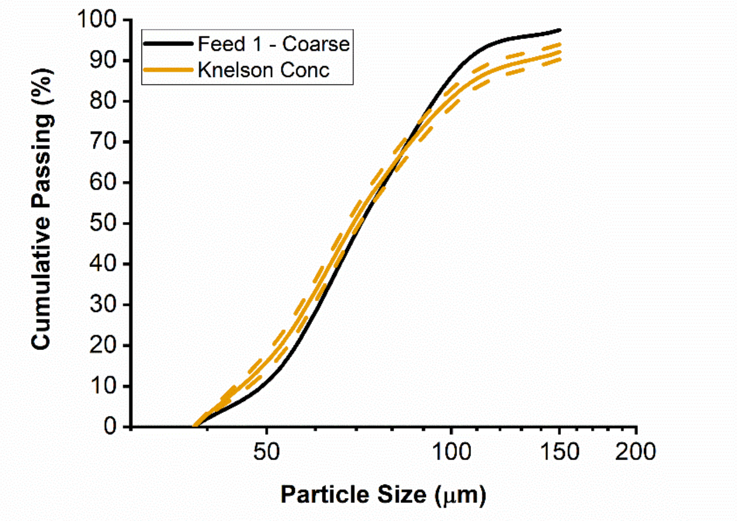

Figure 5.5 – Average particle size distribution of the five Knelson concentrates produced after processing the coarse particle fraction of Feed 1. The dashed line represents the 95 % confidence interval

Table 5.1 – Average mass recovery and SG of the five Knelson concentrates produced after processing the coarse particle fraction of Feed 1

Sample	Mass Recovery (%)	95 % Confidence Interval	SG	95 % Confidence Interval
Feed	100	-	2.6	-
Knelson Concentrate	2.4	0.4	3.1	0.1

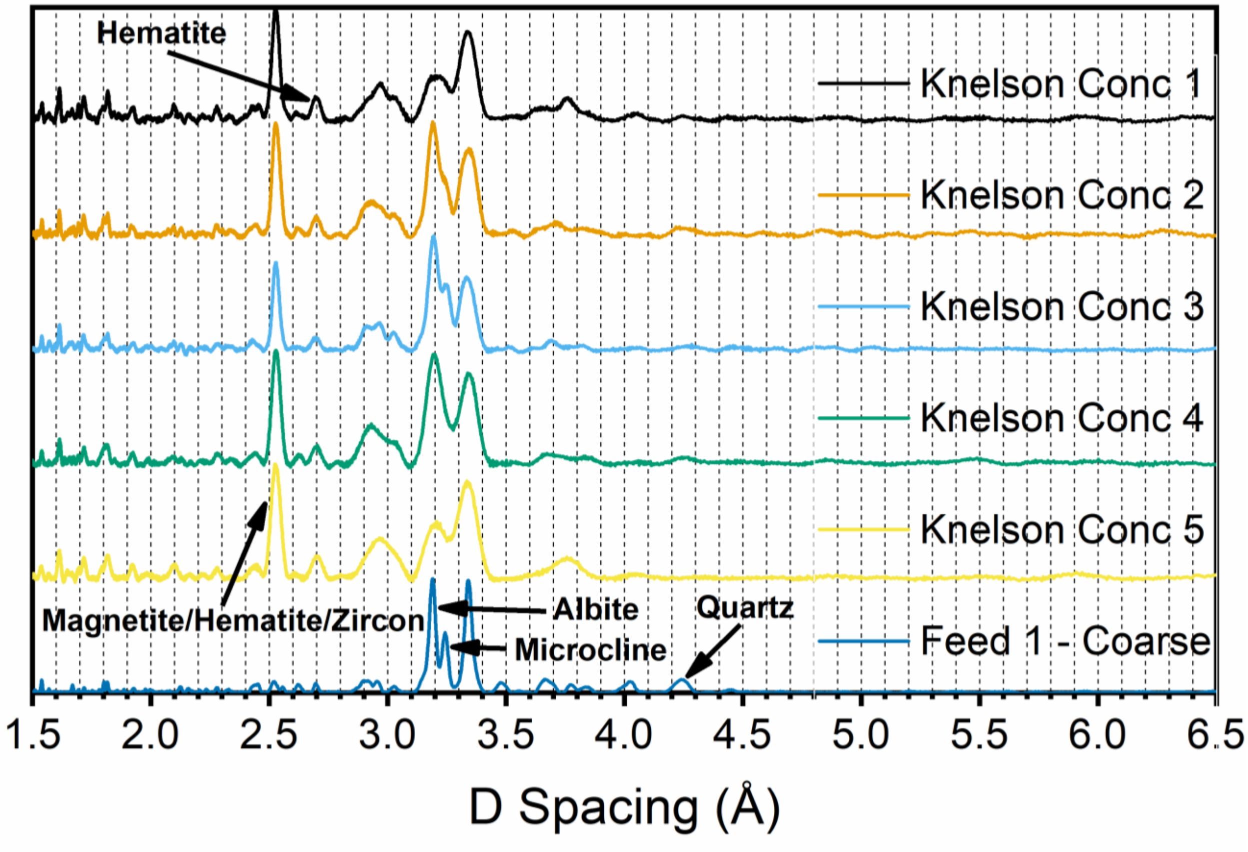

Figure 5.6 – XRD results of the five Knelson concentrates produced after processing the coarse particle fraction of Feed 1

5.5.2.2 Feed 2

The operating conditions used to process Feed 2 were based off results from the work detailed in Appendix A (Section A.3), which examined the impact of feed grade on the beneficiation of a -53 μm synthetic magnetite/quartz ore. SG differences between heavy and light minerals in the Nechalacho deposit are similar to those of magnetite and quartz, respectively. Therefore, the optimum operating parameters determined for the synthetic ore were applied here. The initial conditions used were those which were determined to be optimum when processing the 15 % magnetite ore. The tails from the first pass were then processed using optimum conditions for the 10 % magnetite ore, followed by two more passes performed at the best conditions obtained for the 5 % case. A flowsheet which details the bowl speed (rpm), fluidizing water rate (L/min) and solids feed rate (g/min) used for each pass of the Knelson is shown in Figure 5.7. For each pass the bowl was stopped after 1 kg of material was fed to the equipment to remove accumulated concentrate from the bowl. It is important to note that the conditions used for each pass were assigned prior to any characterization work to determine heavy mineral content prior to each pass. As such the conditions used are outside the optimum ranges determined for the synthetic magnetite/quartz mixture. All products produced from this test work were analyzed by XRD, XRF and QEMSCAN.

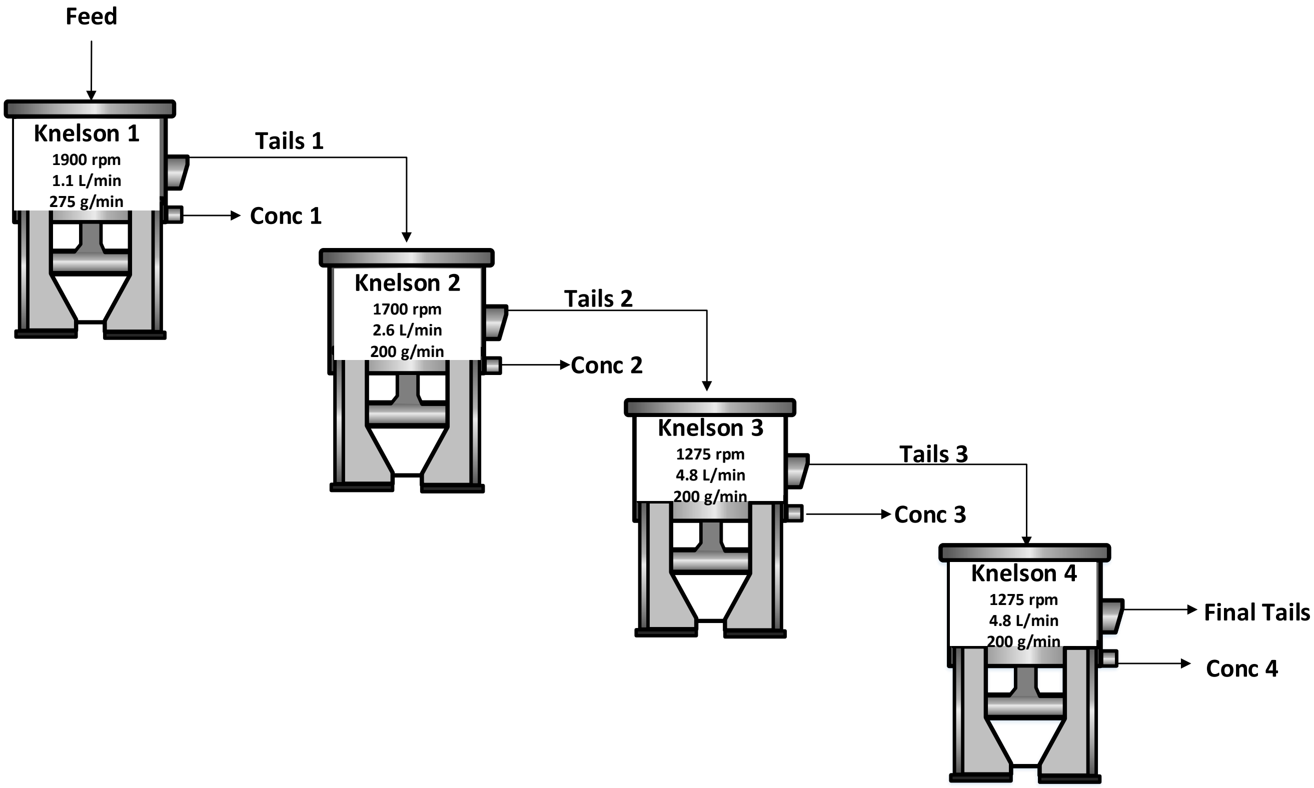

Figure 5.7 – Flowsheet detailing the conditions used for Knelson Concentrator experiments performed on Feed 2

5.5.3 Spiral Concentrator

The spiral separator (Chapter 3, Section 3.3.1.3) used in this work was a Walkabout assembly from Mineral Technologies (Australia). The unit is composed of a four turn Wallaby trough, with a 208 mm pitch and trough diameter of 360 mm. In all cases, the sample was fed as a slurry (20 $\%_{w/w}$ solids) to the top of a spiral, which was fitted with a funnel (for pulse damping), using a diaphragm pump.

5.5.3.1 Feed 1

The coarse particle stream of Feed 1 was processed by the spiral. Concentrate and tailings were collected separately and analyzed by XRD, ICP-MS and QEMSCAN.

5.5.3.2 Feed 4

The coarse particle fraction of Feed 4 was processed with three stages of spiral concentration. The three spiral concentrates were combined and reground to be processed using a Mozley Laboratory Separator Table. A flowsheet detailing this process is provided in Figure 5.8. The spiral concentrates were sampled and analyzed using XRF and QEMSCAN.

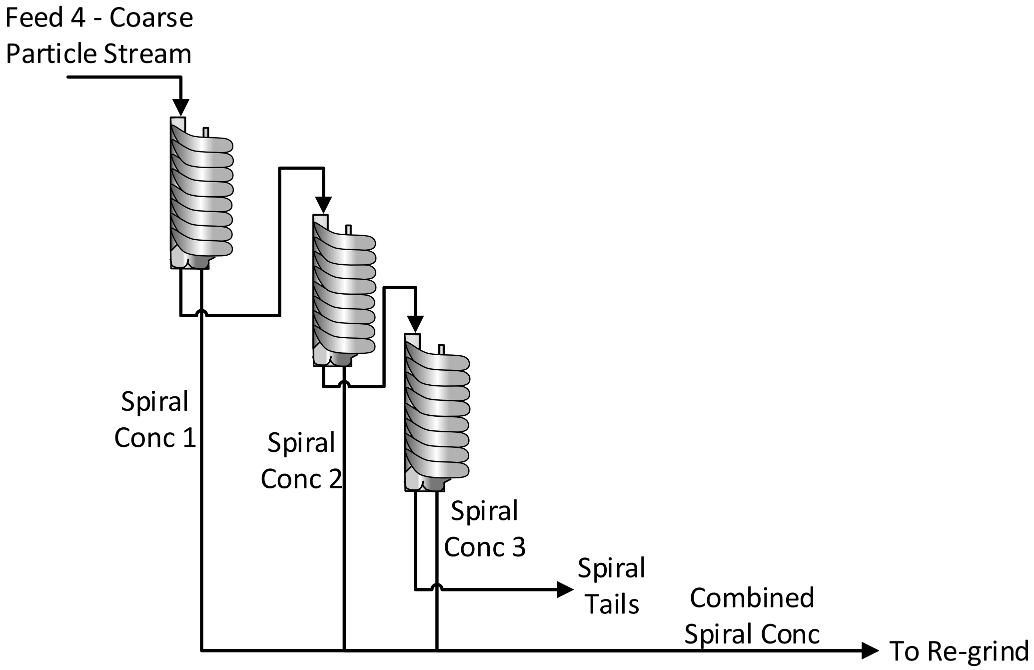

Figure 5.8 – Flowsheet detailing the three stages of spiral concentration to process the coarse particle fraction of Feed 4

5.5.4 Multi-Gravity Separator

The MGS (Chapter 3, Section 3.3.1.3) used in this work was a pilot scale C-900 unit (Richard Mozley Ltd., UK). For all tests the tilt angle, shake amplitude and shake frequency were kept constant at 7.5°, 15 mm and 350 min^{-1}, respectively.

5.5.4.1 Feed 1

The fine particle fraction of Feed 1 was processed using the MGS. Both the conventional and low-profile scrapper systems were employed (Chapter 3, Figure 3.9). Using the conventional scrapper system, tests were performed at drum speeds of 162 rpm (minimum speed required to pull mass to the concentrate) and 168 rpm with wash water rates ranging from 1 – 4 L/min. Tests using the low-profile scraper system were performed at 170 rpm with wash water rates ranging from 2 – 6 L/min. When using the low-profile scrappers, higher drum speeds were required to pull mass to the concentrate, with no mass recovered at drum speeds lower than 170 rpm. The solids feed rate ranged from 860 – 915 g/min. In all cases, after changing operating conditions, the system was allowed to reach a steady state prior to sampling the concentrate and tailings streams. Samples taken at each condition were analyzed by XRF and QEMSCAN.

5.5.4.2 Feed 3

Feed 3 was processed using the MGS equipped with the low-profile scrappers. It was operated as three batch tests, with the tails from each proceeding test acting as the feed for the next. The drum speed (rpm), wash water rate (L/min) and solids flow rate (g/min) used for each pass are detailed in Figure 5.9. At the end of the last pass, the material which remained on the walls of the MGS (while it was still rotating), was collected separately and called “Middlings”. All products were analyzed by XRD, XRF and QEMSCAN.

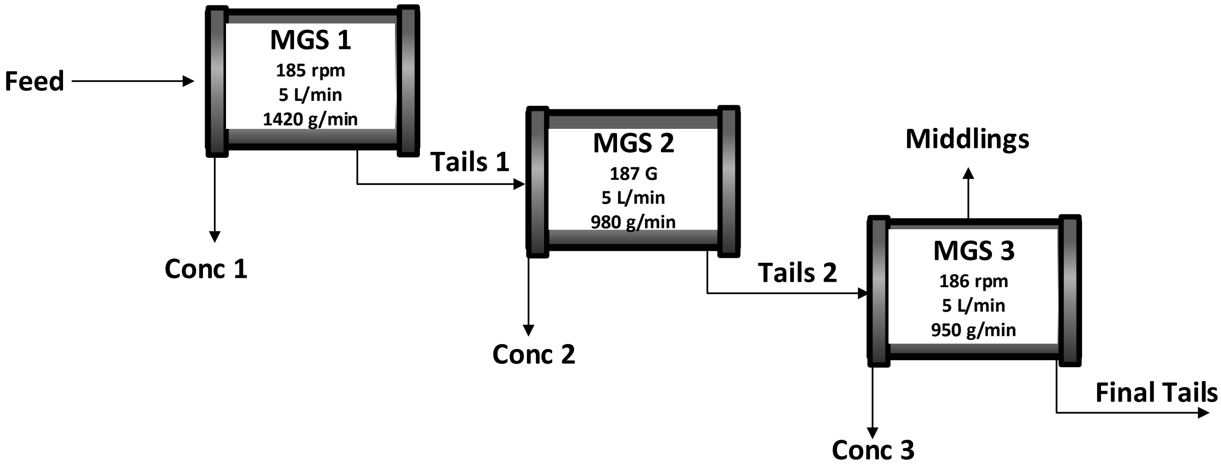

Figure 5.9 – Flowsheet detailing the three stages of MGS concentration to process Feed 3

5.5.5 Mozley Laboratory Shaking Table

Following re-grinding of the spiral concentrate (Section 5.5.3.2) it was recombined with the fine particle fraction of Feed 4 and processed using a Mozley Laboratory Separator Table (Chapter 3, Section 3.3.1.2) equipped with a flat deck for fine particle separation (see flowsheet provided in Figure 5.4). The deck slope was set at 1.5° and it was operated with a stroke length of 5.08 cm and stroke rate of 90 rpm. The material was fed to the table as 100 g representative samples, processing each 100 g sample individually until all the mass had been processed by the shaking table. The concentrate and tailings were then analyzed by XRF and QEMSCAN.

5.6 Magnetic Separations

5.6.1 Wet Magnetic Test Chute

A Wet Magnetic Test Chute (Chapter 3, Section 3.4.1.1) with a ferrite magnet (0.04 T) (Master Magnets, UK) was employed in this work as a LIMS. The gravity concentrates produced after processing Feed 3 with a MGS (Section 5.5.4.2) and Feed 4 with a shaking table (Section 5.5.5) were individually processed. Material was poured wet by hand to the Wet Magnetic Test Chute with non-magnetic material washed down the inclined surface using water. The magnetic fraction produced was analyzed by XRF and QEMSCAN and the non magnetic fraction was processed further using a Wet High Intensity Magnetic Separator (WHIMS).

5.6.2 Wet High Intensity Magnetic Separator

A jaw type WHIMS concentrator (Chapter 3, Section 3.4.1.2) equipped with a coarse expanded metal matrix (Master Magnets, UK) was used to process the non-magnetic fractions of the Wet Magnetic Test Chute. The material was passed through the magnetic matrix as a slurry. The magnetic material trapped in the matrix of the separator was removed as magnetic concentrate. The gravity concentrate of Feed 3 (MGS) was processed at 1.8 T and that of Feed 4 (Mozley Table) was processed at 1.4 T. A flowsheet detailing magnetic separation experiments is provided in Figure 5.10. Magnetic and non magnetic fractions were analyzed by XRF and QEMSCAN.

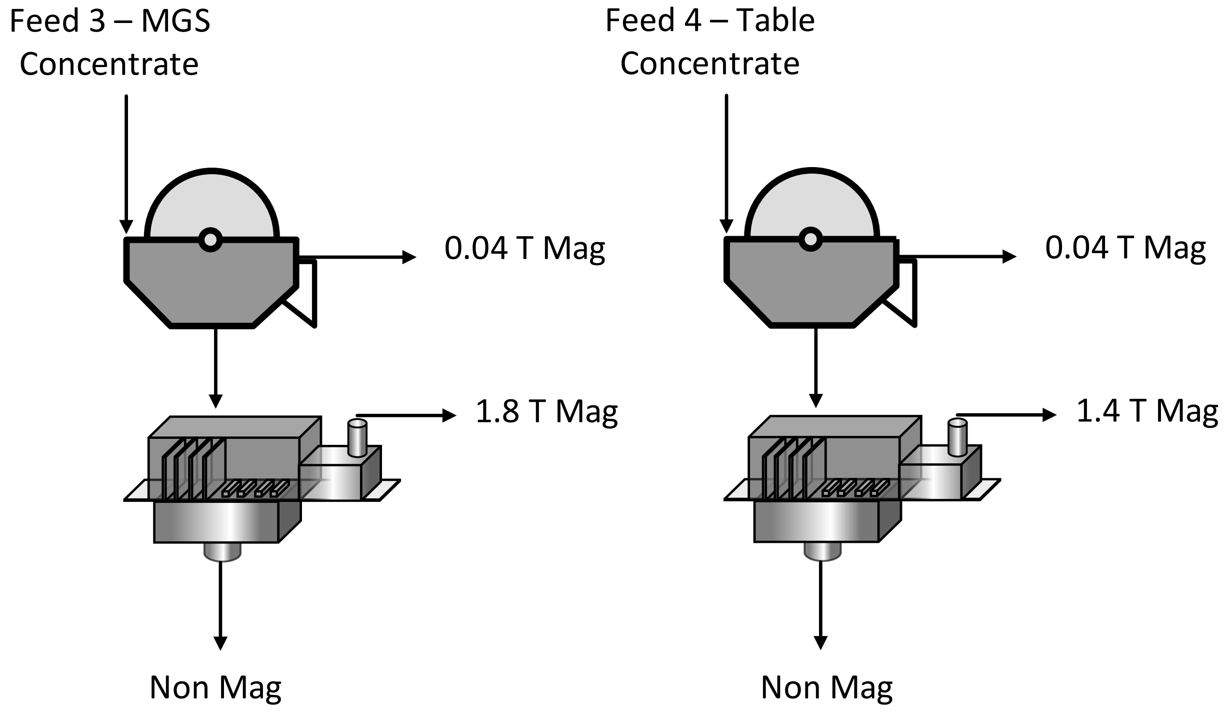

Figure 5.10 – Flowsheet detailing magnetic separation experiments. Note the low-intensity Wet Magnetic Test Chute is represented here by a low-intensity magnetic drum separator.

5.7 Conclusions

The experimental conditions employed throughout this thesis have been detailed in this chapter. Four different feed samples were used with flowsheets detailing the separations performed on each provided. Readers interested the theory of a particular technique are directed to Chapter 3.

Chapter 6

Feed Characteristics

6.1 Introduction

This chapter details the mineralogical characteristics of feed samples 1 – 4 (detailed information of how each feed was prepared can be found in Chapter 5, Section 5.3). Mineral content, grain size distributions, liberation and association characteristics and particle SG distributions (determined from QEMSCAN) were used to characterize each feed sample prior to separation experiments. Both Feed 1 and Feed 4 were split into coarse and fine particle fractions for downstream separation work (Figures 5.1 and 5.4, respectively); however, in Feed 1 there was a significant amount of - 53 + 38 μm material in both coarse and fine fractions, compared to Feed 4 where nearly all the - 53 μm material was sent to the fine particle fraction (4.9 % of the coarse particle fraction was < 53 μm). Therefore, throughout this section Feed 1 will be generally presented as a coarse, fine and reconstructed feed; whereas characteristics of Feed 4 will generally be provided only as the reconstructed feed. For Feed 4 material in the + 53 μm fractions represent the characteristics of the coarse fraction and those in the - 53 μm fractions represent the portion of the feed which bypassed the spiral concentrator and was processed as a fine particle fraction along with the spiral concentrate.

6.2 Mineralogy

The mineralogy and elemental content of the coarse fraction of Feed 1, the fine fraction of Feed 1, reconstructed Feed 1, Feed 2, Feed 3 and Feed 4 are given in Tables 6.1 – 6.11. REM are generally grouped into LREM, comprised of predominantly LREE-bearing minerals (bastnäsite, synchysite, allanite and monazite), and HREM, comprised of HREE-bearing minerals [fergusonite and columbite (Fe)] throughout this thesis. Examining the size by size mineralogy of each feed sample (Tables 6.5, 6.6, 6.8 and 6.10), zircon is significantly concentrated in coarser size fractions. While the same size fractions were not analyzed for each sample, comparing each feed indicates that zircon is specifically enriched in particles > 20 µm. This trend is also demonstrated in the elemental distribution of each size fraction (Tables 6.2, 6.4, 6.6, 6.8 and 6.10), where the concentration of Zr is elevated in the coarse particles. These results correspond well with those of Jordens *et al.* (2016b), who also found zircon was enriched in the + 20 µm after grinding the ore to 80 % passing 40 µm; this suggests that an optimized grinding and classification circuit may provide an opportunity to pre-concentrate zircon in the ore through selective comminution. It should be noted that although there is limited mass in the + 150 µm size fraction of Feed 1 (Table 6.5), it is significantly enriched in both zircon and LREM. This suggests that coarse complex particles containing zircon and LREM in the deposit are more difficult to grind than minerals such as feldspars (K-feldspar and plagioclase), which may provide opportunities for concentration at even coarser particle sizes.

Table 6.1 – Mineralogy (in wt %) of the coarse particle fraction of Feed 1 (determined by QEMSCAN)

	Mineral	**Wt %**					
		Combined	**+ 150 µm**	**- 150 + 106 µm**	**- 106 + 75 µm**	**- 75 + 53 µm**	**- 53 + 38 µm**
Mass Distribution		100	2.5	7.5	34.1	40.8	15.1
LREM	Bastnäsite	1.1	1.6	1.2	1.1	1.1	1.3
	Synchysite	0.5	0.6	0.4	0.4	0.5	0.6
	Allanite	0.9	1.8	0.9	0.9	0.8	0.9
	Monazite	0.2	0.2	0.1	0.1	0.2	0.3
HREM	Fergusonite	0.1	0.1	0.1	0.1	0.1	0.1
	Columbite (Fe)	0.5	0.6	0.4	0.4	0.5	0.6
	Zircon	6.2	7.2	4.1	4.9	6.6	9.4
Silicate Gangue	Quartz	15.4	19.4	16.5	16.1	15.1	13.7
	K-Feldspar	25.8	19.5	29.5	27.4	25.6	21.7
	Plagioclase	28.5	20.1	29.4	30.0	28.6	25.4
	Biotite	7.1	8.3	6.8	6.8	7.2	7.2
Other Gangue	Fe – Oxides	8.0	13.0	5.5	6.1	7.9	12.6
	Other	5.7	7.6	5.0	5.6	5.8	6.0

Table 6.2 – Concentration (in wt %) of REE and ZrO_2 in the coarse particle fraction of Feed 1 (determined by ICP-MS and XRF)

Metals / Equivalent Metal Oxide	**Wt %**					
	Combined	**+ 150 µm**	**- 150 + 106 µm**	**- 106 + 75 µm**	**- 75 + 53 µm**	**- 53 + 38 µm**
Mass Distribution	100	2.5	7.5	34.1	40.8	15.1
ZrO_2	2.5	2.8	1.8	1.9	2.7	3.5
LREE	1.1	1.3	0.9	0.9	1.1	1.4
HREE	0.2	0.3	0.2	0.2	0.2	0.3

Table 6.3 – Mineralogy (in wt %) of the fine particle fraction of Feed 1 (determined by QEMSCAN)

Mineral		Wt % Combined	+ 20 μm	- 20 μm
Mass Distribution		100	42	58
LREM	Bastnäsite	1.0	1.2	0.9
	Synchysite	0.6	0.4	0.6
	Allanite	0.8	0.7	1.0
	Monazite	0.4	0.2	0.5
HREM	Fergusonite	0.1	0.1	0.1
	Columbite (Fe)	0.6	0.5	0.6
	Zircon	4.7	6.1	3.7
Silicate Gangue	Quartz	13.7	14.5	13.1
	K-Feldspar	21.2	23.6	19.4
	Plagioclase	21.0	25.9	17.6
	Biotite	16.7	9.3	21.9
Other Gangue	Fe – Oxides	11.6	11.1	12.0
	Other	7.6	6.2	8.6

Table 6.4 – Concentration (in wt %) of Ce_2O_3 and ZrO_2 in the fine particle fraction of Feed 1 (determined by XRF)

Equivalent Metal Oxide	Wt % Combined	+ 20 μm	- 20 μm
Mass Distribution	100	42	58
ZrO_2	2.2	2.5	2.1
Ce_2O_3	0.6	0.5	0.6

Table 6.5 – Reconstructed mineralogy (in wt %) of Feed 1 (determined by QEMSCAN)

	Mineral	**Wt %**						
		Combined	**+ 150 µm**	**- 150 + 106 µm**	**- 106 + 75 µm**	**- 75 + 53 µm**	**- 53 + 20 µm**	**- 20 µm**
Mass Distribution		100	0.8	2.5	11.3	13.5	33.1	38.9
LREM	Bastnäsite	1.1	1.6	1.2	1.1	1.1	1.2	0.9
	Synchysite	0.5	0.6	0.4	0.4	0.5	0.4	0.6
	Allanite	0.9	1.8	0.9	0.9	0.8	0.7	1
	Monazite	0.3	0.2	0.1	0.1	0.2	0.2	0.5
HREM	Fergusonite	0.1	0.1	0.1	0.1	0.1	0.1	0.1
	Columbite (Fe)	0.5	0.6	0.4	0.4	0.5	0.5	0.6
	Zircon	5.2	7.2	4.1	4.9	6.6	6.6	3.7
Silicate Gangue	Quartz	14.3	19.4	16.5	16.1	15.1	14.4	13.1
	K-Feldspar	22.7	19.5	29.5	27.4	25.6	23.3	19.4
	Plagioclase	23.5	20.1	29.4	30.0	28.6	25.8	17.6
	Biotite	13.5	8.3	6.8	6.8	7.2	9	21.9
Other Gangue	Fe – Oxides	10.4	13.0	5.5	6.1	7.9	11.3	12
	Other	7.0	7.6	5.0	5.6	5.8	6.2	8.6

Table 6.6 – Mineralogy (in wt %) of Feed 2 (determined by QEMSCAN)

Mineral		Wt %			
		Combined	+ 75 µm	- 75 + 38 µm	- 38 µm
Mass Distribution		100	6.4	22.8	70.7
LREM	Bastnäsite	1.0	1.3	1.2	0.9
	Synchysite	0.6	0.4	0.5	0.7
	Allanite	1.7	1.6	1.2	1.9
	Monazite	0.3	0.1	0.2	0.4
HREM	Fergusonite	0.1	0.1	0.1	0.2
	Columbite (Fe)	0.6	0.5	0.5	0.6
	Zircon	6.0	7.4	10.9	4.4
Silicate Gangue	Quartz	15.6	17.1	16.7	15.1
	K-Feldspar	22.2	22.8	20.6	22.6
	Plagioclase	23.6	26.7	25.8	22.6
	Biotite	10.9	6.1	5.2	13.2
Other Gangue	Fe – Oxides	11.5	11.3	12.9	11.1
	Other	5.9	4.6	4.2	6.5

Table 6.7 – Concentration (in wt %) of Ce_2O_3 and ZrO_2 in Feed 2 (determined by XRF)

Equivalent Metal Oxide	Wt %			
	Combined	+ 75 µm	- 75 + 38 µm	- 38 µm
Mass Distribution	100	6.4	22.8	70.7
ZrO_2	2.8	3.0	4.3	2.4
Ce_2O_3	0.6	0.6	0.6	0.6

Table 6.8 – Mineralogy (in wt %) of Feed 3 (determined by QEMSCAN)

Mineral		Wt %			
		Combined	+ 75 µm	- 75 + 20 µm	- 20 µm
Mass Distribution		100	6.6	39.1	54.3
LREM	Bastnäsite	0.9	1.2	1.0	0.8
	Synchysite	0.4	0.5	0.4	0.4
	Allanite	1.6	1.2	1.0	2.0
	Monazite	0.3	0.1	0.2	0.3
HREM	Fergusonite	0.1	0.1	0.1	0.1
	Columbite (Fe)	0.5	0.4	0.5	0.6
	Zircon	4.9	7.1	8.1	2.4
Silicate Gangue	Quartz	14.7	19.4	16.6	12.8
	K-Feldspar	24.3	19.4	22.8	25.9
	Plagioclase	24.7	26.2	27.6	22.4
	Biotite	11.3	5.4	6.5	15.5
Other Gangue	Fe – Oxides	9.6	10.0	10.6	8.9
	Other	6.6	8.9	4.5	7.8

Table 6.9 – Concentration (in wt %) of Ce_2O_3 and ZrO_2 in Feed 3 (determined by XRF)

Equivalent Metal Oxide	Wt %			
	Combined	+ 75 µm	- 75 + 20 µm	- 20 µm
Mass Distribution	100	6.6	39.1	54.3
ZrO_2	2.7	3.2	3.6	1.9
Ce_2O_3	0.6	0.5	0.5	0.6

Table 6.10 – Mineralogy (in wt %) of Feed 4 (determined by QEMSCAN)

Mineral		Wt %				
		Combined	- 150 + 106 μm	- 106 + 53 μm	- 53 +20 μm	-20 μm
Mass Distribution		100	28.9	28.1	25.5	17.5
LREM	Bastnäsite	1.2	1.1	1.4	1.4	1.0
	Synchysite	0.6	0.4	0.6	0.7	0.5
	Allanite	1.2	0.9	0.9	1.0	2.7
	Monazite	0.2	0.2	0.2	0.3	0.3
HREM	Fergusonite	0.1	0.1	0.1	0.1	0.1
	Columbite (Fe)	0.6	0.4	0.6	0.7	0.8
	Zircon	7.1	5.1	9.3	9.6	3.4
Silicate Gangue	Quartz	15.4	17.0	15.8	14.6	13.0
	K-Feldspar	22.1	27.2	22.0	18.8	18.9
	Plagioclase	25.0	29.7	25.4	23.4	19.0
	Biotite	9.2	6.4	6.9	8.1	19.2
Other Gangue	Fe – Oxides	10.6	6.3	10.6	14.7	11.5
	Other	6.6	5.1	6.2	6.5	9.7

Table 6.11 – Concentration (in wt %) of Ce_2O_3 and ZrO_2 in Feed 4 (determined by XRF)

Equivalent Metal Oxide	Wt %				
	Combined	- 150 + 106 μm	- 106 + 53 μm	- 53 +20 μm	-20 μm
Mass Distribution	100	28.9	28.1	25.5	17.5
ZrO_2	3.0	2.2	3.9	3.9	1.7
Ce_2O_3	0.6	0.4	0.7	0.7	0.7

6.3 Grain Size Distributions

The QEMSCAN estimated grain size distributions of zircon, LREM and HREM in each feed sample are shown in Figure 6.1, with the d_{50} and d_{80} of each mineral class provided in the legend of each plot. Examining the grain size of zircon in each feed sample may provide some understanding into the concentration of zircon in the + 20 μm fractions following grinding. The distribution of zircon with a grain size > 20 μm in Feed 1 through 4 are 79 %, 79 %, 76 % and 85 %, respectively. As the majority of zircon remains in coarse grains even when the particle size is significantly reduced (d_{80} of 120 μm in Feed 4 *vs.* 66 μm in Feed 1 and 55 μm in Feed 2 and 3) it is suggested that zircon grains are resistant to grinding and fractures in zircon-bearing particles occur predominantly along the zircon grain boundaries. This would significantly improve the liberation characteristics of zircon allowing for coarser grinds to achieve liberation. Figure 6.1 also demonstrates the very fine-grained RE mineralization, which suggests poor REM liberation at particle sizes > 20 μm.

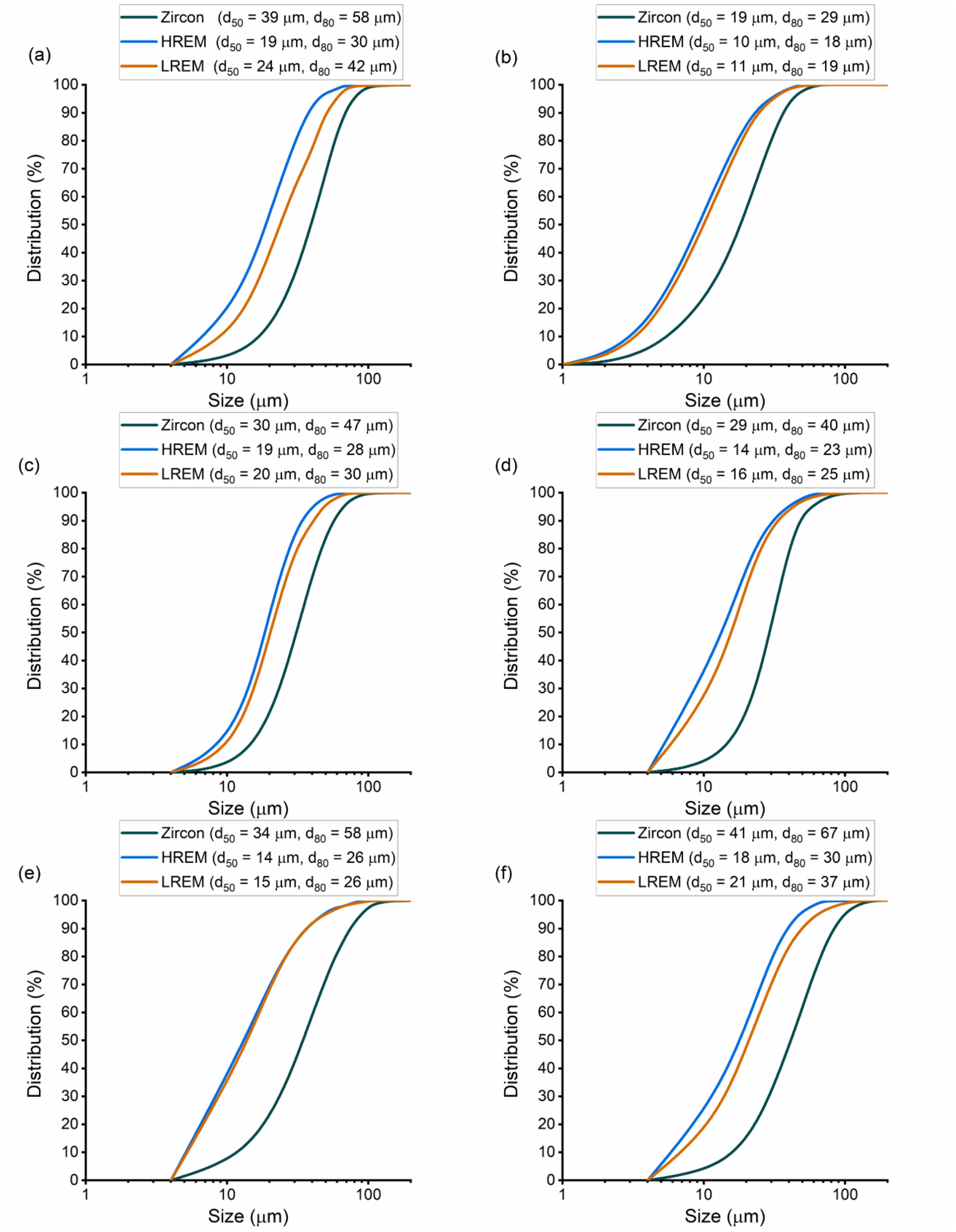

Figure 6.1 – Grain size distribution of zircon, HREM and LREM estimated by QEMSCAN for (a) the coarse fraction of Feed 1, (b) the fine fraction of Feed 1, (c) reconstructed Feed 1, (d) Feed 2, (e) Feed 3 and (f) Feed 4

6.4 Liberation and Association Characteristics

Liberation and association characteristics of zircon, HREM and LREM in each feed are shown in Figures 6.2 – 6.3, respectively. Mineral particles were grouped into free, liberated, binary and complex. Minerals having > 95 % of the particle surface area are referred to as “free”, and those < 95 % and > 80 % of the particle surface area are considered “liberated”.

Figure 6.2 shows that in all feed samples zircon is relatively well liberated. It also provides a visual representation demonstrating that following grinding zircon is concentrated in > 20 μm particles. Across all particle sizes, liberation (free + liberated) of zircon is 59 % in the coarse particle fraction of Feed 1, 79 % in the fine particle fraction of Feed 1, 70 % in Feed 1, 56 % in Feed 2, 68 % in Feed 3 and 55 % in Feed 4 (49 % in the + 53 μm fraction and 74 % in the -53 μm fraction). In the coarse particle stream of Feed 1, approximately 50 % of zircon grains are > 38 μm (the minimum particle size of this feed). Comparing this to the concentration of liberated zircon particles in this feed suggests that most of these coarse zircon grains are liberated. Similar findings were observed for the + 53 μm fraction of Feed 4 for which 55 % of zircon grains are > 53 μm, with 49 % of all zircon being liberated. Although a more detailed study is required to investigate the comminution properties of the ore, the present results further reinforce the notion that fractures in particles containing zircon occur preferentially at grain boundaries, rather than through zircon grains.

Figure 6.3 demonstrates that in Feed 2, 3 and 4 HREM liberation is poor (ranging from 10 – 25 %). In Feed 1, liberation is improved (43 %), with much of the liberated HREM reporting to the -20 μm fraction. In is interesting to note the differences in liberation, specifically in the finest particle size ranges (- 38 μm and - 20 μm) of each feed. In the - 20 μm fraction of Feed 1, 65 % of HREM particles are liberated, whereas in the finest size range investigated of the other feed samples liberation remains low (< 30 %). The main difference between the preparation of Feed 1 and the other feed samples is that a ball mill was used as opposed to a rod mill for the other feed samples. It is likely that the ball mill produces more ultra-fine (< 10 μm) particles, improving liberation, or improved liberation may be as a result of different breakage mechanisms in the ball mill. More work is required for a fundamental understanding of the mechanisms involved.

Figure 6.4 suggests that LREM are more readily liberated than HREM following grinding, with liberation ranging from 40 – 50 % across all feed samples. This is interesting when also comparing grain sizes (Figure 6.1) between HREM and LREM, as their grain sizes do not differ drastically. More work is required to determine the differences in fracturing of HREM and LREM bearing particles, however, these findings suggest that those containing HREM may be more resistant to fracture, particularly when using a rod mill.

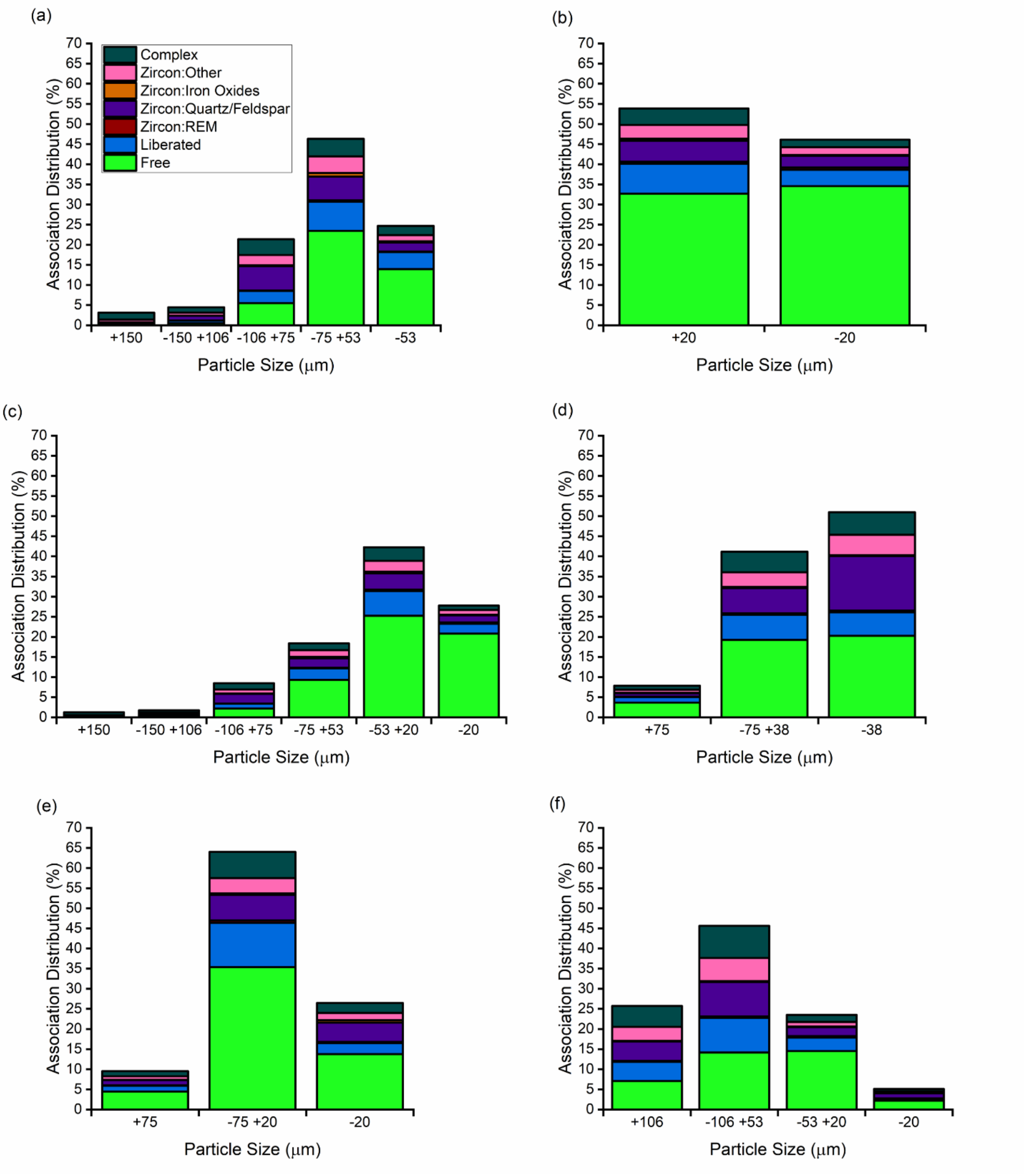

Figure 6.2 – Zircon associations by particle size in (a) the coarse fraction of Feed 1, (b) the fine fraction of Feed 1, (c) reconstructed Feed 1, (d) Feed 2, (e) Feed 3 and (f) Feed 4

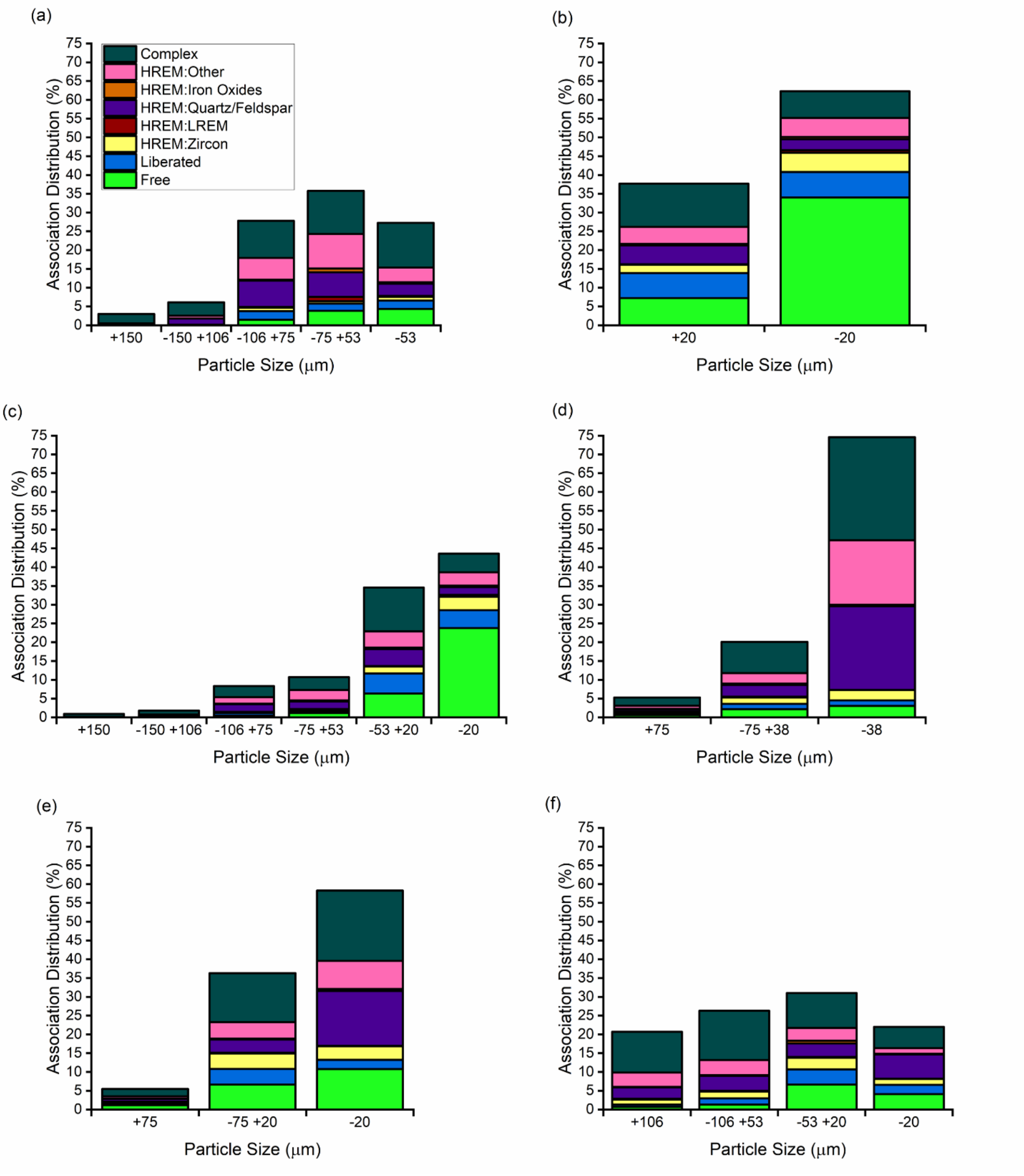

Figure 6.3 – HREM associations by particle size in (a) the coarse fraction of Feed 1, (b) the fine fraction of Feed 1, (c) reconstructed Feed 1, (d) Feed 2, (e) Feed 3 and (f) Feed 4

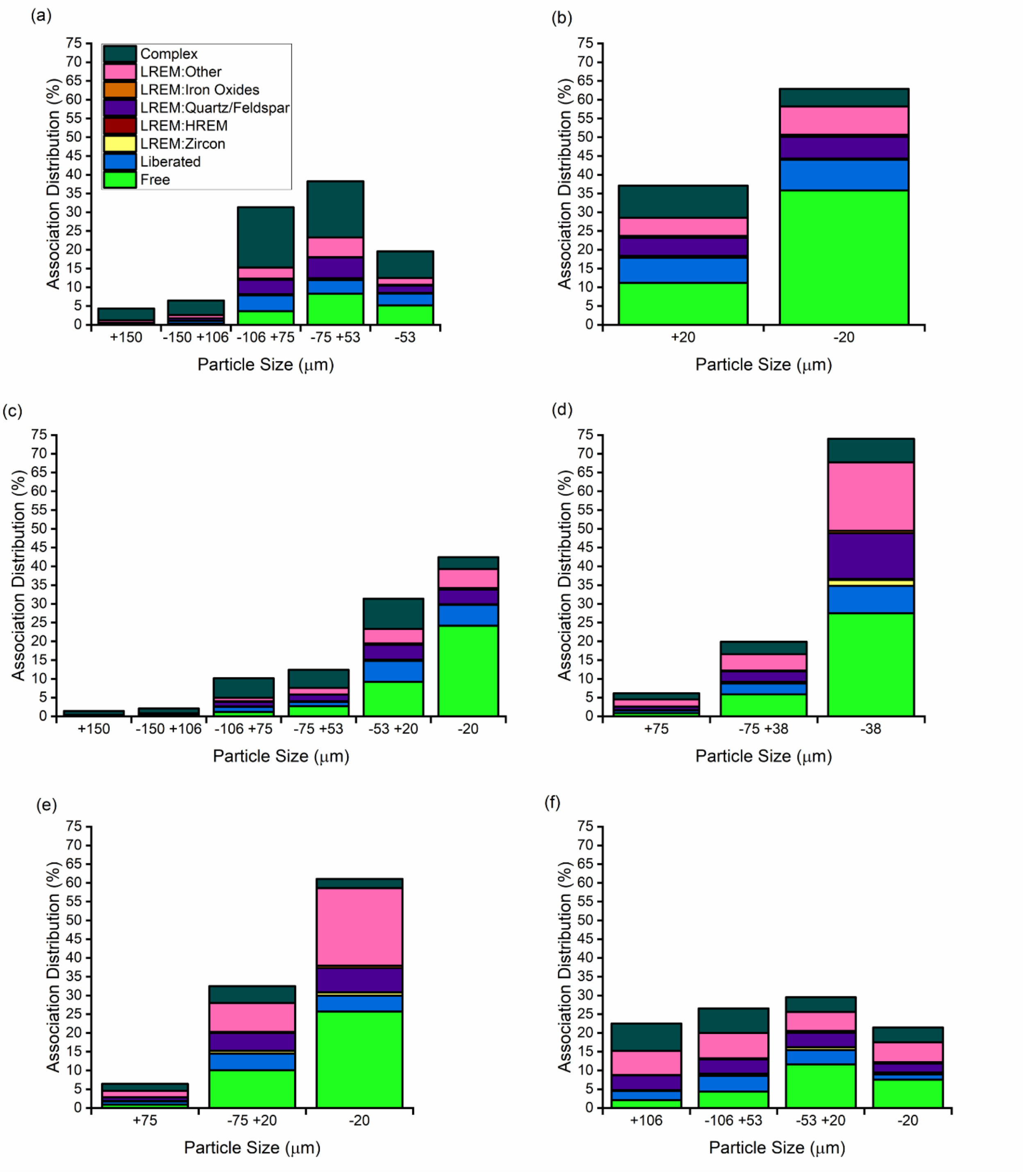

Figure 6.4 – LREM associations by particle size in (a) the coarse fraction of Feed 1, (b) the fine fraction of Feed 1, (c) reconstructed Feed 1, (d) Feed 2, (e) Feed 3 and (f) Feed 4

6.5 QEMSCAN Gravity Modelling

Mineral particles in the feed can be grouped into different SG classes using the QEMSCAN data. This is done by estimating volumetric composition of a particle from the two-dimensional phase map and stereological corrections in the QEMSCAN software (Pascoe et al., 2007). Each mineral is assigned a SG value, and the SG of each particle is calculated based upon its constituents. To avoid repetitive discussion, the SG distributions of value minerals and particles are presented in Chapter 7 and theoretical upgrade ratio and recovery plots are presented here (Figure 6.5). These are produced by artificially splitting the sample at a defined SG. Figure 6.5 shows the data for zircon, LREM and HREM in each feed (except for the fine particle fraction of Feed 1, where SG distributions of HREM were not examined). The results for the reconstructed Feed 1 are not shown here as the coarse and fine particle samples were processed separately. Similarly, Feed 4 is also split into its coarse and fine particle streams. For the coarse particle fraction of Feed 1, the samples were theoretically split at an SG of 2.75, 2.95 [to mimic the SG used for DMS experiments (Chapter 7)] and 3.5. For the fine particle fraction of Feed 1, Feed 2, 3 and 4 the samples were theoretically split at an SG of 3.5. Feed 2, 3 and 4 were also analysed on a size by size basis.

Figure 6.5 indicates zircon is concentrated in high SG particles, with predicted recoveries > 75 % and upgrade ratios > 4.4 for all the feed samples. The high proportion of zircon-bearing particles with SG > 3.5 corresponds well to its liberation characteristics (Figure 6.4). However, it is interesting to note that even at coarse particle sizes (> 75 μm) where zircon liberation is relatively low it remains in high SG particles.

For HREM, predicted recoveries range from 41 % to 71 % and predicted upgrading ranges from 2.4 to 4.5 times, when artificially splitting the feed samples at a SG of 3.5. Examining the impact of particle size on HREM-bearing particles in Feed 2, 3 and 4, it is evident that as particle size is reduced (using a rod mill), HREM become concentrated in lower SG particles (< 3.5) which results in poor estimated recoveries. In all these feeds, < 40 % of HREM-bearing particles in the finest size class (- 38 μm or - 20 μm) are present in particles with an SG > 3.5, whereas, in the coarser size fractions > 60 % of the HREM-bearing particles have an SG > 3.5. This suggests that at coarser particle sizes although HREM are not liberated they remain associated with other high SG minerals. However, as the particle size decreases below 38 µm, the associated high SG material is removed from these particles and HREM remain locked with low SG gangue. These findings indicate that recovery of fine (< 38 µm) HREM-bearing particles produced using a rod mill is likely to be challenging using gravity separation. Nevertheless, at coarser particle sizes mineral associations may provide opportunities to recover these minerals.

LREM are also concentrated in high SG particles in each feed, with predicted recoveries ranging from 66 % - 77 % and upgrade ratios ranging from 3.4 to 4.7 when splitting the ore at a SG of 3.5. LREM follow a similar trend to HREM where they remain in high SG particles at coarse particle sizes where liberation is low. However, as liberation is significantly improved at finer sizes compared with HREM they are also present in more high SG particles at sizes < 38 µm.

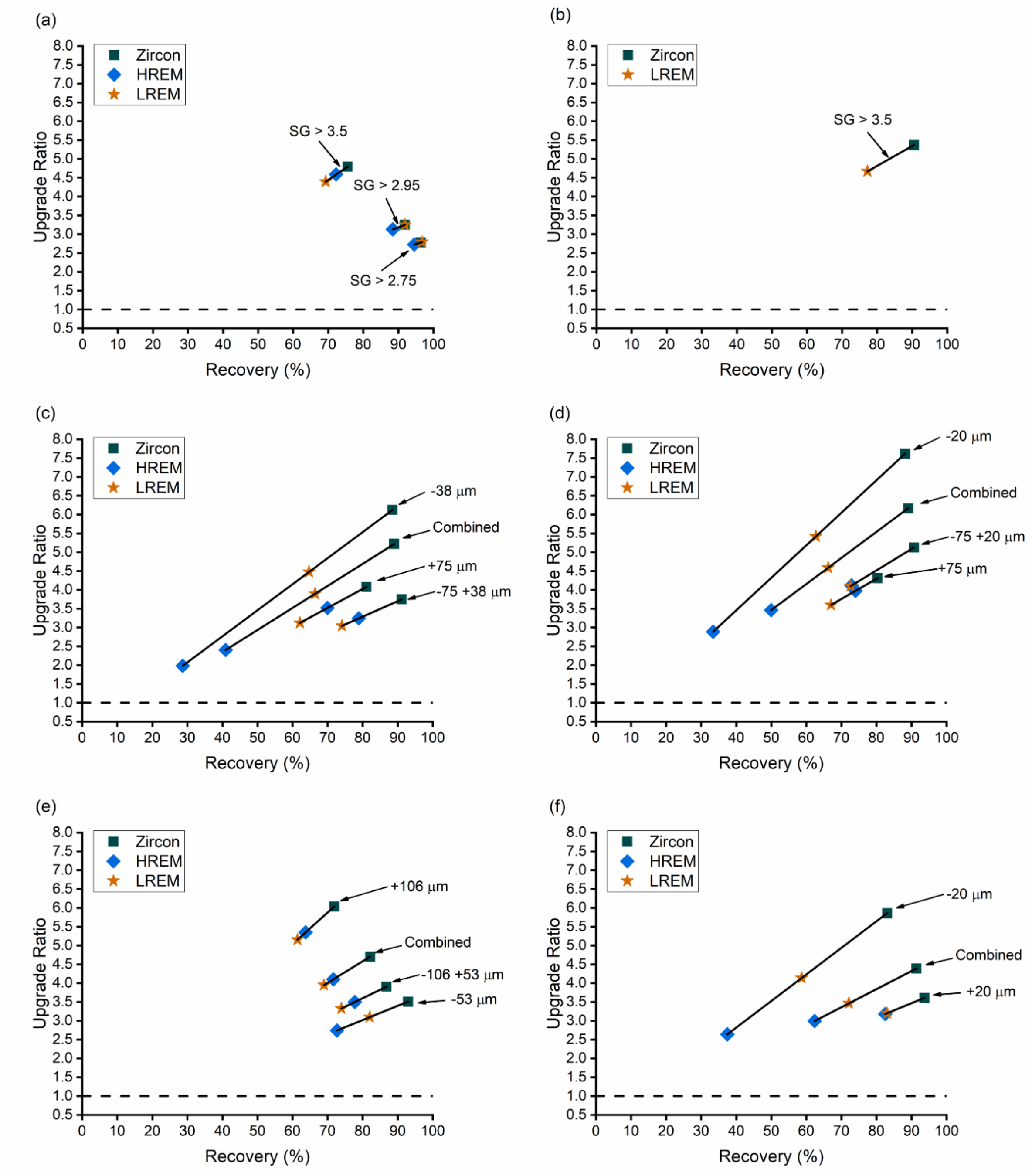

Figure 6.5 – QEMSCAN predicted upgrade ratio and recovery of zircon, HREM and LREM for (a) the coarse particle fraction of Feed 1 split at a SG of 2.75, 2.95 and 3.5, (b) the fine particle fraction of Feed 1 split at a SG of 3.5, (c) Feed 2 split at a SG of 3.5, (d) Feed 3 split at a SG of 3.5, (e) the coarse particle fraction of Feed 4 split at a SG of 3.5 and (f) the fine particle fraction of Feed 4 split at a SG of 3.5

6.6 Conclusions

This chapter has detailed the mineralogical characteristics of the different feed samples which were studied during this thesis. Examining the mineralogy, grain size distributions, liberation and association characteristics and mineral SG distributions the following conclusions can be made:

1. Following grinding, zircon is enriched in coarse particles (> 20 µm), which may provide opportunities for pre-concentration through selective comminution
2. Zircon is relatively well liberated (> 55 %) across each feed and is concentrated in high SG particles even at coarse (+75 µm) particle sizes
3. HREM liberation is low (< 25 %) in Feeds ground using a rod mill, however, when a ball mill is used liberation is improved
4. HREM are concentrated in high SG particles at coarse (> approximately 38 µm) particle sizes, however, at finer sizes most HREM-bearing particles are of low SG
5. LREM are more readily liberated than HREM when using a rod mill and are concentrated in high SG particles

Chapter 7

Gravity Separation

7.1 Introduction

This chapter details gravity separation experiments applied to the Nechalacho ore to asses its application as both a preconcentration and primary separation stage. While some information is provided in this Chapter, readers are referred to Chapter 5 for more details on the operating conditions employed for each technique and the feed samples tested. The behaviour of the various value and gangue minerals when using different gravity separation techniques is understood using multiple characterisation tools, including QEMSCAN, SEM, XRD, ICP-MS and XRF. However, much of the discussion is focussed on information obtained from QEMSCAN with the various other characterisation tools being used to validate the QEMSCAN results.

7.2 Preconcentration

The Nechalacho deposit is composed primarily of finely grained valuable minerals, which require fine grinding for effective liberation. However, previous test work (Jordens *et al.*, 2016b) coupled with the mineralogical analysis performed on the various feed samples studied in this thesis (Chapter 6) suggest that value minerals remain in relatively high SG particles at coarse sizes, providing opportunities to preconcentrate the ore prior to complete liberation, using a gravity separation step. This was assed on coarse particle fractions of Feed 1 and Feed 4 (Chapter 5), which had size distributions (d_{80}) of 97 μm and 133 μm, respectively. The goal of this preconcentration stage is aimed at early gangue rejection which could have significant benefits, including lower energy requirements in the comminution stage, increased feed grades and lower throughputs to downstream processes, and lower operational costs.

7.2.1 Dense Medium Separation

7.2.1.1 Feed 1

Figure 7.1 shows the recovery and upgrade ratio of Zr, LREE and HREE in the DMS sink fractions when using a heavy liquid with a SG of 2.95 and 2.75 to process a representative fraction of the coarse particle fraction of Feed 1. The results indicate that 81 % of Zr and 76 % of REE can be recovered, with upgrade ratios of 4.2 and 3.9 respectively, when processing the material using a heavy liquid with a SG of 2.95. Zr and REE recoveries were increased to 95 % and 92 %, respectively, at a SG of 2.75. However, upgrading was impacted (Zr: 2.9; REE: 2.8), due to the recovery of less liberated material. These results are in good agreement with the mineralogical upgrading and recovery determined by QEMSCAN analysis on the feed sample (Chapter 6, Figure 6.5a). This demonstrates gravity modeling using QEMSCAN can be used, confidently, to predict grade and recovery values by SG for DMS.

SEM-EDS was used to identify Zr, Fe, Ce and Y in the sink and float fractions at a SG of 2.75 (Figure 6.2). While only qualitative, the SEM images provide an empirical check for the conclusions drawn from QEMSCAN (Chapter 6, Section 6.5), which assigns mineral chemistry based on a definition database. This analysis clearly shows valuable minerals (and iron oxides) are concentrated in the DMS sink fraction. Zircon is recovered as both coarse liberated particles and fine-grained material which remains locked with other minerals in the feed. The SEM images show Y alongside Zr, demonstrating the importance of recovering zircon for the recovery of HREE. Minerals bearing LREE, such as Ce, are generally finely grained and poorly liberated. However, they are found in particles containing other REM, zircon and/or Fe oxide grains, confirming that mineral association characteristics provide opportunities for the recovery of less liberated material. Although DMS represents near ideal gravity separation and the upgrade ratios obtained here are likely not possible using conventional or enhanced gravity concentrators, the results indicate that gravity separation may be effective at selectively recovering both zircon and REM, while rejecting low SG gangue.

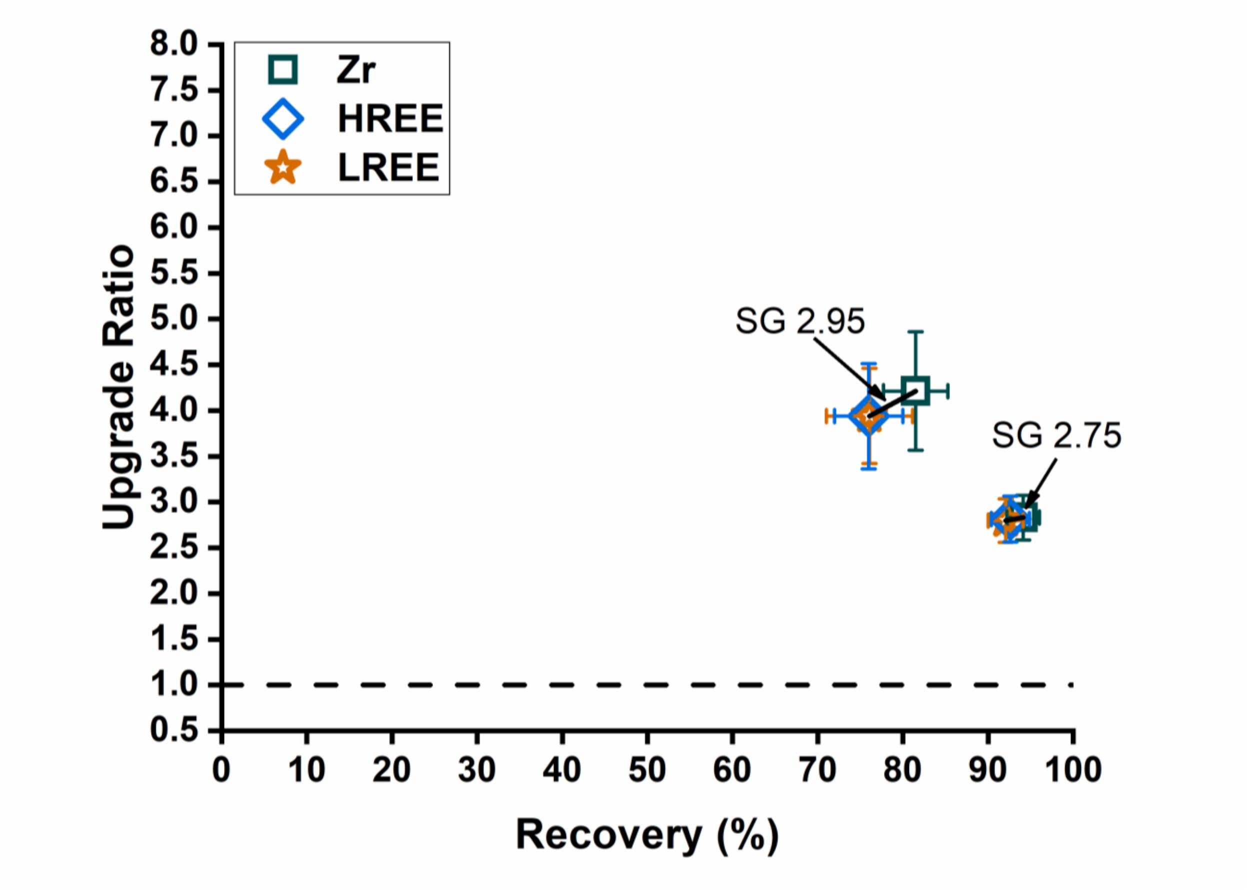

Figure 7.1 – Upgrade ratio and recovery of valuable elements from DMS sink fractions with a heavy liquid of SG 2.95 and 2.75 (Error bars represent 95 % confidence intervals)

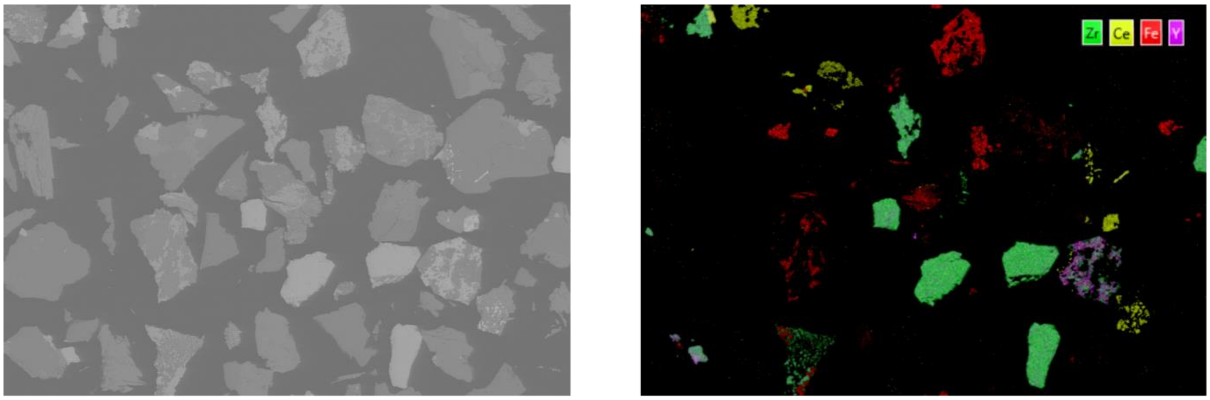

Sink

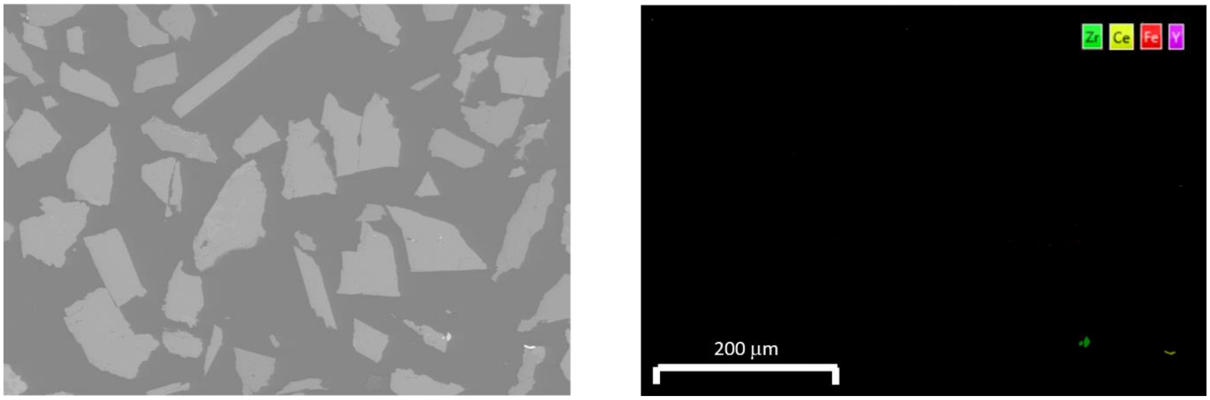

Float

Figure 7.2 – BSE image (left) and elemental (Zr, Ce, Fe, Y) phase identification (right) of the DMS sink and float fraction produced using a heavy liquid with a SG of 2.75

7.2.2 Knelson Concentrator

7.2.2.1 Feed 1

The upgrade ratio *vs.* recovery of the major mineral classes in the concentrate produced after processing a representative sample of the coarse particle fraction of Feed 1 using a Knelson Concentrator is shown in Figure 7.3. The results indicate that all relatively high SG minerals (zircon, Fe oxides and REM) in the deposit are concentrated, while the gangue minerals (quartz and feldspars) are rejected. The Knelson Concentrator was most effective at upgrading iron oxides, with an upgrade ratio of 2.6, followed by zircon (2.3), LREM (2.1) and then HREM (1.8). These findings were verified qualitatively through XRD (Figure 7.4) and quantitatively using ICP-MS (Figure 7.5) which gave elemental upgrade ratios for Zr, LREE and HREE of 1.8, 2.1 and 2.1 respectively. The minor discrepancies between chemical assays and QEMSCAN results (most notably between Zr and zircon) are likely caused by differential settling and density segregation of particles during preparation of the polished sections. This is a common concern when creating polished sections for QEMSCAN (Coetzee et al., 2011; Kwitko-Ribeiro, 2012; Speirs et al., 2008); and in this case (and in other instances throughout this thesis), results in small (negligible) overestimations of zircon. Although the recoveries of relatively high SG minerals in the deposit are low, examining the mineral liberation and association characteristics of the Knelson concentrate and tailings (Figure 7.6), suggests that zircon and iron oxide recoveries are likely low due to the lack of recirculation, rather than insufficient liberation. The findings from Section 6.5 and Section 7.2.1, which indicate REM are present in relatively high SG particles, suggest that multiple stages of concentration using the Knelson may also improve the recovery of REM. Improvements in grade and recovery would additionally be expected through the optimization of Knelson operating parameters.

Figure 7.7 shows the recovery of the major mineral classes relative to each size class investigated. It is suggested that in general when using the Knelson Concentrator there is limited preferential recovery by particle size. The relative recovery of material > 150 μm is greater than the other size classes, however, there is minimal mass in this size fraction and therefore tangible conclusions can not be drawn. At particle sizes > 106 μm the Knelson Concentrator is not effectively rejecting quartz. Although feldspars (which account for the largest proportion of gangue) are rejected, and high SG minerals are recovered preferentially. Thus, the use of a centrifugal gravity separator, such as a Knelson Concentrator, may provide opportunities for processing this deposit at coarser size fractions than those tested here.

Figure 7.8 shows the distribution of zircon and LREM by SG class at each particle size. It can be noted that the Knelson concentrator is favouring the recovery of particles with more elevated SG across all size ranges for both zircon and LREM. It also indicates significant amount of high SG material remains in the tailings fraction, reiterating the fact that multiple processing stages through the Knelson is likely to provide increased recovery of high SG material without a major impact on concentrate grade. Although the mass in the + 106 µm size fraction is low, the Knelson Concentrator does continue to preferentially recover valuable minerals in high SG particles which reiterates that the Knelson may be effective at preconcentrating a coarser feed, under the assumption that at coarser sizes valuable minerals remain enriched in high SG particles.

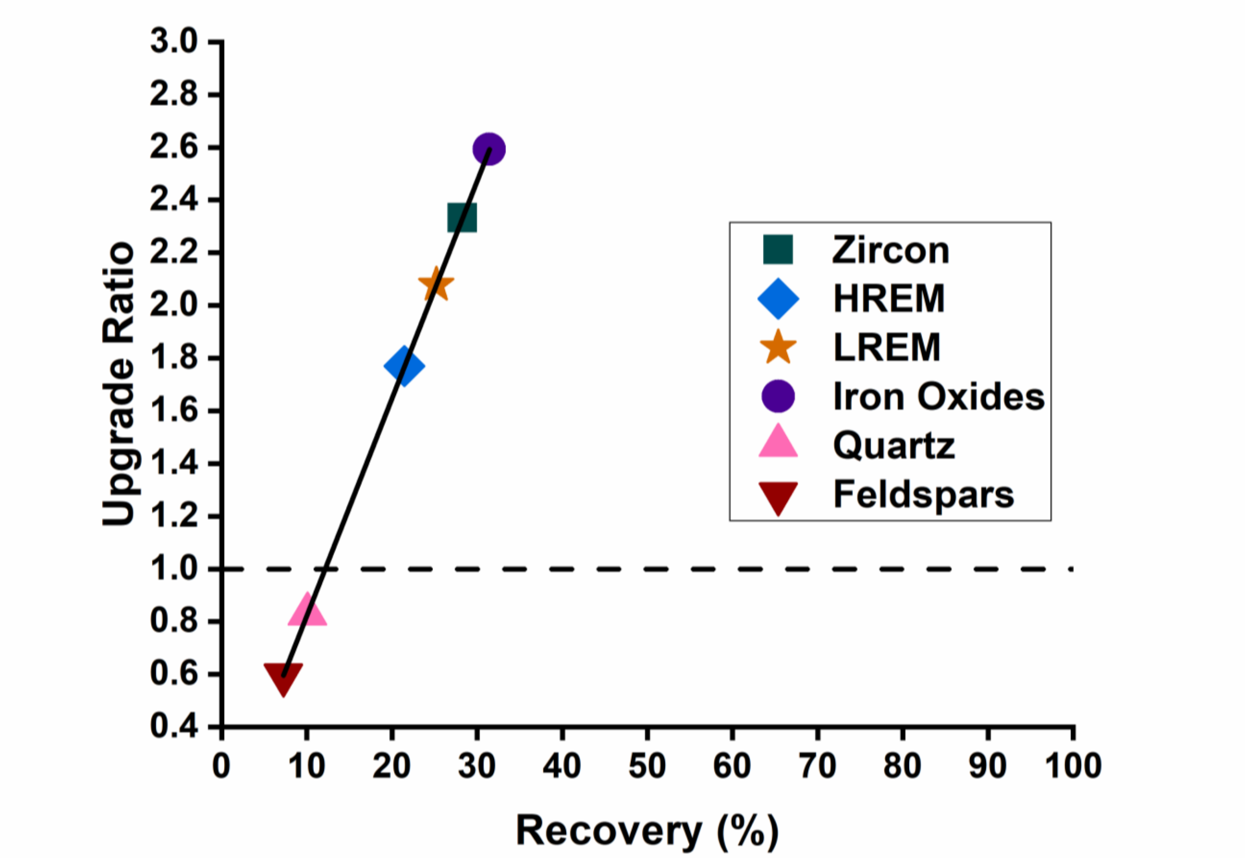

Figure 7.3 – Upgrade ratio and recovery of the major mineral classes in the Knelson concentrate produced from the coarse particle fraction of Feed 1

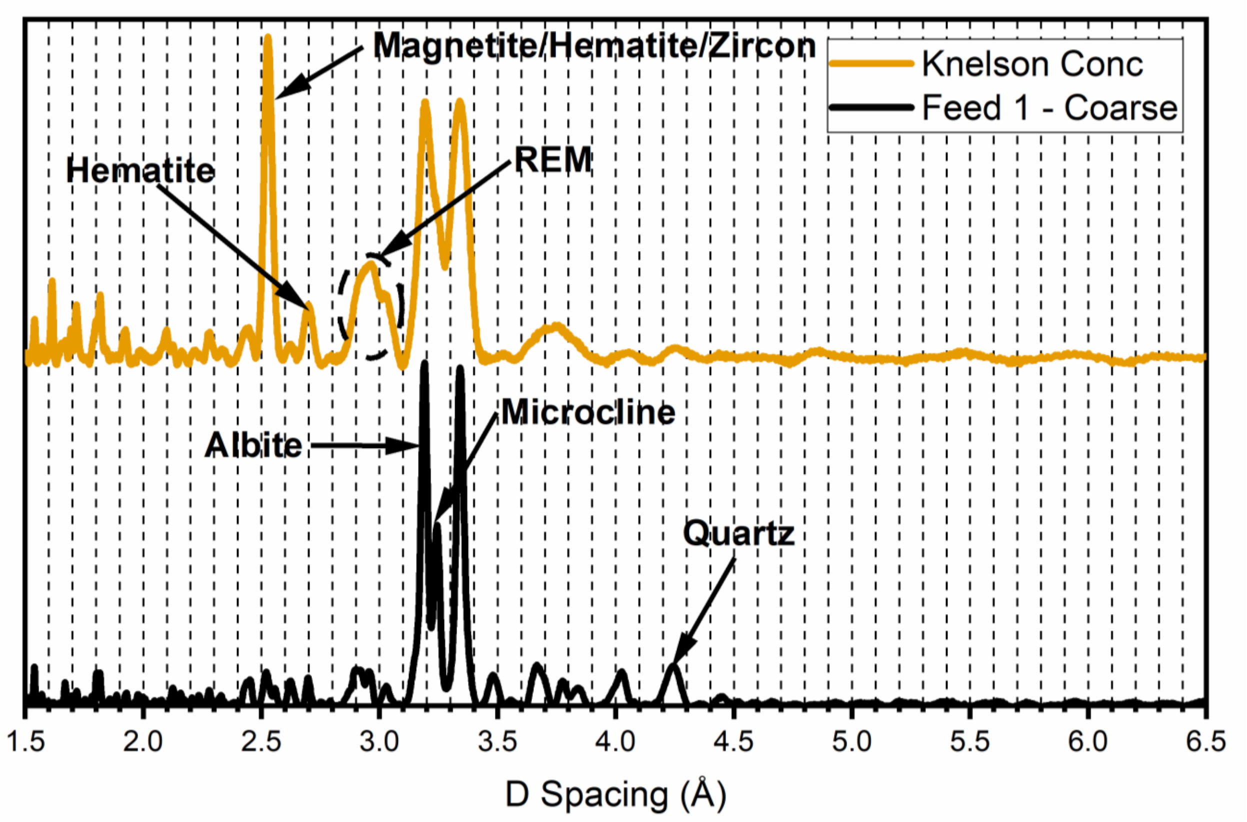

Figure 7.4 – XRD pattern of the Knelson concentrate and the coarse particle fraction of Feed 1

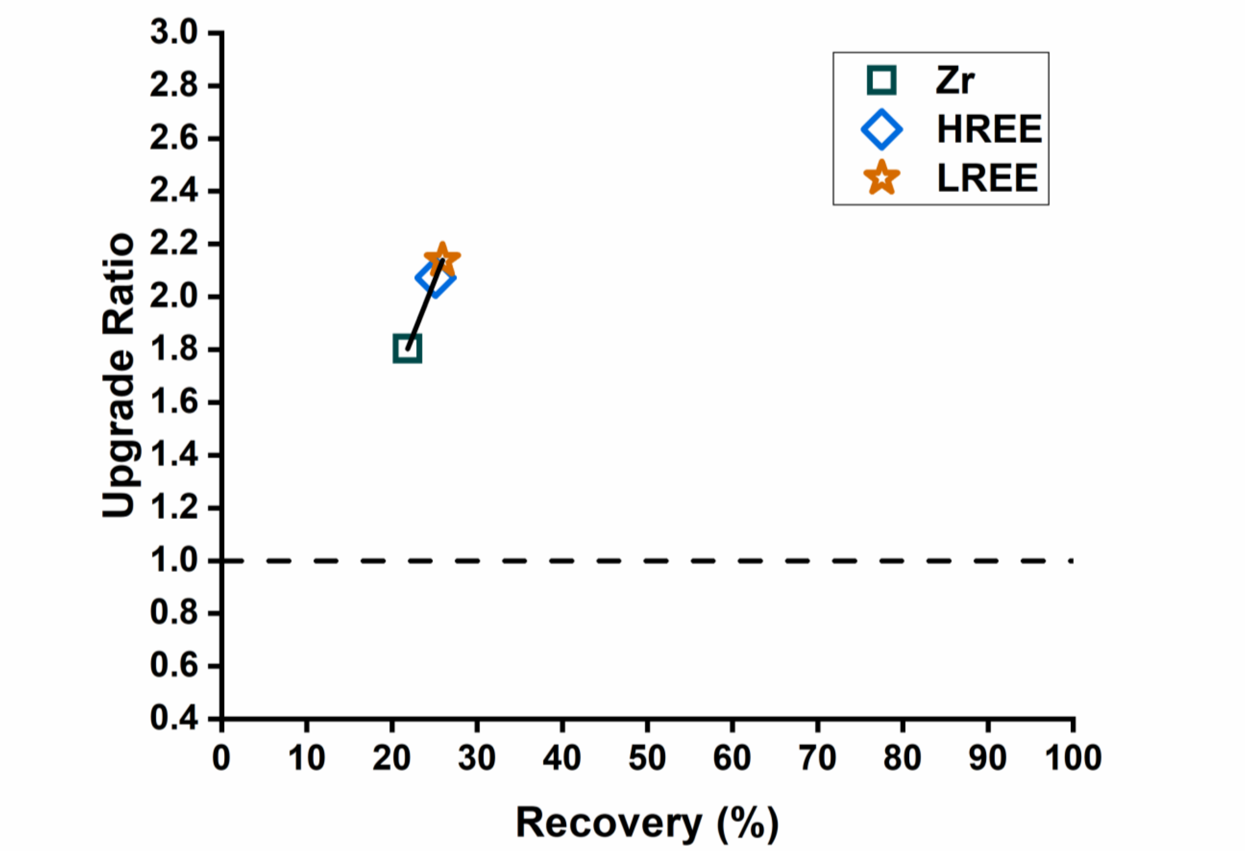

Figure 7.5 – Upgrade ratio and recovery of valuable elements in the Knelson concentrate produced from the coarse particle fraction of Feed 1

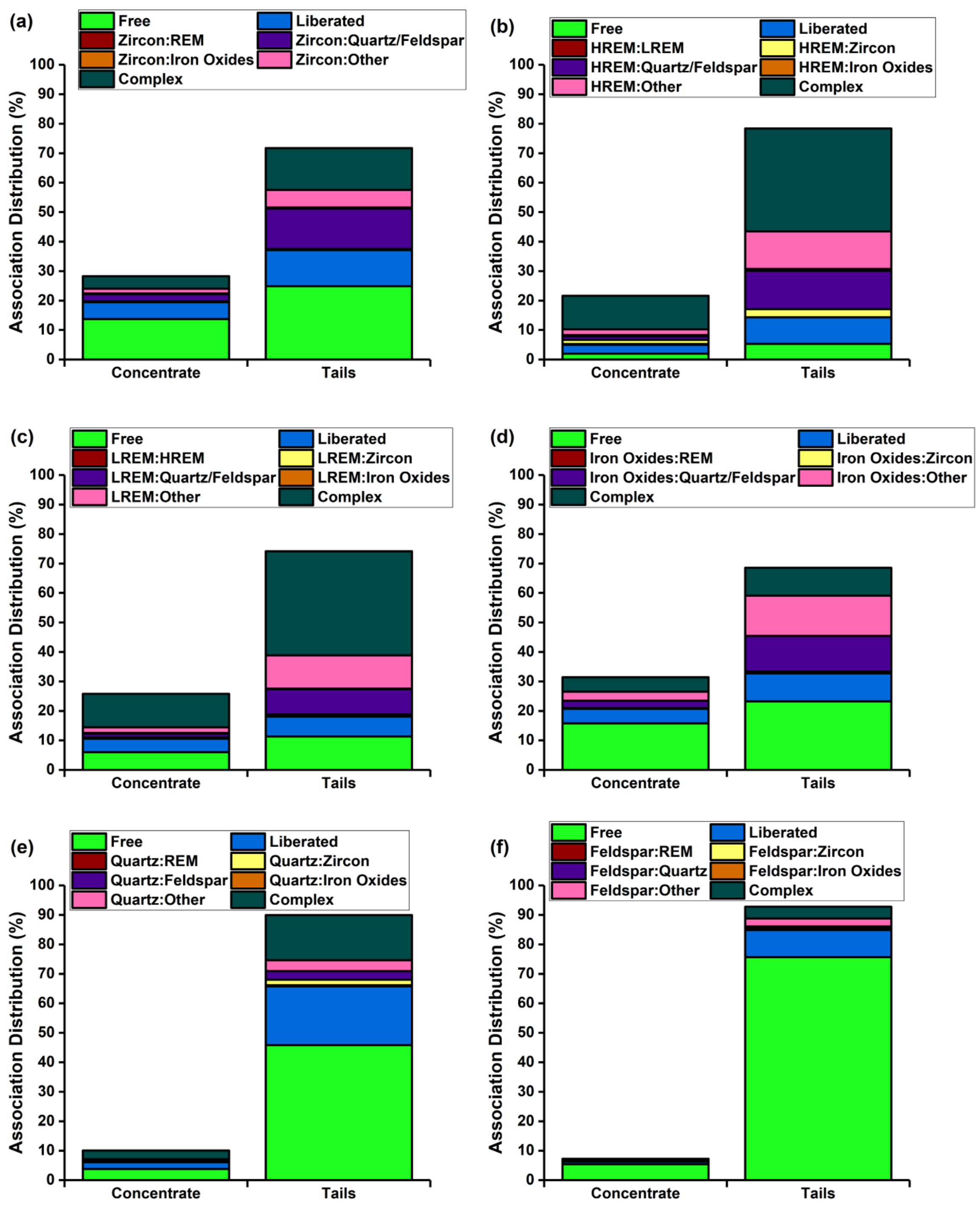

Figure 7.6 – Mineral associations of the Knelson products produced from the coarse particle fraction of Feed 1 for (a) zircon, (b) HREM, (c) LREM, (d) Fe oxides, (e) quartz and (f) feldspars

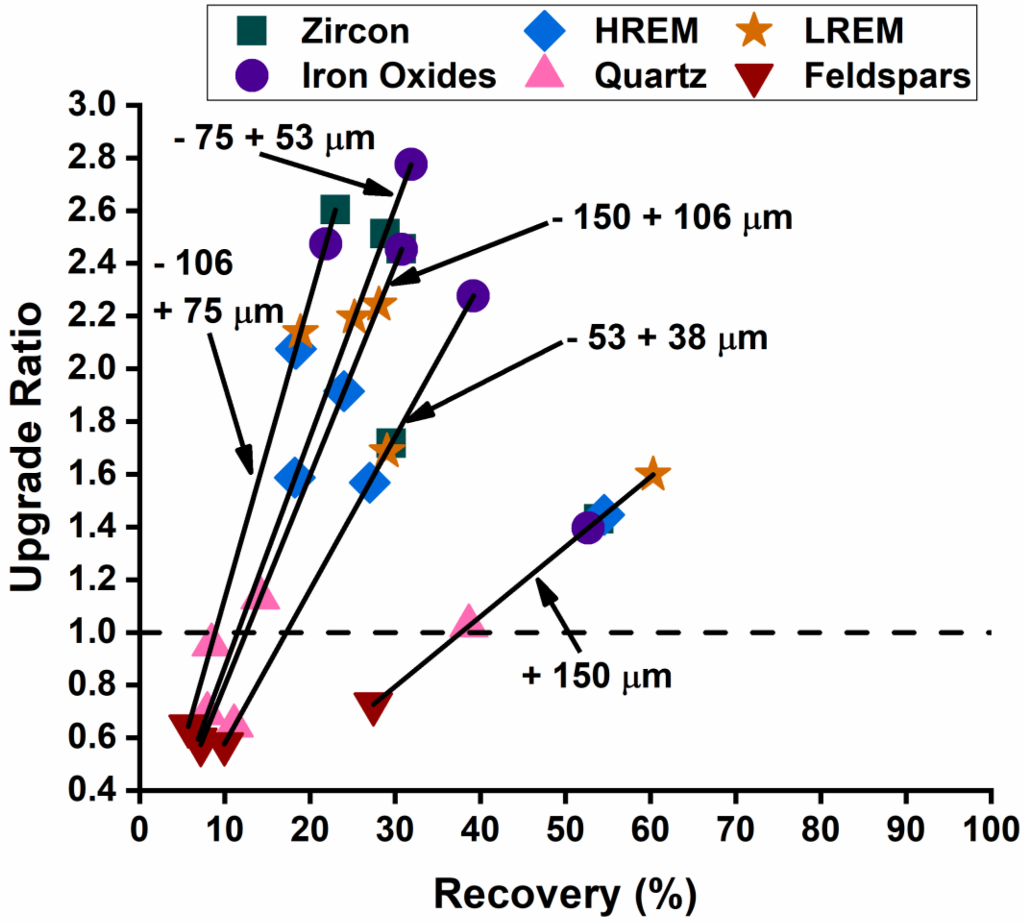

Figure 7.7 – Upgrade ratio and recovery of the major mineral classes in the Knelson concentrate produced from the coarse particle fraction of Feed 1 sorted by size

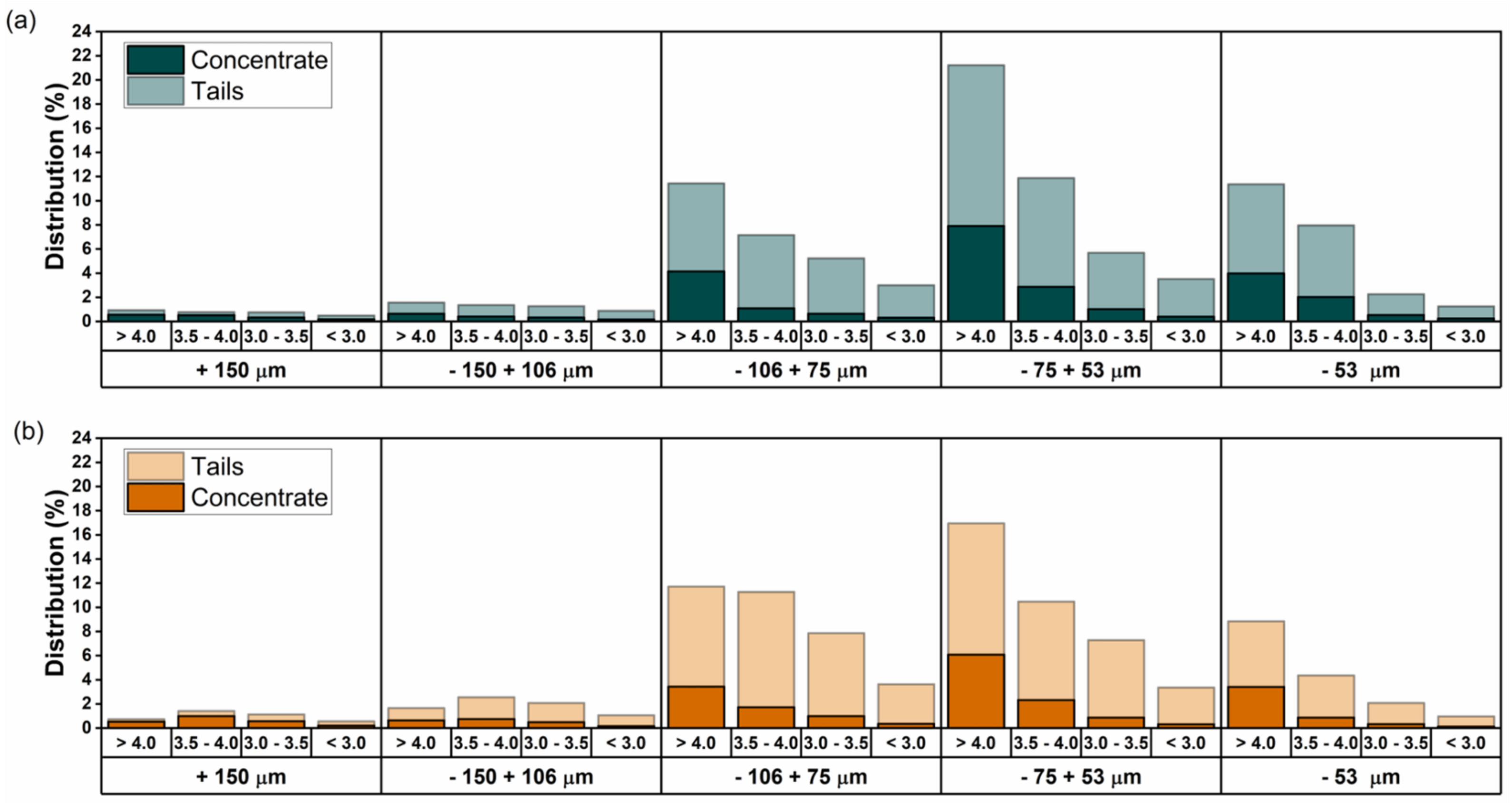

Figure 7.8 – SG distribution of (a) zircon and (b) LREM in the Knelson concentrate and tails produced from the coarse particle fraction of Feed 1, shown cumulatively as such that the total of all bars equates to 100 %

7.2.3 Spiral Concentrator

7.2.3.1 Feed 1

An analysis, similar to that performed on the Knelson products in Section 7.2.2.1, was conducted on the spiral concentrate and tailings produced after processing a representative sample of the same feed. Figure 7.9 shows the upgrade ratio *vs.* recovery for the major mineral classes in the deposit; Figure 7.10 the XRD pattern of the spiral concentrate and feed; Figure 7.11 the upgrade ratio *vs.* recovery of valuable elements (determined by ICP-MS); Figure 7.12 the mineral liberation and association data; Figure 7.13 the size by size upgrading and recovery of each mineral class; and Figure 7.14 the recovery of zircon and LREM by SG class. Comparing the two techniques the Knelson concentrator provides better selectivity over the spiral concentrator, with improved quartz and feldspar rejection; however, recoveries are significantly greater after a single pass of the spiral. The liberation and association data for the Knelson products (Figure 7.5), compared to those obtained for the spiral products (Figure 7.12), suggest that the Knelson concentrator yields improved upgrading through both better rejection of liberated gangue and selectivity for liberated high SG zircon- and LREM-bearing particles (Figure 7.12). The ability to better reject liberated gangue may be partially attributed to the fact that particle size is less of a factor in separation (Figure 7.13 *vs.* Figure 7.7). Figure 7.13 indicates that, in general, the spiral concentrator is preferentially recovering coarse particles in the feed; although this may be an artifact of the low mass in the > 106 μm size fractions. Minimal upgrading is obtainable at particle sizes > 150 μm, but, the spiral concentrator is effective at upgrading the high SG minerals in the finer size fractions. Zircon and REM, in the - 150 + 106 μm fraction, are effectively upgraded and recovered, even though they are poorly liberated (Chapter 6, Section 6.4). This implies grain size differences and mineral associations allow for the separation of coarse unliberated valuable material using a spiral, but it may only be effective at particle size ranges less than 150 μm. However, it is again noted that the mass fraction with a size > 106 μm is low and further work with a coarser feed size should be investigated.

From Figure 7.14, the spiral concentrator is favouring the recovery of particles with more elevated SG across all size ranges for both zircon and LREM, except for the + 150 μm size fraction. Figure 7.14, along with Figure 7.12 suggest similar findings to the those obtained using a Knelson, where greater recoveries are likely possible through multiple stages of separation. It is important to note that the spiral and operating conditions (pulp density, flow rate, *etc.*) used for this study have not been optimized. Thus, the use of a spiral concentrator better suited for fine particle separation (< 100 μm) (Richards *et al.*, 2000) and through further optimization, significant improvements could be achieved.

Although the Knelson Concentrator offers greater potential for higher grades following a preconcentration stage, the goal of this stage is primarily for early gangue rejection. The spiral offers greater simplicity over the Knelson, and these results suggest it can effectively recover valuable minerals while rejecting significant quantities of low SG gangue (particularly feldspars). Therefore, it is likely better suited for this process in an industrial setting.

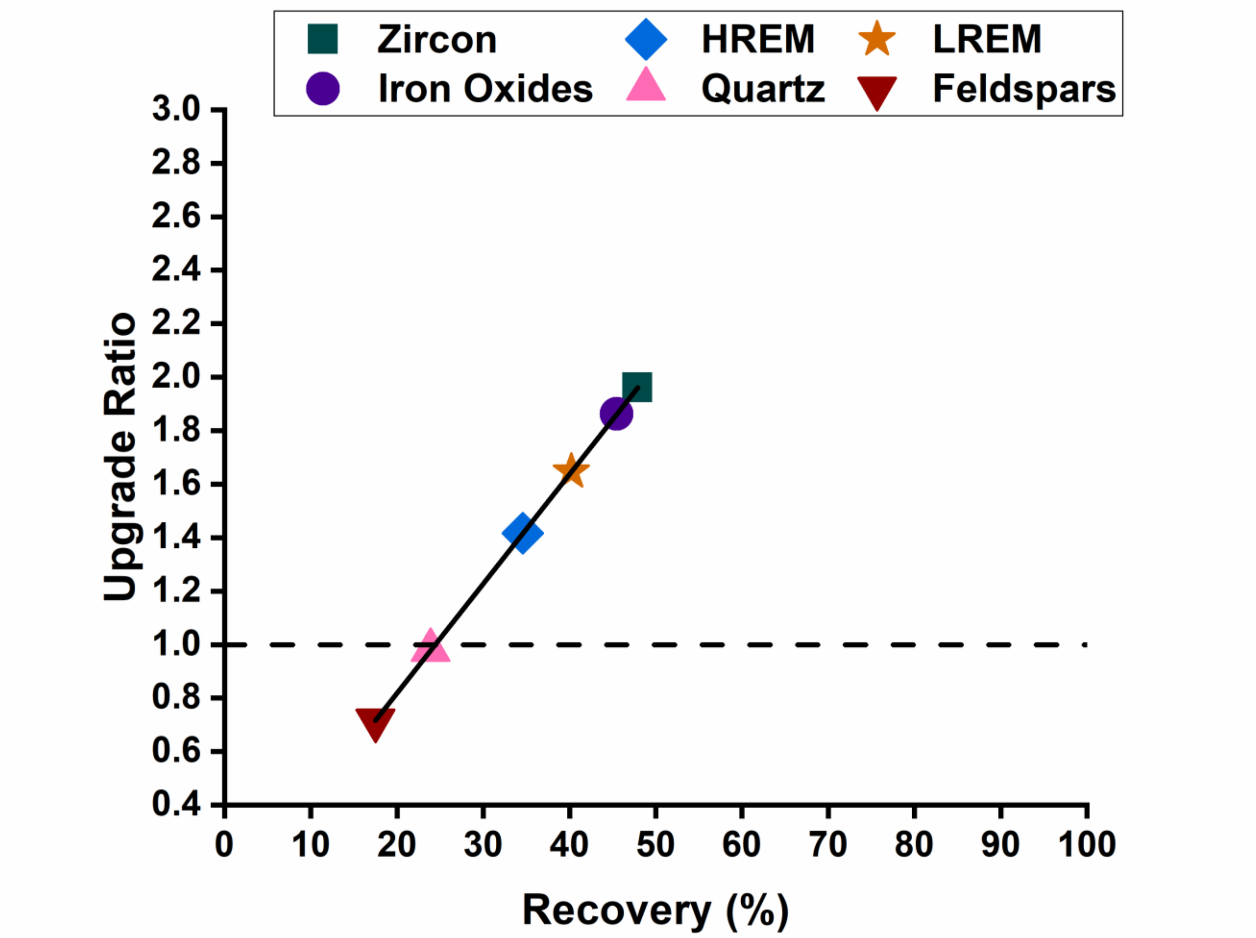

Figure 7.9 – Upgrade ratio and recovery of the major mineral classes in the spiral concentrate produced from the coarse particle fraction of Feed 1

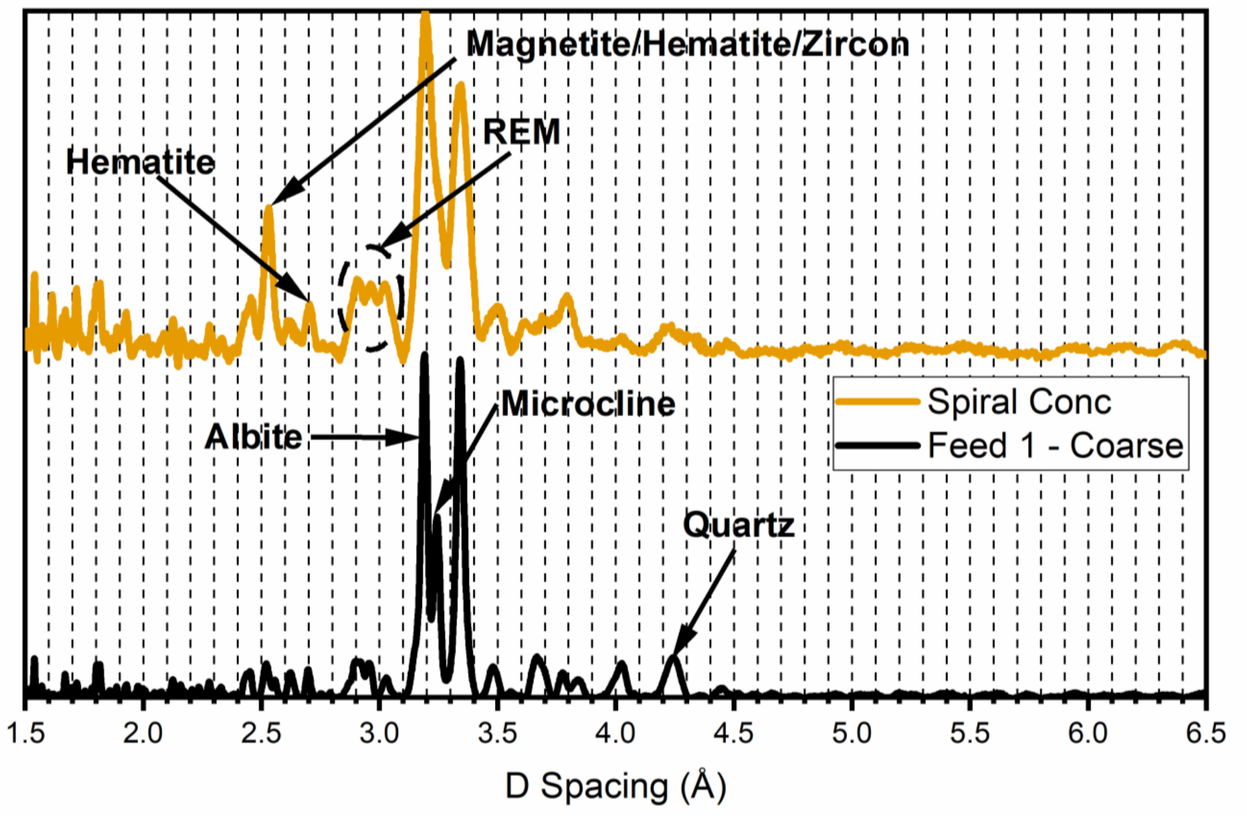

Figure 7.10 – XRD pattern of the spiral concentrate and the coarse particle fraction of Feed 1

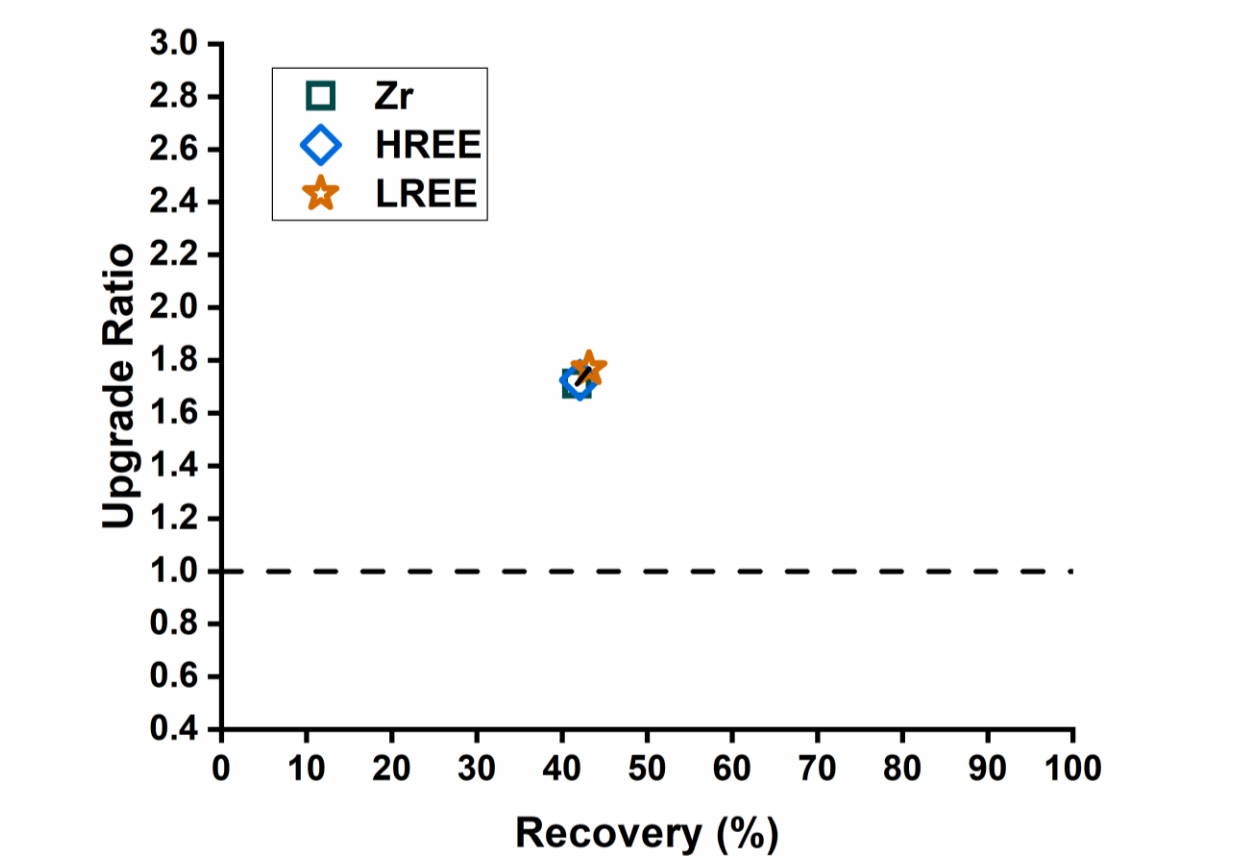

Figure 7.11 – Upgrade ratio and recovery of valuable elements in the spiral concentrate produced from the coarse particle fraction of Feed 1

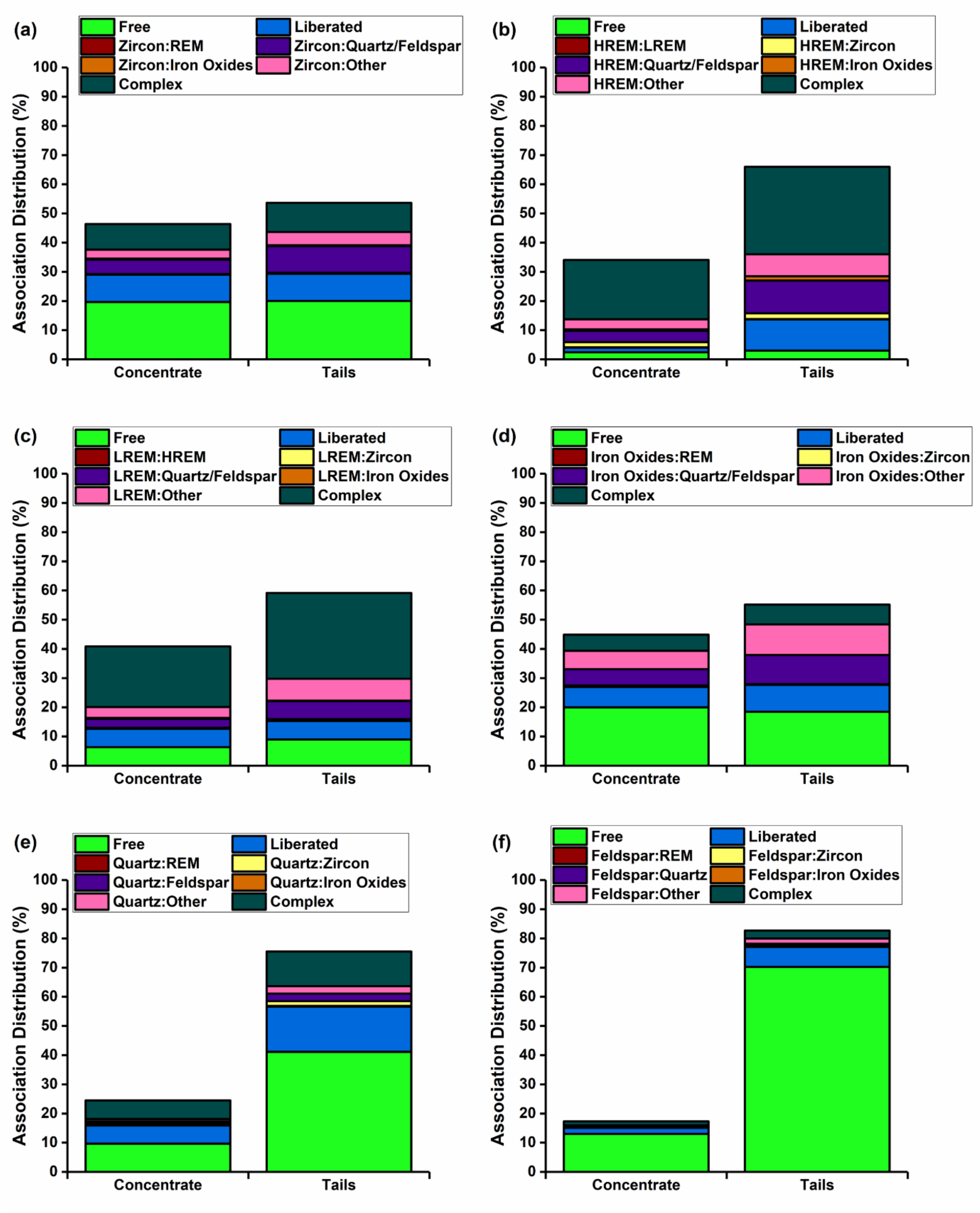

Figure 7.12 – Mineral associations of the spiral products produced from the coarse particle fraction of Feed 1 for (a) zircon, (b) HREM, (c) LREM, (d) Fe oxides, (e) quartz and (f) feldspars

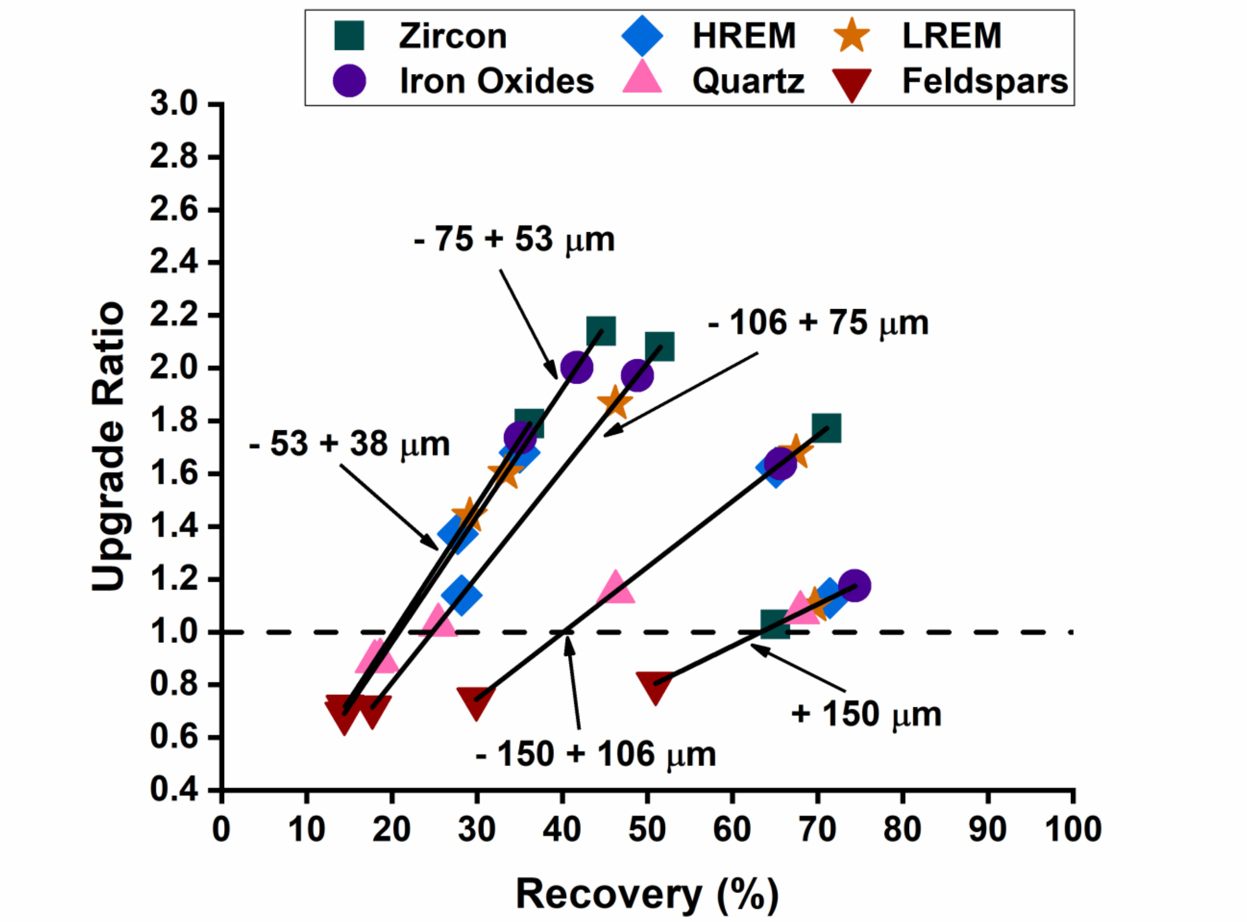

Figure 7.13 – Upgrade ratio and recovery of the major mineral classes in the spiral concentrate produced from the coarse particle fraction of Feed 1 sorted by size

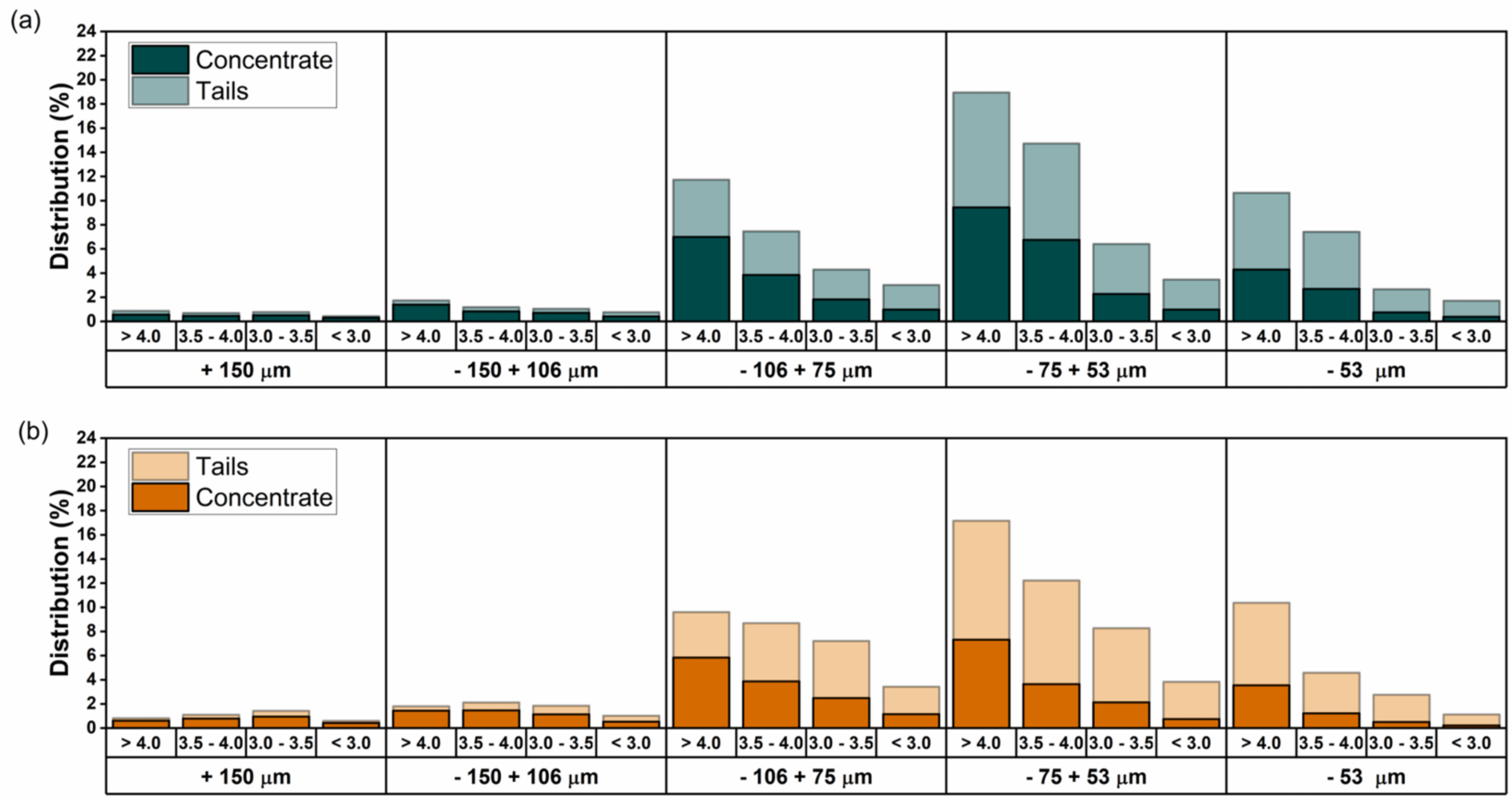

Figure 7.14 – SG distribution of (a) zircon and (b) LREM in the spiral concentrate and tails produced from the coarse particle fraction of Feed 1, shown cumulatively as such that the total of all bars equates to 100 %

7.2.3.2 Feed 4

To asses some of the observations from processing the coarse particle fraction of Feed 1 with a spiral concentrator (Section 7.2.3.1), a coarser feed with a size distribution of d_{80} = 133 μm (- 150 + 53 μm) was produced through stage grinding and sieving (Chapter 5, Section 5.3). The feed was processed with three stages of spiral concentration, producing three concentrates and a tailings fraction.

The cumulative upgrade ratio and recovery plots of the major mineral classes (determined from QEMSCAN) and equivalent metal oxides (ZrO_2 and Ce_2O_3) (determined from XRF) following each pass of the spiral are shown in Figure 7.15 and Figure 7.16, respectively. After a single pass the concentrate recovered 57 % of the iron oxides, 56 % of the zircon, 50 % of the LREM and 47 % of the HREM. Upgrading the feed 2.3 times, 2.3 times, 2.0 times and 1.9 times, respectively. These results are improved over those observed when processing the coarse particle fraction of Feed 1 (Figure 7.9). This is unexpected if one were to compare only the liberation characteristics of these two feed samples (Chapter 6, Section 6.4). However, these improvements are likely realized from the coarser feed being better suited for separation in the spiral, coupled with the fact that the SG of valuable mineral-bearing particles is not significantly impacted at this coarser size (Chapter 6, Section 6.5). Similar to the initial study, the spiral is significantly better at rejecting feldspar than it is quartz.

After reprocessing the tails, zircon, HREM and LREM recoveries respectively increased to 81 %, 73 % and 74 % after a second pass; and 91 %, 86 % and 86 %, after a third. However, upgrading was impacted after each subsequent pass and the grade of valuable material in the third concentrate was lower than that of the initial feed. Further optimization of this process is required; however, these findings do demonstrate that it is possible to recover a high percentage of value minerals while effectively rejecting gangue (particularly feldspar) using a spiral concentrator.

To better investigate the effectiveness of each stage of separation, upgrade ratio *vs.* recovery plots relative to the feed for each separation step (*i.e.* tails of pass 1 are the feed for pass 2 and tails of pass 2 the feed for pass 3) were created (Figure 7.17). These results indicate that although the process becomes less selective with each subsequent pass, and in the case of the third concentrate valuable mineral grades are lower than the initial feed sample, relative to the feed prior to each pass enrichment is still occurring. As such future work should investigate spiral circuits which include rougher, cleaner and scavenger stages with recycling to improve the performance of this pre-concentration step and ideally produce a high-grade pre-concentrate with minimal losses of valuable material for downstream processing.

Figure 7.18 shows the recovery by liberation of the major mineral classes in the ore. After the first pass of the spiral the recovery of liberated valuable minerals exceeded 62 %, with a second pass recovering more than 82 %. The recovery of value minerals which are associated in binary particles with other high SG minerals exceeds 66 % after one pass and 85 % after the second. It is also interesting to note that that the process is effective at recovering zircon, LREM and HREM present in complex particles, with recoveries > 43 % after the first stage and > 72 % after the second. This finding reaffirms that grain size differences and mineral associations allow for the effective separation of coarse unliberated valuable material using a spiral. Figure 7.18 indicates that most of the quartz and feldspar recovered is liberated, which suggests that with optimization of the process parameters and circuit design further improvements in grade could be realized.

Figure 7.19 shows the recovery of mineral particles by SG class. Figure 7.19a shows the recovery of all particles in the feed. After one pass the recovery of particles with an SG > 4.0, from 3.5 to 4.0, from 3.0 to 3.5 and < 3.5 were 65 %, 49 %, 30 % and 15 % respectively. After a second pass the respective cumulative recoveries were 86 %, 77 %, 59 % and 35 %. Similar trends were observed for particles bearing zircon (Figure 7.19b), LREM (Figure 7.19c) and HREM (Figure 7.19d). The spirals effectiveness at recovering and concentrating particles with and SG > 4.0 is particularly useful for the preconcentration of zircon, of which 69 % of is present in particles with an SG > 4.0. Although the liberation of zircon is much greater than that of HREM and LREM, both these mineral classes a primarily found in high SG particles. The concentration of HREM present in particles of SG > 4.0 is 51 % and of SG > 3.5 is 66 %. The concentration of LREM in high SG particles is lower (40 % with SG > 4.0; 69 % with SG > 3.5). As the grain sizes are similar (Chapter 6, Figure 6.1e), this may suggest that HREM are more preferentially associated with other high SG minerals than LREM. It may also be a result of a significant quantity (32 %) of the LREM content being allanite, which as a low SG (3.5 – 4.2) relative to the other major REM in the deposit (SG > ~ 5.0). However, it is noted that the recovery of allanite in this stage does not differ significantly from other REM.

Comparing Figure 7.19b to Figure 7.14a, indicates that although the particle size is coarser the SG distributions for zircon are more advantageous for gravity separation (more valuable material in SG > 4.0 particles). Feed 4 was prepared through stage grinding with a rod mill, whereas, Feed 1 was ground in one stage using a ball mill. This demonstrates that the comminution process is going to play a critical role in the effectiveness of this preconcentration step, and this stage should be optimized to ensure the properties of feed are ideal for separation using a spiral at coarse particle sizes. One area of focus for future work is to examine the SG distributions of valuable minerals at coarser sizes than those investigated here, using various methods of comminution (rod mill, ball mill, high pressure grinding rolls, etc). If valuable minerals remain in high SG particles, the spiral may be effective at preconcentrating a coarser feed, which could have significant benefits, particularly in energy savings in comminution.

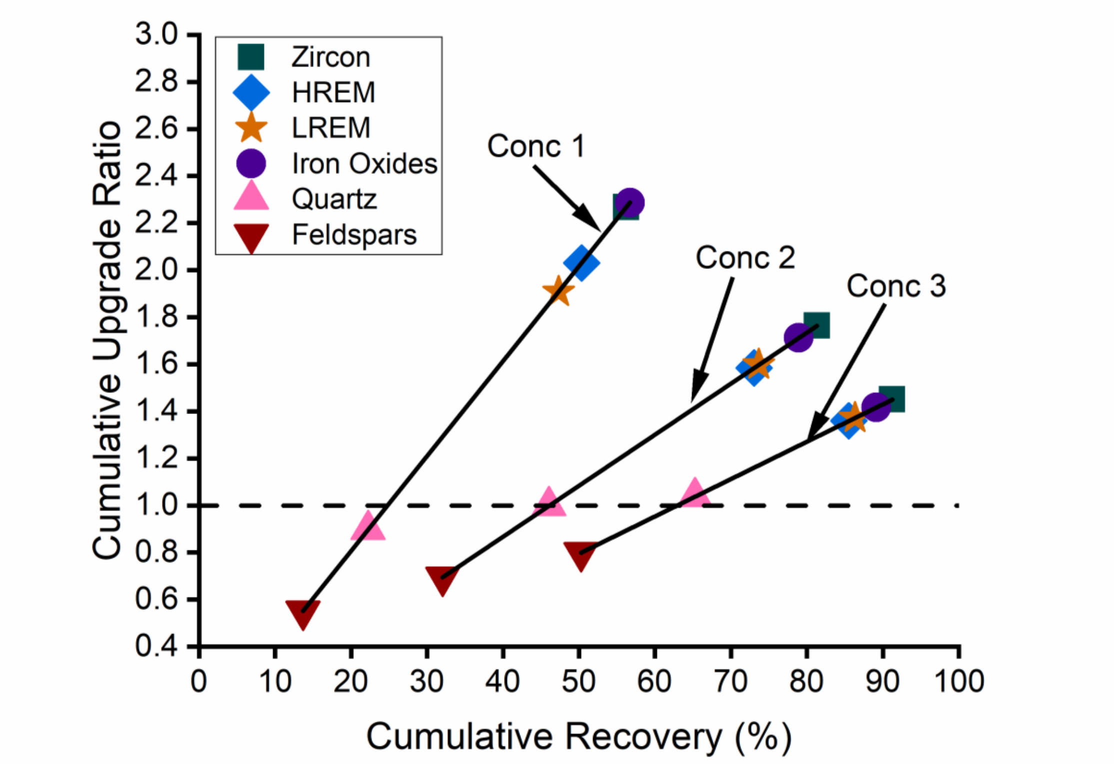

Figure 7.15 – Cumulative upgrade ratio and recovery of the major mineral classes in the spiral concentrates produced from Feed 4

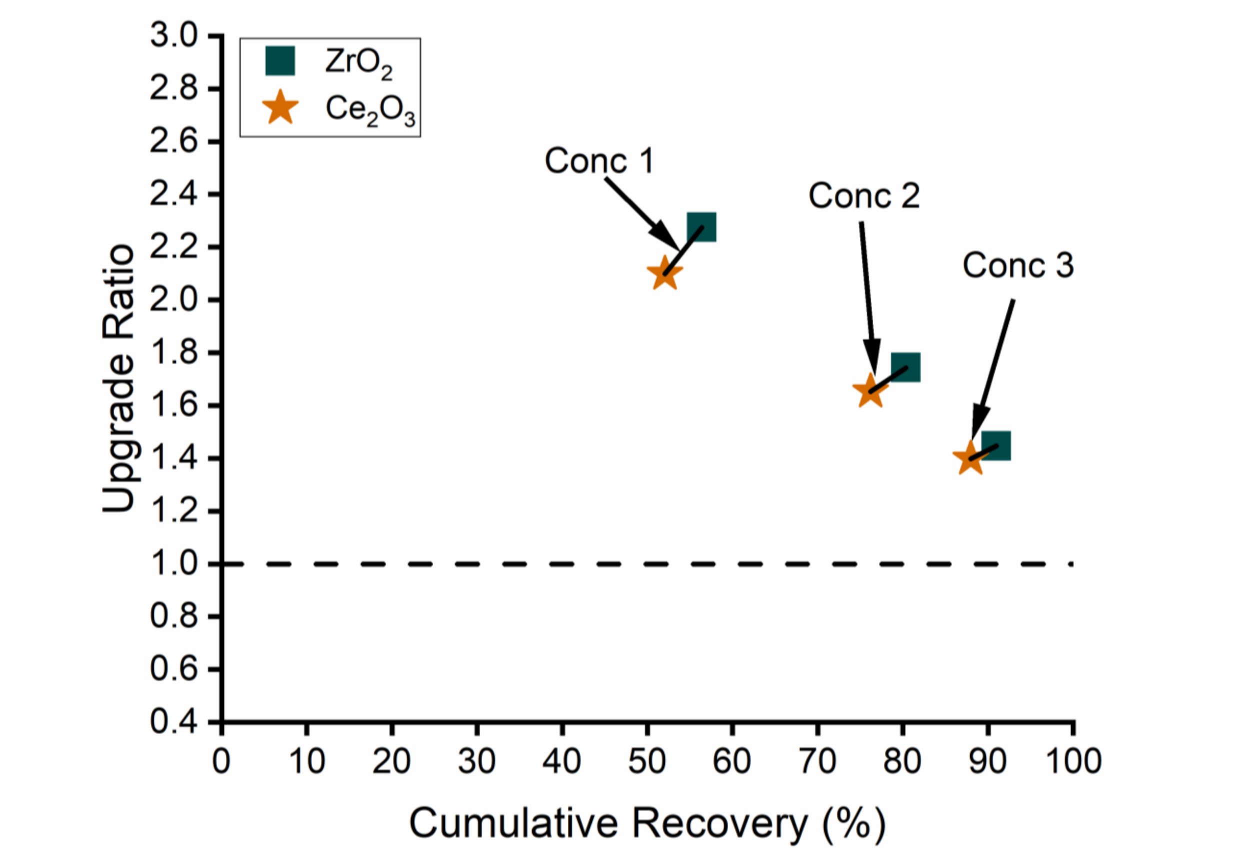

Figure 7.16 – Cumulative upgrade ratio and recovery of ZrO_2 and Ce_2O_3 in the spiral concentrates produced from Feed 4

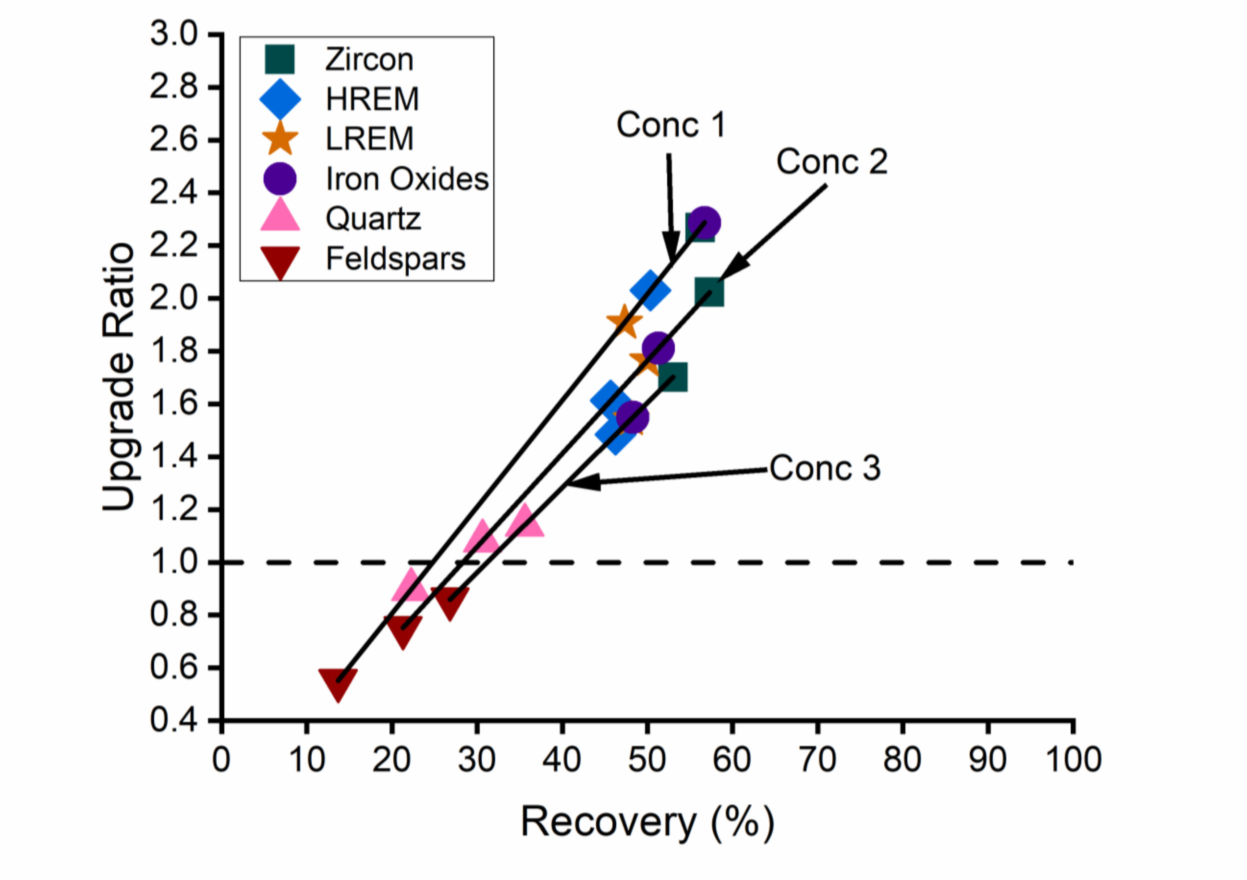

Figure 7.17 – Upgrade ratio and recovery of the major mineral classes in the spiral concentrates produced from the coarse particle fraction of Feed 4, relative to the feed of each pass

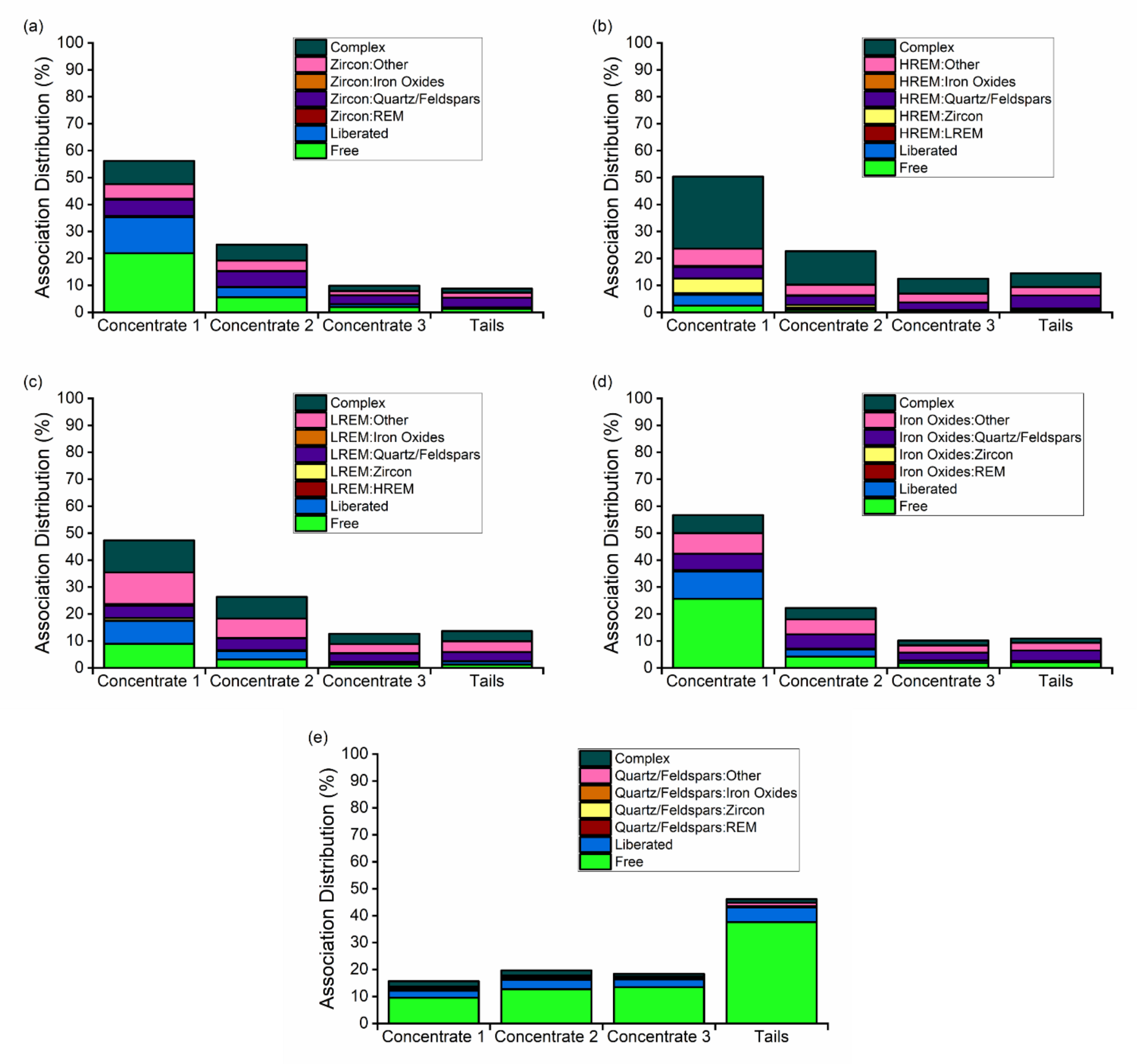

Figure 7.18 - Mineral associations of the spiral products produced from the coarse particle fraction of Feed 4 for (a) zircon, (b) HREM, (c) LREM, (d) Fe oxides, (e) quartz/feldspars

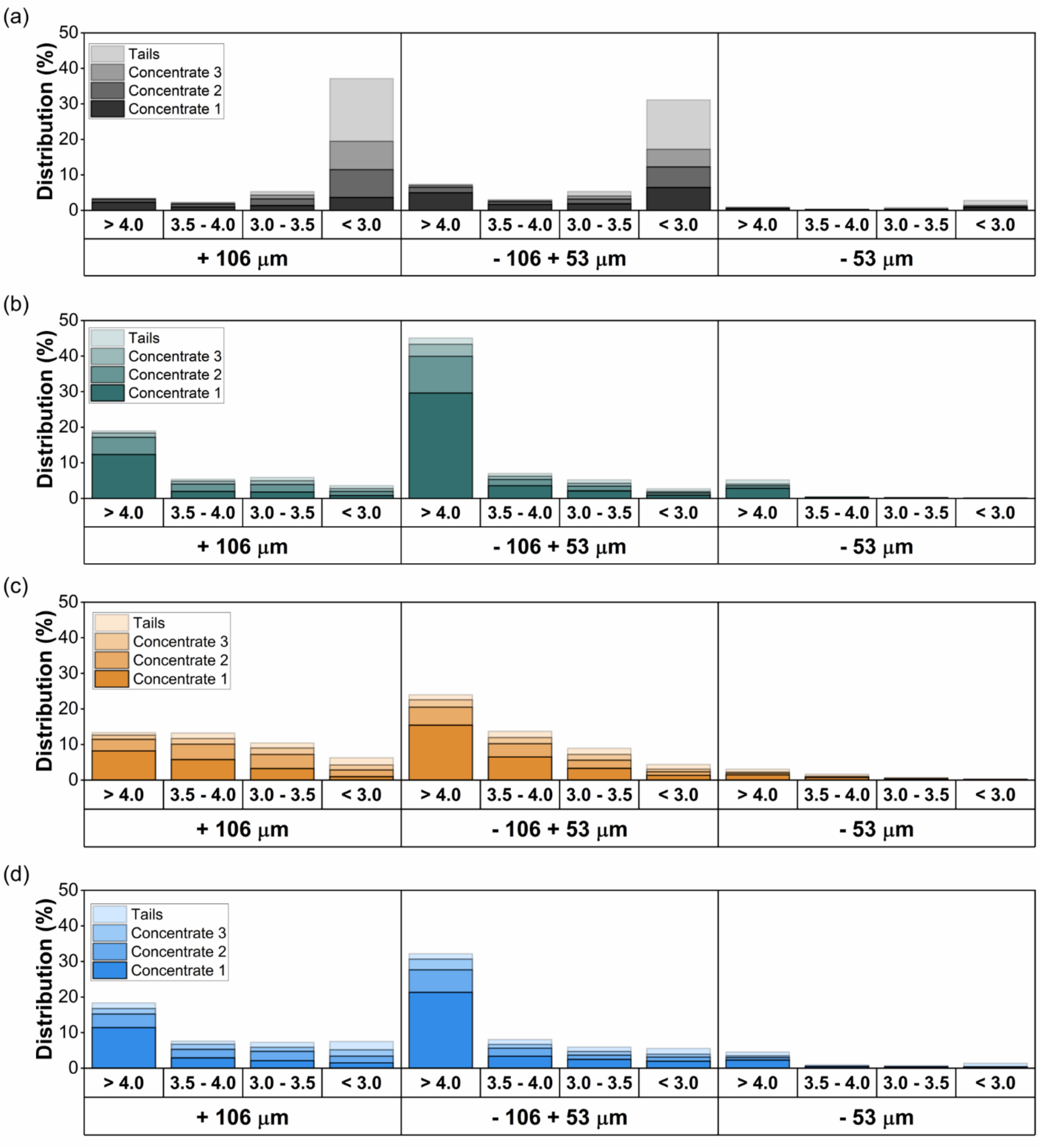

Figure 7.19 – SG distribution of (a) all particles, (b) zircon, (c) LREM and (d) HREM in the spiral products produced from the coarse particle fraction of Feed 4, shown cumulatively as such that the total of all bars equates to 100 %

7.3 Primary Separation

The goal of the work detailed in this section was to asses the application of various gravity separation techniques to concentrate valuable high SG minerals (and iron oxides) at particle sizes much closer to their liberation size than was studied in Section 7.2. As the grain size of REM is very low, the feed size must be reduced below the effective size range of conventional gravity separators, such as the spiral. Therefore, centrifugal gravity separators, specifically a Knelson Concentrator and a Multi-Gravity Separator, are studied here. One of the primary drawbacks of the industrial application of these devices is that they have relatively low capacities, when compared to other processing technologies. However, the Nechalacho deposit plans to process only 2,000 – 4,000 t/day (Ciuculescu *et al.*, 2013). To put this into perspective, some copper plants (employing flotation), such as Escondida in Chile (the largest copper mine in the world), are designed to process over 300,000 t/day (Rode, 2015). At Mount Wright in Canada (an iron ore mine), 8,500 spirals are used to process more than 180,000 t/day (ArcelorMittal, 2019). The capacity of a single CVD Knelson Concentrator is up to 7,200 t/day (FLSmidth Knelson, 2013) and a single industrial scale MGS up to 84 t/day (Gravity Mining Ltd., 2019). The new "Pure Select" MGS, which employs a low-profile scrapper system, is also said to dramatically increase capacity, however, to what extent is not presently reported (Gravity Mining Ltd., 2019). As high capacity systems are not required for the Nechalacho ore, both the Knelson Concentrator and MGS are directly applicable processing techniques. If a preconcentration step, such as that detailed in Section 7.2, is used the throughputs to the Knelson Concentrator or MGS would be even more manageable.

The application of a Knelson Concentrator and MGS was assessed using the fine particle fraction of Feed 1 ($d_{100} = 53$ µm), Feed 2 ($d_{80} = 55$ µm) and Feed 3 ($d_{80} = 55$ µm). Readers are referred to Chapter 5 for more details on the operational parameters used and the feed preparation process. More information on the mineralogical characteristics of each feed can be found in Chapter 6.

7.3.1 Knelson Concentrator

7.3.1.1 Feed 2

The cumulative upgrade ratio and recovery of the major mineral classes after each pass of the Knelson Concentrator is shown in Figure 7.20. The first two passes of the Knelson are effective at upgrading and recovering high SG material, particularly zircon, while rejecting quartz and feldspars. The third and fourth pass are not effective, offering little in terms of additional recovery. This is likely a result of the operational parameters which were used. Similar conclusions can be drawn from the XRD patterns for each concentrate (Figure 7.21) and the upgrade ratio *vs.* recovery of equivalent metal oxides (ZrO_2 and Ce_2O_3) (Figure 7.22).

To better asses the effectiveness of each stage upgrade ratio *vs.* recovery plots of each stage relative to their respective feed are shown in Figure 7.23. This process followed the work detailed in Appendix A (Section A.3), which was focused on determining optimum operating parameters of a synthetic feed of similar properties to the Nechalacho ore. The first stage of separation followed the condition which were determined optimal for a feed consisting of 15 % high SG material (employing a high bowl speed and low fluidizing water rate). The results of the real ore case were not as successful as those for the synthetic ore; producing a product of which 50 % of the minerals which were recovered were high SG minerals (zircon, REM, iron oxides) compared to the synthetic ore case where a product grade above 90 % was achieved. Recoveries were also significantly lower, at < 35 % for the real ore case compared to > 80 % for the synthetic ore. The differences are likely a result of the fact that in the real ore minerals are not all liberated, which lowers the concentrate grade, and the initial feed grade of high SG minerals is significantly higher (22 % *vs.* 15 %) which likely causes the bowl to fill up faster lowering mineral recoveries. The higher feed grades may result in different optimal operating parameters. However, the results from Appendix A (Section A.3) suggest that as the feed grade increases the Knelson should be operated with higher rotational speeds and lower fluidizing water rates, which are already set at close to the maximum and minimum, respectively.

The second stage followed the operating conditions outlined by processing the synthetic ore with a feed grade of 10 %. This resulted in a concentrate of which 45 % of the minerals were of high SG and recoveries ranging from 10 % to 30 %, depending on the mineral. The grade of this product is comparable to that of the synthetic ore (52 %), however, recoveries are again much lower (~ 40 % for the synthetic ore). Operating conditions for the Nechalacho ore were determined without knowledge of the results from subsequent passes. In this case the grade of high SG minerals in the feed (tails of stage 1) was 17 %. Therefore, using the conditions outlined by the synthetic ore with a grade of 15 % which would suggest increasing the bowl speed and lowering the fluidizing water rate may result in improved results. However, it is noted that as not all the high SG minerals are liberated (particularly REM), the grade of particles with a comparable SG to that of magnetite likely falls somewhere between 10 % and 15 %.

As the operating conditions were chosen without knowledge of the results of subsequent passes, those chosen for pass 3 and 4 were not effective. The grade of high SG minerals in the feeds for pass 3 and 4 were still above 15 %. The operating conditions used here were those determined to be best for a feed grade of 5 %, which are to employ relatively low bowl speeds and high fluidizing water rates. When using these conditions with higher feed grades (10 % or 15 %) relatively high grades were achievable (which was observed with the Nechalacho ore only for zircon) but recoveries where severely impacted (as was seen here). Future work following a flowsheet with more optimized conditions may prove the Knelson Concentrator as a highly effective method for concentrating the deposit. However, it is noted that the recovery and upgrading of REM is much lower than that of zircon and iron oxides. As such substantial improvements would be required to avoid significant losses of these minerals.

Figure 7.24 shows the recovery by liberation class for the major minerals in the deposit. The first two stages of separation are effective at recovering the majority of liberated (free + liberated) zircon (72 %), HREM (88%) and iron oxides (75 %). However, only 29 % of the liberated LREM were recovered. This is likely a result of liberated LREM being of fine particle size which the Knelson is not effectively recovering. This is better visualized in Figure 7.25, which shows the recovery of all particles, zircon, HREM and LREM by SG class and particle size. It is evident that the Knelson is highly effective at recovering and concentrating material > 38 μm, whereas it is not effective for the finer size class. Further work is required to determine if improvements at fine particle sizes are possible. If not, the Knelson Concentrator may not be suitable to process this entire deposit, as fine grinding is required to liberate REM. It is also noted that a significant portion of REM remain in low SG particles (particularly HREM) at the fine particle size. It was proposed in Chapter 6 that this was a result of using a rod mill for size reduction and with a ball mill it may not be of issue. But this does demonstrate the need to further explore the effects of comminution on this ore and optimize the size reduction process for all stages of separation.

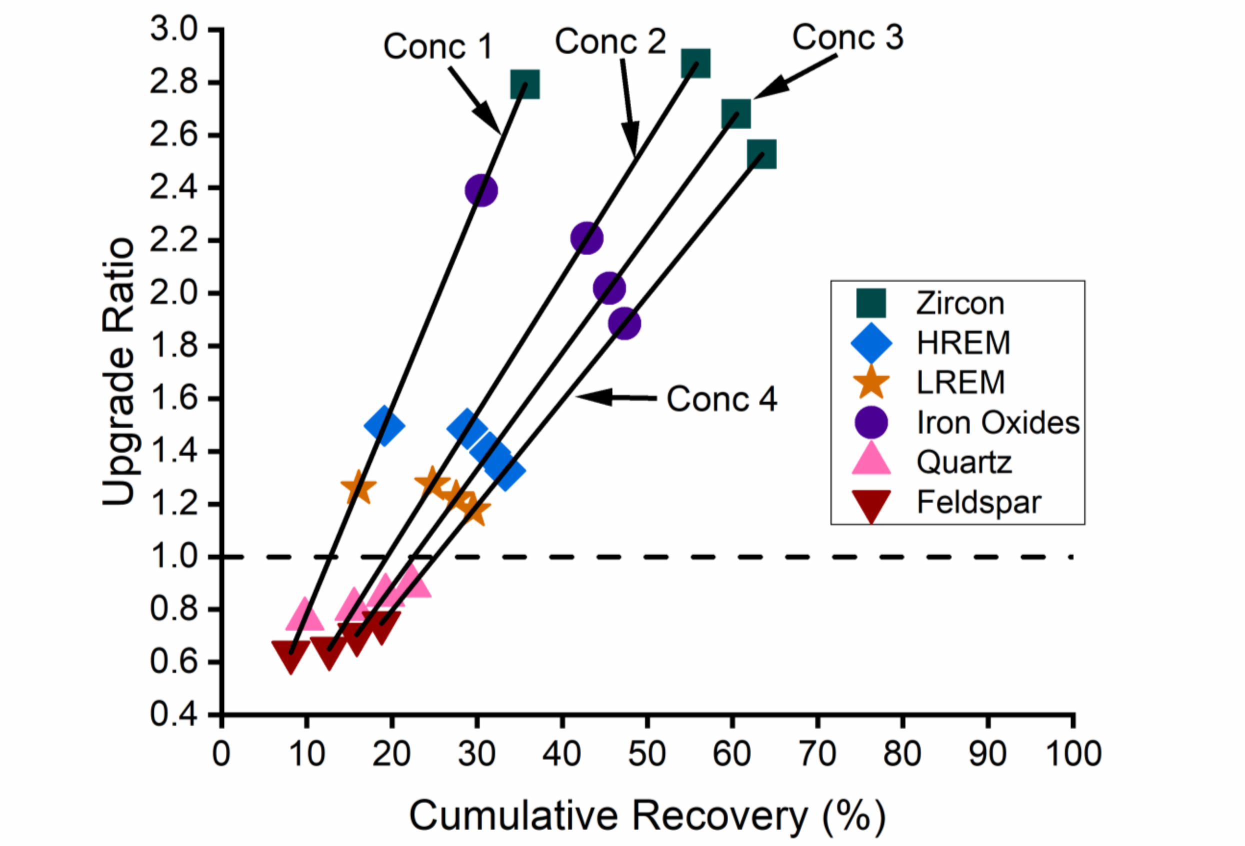

Figure 7.20 – Cumulative upgrade ratio and recovery of the major mineral classes in the Knelson concentrates produced from Feed 2

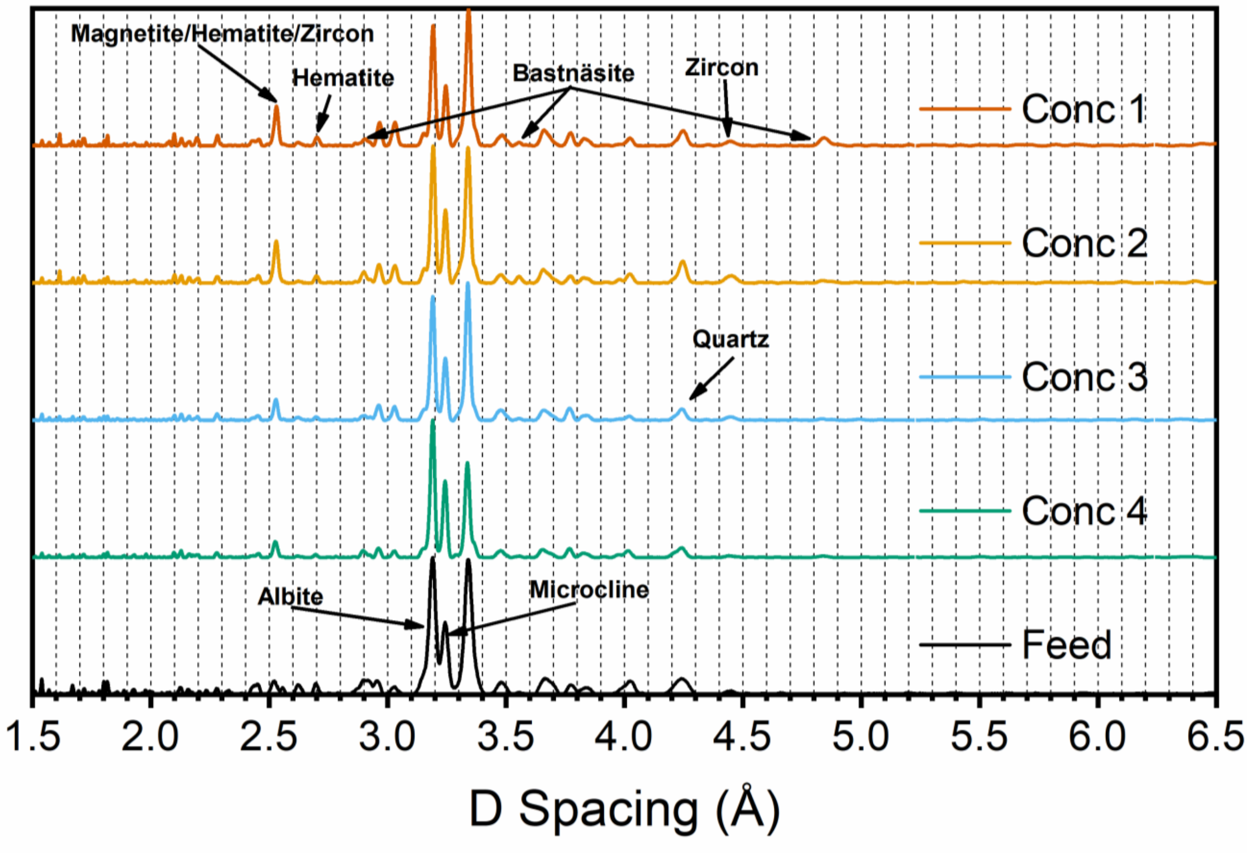

Figure 7.21 – XRD pattern of the Knelson concentrates and Feed 2.

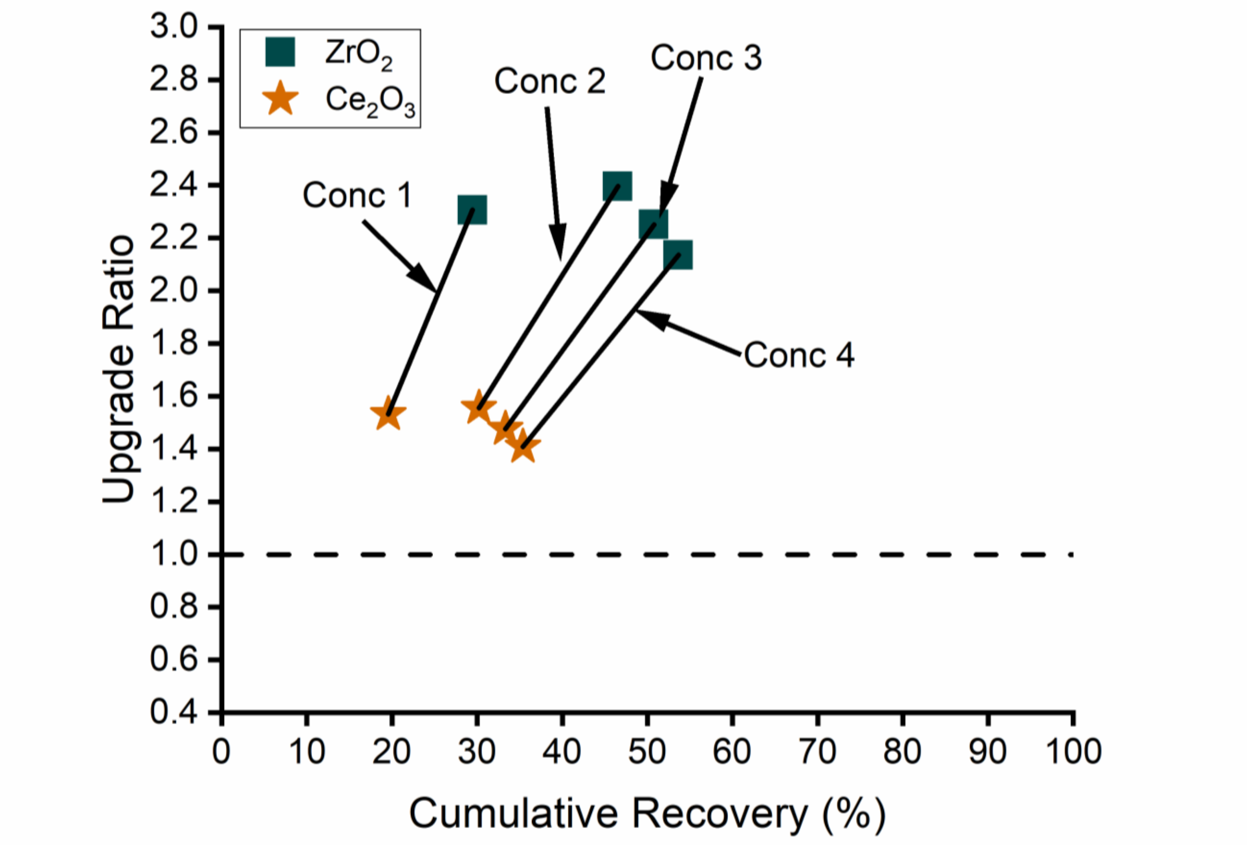

Figure 7.22 – Cumulative upgrade ratio and recovery of ZrO_2 and Ce_2O_3 in the Knelson concentrates produced from Feed 2

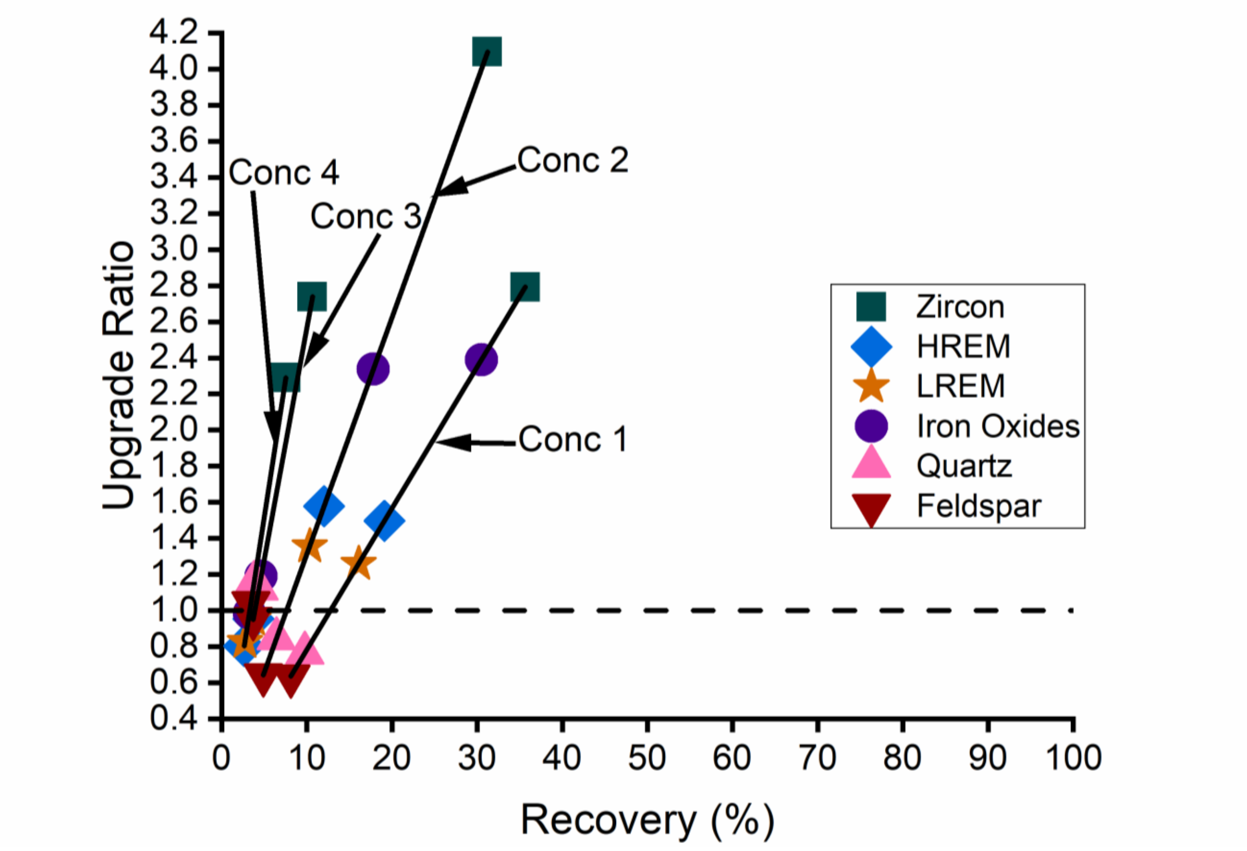

Figure 7.23 – Upgrade ratio and recovery of the major mineral classes in the Knelson concentrates produced from Feed 2, relative to the feed of each pass

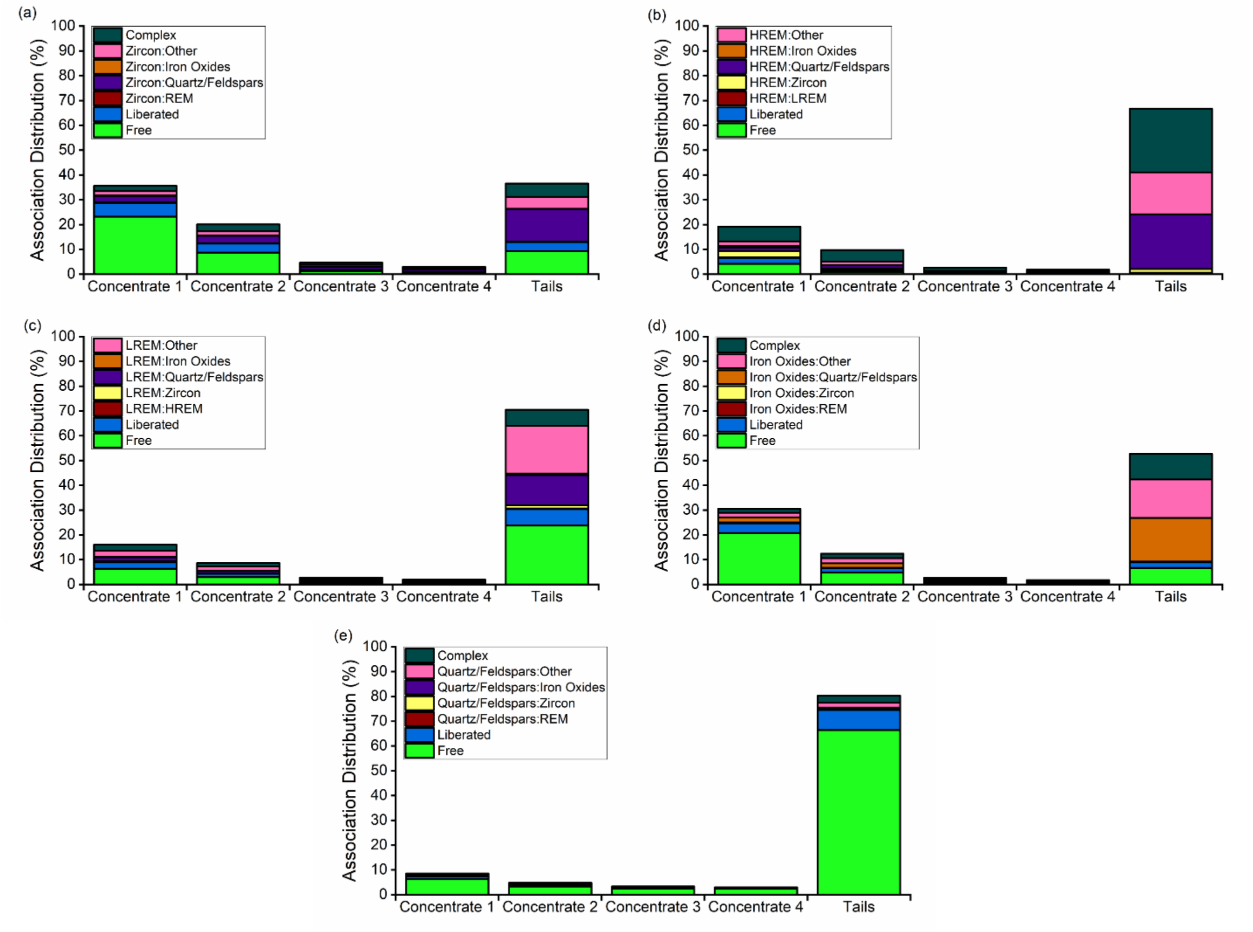

Figure 7.24 - Mineral associations of the Knelson products produced from Feed 2 for (a) zircon, (b) HREM, (c) LREM, (d) Fe oxides, (e) quartz/feldspars

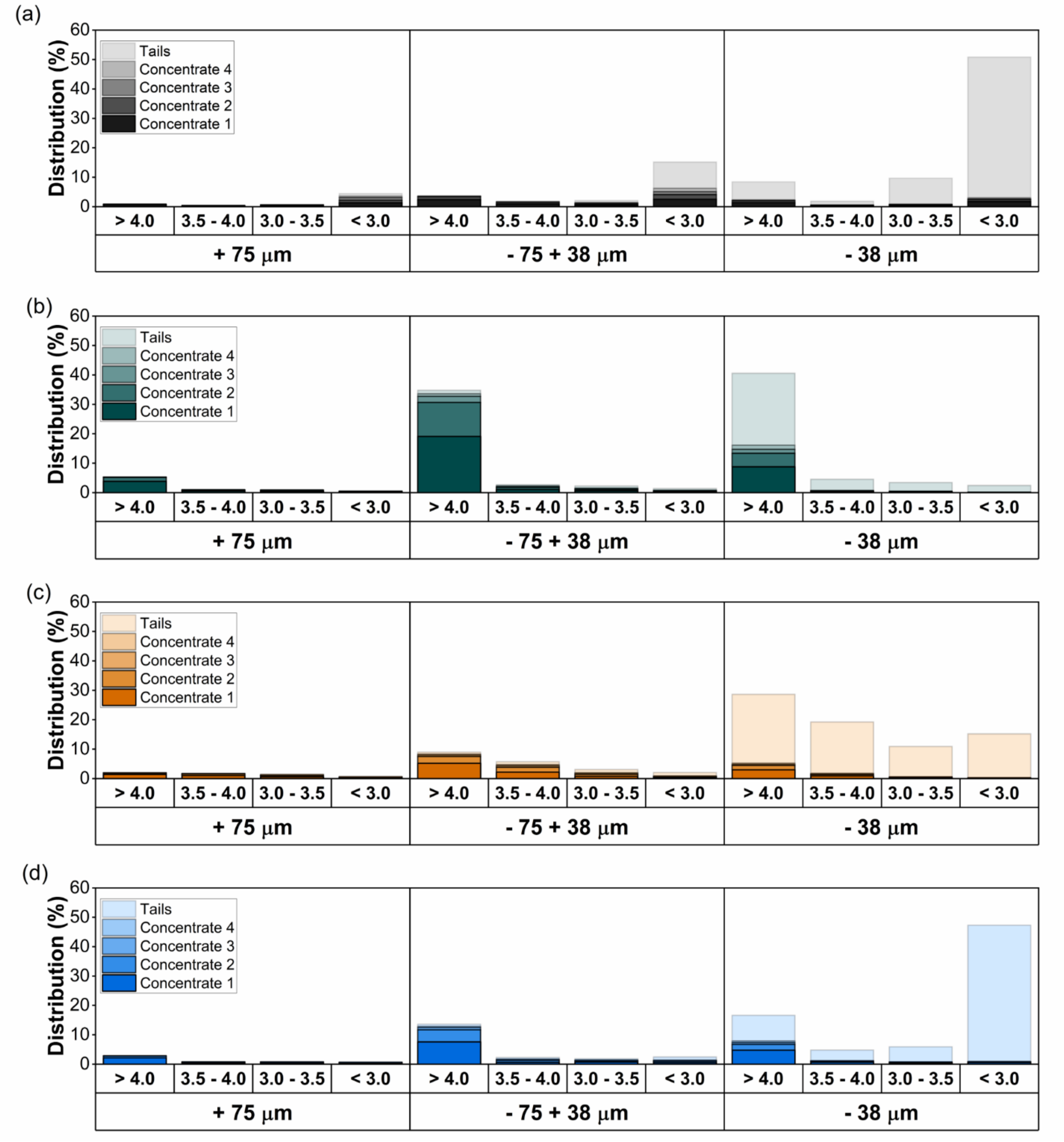

Figure 7.25 – SG distribution of (a) all particles, (b) zircon, (c) LREM and (d) HREM in the Knelson products produced from Feed 2, shown cumulatively as such that the total of all bars equates to 100 %

7.3.2 Multi-Gravity Separator

7.3.2.1 Feed 1

Figure 7.26 shows the upgrade ratio and recovery of the major mineral classes in the ore after processing the fine particle fraction of Feed 1 with an MGS under different operating conditions (drum speed, wash water rate and scrapper system). The QEMSCAN results correspond well to those obtained by XRF (Figure 2.27). The results from this initial test work demonstrate that the MGS was highly effective at upgrading the high SG minerals in the deposit. Under these conditions there is very limited recovery of low SG material. Therefore, wash water has limited impact on grade and simply reduces the recovery of high SG minerals. Comparing the results of the low-profile scrapper system (Figure 7.26c) to those of the traditional scrapper blades (Figure 7.26a and Figure 7.26b), suggests limited differences in the concentrates which can be produced, although more elevated drum speeds were required to achieve comparable recoveries (170 rpm *vs.* 162 rpm).

Examining the recovery by liberation of zircon, HREM, LREM and iron oxides using the traditional scrapper blades at a drum speed of 168 rpm and wash water rate of 2 L/min (best condition studied) (Figure 7.28) demonstrates the MGS is primarily recovering liberated material. While not depicted in Figure 7.28, increasing the wash water rate, decreasing the drum speed or changing the scrapper blade system does not change the recovery by liberation profile, but results in lower recoveries of liberated material. This is depicted in Figure 7.29 and Figure 7.30, which shows the recovery by SG of zircon and LREM, respectively, under various operating conditions. It is evident that in both the + 20 μm and - 20 μm size fractions, these changes cause a lower recovery of high SG material. The major conclusion from this work is that higher drum speeds should be investigated, to determine if greater recoveries can be obtained.

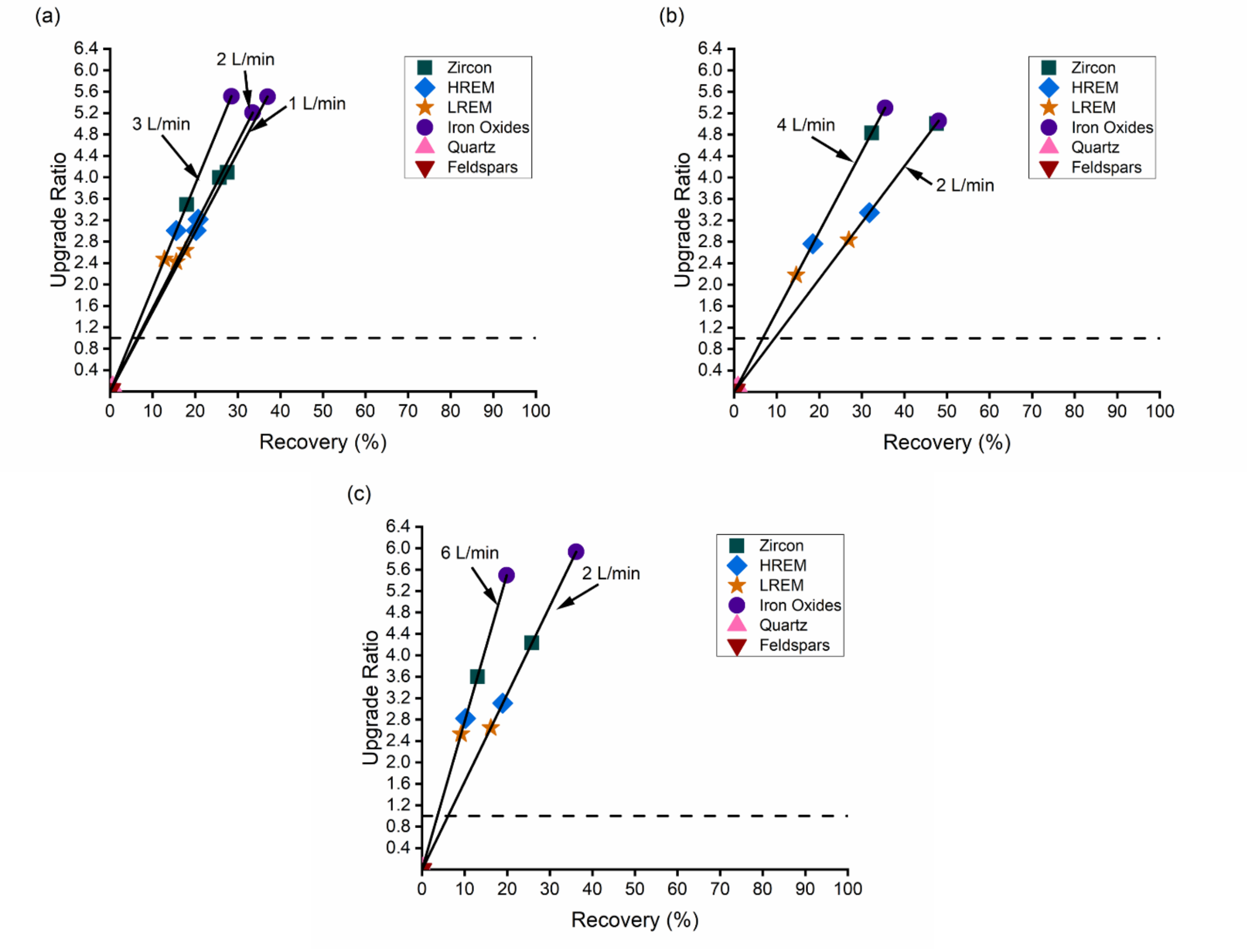

Figure 7.26 – Cumulative upgrade ratio and recovery of the major mineral classes in the MGS concentrates produced from the fine particle fraction Feed 1 with traditional scrapper blades at a drum speed of (a) 162 rpm and (b) 168 rpm, and (c) with the low-profile scrapper system at 170 rpm

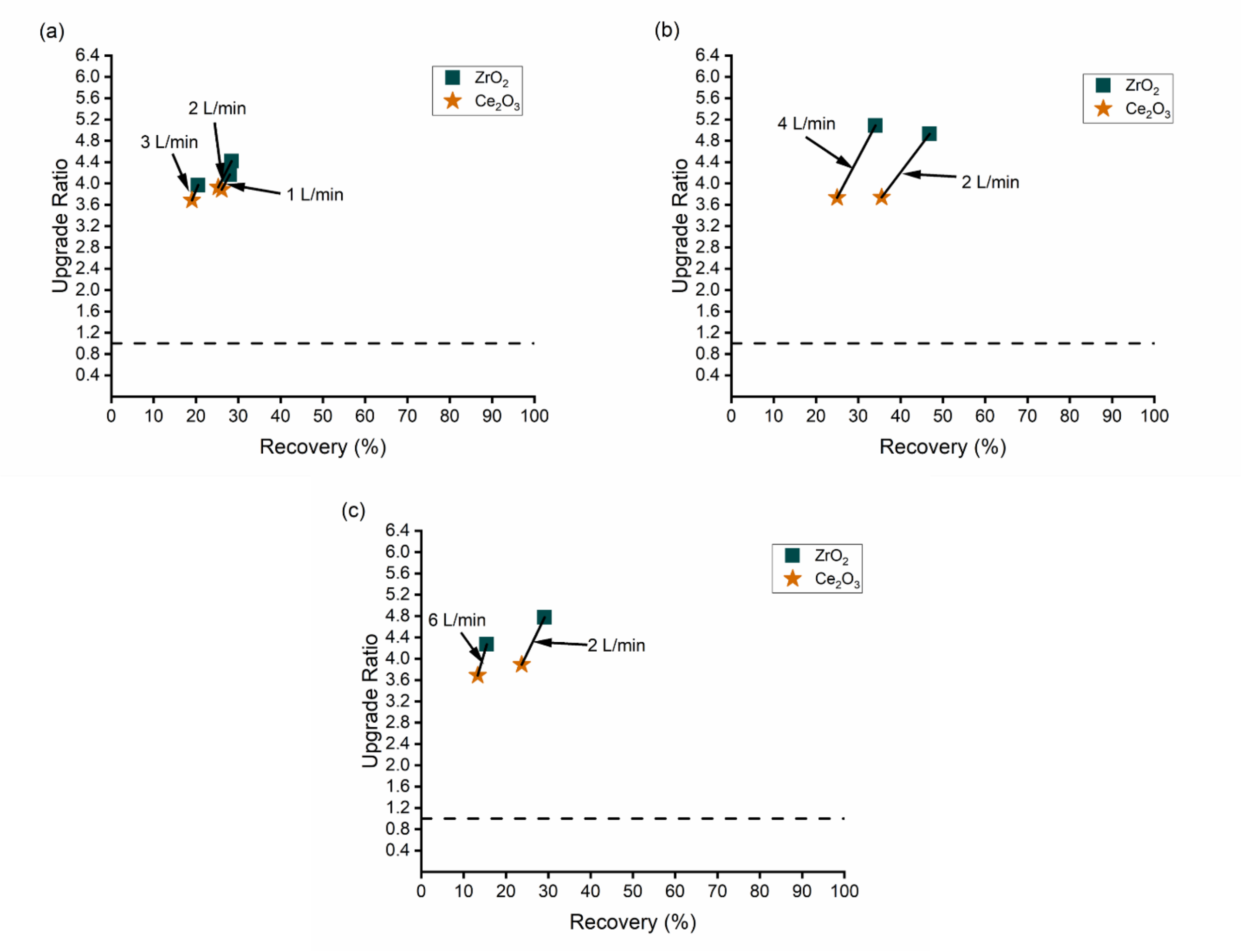

Figure 7.27 – Cumulative upgrade ratio and recovery of ZrO_2 and Ce_2O_3 in the MGS concentrates produced from the fine particle fraction Feed 1 with traditional scrapper blades at a drum speed of (a) 162 rpm and (b) 168 rpm, and (c) with the low-profile scrapper system at 170 rpm

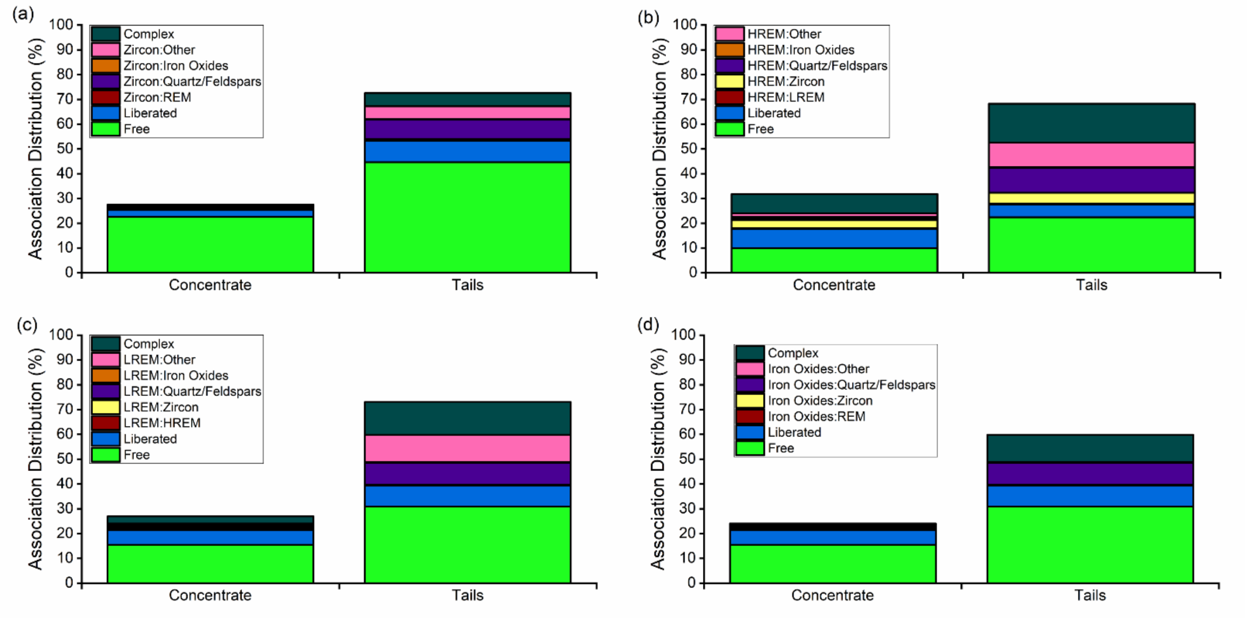

Figure 7.28 – Mineral associations of the MGS products produced from the fine particle fraction of Feed 1, operating with a drum speed of 162 rpm and wash water rate of 2 L/min for (a) zircon, (b) HREM, (c) LREM, (d) Fe oxides

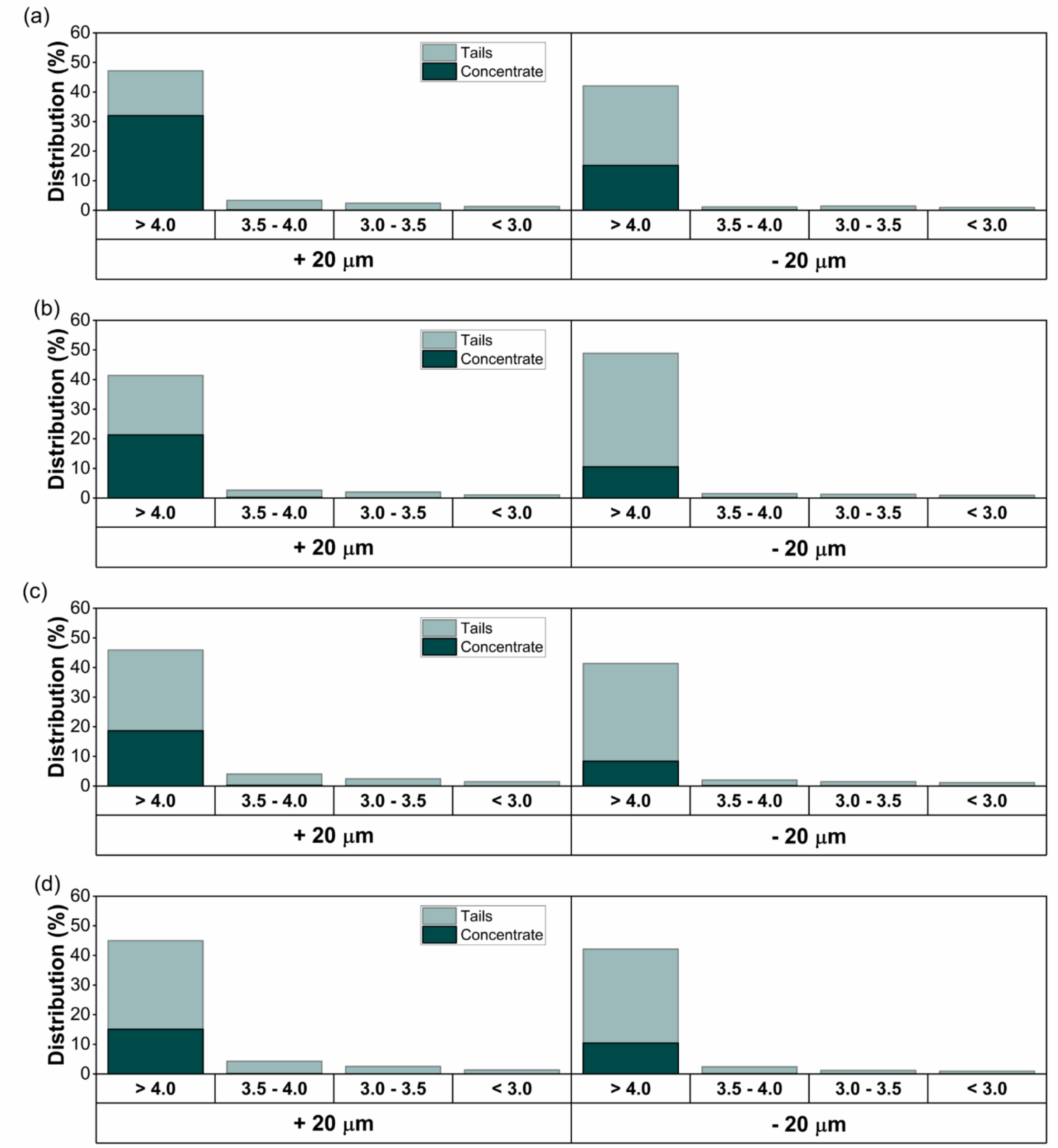

Figure 7.29 – SG distribution of zircon in the MGS concentrates produced from the fine particle fraction of Feed 1, operating with traditional scrapper blades and drum speeds and wash water rates of (a) 168 rpm and 2 L/min, (b) 168 rpm and 4 L/min, (c) 168 rpm and 4 L/min and (d) with the low-profile scrapper system at a drum speed of 170 rpm and wash water rate of 2 L/min, shown cumulatively as such that the total of all bars equates to 100 %

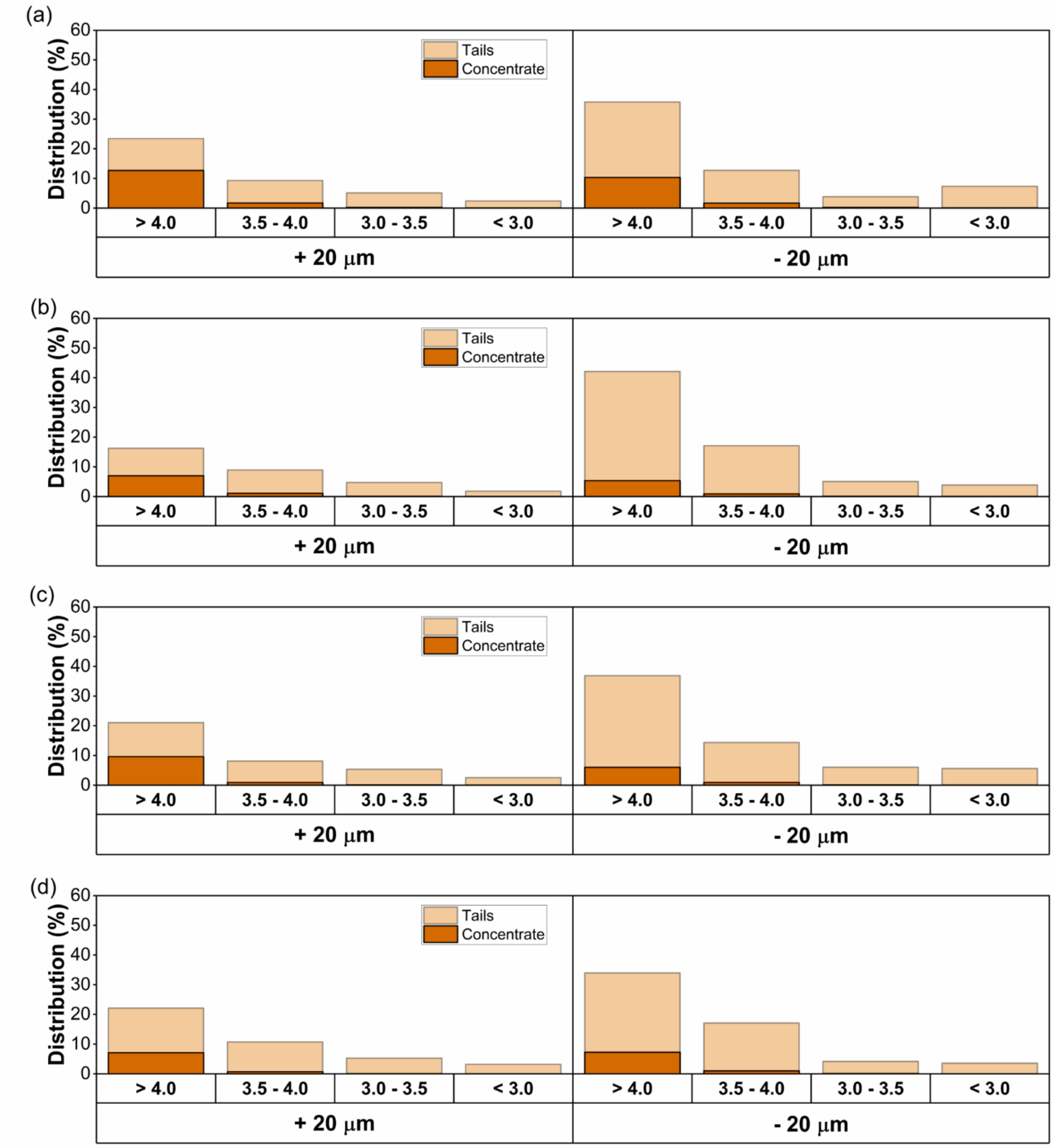

Figure 7.30 – SG distribution of LREM in the MGS concentrates produced from the fine particle fraction of Feed 1, operating with traditional scrapper blades and drum speeds and wash water rates of (a) 168 rpm and 2 L/min, (b) 168 rpm and 4 L/min, (c) 168 rpm and 4 L/min and (d) with the low-profile scrapper system at a drum speed of 170 rpm and wash water rate of 2 L/min, shown cumulatively as such that the total of all bars equates to 100 %

7.3.2.2 Feed 3

To asses the use of higher drum speeds, Feed 3 was processed with an MGS equipped with the low-profile scrapper system at a drum speed of 185 rpm. The tailings from this stage were also reprocessed twice with drum speeds of 187 rpm and 186 rpm, respectively, with the goal of these two subsequent steps to act as a scavenger stage and recover as much of the high SG material as possible. The cumulative upgrade ratio and recovery of the major mineral classes after each pass is shown in Figure 7.31. The QEMSCAN results were validated qualitatively by XRD (Figure 7.32) and quantitatively from XRF results (Figure 7.33). The results demonstrate that the use of higher drum speeds resulted in a greater recovery of high SG minerals (zircon: 63 %, HREM: 38 %, LREM 28 % and iron oxides: 51 %); with limited recovery of quartz (6 %) and feldspar (2 %). With the very low gangue recovery, the upgrade ratios are comparable to those predicted by QEMSCAN; theoretically slitting the ore at an SG of 3.5 (Chapter 6, Figure 6.5d). After three passes, zircon, HREM, LREM and iron oxide recovery increased to 85 %, 62 %, 50 % and 75 %, respectively. However, higher recovery was offset by a lower grade. The recovery of LREM is partly hindered by a poor allanite recovery (17 % after one pass; 34 % after 3), likely as a result of its lower SG. If allanite is excluded 67 % of LREM are recovered after three passes.

Examining the recovery relative to the feed of each pass through the MGS (Figure 7.34), only the first two passes are selective. From Figure 7.35, the first pass recovers primarily only liberated high SG minerals. The second recovers more binary and complex particles, along with some liberated material including liberated quartz and feldspar. The third pass is primarily recovering liberated quartz and feldspar.

Figure 7.36 shows the recovery of all particles, as well as those containing zircon, HREM and LREM by SG class and particle size. This demonstrates that the MGS is highly effective at recovering high SG material with a particle size > 20 μm. After a single pass, 78 % of the particles which have an SG > 4.0 and 75 % of those with an SG > 3.5, in the + 20 μm size class, are recovered. In the - 20 μm size fraction the recovery of material with an SG > 4.0 was only 30 %. The second pass recovered most of the remaining high SG material in the + 20 μm class and some additional (14 %) SG > 4.0 material in the - 20 µm size class. However, this pass also recovered a significant quantity of low SG (< 3.0) particles of size > 20 µm. These particles accounted for 53 % of the concentrate mass. The third pass recovered more low SG coarse particles which accounted for 70 % of the third concentrate.

These initial findings suggest that the MGS can be a highly effective method of separation for the Nechalacho deposit. However, for this to be the case the recovery of fine high SG material and the SG of REM-bearing particles, particularly < 20 µm, must be significantly improved. The recovery of fine material could be improved simply through the optimization of MGS operating conditions. However, processing the coarse and fine material separately may be more successful. As was already suggested in Chapter 6, one method of improving the SG distributions (liberation) of REM is by using a ball mill rather than a rod mill. However, even with improved liberation it is noted that allanite losses may be significant.

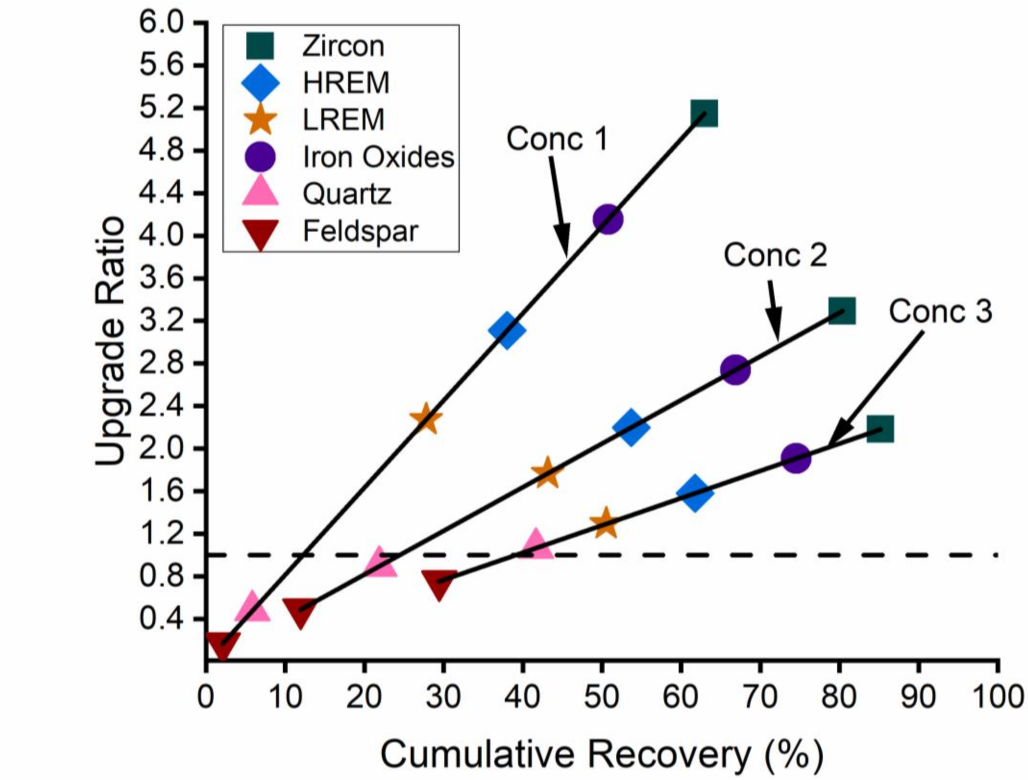

Figure 7.31 – Cumulative upgrade ratio and recovery of the major mineral classes in the MGS concentrates produced from Feed 3

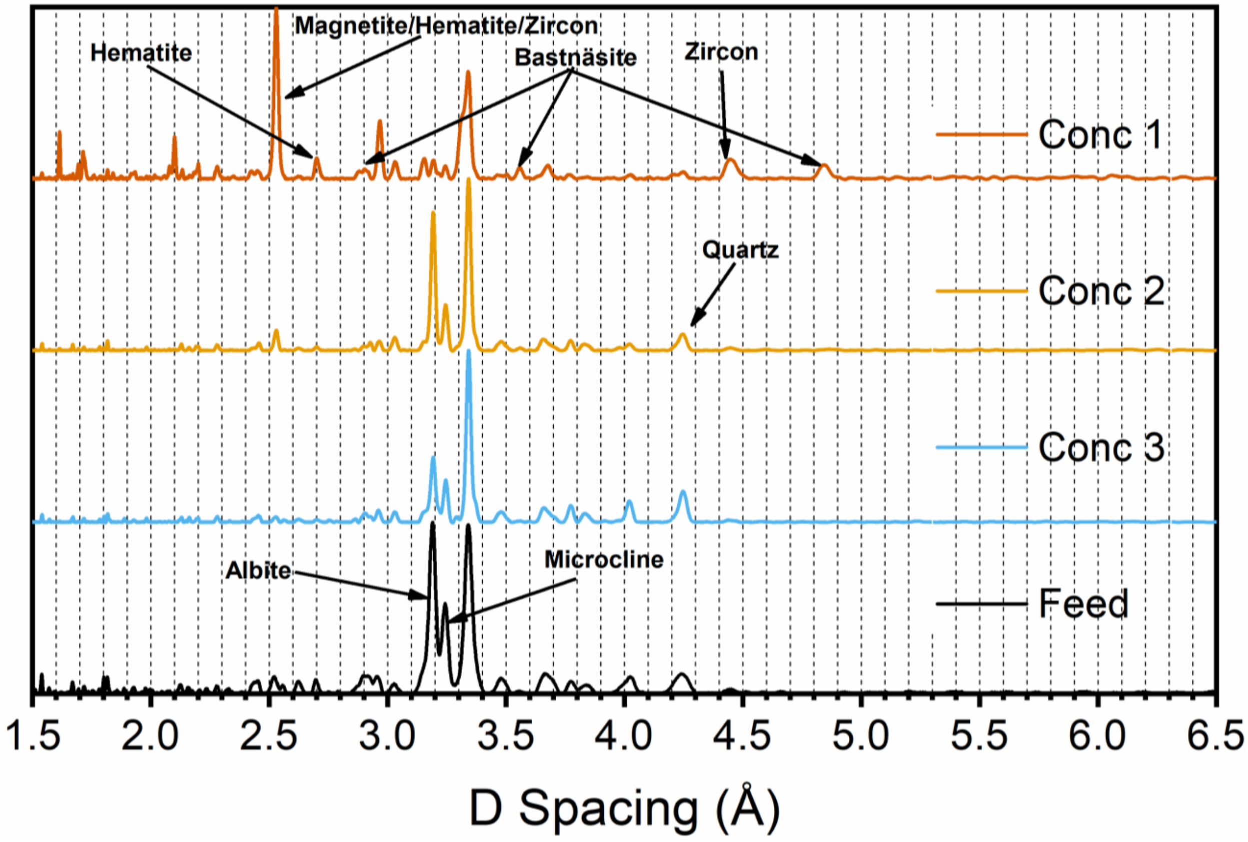

Figure 7.32 – XRD pattern of the MGS concentrates and Feed 3

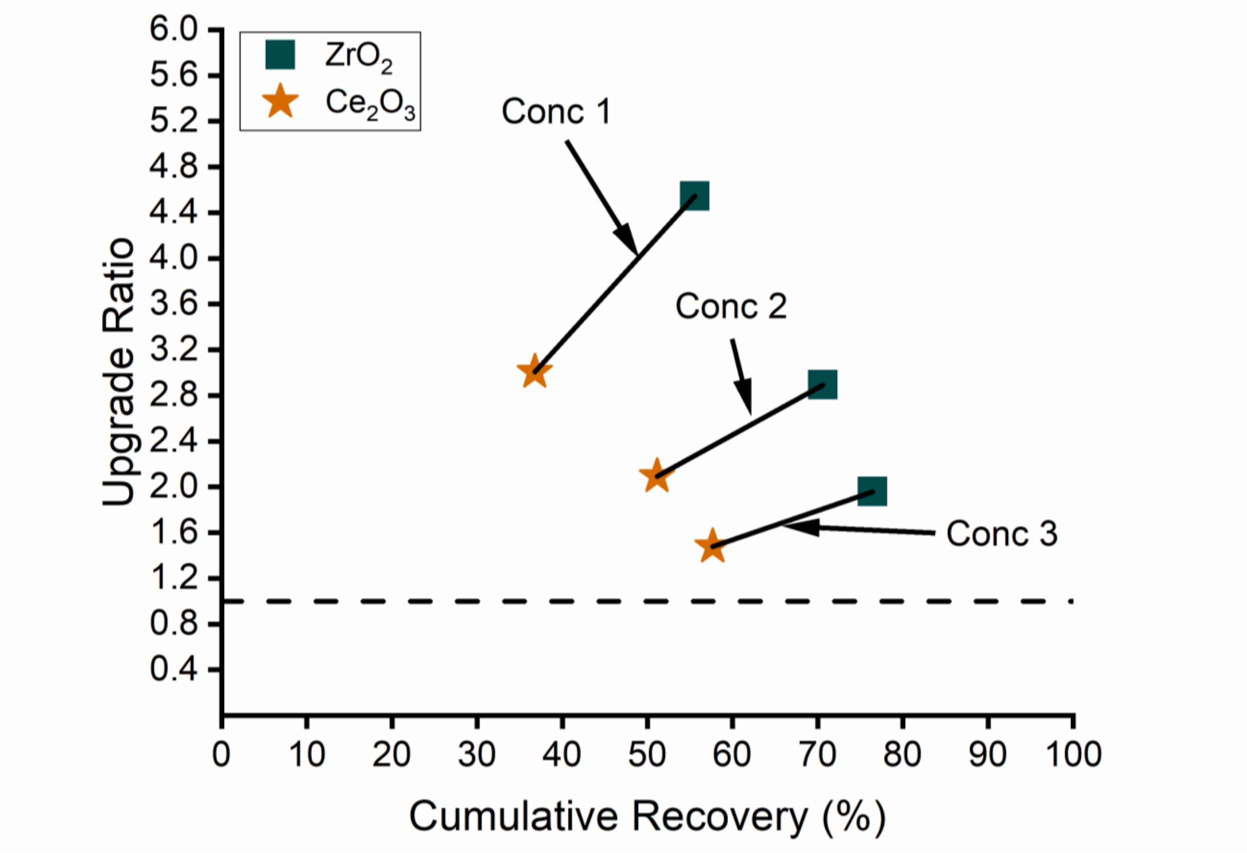

Figure 7.33 – Cumulative upgrade ratio and recovery of ZrO_2 and Ce_2O_3 in the MGS concentrates produced from Feed 3

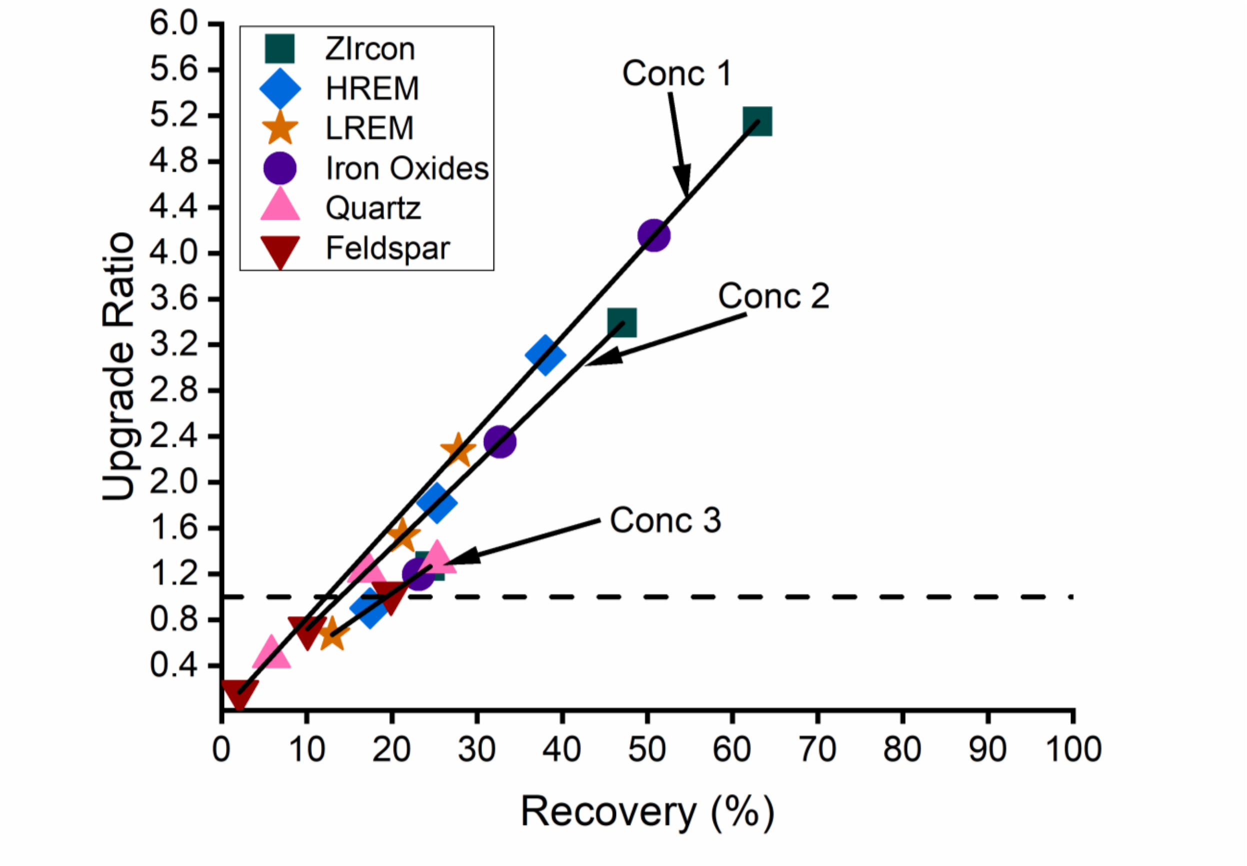

Figure 7.34 – Upgrade ratio and recovery of the major mineral classes in the MGS concentrates produced from Feed 3, relative to the feed of each pass

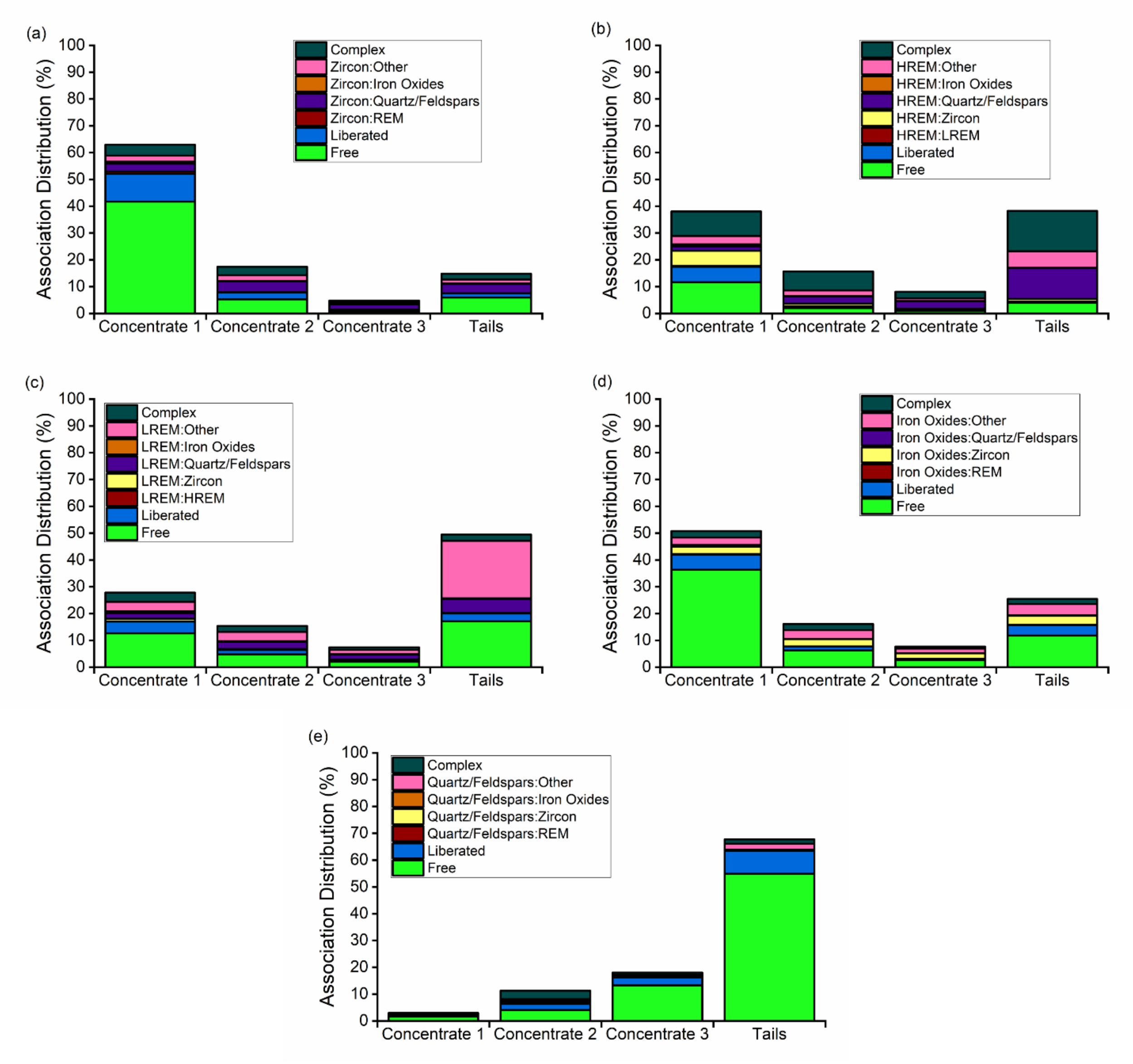

Figure 7.35 - Mineral associations of the MGS products produced from Feed 3 for (a) zircon, (b) HREM, (c) LREM, (d) Fe oxides, (e) quartz/feldspars

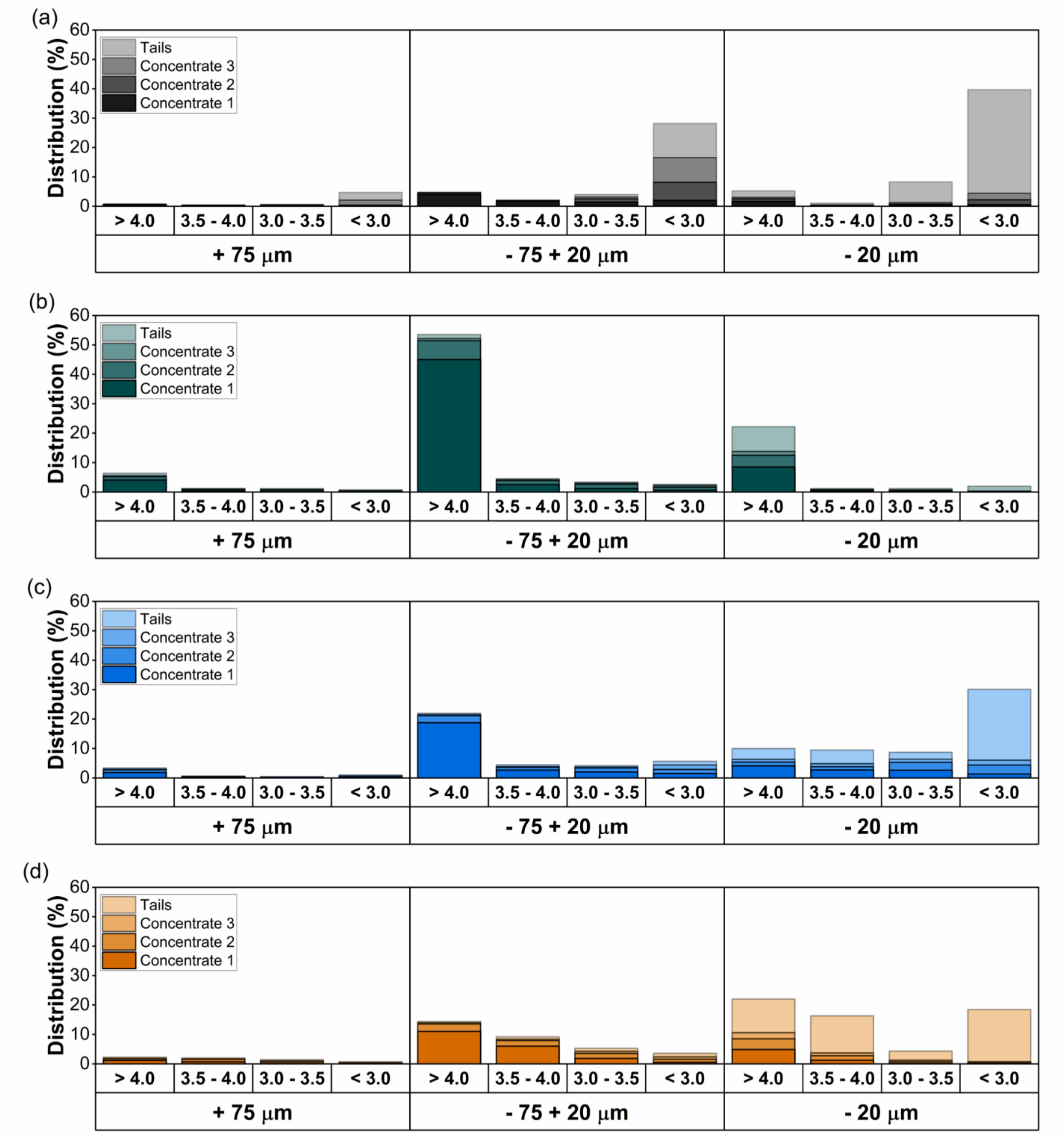

Figure 7.36 – SG distribution of (a) all particles, (b) zircon, (c) HREM and (d) LREM in the MGS products produced from Feed 3, shown cumulatively as such that the total of all bars equates to 100 %

7.3.3 Mozley Laboratory Shaking Table

7.3.3.1 Feed 4

To asses a multi-stage process involving preconcentration at coarse particle size, re-grinding and then a primary gravity separation stage, the spiral concentrate produced from the coarse particle fraction of Feed 4 was re-ground to - 53 µm, combined with the fine particle fraction which was removed prior to spiral concentration and processed using a Mozley Laboratory Separator Table (Chapter 5, Figure 5.4). Although the Mozley Laboratory Separator Table is a laboratory device (does not directly represent an industrial shaking table) and is likely to be much less efficient when compared to a MGS, especially at particle sizes < 20 µm (Traore *et al.*, 1995), it was used as there was insufficient mass available (< 10 kg) to process the material using a MGS. While a MGS is likely to offer superior results and is likely better suited in this flowsheet; it is noted that, industrially, shaking tables are much more commonly employed and have been used in various flowsheets developed for three of the largest REE mines in China: the Bayan Obo deposit, the Maoniuping deposit and the Weishan deposit (Chi *et al.*, 2001; Gupta and Krishnamurthy, 2005; Houot *et al.*, 1991; Jordens *et al.*, 2013; Ling and Yang, 2014; Luo and Chen, 1987).

The upgrade ratio and recovery of the major mineral classes relative to the feed to the shaking table (after spiral concentration) and relative to the initial feed (before spiral concentration) are shown in Figure 7.36. The corresponding ZrO_2 and Ce_2O_3 upgrade ratio and recovery is shown in Figure 7.37. The results indicate that the table is effective at recovering and upgrading high SG minerals. From Figure 7.38, it is suggested that the relatively low recovery of LREM and HREM is again hindered by their association with low SG minerals in fine particles. As has been previously discussed this could be improved by using a ball mill in lieu of a rod mill. Overall compared with the MGS recoveries are improved, however grades are much lower. This is a result of the reduced selectivity at coarse (> 20 µm) particle size, as well as a greater proportion of valuable minerals being present in (high SG) particles of size > 20 µm from stage grinding.

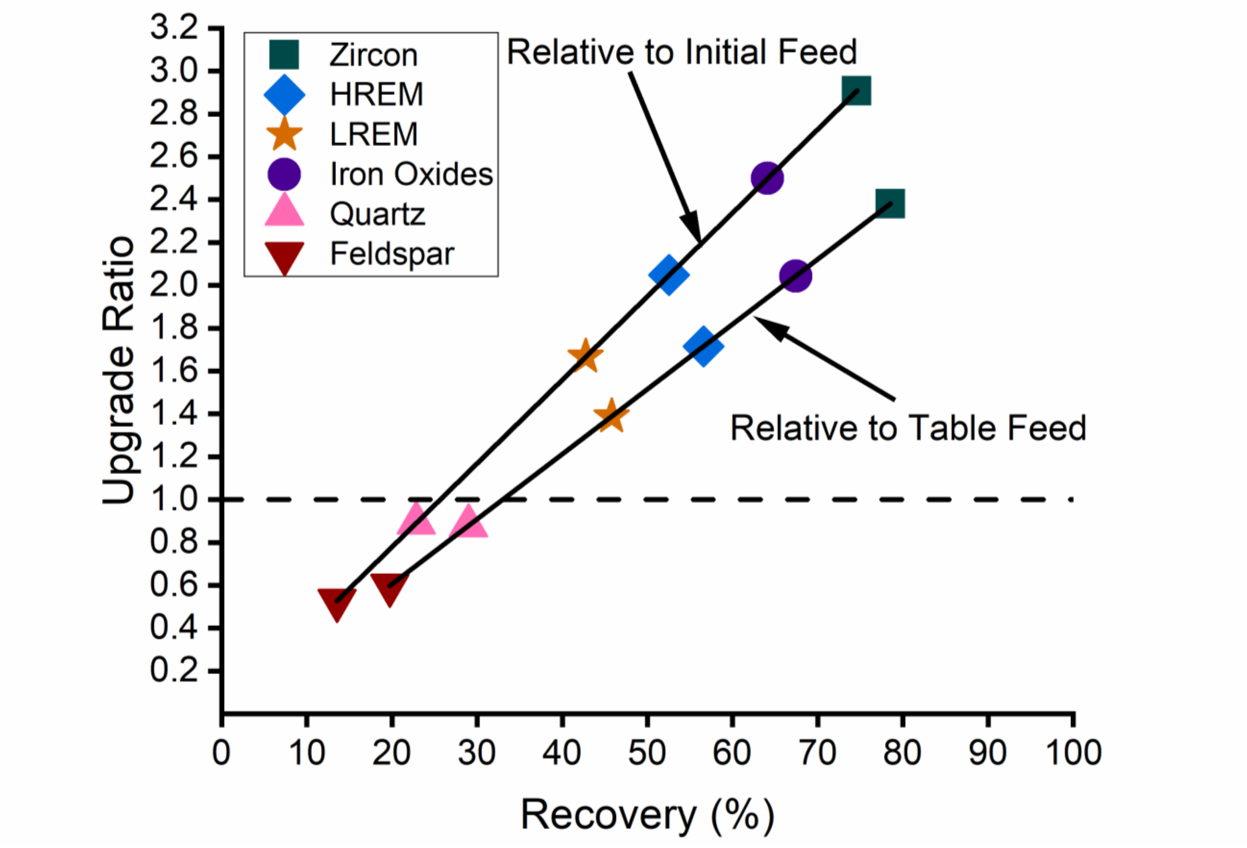

Figure 7.37 – Upgrade ratio and recovery of the major minerals classes in the table concentrate produced from Feed 4, relative to the table feed and the initial feed

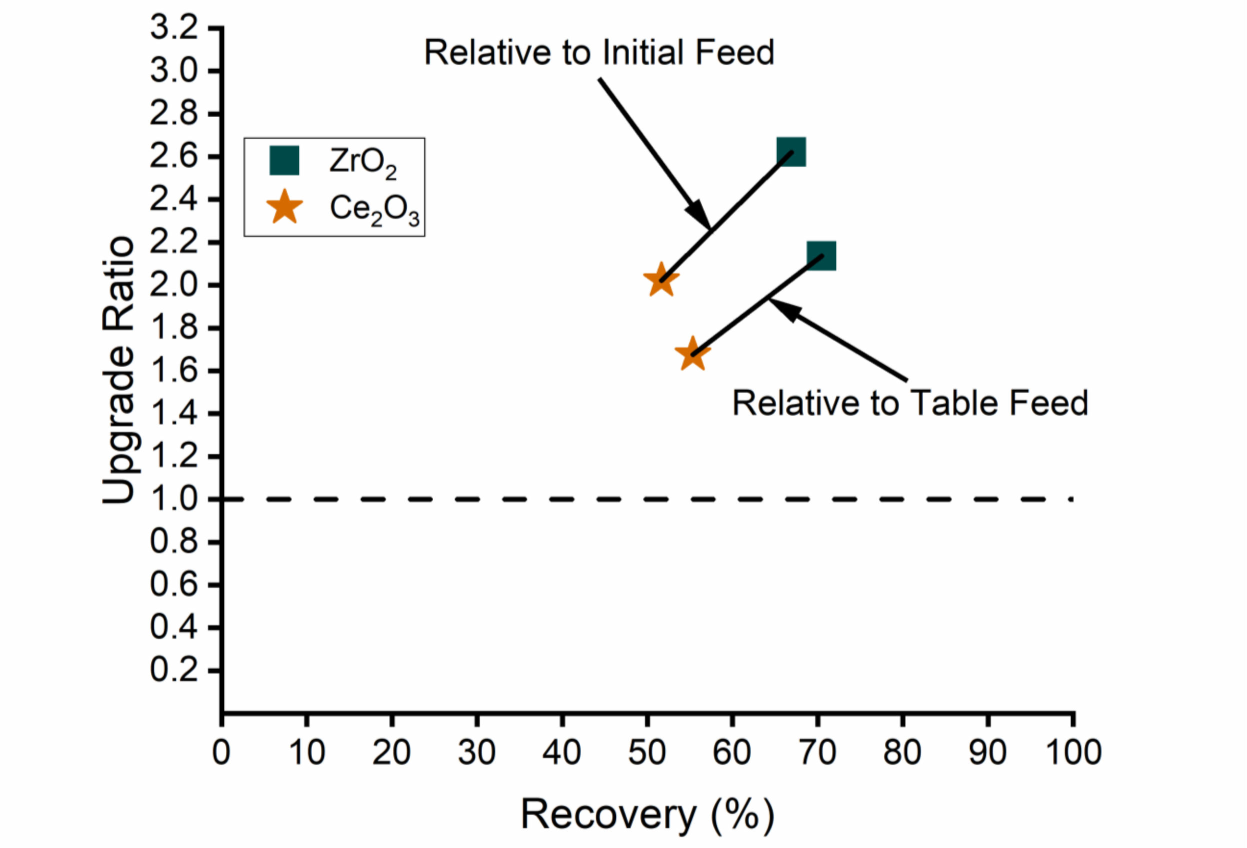

Figure 7.38 – Upgrade ratio and recovery of ZrO_2 and Ce_2O_3 in the table concentrate produced from Feed 4, relative to the table feed and the initial feed

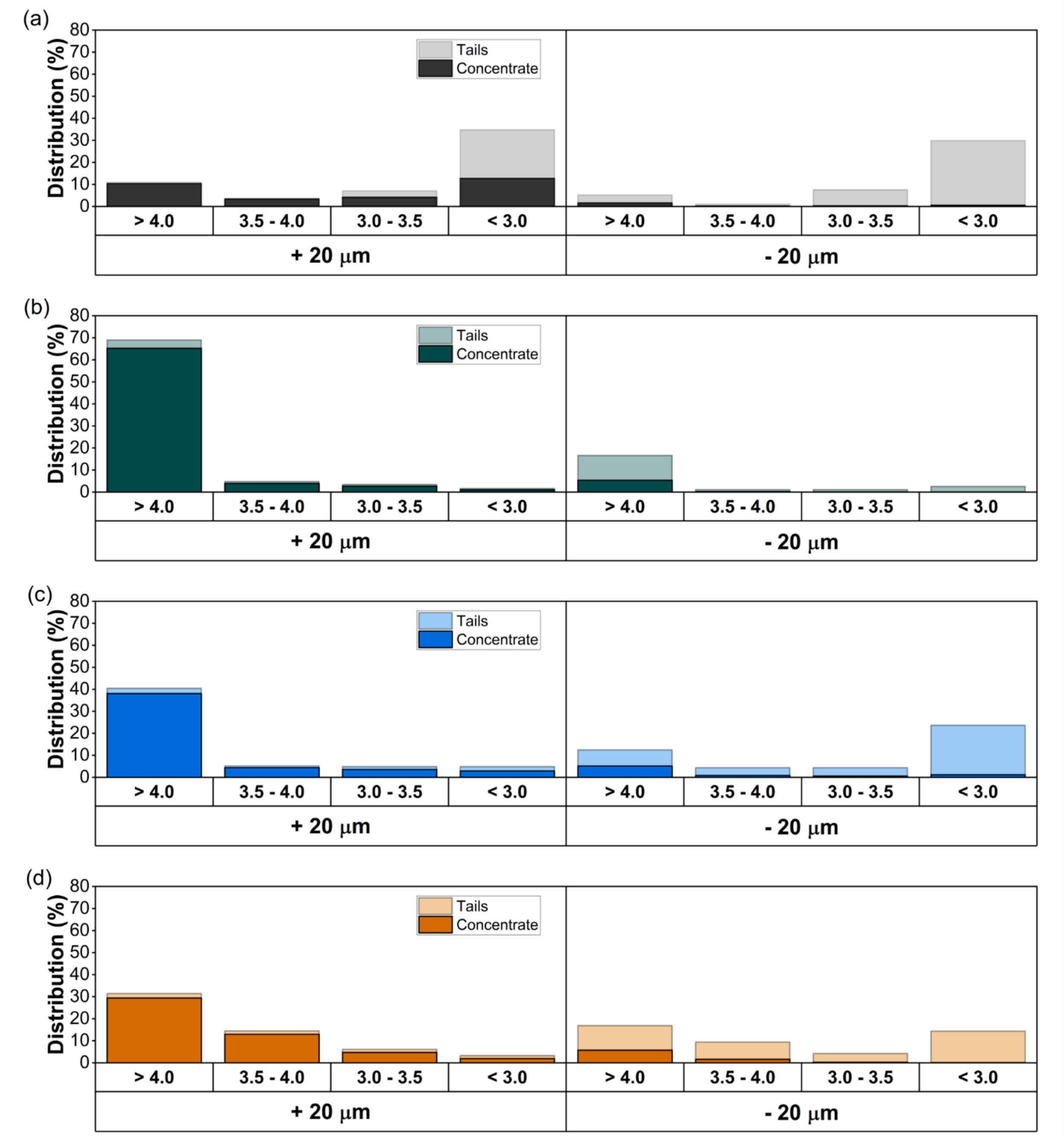

Figure 7.39 – SG distribution of (a) all particles, (b) zircon, (c) HREM and (d) LREM in the table products produced from Feed 4, shown cumulatively as such that the total of all bars equates to 100 %

7.4 Conclusions

This chapter assessed various gravity separation techniques as a preconcentration and primary separation stage for the beneficiation of the Nechalacho ore. The general conclusions of this chapter are:

1. Gravity modeling using QEMSCAN can be used to confidently predict grade and recovery values by SG for DMS.
2. The liberation and association behaviour of the ore following grinding allows for a gravity preconcentration step at relatively coarse particle sizes to be effective. With proper optimization, such a step could result in significant gangue rejection early in the process.
3. Both the Knelson Concentrator and spiral are effective preconcentration steps, but, the simplicity and effectiveness of the spiral makes it a more applicable process in an industrial setting.
4. The Knelson Concentrator, MGS and Mozley Laboratory Separator Table were all capable of producing a high-grade concentrate. They were particularly effective at particle sizes > 20 μm.
5. As the MGS could produce near ideal separation it offers the greatest potential moving forward, however, its ability to recover fine (< 20 μm) high SG material should be addressed
6. When equipped with the low-profile scrapper system the MGS required high drum speeds to produce a similar concentrate to that obtained with the traditional scrapper blades.
7. Optimization of the comminution process for a preconcentration step using spirals and a primary separation stage with an MGS is imperative to achieving acceptable zircon and REM recoveries.

Chapter 8

Magnetic Separation

8.1 Introduction

This chapter details magnetic separation experiments applied to the first MGS concentrate and the shaking table concentrate produced from Feed 3 and Feed 4, respectively. Readers are referred to Chapter 5 for information regarding the operating conditions of magnetic separation devices and the preparation of the feed; and Chapter 7 for the characteristics of the gravity concentrates. The goal of the work detailed in this Chapter is to asses the behaviour of the major minerals in low- and high-intensity magnetic fields. A laboratory wet magnetic test chute was employed as a LIMS (0.04 T) and a WHIMS was used to test the impact of a higher magnetic intensities [1.8 T (Feed 3) and 1.4 T (Feed 4)]. The products of each separation stage were analyzed by QEMSCAN and XRF.

8.2 Laboratory Wet Magnetic Test Chute

The upgrade ratio and recovery of the major mineral classes in the products of the laboratory wet magnetic test chute performed on the MGS concentrate (Feed 3) are shown in Figure 8.1; with elemental (ZrO_2, Ce_2O_3 and Fe_2O_3) upgrade ratio and recovery values determined by XRF shown in Figure 8.2. Similar plots detailing the results of test work on the table concentrate (Feed 4) are provided in Figure 8.3 and Figure 8.4. The results are presented relative to the feed to the LIMS (the gravity concentrate) as well as relative to the overall feed sample prior to gravity separation. Both concentrates respond similarly to the LIMS step, which effectively removed iron oxides (80 % recovery); leaving approximately 80 % of REM and zircon in the non-magnetic fraction. Mineral recovery and upgrading relative to the initial feeds are a direct result of the effectiveness of the preceding gravity separation stage. The non-magnetic fraction of the MGS achieved significantly higher grades than that of the table, with slightly lower recoveries.

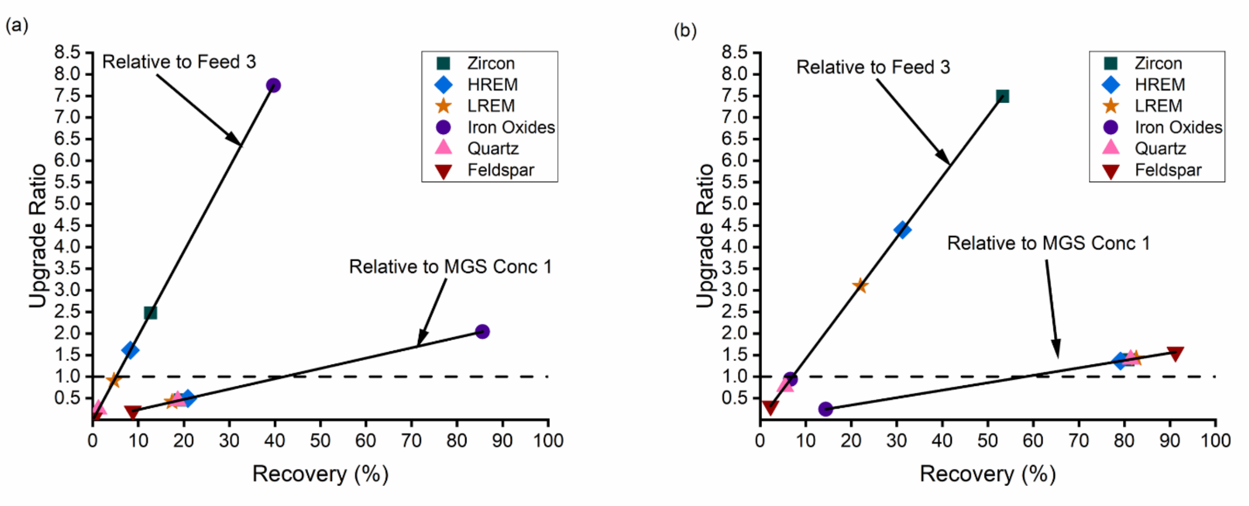

Figure 8.1 – Upgrade ratio and recovery of the major mineral classes in the (a) magnetic fraction and (b) non-magnetic fraction following LIMS of the first MGS concentrate (Feed 3). Results are presented relative to the MGS concentrate and the initial feed sample

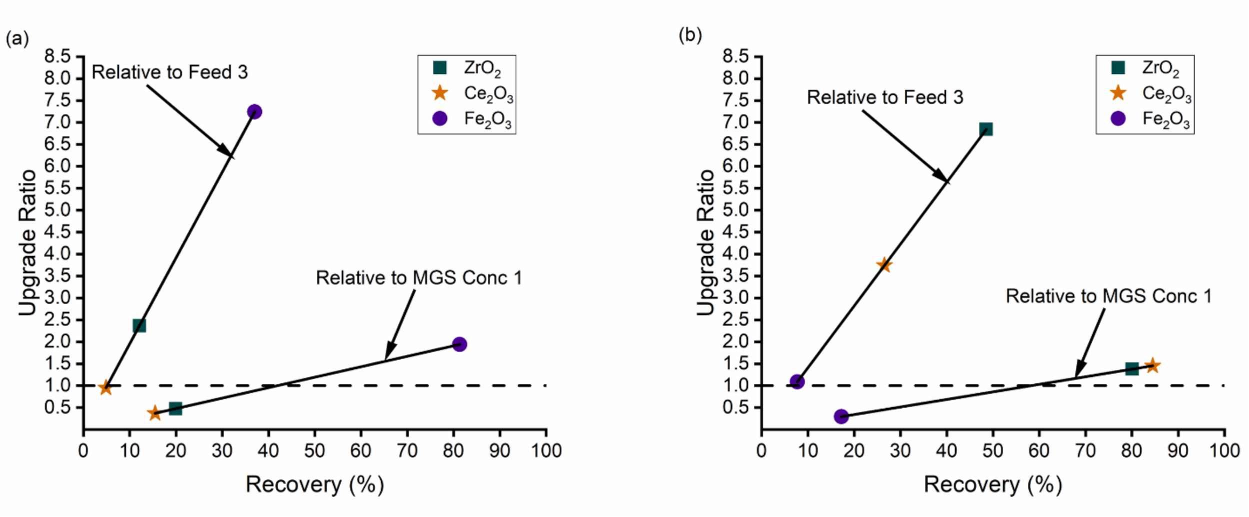

Figure 8.2 – Upgrade ratio and recovery of ZrO_2, Ce_2O_3 and Fe_2O_3 in the (a) magnetic fraction and (b) non-magnetic fraction following LIMS of the first MGS concentrate (Feed 3). Results are presented relative to the MGS concentrate and the initial feed sample

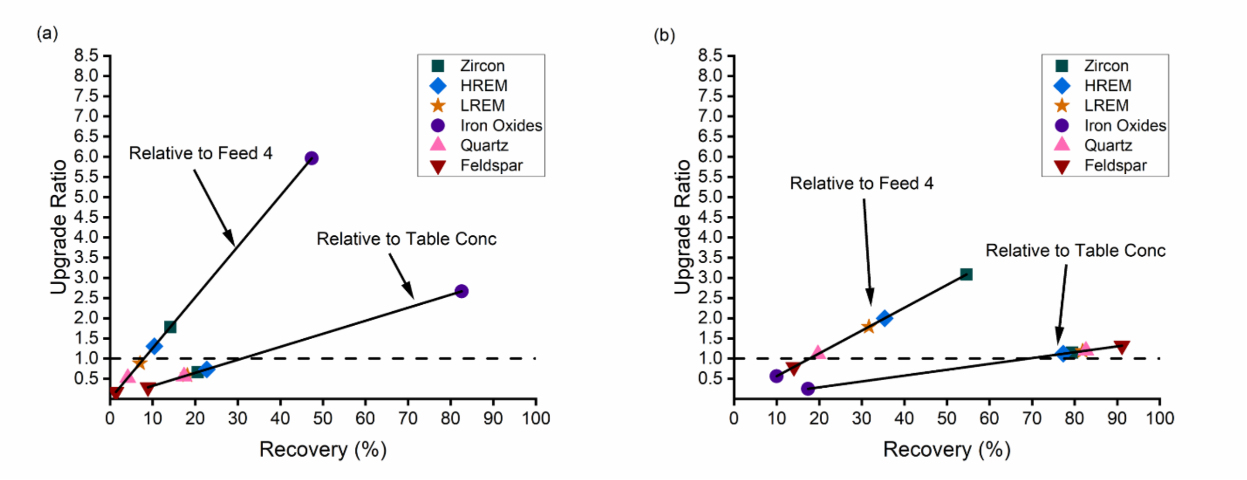

Figure 8.3 – Upgrade ratio and recovery of the major mineral classes in the (a) magnetic fraction and (b) non-magnetic fraction following LIMS of the table concentrate (Feed 4). Results are presented relative to the table concentrate and the initial feed sample

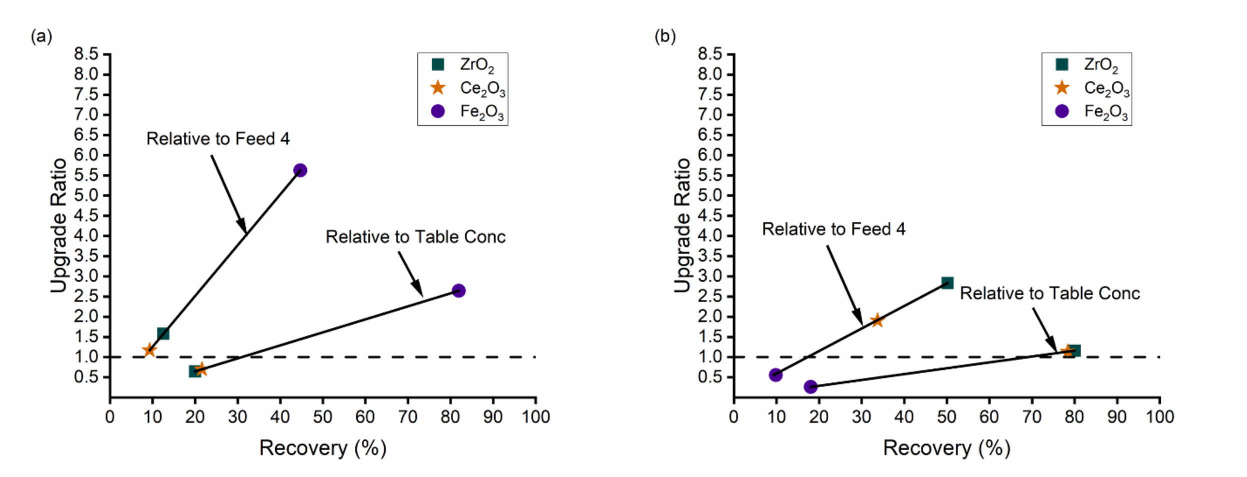

Figure 8.4 – Upgrade ratio and recovery of ZrO_2, Ce_2O_3 and Fe_2O_3 in the (a) magnetic fraction and (b) non-magnetic fraction following LIMS of the table concentrate (Feed 3). Results are presented relative to the MGS concentrate and the initial feed sample

Although the LIMS step is effective at removing iron oxides from the gravity concentrate, losses of zircon and REM to this stream are significant (20 %). These minerals are paramagnetic or diamagnetic (Chapter 4, Section 4.3.1), therefore, they are not expected to report to the magnetic fraction following LIMS. As such it is likely they are recovered as a result of being entrapped by magnetic material (iron oxides) or due to their mineral association with highly magnetic material.

The liberation and association distribution of minerals in the magnetic and non-magnetic fractions are given in Figure 8.5 and Figure 8.6. The results indicate that most the valuable mineral-bearing particles (particularly zircon) in the magnetic fraction are free. As such, one would suspect this material is recovered by entrapment. However, the QEMSCAN definition of a free particle is that > 95 % of the particle surface area is a single mineral. Using SEM-EDS, to take a closer look at these particles it was determined that many of the valuable mineral-bearing particles, which would be classified as free or liberated by QEMSCAN, are associated with minor amounts of iron (Figure 8.7). This minor association with highly magnetic (ferromagnetic) material likely results in the particles having sufficient attraction to the magnetic field, causing them to be recovered. Therefore, without any further breakage, to free this material from iron oxides, these losses may be unavoidable.

As an alternative to the upgrade ratio and recovery plots given in Figure 8.1 and Figure 8.3, the grade and recovery (relative to the initial feeds) of the non-magnetic fractions is given in Figure 8.8. It is evident that a flowsheet employing gravity and magnetic separation can produce a high-grade concentrate (grade of valuable material in the non-magnetic fraction of the MGS concentrate is 50 %). However, in this case recoveries (particularly of REM) are quite low. The low recoveries are a direct result of the lack of optimization carried out in this research program. The results of Chapter 6 indicate that with proper optimization of the comminution circuit and gravity separation stages (both preconcentration using a spiral and primary separation using a MGS), a high grade product with adequate recoveries is achievable. Future work should be focussed on directly assessing this conclusion.

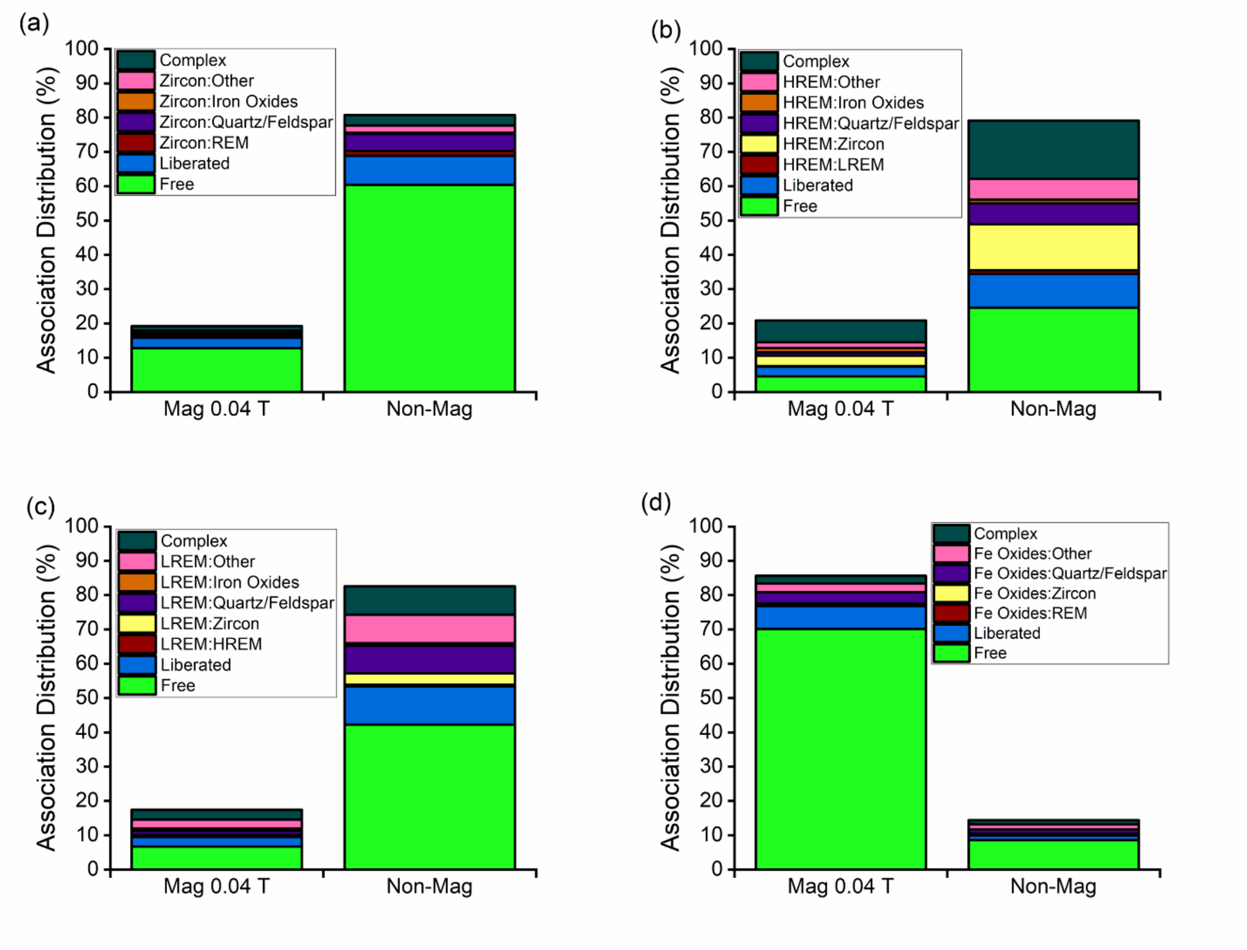

Figure 8.5 – Mineral associations of the magnetic and non-magnetic fractions produced from the LIMS step on the MGS concentrate (Feed 3) for (a) zircon, (b) HREM, (c) LREM and (d) iron oxides

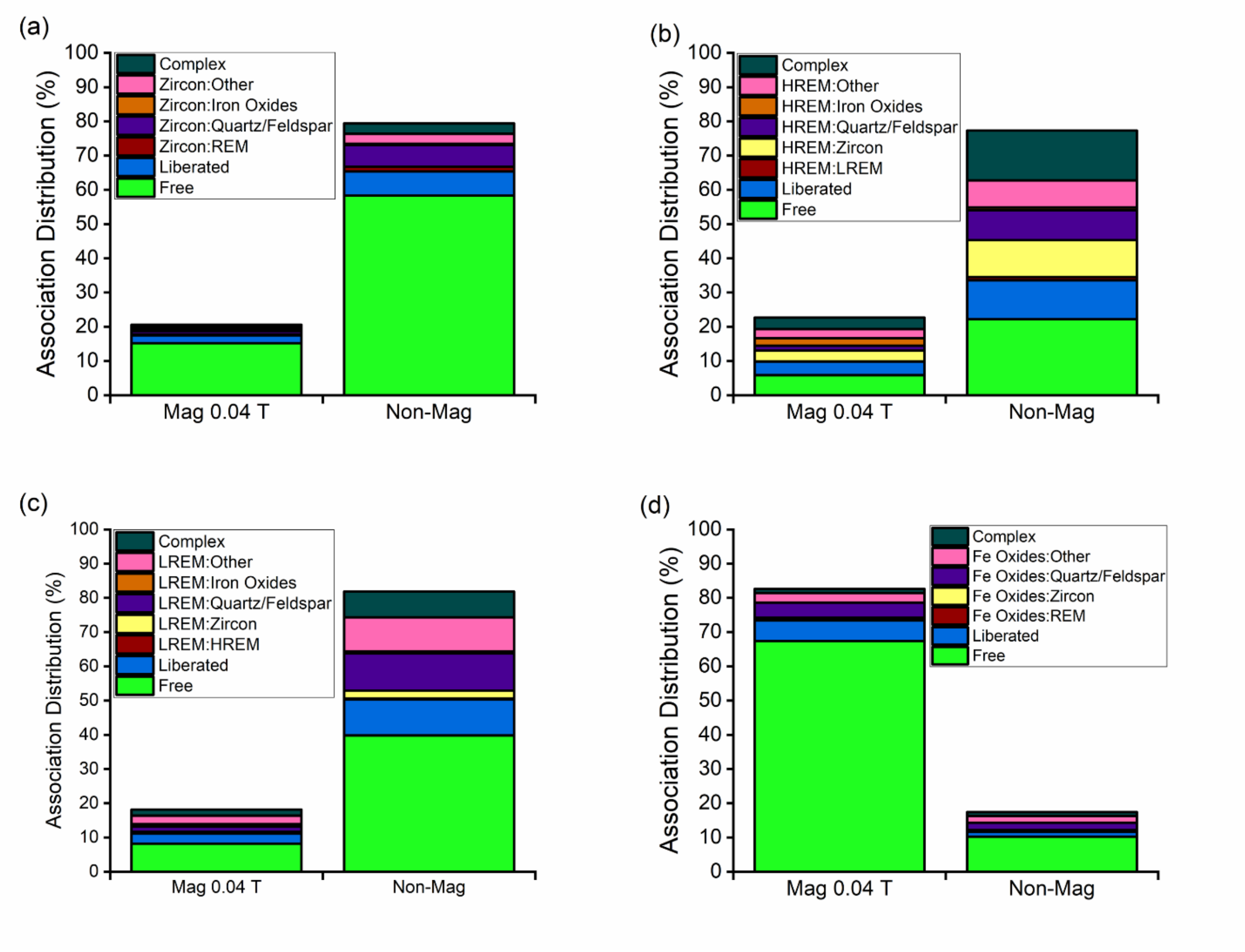

Figure 8.6 – Mineral associations of the magnetic and non-magnetic fractions produced from the LIMS step on the table concentrate (Feed 4) for (a) zircon, (b) HREM, (c) LREM and (d) iron oxides

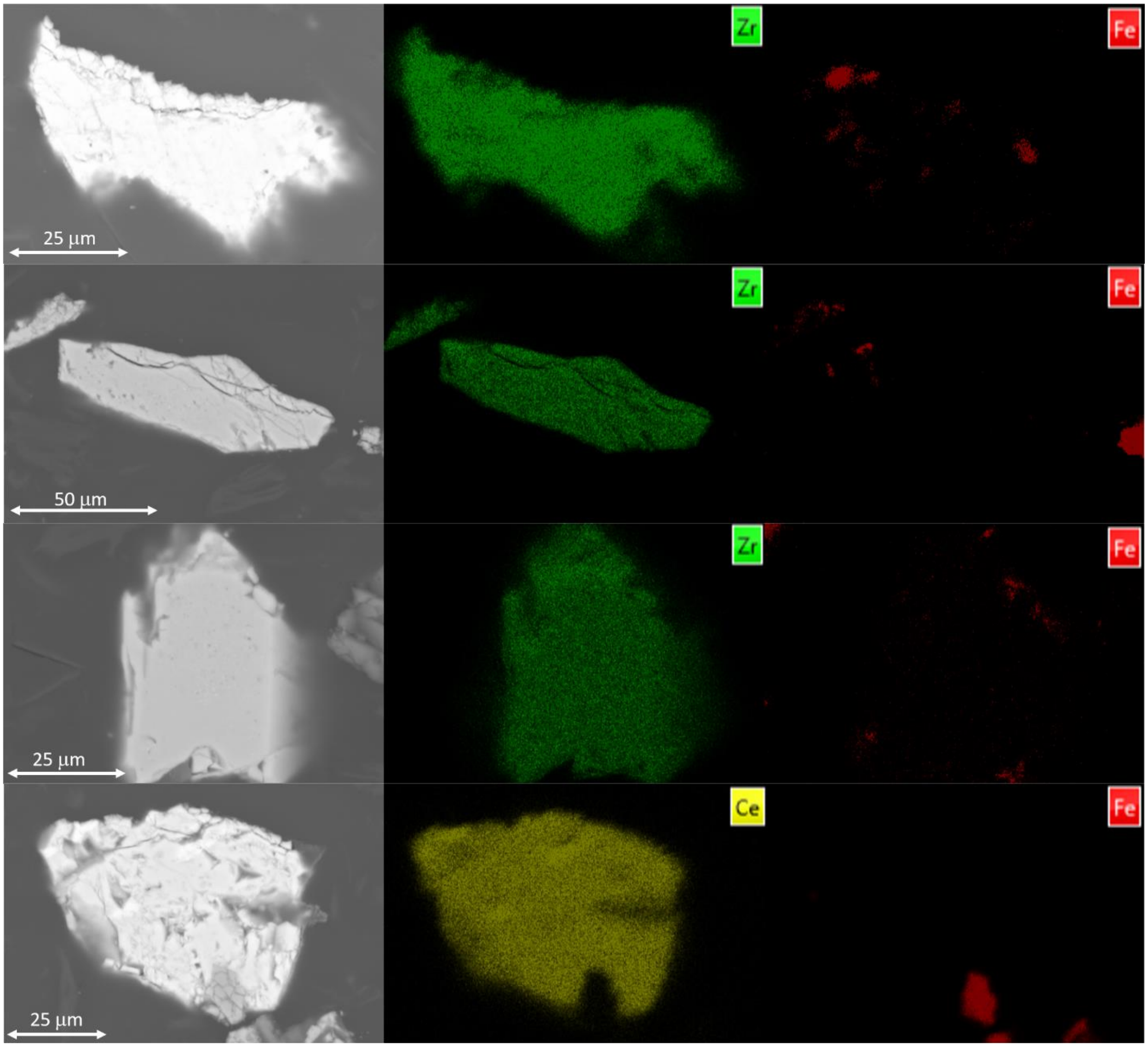

Figure 8.7 – BSE image (left) and elemental phase [Ce, Zr (centre) and Fe (right)] identification of zircon and REM particles in the LIMS magnetic fraction of the MGS concentrate (Feed 3); showing minor iron association with particles which would be defined as “free” or “liberated” by QEMSCAN

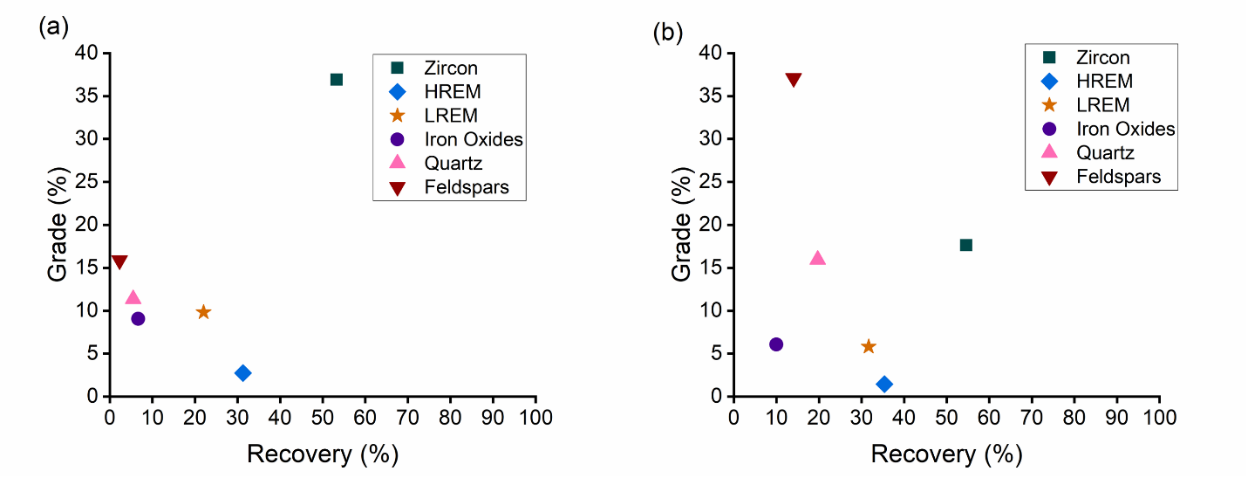

Figure 8.8 – Grade and recovery of the major mineral classes in the non-magnetic fraction of (a) the MGS concentrate (Feed 3) and (b) the table concentrate (Feed 4) after LIMS, relative to the initial feed.

8.3 Wet High-Intensity Magnetic Separation

The results of Section 8.2 along with those of Chapter 7 suggest that a high-grade bulk zircon/REM concentrate can be produced, and with proper optimization this could occur with adequate valuable mineral recoveries. It may be of interest to then separate REM from zircon as their response in downstream elemental extraction and separation processes is very different (leaching and digestion of zircon is orders of magnitude more difficult than a mineral such as bastnäsite). As most of the REM in the deposit (apart from synchysite) are paramagnetic and zircon is diamagnetic, a WHIMS was tested with the goal of separating REM from zircon.

The upgrade ratio and recovery of the major mineral phases in the WHIMS (operated at 1.8 T) products of the LIMS non-magnetic fraction of the MGS concentrate are shown in Figure 8.9. The elemental (ZrO_2, Ce_2O_3 and Fe_2O_3) upgrading and recovery can be seen in Figure 8.10. The results indicate that HREM and LREM are concentrated in the WHIMS magnetic fraction, with most of the zircon reporting to the non-magnetic fraction. Although this demonstrates that REM can be concentrated, the recovery (relative to the WHIMS feed) of HREM and LREM is only 60 % and 50 %, respectively. Apart from synchysite, which has been reported as a diamagnetic mineral (Al-

Ali *et al.*, 2019), all other REM are paramagnetic. Therefore, those which report to the non-magnetic fraction may be insufficiently liberated or too fine (relative to their magnetic susceptibility) to be recovered with the WHIMS conditions (matrix type, field strength and/or field gradient) which were employed. The results of the WHIMS (operated at 1.4 T) step performed on the LIMS non-magnetic fraction of the table concentrate, provided on a mineral basis in Figure 8.11 and elemental one in Figure 8.12, demonstrate similar findings. However, lower REM recoveries were observed, due to the lower field strength; and lower grades were observed, due to the increased quantity of quartz and feldspar present in the table concentrate.

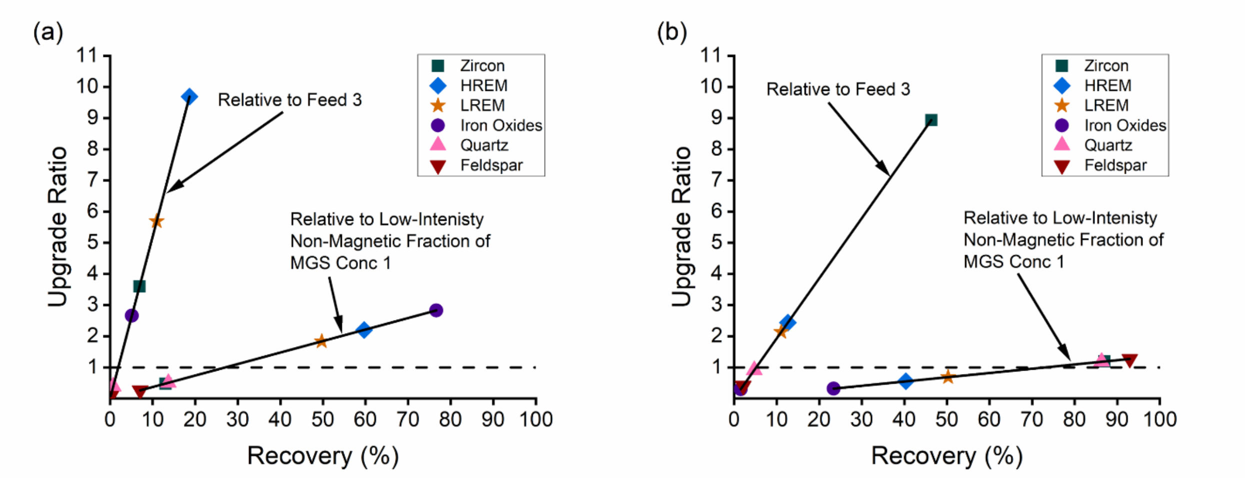

Figure 8.9 – Upgrade ratio and recovery of the major mineral classes in the (a) magnetic fraction and (b) non-magnetic fraction following WHIMS of the LIMS non-magnetic fraction of the MGS concentrate (Feed 3). Results are presented relative to the MGS concentrate and the initial feed sample

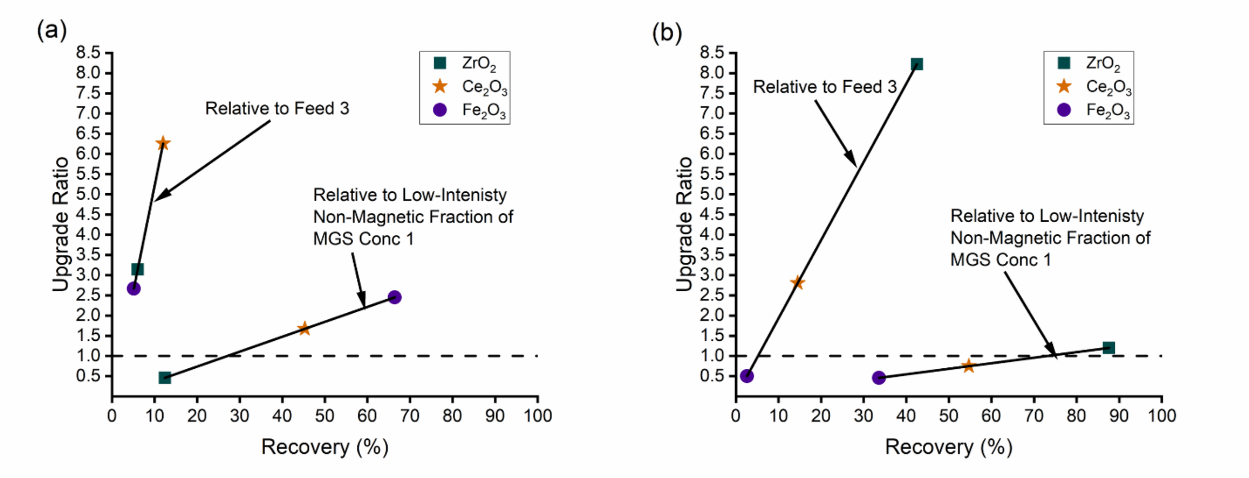

Figure 8.10 – Upgrade ratio and recovery of ZrO_2, Ce_2O_3 and Fe_2O_3 in the (a) magnetic fraction and (b) non-magnetic fraction following WHIMS of the LIMS non-magnetic fraction of the MGS concentrate (Feed 3). Results are presented relative to the MGS concentrate and the initial feed sample

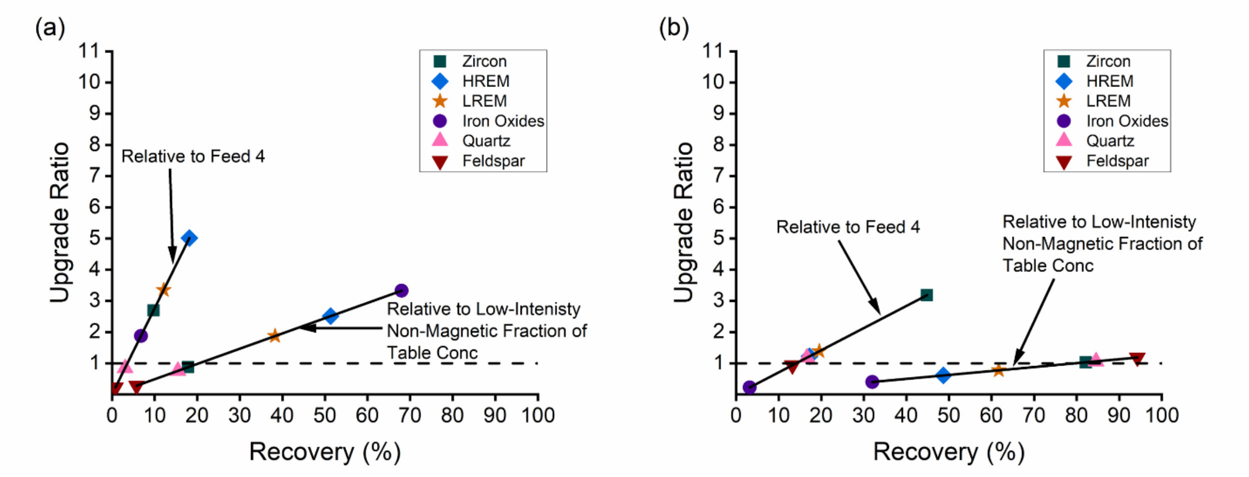

Figure 8.11 – Upgrade ratio and recovery of the major mineral classes in the (a) magnetic fraction and (b) non-magnetic fraction following WHIMS of the LIMS non-magnetic fraction of the table concentrate (Feed 4). Results are presented relative to the MGS concentrate and the initial feed sample

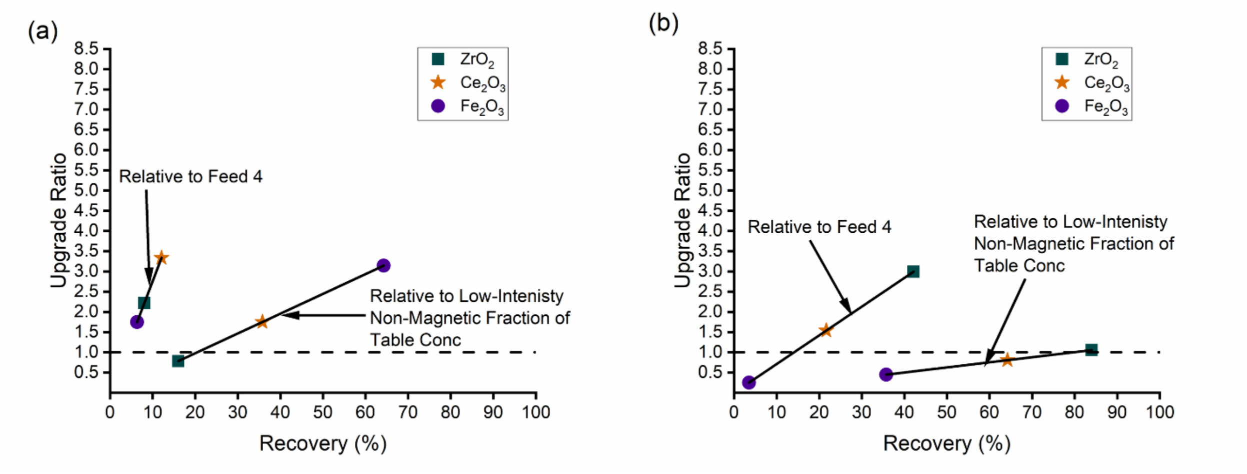

Figure 8.12 – Upgrade ratio and recovery of ZrO_2, Ce_2O_3 and Fe_2O_3 in the (a) magnetic fraction and (b) non-magnetic fraction following WHIMS of the LIMS non-magnetic fraction of the table concentrate (Feed 4). Results are presented relative to the MGS concentrate and the initial feed sample

To asses the magnetic response of individual REM, their upgrade ratio and recovery values were plotted in Figure 8.13. These results demonstrate that the relative magnetic response of REM is allanite > fergusonite > columbite (Fe) > monazite > bastnäsite > synchysite. These results correspond to the magnetic susceptibilities reported by Rosenblum and Brownfield (2000), Jordens et al. (2014) and Al-Ali et al. (2019) (Chapter 4, Section 4.3.1). Comparing the WHIMS magnetic product of the MGS concentrate (operated at 1.8 T) to that of the table concentrate (operated at 1.4 T), increasing the field strength increased REM recovery. The recovery increased 7 - 10 % for all REM apart from allanite, which saw a 19 % increase in recovery. Further increases in magnetic field strength may be beneficial, however, as discussed in Chapter 3 (Section 3.4.1), increases in the magnetic field strength can result in a lower magnetic force acting on particles, and it may be more effective to increase the magnetic field gradient employing a different matrix design, or using a different technique all together, such as a high-gradient magnetic separator (HGMS) (*i.e.* SLon).

The liberation and association characteristics of zircon, HREM, LREM and iron oxides in the WHIMS magnetic and non-magnetic fraction of the MGS concentrate can be seen in Figure 8.14. The recovery of liberated HREM and LREM, to the magnetic fraction, was 74 % and 54 %, respectively. Most of the liberated LREM reporting to the non-magnetic fraction are bastnäsite, monazite and synchysite. The relatively low recovery of liberated paramagnetic material reiterates a higher magnetic force is required to recover these minerals at this particle size and methods with an increased magnetic field gradient should be investigated. The significant association of HREM with zircon should also be acknowledged. While < 1 % of the zircon mass is associated with HREM, it does account for 15 % of the HREM mass which may impact downstream processing (leaching).

The grade and recovery values (relative to the initial feed) of the WHIMS magnetic and non-magnetic fractions for the MGS and table concentrates are shown in Figure 8.15 and Figure 8.16, respectively. The WHIMS magnetic product of the MGS concentrate recovered 28 % of REM at a grade of 24 %, and the non-magnetic product recovered 46 % of zircon at a grade of 44 %. As previously stated, with proper optimization of the comminution and gravity separation steps significant improvements in recovery are expected. However, the test work detailed in Chapter 7 (Section 7.3.2) suggested that the MGS is less effective at recovering allanite, compared to the other value minerals in the deposit. Therefore, an additional step to recover allanite may be required. As the WHIMS results indicate that it is highly effective at recovering allanite, it could be employed on the MGS tails. If such a step is successful it would have a significant impact on the overall REE recovery.

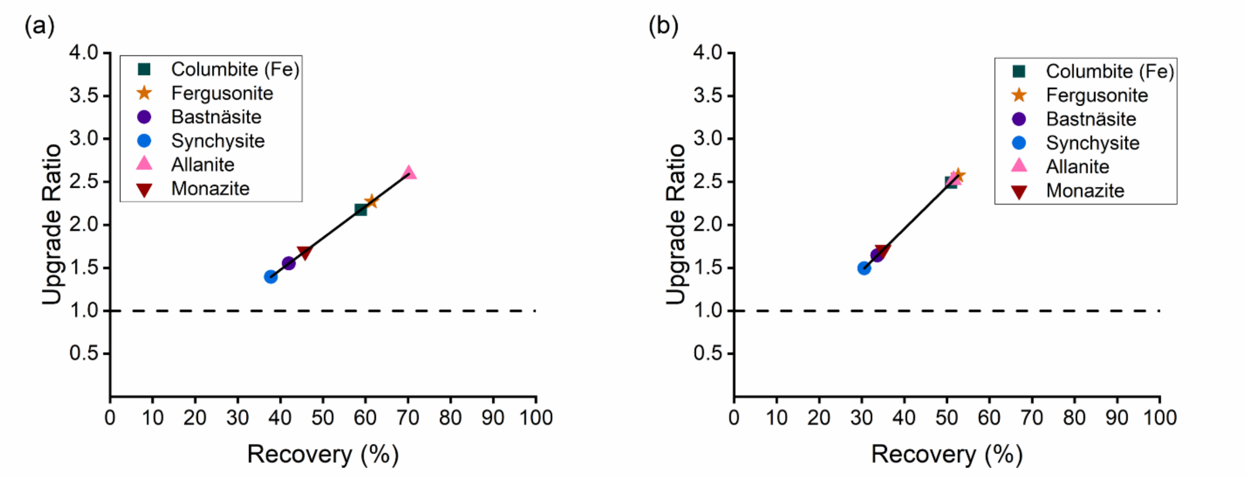

Figure 8.13 – Upgrade ratio and recovery of REM in the WHIMS magnetic fraction of the LIMS non-magnetic fraction of the (a) MGS concentrate and (b) table concentrate, relative to the WHIMS feed

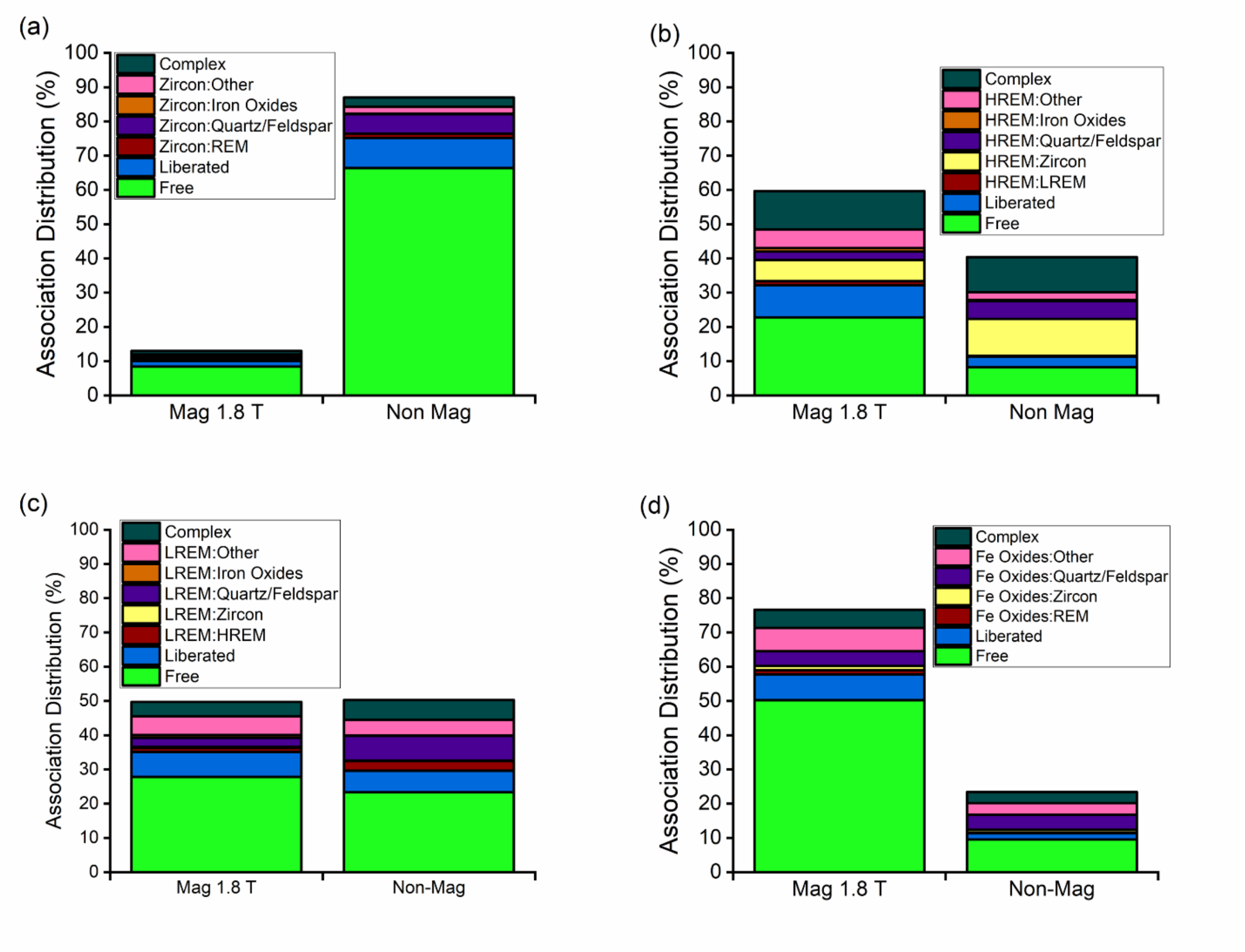

Figure 8.14 – Mineral associations of the magnetic and non-magnetic fractions produced from WHIMS of the LIMS non-magnetic fraction of the MGS concentrate (Feed 3) for (a) zircon, (b) HREM, (c) LREM and (d) iron oxides

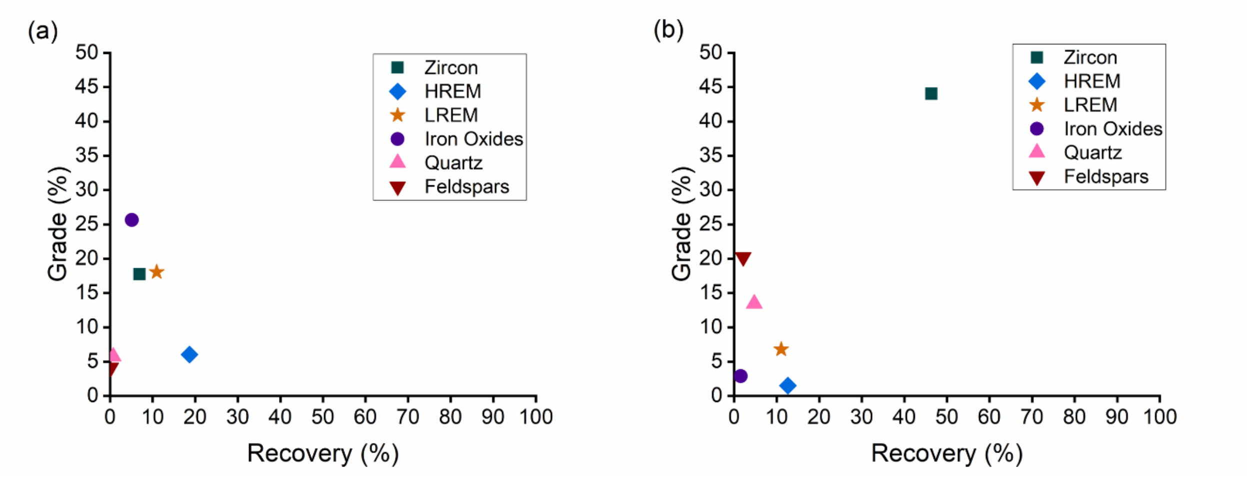

Figure 8.15 – Grade and recovery of the major mineral classes in the WHIMS (a) magnetic and (b) non-magnetic fraction of the LIMS non-magnetic fraction of the MGS concentrate, relative to the initial feed (Feed 3)

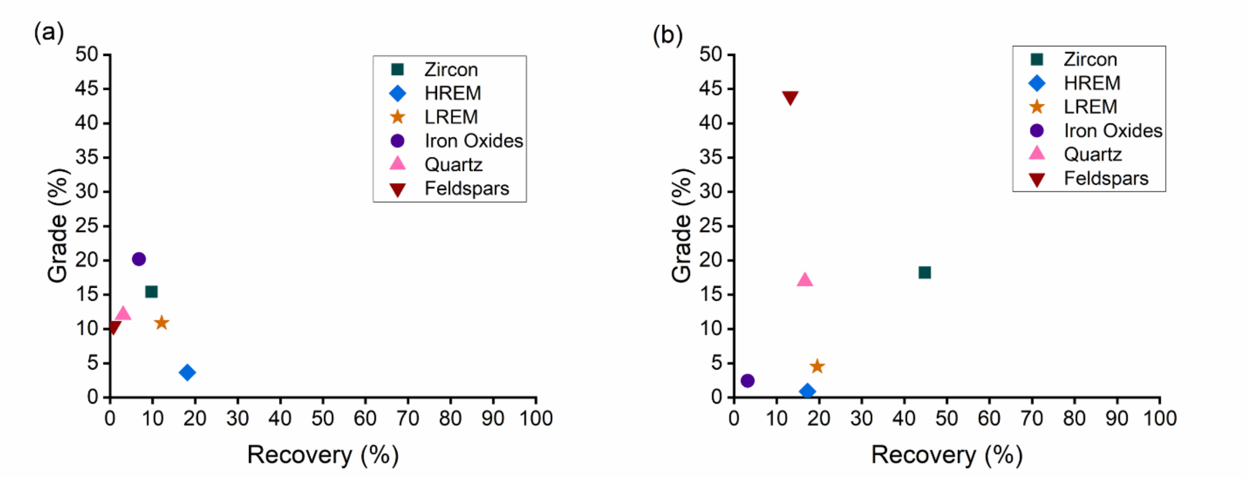

Figure 8.16 – Grade and recovery of the major mineral classes in the WHIMS (a) magnetic and (b) non-magnetic fraction of the the LIMS non-magnetic fraction of the table concentrate, relative to the initial feed (Feed 4)

8.4 Proposed Flowsheet

Following the results of gravity (Chapter 7) and magnetic separation (Chapter 8) experiments undertaken in this thesis, a potential flowsheet, employing gravity and magnetic separation, is proposed to beneficiate the Nechalacho deposit. A simplified version of this flowsheet can be seen in Figure 8.17. The feed would initially be pre-concentrated using a spiral to reject a significant portion of silicate gangue (quartz and feldspars) at a relatively coarse particle size. The gravity concentrate would then be re-ground and processed using a MGS. The MGS concentrate would undergo subsequent stages of magnetic separation; removing iron oxide gangue with a LIMS and then separating zircon and REM using a WHIMS. The MGS tails would be processed using a WHIMS to recover additional allanite. The application of this flowsheet is highly dependant upon an in-depth study into the comminution behaviour of the ore to optimize the feed for each separation stage. Optimization of the operating parameters in each separation stage is also imperative.

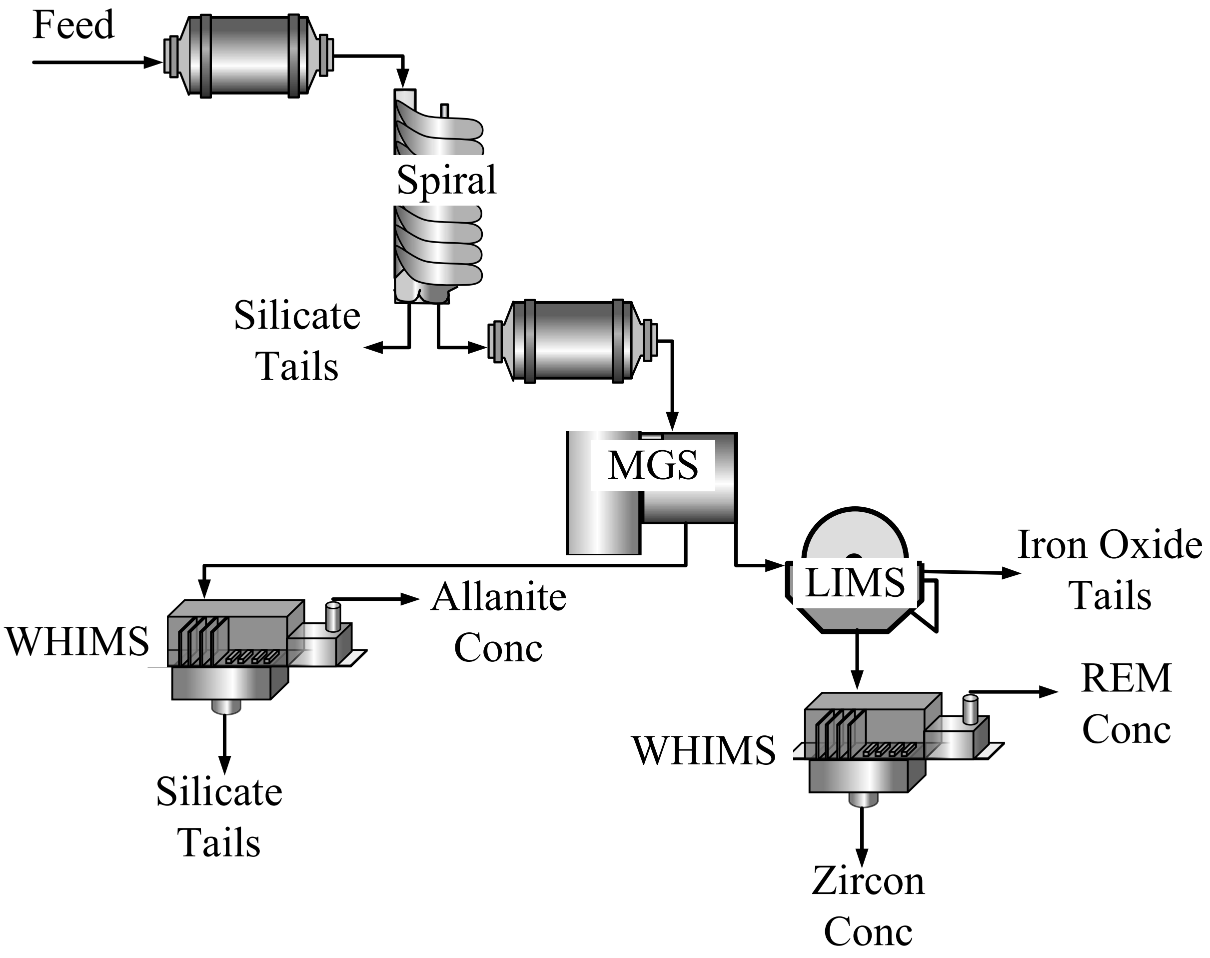

Figure 8.17 – Simplified flowsheet proposed to beneficiate the Nechalacho deposit

8.5 Conclusions

Chapter 8 has detailed the magnetic response of minerals in the MGS and table concentrates to LIMS and WHIMS. The conclusions are as follows:

1. The LIMS step is effective are removing iron oxides from REM and zircon in the gravity concentrates.
2. Some zircon and REM losses are expected to the magnetic fraction of the LIMS step, due to their association with iron oxides.

3. WHIMS was effective at producing a high REM concentrate, leaving zircon in the non-magnetic fraction. However, as the recovery of REM (particularly bastnäsite and monazite) was low, the use of higher magnetic field gradients is recommended.
4. The relative magnetic response of REM in the Nechalcho ore followed allanite > fergusonite > columbite (Fe) > monazite > bastnäsite > synchysite.
5. The magnetic response of allanite to the WHIMS suggests its use on the MGS tails to limit allanite losses.
6. A flowsheet employing gravity and magnetic separation was suggested

Chapter 9

Conclusions, Contributions and Future Work

9.1 Conclusions

This chapter summarizes the main conclusions from this thesis, details the claims to original work and highlights the areas identified as requiring future work.

This research program has focussed on the constructing a process for the beneficiation of the Nechalacho REM deposit that is based on sound mineral processing fundamentals; while adding to the body of knowledge surrounding the beneficiation of REM, which is quite limited. The conclusions of this work are as follows:

1. The liberation and association behaviour of zircon and REM was identified as a significant opportunity to concentrate the Nechalacho ore using gravity separation
2. The method of comminution has a significant impact on the liberation and association behaviour of the ore, particularly for REM
3. Gravity modeling using automated mineralogy has been shown to be capable of accurately predicting grade and recovery values by SG for DMS
4. A spiral concentrator can be used to preconcentrate zircon and REM in the Nechalcho ore at particle sizes above their liberation size
5. A MGS can produce near ideal separation of REM and zircon from silicate gangue at particle sizes close to their liberation size; resulting in a bulk heavy mineral (zircon, REM and iron oxides) concentrate

6. A LIMS step was successful at removing iron oxides from the gravity concentrate, resulting in a bulk zircon and REM concentrate. However, due to the association of iron oxides with value minerals, some losses are expected

7. A WHIMS can separate REM from zircon, however, for this stage to be effective high magnetic field gradients are recommended. The relative response of REM to this step followed allanite > fergusonite > columbite (Fe) > bastnäsite > monazite > synchysite which corresponds well to reported magnetic susceptibilities in literature

8. A flowsheet was proposed to beneficiate the Nechalcho ore using only physical separations

9.2 Contributions to Original Knowledge

This thesis involved the application of automated mineralogy to understand the behaviour of a novel class of minerals in established separation techniques. In the literature, there is generally a poor understanding of how to process complex REM deposits, such as the Nechalacho deposit. As such, the contributions of this work can be generally stated as the development of a framework of REM beneficiation knowledge which future researchers can build on. The major contributions are summarized as follows:

1. A physical separation (gravity and magnetic) process capable of processing the Nechalcho deposit was proposed

2. Automated mineralogy was used extensively to characterize each process which was studied; developing an improved fundamental understanding of each technique which was employed and their application to REM beneficiation

3. For the first time, a MGS was applied to an ore containing multiple REM and their response was understood on a mineralogical basis

4. The separation of iron oxides, REM and zircon using magnetic separation was studied and the relative response of the various REM present in the Nechalacho deposit was reported

5. Automated mineralogy was demonstrated as an important and highly effective tool when developing a beneficiation process for complex ore deposits

9.3 Future Work

Although REM beneficiation has received an extensive amount of research over the last decade there continues to be significant gaps in knowledge. Certain areas in need of investigation for the field of REM beneficiation include:

1. Fundamental physicochemical characterisation of valuable REM to determine bulk properties (specific gravities, magnetic properties, *etc.*) and surface properties (for flotation) which control separation behaviour

2. Applying automated mineralogy to understand the behaviour of REM in other established separation techniques (i.e. flotation, HGMS, *etc.*)

In the context of the Nechalacho deposit the following areas should be investigated:

1. A fundamental investigation into the comminution behavior of the ore, to optimize the feed for downstream separation processes

2. Spiral circuits which include rougher, cleaner and scavenger stages with recycling to determine an optimal process for preconcentration

3. Optimization work of the MGS to ensure grade and recovery targets are met

4. The use of different WHIMS matrix designs to optimize the magnetic force acting on REM

5. The use of a HGMS (*i.e* SLon) in place of a WHIMS

References

Abaka-Wood, G.B., Quast, K., Zanin, M., Addai-Mensah, J., Skinner, W., 2019a. A Study of the Feasibility of Upgrading Rare Earth Elements Minerals from Iron-Oxide-Silicate Rich Tailings Using Knelson Concentrator and Wilfley Shaking Table. Powder Technology 344, 897-913.

Abaka-Wood, G.B., Zanin, M., Addai-Mensah, J., Skinner, W., 2019b. Recovery of Rare Earth Elements Minerals from Iron Oxide–Silicate Rich Tailings – Part 1: Magnetic Separation. Minerals Engineering 136, 50-61.

Aktaş, Z., Karacan, F., Olcay, A., 1998. Centrifugal Float–Sink Separation of Fine Turkish Coals in Dense Media. Fuel Processing Technology 55, 235-250.

Al-Ali, S., Wall, F., Sheridan, R., Pickles, J., Pascoe, R., 2019. Magnetic Properties of REE Fluorcarbonate Minerals and Their Implications for Minerals Processing. Minerals Engineering 131, 392-397.

Ali, S.H., 2014. Social and Environmental Impact of the Rare Earth Industries. Resources 3, 123-134.

Anderson, C., 2015. Improved Understanding of Rare Earth Surface Chemistry and Its Application to Froth Flotation, PhD Thesis, Metallurgical and Materials Engineering. Colorado School of Mines, Colorado, USA.

Anthony, J.W., Bideaux, R.A., Bladh, K.W., Nichols, M.C., 2001. Handbook of Mineralogy. Mineralogical Society of America, Chantilly, USA.

ArcelorMittal, 2019. Mining Sites (Mount-Wright and Fire Lake). Retrieved Nov 2019 from https://www.transformerlavenir.com.

Argus Media Ltd., 2015. Argus White Paper: Impact of Changes to Chinese Policy on the Rare Earths Market in 2015. Argus Media Ltd., London, UK.

Arol, A.I., Aydogan, A., 2004. Recovery Enhancement of Magnetite Fines in Magnetic Separation. Colloids and Surfaces A: Physicochemical and Engineering Aspects 232, 151-154.

Aslan, N., 2007a. Application of Response Surface Methodology and Central Composite Rotatable Design for Modeling the Influence of Some Operating Variables of a Multi-Gravity Separator for Coal Cleaning. Fuel 86, 769-776.

Aslan, N., 2007b. Modeling and Optimization of Multi-Gravity Separator to Produce Celestite Concentrate. Powder Technology 174, 127-133.

Aslan, N., 2008a. Application of Response Surface Methodology and Central Composite Rotatable Design for Modeling and Optimization of a Multi-Gravity Separator for Chromite Concentration. Powder Technology 185, 80-86.

Aslan, N., 2008b. Multi-Objective Optimization of Some Process Parameters of a Multi-Gravity Separator for Chromite Concentration. Separation and Purification Technology 64, 237-241.

Avalon Rare Metals Inc., 2013. Avalon Reports on Summer Work Program at the Nechalacho Rare Earth Elements Project and Provides Mineral Resource Update. Avalon Rare Metals Inc. Retrieved Nov 2019 from http://www.avalonadvancedmaterials.com.

Bagnold, R.A., 1954. Experiments on a Gravity-Free Dispersion of Large Solid Spheres in a Newtonian Fluid under Shear. Proceedings of the Royal Society of London. Series A. Mathematical and Physical Sciences 225, 49-63.

Becker, M., Harris, P.J., Wiese, J.G., Bradshaw, D.J., 2009. Mineralogical Characterisation of Naturally Floatable Gangue in Merensky Reef Ore Flotation. International Journal of Mineral Processing 93, 246-255.

Binnemans, K., Jones, P.T., 2015. Rare Earths and the Balance Problem. Journal of Sustainable Metallurgy 1, 29-38.

Binnemans, K., Jones, P.T., Blanpain, B., Van Gerven, T., Yang, Y., Walton, A., Buchert, M., 2013. Recycling of Rare Earths: A Critical Review. Journal of Cleaner Production 51, 1-22.

Binnemans, K., Jones, P.T., Müller, T., Yurramendi, L., 2018. Rare Earths and the Balance Problem: How to Deal with Changing Markets? Journal of Sustainable Metallurgy 4, 126-146.

Brown, M., Eggert, R., 2018. Simulating Producer Responses to Selected Chinese Rare Earth Policies. Resources Policy 55, 31-48.

Bulatovic, S.M., 2010. Flotation of Reo Minerals, in: Bulatovic, S.M. (Ed.), Handbook of Flotation Reagents: Chemistry, Theory and Practice. Elsevier, Amsterdam, pp. 151-173.

Butcher, A., 2010. A Practical Guide to Some Aspects of Mineralogy That Affect Flotation. Flotation Plant Optimisation A Metallurgical Guide to Identifying and Solving Problems in Flotation Plants, 191-200.

Castor, S.B., 2008. Rare Earth Deposits of North America. Resource Geology 58, 337-347.

Chan, T.N., 1992. A New Beneficiation Process for Treatment of Supergene Monazite Ore, in: Bautista, R.G., Jackson, N. (Eds.), Rare Earths, Resources, Science, Technology and Applications. Minerals, Metals & Materials Society.

Chaurasia, R.C., Nikkam, S., 2017a. Beneficiation of Low-Grade Iron Ore Fines by Multi-Gravity Separator (MGS) Using Optimization Studies. Particulate Science and Technology 35, 45-53.

Chaurasia, R.C., Nikkam, S., 2017b. Optimization Studies on a Multi-Gravity Separator Treating Ultrafine Coal. International Journal of Coal Preparation and Utilization 37, 195-212.

Chi, R., Xu, S., Zhu, G., Xu, J., Qiu, X., 2001. Beneficiation of Rare Earth Ore in China, in: Anjier, J.L. (Ed.), Light Metals. The Minerals, Metals & Materials Society, New Orleans, USA.

Ciuculescu, T., Foo, B., Gowans, R., Hawton, K., Jacobs, C., Spooner, J., 2013. Technical Report Disclosing the Results of the Feasibility Study on the Nechalacho Rare Earth Elements Project. Avalon Rare Metals Inc.. Retrieved Nov 2019 from http://www.avalonadvancedmaterials.com.

Cobb, H.M., 2012. Dictionary of Metals. ASM International, Materials Park, USA.

Coetzee, L.L., Theron, S.J., Martin, G.J., Merwe, J.-D.v.d., Stanek, T.A., 2011. Modern Gold Deportments and Its Application to Industry. Minerals Engineering 24, 565-575.

Cordier, D.J., 2011. Rare Earths, Mineral Commodity Summaries. United States Geological Survey. Retrieved Nov 2019 from https://www.usgs.gov.

Cordier, D.J., 2012. Rare Earths, Mineral Commodity Summaries. United States Geological Survey. Retrieved Nov 2019 from https://www.usgs.gov.

Cui, H., 2015. Beneficiation of Rare Earth Elements Bearing Ancylite, MSc Thesis, Metallurgical & Materials Engineering. Colorado School of Mines, Colorado, USA.

Dehaine, Q., Filippov, L.O., 2015. Rare Earth (La, Ce, Nd) and Rare Metals (Sn, Nb, W) as by-Product of Kaolin Production, Cornwall: Part1: Selection and Characterisation of the Valuable Stream. Minerals Engineering 76, 141-153.

Dehaine, Q., Filippov, L.O., Joussemet, R., 2017. Rare Earths (La, Ce, Nd) and Rare Metals (Sn, Nb, W) as by-Products of Kaolin Production – Part 2: Gravity Processing of Micaceous Residues. Minerals Engineering 100, 200-210.

Dostal, J., 2016. Rare Metal Deposits Associated with Alkaline/Peralkaline Igneous Rocks, in: Verplanck, P.L., Hitzman, M.W. (Eds.), Rare Earth and Critical Elements in Ore Deposits. Society of Economic Geologists.

Ebner, A.D., Ritter, J.A., Ploehn, H.J., 1997. Feasibility and Limitations of Nanolevel High Gradient Magnetic Separation. Separation and Purification Technology 11, 199-210.

Espiritu, E.R.L., 2018. Beneficiation of Rare Earth Minerals from Niobec Ore: Froth Flotation, PhD Thesis, Department of Mining and Materials Engineering. McGill University, Montreal, Canada.

European Commission, 2017. Study on the Review of the List of Critical Raw Materials: Criticality Assesments. European Commission. Retrieved Nov 2019 from https://op.europa.eu.

Falconer, A., 2003. Gravity Separation: Old Technique/New Methods. Physical Separation in Science and Engineering 12, 31-48.

Fekete, J., 2014. Canada Looking to Break into 'Critical' Rare Earth Elements Mining. Ottawa Citizen Ottawa Canada. Retrieved Nov 2019 from https://o.canada.com.

Feng, Q., Zhao, W., Wen, S., Cao, Q., 2017. Activation Mechanism of Lead Ions in Cassiterite Flotation with Salicylhydroxamic Acid as Collector. Separation and Purification Technology 178, 193-199.

Ferron, C.J., Bulatovic, S.M., Salter, R.S., 1991. Beneficiation of Rare Earth Oxide Minerals, in: Siribumrungsukha, B., Arrykul, S., Sanguansai, P., Pungrassami, T., Sikong, L., Kooptarnond, K. (Ed.), International Conference on Rare Earth Minerals and Minerals for Electronic Uses, Prince of Songklia University, Hat Yai, Thailand.

Filippov, L.O., Dehaine, Q., Filippova, I.V., 2016. Rare Earths (La, Ce, Nd) and Rare Metals (Sn, Nb, W) as by-Products of Kaolin Production – Part 3: Processing of Fines Using Gravity and Flotation. Minerals Engineering 95, 96-106.

Fitzpatrick, R., Hegarty, P., Fergusson, K., Rollinson, G., Xie, W., Mildren, T., 2018. Optimisation of a Multi-Gravity Separator with Novel Modifications for the Recovery of Ferberite. Minerals 8, 191.

FLSmidth Knelson, 2013. Kneslon Concentrator Model Kc-Cvd64 Specification Sheet. FLSmidth Ltd., Langley, Canada. Retrieved Nov 2019 from https://www.consep.com.au.

Foner, S., 1959. Versatile and Sensitive Vibrating-Sample Magnetometer. Review of Scientific Instruments 30, 548-557.

Gambogi, J., 2013. Rare Earths, Mineral Commodity Summaries. United States Geological Survey. Retrieved Nov 2019 from https://www.usgs.gov.

Gambogi, J., 2015. Rare Earths, 2015 Minerals Yearbook. United States Geological Survey. Retrieved Nov 2019 from https://www.usgs.gov.

Gambogi, J., 2018. Rare Earths, Mineral Commodity Summaries. United States Geological Survey. Retrieved Nov 2019 from https://www.usgs.gov.

Ge, W., Encinas, A., Araujo, E., Song, S., 2017. Magnetic Matrices Used in High Gradient Magnetic Separation (HGMS): A Review. Results in Physics 7, 4278-4286.

Goodenough, K.M., Wall, F., Merriman, D., 2018. The Rare Earth Elements: Demand, Global Resources, and Challenges for Resourcing Future Generations. Natural Resources Research 27, 201-216.

Gottlieb, P., Wilkie, G., Sutherland, D., Ho-Tun, E., Suthers, S., Perera, K., Jenkins, B., Spencer, S., Butcher, A., Rayner, J., 2000. Using Quantitative Electron Microscopy for Process Mineralogy Applications. JOM 52, 24-25.

Grammatikopoulos, T., Mercer, W., Gunnning, C., Prout, S., 2011. Quantitative Characterization of the REE Minerals by QEMSCAN from the Nechalacho Heavy Rare Earth Deposit, Thor Lake Project, Nwt, Canada, 43rd Annual Meeting of the Canadian Mineral Processors, Ottawa, Canada.

Gravity Mining Ltd., 2019. Home Page. Retrieved Nov 2019 from http://www.gravitymining.com.

Greinacher, E., 1981. History of Rare Earth Applications, Rare Earth Market Today, Industrial Applications of Rare Earth Elements. American Chemical Society, pp. 3-17.

Gupta, C.K., Krishnamurthy, N., 2005. Extractive Metallurgy of Rare Earths. CRC press, Boca Raton.

Guy, P.J., Bruckard, W.J., Vaisey, M.J., 2000. Beneficiation of Mt Weld Rare Earth Oxides by Gravity Concentration, Flotation and Magnetic Separation, Seventh Mill Operators' Conference. The Australasian Institute of Mining and Metallurgy, Kalgoorlie, Australia.

Haapala, I., Ervamaa, P., Löfgren, A., Ojanperä, P., 1969. An Occurrence of Monazite in Puumala, Eastern Finland. Bulletin of the Geological Society of Finland 41, 117-124.

Hatch, G.P., 2015. TMR Advanced Rare-Earth Projects Index. Technology Metal Research. Retrieved Nov 2019 from https://www.techmetalsresearch.com.

Hedrick, J.B., 1999. Rare Earths, Mineral Commodity Summaries. United States Geological Survey. Retrieved Nov 2019 from https://www.usgs.gov.

Hedrick, J.B., 2003. Rare Earths, Mineral Commodity Summaries. United States Geological Survey. Retrieved Nov 2019 from https://www.usgs.gov.

Hedrick, J.B., Sinha, S.P., Kosynkin, V.D., 1997. Loparite, a Rare-Earth Ore (Ce, Na, Sr, Ca)(Ti, Nb, Ta, Fe^{+3})O_3. Journal of Alloys and Compounds 250, 467-470.

Heiskanen, K., 1993. Particle Classification. Chapman & Hall, London.

Hendrick, J.B., 2005. Rare Earths, Mineral Commodity Summaries. United States Geological Survey. Retrieved Nov 2019 from https://www.usgs.gov.

Hendrick, J.B., 2006. Rare Earths, Mineral Commodity Summaries. United States Geological Survey. Retrieved Nov 2019 from https://www.usgs.gov.

Hendrick, J.B., 2007. Rare Earths, Mineral Commodity Summaries. United States Geological Survey. Retrieved Nov 2019 from https://www.usgs.gov.

Hendrick, J.B., 2008. Rare Earths, Mineral Commodity Summaries. United States Geological Survey. Retrieved Nov 2019 from https://www.usgs.gov.

Hendrick, J.B., 2009. Rare Earths, Mineral Commodity Summaries. United States Geological Survey. Retrieved Nov 2019 from https://www.usgs.gov.

Hendrick, J.B., 2010. Rare Earths, Mineral Commodity Summaries. United States Geological Survey. Retrieved Nov 2019 from https://www.usgs.gov.

Henley, K., 1983. Ore-Dressing Mineralogy - A Review of Techniques, Applications and Recent Developments, in: De Villiers, J.P.R., Cawthron, P.A. (Eds.), First International Congress on Applied Mineralogy (ICAM 81). Special Publication of the Geological Society of South Africa, Johannesburg, South Africa, pp. 175-200.

Hiemstra, S.A., 1985. The Role of Mineralogy in Ore Beneficiation as Illustrated by Case Histories, in: Park, W.C., Hausen, D.M., Hagni, R.D. (Eds.), Second International Congress on Applied Mineralogy in the Minerals Industry. Metallurgical Society of the American Institute of Mining, Metallurgical, and Petroleum Engineers, Los Angeles, USA, pp. 9-20.

Hirajima, T., Sasaki, K., Bissombolo, A., Hirai, H., Hamada, M., Tsunekawa, M., 2005. Feasibility of an Efficient Recovery of Rare Earth-Activated Phosphors from Waste Fluorescent Lamps through Dense-Medium Centrifugation. Separation and Purification Technology 44, 197-204.

Holtham, P.N., 1990. Flow Visualisation of Secondary Currents on Spiral Separators. Minerals Engineering 3, 279-286.

Houot, R., Cuif, J.P., Mottot, Y., Samama, J.C., 1991. Recovery of Rare Earth Minerals with Emphasis on Flotation Process, in: Siribumrungsukha, B., Arrykul, S., Sanguansai, P., Pungrassami, T., Sikong, L., Kooptarnond, K. (Ed.), International Conference on Rare Earth Minerals and Minerals for Electronic Uses, Hat Yai, Thailand, pp. 301-324.

Hu, A.H., Kuo, C.-H., Huang, L.H., Su, C.-C., 2017. Carbon Footprint Assessment of Recycling Technologies for Rare Earth Elements: A Case Study of Recycling Yttrium and Europium from Phosphor. Waste Management 60, 765-774.

Ito, S., Yotsumoto, H., Sakamoto, H., 1991. Magnetic Separation of Monazite and Xenotime, in: Siribumrungsukha, B., Arrykul, S., Sanguansai, P., Pungrassami, T., Sikong, L., Kooptarnond, K. (Eds.), International Conference on Rare Earth Minerals and Minerals for Electronic Uses, Prince Songkla University, Hat Yai, Thailand, pp. 279-300.

Jiles, D., 2015. Introduction to Magnetism and Magnetic Materials. CRC press, Boca Raton.

Jordens, A., 2016. The Beneficiation of Rare Earth Element-Bearing Minerals, PhD Thesis, Department of Mining and Materials Engineering. McGill University, Montreal, Canada.

Jordens, A., Cheng, Y.P., Waters, K.E., 2013. A Review of the Beneficiation of Rare Earth Element Bearing Minerals. Minerals Engineering 41, 97-114.

Jordens, A., Marion, C., Grammatikopoulos, T., Hart, B., Waters, K.E., 2016a. Beneficiation of the Nechalacho Rare Earth Deposit: Flotation Response Using Benzohydroxamic Acid. Minerals Engineering 99, 158-169.

Jordens, A., Marion, C., Langlois, R., Grammatikopoulos, T., Rowson, N.A., Waters, K.E., 2016b. Beneficiation of the Nechalacho Rare Earth Deposit. Part 1: Gravity and Magnetic Separation. Minerals Engineering 99, 111-122.

Jordens, A., Marion, C., Langlois, R., Grammatikopoulos, T., Rowson, N.A., Waters, K.E., 2016b. Beneficiation of the Nechalacho Rare Earth Deposit. Part 1: Gravity and Magnetic Separation. Minerals Engineering 99, 111-122.

Jordens, A., McCarthy, S., Waters, K.E., 2014. The Effect of Activating Ions on the Adsorption of a Benzohydroxamic Acid Collector onto a Rare Earth Silicate, Conference of Metallurgists, Vancouver, Canada.

Jowitt, S.M., Werner, T.T., Weng, Z., Mudd, G.M., 2018. Recycling of the Rare Earth Elements. Current Opinion in Green and Sustainable Chemistry 13, 1-7.

Katzmarzyk, J., Gronen, L., Wotruba, H., Sindern, S., Meyer, F.M., Hellmann, A., 2018. Geometallurgical Investigation of the Processing of REE-Y-Nb-Zr Complex Ore, XXIX International Mineral Processing Congress, Moscow, Russia.

Kelly, T.D., Matos, G.R., 2015. Rare Earths End-Use Statistics Historical Statistics for Mineral and Material Commodities in the United States (2016 Version). United States Geological Survey. Retrieved Nov 2019 from https://www.usgs.gov.

Kennedy, J., 2019. China Solidifies Dominance in Rare Earth Processing. National Defence. Retrieved Nov 2019 from https://www.nationaldefensemagazine.org.

Kingsnorth, D., 2018. The Rare Earth Market in 2018, Driven by E-Mobility. Industrial Minerals Company of Australia and Curtain University, Perth, Australia.

Kingsnorth, D.J., 2010. Rare Earths: Facing New Challenges in the New Decade, Presentation at the SME Annual Meeting, Phoenix, USA.

Klima, M., Xu, D., Cho, H., 1995. A Preliminary Investigation of Dense-Medium Centrifugation for Fine Coal Separations, 19th International Mineral Processing Congress. Society for Mining, Metallurgy, and Exploration, San Francisco, pp. 138-142.

Krishnamurthy, N., Gupta, C., 2016. Extractive Metallurgy of Rare Earths. CRC Press, Boca Raton.

Kwitko-Ribeiro, R., 2012. New Sample Preparation Developments to Minimize Mineral Segregation in Process Mineralogy, in: Broekmans, M.A.T.M. (Ed.), Proceedings of the 10th International Congress for Applied Mineralogy (Icam). Springer Berlin Heidelberg, Berlin, Heidelberg, pp. 411-417.

Lätti, D., Adair, B.J.I., 2001. An Assessment of Stereological Adjustment Procedures. Minerals Engineering 14, 1579-1587.

Lewis, B., Scheyder, E., 2018. China Cutting Rare Earth Output, Unnerving Global Manufacturers, Reuters. Retrieved May 2019 from https://www.reuters.com.

Li, X., Chen, Z., Chen, Z., Zhang, Y., 2013. A Human Health Risk Assessment of Rare Earth Elements in Soil and Vegetables from a Mining Area in Fujian Province, Southeast China. Chemosphere 93, 1240-1246.

Lin, D., Lastra, R., Finch, J., 1999. Comparison of Stereological Correction Procedures for Liberation Measurements by Use of a Standard Material. Transactions of the Institution of Mining and Metallurgy. Section C. Mineral Processing and Extractive Metallurgy 108.

Ling, Z.L., Yang, X., 2014. China's Rare Earth Ore Deposits and Beneficiation Techniques, 1st European Rare Earth Resources Conference, Milos Island, Greece.

Long, K.R., Van Gosen, B.S., Foley, N.K., Cordier, D., 2012. The Principal Rare Earth Elements Deposits of the United States: A Summary of Domestic Deposits and a Global Perspective, in: Sinding-Larsen, R., Wellmer, F.-W. (Eds.), Non-Renewable Resource Issues: Geoscientific and Societal Challenges. Springer Netherlands, Dordrecht, pp. 131-155.

Lorenz, T., Bertau, M., 2019. Recycling of Rare Earth Elements from Fendb-Magnets Via Solid-State Chlorination. Journal of Cleaner Production.

Luo, J., Chen, X., 1987. Research into the Recovery of High-Grade Rare-Earth Concentrate from Baotou Complex Iron Ore, China. Beijing Mining and Metallurgical Research Institute, China.

Mancheri, N.A., Sprecher, B., Bailey, G., Ge, J., Tukker, A., 2019. Effect of Chinese Policies on Rare Earth Supply Chain Resilience. Resources, Conservation and Recycling 142, 101-112.

Meng, Q., Yuan, Z., Yu, L., Xu, Y., Du, Y., 2018. Study on the Activation Mechanism of Lead Ions in the Flotation of Ilmenite Using Benzyl Hydroxamic Acid as Collector. Journal of Industrial and Engineering Chemistry 62, 209-216.

Menzel, K., Lindner, J., Nirschl, H., 2012. Removal of Magnetite Particles and Lubricant Contamination from Viscous Oil by High-Gradient Magnetic Separation Technique. Separation and Purification Technology 92, 122-128.

Moss, R.L., Tzimas, E., Willis, P., Arendorf, J., Thompson, P., Chapman, A., Morley, N., Sims, E., Bryson, R., Pearson, J., Tercero Espinoza, L., Marscheider-Weidemann, F., Soulier, M., Lüllmann, A., Sartorius, C., Ostertag, K., 2013. Critical Metals in the Path Towards the Decarbonisation of the Eu Energy Sector: Assessing Rare Metals as Supply-Chain Bottlenecks in Low-Carbon Energy Technologies. European Commission's Joint Research Centre, Luxembourg.

Moustafa, M.I., Abdelfattah, N.A., 2010. Physical and Chemical Beneficiation of the Egyptian Beach Monazite. Resource geology 60, 288-299.

Napier-Munn, T., Bosman, J., Holtham, P., 2014. Innovations in Dense Media Separation Technology. Mineral processing and extractive metallurgy 100, 265-275.

Oberteuffer, J., 1974. Magnetic Separation: A Review of Principles, Devices, and Applications. IEEE Transactions on Magnetics 10, 223-238.

Özbayoğlu, G., Ümit Atalay, M., 1995. Beneficiation of Beylikahir Complex Rare Earth Deposit of Turkey. Physicochemical Problems of Mineral Processing 29, 19-30.

Özbayoğlu, G., Ümit Atalay, M., 2000. Beneficiation of Bastnaesite by a Multi-Gravity Separator. Journal of Alloys and Compounds 303-304, 520-523.

Özgen, S., 2012. Clean Chromite Production from Fine Chromite Tailings by Combination of Multi Gravity Separator and Hydrocyclone. Separation Science and Technology 47, 1948-1956.

Packey, D.J., Kingsnorth, D., 2016. The Impact of Unregulated Ionic Clay Rare Earth Mining in China. Resources Policy 48, 112-116.

Pan, Y., Li, H., 2016. Investigating Heavy Metal Pollution in Mining Brownfield and Its Policy Implications: A Case Study of the Bayan Obo Rare Earth Mine, Inner Mongolia, China. Environmental Management 57, 879-893.

Parak, T., 1973. Rare Earths in the Apatite Iron Ores of Lappland Together with Some Data About the Sr, Th and U Content of These Ores. Economic Geology 68, 210-221.

Petruk, W., 1985. Image Analysis Measurements and Data Presentation for Mineral Dressing Applications, in: Park, W.C., Hausen, D.M., Hagni, R.D. (Eds.), Second International Congress on Applied Mineralogy in the Minerals Industry. Metallurgical Society of the American Institute of Mining, Metallurgical, and Petroleum Engineers, Los Angeles, pp. 9-20.

Petruk, W., 2000. Chapter 1 - General Principles of Applied Mineralogy, in: Petruk, W. (Ed.), Applied Mineralogy in the Mining Industry. Elsevier, Amsterdam, pp. 1-26.

Pooler, R., Dold, B., 2017. Optimization and Quality Control of Automated Quantitative Mineralogy Analysis for Acid Rock Drainage Prediction. Minerals 7, 12.

Raslan, M.F., 2009. Mineralogical and Minerallurgical Characteristics of Samarskite-Y, Columbite and Zircon from Stream Sediments of the Ras Baroud Area, Central Eastern Desert, Egypt. Mining Science 128, 179.

Ren, L., Qiu, H., Zhang, M., Feng, K., Liu, P., Guo, J., Feng, J., 2017. Behavior of Lead Ions in Cassiterite Flotation Using Octanohydroxamic Acid. Industrial & Engineering Chemistry Research 56, 8723-8728.

Richards, R.G., MacHunter, D.M., Gates, P.J., Palmer, M.K., 2000. Gravity Separation of Ultra-Fine (−0.1mm) Minerals Using Spiral Separators. Minerals Engineering 13, 65-77.

Rode, H., 2015. Escondida: Enhancing Our Competitive Advantage, BHP Billiton Investor Briefing, Excondida, Chile. Retrieved Nov 2019 from https://www.bhp.com.

Rogers, J., Stringer, D., Ritchie, M., 2019. China Gears up to Use Rare Earths as a Weapon in Trade War as Summit Approaches. Los Angeles Times. Retrieved Nov 2019 from https://www.latimes.com.

Rosenblum, S., Brownfield, I.K., 2000. Magnetic Susceptibility of Minerals. United States Geological Survey, Reston, USA.

Roy, S., 2012. Recovery Improvement of Fine Magnetic Particles by Floc Magnetic Separation. Mineral Processing and Extractive Metallurgy Review 33, 170-179.

Rudnick, R.L., Gao, S., 2003. Composition of the Continental Crust. Treatise on geochemistry 3, 659.

Sakuhuni, G., Altun, N.E., Klein, B., Tong, L., 2016. A Novel Laboratory Procedure for Predicting Continuous Centrifugal Gravity Concentration Applications: The Gravity Release Analysis. International Journal of Mineral Processing 154, 66-74.

Sanematsu, K., Watanabe, Y., 2016. Characteristics and Genesis of Ion Adsorption-Type Rare Earth Element Deposits, in: Verplanck, P.L., Hitzman, M.W. (Eds.), Rare Earth and Critical Elements in Ore Deposits. Society of Economic Geologists, Littleton.

Schriner, D., 2016. Advanced Beneficiation of Bastnaesite Ore through Centrifugal Concentration and Froth Flotation, MSc Thesis, Metallurgical and Materials Engineering. Colorado School of Mines, Colorado, USA.

Sengupta, D., Gosen, B.S.V., 2016. Placer-Type Rare Earth Element Deposits in: Verplanck, P.L., Hitzman, M.W. (Eds.), Rare Earth and Critical Elements in Ore Deposits. Society of Economic Geologists, Littleton.

Sivamohan, R., Forssberg, E., 1985. Principles of Spiral Concentration. International Journal of Mineral Processing 15, 173-181.

Smythe, D.M., Lombard, A., Coetzee, L.L., 2013. Rare Earth Element Deportment Studies Utilising Qemscan Technology. Minerals Engineering 52, 52-61.

Speirs, J.C., McGowan, H.A., Neil, D.T., 2008. Polar Eolian Sand Transport: Grain Characteristics Determined by an Automated Scanning Electron Microscope (Qemscan®). Arctic, Antarctic, and Alpine Research 40, 731-743.

Spencer, J.F., 1919. The Metals of the Rare Earths. Longmans, Green and Co., London.

Stark, T., Silin, I., Wotruba, H., 2017. Mineral Processing of Eudialyte Ore from Norra Kärr. Journal of Sustainable Metallurgy 3, 32-38.

Svoboda, J., 1994. The Effect of Magnetic Field Strenght on the Efficiency of Magnetic Separation. Minerals Engineering 7, 747-757.

Svoboda, J., 2004. Magnetic Techniques for the Treatment of Materials. Kluwer Academic Publishers, Dordrecht, Netherlands.

Svoboda, J., Fujita, T., 2003. Recent Developments in Magnetic Methods of Material Separation. Minerals Engineering 16, 785-792.

Tian, M., Gao, Z., Sun, W., Han, H., Sun, L., Hu, Y., 2018. Activation Role of Lead Ions in Benzohydroxamic Acid Flotation of Oxide Minerals: New Perspective and New Practice. Journal of Colloid and Interface Science 529, 150-160.

Tong, S.-L., Zhu, W.-Z., Gao, Z.-H., Meng, Y.-X., Peng, R.-L., Lu, G.-C., 2004. Distribution Characteristics of Rare Earth Elements in Children's Scalp Hair from a Rare Earths Mining Area in Southern China. Journal of Environmental Science and Health, Part A 39, 2517-2532.

Traore, A., Conil, P., Houot, R., Save, M., 1995. An Evaluation of the Mozley Mgs for Fine Particle Gravity Separation. Minerals Engineering 8, 767-778.

Trifonov, D.N., 1963. The Rare-Earth Elements. The MacMillan Company, New York, USA.

Turner, J.W.G., Hallewell, M.P., 1993. Process Improvements for Fine Cassiterite Recovery at Wheal Jane. Minerals Engineering 6, 817-829.

United States Department of Energy, 2011. Critical Materials Stategy. United States Department of Energy. Retrieved Nov 2019 from https://www.energy.gov.

Verplanck, P.L., Mariano, A.N., Mariano, A., Jr., 2016. Rare Earth Element Ore Geology of Carbonatites, in: Verplanck, P.L., Hitzman, M.W. (Eds.), Rare Earth and Critical Elements in Ore Deposits. Society of Economic Geologists, Littleton.

Vijayan, S., Meinyk, A.J., Singh, R.D., Nuttall, K., 1989. Rare Earths: Their Mining, Processing, and Growing Industrial Usage. Mining Engineering 41, 97-114.

Williams, N., 2018. Bastnaesite Beneficiation by Froth Flotation and Gravity Separation, MSc Thesis Metallurgical and Materials Engineering. Colorado School of Mines, Colorado, USA.

Wills, B.A., Finch, J., 2016a. Wills' Mineral Processing Technology (Eighth Edition): An Introduction to the Practical Aspects of Ore Treatment and Mineral Recovery. Butterworth-Heinemann, Boston.

Wills, B.A., Finch, J.A., 2016b. Chapter 1 - Introduction, in: Wills, B.A., Finch, J.A. (Eds.), Wills' Mineral Processing Technology (Eighth Edition). Butterworth-Heinemann, Boston, pp. 1-27.

Wills, B.A., Finch, J.A., 2016c. Chapter 10 - Gravity Concentration, in: Wills, B.A., Finch, J.A. (Eds.), Wills' Mineral Processing Technology (Eighth Edition). Butterworth-Heinemann, Boston, pp. 223-244.

Wills, B.A., Finch, J.A., 2016d. Chapter 11 - Dense Medium Separation (Dms), in: Wills, B.A., Finch, J.A. (Eds.), Wills' Mineral Processing Technology (Eighth Edition). Butterworth-Heinemann, Boston, pp. 245-264.

Wills, B.A., Finch, J.A., 2016e. Chapter 13 - Magnetic and Electrical Separation, in: Wills, B.A., Finch, J.A. (Eds.), Wills' Mineral Processing Technology (Eighth Edition). Butterworth-Heinemann, Boston, pp. 381-407.

Xia, L., Hart, B., Loshusan, B., 2015. A Tof-Sims Analysis of the Effect of Lead Nitrate on Rare Earth Flotation. Minerals Engineering 70, 119-129.

Xiong, W., Deng, J., Chen, B., Deng, S., Wei, D., 2018. Flotation-Magnetic Separation for the Beneficiation of Rare Earth Ores. Minerals Engineering 119, 49-56.

Xu, L., Tian, J., Wu, H., Lu, Z., Yang, Y., Sun, W., Hu, Y., 2017. Effect of Pb^{2+} Ions on Ilmenite Flotation and Adsorption of Benzohydroxamic Acid as a Collector. Applied Surface Science 425, 796-802.

Yang, H., Rong, Y., Tang, R., Xue, X.-X., Li, Y., 2013a. Recovery of Iron from Baotou Rare Earth Tailings by Magnetizing Roast. Rare Metals 32, 616-621.

Yang, X., Satur, J.V., Sanematsu, K., Laukkanen, J., Saastamoinen, T., 2015. Beneficiation Studies of a Complex Ree Ore. Minerals Engineering 71, 55-64.

Yang, X.J., Lin, A., Li, X.-L., Wu, Y., Zhou, W., Chen, Z., 2013b. China's Ion-Adsorption Rare Earth Resources, Mining Consequences and Preservation. Environmental Development 8, 131-136.

Yin, X., Tian, X., Wu, Y., Zhang, Q., Wang, W., Li, B., Gong, Y., Zuo, T., 2018. Recycling Rare Earth Elements from Waste Cathode Ray Tube Phosphors: Experimental Study and Mechanism Analysis. Journal of Cleaner Production 205, 58-66.

Zepf, V., 2013. Rare Earth Elements: A New Approach to the Nexus of Supply, Demand and Use: Exemplified Along the Use of Neodymium in Permanent Magnets. Springer, Berlin.

Zepf, V., 2016. Chapter 1 - an Overview of the Usefulness and Strategic Value of Rare Earth Metals, in: Borges De Lima, I., Leal Filho, W. (Eds.), Rare Earths Industry. Elsevier, Boston, pp. 3-17.

Zhang, J., Edwards, C., 2012. A Review of Rare Earth Mineral Processing Technology, 44th Annual Canadian Mineral Processors Operators Conference, Ottawa, Canada.

Zhang, Y., 2016. Froth Flotation of Xenotime, MSc Thesis, Metallurgical and Materials Engineering. Colorado School of Mines, Colorado, USA.

Appendix A

Preliminary Experimental Work

A.1 Overview of Appendix A

Appendix A contains two published manuscripts containing preliminary experimental work which was completed during this research program. Both studies provided insightful information to direct the studies found in the thesis, however, are generally outside of its main scope. The first, titled "The potential for dense medium separation of mineral fines using a laboratory Falcon Concentrator", is published in *Minerals Engineering* and details a novel use of a Falcon Concentrator to process Nechalcho gravity tails by dense medium separation. This paper details some early work demonstrating the potential of using gravity separation to process this ore, even at ultra fine particle sizes (d_{80} = 11 μm). The second, also published in *Minerals Engineering,* is titled "A design of experiments investigation into the processing of fine low specific gravity minerals using a laboratory Knelson Concentrator". This manuscript focuses on determining optimal operating conditions of a Knelson Concentrator when processing a synthetic ore of magnetite and quartz sized at – 53 μm. Although this work is not performed on REM, magnetite is used instead as it is easy to obtain in large quantities and has a similar specific gravity to many of the REM in the Nechalacho deposit. The operating conditions determined in this paper to provide the best grade and recovery of magnetite were those used for the Knelson Concentrator testwork in this thesis.

A.2 The Potential for Dense Medium Separation of Mineral Fines Using a Laboratory Falcon Concentrator

Dense medium separation (DMS) is a technique used to separate particles based on specific gravity. While industrially limited by particle size, this technique is an effective method to asses the applicability of gravity separation to an ore at the laboratory scale. At the laboratory scale, separation using a static bath or centrifuge can be used. This study examined the use of a traditional laboratory centrifuge as well as a Falcon Concentrator, modified to act as a DMS centrifuge. While the primary focus of this work was the development and testing of the modified Falcon Concentrator, it does demonstrate that gravity separation may be an effective method of concentrating the ore. This manuscript has been published in the peer-reviewed journal *Minerals Engineering* (Marion, C., Williams, H., Langlois, R., Kökkılıç, O., Coelho, F., Awais, M., Rowson, N.A., Waters, K.E., 2017. The Potential for Dense Medium Separation of Mineral Fines Using a Laboratory Falcon Concentrator. Minerals Engineering 105, 7-9) and is reproduced below.

Abstract

Dense medium separation (DMS) is a technique used to separate particles based on specific gravity. Conventional DMS is, however, limited to coarse particle sizes and is not practical when processing fines. To improve the separation efficiency when processing fine particles, centrifugal separators have been employed. This work investigated DMS in a lab centrifuge and a modified Falcon Concentrator, in order to process the slimes of a rare earth ore. It has been shown that centrifugal concentration using a dense medium is possible when recovering values from a slimes fraction. Both the lab centrifuge and modified Falcon Concentrator resulted in a similar performance.

A.2.1 Introduction

Dense medium separation (DMS) is a process by which particles are separated based on differences in specific gravity (SG). The process can be controlled with a high degree of precision over a wide range of separating densities and is commonly applied as a pre-concentration step for minerals (such as cassiterite) and in the separation of coal from contaminants (Wills and Finch, 2016). An aqueous suspension of fine particles (significantly finer than the particles that are being separated) or a heavy liquid with a predetermined density is utilised as the medium and particles with a SG less than the liquid will float and those with a SG greater than the liquid will sink. Traditionally, DMS is performed using static bath separators, for which separation is only practical at coarse particle sizes (> 4 mm) as the slow settling rates of fine particles result in a poor separation efficiency (Wills and Finch, 2016). To improve the separation efficiency of finer particles, centrifugal separators have been employed to aid in their migration through the dense medium. Industrially, centrifugal DMS is considered practical for particle sizes down to 0.5 mm in diameter (Wills and Finch, 2016), however, several initiatives to beneficiate fine coal have shown that good separation can be achieved for particle sizes down to 25 μm (Aktaş *et al.*, 1998; Klima *et al.*, 1995), and more recently, work by Hirajima *et al.* (2005), investigating centrifugal DMS for the recycling of rare earth-activated phosphors from waste fluorescent lamps, demonstrated effective separation of particles with a size of 3 – 13 μm.

The use of a centrifuge to separate material on the basis of density is not only limited to DMS. A similar process to centrifugal DMS, known as density gradient centrifugation, is widely used in molecular biology for separating particles such as viruses, ribosomes or molecules (such as DNA) (Brakke, 1951; Hinton and Dobrota, 1978). Centrifuges are also employed to separate suspended solids from liquids in other industries, such as food and agriculture, pharmaceutical and biotechnology, environmental industries, and chemical industries (Beveridge, 2000).

This work investigates using a modified laboratory scale Falcon Concentrator as a DMS centrifuge to process fines from the Nechalacho deposit in Canada, which is being investigated for its rare earth potential (Jordens *et al.*, 2013; Jordens *et al.*, 2014; Xia *et al.*, 2015). While there are multiple rare earth minerals in this deposit, zircon is the mineral of greatest importance due to its high content of the significantly more valuable rare earth elements (Ciuculescu *et al.*, 2013; Grammatikopoulos *et al.*, 2011).

A.2.2 Materials and Experimental Methodology

A.2.2.1 Materials

The raw material used in this work was obtained from the Nechalacho Deposit (Avalon Advanced Materials Inc., Canada) located in the Northwest Territories of Canada. Prior to DMS experiments, the ore was subject to a series of gravity and magnetic separation experiments detailed in Jordens *et al.* (2016a). The gravity tailings were then passed through a lab-scale model WD(20) wet drum permanent magnet to remove magnetite. The non-magnetic fraction was then passed through a 2" de-sliming hydrocyclone (Salter Cyclones Ltd, UK) with a cut size of approximately 4 μm and operating pressure of 30 psi. The slimes fraction (overflow) of the hydrocyclone was then used as the feed (d_{50} = 3.9 μm, d_{80} = 11.2 μm) for the DMS experiments. Lithium metatungstate (LMT) [LMT Liquid, LLC (USA)] with a density of 2.95 was used for all DMS experiments.

A.2.2.2 Dense Medium Separation in Lab Centrifuge

Centrifugal DMS was performed using an IEC Centra CL2 centrifuge (Thermo Electron Corporation, USA). Samples were added to 35 mL of heavy liquid solution to give a solid content of 12.5 $\%_{w/w}$ in 50 mL centrifuge tubes. The suspensions were then mixed by hand shaking the sample and centrifuged for 15 min at 4400 rpm. Six repeat tests were performed and the heavy and light fractions from each were mass balanced and analyzed separately using x-ray fluorescence (XRF) analysis. All XRF analysis in this work was performed using a Niton XL3t GOLDD+ XRF analyzer (Thermo Fisher Scientific, USA).

A.2.2.3 Dense Medium Separation in a Modified Falcon Concentrator

The Falcon Concentrator (model SB-6A manufactured by Sepro Mineral Systems, Canada) used in this work was equipped with an ultrafine (U/F) bowl. The unit was modified with a lid to seal the bowl, allowing for the sample and heavy liquid to be contained throughout the experiment. The bottom of the bowl was filled with a mouldable plastic to create a flat base for ease of emptying. A schematic of the modified Falcon U/F bowl can be seen in Figure A.1. Prior to beginning the test, the sample was added to 200 mL of heavy liquid solution to ensure a solid content of 12.5 $\%_{w/w}$. The Falcon Concentrator was operated at 1550 rpm for 60 min. Particles which remained attached to the bowl walls after operation were considered the "heavy" fraction and the remaining particles made up the "light" fraction. Four repeat tests were performed and light and heavy fractions from each test were then individually analyzed using XRF analysis.

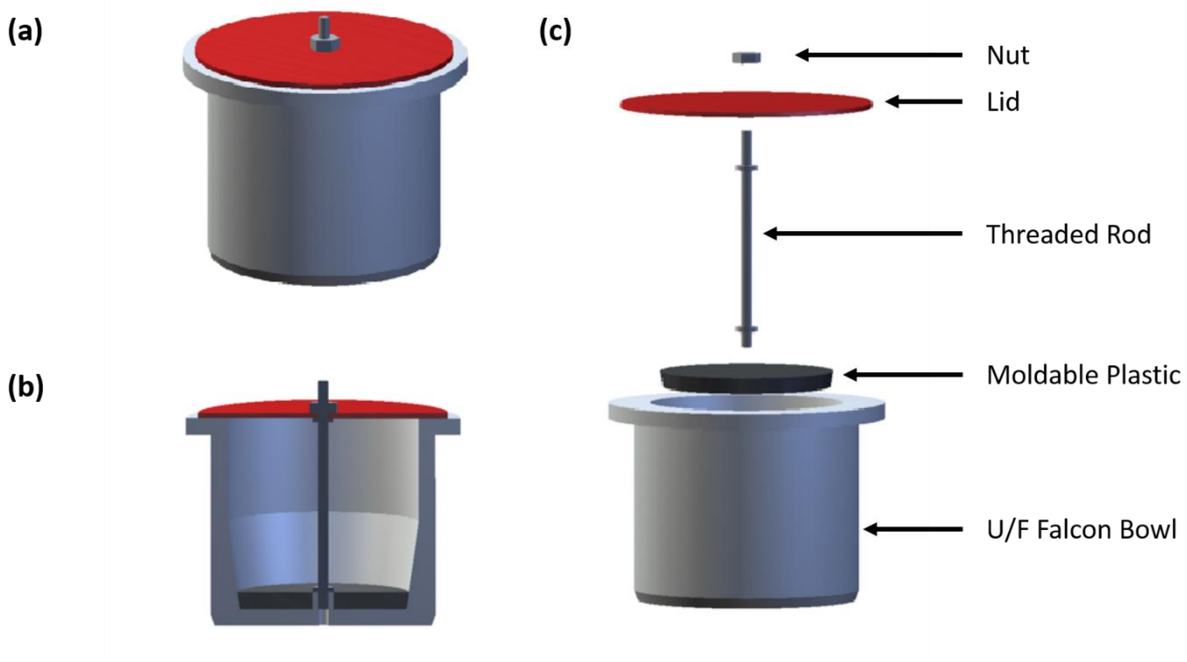

Figure A.1 (a) front view, (b) cross-sectional view and (c) exploded view of the modified Falcon U/F bowl

A.2.3 Results and Discussion

A.2.3.1 Dense Medium Separation in Lab Centrifuge

The elemental grades and recovery of the heavy and light fractions produced from DMS performed in a lab centrifuge are shown in Table A.1 and A.2 respectively. The elemental distribution indicates that Zr, and therefore zircon (SG 4.65) (as it is the only Zr bearing mineral in the deposit), is more abundant in the heavy fraction, with an upgrade ratio of 2.9. The recovery of zircon to the heavy fraction is 71 %. The increased Fe content in the heavy fraction also suggests that iron oxide minerals [magnetite (SG 5.17) and hematite (SG 5.26)] are being concentrated. However, the relatively low recovery of Fe (46.9 %) in the heavy fraction may suggest that these minerals remain locked to silicate gangue, causing them to report to the light fraction. The elevated Si content in the light fraction, suggests that silicate gangue minerals [quartz (SG 2.65) and feldspars (SG 2.55-2.76)] are reporting to the light fraction.

Table A.1 Elemental grade of heavy and light fractions produced from DMS in a lab centrifuge

Sample	Si (%)	95 % confidence	Fe (%)	95 % confidence	Zr (%)	95 % confidence	W (%)	95 % confidence
Feed	12.0	0.7	8.3	0.5	1.2	1.0×10^{-2}	1.4×10^{-2}	4.2×10^{-3}
Heavy	7.1	1.0	16.6	0.9	3.5	0.2	1.6	0.5
Light	14.8	1.6	5.5	1.0	0.4	0.1	0.5	0.1

Table A.2 Elemental recovery of heavy and light fractions produced from DMS in a lab centrifuge

Sample	Si (%)	95 % confidence	Fe (%)	95 % confidence	Zr (%)	95 % confidence
Heavy	12.2	2.2	46.9	4.9	70.8	5.7
Light	87.8	2.2	53.1	4.9	29.2	5.7

While Table A.1 suggests that heavy (SG > 2.95) minerals, most notably zircon, are being concentrated in the heavy fraction it is important to note that there are some discrepancies in the reported values when compared to the feed sample (average of 5 samples analyzed by XRF analysis). This is due to the LMT remaining in the samples after DMS (indicated by the elevated concentration in W in both the heavy and light fractions). This indicates that more work is required to ensure all entrained heavy liquid is removed from the samples, however, W content remains relatively low and is likely to have minimal effect on the values reported in this work.

A.2.3.2 Dense Medium Separation in a Modified Falcon Concentrator

The elemental grades and recoveries of the heavy and light fractions produced from DMS performed in a modified Falcon Concentrator are shown in Table A.3 and A.4 respectively. Similar to the results obtained for the lab centrifuge, the results suggest that heavy minerals (SG > 2.95) are being concentrated in the heavy fraction while minerals with relatively low densities (such as silicate gangue) are reporting to the light fraction. Using the modified Falcon Concentrator results in similar grades to those obtained when using the lab centrifuge, however, significant decreases in recovery are observed. The decreases in Zr and Fe recovery are likely due to the fact that the centrifugal acceleration in the modified Falcon Concentrator (130 times Earth's gravitational acceleration) is much lower than that in the lab centrifuge (2100 times Earth's gravitational acceleration). The significant reduction in centrifugal acceleration likely prevents ultrafine particles from migrating to the wall of the U/F bowl to be collected. This may be a limitation for DMS in a modified Falcon Concentrator, however, more work is required to optimize the process to determine if further improvements in recovery can be made.

Table A.3 Elemental grade of heavy and light fractions produced from DMS in a modified Falcon concentrator

Sample	**Si (%)**	**95 % confidence**	**Fe (%)**	**95 % confidence**	**Zr (%)**	**95 % confidence**	**W (%)**	**95 % confidence**
Feed	12.0	0.7	8.3	0.5	1.2	1.0 x 10^{-2}	1.4 x 10^{-2}	4.2 x 10^{-3}
Heavy	9.5	0.8	16.0	1.0	4.0	0.3	0.4	0.1 0.07
Light	14.8	2.2	5.8	0.5	0.7	0.1	0.5	0.2

Table A.4 Elemental recovery of heavy and light fractions produced from DMS in a modified Falcon concentrator

Sample	**Si (%)**	**95 % confidence**	**Fe (%)**	**95 % confidence**	**Zr (%)**	**95 % confidence**
Heavy	9.6	2.3	31.4	2.6	48.4	4.3
Light	90.5	2.3	68.6	2.6	51.6	4.3

A.2.4 Conclusions

It has been shown that centrifugal concentration using a dense medium is possible when recovering values from a slimes fraction. The use of a modified Falcon Concentrator U/F bowl resulted in a similar performance to that of the standard centrifuge used. Further work is required to optimise this process, and to remove all entrained heavy liquid.

This technique has potential for processing high value slimes, where any loss of value may have a significant impact on the profitability of a mineral processing plant.

A.2.5 Acknowledgments

The authors would like to acknowledge the Natural Sciences and Engineering Research Council of Canada (NSERC) and Avalon Advanced Materials Inc. for providing funding for this work through the Collaborative Research and Development (CRD) program (CRDPJ 445372-12). C. Marion would also like to acknowledge funding from the McGill Engineering Doctoral Award. M. Awais and F. Coelho received funding from the European Community's Horizon 2020 Programme ([H2020/2014-2019]) under Grant Agreement no. 674973 (MSCA-ETN DEMETER – Project website: http://etn-demeter.eu). This publication reflects only the authors' views, exempting the Community from any liability.

A.3 A Design of Experiments Investigation into the Processing of Fine Low Specific Gravity Minerals Using a Laboratory Knelson Concentrator

This study was performed to determine operating conditions which could provide more ideal separation when using the Knelson Concentrator to beneficiate the Nechalacho ore after it is ground to a particle size range below 53 µm. The work employed a synthetic ore comprised of magnetite (which has a similar SG to the heavy minerals found in the Nechalacho deposit) and quartz (similar SG to the deposits gangue). The conditions determined from this study were those which were used for the Knelson Concentrator test work in this thesis. This manuscript has been published in the peer-reviewed journal *Minerals Engineering* (Marion, C., Langlois, R., Kökkılıç, O., Zhou, M., Williams, H., Awais, M., Rowson, N.A., Waters, K.E., 2019. A Design of Experiments Investigation into the Processing of Fine Low Specific Gravity Minerals Using a Laboratory Knelson Concentrator. Minerals Engineering 135, 139-155) and is reproduced below.

Abstract

Fine grinding, required to liberate valuable minerals in finely disseminated deposits, creates significant challenges for beneficiation. For these deposits, traditional gravity separation techniques are often ineffective, and centrifugal separators, such as the Knelson Concentrator, are required. The Knelson Concentrator is well established for treating gold ores, and due to its relatively low cost and small environmental impact when compared to other separation techniques, it has become an active area of research for the processing of lower specific gravity (SG) minerals. This work investigates the optimum operating conditions when processing fine (-53 μm) low SG material using a laboratory Knelson Concentrator. A synthetic feed comprised of magnetite (SG 5.2) and quartz (SG 2.65), with grades of 5 %, 10 % and 15 % magnetite, was used to mimic a low-density ore. Central composite design was used to design the experiments and response surface method was used for optimization, with the experimental variables being bowl speed (G), fluidizing water rate (L/min) and solids feed rate (g/min). The results indicate, for 5 % and 10 % magnetite feeds, that bowl speed impacts concentrate grade negatively and heavy mineral recovery positively, while the fluidizing water rate has an opposite effect on separation. A trade off between grade and recovery must therefore be made when processing this material. When processing the 15 % feed, maximum concentrate grade and magnetite recovery were achieved at high bowl speeds and low fluidizing water rates.

A.3.1 Introduction

As mineral deposits are becoming increasingly more finely disseminated, the recovery of valuable minerals is exceedingly more difficult. Fine grinding, required for liberation, creates many challenges when trying to treat these ores, and many separation techniques become ineffective. Gravity separation techniques, used to separate minerals based on differences in specific gravity (SG), traditionally require relatively coarse material to efficiently concentrate valuable minerals. However, the development of centrifugal gravity separators, such as the Knelson Concentrator, has allowed for the processing of much finer material. The Knelson Concentrator is a compact centrifugal separator with an active fluidized bed to concentrate high SG minerals (Knelson, 1992; Knelson and Jones, 1994). It was initially developed for gold processing, which commonly employed semi-batch units, as the yield to the concentrate was typically below 1 %. However, due to its relatively low cost, small environmental impact when compared to other separation techniques (such as froth flotation), and the development of the Continuous Variable Discharge (CVD) concentrator, the Knelson has become an active area of research for the processing of many low-SG deposits. A summary of the various low-SG minerals for which the Knelson Concentrator has been applied is shown in Table A.5. Although these studies demonstrate that the Knelson Concentrator can be an effective step in the processing of these ores, they are predominately focused on relatively coarse material with little work on optimizing operating variables for separation. Those which do investigate the impact of operating variables, generally do so studying one factor at a time (OFAT). While OFAT analysis can give some basic understanding of how operating variables impact separation, it would require a significant amount of test work to determine optimum conditions and gives no information regarding the interaction of the factors investigated. The type of analysis (single condition, OFAT, experimental design) and the best conditions found by each study are shown in Table A.5.

In this study central composite design (CCD) is used to design the experiments and response surface method (RSM) is used for optimization. The experimental variables are bowl speed (G), fluidizing water rate (L/min) and solids feed rate (g/min). A synthetic feed comprised of magnetite and quartz was used to mimic a low-density ore. Three different feed samples with varying magnetite grades (5 %, 10 % and 15 %) were investigated to determine how feed grade impacts the optimum operating conditions. The rational behind this study is to determine ideal operating conditions for processing fine (-53 µm) low-density material using a laboratory Knelson Concentrator; and to serve as a reference for the optimization of plant operations.

Table A.5 – Summary of literature focused on the use of a Knelson Concentrator to process low-SG minerals

Value Mineral	Specific Gravity	Feed Particle Size (µm)	Feed Grade (%) [3]	Knelson Unit	Enrichment Ratio	Method of Analysis	Best Operating Conditions			Reference
							BS [4]	FWR [4]	FR [4]	
Cassiterite	7	$d_{80} = 160$	7^{M}	KC-MD3	2	Single Condition	40 G	1.6 L/min	50 g/min	(Angadi *et al.*, 2017)
Chromite	4.6	$d_{80} = 150$	25^{O}	KC-MD3	1.7	Experimental Design	60 G	11 L/min	200 g/min	(Akar Sen, 2016)
Colemanite [1]	2.4	-500	2.4^{E}	KC-MD3	0.41	OFAT	11 G	1 L/min	-	(Savas, 2016)
Coal [1]	1.1 – 1.4	-1000	11^{A}	KC-MD3	Not Reported	OFAT	60 G	30 kPa	-	(Butcher and Rowson, 1995)
		$d_{70} = 250$	36^{A}	KC-MD3	0.47	OFAT	30 G	20 kPa	-	(Majumder *et al.*, 2007)
		-200	19^{A}	KC-MD3	0.79	OFAT	60 G	14 kPa	-	(Rubiera *et al.*, 1997)
		-106	20^{A}	KC-MD3	Not Reported	OFAT	60 G	20 kPa	-	(Uslu *et al.*, 2012)
		-210 +44	39^{A}	CVD6	0.38	Experimental Design	900 rpm	8.2 L/min	-	(Honaker *et al.*, 2005)
		-150 +44	21^{A}	CVD6	0.40	Experimental Design	1100 rpm	7.5 L/min	-	(Honaker and Das, 2004)
Magnetite	5.2	Not Reported	$\leq 5^{M}$	CVD6	≥ 14	OFAT	40 G	-	-	(Fullam and Grewal, 2001)
		-180 +150	4^{M}	KC-MD3	8	Experimental Design	30 G	34 kPa	300 g/min	(Ghaffari and Farzanegan, 2017)
		$d_{80} = 125$	4^{M}	CVD6	20	OFAT	700 rpm	23 L/min	-	(McLeavy *et al.*, 2001)
		Not Reported	5^{M}	CVD6	5	OFAT	60 G	30 L/min	-	(Sakuhuni *et al.*, 2015)
		$d_{80} = 135$	5^{M}	KC-MD3	5	Single Condition	60 G	13 L/min	500 g/min	(Sakuhuni *et al.*, 2016)
Pentlandite	4.6 – 5	$d_{80} = 94$	0.5^{E}	KC-MD3	1.5	Single Condition	-	-	-	(Klein *et al.*, 2016)
				CVD6	1.5	OFAT	60 G	30 L/min	-	
Rare Earth Minerals	3.8 – 6.3	$d_{80} = 40$	20^{M}	KC-MD3	1.6 – 3.3	Single Condition	40 G	6 L/min	200 g/min	(Jordens *et al.*, 2016b)
Gold Bearing Sulphides [2]	5.0 – 7.6	Not Reported	0.7 ppm^{E}	KC-MD3	2 - 7	Single Condition	60 G	13 L/min	500 g/min	(Sakuhuni *et al.*, 2016)
	5.0 – 7.6	Not Reported	0.7 ppm^{E}	CVD6	1.5 - 4	Single Condition	-	-	-	(Sakuhuni *et al.*, 2016)
	3.9 – 7.6	$d_{50} = 150$	16 ppm^{E}	CVD6	4	OFAT	30 G	30 L/min	1 t/hr	(Altun *et al.*, 2015)
	3.9 – 4.2	$d_{80} = 103$	5 ppm^{E}	CVD6	7	OFAT	700 rpm	23 L/min	-	(McLeavy *et al.*, 2001)
	5.0 – 6.2	$d_{80} = 130$	1 ppm^{E}	KC-MD3	5	Single Condition	-	-	-	(Klein *et al.*, 2010)
	5.0 – 6.2	$d_{80} = 130$	1 ppm^{E}	CVD6	10	OFAT	60 G	43 L/min	-	(Klein *et al.*, 2010)
Tantalum Bearing Minerals	6.5 – 7.2	$d_{45} = 12$	0.1^{O}	KC-MD3	6	Single Condition	-	-	-	(Burt *et al.*, 1995)
		$d_{85} = 212$	0.04^{O}	CVD6	34	OFAT	30 G	33	1.1 t/hr	(Fullam and Grewal, 2001)
Heavy Mineral Sands	4.2 – 4.7	$d_{80} = 190$	2.4^{M}	KC-MD3	3.3	Single Condition	-	-	-	(Gonçalves and Braga, 2016)
	4.2 – 4.8	- 125 + 63	33^{E}	KC-MD3	1.2	OFAT	60 G	62.1 kPa	-	(Premaratne and Rowson, 2004)

[1] For coal and colemanite the Knelson Concentrator is used to remove relatively high SG contaminates. Enrichment ratios are those of the contaminate in the valuable (Knelson tailings) fraction.

[2] The SG presented for gold bearing sulphides is that of the associated minerals. The actual value may be slightly elevated due to the inclusions of gold. Feed grades reported are that of gold and not the associated sulphide minerals

[3] Feed grades reported as mineral (^{M}), metal oxide (^{O}), elemental (^{E}) or ash (^{A}) content.

[4] BS, FWR and FR refer to bowl speed, fluidizing water rate and feed rate respectively.

A.3.2 Materials and Methods

A.3.2.1 Materials

Magnetite used for this work was obtained from Gem and Mineral Miners Inc. (USA) and the quartz used in this study was purchased from U.S. Silica (USA). Magnetite was pulverized using a LM2 laboratory pulverizing mill (Labtechnics, Australia) and screened to -53 ,μm and subsequently purified using a lab-scale WD(20) wet drum permanent magnetic separator (Carpco Inc., USA), equipped with an iron-based permanent magnet (low intensity; 0.03 T at drum surface). The quartz was screened wet at 53 μm to remove any oversize quartz particles. The particle size distribution [determined using a LA-920 particle size analyser (Horiba, Japan)] of magnetite and quartz are shown in Figure A.2. Magnetite and quartz were then sampled to produce 1 kg samples with a feed grades of 5 %, 10 % and 15 %. Hydrochloric acid used in this work was purchased from Fisher Scientific (USA).

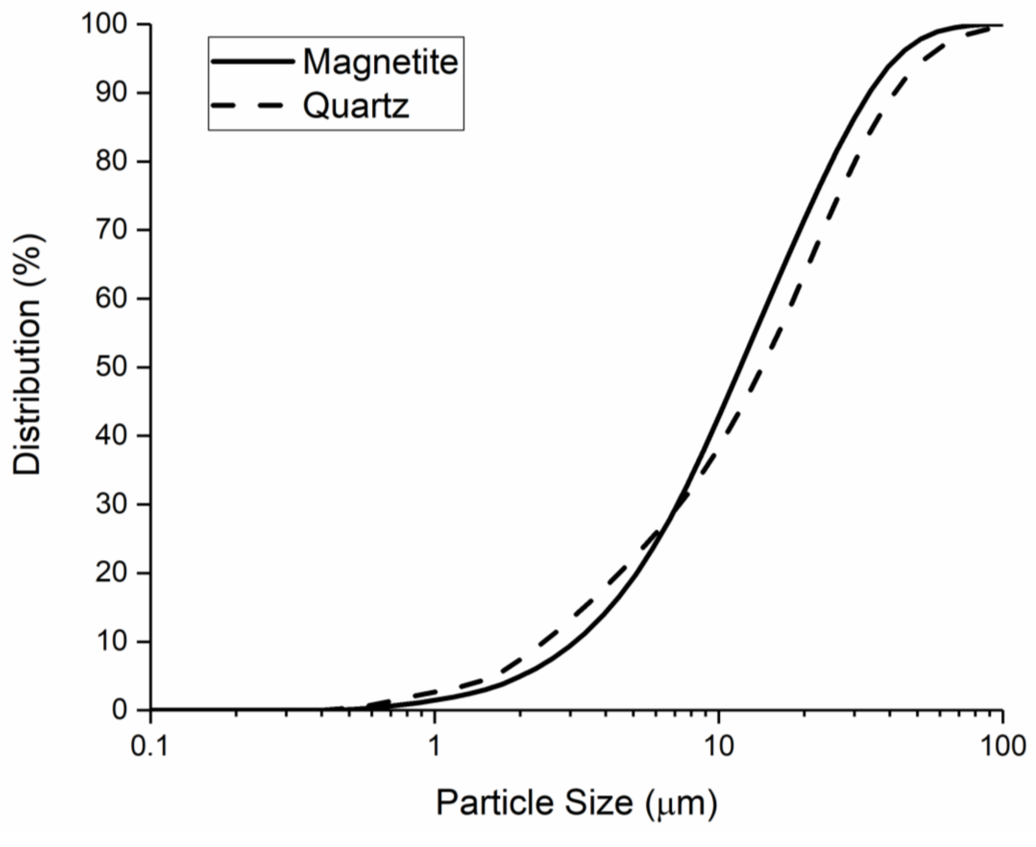

Figure A.2 – Particle size distribution of magnetite and quartz samples

A.3.2.2 Methods

A lab scale KC-MD3 Knelson Concentrator (FLSmidth, Canada) was used for this study. For each test, 1 kg of synthetic sample was used. Independent variables [bowl speed (G), fluidizing water rate (L/min) and solids feed rate (g/min)] were set to their desired conditions. The range used for bowl speed and fluidizing water rater were based on the limitations of the equipment (maximum and minimum possible speeds of the unit; maximum fluidizing water rate to prevent washing of all the material from the bowl and minimum to maintain for sufficient fluidization for separation). The range of feed rate was based on the work of Prof. Laplante who suggested feed rates of 300 g/min for 75 µm material when performing gravity recovery gold test work (Clarke, 2005; Xiao *et al.*, 2009). This feed rate was set as the maximum value studied here. The feed was fed dry to the feed cone where it was slurried with water at a rate of approximately 1.5 L/min. Slurrying water rate was not considered as an independent variable, as the effect of solids concentration over the range of feed blends investigated is expected to be minimal. Following each test, the bowl was emptied, filtered and dried. Three representative samples from each concentrate were analysed by digesting magnetite with hydrochloric acid. The residual mass was then dried, weighed and compared to the original mass of the digested sample to calculate magnetite grade and recovery.

RSM was used to investigate the relationship between independent variables and the response; and possible interactions between the independent variables and their effects on the separation performance of a Knelson Concentrator. CCD, a well-suited RSM for fitting a second-order response surface, was used to design the experiments (Box and Hunter, 1957; Box and Wilson, 1992; Chen and Parlar, 2013; Montgomery, 2009; Yi *et al.*, 2010). Each variable has five levels ($\pm\beta$, ±1, 0 where $\beta = 2^{3/4} = 1.682$), with grade and recovery of magnetite chosen as the responses.

The number of tests required for the CCD can be calculated using equation A.1, which contains the standard 2^k factorial with its origin at the centre, $2k$ points at a distance, β, from the centre to generate the quadratic terms, and replicate tests at the centre (Box and Hunter, 1957; Kökkılıç *et al.*, 2015; Montgomery, 2009; Zhou *et al.*, 2016).

$$N = 2^k + 2k + n_0 \tag{A.1}$$

With three variables (k) and six replicates at the centre point (n_0), the number of tests required for each feed grade investigated is 20 (Kökkılıç *et al.*, 2015; Montgomery, 2009; Obeng *et al.*, 2005;

Zhou *et al.*, 2016). The independent variables are designated as x_1, x_2 and x_3 and the predicted responses, grade and recovery, are designated as y_1 and y_2 respectively. The coded values were calculated as shown in Table A.6. These were used to determine the levels of the independent variables for each of the 20 experiments.

Table A.6 – Independent variables and their levels

Independent Variables	Symbol	Coded Variable Level				
		Lowest	**Low**	**Centre**	**High**	**Highest**
		-β[a]	**-1**	**0**	**+1**	**+β[a]**
Bowl Speed (G)	x_1	10	30	60	90	110
Fluidizing water rate (L/min)	x_2	1	1.8	3	4.2	5
Solids feed rate (g/min)	x_3	100	140	200	260	300

[a] : 1.682

For each Knelson test, the bowl speed, fluidizing water rate and solids feed rate were changed successively during the tests with respect to the central composite design. The mathematical relationship between the three independent variables and responses can be approximated by a second order model, such as equation A.2:

$$y = \beta_0 + \beta_1 x_1 + \beta_2 x_2 + \beta_3 x_3 + \beta_{11} x_1^2 + \beta_{22} x_2^2 + \beta_{33} x_3^2 + \beta_{12} x_1 x_2 + \beta_{13} x_1 x_3 + \beta_{23} x_2 x_3 + \varepsilon \quad \text{(A.2)}$$

where y is the predicted response; β_0 is the model constant; x_1, x_2 and x_3 are the variables; β_1, β_2 and β_3 are linear coefficients; β_{12}, β_{13} and β_{23} are cross-product coefficients; and β_{11}, β_{22} and β_{33} are the quadratic coefficients (Kökkılıç *et al.*, 2015; Kwak, 2005; Montgomery, 2009; Zhou *et al.*, 2016). Minitab Statistical Software 17® (Minitab, USA) was used to estimate these coefficients [the main effect (β_i), the quadratic effect (β_{ii}) and two-factor interactions (β_{ij})] from the experimental results.

Using experimental data (grade and recovery) from each experiment, a second order regression model which describes the concentration process was produced. Analysis of Variance (ANOVA) was used to determine the regression coefficients and detect the agreement of the model. Statistical importance of each variable on the response was found at a 95 % confidence level by using Fischer (F) test and p-values. RSM was used to analyse the proposed model and optimization was realized using response surface and contour plots for different interactions of any two independent variables (holding the value of the third variable constant at the centre level). All statistical analyses were conducted using Minitab Statistical Software 17® (Minitab, USA).

A.3.3 Results and Discussion

The responses (grade and recovery) for each test run for the 5 %, 10 % and 15 % feed grades are shown in Tables A.7 – A.9. Due to the difficulty of ensuring the solids feed rate and fluidizing water rate were the same as the coded variables (Table A.6), the actual measured values (shown in Tables A.7 – A.8) were used for statistical analysis. The second order response functions representing grade (y_1) and recovery (y_2) of magnetite in the Knelson concentrate, were expressed as a function of bowl speed (x_1), fluidizing water rate (x_2) and solids feed rate (x_3). The coded model equations are presented in equations A.3 – A.8:

$$y_{1\,5\,\%} = 35.13 - 3.015x_1 + 6.724x_2 - 0.386x_3 + 0.555x_1^2 + 0.469x_2^2 - 0.601x_3^2 - 5.363x_1x_2 + 0.130x_1x_3 + 0.657x_2x_3 \qquad \text{(A.3)}$$

$$y_{2\,5\,\%} = 49.12 + 6.48x_1 + 0.37x_2 - 1.56x_3 - 6.44x_1^2 - 0.36x_2^2 - 0.605x_3^2 - 2.44x_1x_2 - 0.03x_1x_3 + 1.02x_2x_3 \qquad \text{(A.4)}$$

$$y_{1\,10\,\%} = 56.9 - 2.054x_1 + 6.052x_2 + 0.615x_3 - 1.929x_1^2 - 0.686x_2^2 - 0.098x_3^2 + 0.75x_1x_2 + 0.368x_1x_3 - 0.83x_2x_3 \qquad \text{(A.5)}$$

$$y_{2\,10\,\%} = 40.31 + 8.601x_1 - 4.763x_2 + 0.429x_3 - 4.398x_1^2 - 0.835x_2^2 - 0.187x_3^2 + 2.40x_1x_2 - 0.89x_1x_3 + 0.83x_2x_3 \qquad \text{(A.6)}$$

$$y_{1\,15\,\%} = 65.44 + 3.40x_1 + 3.25x_2 + 4.50x_3 + 1.14x_1^2 + 0.22x_2^2 + 1.56x_3^2 - 1.85x_1x_2 + 3.89x_1x_3 - 2.77x_2x_3 \qquad \text{(A.7)}$$

$$y_{2\,15\,\%} = 36.34 + 12.27x_1 - 6.53x_2 + 3.511x_3 - 2.41x_1^2 + 0.329x_2^2 + 1.696x_3^2 - 1.96x_1x_2 + 3.92x_1x_3 - 2.47x_2x_3 \qquad \text{(A.8)}$$

Table A.7 – Results of magnetite grade and recovery for the 5% feed

Run	Coded Level of Variables			Actual Measured Level of Variables			Response	
	x_1	x_2	x_3	Bowl Speed (G)	Fluidizing Water Rate (L/min)	Solids Feed Rate (g/min)	Grade (%)	Recovery (%)
1	1	1	-1	90	4.2	152.1	31.1	41.4
2	0	0	-1.68	60	3.1	94.2	35.5	53.6
3	0	1.68	0	60	5.0	204.1	46.7	49.0
4	-1.68	0	0	10	3.0	197.4	41.8	18.9
5	-1	-1	-1	30	1.9	130.2	26.5	31.2
6	0	0	0	60	3.0	205.5	37.8	50.8
7	-1	1	1	30	4.1	270.3	48.5	36.0
8	1	-1	-1	90	1.9	133.3	32.5	51.1
9	1	1	1	90	4.2	257.5	35.0	46.9
10	0	0	0	60	3.0	210.5	35.5	46.7
11	0	-1.68	0	60	1.0	187.5	28.1	51.7
12	0	0	0	60	3.0	202.7	37.6	53.6
13	0	0	0	60	3.0	199.3	35.8	51.4
14	-1	-1	1	30	1.9	254.2	27.2	32.6
15	1.68	0	0	110	2.9	209.8	33.3	46.8
16	0	0	0	60	3.0	202.0	30.8	45.4
17	0	0	0	60	3.0	192.0	32.7	45.9
18	1	-1	1	90	1.8	263.2	28.0	42.3
19	-1	1	-1	30	4.2	135.1	51.9	40.4
20	0	0	1.68	60	3.0	317.5	32.5	43.8

Table A.8 – Results of magnetite grade and recovery for the 10% feed

Run	Coded Level of Variables			Actual Measured Level of Variables			Response	
	x_1	x_2	x_3	Bowl Speed (G)	Fluidizing Water Rate (L/min)	Solids Feed Rate (g/min)	Grade (%)	Recovery (%)
1	1	1	-1	90	4.2	129	58.0	39.7
2	0	0	-1.68	60	3.0	83	54.1	39.1
3	0	1.68	0	60	5.0	190	66.6	29.8
4	-1.68	0	0	10	3.1	210	50.6	7.7
5	-1	-1	-1	30	1.8	103	51.6	34.1
6	0	0	0	60	3.0	237	55.0	38.9
7	-1	1	1	30	4.3	268	63.4	24.8
8	1	-1	-1	90	1.8	135	43.2	45.1
9	1	1	1	90	4.2	243	55.8	38.1
10	0	0	0	60	3.0	196	57.6	40.8
11	0	-1.68	0	60	1.1	180	41.1	45.1
12	0	0	0	60	3.0	178	56.0	41.3
13	0	0	0	60	3.0	206	58.1	40.3
14	-1	-1	1	30	1.8	248	55.1	37.5
15	1.68	0	0	110	3.1	213	51.4	46.7
16	0	0	0	60	3.0	199	57.9	39.7
17	0	0	0	60	3.0	191	57.2	40.5
18	1	-1	1	90	1.8	253	47.5	43.8
19	-1	1	-1	30	4.2	157	61.9	19.1
20	0	0	1.68	60	3.1	390	57.6	39.1

Table A.9 – Results of magnetite grade and recovery for the 15% feed

Run	Coded Level of Variables			Actual Measured Level of Variables			Response	
	x_1	x_2	x_3	Bowl Speed (G)	Fluidizing Water Rate (L/min)	Solids Feed Rate (g/min)	Grade (%)	Recovery (%)
1	1	1	-1	90	4.1	131	69.3	38.7
2	0	0	-1.68	60	2.9	103	62.5	35.7
3	0	1.68	0	60	5.1	122	74.8	28.3
4	-1.68	0	0	10	3.0	160	63.9	8.7
5	-1	-1	-1	30	1.7	103	58.2	31.8
6	0	0	0	60	3.0	148	57.0	32.1
7	-1	1	1	30	4.2	226	71.6	21.7
8	1	-1	-1	90	1.7	114	51.6	41.3
9	1	1	1	90	4.1	247	73.6	40.6
10	0	0	0	60	3.0	148	67.3	36.5
11	0	-1.68	0	60	1.0	162	57.0	42.9
12	0	0	0	60	2.9	156	65.0	36.4
13	0	0	0	60	3.1	172	59.7	30.8
14	-1	-1	1	30	1.8	251	60.0	28.7
15	1.68	0	0	110	3.0	167	70.3	45.1
16	0	0	0	60	3.1	195	66.2	35.1
17	0	0	0	60	3.1	175	64.4	36.8
18	1	-1	1	90	1.9	236	78.0	64.9
19	-1	1	-1	30	4.3	139	70.5	20.6
20	0	0	1.68	60	3.1	305	78.9	46.3

To estimate the significance and accuracy of the developed models, ANOVA was applied (Table A.10). *F*-values for all cases are greater than the *F*-value found in the *F*-statistics Table with P=0.05 ($F_{0.05(9,10)}$=3.14); *p*-values of the regression models are smaller than 0.05 and standard deviations are relatively low. Normal probability plots of the residuals and a plot of the residuals versus the fitted response are presented in the Appendix (Figures A.S1 – A.S6). Residuals generally lie on a straight line, indicating errors are distributed normally; and the residuals scatter randomly, suggesting model predictions are adequate. The quality of fit of the polynomials, expressed by R^2 values (Table A.10), is acceptable ($R^2 \geq 0.80$) (Azizi *et al.*, 2012; Joglekar *et al.*, 1987; Saguy and Graf, 1990). Thus, it can be concluded that regression models are significant and accurate.

Once the model was verified, the Student's *t*-test was performed to estimate the quantitative effects of the variables and their interactions. Tables A.11 – A.13 show the summarized Student's *t*-test, for each feed grade, which includes the *p*-value and T-value of each variable. The *p*-values indicate the significance of variables and their interactions, with 95 % confidence; and T-values are the result of the Student's *t*-test and indicate whether each significant variable has a positive or negative effect on the response, as well as how significant they are. All variables and interactions with a p-value ≤ 0.05 are considered as significant, with the magnitude of the T-values indicating the level of significance (greater the magnitude greater the significance). Response surface plots further demonstrating the impact of an input variable on grade and recovery when processing 5 %, 10 % and 15 % magnetite feeds can be found in the Appendix (Figures A.S7 – A.S12).

Table A.10 – Summary of ANOVA for regression models

Feed Grade	Response	*F*-value	*p*-value	R^2	R^2_{adj}	Standard deviation
5 %	Grade	14.66	0.000	0.93	0.87	2.58
	Recovery	7.03	0.003	0.86	0.74	4.46
10 %	Grade	8.30	0.001	0.88	0.78	2.94
	Recovery	17.13	0.000	0.94	0.88	3.26
15 %	Grade	6.75	0.003	0.86	0.73	3.86
	Recovery	18.06	0.000	0.94	0.89	3.79

Table 7 indicates that when processing the 5 % magnetite feed, the two responses are affected by the independent variables differently. Bowl speed (x_1) has significant and opposite effects on grade (negative) and recovery (positive); fluidizing water rate (x_2) has a strong positive influence on grade, however, did not affect recovery significantly; and solids feed rate does not have any significant effect on the response. There is a negative interaction effect on grade, between bowl speed and fluidizing water rate (x_1x_2). Bowl speed also has a negative quadratic effect on recovery. The significant and opposite influence of bowl speed on grade and recovery suggests that different operating conditions will be required to obtain a maximum grade or a maximum recovery.

Similar results were observed when processing the 10 % magnetite feed (Table 8), where high grade and high recovery will occur at different conditions. In this case both bowl speed and fluidizing water rates have significant and opposite effects on grade and recovery. Bowl speed also has a negative quadradic effect on both grade and recovery.

Table 9 shows the influence of independent variables on responses for the 15 % magnetite feed. Bowl speed, fluidizing water rate and solids feed rate are all significant variables for both responses. Grade is affected by all three independent variables positively with their significance decreasing according to solids feed rate > bowl speed > fluidizing water rate. The order of significance of the independent variables on recovery is bowl speed positively > fluidizing water rate negatively > solids feed rate positively. An interaction effect, between bowl speed and solids feed rate, is observed for both responses; and bowl speed has a positive quadratic effect on recovery.

Table A.11 – Summarized Student's t-test for 5 % feed grade

Term	Grade		Recovery	
	***p*-value**	**T-value**	***p*-value**	**T-value**
x_1	**0.001**	-4.33	**0.000**	5.38
x_2	**0.000**	8.82	0.769	0.30
x_3	0.567	-0.59	0.195	-1.39
x_1^2	0.435	0.81	**0.000**	-5.46
x_2^2	0.521	0.66	0.775	-0.29
x_3^2	0.305	-1.08	0.543	-0.63
x_1x_2	**0.000**	-5.79	0.158	-1.52
x_1x_3	0.886	0.15	0.984	-0.02
x_2x_3	0.481	0.73	0.524	1.02

Table A.12 – Summarized Student's t-test for 10 % feed grade

Term	Grade		Recovery	
	***p*-value**	**T-value**	***p*-value**	**T-value**
x_1	**0.029**	-2.55	**0.000**	9.66
x_2	**0.000**	7.33	**0.000**	-5.21
x_3	0.388	0.90	0.582	0.57
x_1^2	**0.035**	-2.44	**0.001**	-5.03
x_2^2	0.425	-0.83	0.382	-0.91
x_3^2	0.776	-0.29	0.627	-0.50
x_1x_2	0.496	0.71	0.067	2.05
x_1x_3	0.720	0.37	0.439	-0.81
x_2x_3	0.434	-0.81	0.477	0.74

Table A.13 – Summarized Student's t-test for 15 % feed grade

Term	Grade		Recovery	
	p-value	T-value	*p*-value	T-value
x_1	**0.018**	2.82	**0.000**	10.36
x_2	**0.034**	2.45	**0.001**	-5.02
x_3	**0.001**	4.50	**0.005**	3.58
x_1^2	0.294	1.11	**0.039**	-2.38
x_2^2	0.835	0.21	0.749	0.33
x_3^2	0.152	1.55	0.116	1.72
x_1x_2	0.213	-1.33	0.181	-1.44
x_1x_3	**0.017**	2.86	**0.015**	2.95
x_2x_3	0.057	-2.15	0.079	-1.96

Although the findings from Tables A.11 – A.13 give a general idea of how independent variables affect the responses, and contour plots (Figures A.S7 – A.S12) show regions where high grade and recovery can be obtained, they do not indicate the optimum separation conditions. More accurate information about the optimum operating conditions and how they affect both grade and recovery simultaneously can be obtained by drawing overlaid contour plots (Figures A.3 – A.5). As both grade and recovery cannot be maximized simultaneously for the 5 % and 10 % magnetite feeds, three points are presented on the overlaid plots (a blue dot for maximum grade, a red dot for maximum recovery and a black dot for the conditions where both grade and recovery are maximized simultaneously). In this study, the optimum operating conditions when considering both grade and recovery were chosen to be where an increase in one did not result in a decrease in the other. For the 15 % magnetite feed a single optimum point could be obtained for both grade and recovery (shown in Figure A.5). The actual predicted values for the optimum conditions of all three feed grades are shown in Table A.14. In some cases, the confidence intervals (95 %) associated with the predicted responses are large, as they are well outside the range of predictor levels (measured responses) used to fit the model. For example, when processing the 15 % magnetite feed the maximum measured grade and recovery were 78.9 % and 64.9 % respectively. However, the model predicts a maximum grade of 91.8 % and recovery 82.7 %, leading to large confidence intervals. To validate the responses at the optimum conditions determined by the model, further experiments were carried out for each feed grade. The validation tests were repeated three times and the results were compared to those predicted by the model (Table A.15). It can be concluded that the proposed equations adequately predict magnetite grade and recovery for all three feed grade conditions (Error < 10 %).

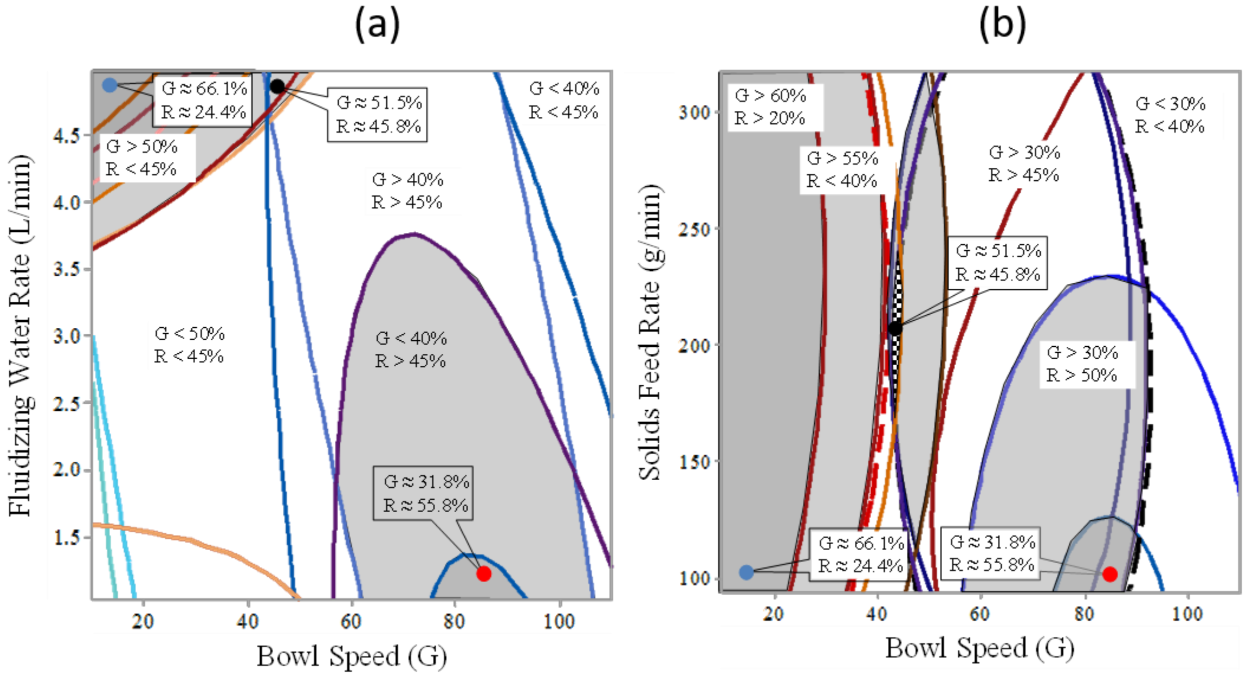

Figure A.3 – Grade and recovery behaviour at different (a) fluidizing water rates and bowl speeds and (b) solids feed rate and bowl speeds for the 5 % magnetite feed

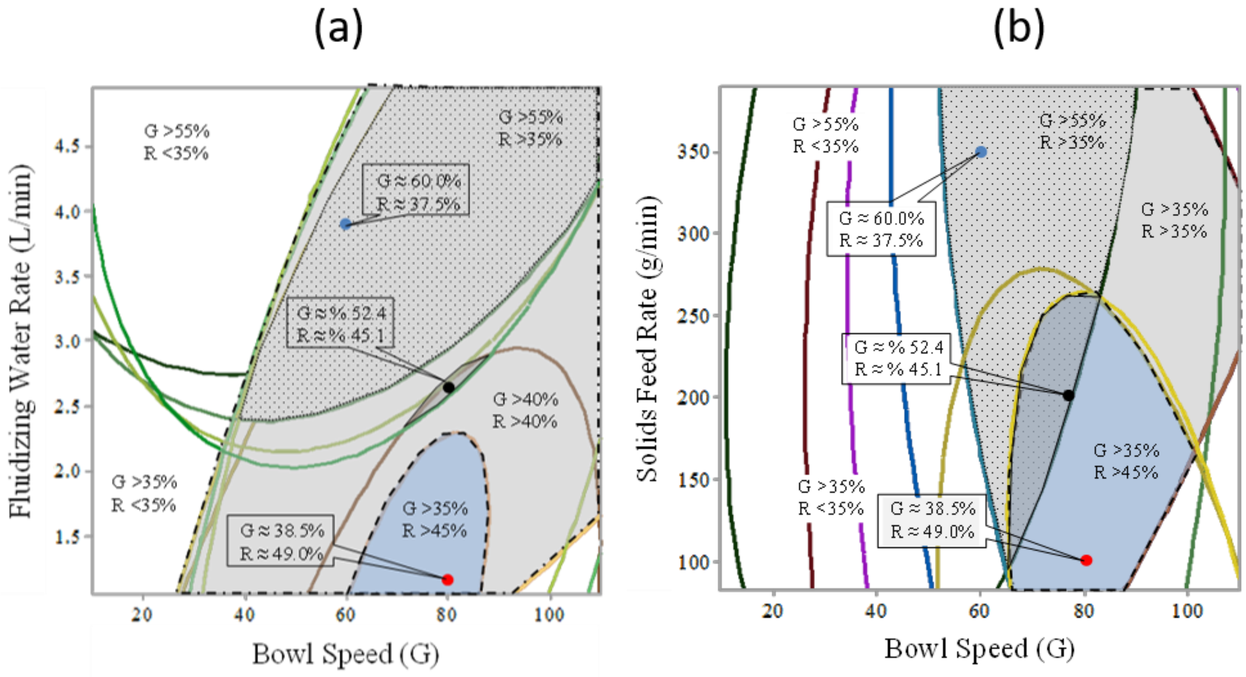

Figure A.4 – Grade and recovery behaviour at different (a) fluidizing water rates and bowl speeds and (b) solids feed rate and bowl speeds for the 10 % magnetite feed

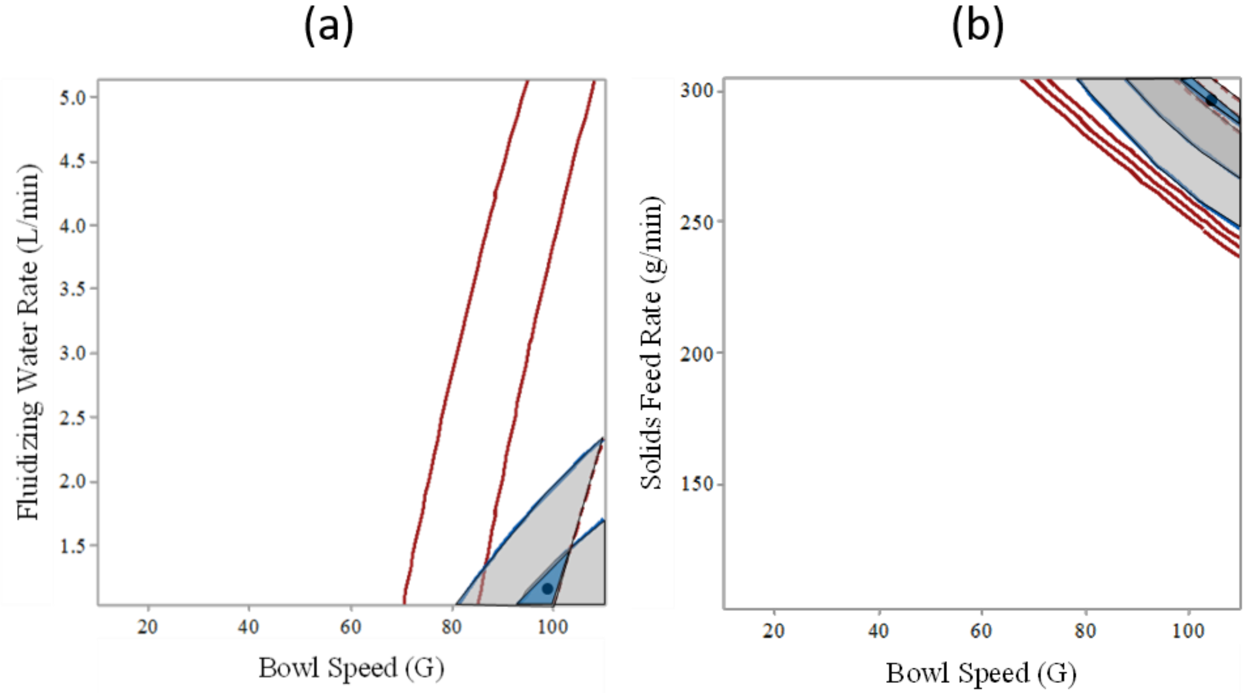

Figure A.5 – Grade and recovery behaviour at different (a) fluidizing water rates and bowl speeds and (b) solids feed rate and bowl speeds for the 15 % magnetite feed

Table A.14 – Optimum conditions for grade and recovery

Feed Grade	Optimized for	Operating Variables Bowl Speed (G)	Fluidizing Water Rate (L/min)	Solids Feed Rate (g/min)	Predicted Response Grade (%)[1]	Recovery (%)[1]
5 %	Grade	10	5.0	100	66.1 ± 11.7	24.4 ± 20.0
	Recovery	85	1.0	100	31.8 ± 8.9	55.7 ± 15.0
	Grade and Recovery	45	4.8	200	51.5 ± 4.2	45.8 ± 7.2
10 %	Grade	60	3.9	350	60.4 ± 5.8	37.7 ± 6.9
	Recovery	80	1.1	100	38.4 ± 8.3	49.0 ± 9.3
	Grade and Recovery	80	2.6	200	52.4 ± 2.6	45.1 ± 2.9
15 %	Grade and Recovery	100	1.1	275	91.8 ± 16.6	82.7 ± 16.2

[1] Error shown for predicted responses represents 95 % confidence intervals

Table A.15– Comparative data at optimum conditions for validation

	Operating Variables			Predicted Response		Validation Tests			
Feed Grade	Bowl Speed (G)	Fluidizing Water Rate (L/min)	Solids Feed Rate (g/min)	Grade (%)	Recovery (%)	Grade (%)[1]	% Error	Recovery (%)[1]	% Error
5 %	45	4.8	200	51.5	45.8	49.6 ± 2.7	-3.7	41.7 ± 1.9	-9.0
10 %	80	2.6	200	52.4	45.1	52.4 ± 1.4	0.0	44.3 ± 2.1	-1.8
15 %	100	1.1	275	91.8	82.7	91.3 ± 1.2	-0.5	84.6 ± 1.2	2.3

[1] Error shown for validation tests represents 95 % confidence intervals

The above findings demonstrate that when processing relatively low grade (≤ 10 %) feed a balance between both bowl speed and fluidizing water rate is required. For high grade feeds (15 %), high grade and high recovery is realized at high bowl speeds, low fluidizing water rates and high solid feed rates. Comparing the significant parameters from each data set it can be concluded that with low feed grades, the force balance acting on particles plays a much greater role in optimizing separation; whereas, with high feed grades optimizing the properties of the fluidizing bed becomes more important.

For the 5 % magnetite feed, product grade is influenced by only bowl speed (negative), fluidizing water rate (positive) and an interaction between bowl speed and fluidizing water rate (negative); whereas, recovery is influenced by only bowl speed (positive) and a quadratic effect of bowl speed (negative). This suggests that high grade is predominantly achieved with low centrifugal force and high drag force to reject as much low SG material as possible and recover only the heaviest material (resulting in low recovery). High recovery is obtained by using high bowl speeds to induce a high centrifugal acceleration on particles and recover as much high SG material as possible. However, this also results in high recovery of low SG material (and therefore low product grades) and after a certain point, further increases in bowl speed result in the process becoming completely unselective and becomes detrimental to recovery.

For the 10 % magnetite feed, it is similarly suggested that a balance between drag force and centrifugal acceleration is required to achieve ideal separation. However, in this case there is a larger quantity of high SG material to replace the low SG particles which are recovered in the concentrating bed throughout the process. This allows for greater substitution of material and the properties of the fluidizing bed become more important. In this case slightly higher bowl speeds are recommended (bowl speed now has a quadratic influence on both product grade and recovery) and fluidizing water rate becomes an important variable for the recovery of magnetite. The negative influence of fluidizing water rate on recovery suggests a tightly packed fluidized particle bed is beneficial.

For the 15 % magnetite feed there is now sufficient high SG material to achieve high grade and recovery simultaneously through the optimization of the properties of the fluidizing bed. High drag forces acting on particles are no longer required to reject low SG material. This now occurs mainly through the substitution of low SG particles for high SG material in the concentrating bed. At this feed grade, elevated bowl speeds are recommended along with low fluidizing water rates to keep a tightly packed concentrating bed. Feed rate is also an important variable with high feed rates desired for optimum separation. There is also a positive interaction between bowl speed and feed rate suggesting higher feed rates are recommended at higher bowl speeds. The influence of feed rate suggests that bringing high SG material into the concentrating bed quicker likely prevents the settling of low SG material allowing for easier substitution.

It is important to note that the findings of this study are specific for the processing of 1 kg feed samples. For low-grade feeds (≤ 10 %), processing more material is likely to result in an improved concentrate grade, as feeding more material will result in greater substitution of quartz with magnetite in the concentrating bed. This, however, is not likely to have a beneficial effect on recovery and after a certain point (when the bowl is overloaded) will be detrimental to the recovery of magnetite. It is also important to note that the industrial application of a Knelson Concentrator to feeds like those studied here, would require the use of a continuous system, however, work by Sakuhuni et al 2016, has demonstrated a lab scale Knelson Concentrator can be used for predicting CVD performance.

The findings from this work could also be extended to the processing of a high-grade low-SG deposit where any loss of value may have a significant impact on the profitability of a mineral processing plant. A high grade (15 % or 10 %) feed could first be processed at its optimum conditions and then the tailings could be reprocessed at more optimal conditions for a low-grade feed (5 %). An example of such a flowsheet is shown in Figure A.6, where the values shown for the second Knelson concentrator are those found for the 5 % magnetite feed.

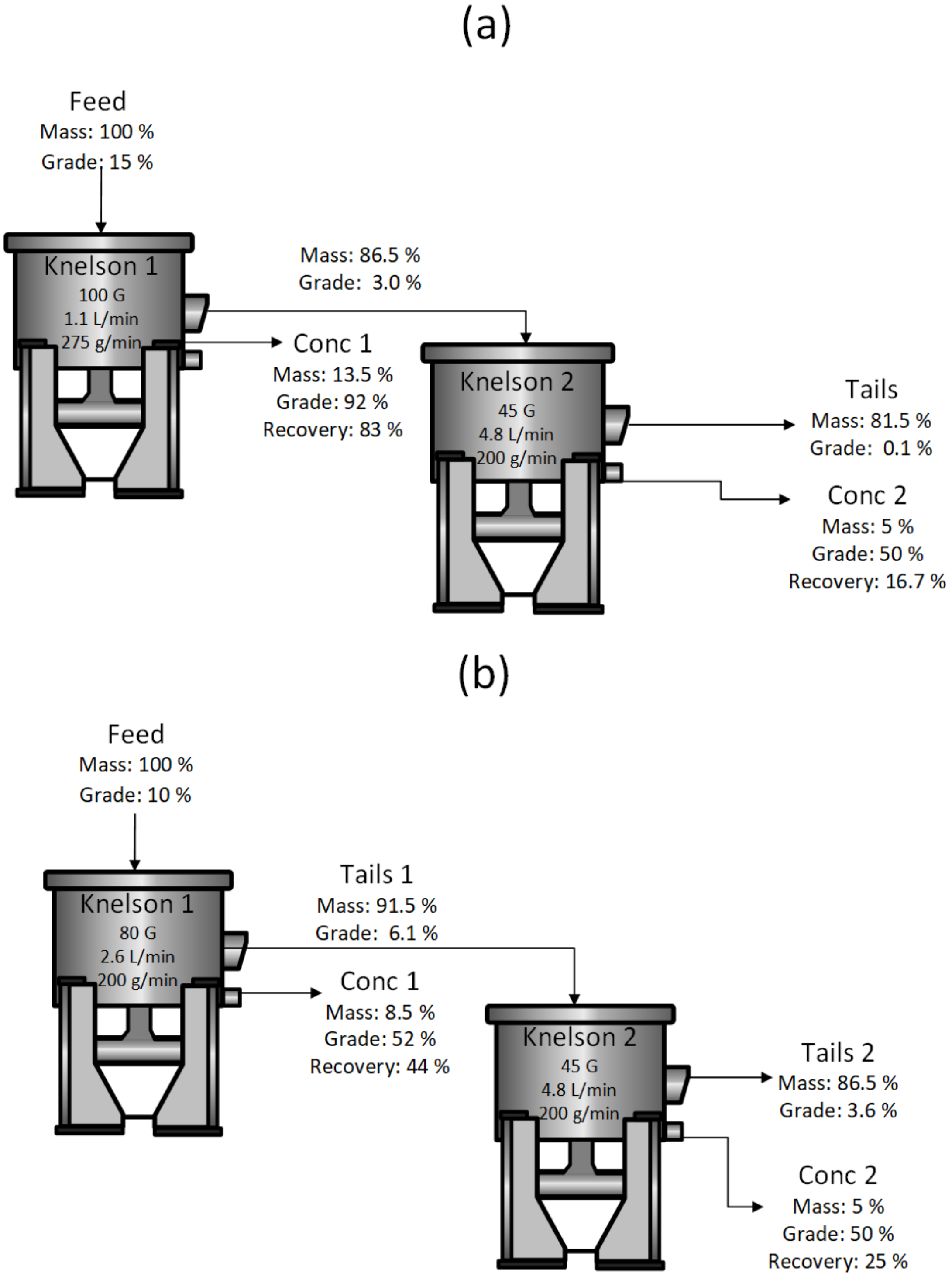

Figure A.6 – Example flowsheet for processing (a) a 15 % and (b) 10 % feed with a series of Knelson Concentrators

A.3.4 Conclusions

This study utilized response surface design experiments to determine the effect of Knelson operating variables (bowl speed, fluidizing water rate and solids feed rate) on grade and recovery of magnetite from a synthetic sample consisting of magnetite and quartz with three different feed grades. The conclusions are as follows:

1. The empirical regression equations as a function of the independent variables were derived by the RSM model for the grade and recovery of magnetite from feeds with 5 %, 10 % and 15 % magnetite.
2. The regression models are considered acceptable and fit well for all three feed grades examined. The regression models for each feed grade have p – values less than 0.05 for magnetite grade and recovery, indicating that the selected models are significant to the responses.
3. Feed grade has a significant effect on the optimal operating conditions for grade and recovery. Bowl speed and fluidizing water rate are significant operating variables for all three feed grades examined. Solids feed rate only had a significant impact when processing the 15 % magnetite feed.
4. A trade off between grade and recovery must be made when processing material with low feed grades (≤ 10 %). Grade and recovery can be simultaneously maximized for the 15 % magnetite feed.
5. Comparing the significant parameters from each data set it can be concluded that with low feed grades, the force balance acting on particles plays a much greater role in optimizing separation; whereas with high feed grades optimizing the properties of the fluidizing bed becomes more important.
6. Optimum operating conditions were obtained at a bowl speed, fluidizing water rate and solids feed rate of 45 G, 4.8 L/min and 200 g/min, for the 5 % feed; 80 G, 2.6 L/min and 200 g/min, for the 10 % feed; and 100 G, 1.1 L/min and 275 g/min for the 15 % feed.

A.3.5 Acknowledgements

The authors would like to acknowledge the Natural Science and Engineering Research Council of Canada (NSERC) in conjunction with SGS Canada Inc., Shell Canada, Barrick Gold Corp, COREM, Teck Resources Ltd., Vale Base Metals, CheMIQA, and XPS Testwork and Consulting Services (A Glencore Company) for funding this work through the Collaborative Research and Development Grant Program (CRDPJ-445682-12). C. Marion and M. Zhou would also like to acknowledge funding from the McGill Engineering Doctoral Award. In addition, C. Marion would like to acknowledge funding from an NSERC Alexander Graham Bell Canada Graduate Scholarship.

A.3.6 Supplementary Material

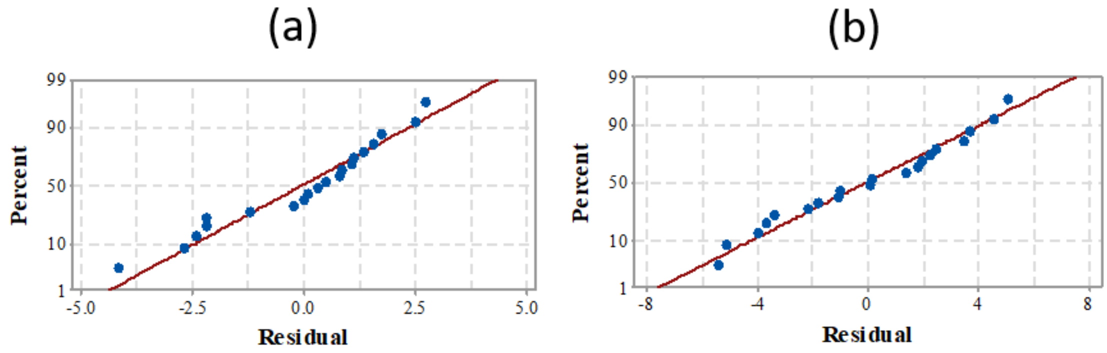

Figure A.7 – Normal probability plot of the residuals for (a) grade and (b) recovery for the 5 % magnetite feed

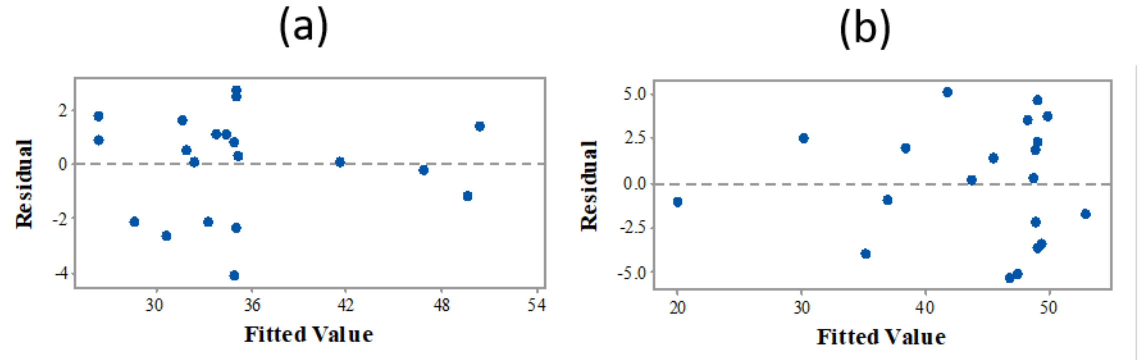

Figure A.8 – Plot of the residuals versus fitted response for (a) grade and (b) recovery for the 5 % magnetite feed

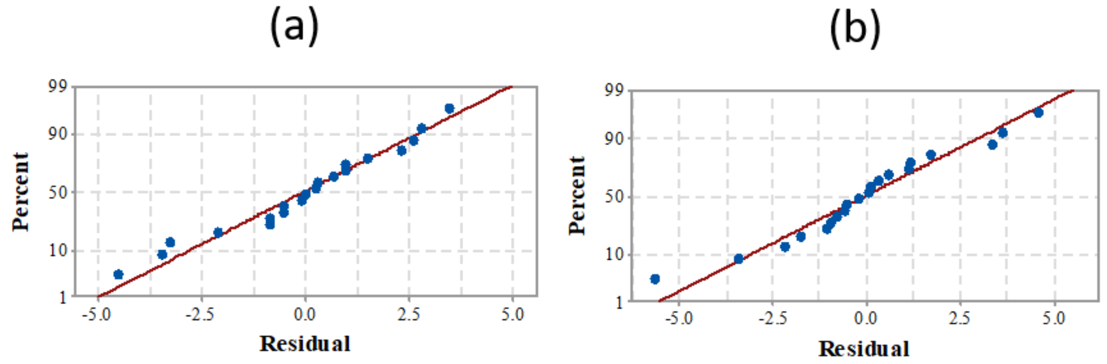

Figure A.9 – Normal probability plot of the residuals for (a) grade and (b) recovery for the 10 % magnetite feed

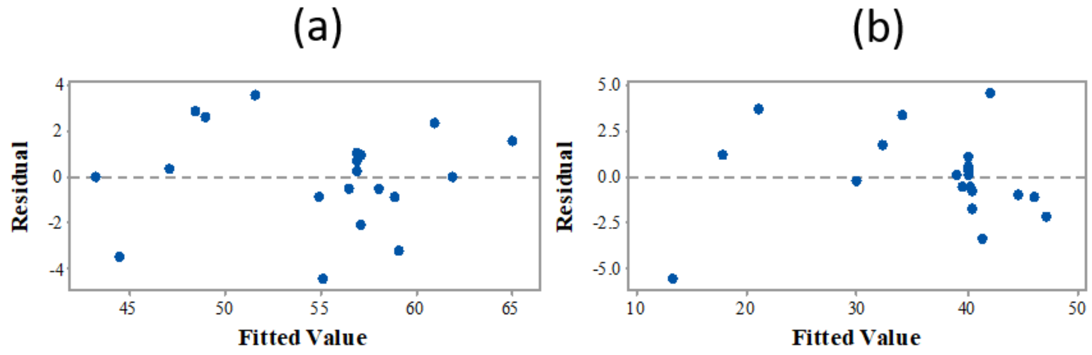

Figure A.10 – Plot of the residuals versus fitted response for (a) grade and (b) recovery for the 10 % magnetite feed

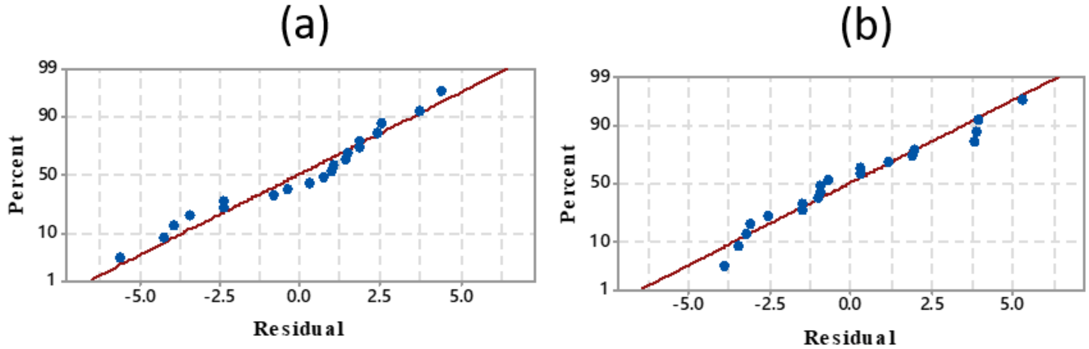

Figure A.11 – Normal probability plot of the residuals for (a) grade and (b) recovery for the 15 % magnetite feed

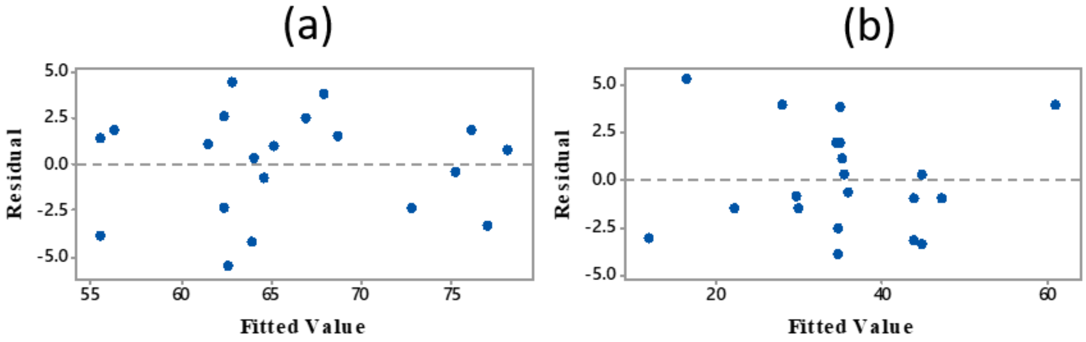

Figure A.12 – Plot of the residuals versus fitted response for (a) grade and (b) recovery for the 15 % magnetite feed

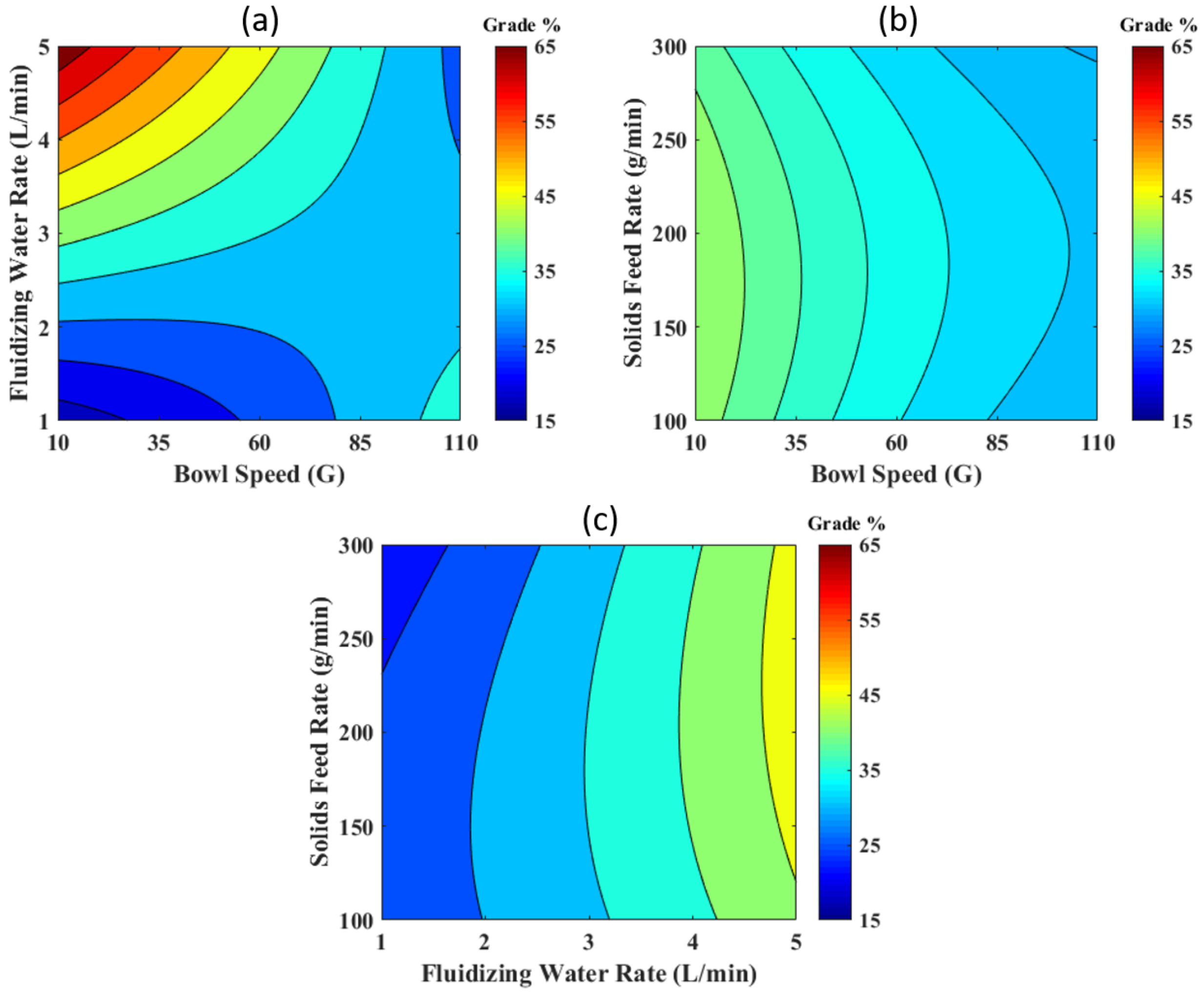

Figure A.13 – Response surface plots for grade showing the relationship between (a) bowl speed and fluidizing water rate, (b) bowl speed and solids feed rate and (c) fluidizing water rate and solids feed rate when processing the 5 % magnetite feed. In all cases the third variable is held constant at the centre (0) level

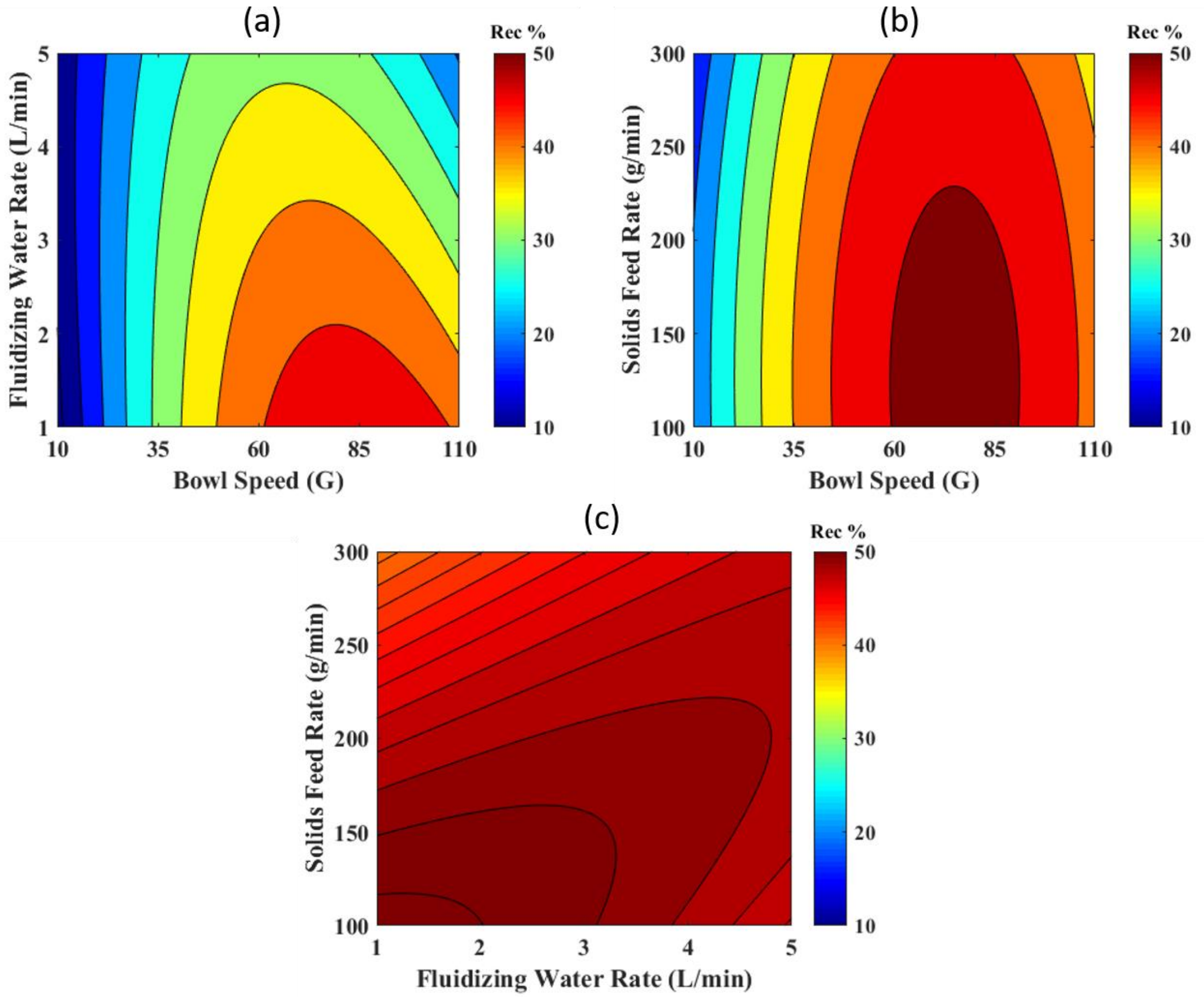

Figure A.14 – Response surface plots for recovery showing the relationship between (a) bowl speed and fluidizing water rate, (b) bowl speed and solids feed rate and (c) fluidizing water rate and solids feed rate when processing the 5 % magnetite feed. In all cases the third variable is held constant at the centre (0) level

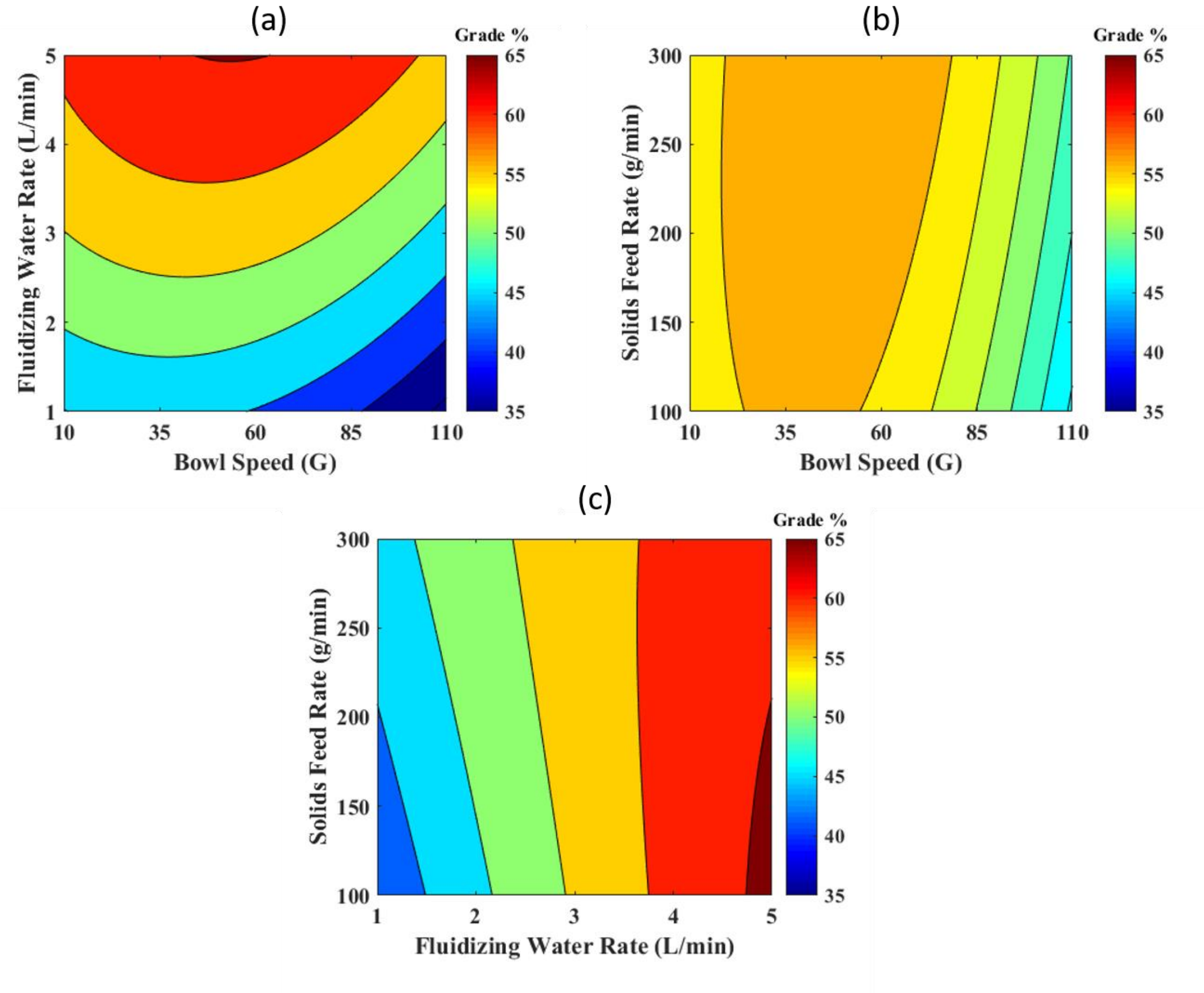

Figure A.15 – Response surface plots for grade showing the relationship between (a) bowl speed and fluidizing water rate, (b) bowl speed and solids feed rate and (c) fluidizing water rate and solids feed rate when processing the 10 % magnetite feed. In all cases the third variable is held constant at the centre (0) level

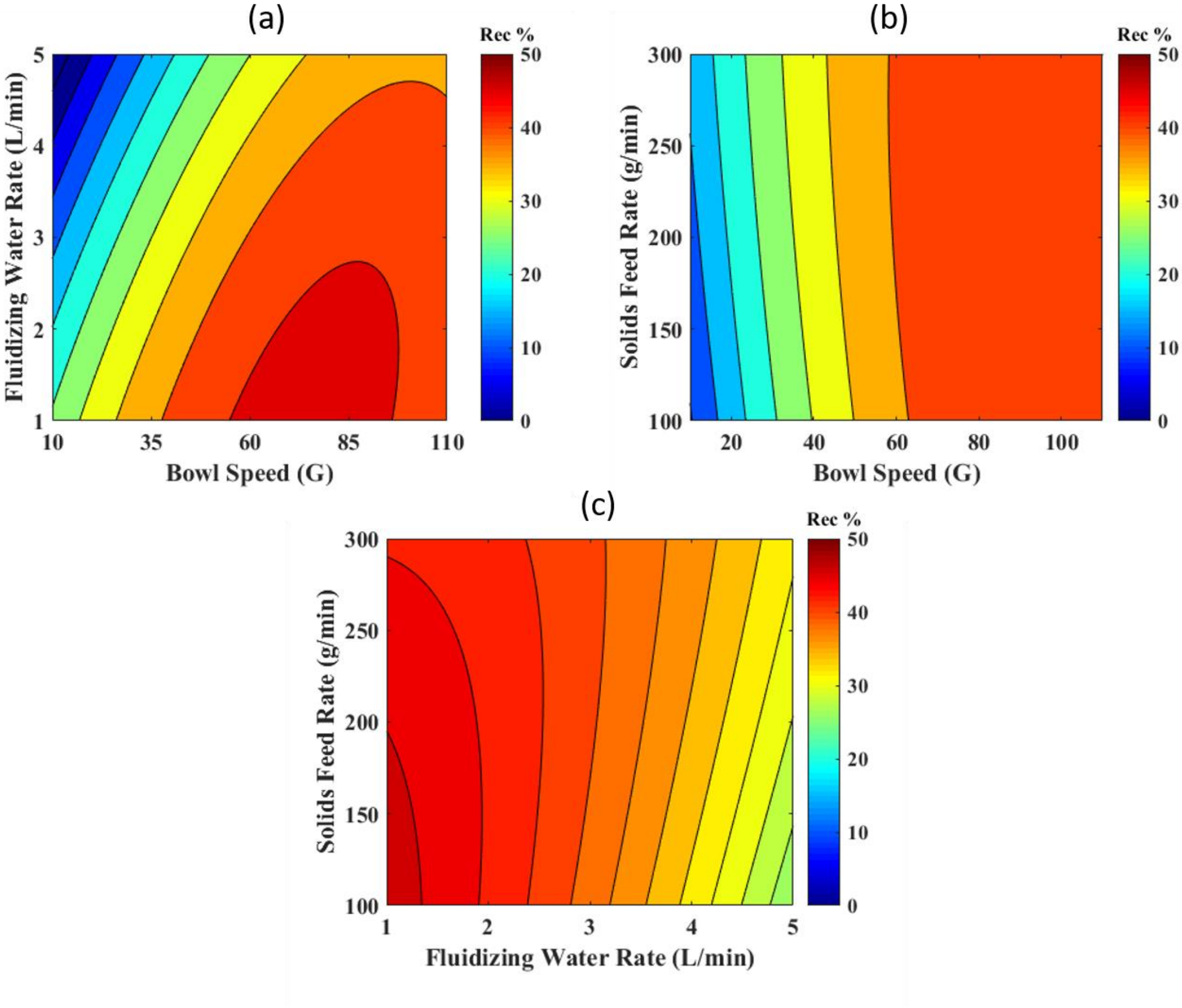

Figure A.16 – Response surface plots for recovery showing the relationship between (a) bowl speed and fluidizing water rate, (b) bowl speed and solids feed rate and (c) fluidizing water rate and solids feed rate when processing the 10 % magnetite feed. In all cases the third variable is held constant at the centre (0) level

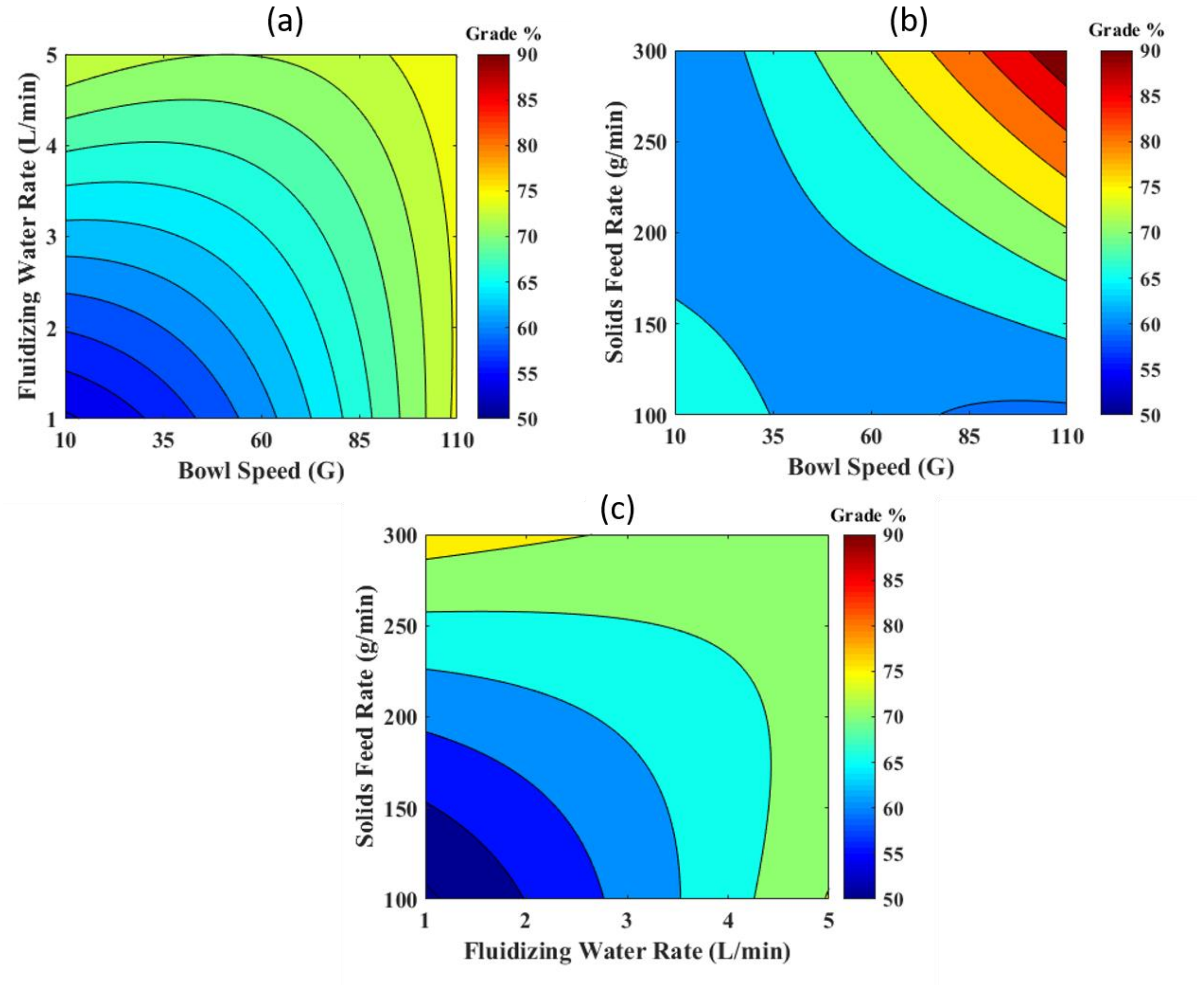

Figure A.17 – Response surface plots for grade showing the relationship between (a) bowl speed and fluidizing water rate, (b) bowl speed and solids feed rate and (c) fluidizing water rate and solids feed rate when processing the 15 % magnetite feed. In all cases the third variable is held constant at the centre (0) level

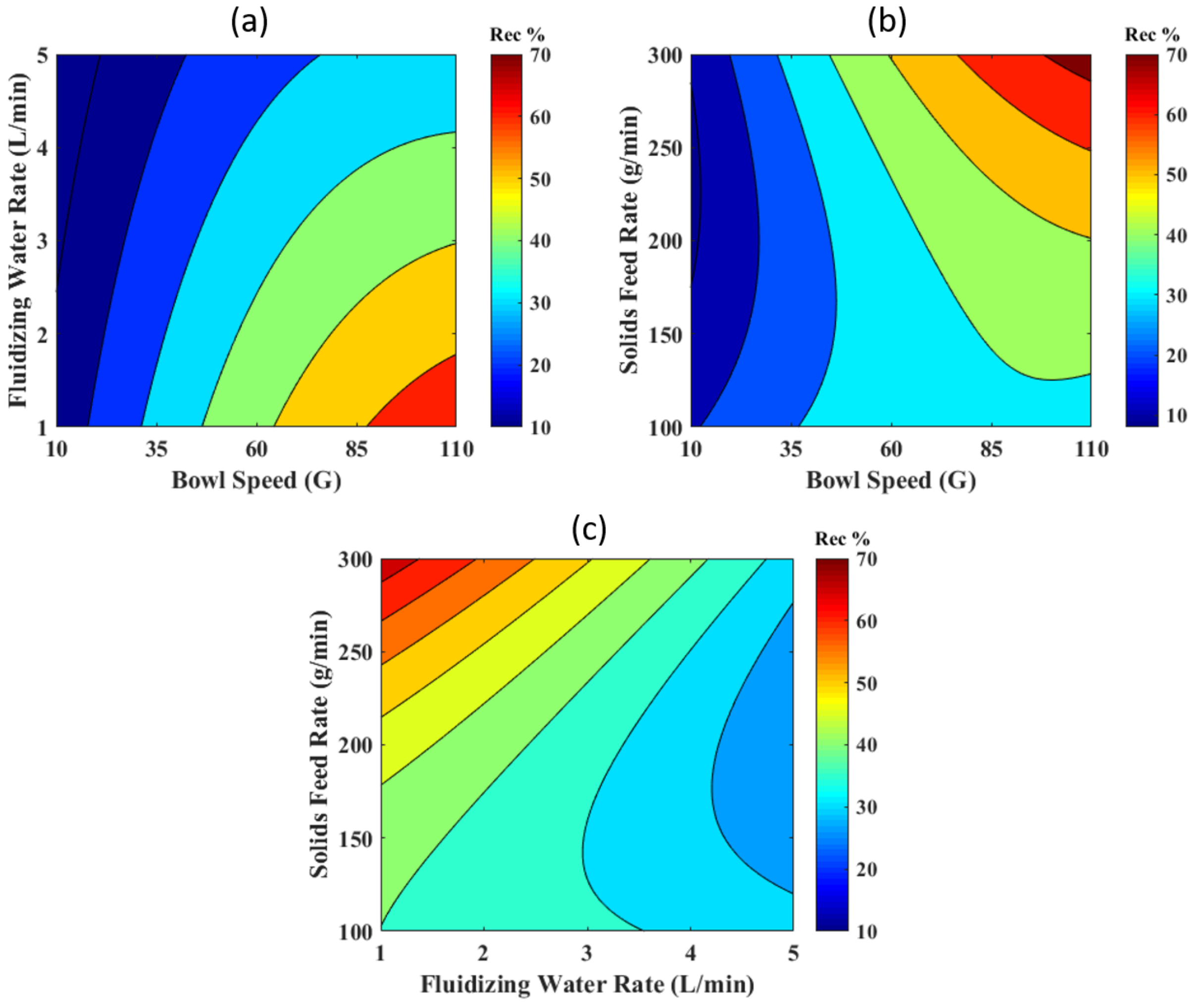

Figure A.18 – Response surface plots for recovery showing the relationship between (a) bowl speed and fluidizing water rate, (b) bowl speed and solids feed rate and (c) fluidizing water rate and solids feed rate when processing the 15 % magnetite feed. In all cases the third variable is held constant at the centre (0) level

References

Akar Sen, G., 2016. Application of Full Factorial Experimental Design and Response Surface Methodology for Chromite Beneficiation by Knelson Concentrator. Minerals 6, 5-16.

Aktaş, Z., Karacan, F., Olcay, A., 1998. Centrifugal Float–Sink Separation of Fine Turkish Coals in Dense Media. Fuel Processing Technology 55, 235-250.

Altun, N.E., Sakuhuni, G., Klein, B., 2015. The Use of Continuous Centrifugal Gravity Concentration in Grinding Circuit. Modified Approach for Improved Metallurgical Performance and Reduced Grinding Requirements. Physicochemical Problems of Mineral Processing 51, 115-126.

Angadi, S.I., Eswaraiah, C., Jeon, H.-S., Mishra, B.K., Miller, J.D., 2017. Selection of Gravity Separators for the Beneficiation of the Uljin Tin Ore. Mineral Processing and Extractive Metallurgy Review 38, 54-61.

Azizi, D., Shafaei, S.Z., Noaparast, M., Abdollahi, H., 2012. Modeling and Optimization of Low-Grade Mn Bearing Ore Leaching Using Response Surface Methodology and Central Composite Rotatable Design. Transactions of Nonferrous Metals Society of China 22, 2295-2305.

Beveridge, T., 2000. Large-Scale Centrifugation. ID Wilson, ER Adlard, M. Cooke and CF Poole, Encyclopedia of Separation Science, Academic Press, London, 320-342.

Box, G.E., Hunter, J.S., 1957. Multi-Factor Experimental Designs for Exploring Response Surfaces. The Annals of Mathematical Statistics 28, 195-241.

Box, G.E., Wilson, K., 1992. On the Experimental Attainment of Optimum Conditions, Breakthroughs in Statistics. Springer, pp. 270-310.

Brakke, M.K., 1951. Density Gradient Centrifugation: A New Separation Technique1. Journal of the American Chemical Society 73, 1847-1848.

Burt, R., Korinek, G., Young, S., Deveau, C., 1995. Ultrafine Tantalum Recovery Strategies. Minerals Engineering 8, 859-870.

Butcher, D.A., Rowson, N.A., 1995. Desulphurisation of Coal in Intensified Magnetic, Electrostatic and Gravitational Fields. New Trends in Coal Preparation Technologies and Equipment 1, 223-228.

Chen, Y.C., Parlar, H., 2013. Enrichment Behavior of Immunoglobulin by Foam Fractionation Using Response Surface Methodology. Separation and Purification Technology 107, 102-108.

Ciuculescu, T., Foo, B., Gowans, R., Hawton, K., Jacobs, C., Spooner, J., 2013. Technical Report Disclosing the Results of the Feasibility Study on the Nechalacho Rare Earth Elements Project. Avalon Rare Metals Inc.. Retrieved Nov 2019 from http://www.avalonadvancedmaterials.com.

Clarke, J., 2005. A Simplified Gravity-Recoverable-Gold Test. MEng Thesis, Department of Mining and Materials Engineering. Mcgill University, Montreal, Canada.

Fullam, M., Grewal, I., 2001. The Knelson Continuous Variable Discharge (Cvd) Concentrator. The Knelson Group, 1-6.

Ghaffari, A., Farzanegan, A., 2017. An Investigation on Laboratory Knelson Concentrator Separation Performance: Part 2: Two-Component Feed Separation Modelling. Minerals Engineering 112, 114-124.

Gonçalves, C., Braga, P., 2016. In-Depth Characterization and Preliminary Beneficiation Studies of Heavy Minerals from Beach Sands in Brazil, The Tenth International Heavy Minerals Conference, Sun City, South Africa.

Grammatikopoulos, T., Mercer, W., Gunnning, C., Prout, S., 2011. Quantitative Characterization of the REE Minerals by QEMSCAN from the Nechalacho Heavy Rare Earth Deposit, Thor Lake Project, Nwt, Canada, 43rd Annual Meeting of the Canadian Mineral Processors, Ottawa, Canada.

Hinton, R., Dobrota, M, 1978. Density Gradient Centrifugation, in: Work, T.S., Work, E. (Eds.), Laboratory Techniques in Biochemistry and Molecular Biology. North Holland Publishing Company, Amsterdam.

Hirajima, T., Sasaki, K., Bissombolo, A., Hirai, H., Hamada, M., Tsunekawa, M., 2005. Feasibility of an Efficient Recovery of Rare Earth-Activated Phosphors from Waste Fluorescent Lamps through Dense-Medium Centrifugation. Separation and Purification Technology 44, 197-204.

Honaker, R., Das, A., Nombe, M., 2005. Improving the Separation Efficiency of the Knelson Concentrator Using Air Injection. Coal Preparation 25, 99-116.

Honaker, R.Q., Das, A., 2004. Ultrafine Coal Cleaning Using a Centrifugal Fluidized-Bed Separator. Coal Preparation 24, 1-18.

Joglekar, A.M., May, A.T., Graf, E., Saguy, I., 1987. Product Excellence through Experimental Design. Food Product and Development: From Concept to the Marketplace, 211-230.

Jordens, A., Cheng, Y.P., Waters, K.E., 2013. A Review of the Beneficiation of Rare Earth Element Bearing Minerals. Minerals Engineering 41, 97-114.

Jordens, A., Marion, C., Langlois, R., Grammatikopoulos, T., Rowson, N.A., Waters, K.E., 2016a. Beneficiation of the Nechalacho Rare Earth Deposit. Part 1: Gravity and Magnetic Separation. Minerals Engineering 99, 111-122.

Jordens, A., Marion, C., Langlois, R., Grammatikopoulos, T., Sheridan, R.S., Teng, C., Demers, H., Gauvin, R., Rowson, N.A., Waters, K.E., 2016b. Beneficiation of the Nechalacho Rare Earth Deposit. Part 2: Characterisation of Products from Gravity and Magnetic Separation. Minerals Engineering 99, 96-110.

Jordens, A., Sheridan, R.S., Rowson, N.A., Waters, K.E., 2014. Processing a Rare Earth Mineral Deposit Using Gravity and Magnetic Separation. Minerals Engineering 62, 9-18.

Klein, B., Altun, N.E., Ghaffari, H., 2016. Use of Centrifugal-Gravity Concentration for Rejection of Talc and Recovery Improvement in Base-Metal Flotation. International Journal of Minerals, Metallurgy, and Materials 23, 859-867.

Klein, B., Altun, N.E., Ghaffari, H., McLeavy, M., 2010. A Hybrid Flotation–Gravity Circuit for Improved Metal Recovery. International Journal of Mineral Processing 94, 159-165.

Klima, M., Xu, D., Cho, H., 1995. A Preliminary Investigation of Dense-Medium Centrifugation for Fine Coal Separations, 19th International Mineral Processing Congress. Society for Mining, Metallurgy, and Exploration, San Francisco, pp. 138-142.

Knelson, B., 1992. The Knelson Concentrator. Metamorphosis from Crude Beginning to Sophisticated World Wide Acceptance. Minerals Engineering 5, 1091-1097.

Knelson, B., Jones, R., 1994. "A New Generation of Knelson Concentrators" a Totally Secure System Goes on Line. Minerals Engineering 7, 201-207.

Kökkılıç, O., Langlois, R., Waters, K.E., 2015. A Design of Experiments Investigation into Dry Separation Using a Knelson Concentrator. Minerals Engineering 72, 73-86.

Kwak, J.-S., 2005. Application of Taguchi and Response Surface Methodologies for Geometric Error in Surface Grinding Process. International Journal of Machine Tools and Manufacture 45, 327-334.

Majumder, A., Tiwari, V., Barnwal, J., 2007. Separation Characteristics of Coal Fines in a Knelson Concentrator–a Hydrodynamic Approach. Coal preparation 27, 126-137.

McLeavy, M., Klein, B., Grewal, I., 2001. Knelson Continuous Variable Discharge Concentrator: Analysis of Operating Variables, International Heavy Minerals Conferences, Fremantle, Australia, pp. 119-125.

Montgomery, D.C., 2009. Design and Analysis of Experiments. John Wiley & Sons, New Jersey.

Obeng, D.P., Morrell, S., Napier-Munn, T.J., 2005. Application of Central Composite Rotatable Design to Modelling the Effect of Some Operating Variables on the Performance of the Three-Product Cyclone. International Journal of Mineral Processing 76, 181-192.

Premaratne, W., Rowson, N., 2004. Recovery of Titanium from Beach Sand by Physical Separation. The European J. Mineral Processing and Environmental Protection 4, 183-193.

Rubiera, F., Hall, S.T., Shah, C.L., 1997. Sulfur Removal by Fine Coal Cleaning Processes. Fuel 76, 1187-1194.

Saguy, I.S., Graf, E., 1990. Food Product Development: From Concept to the Marketplace. Aspen Publishers, Inc., Maryland.

Sakuhuni, G., Altun, N.E., Klein, B., Tong, L., 2016. A Novel Laboratory Procedure for Predicting Continuous Centrifugal Gravity Concentration Applications: The Gravity Release Analysis. International Journal of Mineral Processing 154, 66-74.

Sakuhuni, G., Klein, B., Altun, N.E., 2015. A Hybrid Evolutionary Performance Improvement Procedure for Optimisation of Continuous Variable Discharge Concentrators. Separation and Purification Technology 145, 130-138.

Savas, M., 2016. Recovery of Colemanite from Tailing Using a Knelson Concentrator. Physicochemical problems of mineral processing 52, 1036-1047.

Uslu, T., Sahinoglu, E., Yavuz, M., 2012. Desulphurization and Deashing of Oxidized Fine Coal by Knelson Concentrator. Fuel Processing Technology 101, 94-100.

Wills, B.A., Finch, J.A., 2016. Chapter 11 - Dense Medium Separation (Dms), in: Wills, B.A., Finch, J.A. (Eds.), Wills' Mineral Processing Technology (Eighth Edition). Butterworth-Heinemann, Boston, pp. 245-264.

Xia, L., Hart, B., Douglas, K., 2015. The Role of Citric Acid in the Flotation Separation of Rare Earth from the Silicates. Minerals Engineering 74, 123-129.

Xiao, Z., Laplante, A.R., Finch, J.A., 2009. Quantifying the Content of Gravity Recoverable Platinum Group Minerals in Ore Samples. Minerals Engineering 22, 304-310.

Yi, S., Su, Y., Qi, B., Su, Z., Wan, Y., 2010. Application of Response Surface Methodology and Central Composite Rotatable Design in Optimizing the Preparation Conditions of Vinyltriethoxysilane Modified Silicalite/Polydimethylsiloxane Hybrid Pervaporation Membranes. Separation and Purification Technology 71, 252-262.

Zhou, M., Kökkılıç, O., Langlois, R., Waters, K.E., 2016. Size-by-Size Analysis of Dry Gravity Separation Using a 3-In. Knelson Concentrator. Minerals Engineering 91, 42-54.

Appendix B

Flotation of Rare-Earth Minerals

B.1 Froth Flotation

Froth flotation is a separation process that exploits natural and induced differences in the wettability of minerals. A slurry is introduced to a flotation cell (Figure B.1), where rising air bubbles collide with mineral particles. Particles with a hydrophobic surface may attach to an air bubble and rise to create the froth phase, which overflows over the edge of the cell and is continually collected. Hydrophilic mineral particles will remain in suspension, and after a given collection time all material remaining in the pulp of the flotation cell reports to the tailings of the flotation process. Generally, the collected froth phase is the considered concentrate, however, in some cases, “reverse flotation” is used to preferentially float gangue minerals and retain the valuable material in the flotation tailings.

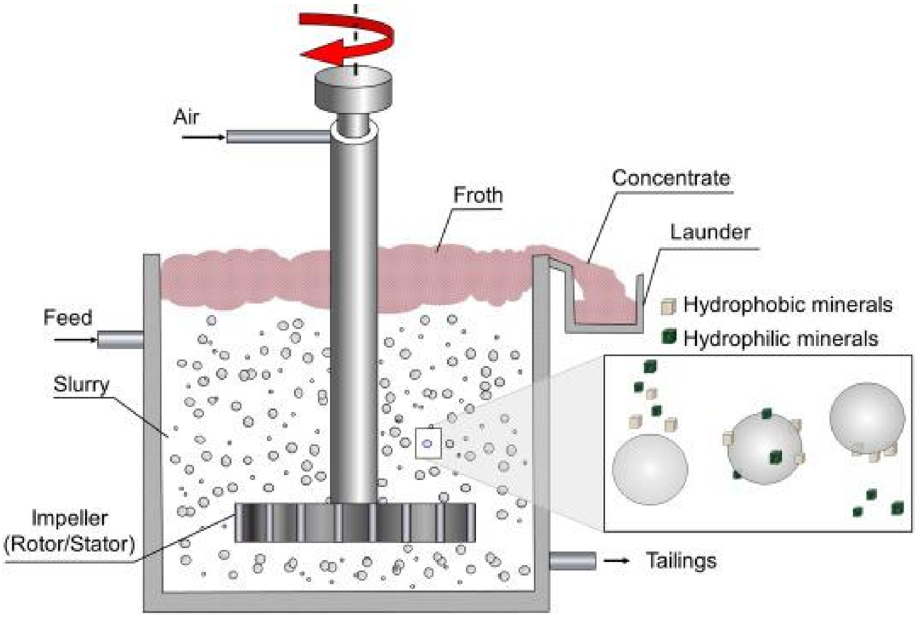

Figure B.1 – Example of a froth flotation cell, reproduced from Wills and Finch (2016b)

Flotation is a complex, three phase (solids, water and air) process, which involves both chemical and physical variables. The chemical variables aim to control the wettability of mineral particles and the physical variables include those resulting from ore properties (particle size, composition, liberation characteristics, *etc.*) and machine derived factors (air rate, bubble size, *etc.*). To achieve the desired flotation results, most ores require surfactants to be added to the flotation system. These surfactants have multiple different classifications, including frothers, collectors, depressants and activators. Frothers act at the air-water interface of bubbles, to preserve their size and stabilize the froth phase. Collectors interact selectively with mineral surfaces to enhance their hydrophobicity. Depressants act to selectively render mineral surfaces more hydrophilic, preventing them from floating. Activators selectively alter mineral surfaces to render them more amenable to adsorbing collectors. There is a large body of literature available for readers interested in a more in-depth discussion into flotation fundaments, such as Wills and Finch (2016b).

B.2 A Review of Reagent Applied to Rare-Earth Mineral Flotation

The most applied beneficiation technique for REM is froth flotation. Section B.2 provides a review of available literature on REM flotation, covering their surface chemical properties as well as the various flotation reagents which have been employed. This review has been published in the peer-reviewed journal *Advances in Colloid and Interface Science* (Marion, C., Li, R., Waters, K.E., 2020. An Evaluation of Hydroxamate Collectors for Malachite Flotation. Separation and Purification Technology, In Press) and is reproduced below.

Abstract

The rare-earth elements (REE), which encompass the fifteen metallic elements of the lanthanoid series of the periodic table, yttrium and occasionally scandium, have gained enormous public, economic and scientific attention in recent years. These elements, which have been found in over 250 minerals, are of high economic and strategic importance to many high-technology industries. As such they have been designated as critical materials by several countries and many new deposits are being developed. Rare-earth mineral (REM) deposits can be broadly classified into four geological environments: carbonates, alkaline/peralkaline igneous rocks, placers and ion adsorption clays. Apart from ion adsorption clay deposits, which require no mineral processing steps, froth flotation is the most applied beneficiation technique. This paper reviews the flotation of REM, covering their surface chemical properties as well as the various flotation reagents which have been employed.

B.2.1 Introduction

The rare-earth elements (REE) have gained enormous public, economic and scientific attention in recent years. They are strategic metals which are indispensable to the development of modern defense systems, electronic applications and green technologies. The growing economic and strategic importance of these sectors, coupled with uncertainty in the global supply of REE from China, have led to concerns about the future availability of many of these metals. Due to these supply concerns and the increasing demand of REE, they have been designated as a critical resource by several countries, including the USA (Department of the Interior, 2018), the EU (European Commission, 2017) and Canada (Fekete, 2014).

The REE comprise the fifteen metallic elements of the lanthanoid series of the periodic table, as well as chemically similar yttrium, and occasionally scandium (Connelly *et al.*, 2005). These elements are usually classified into two different sub-groups: the cerium sub-group of “light” rare-earth elements (LREE) and the yttrium sub group of “heavy” rare-earth elements (HREE) (Gambogi, 2015; Krishnamurthy and Gupta, 2016). A third sub-group, “medium” rare-earth elements (MREE), is also sometimes used (Kingsnorth, 2010; Krishnamurthy and Gupta, 2016; Zepf, 2013). The grouping of REE in these sub groups is not consistent among different authors, however, the most logical grouping is based on electron configuration (Gambogi, 2015; Zepf, 2013). Using this distinction, the LREE consist of cerium (atomic number 58) to gadolinium (atomic number 64), which have unpaired electrons in the 4f electron shell, and the HREE include terbium (atomic number 65) to lutetium (atomic number 71), which have paired electrons in the 4f electron shell (Gambogi, 2015; Zepf, 2013). Lanthanum (atomic number 57) does not have electrons in f-orbitals, however, it is generally grouped with the LREE (Gambogi, 2015; Zepf, 2013). Yttrium is generally classed as a HREE, as its ionic radius and chemical behaviour is similar to holmium (Zepf, 2013). Scandium, when classified as a REE, is not included in either the LREE or HREE classifications (Krishnamurthy and Gupta, 2016). While this sub-grouping is at present sufficient for REM exploitation and is what will be used here, it is important to note that the use of three groups may become more common, because, Chinese resource tax rates use this distinction (Argus Media Ltd., 2015; Zepf, 2016).

As of 2019, there are more than 250 REM that have been discovered; however, not all of them are of economic value (Bulatovic, 2010; Ferron *et al.*, 1991; Jordens *et al.*, 2013; Krishnamurthy and

Gupta, 2016). These minerals can be considered as complex (containing all the REE), or selective (containing either predominately LREE or HREE) (Ferron *et al.*, 1991). Selective REM which contain mainly LREE are grouped as cerium type minerals or light rare-earth minerals (LREM), whereas those containing HREE are called yttrium type minerals or heavy rare-earth minerals (HREM). A list of REM mentioned in this review is provided in Table B.1. For a more extensive list of common REM, readers are referred to Jordens *et al.* (2013).

Table B.1 – List of REM discussed in this review paper

Mineral Type	Mineral Name	Chemical Formula
Carbonate	Ancylite	$Sr(Ce,La)(CO_3)_2(OH)\cdot H_2O$
	Bastnäsite	$(Ce,La)(CO_3)F$
	Cebait	$Ba_3Ce_2(CO_3)_5F_2$
	Huanghoite	$BaCe(CO_3)_2F$
	Parisite	$Ca(Ce,La)_2(CO_3)_3F_2$
	Synchysite	$Ca(Ce,La)(CO_3)_2F$
Oxide	Cerianite	$(Ce^{4+},Th)O_2$
	Columbite	$(Fe, Mn)Nb_2O_6$
	Fergusonite	$YNbO_4$
	Loparite	$(Ce,Na,Ca)(Ti,Nb)O_3$
	Priorite	$(Y,Ca,Fe,Th)(Ti,Nb)_2(O,OH)_6$
	Pyrochlore	$(Na,Ca)_2Nb_2O_6(OH,F)$
Phosphate	Apatite	$(Ca,REE)_5(PO_4)_3(F,Cl,OH)$
	Cheralite	$(Ce,Ca,Th)(P,Si)O_4$
	Florencite	$CeAl_3(PO_4)_2(OH)_6$
	Monazite	$(Ce,La,Nd,Th)PO_4$
	Rhabdophane	$(Ce,La)PO_4\cdot H_2O$
	Xenotime	YPO_4
Silicate	Allanite	$(Ca,Ce,Y)_2(Al,Fe^{2+},Fe^{3+})_3(SiO_4)_3(OH)$
	Elpidite	$Na_2ZrSi_6O_{15}\cdot 3H_2O$
	Eudialyte	$Na_4(Ca,Ce)_2(Fe^{2+},Mn^{2+},Y)ZrSi_8O_{22}(OH,Cl)_2$
	Gadolinite	$(Ce,La,Nd,Y)_2Fe^{2+}Be_2Si_2O_{10}$
	Gerenite	$(Ca,Na)_2(Y,REE)_3Si_6O_{18}\cdot 2H_2O$
	Gittinsite	$CaZrSi_2O_7$
	Kainosite	$Ca_2(Y,Ce)_2Si_4O_{12}(CO_3)\cdot H_2O$
	Steenstupine	$Na_{14}Ce_6Mn_2Fe_2(Zr,Th)(Si_6O_{18})_2(PO_4)_7\cdot 3H_2O$
	Titanite	$Ca(Ti,REE)SiO_5$
	Thorite	$(Th,U)SiO_4$
	Zircon	$(Zr,REE)SiO_4$

B.2.2 Resources

The majority of the world's REE are derived from natural resources. These deposits can be divided into various categories based on their formation and major mineral types. They can be broadly classified into four geologic environments: carbonatites, alkaline/peralkaline igneous rocks, placers (mineral sands), and ion adsorption clays (Castor, 2008; Goodenough *et al.*, 2018).

For more than 50 years, the majority of REE have been derived from carbonatite deposits; these are defined as an igneous rock deposit containing > 50 % carbonate minerals. These deposits tend to be large, high-grade, and generally contain a high content of LREE. There are currently several operating REE-bearing carbonatite deposits, as well as many others under investigation (Verplanck *et al.*, 2016). The world's largest REE mine, the Bayan Obo mine in China, and the Mountain Pass mine (the world's primary producer from 1965 to 1995) in the USA, are both carbonatite deposits (Castor, 2008; Verplanck *et al.*, 2016). Other current mining operations associated with carbonatites are the Maoniuping, Weishan and Dalucao deposits in China and the Mount Weld deposit in Australia (Verplanck *et al.*, 2016). There also exists numerous deposits of this type which are being explored, including Bear Lodge (USA), Montviel (Canada), Niobec (Canada) and Songwe Hill (Africa). Carbonatite deposits can contain a variety of REE-rich mineral phases, however, bastnäsite is generally the primary mineral mined (Castor, 2008; Verplanck *et al.*, 2016). The primary method of beneficiation for these deposits is froth flotation.

The other group of "hard-rock" REE deposits are classified as alkaline/peralkaline igneous rock deposits. These deposits tend to have a much "flatter" REE distribution than carbonatite deposits, making them one of the most economically important resources of HREE (Dostal, 2016; Goodenough *et al.*, 2018). They are, however, often much more complex than carbonatite deposits, with highly variable mineralogy, both within individual deposits and particularly among the various deposits (Dostal, 2016). The only active REE deposits of this type are in the Kola Peninsula in Russia (Lovozero and Khibiny deposits), where the main REE bearing mineral is loparite (Dostal, 2016; Goodenough *et al.*, 2018; Hedrick *et al.*, 1997). However, there are many alkaline/peralkaline igneous rock deposits which are currently being investigated, including Kvanefjeld (Greenland), Norra Kärr (Sweeden), Nechalacho (Canada) and Strange Lake (Canada) (Castor, 2008).

Placers, or mineral sands, are sedimentary deposits formed by the natural physical concentration of minerals from weathering processes. Although placer deposits are most commonly processed for other commodities such as gold, tin (in cassiterite), titanium (in ilmenite and rutile) and zirconium (in zircon), many have potential to produce REE as a co-product (Goodenough *et al.*, 2018; Sengupta and Gosen, 2016). In fact, before full scale production began at the Mountain Pass mine in 1965, placer mines were the world's chief REE supplier (Sengupta and Gosen, 2016). The REM found in these deposits are primarily monazite and sometimes xenotime. As they are generally more enriched in monazite, they contain more LREE than HREE, however, xenotime offers potential for HREE production (Goodenough *et al.*, 2018; Sengupta and Gosen, 2016). Although placer deposits are generally smaller and have lower REE grades than carbonatite ores, they have very simple and well-established processing routes (with little to no comminution required) and can produce multiple salable products to offset mining costs (Goodenough *et al.*, 2018; Jordens *et al.*, 2013; Sengupta and Gosen, 2016).

The final REE deposit type is classified as ion adsorption clays. Ion adsorption clays are currently the second major producer of REE and the world's chief source of HREE, with a large proportion coming from illegal Chinese producers (Brown and Eggert, 2018; Goodenough *et al.*, 2018; Sanematsu and Watanabe, 2016). These deposits are primarily located in China, with a few specific locations elsewhere in the world (Goodenough *et al.*, 2018; Sanematsu and Watanabe, 2016). In ion adsorption clay deposits, REE are not held within minerals but adsorbed onto clay surfaces (Goodenough *et al.*, 2018; Sanematsu and Watanabe, 2016). Therefore, REE from these deposits can be easily extracted by ion-exchange using a dilute electrolyte solution, such as ammonium sulfate, and do not require any mineral processing steps such as flotation (Goodenough *et al.*, 2018; Sanematsu and Watanabe, 2016).

Froth flotation is commonly applied to REE-bearing ores due to its ability to process a wide range of fine particle sizes and it can be tailored to the mineralogy of a specific deposit. As such, when compared to other beneficiation techniques, flotation has received the most research. Research has focused primarily on bastnäsite and monazite surface characteristics and their relation to flotation response. Most of the work focused on the flotation of ore deposits has been performed on Bayan Obo (China) and Mountain Pass (USA) ores, where bastnäsite is the main REE-bearing mineral. There is limited information with regards to the flotation of other REE deposits.

B.2.3 Surface Chemistry

Froth flotation is a complex, three-phase (solids, water and air), separation process that exploits natural and induced differences in the wettability of minerals. To achieve the desired flotation results, most ores require surfactants to be added to the flotation system. These surfactants have multiple different classifications, including frothers, collectors, depressants and activators. There is a large body of literature available for readers interested in a more in-depth discussion into flotation fundamentals, such as Wills and Finch (2016).

In froth flotation, the electrical double layer governs the adsorption of flotation reagents (Fuerstenau and Pradip, 2005). An important mineral property in characterizing the electrical double layer is the isoelectric point (IEP), which is the pH value where the zeta potential is zero (Pope and Sutton, 1973). If the IEP of a mineral is known, the sign of the charge on a mineral surface in a given pH range can be predicted (Pope and Sutton, 1973). This information coupled with knowledge of a surfactant's ionization behaviour can help understand mechanisms of reagent adsorption and select optimal flotation conditions to effectively separate a valuable mineral from gangue minerals (Cheng *et al.*, 1993; Jordens *et al.*, 2014b; Pope and Sutton, 1973). In systems where collector adsorption occurs through electrostatic attraction and hydrophobic bonding, the adsorption process is characterized as physisorption and the extent of reagent adsorption is controlled by the sign and magnitude of the surface charge (Fuerstenau and Pradip, 2005; Pope and Sutton, 1973). When collector adsorption occurs through the formation of strong covalent or coordinate bonds with surface species, the process is characterized as chemisorption. Chemisorbing surfactants can adsorb onto the surface of similarly charged minerals, however, an elevated surface charge can inhibit adsorption via electrostatic repulsion (Fuerstenau and Pradip, 2005). For an introduction to the concept of surface charge and zeta potentials and their application in flotation, interested readers should consult Riley (2009) and Fuerstenau and Pradip (2005). IEP values for many common minerals are listed in Parks (1965) and Kosmulski (2002, 2004, 2006, 2009, 2011, 2014, 2018, 2020).

Different methods can be used to measure the zeta potential of a suspension, including electrophoretic, electroacoustic and streaming potential techniques. Electrophoresis is the most commonly employed method, in which an electric field is applied across a dilute ($< 1\%_{w/w}$)

suspension of very fine particles (< 10 μm), which induces charged particles to move (Babchin *et al.*, 1989; Hunter, 1998; Johnson, 1999; Miller and Berg, 1991; Riley, 2009). The zeta potential can then be calculated using the direction and velocity (electrophoretic mobility) of the particles. Electroacoustic zeta potential measurements are based on the application of high-frequency alternating electric fields to a suspension of particles, causing charged particles to oscillate and produce a sound wave of the same frequency (O'Brien, 1990; O'Brien, 1995; O'Brien *et al.*, 1990). The zeta potential of the sample can be calculated from the phase and magnitude of the resulting sound wave. The electroacoustic method offers distinct advantages over electrophoresis. As it is a non-optical measurement technique, electroacoustic methods are free of the limitations associated with optical electrophoretic measurements, and have been shown to be effective in analysing sizes ranging from a few nanometers to several micrometers (Greenwood, 2003; Hunter, 1998; Klein *et al.*, 2012; Marlow *et al.*, 1988), concentrated and complex mineral suspensions (Hunter, 1998; Marlow *et al.*, 1988) in excess of $60\%_{w/w}$ (Greenwood, 2003; Greenwood *et al.*, 2007; Klein *et al.*, 2012), opaque or photosensitive materials (Babchin *et al.*, 1989; Marlow *et al.*, 1988) and flowing streams (Marlow *et al.*, 1988). However, this technique is poorly suited for cases where only very small quantities of pure mineral sample are available, which is generally the case for REM. Rather than applying an electric field or sound wave to cause the particles in suspension to move, streaming potential measurements are conducted by applying a pressure gradient to cause an electrolyte solution to flow through a bed of particles (Fuerstenau, 1956; Fuerstenau and Pradip, 2005; Neale, 1946). The fluid travelling through the solid bed carries mobile ions with it, creating a potential difference (Neale, 1946). This potential difference is the “streaming potential”, which can be used to calculate the zeta potential (Fuerstenau, 1956; Neale, 1946).

A summary of the surface chemical studies focused on REM is shown in Table B.2 to Table B.4. These tables contain the origin of the mineral sample, the measurement technique used and reported IEPs. Zircon is included in Table B.4, as in some REM deposits, such as the Nechalacho deposit, it is an important REE-bearing mineral (Ciuculescu *et al.*, 2013; Grammatikopoulos *et al.*, 2011). It should be noted that in all published surface chemical studies investigating zircon the REE content is not indicated. Apart from bastnäsite (Table B.2) and monazite (Table B.3), which have been extensively characterized, test work investigating REM (Table B.4) is limited. The large differences in reported IEP values, for bastnäsite (4.6 to 9.5), monazite (1.1 to 9.0), xenotime (2.3

to 7.0), fergusonite (2.7 to 6.3) and zircon (2.3 to 6.0) have been suggested to be a result of variations in potential determining ions, mineral composition and the structure of the mineral surfaces, as well as differences in the procedure and/or technique used to determine the IEP (Cheng, 2000; Jordens *et al.*, 2014b). For semi-soluble minerals, such as bastnäsite, it is likely that differences in procedure or techniques used have a larger impact than mineral origin. This is evident by the fact that bastnäsite from a single source, the Mountain Pass deposit, has a wide range of reported IEP values (Azizi *et al.*, 2016; Herrera-Urbina *et al.*, 2013; Jordens *et al.*, 2014b; Pradip *et al.*, 2015; Sarvaramini *et al.*, 2016; Smith and Shonnard, 1986; Smith and Steiner, 1980). Variations in solids concentration and conditioning time will impact mineral dissolution, and therefore result in differences in the amount of potential determining ions in the bulk. This has been demonstrated by Smith and Steiner (1980), who noted that after 30 min of conditioning the IEP was at pH 5.3, whereas after 24 hours it increased to pH 7.2. Similarly, Jordens *et al.* (2014b) measured the same bastnäsite sample using both electrophoretic and electroacoustic techniques. The electroacoustic technique, which used a much greater solids concentration, measured an IEP of 8.1, compared to 6.8 measured using electrophoresis. As monazite has a low dissolution rate (Oelkers and Poitrasson, 2002), it is unlikely that variations in its IEP are due to the same mechanism as bastnäsite. However, Geneyton *et al.* (2018) tested three synthetic monazites with different REE in their lattice and have suggested that IEP variations are due to procedural differences and not substitutions of REE in the mineral lattice. The authors indicated that ions resulting from CO_2 dissociation are potential determining ions for monazite which influence its zeta potential significantly. Therefore, if the suspension has not reached an equilibrium with dissolved CO_2 from the atmosphere, variations in the IEP will exist.

Although there exists a wide discrepancy of reported IEPs for bastnäsite and monazite, most work indicates their IEPs occur between pH 6 to 8 and pH 5 to 6, respectively. This does demonstrate the importance of obtaining a similarly large database of surface chemical studies for other REM. To expand this database, the IEP of several REM (bastnäsite, monazite, allanite, columbite, fergusonite and zircon) were measured and are shown in bold in Tables B.2 to B.5. The procedure which was followed to obtain these measurements is detailed in the Appendix. Apart from fergusonite, the IEP values measured for the various minerals all correspond well with those reported by previous authors. The IEP of the natural fergusonite sample corresponds well to the value reported by Fawzy (2018) (IEP at pH 2.7), but, not that of Malas *et al.* (2013) (IEP at pH

6.3); who studied a fergusonite sample from the same origin and followed a similar procedure to that employed here. However, the fergusonite sample tested by Malas *et al.* (2013) remained embedded in a matrix of magnesium and aluminum silicate, whereas the sample used here was of relatively high purity; likely explaining the difference. The observed differences in the IEP of synthetic $YNbO_4$ versus natural fergusonite should be noted. The synthesis of $YNbO_4$ uses reagent grade materials providing clean mineral surfaces, whereas the surface properties of the natural sample are likely affected by contamination of other minerals and lattice damage caused by radiation due to the presence of uranium and thorium. Therefore, surface chemical studies on a synthetic sample may not represent a real-world situation, which should be acknowledged by any researchers performing such studies on synthetic specimens.

Table B.2 – Summary of measured IEPs for bastnäsite. Measurements taken during the current research program are in bold.

Mineral	Sample Origin	Measurement Technique	Background Electrolyte	IEP	Reference
Bastnäsite	Mountain Pass, USA	Electrophoresis	Not Indicated	4.6	Smith and Shonnard (1986)
		Electrophoresis	Not Indicated	5.3	Smith and Steiner (1980)
		Electrophoresis	10^{-3} M KCl	6.4	Jordens *et al.* (2014b)
		Electrophoresis	Not Indicated	6.8	Smith and Steiner (1980)
		Electrophoresis	10^{-1} M KNO_3	7.0	Sarvaramini *et al.* (2016)
		Electrophoresis	10^{-1} M KNO_3	7.0	Azizi *et al.* (2016) and Azizi *et al.* (2017)
		Electrophoresis	Not Indicated	7.2	Smith and Steiner (1980)
		Electrophoresis	10^{-3} M $NaNO_3$ 10^{-3} M NaF	9.3	Pradip *et al.* (2015)
		Electrophoresis	1 M $NaNO_3$	9.3	Herrera-Urbina *et al.* (2013)
	Bayan Obo, China	Electrophoresis	10^{-3} M KNO_3	7.0	Luo and Chen (1984)
		Electrophoresis	KCl	7.1	Li *et al.* (2018)
		Electrophoresis	Not Indicated	8.1	Yang *et al.* (2017)
	Not Given	Not Indicated	Not Indicated	4.7	Kim *et al.* (2010)
	Poços de Caldas, Brazil	Electrophoresis	10^{-3} M KCl	4.9	Pavez *et al.* (1996)
	Not Given	Electrophoresis	10^{-2} M KCl	5.3	Zhou *et al.* (2014)
	Madagascar	Electrophoresis	10^{-3} M KCl	6.2	Jordens *et al.* (2014b)
		Electrophoresis	**10^{-3} M KCl**	**6.8**	**This Work**
		Electroacoustics	10^{-3} M KCl	8.1	Jordens *et al.* (2014b)
	Weishan, China	Electrophoresis	10^{-3} M KNO_3	6.8	Cao *et al.* (2019)
	Gakara Mine, Burundi	**Electrophoresis**	**10^{-3} M KCl**	**6.4**	**This Work**
		Electrophoresis	10^{-3} M NaCl	7.5	Espiritu *et al.* (2018a)
		Electrophoresis	10^{-3} M NaCl	8.0	Espiritu *et al.* (2018b)
	Maoniuping, China	Electrophoresis	Mot Indicated	7.8	Ren *et al.* (2000)
		Electrophoresis	Not Indicated	8.0	Ren *et al.* (1997)
	Synthetic	Electrophoresis	10^{-3} M $NaNO_3$ 10^{-3} M NaF	7.8	Pradip *et al.* (2015)
	Zagi Mountains, Pakistan	Electrophoresis	Not Indicated	8.1	Zhang *et al.* (2013)
		Electrophoresis	10^{-3} M KCl	9.0	Liu *et al.* (2016) and Liu *et al.* (2018)
	Zaozhuang, China	Electrophoresis	Not Indicated	9.0	Cao *et al.* (2018a)
	Synthetic	Electrophoresis	10^{-3} M $NaNO_3$	9.3	Pradip (1981)

Table B.3 – Summary of measured IEPs for monazite. Measurements taken during the current research program are in bold.

Mineral	Sample Origin	Measurement Technique	Background Electrolyte	IEP	Reference
Monazite	Not Given	Not Indicated	Not Indicated	1.1 – 9.0	Reported by Houot *et al.* (1991)
	USA	Electrophoresis	10^{-3} M NaCl	3.0	Harada *et al.* (1993)
	Korea	Electrophoresis	Not Indicated	3.5	Hyung and Ki (1963)
	Bayan Obo, China	Electrophoresis	10^{-3} M KNO_3	5.0	Luo and Chen (1984)
		Electrophoresis	10^{-2} M KCl	5.4	Li *et al.* (2018)
	Eureka Farm 99, Namibia	Electrophoresis	10^{-3} M KCl	5.0	Espiritu and Waters (2018)
		Electrophoresis	10^{-3} M NaCl	7.0	Espiritu *et al.* (2018a) and Espiritu *et al.* (2018b)
	Yard Mine (USA)	**Electrophoresis**	**10^{-3} M KCl**	**5.1**	**This Work**
	Brazil	Electrophoresis	10^{-3} M KCl	5.2	Pavez and Peres (1993a) and Pavez *et al.* (1996)
	New Mexico, USA	Streaming Potential	Not Indicated	5.3	Nduwa-Mushidi and Anderson (2017)
	Australia	Electrophoresis	Not Indicated	5.3	Cheng *et al.* (1993)
	Egypt	Streaming Potential	None	5.5	Abeidu (1972)
	Malaysia	Electrophoresis	10^{-3} M NaCl	5.5	Harada *et al.* (1993)
	Synthetic (Ce)	Electrophoresis	10^{-3} M KCl	5.9	Geneyton *et al.* (2018)
	Synthetic (La)	Electrophoresis	10^{-3} M KCl	5.9	Geneyton *et al.* (2018)
	Synthetic (Nd)	Electrophoresis	10^{-3} M KCl	5.9	Geneyton *et al.* (2018)
	Itambé, Brazil	Electrophoresis	10^{-1} M KNO_3	5.9	Azizi *et al.* (2016) and Azizi *et al.* (2017)
		Electrophoresis	10^{-1} M KNO_3	5.9	Sarvaramini *et al.* (2016)
	China	Electrophoresis	10^{-3} M KCl	6.0	Zhang *et al.* (2016)
	China	Electrophoresis	10^{-3} M KCl	6.5	Zhang *et al.* (2017)
	Australia	Electroacoustics	10^{-3} M KNO_3	6.5	Abaka-Wood *et al.* (2017)
	Australia	Electrophoresis	10^{-3} M NaCl	7.0	Harada *et al.* (1993)

Table B.4 – Summary of measured IEPs for other REM. Measurements taken during the current research program are in bold.

Mineral	Sample Origin	Measurement Technique	Background Electrolyte	IEP	Reference
Xenotime	Pitinga, Brazil	Electrophoresis	10^{-2} M NaCl	2.3	Pereira and Peres (1997)
	Australia	Electrophoresis	Not Indicated	< 3	Cheng *et al.* (1993)
	Not Given	Not Indicated	Not Indicated	4.0 – 5.0	Reported by Pereira and Peres (1997)
	Hainan, China	Streaming Potential	None	4.7	Zhang and Anderson (2017a) and Zhang and Anderson (2017b)
	Malaysia	Electrophoresis	10^{-3} M NaCl	7.0	Harada *et al.* (1993)
Allanite	Nevada, USA	**Electrophoresis**	**10^{-3} M KCl**	**3.5**	**This Work**
		Electrophoresis	10^{-3} M KCl	4.0	Jordens *et al.* (2014a)
Ancylite	Not Given	Streaming Potential	None	5.5	Cui and Anderson (2017b)
Apatite	Jacupiranga, Brazil	Streaming Potential	Not Indicated	3.8	Owens *et al.* (2019)
	Synthetic	Electrophoresis	Not Indicated	< 5	Chen *et al.* (2016)
	Fort Dauphin, Madagascar	Electrophoresis	10^{-1} M KCl	2 – 3	Filippova *et al.* (2014)
	Fort Dauphin, Madagascar	Electrophoresis	10^{-1} M $NaNO_3$	1 – 2	Filippov *et al.* (2012)
	Not Given	Electrophoresis	10^{-3} M KCl	4.2	Zhou *et al.* (2015)
Columbite	**Madagascar**	**Electrophoresis**	**10^{-3} M KCl**	**< 3**	**This Work**
	Japan	Electrophoresis	10^{-3} M NaCl	4.0	Harada *et al.* (1993)
	Brazil	Electrophoresis	10^{-3} M NaCl	4.5	Harada *et al.* (1993)
Eudialyte	Not Given	Not Indicated	Not Indicated	3.5	Reported by Stark *et al.* (2017)
	Not Given	Not Indicated	Not Indicated	4.5	
Fergusonite	Egypt	Electrophoresis	10^{-2} M $NaNO_3$	2.7	Fawzy (2018)
	Cole Quarry, Canada	**Electrophoresis**	**10^{-3} M KCl**	**< 3**	**This Work**
		Electrophoresis	10^{-3} M KCl	6.3	Malas *et al.* (2013)
	Synthetic $YNbO_4$	**Electrophoresis**	**10^{-3} M KCl**	**6.9**	**This Work**
Parisite	USA	Streaming Potential	Not Indicated	5.6	Owens *et al.* (2018)
	Blackbird Mine, USA	**Electrophoresis**	**10^{-3} M KCl**	**7.2**	**This Work**
Zircon[1]	Pitinga, Brazil	Electrophoresis	10^{-2} M NaCl	2.3	Pereira and Peres (1997)
	Thailand	Electrophoresis	Not Indicated	2.9	Gül (2004)
	Egypt	Streaming Potential	None	3.7	Abeidu (1972)
	Brazil	Electrophoresis	10^{-3} M KCl	4.1	Pavez and Peres (1993a)
	Malawi	**Electrophoresis**	**10^{-3} M KCl**	**5.5**	**This Work**
	Australia	Electrophoresis	10^{-3} M NaCl	4.5	Peng *et al.* (2017)
	Not Given	Not Indicated	Not Indicated	4.7	Reported by Pereira and Peres (1997)
	Not Given	Electrophoresis	Not Indicated	5.0	Choi and Whang (1963)
	Australia	Electrophoresis	10^{-2} M KNO_3	5.5	Mao *et al.* (1994)
	Australia	Electrophoresis	10^{-2} M KNO_3	5.7	Mao *et al.* (1994)
	Not Given	Not Indicated	Not Indicated	6.0	Reported by Pereira and Peres (1997)

[1] Cited studies do not state REE content of zircon

B.2.4 Collectors

REM often have physical and chemical properties which are similar to the gangue minerals with which they are found. Therefore, highly selective flotation reagents are typically required (Bulatovic, 2010; Ren *et al.*, 2003). The flotation of REM, particularly bastnäsite and monazite, is typically accomplished using oxhydryl collectors, such as hydroxamates, carboxylates and phosphoric acid esters (Bulatovic, 2010; Jordens *et al.*, 2013; Ren *et al.*, 2003). This class of collectors is called oxhydryl collectors, as their functional groups consist of an oxygen anion and a double-bonded oxygen to which a metal cation will bind, with the key difference between these three collectors being the atom to which the oxygen atoms are attached (nitrogen, carbon and phosphorous) (Bulatovic, 2007a). Depending on the mineralogy of the ore, these collectors may be used in conjunction with a variety of different depressants and activators.

B.2.4.1 Hydroxamic Acids

Hydroxamic acids are a group of chelating collectors, which form complexes with metal cations present at the surface of minerals. Multiple researchers have suggested hydroxamate-metal complexation occurs through the substitution of the hydrogen atom of the hydroxyamide group with a metal cation and ring closure via the carbonyl oxygen atom (Cao *et al.*, 2019; Cui *et al.*, 2012; Espiritu *et al.*, 2018a; Gao *et al.*, 2018; Hope *et al.*, 2010; Li *et al.*, 2018; Pradip and Fuerstenau, 1983; Zhang *et al.*, 2017). The strength of the interaction varies depending on the metal cation (Figure B.2). The most stable complexes are formed with Fe^{3+}, Al^{3+}, Cu^{2+}, Cr^{3+} and Pb^{2+}, followed by rare-earth metal cations; and the weakest complexes are formed with alkaline-earth metal cations (Fuerstenau, 2005; Khairy *et al.*, 1996; Khalil and Fazary, 2004; Sastri *et al.*, 2003). It has been suggested that the larger the difference in stability constant of the complexes formed with surface cations the greater the selectivity (Pavez and Peres, 1993b; Pradip and Fuerstenau, 1983). Others believe that the selectivity of hydroxamic acid collectors is more closely related to adsorption kinetics (Assis *et al.*, 1996). It has been suggested that hydroxamic acid collectors may interact with metal cations at the mineral surface in two ways: chemisorption and surface reactions (Pradip and Fuerstenau, 1983). Chemisorption involves the chelation reaction with the surface metal cation fixed in the mineral lattice. Surface reactions involve the hydrolysis of lattice cations, the formation of hydroxyl-complexes in solution, followed by re-adsorption (or precipitation) at the mineral surface, providing sites for hydroxamic acid adsorption. Adsorption through surface reactions are believed to be much faster than chemisorption, and therefore the selectivity of the collector is strongly related to mineral solubility (Assis *et al.*, 1996). More soluble minerals will exhibit faster adsorption kinetics compared to less soluble ones. Deng *et al.* (2016) and Gao *et al.* (2018) have also suggested mineral O-O bond distances dictate the degree to which collector adsorption occurs. Minerals with O-O distances similar to those of the hydroxamate collector are readily able to form stable chelates, whereas those whose O-O distances do not match cannot. Bulk precipitation is another important factor to consider in hydroxamic acid flotation. Undesirable precipitates can form when the collector reacts with dissolved metal cations in the bulk solution. This may consume collector or potentially adsorb onto mineral surfaces, altering the flotation response.

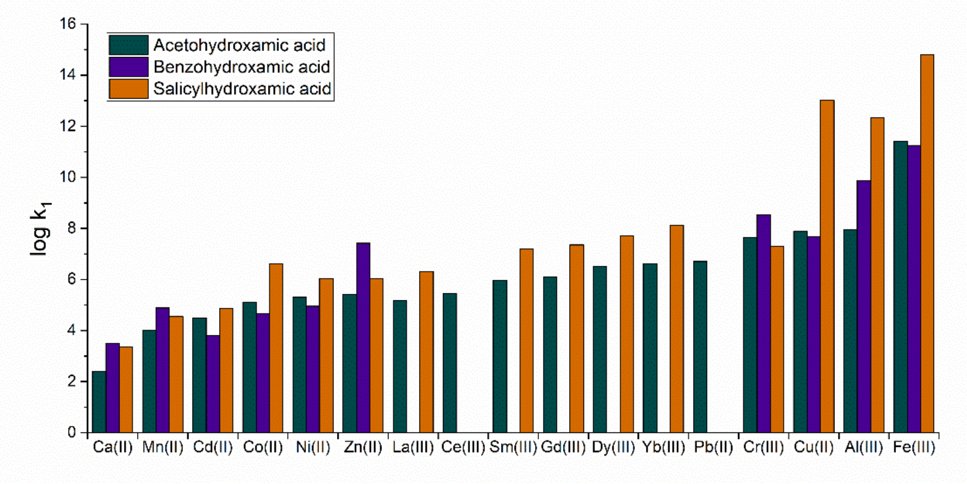

Figure B.2 - Stability constants for metal complexes with AHA, SHA and BHA. Adapted from (Fuerstenau, 2005; Khairy *et al.*, 1996; Khalil and Fazary, 2004; Sastri *et al.*, 2003)

Hydroxamic acids and their salts (collectively referred to as hydroxamates) are, generally, considered to be the most effective collectors for bastnäsite and monazite flotation. There is a large body of work demonstrating their selectivity and collectivity for bastnäsite and monazite; and they are used to process the Bayan Obo deposit (Zhang and Edwards, 2012). A summary of the literature available for REM flotation using hydroxamic acids is given in Tables B.5 to B.9. It should be noted that the optimum pH for flotation often occurs at around pH 9. This is roughly the pKa of hydroxamic acid collectors (Fuerstenau and Pradip, 2005; Gupta, 2013; Pradip and Fuerstenau, 1983). Fuerstenau and Pradip (2005) suggested that, in some mineral systems, at the pKa of the hydroxamic acid collector the hydroxamate anion adsorbs alongside the neutral molecule, resulting in multilayers of collector adsorption. At this pH, elevated concentrations of rare-earth hydroxy species are also present providing ideal conditions for collector adsorption (Assis *et al.*, 1996).

As cerium is typically the primary REE in bastnäsite and monazite, much of the work focused on understanding mechanisms of collector adsorption are focussed on the interaction of the collector with solvated cerium species. The findings to date strongly suggest that hydroxylated cerium complexes, $Ce(OH)^{2+}$ and $Ce(OH)_2^{+}$, at the mineral surface provide adsorption sites for the hydroxamate collector (Jordens *et al.*, 2014b; Pradip and Fuerstenau, 1985; Sarvaramini *et al.*, 2016). Quantum mechanical simulations using density functional theory (DFT) have indicated that the interaction of $Ce(OH)^{2+}$ and $Ce(OH)_2^{+}$ with up to three heptylhydroxamic acid (HHA) anions is thermodynamically favourable, which leads to the formation of $[Ce(OH)(HHA)_3(H_2O)]^{-}$ and $[Ce(OH)_2(HHA)_3]^{2-}$ at the mineral surface (Sarvaramini *et al.*, 2016).

Although hydroxylated REE complexes are understood to be important for the flotation of both bastnäsite and monazite (Cheng *et al.*, 1993; Espiritu and Waters, 2018), the specific manner by which hydroxamates interact with each mineral is believed to be different. It has been demonstrated that below monolayer coverage, hydroxamates adsorb on semi-soluble minerals, such as bastnäsite, through endothermic surface precipitation (Pradip and Fuerstenau, 1985, 1991; Zhang and Honaker, 2017). Adsorption onto minerals with low solubility, such as monazite, occurs through exothermic chemisorption (Zhang and Honaker, 2017). As the collector concentration increases above monolayer coverage, the adsorption mechanism changes from exothermic chemisorption to endothermic surface precipitation (Zhang and Honaker, 2017). Both these processes are entropy-driven reactions (positive change in entropy) (Pradip and Fuerstenau, 1985; Zhang and Honaker, 2017); therefore, increases in temperature are likely to play a beneficial role in adsorption. It has been demonstrated for both minerals that temperature increases result in increased adsorption densities and flotation recoveries (Pavez and Peres, 1993b; Pradip and Fuerstenau, 1985; Zhang and Honaker, 2017). Improvements in selectivity as a result of temperature increases have also been demonstrated (Pavez and Peres, 1993b; Pradip and Fuerstenau, 1985). Li *et al.* (2018) suggested that at low temperatures (35°C) naphthyl hydroxamic acid adsorption to bastnäsite and monazite was unstable and as temperature increased (75°C) the adsorption stability increased. Pavez and Peres (1993b) found greater improvements of monazite recovery compared to zircon and rutile with increased temperatures (up to 65°C) and Pradip and Fuerstenau (1985) demonstrated increased temperatures (up to 61°C) favoured bastnäsite flotation over calcite and barite, using octylhydroxamic acid (OHA) and potassium octylhydroxamate (POH), respectively. Pradip and Fuerstenau (1985) suggested that at room temperature POH adsorbed to bastnäsite, calcite and barite, but with different free energies of adsorption; thermodynamically favouring bastnäsite. As the temperature increased, so did collector adsorption onto all three minerals, but it did so disproportionately: increasing the difference in free energies of adsorption, hence improving selectivity. While temperature increases have been generally shown to improve both selectivity and REM recovery (Li *et al.*, 2018; Pavez and Peres, 1993b; Pradip and Fuerstenau, 1985, 1991; Zhang and Honaker, 2017), there are instances where temperature increases have been detrimental to REM flotation with hydroxamate collectors (Pavez and Peres, 1993b; Wang *et al.*, 2012). Although Pavez and Peres (1993b) found a positive impact of temperature when using OHA, they also found that when using the commercial hydroxamate Flotinor V3759, monazite recovery dropped and zircon and rutile recovery increased slightly with increasing temperature. Wang *et al.* (2012) found that increased temperature (up to 35 °C) resulted in minor improvements in grade and recovery when floating the Maoniuping bastnäsite ore with a modified hydroxamate collector. However, further temperature increases were detrimental to bastnäsite recovery and increases above 50°C were detrimental to grade.

Extensive literature exists demonstrating the effectiveness of hydroxamic acid-based collectors for the flotation of REM and other minerals; however, a wide variety of different hydroxamate collectors have been studied, with very few fundamental studies examining the impact of the collector's structure on flotation. Some work has been conducted investigating the effect of the hydrocarbon chain length of alkyl hydroxamates (Palmer *et al.*, 1973; Sreenivas and Padmanabhan, 2002), suggesting that an improved flotation performance can be achieved with a longer hydrocarbon chain. Others, however, have noted a reduced flotation performance with hydroxamates which have carbon chains longer than C_9 (Bulatovic, 2007a). While most laboratory work to date investigating the flotation of minerals with hydroxamate collectors focuses on the use of alkyl hydroxamates, a modified naphthyl hydroxamate (known as H_{205}) has been widely used to process Chinese bastnäsite ores, producing rare-earth oxide (REO) concentrates with grades above 50 % (Jordens *et al.*, 2013; Li *et al.*, 1988; Zhang and Edwards, 2012). Li *et al.* (1988) compared this collector to a commercial C_5-C_9 alkyl hydroxamate mixture and naphthyl hydroxamate for the flotation of the Bayan Obo deposit. Although higher dosages of H_{205} were required, it resulted in improvements in both grade and recovery, while eliminating the use of sodium fluorosilicate as a depressant. This work also suggested that the naphthyl collector offered greater selectivity over the alkyl hydroxamate, albeit at lower recoveries. More recently, the use of H_{205} has been compared to cheaper modified naphthyl hydroxamates, known as Dh and L_{102} (Che *et al.*, 2003; Jordens *et al.*, 2013). These collectors both resulted in a comparable flotation performance to H_{205}, with expected cost reductions. In the case of Dh the reductions in cost are estimated to be as high as 50 % (Che *et al.*, 2003). Xia *et al.* (2014) compared the use of three different aromatic hydroxamates (BHA, SHA and H_{205}) in the flotation of the Nechalacho ore. The authors found that all three collectors were effective at recovering REM; however, depending on the rare earth cation present in the mineral lattice each collector produced a different flotation response. SHA was most effective at recovering LREM, whereas BHA was most effective at recovering HREM. Subsequently, a more extensive study on the same ore was performed, investigating 3 aromatic hydroxamates (BHA, SHA and tert-butyl benzo hydroxamate), a cyclic alkyl hydroxamate (cyclohexylhydroxamate) and an alkyl hydroxamate (OHA) (Hart *et al.*, 2014). It is important to note that there is currently no commercial process for manufacturing tert-butyl benzo hydroxamate; however, all other hydroxamate collectors which were investigated are manufactured commercially. Similar results were obtained to those of Xia *et al.* (2014), however, in this case the authors also indicated that lower dosages of OHA were required to obtain similar recoveries to the other collectors investigated (Hart *et al.*, 2014). From the above studies it can be concluded that the hydroxamate structure plays a significant role in flotation, and while aromatic hydroxamates generally offer greater selectivity, they typically require elevated dosages to achieve similar recoveries to alkyl hydroxamates. It is also likely that the optimal hydroxamate collector will vary depending on the mineral deposit.

As evident from the preceding discussion, the response of REM to hydroxamic acid collectors varies not only by the collector's structure but also by mineral type. Literature suggests that carbonate, phosphate and niobate minerals tend to float without much difficulty, whereas silicate minerals do not appear to respond well without excessively high collector dosages or the use of metal activators to promote collector adsorption.

The carbonate REM which have been examined by single mineral flotation experiments are bastnäsite, parisite, and ancylite. Other studies on various ore deposits have also provided some insight into the flotation of synchysite and various barium-rich fluorocarbonate REM found in the Montviel deposit (Canada). The successful flotation of bastnäsite is well documented with a variety of hydroxamate collectors in both single mineral (Table B.5) and ore flotation (Table B.8) experiments. While there is limited work documenting the other minerals, they have been shown to respond well to the hydroxamates tested (Cui and Anderson, 2017a, b; Deng and Hill, 2014; Jordens *et al.*, 2016a; Owens *et al.*, 2018). Parisite and synchysite are a part of a polysomatic series of fluorocarbonate minerals, along with bastnäsite and röntgenite. As such, it is expected that these minerals would respond similarly to hydroxamates (and other flotation reagents). This has been suggested through zeta potential measurements by Owens *et al.* (2018), who demonstrated that parisite and bastnäsite have a similar zeta potential response to the presence of a commercial hydroxamate collector. Likewise, it has been demonstrated in a real ore system by Jordens *et al.* (2016a), who found a similar flotation response between synchysite and bastnäsite when floating a gravity concentrate from the Nechalacho deposit using BHA. It should be noted, however, that although the minerals exhibited only small differences in flotation response both the recovery and kinetics of bastnäsite was greater than that of synchysite. This could be as a result of the lower REE content of synchysite compared to bastnäsite, providing less sites for collector adsorption. Another possibility is that the average grain size of synchysite is less than that of bastnäsite, resulting in reduced liberation and floatability. The grain size of synchysite in ore deposits is typically very small, which makes its flotation in real ore systems challenging, as well as difficulty in obtaining enough pure crystals for fundamental flotation studies. Deng and Hill (2014) found a commercial SHA collector (TR047) to be highly selective when floating a Canadian synchysite ore, however, recoveries were low; the authors attributed this to poor liberation. The specific REM of the Montviel deposit are difficult to define and different mineralogical studies have identified different REM (Nadeau *et al.*, 2015; Negeri and Boisclair, 2016). The major REM which have been identified, however, belong to a series of barium rich fluorocarbonate minerals, which have highly similar structures to bastnäsite. Therefore, similar flotation responses are expected. Flotation work on the Montviel deposit is limited, and as REM in this ore are difficult to define there exists little understanding of each mineral's exact response to hydroxamates, although, high REE recoveries have been obtained using Aero 6493 (an industrial alkyl hydroxamate). The final

RE-bearing carbonate mineral for which literature exists is ancylite. Single mineral studies have shown that high recoveries can be achieved using OHA (Cui and Anderson, 2017b), which translates well to its response in the flotation of the Bear Lodge (USA) deposit, where ancylite is the primary REM (Cui and Anderson, 2017a).

The second class of minerals which have received the most research are phosphate minerals. To date hydroxamates have only been tested for monazite and xenotime, which have been studied primarily in single mineral systems (Table B.6 and Table B.7). There also exists a small amount of literature regarding the flotation of ores where monazite is the primary REM (Table B.8). Monazite also exists as a secondary mineral in many REM deposits; however, these studies generally report REE or REO information, rather than specific information regarding the response of each REM present in the deposit. Although both these minerals can be floated using hydroxamates, the study by Jordens *et al.* (2016a), which investigated the flotation of the Nechalacho deposit using BHA, found monazite to have a much lower recovery and rate of recovery when compared to carbonate minerals such as bastnäsite and synchysite. Similar findings were observed by Li *et al.* (2018), who found bastnäsite floatability was greater than that of monazite when floating the Bayan Obo ore with a napthyl hydroxamic acid collector. This is likely due to differences in mineral solubility, supporting the hypothesis of Assis *et al.* (1996). Although there is no literature demonstrating this effect, xenotime may have a greater flotation response compared to monazite, as free energy of adsorption measurements suggest the adsorption of OHA to the surface of xenotime is through endothermic surface precipitation, most likely similar to that of bastnäsite (Zhang and Honaker, 2017). Apatite is a secondary phosphate mineral which can contain economic concentrations of REE. There exists no literature exploring the use of hydroxamates to process REE-bearing apatite, however, Yu *et al.* (2016b) demonstrated that apatite can be easily separated from dolomite using an alkylhydroxamate. The mechanism of hydroxamate adsorption was described as chemisorption: bonding to calcium at the surface of the mineral.

Although niobates are traditionally recovered for their niobium content, they often contain significant concentrations of REE. The minerals for which literature exists detailing their flotation response to hydroxamates are pyrochlore, columbite and fergusonite. The most widely studied mineral is pyrochlore, for which a review detailing its flotation can be found in Gibson *et al.*

(2015). Both BHA and alkyl hydroxamates have been used to float this mineral. For columbite and fergusonite there exists limited literature detailing their flotation. However, as these minerals are relatively soluble and contain niobium and REE (in some cases), which hydroxamic acids are known to form strong complexes with, it is expected that they will have a strong flotation response. This was demonstrated by Jordens *et al.* (2016a), in the flotation of the Nechalacho deposit using BHA, where both fergusonite and columbite recovery and recovery rate were comparable to that of bastnäsite.

As mineral solubility plays an important role in the adsorption of hydroxamate collectors to mineral surfaces, it is expected that silicate minerals, which are highly insoluble, have a significantly reduced response to hydroxamates. This has been demonstrated both in single mineral systems and ore systems. In a surface chemical study of allanite flotation, Jordens *et al.* (2014a) found that even with very high dosages of BHA, recovery of allanite was limited. Zircon has been shown to float using alkyl hydroxamic acids (Pavez and Peres, 1993a; Pavez and Peres, 1993b), however, when using a commercial aromatic hydroxamate zircon is not recovered (Marion *et al.*, 2019). These results may suggest that aromatic hydroxamates, such as BHA, tends to adsorb to mineral surfaces primarily through surface reactions and therefore mineral solubility is important. Alkyl hydroxamates, such as OHA, however, can more readily form coordinate and/or covalent bonds with surface metal cations fixed in the mineral lattice. In real ore systems, hydroxamates have been shown to be ineffective for the flotation of REE-bearing silicates without the use of activators. Jordens *et al.* (2016a) found relatively poor zircon and allanite recoveries when floating the Nechalacho deposit with BHA. Although a second addition of BHA resulted in slight increases in recovery of both minerals, significant increases in recovery only occurred after the addition of lead chloride as an activator. Although this did result in the preferential recovery of these minerals, it also increased the recovery of silicate gangue minerals. Similarly, Oyediran *et al.* (2014) and Yu *et al.* (2016a) studied the use of an unidentified alkyl and aromatic hydroxamate, along with a commercial aromatic collector (Florrea 7510) for the flotation of the Strange Lake ore (Canada) - a highly complex ore consisting of primarily REE-bearing silicates, such as gadolinite, gerenite, kainosite, zircon, gittensite, thorite and allanite. In both studies the authors provide only limited information how the various minerals responded to different collector systems, and instead used elemental information to asses flotation performance. In the initial study the unnamed aromatic hydroxamate resulted in low REE recoveries and minimal upgrading (Oyediran *et al.*, 2014). The alkyl hydroxamate was found to be the best collector for this ore when compared to various fatty acid and phosphoric acid ester collectors with REE recoveries of 91 % and upgrade ratios of 2.2 (Oyediran *et al.*, 2014). Yu *et al.* (2016a) later tested Florrea 7510 to improve the selectivity of the process. Using this collector alone resulted in a much lower recovery. However, the addition of other surfactants such as alkyl succinamate, octyl phosphonic acid, citric acid and oxalic acid all resulted in increased recovery of zirconium-, cerium- and yttrium-bearing minerals, with phosphonic acid offering the greatest recovery improvements. While this reagent scheme was effective at recovering and upgrading monazite, allanite and to a lesser extent zircon and other REE-bearing silicates, the recovery of gittensite remained poor. The process was also not effective at rejecting iron oxide or aegirine gangue. However, it did offer improvements over the alkyl hydroxamate tested previously. Another ore in which REE are present in silicate minerals was studied by Yang *et al.* (2015). In this case the primary REE-bearing minerals were the silicate minerals, elpidite, zircon, cerite and gittinsite and carbonate minerals, parasite, bastnäsite and synchysite. In this case, the authors found the commercial alkyl hydroxamate Aero 6494 could achieve high REE recoveries, but, with minimal upgrading.

Table B.5 – Summary of single mineral flotation studies on bastnäsite using hydroxamate collectors

REM	Hydroxamate Collector	Gangue Minerals	Other Surfactants	pH	Reference
Bastnäsite	POH			9.3	Pavez *et al.* (1996)
		Barite, Calcite	Sodium carbonate^{d,pH} Lignin sulfonate^{d}	8-9	Pradip and Fuerstenau (1991)
	OHA	Fluorite	Ethylenediamine-tetraacetic acid^{d}	9	Cao *et al.* (2018b)
	C_5 – C_9 alkyl	Barite, Fluorite, Calcite	Sodium carbonate^{d,pH} Sodium silicate^{d} Sodium fluorosilicate^{d}	9.3	Luo and Chen (1984)
	Aero 6493 (C_6 -C_{10} alkyl)			7-9	Sarvaramini *et al.* (2016)
		Calcite, Dolomite, Quartz		9	Azizi *et al.* (2016)
	BHA	Quartz		9	Jordens *et al.* (2014b)
		Dolomite		9	Espiritu *et al.* (2018b)
		Dolomite		9	Espiritu *et al.* (2018a)
	H_{205}	Barite, Calcite		8-10	Yang *et al.* (2017)
	SHA	Barite, Fluorite, Calcite	Strontium chloride hexahydrate^{o}	6.5 - 9	Cao *et al.* (2018a)
	Modified SHA			9	Ren *et al.* (1997)

The purpose of the other surfactant tested is detailed by d for depressant, pH for pH modifier and o for other reagents

Table B.6 – Summary of single mineral flotation studies on monazite using hydroxamate collectors

REM	Hydroxamate Collector	Gangue Minerals	Other Surfactants	pH	Reference
Monazite	POH			9	Pavez *et al.* (1996)
		Zircon Rutile	Sodium metasilicate^{d}	10	Pavez and Peres (1993b)
	OHA	Calcite		9	Zhang *et al.* (2017)
		Calcite		9	Zhang *et al.* (2016)
				9	Zhang and Honaker (2017)
		Calcite	Sodium silicate^{d} Sodium hexametaphosphate^{d} Citric acid^{d} Ethylenediamine-tetraacetic acid^{d}	9	Zhang and Honaker (2018)
		Apatite Ilmenite Quartz Rutile Zircon		7-10	Nduwa-Mushidi and Anderson (2017)
	C_5 – C_9 alkyl	Barite Fluorite Calcite	Sodium carbonate^{d,pH} Sodium silicate^{d} Sodium fluorosilicate^{d}	9.3	Luo and Chen (1984)
	Aero 6493 (C_6 -C_{10} alkyl)			7-9	Sarvaramini *et al.* (2016)
	BHA	Dolomite		7-9	Espiritu *et al.* (2018b)
		Dolomite		7	Espiritu and Waters (2018)
		Dolomite		9	Espiritu *et al.* (2018a)
	Flotinor V3759	Zircon Rutile	Sodium metasilicate^{d}	9 - 10	Pavez and Peres (1993b)
	AEROFLOAT 6494	Hematite Quartz		7 – 9	Abaka-Wood *et al.* (2017)

The purpose of the other surfactant tested is detailed by d for depressant and pH for pH modifier

Table B.7 – Summary of single mineral flotation studies on other REM using hydroxamate collectors

REM	Hydroxamate Collector	Gangue Minerals	Other Surfactants	pH	Reference
Xenotime	Flotinor V3759	Zircon	Lignin sulfonate[d] Quebracho[d] Corn starch[d] Amylopectin[d] Sodium metasilicate[d]	10	Pereira and Peres (1997)
	OHA	Ilmenite Zircon Schorl Staurolite		9	Zhang and Anderson (2017b)
		Ilmenite Zircon Schorl Staurolite	Sodium silicate[d] Lignin sulfonate[d]	5 – 9	Zhang and Anderson (2017a)
Allanite	BHA	Quartz		None	Jordens *et al.* (2014a)
		Quartz	Iron chloride[a]	4	Jordens *et al.* (2014c)
Ancylite	OHA	Calcite Strontianite		6 – 10	Cui and Anderson (2017b)
Collophane	Alkyl	Dolomite		2 – 12	Yu *et al.* (2016b)

The purpose of the other surfactant tested is detailed by d for depressant and a for activator

Table B.8 – Summary of bastnäsite and monazite ore flotation studies using hydroxamate collectors

Deposit	REM	Major Gangue Minerals	Hydroxamate Collector	Other Surfactants	pH	Reference
Bayan Obo	Bastnäsite Monazite	Fluorite Iron minerals Barite Apatite Calcite Quartz	C_{5-9} alkyl	Sodium silicate^{d} Sodium carbonate^{d} Sodium fluorosilicate^{d}	-	Li *et al.* (1988)
					9.3	Luo and Chen (1984)
			Naphthyl	Sodium silicate^{d} Sodium carbonate^{d} Sodium fluorosilicate^{d}	-	Li *et al.* (1988)
				Sodium silicate^{d}	8.5	Li *et al.* (2018)
			H_{205}	Sodium silicate^{d} Sodium carbonate^{d}	8.5 – 9	Li *et al.* (1988)
			Modified	Sodium silicate^{d} $H_{103}{}^{d}$	9	Ren *et al.* (1997)
Mountain Pass	Bastnäsite	Calcite Barite Celestite	POH	Sodium carbonate^{d} Lignin sulfonate^{d}	8-9	Pradip and Fuerstenau (1991)
Maoniuping	Bastnäsite	Barite Fluorite Calcite Quartz	Modified	Sodium silicate^{d} $H_{103}{}^{d}$	9	Ren *et al.* (1997)
			Modified	Sodium silicate^{d}	-	Wang *et al.* (2012)
			C_{5-9} alkyl	Sodium carbonate^{d} Sodium silicate^{d} Sodium fluorosilicate^{d}	-	Reported by Chi *et al.* (2001)
Weishan	Bastnäsite	Barite Fluorite Silicates	Modified	Sodium silicate^{d} $H_{103}{}^{d}$	9	Ren *et al.* (1997)
			L_{101}	Sodium silicate^{d}		Reported by Chi *et al.* (2001)
Niobec	Bastnäsite Monazite	Dolomite Calcite	Aero-6493		9	Azizi *et al.* (2016)
			Florrea 7510	Sodium silicate^{d} Guar gum^{d}	8 – 9	Boulanger *et al.* (2019)
Kaolin deposit in St Austell	Monazite	Quartz Micas Tourmaline Feldspars Kaolinite	AC-3	Sodium polyacrylate^{o}	10	Filippov *et al.* (2016)
Deposit in Zhijin, China	Bastnäsite Monazite	Carbonates Iron minerals	Florrea 8920	Sodium silicate^{d}	8.5	Jordens *et al.* (2016b)
Deposit in Sao Goncalo do Sapucai, Brazil	Monazite	Ilmenite Quartz Zircon Rutile	Flotinor V3759	Sodium metasilicate^{d}	10	Pavez and Peres (1994)
Unnamed Chinese Deposits	Bastnäsite Monazite	Barite Fluorite	H_{205}	Sodium silicate^{d}	8-9	Che (1993)
			Dh	Silica gel^{d}	8	Che *et al.* (2003)

The purpose of the other surfactant tested is detailed by d for depressant and o for other reagents

Table B.9 – Summary of other REM ore flotation studies using hydroxamate collectors

Deposit	REM	Major Gangue Minerals	Hydroxamate Collector	Other Surfactants	pH	Reference
Nechalacho	Zircon Bastnäsite Synchysite Allanite Monazite Fergusonite Columbite	Feldspars Quartz Iron Oxides	POH	Sodium silicate[d]	8.5 – 9	Hart *et al.* (2014)
			BHA	Lead chloride[a]	9	Jordens *et al.* (2016a)
				Lead nitrate[a]	9	Xia *et al.* (2015)
				Sodium silicate[d]	8.5-9	Xia *et al.* (2014)
			SHA	Sodium silicate[d]	8.5-9	Xia *et al.* (2014)
				Sodium silicate[d]	8.5 – 9	Hart *et al.* (2014)
			LF-P81	Lead nitrate[a]	9	Xia *et al.* (2015)
			H_{205}	Sodium silicate[d]	8.5-9	Xia *et al.* (2014)
				Sodium silicate[d]	8.5 – 9	Hart *et al.* (2014)
			Cyclohexyl	Sodium silicate[d]	8.5 – 9	Hart *et al.* (2014)
			Tetra-butyl benzyl	Sodium silicate[d]	8.5 – 9	Hart *et al.* (2014)
Bear Lodge	Ancylite	Calcite Pyrite Strontianite Feldspar	OHA	Sodium carbonate[d,pH] Strontium nitrate[o]	9-10	Cui and Anderson (2017a)
Montviel	Huanghoite Cebaite 17 trace REM	Ankerite Dolomite Siderite Quartz Calcite	Aero 6493	Sodium silicate[d] Carboxymethyl Cellulose[d]	10	Negeri and Boisclair (2016)
Strange Lake	Gadolinite Gerenite Kainosite Zircon Gittinsite Thorite Allanite Monazite Bastnäsite	Quartz Feldspars	Florrea 7510	Sodium silicate[d] Alkyl succimate[a] Phosphinic acid[a] Citric acid[a,d] Oxalic acid[a]	8.5	Yu *et al.* (2016a)
			Alkyl	Sodium silicate[d]	10	Oyediran *et al.* (2014)
Unnamed Deposit	Zircon Elpidite Cerite Allanite Parisite Bastnäsite Synchysite Pyrochlore	Feldspar Quartz	Aero 6494	Sodium silicate[d]	8.8 – 9.3	Yang *et al.* (2015)
Unnamed Canadian Deposit	Synchysite	Ankerite Dolomite	TR047	Sodium silicate[d]	8.2	Deng and Hill (2014)

The purpose of the other surfactant tested is detailed by d for depressant, a for activator, pH for pH modifier and o for other reagents

B.2.4.2 Carboxylates

Carboxylates are the most widely used collectors in industrial practice and were traditionally the collector of choice for REM flotation, prior to the development of hydroxamates as viable flotation collectors (Bulatovic, 2007a; Jordens *et al.*, 2013). Various carboxylate collectors exist, with the most commonly employed being oleic acid, sodium oleate, tall oils (mixtures of oleic, linoleic, conjugated linoleic, palmitic and stearic acids), and some oxidized petroleum derivatives (Bulatovic, 2007a). Although they were industrially employed at Mountain Pass and are used in a primary flotation stage for the processing of the Bayan Obo deposit, these collectors are generally unselective and require elevated temperatures and the addition of large quantities of depressants to be effective (Bulatovic, 2010; Houot *et al.*, 1991; Jordens *et al.*, 2013; Zhang and Edwards, 2012). As such, much of the recent studies focused on REM flotation use hydroxamates and there exists limited work studying the flotation of REM other than bastnäsite, monazite and xenotime. A summary of the work focused on carboxylate flotation of pure REM and various REM deposits is given in Tables B.10 to B.12. As can be seen from these tables most of the studies use sodium oleate or oleic acid as carboxylate collector. However, tall oil fatty acids have been suggested to offer improved results (Bulatovic, 2010).

The adsorption of sodium oleate to the surface of bastnäsite has been well documented in literature. It has been shown to chemisorb to the bastnäsite surface with the maximum adsorption and floatability occurring at pH 9 (Jordens *et al.*, 2014b; Pavez *et al.*, 1996). More recent work, however, found maximum bastnäsite recovery to occur from pH 4 to 8, after which further increases in pH resulted in decreases in recovery (Espiritu *et al.*, 2018b). The authors did not provide any explanation for the observed differences between their study and those by Jordens *et al.* (2014b) and Pavez *et al.* (1996), however, these differences may be a result of differences in the origin of the bastnäsite sample used, or minor impurities in the sample causing a different flotation response. Similar to hydroxamate flotation, it is suggested that hydroxylated REE species at the surface of the mineral provide sites for collector adsorption (Pavez *et al.*, 1996). The application of fatty acid collectors to bastnäsite deposits is primarily discussed with regards to the Mountain Pass deposit, which employed a tall oil collector, elevated temperatures and various depressants to achieve selective separation (Ferron *et al.*, 1991; Houot *et al.*, 1991; Jordens *et al.*, 2013). The improved selectivity at elevated temperatures has been explained by the increased solubility of the collector, an increase in dissolved REE species at the bastnäsite surface, and the preferentially enhanced collector adsorption on the surface of bastnäsite relative to gangue minerals (Jordens *et al.*, 2013). The preferential increase in collector adsorption to the surface of bastnäsite may be described by Figure B.3. Using this description, it is suggested that bastnäsite has made the transition from physisorption to chemisorption at the temperatures being used, whereas, gangue minerals (calcite and barite) fall into a regime where collector adsorption decreases (Jordens *et al.*, 2013). For the Mountain Pass deposit, temperature increases above 75 °C were detrimental, resulting in increased gangue recovery (Jordens *et al.*, 2013). Another explanation for the improvements observed at elevated temperatures could be similar to that given for hydroxamic acids, where temperature increases cause disproportionate increases in the free energies of adsorption, thermodynamically favoring adsorption to the surface of bastnäsite over gangue (Jordens *et al.*, 2013). However, there is no published literature demonstrating this effect. At the Bayan Obo deposit, the lack of selectivity of fatty acid collectors is overcome by only employing them in an initial unselective flotation stage, and subsequently using a hydroxamate to selectively recover REM (Houot *et al.*, 1991; Jordens *et al.*, 2013; Zhang and Edwards, 2012). The removal of fatty acid from the surface of gangue minerals prior to a more selective flotation stage is imperative to facilitate selective REM flotation (Luo and Chen, 1984). Fatty acids have also been employed at the Weishan deposit in China, where an oleic acid type collector was used to produce a concentrate containing > 60 % REO (Chi *et al.*, 2001). There exists little information (in English literature) detailing the exact process used, however, they have since moved to using more selective hydroxamate collectors (Chi *et al.*, 2001).

The use of fatty acid collectors for monazite and xenotime flotation has also been well described, primarily in the context of heavy mineral sands deposits. Compared to bastnäsite, the adsorption of sodium oleate (and oleic acid) to the surface of both minerals has been shown to occur over a wider pH range (pH 3 – 11). Maximum monazite recoveries are generally reported at pH 3 and in the pH range 6-9 (Abaka-Wood *et al.*, 2017; Abeidu, 1972; Cheng *et al.*, 1993; Espiritu *et al.*, 2018b; Pavez *et al.*, 1996; Pavez and Peres, 1993a). It is noted that while similar trends were observed by these authors there were differences in flotation response. Abeidu (1972) tested the pH range 4 – 10 and observed elevated recoveries from 5 to 9, with a maximum at pH 7. Cheng *et al.* (1993) observed high recoveries from pH 3 to 10. Pavez and Peres (1993a) and Pavez *et al.* (1996) observed recovery maximums at pH 3 and 7, with elevated recovery across the pH range investigated (2 – 10). Abaka-Wood *et al.* (2017) observed a maximum at pH 9, with relatively high recovery from pH 5 – 9 and a drastic decrease at pH 3 and 11. Espiritu *et al.* (2018b) found maximum recoveries in the pH range of 6 – 7, and low recoveries at pH 4 and from pH 8 – 11. These differences between authors may indicate that different monazites will have differences in flotation response when using sodium oleate or oleic acid. Maximum xenotime recovery has been reported to occur in the pH range of 7 – 9 (Cheng *et al.*, 1993; Cheng *et al.*, 1994; Zhang and Anderson, 2017a). The mechanism of fatty acid adsorption to the surface of monazite has been reported as physisorption at pH 3 and chemisorption in the pH range 6 – 9 (Pavez *et al.*, 1996). The mechanism of adsorption to the surface of xenotime is reported to be chemisorption (Cheng *et al.*, 1994; Zhang and Anderson, 2017a). As described for bastnäsite, it has been suggested that hydroxylated REE species at the surface of these minerals provide sites for fatty acid adsorption (Cheng *et al.*, 1993). Increases in temperature have also been shown to be beneficial to the flotation of both minerals (Jordens *et al.*, 2013; Pavez and Peres, 1993b; Zhang and Anderson, 2017a). The application of fatty acids to REM deposits containing monazite and/or xenotime is generally reported to be more successful than that of bastnäsite, which is primarily a result of the different mineralogy of these deposits. Several authors have reported high grades and recoveries can be achieved using fatty acids in combination with depressants to recover monazite and xenotime from heavy mineral sands deposits (Andrews *et al.*, 1990; Pavez and Peres, 1994). The use of fatty acids has also been shown to be successful for the flotation of xenotime from a relatively simple Australian deposit (Hadley and Catovic, 2014). However, for more complex monazite and/or xenotime bearing ores, they are generally ineffective (Filippov *et al.*, 2016; Goode *et al.*, 2014; Jeong and Cho, 2014; Satur *et al.*, 2016). The only exception to this, so far, is for the Mount Weld deposit in Australia (Chan, 1992; Guy *et al.*, 2000), where two different flotation schemes employing fatty acids have been proposed. The first uses a blended collector emulsion of fatty acid, with an emulsifier, typically a secondary amino modified sulfonated fatty acid, along with sodium silicate, sodium sulfide and a starch as depressants (Chan, 1992). The second method employs an unnamed fatty acid collector in combination with similar depressants (Guy *et al.*, 2000). Although the Mount Weld deposit is currently operational, there exists no literature reporting the specifics of their flotation process.

Other minerals for which a minor amount of literature exists detailing their interaction with carboxylates are apatite, allanite, columbite, fergusonite, steenstruspine, cerite, zircon and elpidite. Flotation processes for REE-bearing apatites are similar to those used to recover apatite for the phosphate industry (Beer *et al.*, 2014; Harbi *et al.*, 2011; Houot, 1982), where fatty acid flotation is well established (Lu *et al.*, 1998). The flotation of allanite using fatty acids was described by Jordens *et al.* (2014a). The authors found allanite could be recovered at elevated sodium oleate dosages with a maximum recovery occurring at pH 7. However, very high (1 kg/t) dosages were required. The flotation of columbite using sodium oleate was reported by Harada *et al.* (1993). The authors did not note if the columbite sample used contained REE; however, high recoveries were reported over the pH range of 2 – 10, with maximum recovery occurring at pH 2 and 6 – 10. Fergusonite flotation using sodium oleate was reported by Fawzy (2018). Flotation occurred from pH 2 – 10, with highest recovery at pH 5. The authors suggested using Span 80 to enhance the floatability of fergusonite. The flotation of steenstruspine (and monazite) from the Kvanefjeld deposit in Greenland using different carboxylate collectors was described by Sorensen and Lundgaard (1966). They also explored the use of lanthanum ions as an activator, with limited success. The use of sodium oleate was shown to outperform a hydroxamate and a phosphoric acid ester for the flotation of a complex ore containing primarily REE-bearing silicates (Yang *et al.*, 2015). However, the results suggested that only REE-bearing carbonates demonstrated a good flotation response. Cerite and allanite, had significantly reduced recovery and recovery rates compared to bastnäsite, parisite and synchysite; and zircon, elpidite and pyrochlore recoveries were less then 20 %. The flotation of eudialyte using sodium oleate and oleic acid has also been reported by Ferron *et al.* (1991), however, there exists no detailed information in English literature.

Table B.10 – Summary of single mineral flotation studies using carboxylate collectors

Mineral	Collector	Other Surfactants	Gangue Minerals	pH	Reference
Bastnäsite	Sodium oleate			9	Pavez *et al.* (1996)
			Dolomite	4 - 8	Espiritu *et al.* (2018b)
			Quartz	9	Jordens *et al.* (2014b)
	Benzoic acid	Potassium alum[d]		4 - 5	Ren *et al.* (2000)
Monazite	Sodium oleate			3, 6-8	Pavez *et al.* (1996)
			Hematite Quartz	9	Abaka-Wood *et al.* (2017)
			Dolomite	6-7	Espiritu *et al.* (2018b)
			Dolomite	7	Espiritu and Waters (2018)
			Zircon Rutile	3, 7	Pavez and Peres (1993a)
				8-9	Cheng *et al.* (1993)
		Sodium metasilicate[d] Sodium sulfide[d]	Zircon Rutile	6-9	Pavez and Peres (1993b)
		Sodium sulfide[d]	Zircon Pyrochlore	7	Zakharov *et al.* (1967)
	Oleic acid	Sodium sulfide[d]	Zircon	6-9	Abeidu (1972)
				4 - 11	Hyung and Ki (1963)
	Linoleic acid			4 – 9	Hyung and Ki (1963)
Xenotime	Sodium oleate			7	Cheng *et al.* (1994)
				7-8	Cheng *et al.* (1993)
	Sodium oleate	Sodium silicate[d] Lignosulfonate[d]	Ilmenite Zircon Schorl Staurolite	7 – 9	Zhang and Anderson (2017a)
Columbite	Sodium oleate			2, 6 – 10	Harada *et al.* (1993)
Allanite	Sodium oleate		Quartz	7.5	Jordens *et al.* (2014a)
Fergusonite	Sodium oleate	Span 80[a] Sodium metasilicate[d] Oxalic acid[d] Citric acid[d]	Zircon Quartz Feldspar	5	Fawzy (2018)

The purpose of the other surfactant tested is detailed by d for depressant and a for activator

Table B.11 – Summary of bastnäsite, monazite and xenotime ore flotation studies using carboxylate collectors

Deposit	REM	Major Gangue Minerals	Collector	Other Surfactants	pH	Reference
Mountain Pass	Bastnäsite	Calcite Barite Celestite	Oleic acid Linoleic acid Linolenic acid Westvaco L-1 Westvaco L-5 Westvaco M-28B	Lignin sulfonates[d] Sodium fluoride[d] Sodium fluorosilicate[d] Sodium carbonate[d,pH]	10	Morrice and Wong (1982)
Bayan Obo	Bastnäsite Monazite	Fluorite Iron minerals Barite Calcite	Paraffin soap	Sodium carbonate[d] Sodium silicate[d]	10.3	Luo and Chen (1984)
Mount Weld	Monazite Cheralite Cerianite Florencite Rhabdophane	Geotite Apatite Crandalite Dolomite Cryptomelane Jacobsite	Tall oil	Sodium silicate[d]	9.8	Wen Qi (1993)
			Unnamed fatty acid	Sodium sulfide[d] Sodium silicate[d] Starch[d]	10.5	Guy *et al.* (2000)
			Fatty acid collector mixture	Sodium sulfide[d] Sodium silicate[d] Starch[d]	-	Chan (1992)
Weishan	Bastnäsite	Barite Fluorite Silicates	Oleic acid	Sodium silicate[d]	8-8.5	Reported by Chi *et al.* (2001)
Sands deposit in Horsham, Australia	Monazite Xenotime	Zircon Rutile Leucoxene Quartz	Acintol FA2	Sodium silicate[d] Sodium fluorosilicate[d]	10	Andrews *et al.* (1990)
Deposit in Sao Goncalo do Sapucai, Brazil	Monazite	Ilmenite Quartz Zircon Rutile	Sodium oleate	Sodium metasilicate[d]	10	Pavez and Peres (1994)
Wolverine	Xenotime	Quartz	Modified	Sodium silicate[d]	-	Hadley and Catovic (2014)
Eco Ridge	Monazite Bastnäsite Synchysite Allanite	Quartz Pyrite	LR19 Oleic acid	Petroleum sulphonate[d] Kerosene[d]		Goode *et al.* (2014)
Kaolin deposit in Saint Austel	Monazite	Quartz Micas Tourmaline Feldspars Kaolinite	Sodium oleate	Sodium polyacrylate[d]	10	Filippov *et al.* (2016)
Chennai beach sand	Monazite	Ilmenite Rutile Zircon Garnet Quartz	Sodium laurate Sodium oleate Neofat 140 Acintol FA1 Actinol FA2 Actinol FAX	Sodium silicate[d]	9.2 – 9.8	Bulatovic (2010)
Unnamed deposit	Xenotime Monazite RE carbonates	Quartz Nontronite Hematite	Aero 704 Sylfat FA2	Lignin sulfonate[d] Sodium metasilicate[d] Sodium fluoride[d] Starch[d]	10.5	Satur *et al.* (2016)

The purpose of the other surfactant tested is detailed by d for depressant and pH for pH modifier

Table B.12 – Summary of other REM ore flotation studies using carboxylate collectors

Deposit	REM	Major Gangue Minerals	Collector	Other Surfactants	pH	Reference
Songwe	Apatite Synchysite	Ankerite Calcite	Betacol CKF30B	Lignin sulfonate^d Sodium carbonate^d Sodium fluorosilicate^d	-	Beer *et al.* (2014)
Kola	Apatite Titanite	Nepheline Feldspar Clinopyroxene	Tall oil	Sodium silicate^d	-	Houot (1982)
Wadi Khamal Nelsonite	Apatite	Ilmenite Magnetite	Oleic acid	Sodium silicate^d	9.5	Harbi *et al.* (2011)
Kvanefjeld	Steenstrupine Monazite	Silicates	Oleic acid Sodium oleate Linoleic acid	Sodium silicate^d Lanthanum nitrate^o	8-9	Sorensen and Lundgaard (1966)
Unnamed Deposit	Zircon Elpidite Cerite Allanite Parisite Bastnäsite Synchysite Pyrochlore	Feldspar Quartz	Sodium oleate	Sodium silicate^d Starch^d	8.8 – 9.3	Yang *et al.* (2015)

The purpose of the other surfactant tested is detailed by d for depressant and o for other reagents

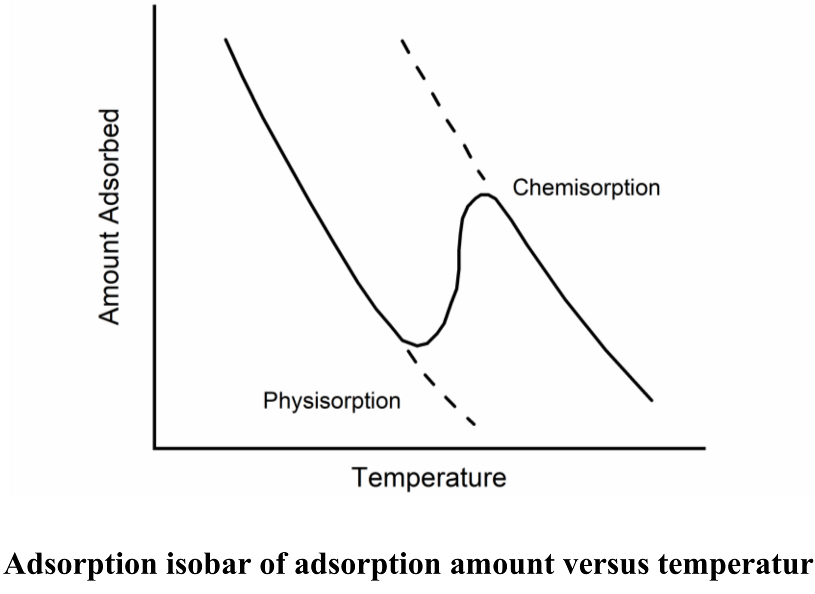

Figure B.3 – Adsorption isobar of adsorption amount versus temperature showing the transition between physical and chemical adsorption. Adapted from Pradip (1981)

B.2.4.3 Phosphoric Acids

After hydroxamates and carboxylates, the next most examined collectors are phosphoric acid-based collectors. Studies examining their application to REM are detailed in Tables B.13 and B.14. These collectors are believed to interact with REM through chemisorption, in a similar manner to hydroxamates and carboxylates (Rao, 2013). Flotation of bastnäsite and monazite has been shown to occur over a wide range of pH (4 – 9 for bastnäsite and 4 – 11 for monazite) (Espiritu *et al.*, 2018b). However, they are typically less selective than hydroxamates (Espiritu *et al.*, 2018b; Jordens *et al.*, 2014b). The selectivity of oxhydryl collectors has been explained by the polarity of the oxygen atoms involved in the collector mineral interactions (Nagaraj, 2018). Nitrogen (in hydroxamates) is the most electronegative, followed by carbon (in carboxylates) and then phosphorous (phosphoric acids) (Nagaraj, 2018). Therefore, the single bonded oxygen present in hydroxamates will be the weakest electron donor and be less available to interact with metal cations (Nagaraj, 2018); whereas, the oxygen in phosphoric acids are more available for complex formation with metal cations and therefore they are typically the least selective (Nagaraj, 2018).

As these collectors are generally unselective, their application to REM deposits is limited. However, there does exist some literature demonstrating their effective use. Andrews *et al.* (1990) tested four different phosphoric acid collectors to recover monazite and xenotime from a heavy minerals sands deposit and found improved selectivity over fatty acids. They also noted that it was possible to float at less alkaline pH when using the phosphoric acid collectors. Yu *et al.* (2016a) compared a hydroxamate collector (with the addition of phosphonic acid) to a phosphoric acid collector (with the addition of citric and oxalic acids) for the flotation of the Strange Lake deposit. In this case both collectors offered similar selectivity, but the phosphoric acid collector scheme was much better at recovering HREE-bearing minerals such as zircon and gittensite. The phosphoric acid ester SM15 has also been demonstrated as an effective collector for recovering eudialyte from the Norra Karr deposit (Stark *et al.*, 2017).

Table B.13 – Summary of single mineral flotation studies using phosphoric acid-based collectors

REM	Collector	Other Surfactants	Gangue Minerals	pH	Reference
Bastnäsite	Flotinor 1682		Dolomite	4 - 8	Espiritu *et al.* (2018b)
	SM15		Quartz	5 - 9	Jordens *et al.* (2014b)
Monazite	Flotinor 1682		Dolomite	4 - 8	Espiritu *et al.* (2018b)
			Dolomite	4 - 7	Espiritu and Waters (2018)

Table B.14 – Summary of REM ore flotation studies using phosphoric acid-based collectors

Deposit	REM	Major Gangue Minerals	Collector	Other Surfactants	pH	Reference
Norra Karr	Eudialyte	Nepheline Feldspars Aegirine	SM15	Oxalic acid^{d} Sodium hexametaphosphate^{d}	<4	Stark *et al.* (2017)
Strange Lake	Gadolinite Gerenite Kainosite Zircon Gittinsite Thorite Allanite Monazite Bastnäsite	Quartz Feldspars	Flotinor 1682	Oxalic acid^{d} Citric acid^{d}	8.5	Yu *et al.* (2016a)
Sands deposit in Horsham, Australia	Monazite Xenotime	Zircon Rutile Leucoxene Quartz	Various phosphoric acid esters	Sodium silicate^{d} Sodium fluorosilicate^{d}	8.5	Andrews *et al.* (1990)

The purpose of the other surfactant tested is detailed by d for depressant

B.2.4.4 Other Collectors

Other collectors which have been examined for REM flotation are alkyl sulfates, sulfonates, amines, ionic liquids and various unique collector blends. These are summarized in Tables B.15 and 16. Alkyl sulfates have been reported as collectors for monazite flotation (Abaka-Wood *et al.*, 2017; Abeidu, 1972; Choi and Whang, 1963; Ferron *et al.*, 1991). Choi and Whang (1963) and Abeidu (1972) reported good monazite floatability at pH below its IEP (pH ≤ ~4), suggesting collector adsorption through electrostatic interactions. Abaka-Wood *et al.* (2017) found contradictory results indicating monazite floats well across the pH range 3 – 11. This would seem to indicate some degree of chemisorption; however, the study did not provide any fundamental explanation for mineral recovery above the IEP of monazite. Sulfonates have also been used as a monazite collector at acidic pH (McEwen *et al.*, 1976). At pH above the IEP, amines have been used as physisorbing collectors to recover REM. Choi and Whang (1963) and Abeidu (1972) found monazite recovery above the IEP using dodecylamonium chloride and dodecylamine, respectively. Ferron *et al.* (1991) reported their use to recover fergusonite and priorite from complex ores and in a double reverse flotation scheme for eudialyte. Eudialyte was reported as being easy to depress, therefore, it was depressed and a fatty acid was used to first remove aegirine and arfredsonite followed by amine flotation to remove feldspars. Amine collectors have also been shown to recover allanite in the pH range 4 – 10 (Jordens *et al.*, 2014a). However, elevated dosages were required to recover allanite when compared to quartz, suggesting the potential for separation by reverse flotation (Jordens *et al.*, 2014a). Flotation using any of these collectors has not been extensively applied or tested in any industrial setting. As gangue minerals typically have similar surface properties and charge as REM, the application of collectors which rely primarily on physisorption is likely to be challenging.

More novel collectors known as ionic liquids have been recently tested for REM flotation, due to their effectiveness in REE extraction and separation (Baba *et al.*, 2011; Binnemans, 2007; Sun *et al.*, 2009; Sun *et al.*, 2012; Sun and Waters, 2014). Tetrabutylammonium bis(2-ethylhexyl)-phosphate, or $[N_{4444}]$[DEHP], was found to offer improved selectivity and collectivity for monazite and bastnäsite in the Niobec deposit compared to an alkyl hydroxamate collector (Azizi *et al.*, 2016). However, these improvements were negligible as both collectors recovered significant amounts of calcite and dolomite. Similarly, Li (2018) tested tetraethylammonium mono-(2-ethylhexyl)2-ethylhexyl phosphonate, or $[N_{2222}]$[EHEHP], as a collector for bastnäsite. It was found that the bastnäsite could be recovered at pH 5; however, the collector had a higher affinity for hematite (recovered from pH 3 – 7).

Collector blends and emulsions have also been reported for the flotation of REM. These include a secondary amine-modified sulphonated fatty acid for bastnäsite flotation (Bulatovic, 1988); an emulsion of a fatty acid, an emulsifier, a phosphonic acid derivative and optional oil/amine additions for monazite flotation (Bulatovic and Willett, 1991); a tallow, fatty acid primary amine acetate (Armac T) for monazite flotation (McEwen *et al.*, 1976); a mixture of Armac T and Reagent

308 for monazite flotation (McEwen *et al.*, 1976); mixtures of alkyl sulphate and phosphate esters (Bulatovic, 2010); a fatty acid/hydroxamate mixture for monazite flotation (Ferron *et al.*, 1991); the blended collector emulsion of fatty acid, with an emulsifier such as a secondary amino modified sulfonated fatty acid described in Section B.2.4.2 for the flotation of the Mount Weld deposit (Chan, 1992); a mixture of sulphosuccinamate and phosphate ester modified with alkylsulphate (known as KBX3) for REM and zircon recovery (Bulatovic, 2010; Yu *et al.*, 2016a); and amine/ester mixtures for fergusonite and priorite flotation (Ferron *et al.*, 1991).

Table B.15 – Summary of single mineral flotation studies using other collectors

REM	**Collector**	**Other Surfactants**	**Gangue Minerals**	**pH**	**Reference**
Bastnäsite	Ionic Liquid: $[N_{2222}]$[EHEHP]		Quartz Hematite	5	Li (2018)
Monazite	Sodium dodecyl sulphate		Zircon	1.5 – 4.5	Abeidu (1972)
				1.5 - 3	Hyung and Ki (1963)
			Hematite Quartz	9	Abaka-Wood *et al.* (2017)
	Armac T		Orthoclase Rutile Plagioclase Ilmenite Garnet	2.5	McEwen *et al.* (1976)
	Reagent 308		Orthoclase Rutile Plagioclase Ilmenite Garnet	2.5	McEwen *et al.* (1976)
	Dodecylamonium chloride			8 – 11	Hyung and Ki (1963)
	Dodecylamine		Zircon	8 – 10	Abeidu (1972)
Allanite	Dodecylamine		Quartz	4 – 10	Jordens *et al.* (2014a)

Table B.16 – Summary of REM ore flotation studies using other collectors

Deposit	REM	Major Gangue Minerals	Collector	Other Surfactants	pH	Reference
Bunbury	Xenotime Monazite	Ilmenite Zircon Garnet Tourmaline Other Silicates	F74286 (Undescribed amphoteric collector)	Sodium silicate^{d}	10	Ozeren and Hutchinson (1990)
Niobec	Monazite Bastnäsite	Calcite Dolomite Quartz	Ionic Liquid: [N_{4444}][EHEHP]	Sodium silicate^{d}	9	Azizi *et al.* (2016)
Rosetta sands deposit	Monazite	Rutile Ilmenite Zircon	Sulphonate 231 Aeropromoter 710 R260 R376 R276R	Sodium oxalate^{d}	-	Bulatovic (2010)

The purpose of the other surfactant tested is detailed by d for depressant

As is evident from Tables B.5 to B.16, the successful separation of REM from gangue, in real ore systems, typically requires the use of other modifying agents. The specific reagents used are ore specific, but generally function to control the ionic composition of the pulp, depress gangue and/or act as activators for REM. The effectiveness of REM flotation is often affected by the ionic composition and hardness of the water which they are floated in. In most cases the presence of dissolved species in solution, from semi-soluble REM and/or accompanying gangue of a semi-soluble nature, have a significant impact on flotation. For example, excess calcium, magnesium or strontium cations in solution from semi-soluble gangue minerals such as calcite, fluorite, dolomite and celestite have been shown to consume collector and result in significantly lower concentrate grades and REM recoveries (Cao *et al.*, 2018a; Espiritu *et al.*, 2018a; Li *et al.*, 1988; Zhang *et al.*, 2017). Some commonly used modifying agents are sodium silicates, sodium carbonate, lignin sulfonates, sodium fluorosilicates, sodium fluoride, starches, sodium sulfide and sodium oxalate. Although some of the reagents listed below are multi-functional they are listed under their primary function.

B.2.5 Pulp/Surface Modifying Agents

B.2.5.1 Sodium Carbonate

Sodium carbonate is used extensively in bastnäsite flotation to regulate the supply of carbonate ions in solution (Houot *et al.*, 1991; Jordens *et al.*, 2013; Pradip and Fuerstenau, 1991). Carbonate ions will affect both the solution pH and the surface properties of bastnäsite and gangue minerals such as calcite and barite (carbonate anions are potential-determining ions for these minerals) (Pradip and Fuerstenau, 1991). Pradip and Fuerstenau (1991) suggested that through the addition of sodium carbonate the surface charge of calcite and barite is positive at pH 9 while bastnäsite is negative. This helps a negatively charged depressant, such as lignin sulfonate, adsorb to the surface of calcite and barite, and allows for fatty acid or hydroxamic acid molecules to adsorb in greater quantities to the surface of bastnäsite. Excess sodium carbonate addition will depress the flotation of bastnäsite (Pradip and Fuerstenau, 1991).

B.2.5.2 Citric Acid

Citric acid has been shown to aid in the flotation of monazite (Zhang and Honaker, 2018). It is suggested that citric acid provides a cleaning action for the monazite surface by chelating with and removing calcium ions (Zhang and Honaker, 2018). Citric acid was tested as a reagent for the flotation of the Strange Lake ore (Yu *et al.*, 2016a). It was shown to result in increased REM recovery using Florrea 7510, Flotinor 1682 and KBX3 (Yu *et al.*, 2016a). The authors suggested the best flotation results occurred with Flotinor 1682 in combination with oxalic acid and citric acid (Yu *et al.*, 2016a). Citric acid combined with sodium metasilicate was suggested to be effective at depressing zircon, quartz, and feldspar in the flotation of fergusonite (Fawzy, 2018).

B.2.5.3 Ethylenediaminetetraacetic acid (EDTA)

EDTA has been used to clean calcium ions from the surface of monazite (Zhang and Honaker, 2018). It offered improvements over citric acid, resulting in greater monazite recovery at optimal dosage and having a lower depressing effect on monazite at elevated dosages (Zhang and Honaker, 2018). It has also been suggested as an effective depressant for fluorite in the flotation of bastnäsite (Cao *et al.*, 2018b). The authors suggested EDTA could remove adsorbed hydroxamate from the surface of fluorite through the formation of dissolved calcium EDTA complexes. Bastnäsite remained unaffected resulting in selective flotation (Cao *et al.*, 2018b).

B.2.5.4 Sodium Polyacrylate

Filippov *et al.* (2016) studied the use of the dispersant sodium polyacrylate for the recovery of monazite from kaolin micaceous residue. It was found to offer significant improvements when compared to flotation without dispersion, resulting in a recovery increase of 50 % and grade improvements of approximately 1.6 times.

B.2.6. Depressants

B.2.6.1 Sodium Silicate

Sodium silicates (also known as water glass) have been employed in the context of REM flotation for the depression of silicate gangue (Chan, 1992; Satur *et al.*, 2016), salt minerals (fluorite, barite, calcite and dolomite) (Boulanger *et al.*, 2019; Li *et al.*, 2018; Luo and Chen, 1984; Ren *et al.*, 1997; Wang *et al.*, 2012; Zhang and Honaker, 2018), iron minerals (Satur *et al.*, 2016; Wen Qi, 1993) and minerals associated with monazite (Pavez and Peres, 1993b) and xenotime (Pereira and Peres, 1997; Zhang and Anderson, 2017a) in placer deposits (zircon, rutile, schorl and staurolite). They have been shown to depress both bastnäsite and monazite, although, they have a greater effect on gangue (Houot *et al.*, 1991; Luo and Chen, 1984; Pavez and Peres, 1993b; Zhang and Honaker, 2018). Sodium silicate has been identified as one of the most important reagents for the successful flotation of the Bayan Obo ore (Jordens *et al.*, 2013). Large dosages are added to depress the flotation of all minerals, and then a small amount of hydroxamic acid is added to selectively float only the REM (Jordens *et al.*, 2013). The large sodium silicate requirement can be reduced by using it in combination with either alum or carboxymethyl cellulose (CMC) (Jordens *et al.*, 2013). The depression mechanism of fluorite, barite and calcite in the Bayan Obo ore has been described as negatively charged colloidal particles of sodium silicate adsorbing to positive calcium and barium hydroxylated complexes at the minerals surface (formed from calcium and barium ions transferring from the mineral surfaces to the highly alkaline solution), forming a hydrophilic film on the surface of these minerals (Luo and Chen, 1984). It has been suggested that sodium silicate further benefits the process by removing excess calcium and magnesium ions in solution, which consume collector, through the formation of precipitates (Bulatovic, 2007a, c; Li *et al.*, 1988). The reagent's impact on pH (renders pH more alkaline) is another important consideration when evaluating its effect on REM flotation (Jordens *et al.*, 2016b).

B.2.6.2 Lignin Sulfonate

Lignin sulfonate is used in REM flotation as a selective depressant for barite (Pradip and Fuerstenau, 1991). It has been shown to adsorb to the surface of barite, calcite and bastnäsite. However, it exhibits a higher affinity for barite and as such it is the only mineral in the Mountain Pass ore for which its depressing action is significant (Pradip and Fuerstenau, 1991). Elevated temperatures are believed to have no impact on the selectivity on the depression of barite or calcite with lignin sulfonate (Pradip and Fuerstenau, 1991). Excessive dosage of this depressant is detrimental to bastnäsite flotation (Morrice and Wong, 1982).

B.2.6.3 Sodium Fluorosilicate

Sodium fluorosilicate has been used as a generic depressant for barite, calcite and fluorite in the Bayan Obo and Mountain Pass ores (Houot *et al.*, 1991; Luo and Chen, 1984; Morrice and Wong, 1982). Sodium fluorosilicate, which was used at Bayan Obo to depress gangue as well as act as an activator for REM flotation (Luo and Chen, 1984), is no longer required due to the use of the more selective H_{205} hydroxamic acid collector (Li *et al.*, 1988). For the Mountain Pass ore, sodium fluorosilicate drastically reduced the pH which had to be offset by excessive sodium carbonate addition, rendering it less effective than sodium fluoride (Morrice and Wong, 1982). Sodium fluorosilicate is also a depressant for silicates (Bulatovic, 2007c).

B.2.6.4 Sodium Fluoride

Sodium fluoride is an important depressant used exclusively in the flotation of non-sulfide minerals (Bulatovic, 2007c). Although it is believed to be a depressant for silicate and oxide minerals, studies have shown it does not depress them, rather it improves depression when used with other depressants (Bulatovic, 2007c). Sodium fluoride was shown to offer improvements for the flotation of REM from the Mountain Pass ore compared to sodium fluorosilicate as it had much less impact on pH (Morrice and Wong, 1982).

B.2.6.5 Sodium Sulphide

Sodium sulphide has been reported as an activator for monazite and a depressant for zircon when using a fatty acid collector (Abeidu, 1972; Zakharov *et al.*, 1967). The depression of zircon is, however, dependant on dosage. At low dosages, sodium sulphide has been shown to activate monazite, zircon and pyrochlore (Zakharov *et al.*, 1967). As the dosage increased, pyrochlore and zircon were depressed, and monazite was unaffected (Zakharov *et al.*, 1967). Zakharov *et al.* (1967) described the depression of zircon and pyrochlore by the adsorption of S^{2-} and SH^- ions to its surface, preventing collector adsorption. The activation of monazite was explained by the lack of SH^- ions on its surface, with the attached sulfur in its oxidized form providing sites for collector adsorption. An alternative explanation is the selective desorption of sodium oleate from the mineral surfaces (Pol'kin *et al.*, 1967). Pol'kin *et al.* (1967) found that the collector was almost completely removed from zircon and pyrochlore, while desorption from monazite was incomplete allowing it to float. Abeidu (1972) provided a third explanation where it was suggested that some phosphate sites at the monazite surface are displaced by S^{2-} and SH^- ions followed by attachment of oleate ions to the adsorbed activating sites.

B.2.6.6 Sodium Hexametaphosphate

Sodium hexametaphosphate has been suggested as a depressant in the separation of monazite from calcite (Zhang and Honaker, 2018). However, removal of calcium ions from the surface of monazite (using citric acid or EDTA) is crucial or it will also be significantly depressed (Zhang and Honaker, 2018). Sodium hexametaphosphate was also used in combination with oxalic acid to depress pyroxenes and nepheline feldspars in the flotation of eudialyte from the Norra Karr deposit (Stark *et al.*, 2017).

B.2.6.7 Starches

Starches are a group of organic polymers which selectively coat mineral surfaces to prevent collector adsorption (Bulatovic, 1999). They are important depressants used in the flotation of xenotime and monazite from mineral sands deposits, where they act as depressants for rutile, ilmenite and zircon (Bulatovic, 2007c; Pereira and Peres, 1997). The have also been employed in flotation schemes proposed for the Mount Weld deposit (Guy *et al.*, 2000).

B.2.6.8 Amylopectin

Amylopectin is one of the two main components of starch (the other being amylose). It has been tested to depress zircon in the flotation of xenotime (Pereira and Peres, 1997). While zircon was depressed, amylopectin also had a small depressing action on xenotime and separation was not as efficient as when using sodium silicate or starch as depressants (Pereira and Peres, 1997).

B.2.6.9 Quebracho

Quebracho is an organic polymer derived from the heartwood of the trees *Shinopsis balansae* and *Shinopsis lorentzii* (Bulatovic, 2007b; Pearse, 2005). It has been tested as a depressant for the flotation of heavy mineral sands deposits, where it has been shown to depress both xenotime and zircon (Pereira and Peres, 1997). The exact mechanism causing xenotime and zircon depression was not described, but, in most other mineral systems it is believed that the depressing action of quebracho is a result of it displacing collector from the mineral surface (Bulatovic, 2007b).

B.2.6.10 Guar Gum

Guar gums are organic polymers produced from the seed of two plants: *Cyamopsis tetragonalobus* and *Cyamopsis psoraloide*. They are effective for the depression of naturally hydrophobic gangue (talc) and silicates (Bulatovic, 2007b). The application of guar gum as a depressant in REM flotation was tested by Boulanger *et al.* (2019). They studied its use for the flotation of the Niobec ore and found that although it resulted in higher bastnäsite and monazite recoveries, it also promoted gangue recovery and was deemed ineffective. The authors noted that the addition of guar gum resulted in a slurry which appeared more viscous, which may have been promoting gangue recovery through non-selective entrainment.

B.2.6.11 Silica Gel

Silica gel has been shown to be a good depressant for gangue minerals barite, fluorite and calcite in the flotation of a Chinese rare earth deposit (Che *et al.*, 2003). The depressing action was explained as an active siliceous colloid which selectively adsorbs to gangue minerals rendering them hydrophilic (Che *et al.*, 2003). The authors suggested silica gel as a more suitable depressant than sodium silicate, however, dosage control is important. When added in excess, silica gel also depressed bastnäsite and monazite.

B.2.7 Activators

B.2.7.1 Metal Activators

Various metal activators have been tested to promote hydroxamate adsorption to the surface of REM. Xia *et al.* (2015) investigated the use of lead nitrate as an activator during the flotation of the Nechalacho deposit. The authors found improvements in both REE grade and recovery when compared to hydroxamate flotation alone. Similarly, Jordens *et al.* (2016a) tested the use of lead chloride for the flotation of the same ore. In this case lead ions were employed to activate REM which were not recovered in an initial flotation stage using BHA. Although the addition of lead was suggested to be beneficial in both cases, lead ions were also shown to activate gangue minerals (Jordens *et al.*, 2016a; Xia *et al.*, 2015). Although it has been shown to be effective for REM flotation, the potential environmental concerns must be noted. There exists a great deal of literature highlighting the potential danger small amounts of lead can have on public health and the environment (Dudka and Adriano, 1997; Duruibe *et al.*, 2007; Förstner and Wittmann, 2012; Harrison and Laxen, 1981). Lead present in a plant's tailings stream would be environmentally concerning and any plant employing a flotation scheme of this nature must mitigate this. As an alternative to the use of lead as an activator, Anderson (2015) demonstrated that cobalt nitrate could effectively activate bastnäsite. This resulted in a shift in the optimum pH for flotation from pH 9 to pH 7, which is the pH where $CoOH^+$ ions are most present (Anderson, 2015). A similar shift in optimum pH was observed by Jordens *et al.* (2014c), when testing the impact of ferric chloride and ferrous chloride as an activator for allanite flotation. Allanite was previously shown to not float in the presence of BHA (Jordens *et al.*, 2014a); however, after the addition of ferrous chloride, allanite demonstrated a maximum recovery at pH 4. This was assumed to be a result of the monohydroxy form of ferric iron species (ferrous ions were at least partially oxidized to their ferric form) providing sites for collector adsorption. It was noted that the addition of ferric chloride was not effective at the pH investigated. The authors did not determine the exact reason for this; however, it was suggested the presence of both divalent and trivalent iron ions with the addition of ferrous chloride may play a role. They also noted that at pH 4 there may be excess ferric hydroxide formation when using ferric chloride, and more favourable results may be possible at pH 3. Lastly, it was noted that improved results may be possible using a metal activator whose monohydroxy species is present at a pH near the pK_a of BHA.

B.2.7.2 Sodium Oxalate/Oxalic acid

Sodium oxalate has been studied as an activator for monazite flotation when using sulfonate collectors (Bulatovic, 2010; Houot *et al.*, 1991). The specific sulfonate collector and conditioning time have a significant impact on flotation (Bulatovic, 2010). Oxalic acid has been studied as an activator in the flotation of the Strange Lake deposit using the hydroxamate collector Florrea 7510, the phosphoric acid Flotinor 1682 and the collector mixture KBX3. In all cases oxalic acid resulted in improved REM recovery (Yu *et al.*, 2016a). Oxalic acid has also been studied as a depressant for pyroxenes and nepheline feldspars in the flotation of eudialyte (Stark *et al.*, 2017), and a co-depressant, in conjunction with sodium metasilicate, for zircon, quartz and feldspar in the flotation of fergusonite (Fawzy, 2018).

B.2.8 Summary and Conclusions

This review has summarized the current available literature on REM flotation. The general findings can be summarized as follows:

- There are large differences in REM IEPs reported by different surface chemical studies. This is particularly the case for bastnäsite and monazite. It is suggested that these variations are a result of procedural differences rather than differences in mineral origin or structure.

- REM other than bastnäsite and monazite could benefit from fundamental surface chemical studies which are limited to date.

- Hydroxamates are currently the most effective collectors available for the flotation of carbonate, phosphate and niobate minerals. However, they do not offer the same degree of recoverability and selectivity for REE-bearing silicate minerals. Mineral solubility plays a significant role on flotation, with more soluble REM generally having a greater flotation response to hydroxamates.

- Aromatic hydroxamates such as BHA and various modified naphthyl hydroxamates seem to offer improved selectivity over alkyl hydroxamates, although higher collector dosages are required to achieve similar recoveries.

- Carboxylate and phosphoric acid collectors are often much less selective than hydroxamates. However, they have been shown to be effective collectors for heavy mineral sands deposits; and may offer improved results for the flotation of silicate REM.

- Regardless of the collectors being used other modifying reagents such as depressants and activators are required to achieve selective separation. While several different reagents have been studied for this purpose, much of the work to date has focussed on depressing gangue minerals found in carbonate deposits (calcite, barite and fluorite) or mineral sands deposits (zircon, rutile and ilmenite). In most cases, the tested depressants also impact REM flotation, and activators for REM flotation also activate gangue minerals. Further work focussed on finding highly selective depressants and activators, specifically for minerals found in more complex alkaline/peralkaline igneous rock deposits, would benefit the future of REM flotation.

- Flotation studies focussed on mineral deposits which contain multiple REM should provide mineralogical information, rather than, or along with, elemental information. This would provide a more fundamental understanding of how REM other than bastnäsite and monazite respond to the various flotation schemes which are tested.

B.2.9 Acknowledgements

The authors would like to acknowledge the Natural Sciences and Engineering Research Council of Canada (NSERC) and Avalon Advanced Materials Inc. for providing funding for this work through the Collaborative Research and Development (CRD) Program (CRDPJ 44537-12). C. Marion would also like to acknowledge funding from the McGill Engineering Doctoral Award and the NSERC Alexander Graham Bell Canada Graduate Scholarships Program. R. Li would also like to thank the McGill Engineering Doctoral Award for funding.

B.2.10 Supplementary Material – Methods Used for Zeta Potential Measurements

B.2.10.1 Materials

The REM used in this work, their origin and the source from which they were obtained are summarized in Table B.17. The procedure for synthesis of $YNbO_4$ follows the protocol described by Hirano and Dozono (2013). The as-received natural mineral samples were stage ground dry using a Pulverisette 6 planetary monomill (Fritsch, Germany) with ceramic grinding media and sieved to produce samples in the size range of – 150 + 38 μm. Minerals which were not received pure were purified using a Mozley MKII Laboratory Separator (Mozley, UK) and/or a Frantz Isodynamic Separator (Frantz, USA). X-ray diffraction (XRD) was employed to verify the success of the purification steps. The XRD analyses were performed using a Bruker D8 Discovery X-ray Diffractometer equipped with a cobalt X-ray generating source. The resulting diffraction patterns and corresponding mineral reference files are provided in Figures B.4-B.11. The XRD patterns for the allanite and fergusonite sample were less conclusive at determining mineral purity than the others. The allanite sample is the same sample as used by Jordens *et al.* (2014a), which was received as 65 % allanite (as determined by QEMSCAN analysis) and then concentrated using a Frantz Isodynamic Separator. Concentration steps were deemed successful and any differences in XRD patterns compared to available reference patterns were said to be due to differences in allanite composition (Jordens *et al.*, 2014a). To ensure mineral purity of fergusonite it was analyzed using a scanning electron microscope (SEM) and energy dispersive X-ray spectroscopy (EDS). The SEM used was a Hitachi SU8000 cold field emission SEM (Hitachi High-Technologies, Canada), equipped with an 80 mm^2 X-Max^N Silicon Drift EDS detector (Oxford Instruments, UK). The X-ray map of the fergusonite sample is provided in Figure B.12. From XRD and SEM analyses it can be concluded that all minerals are of relatively high purity. Once determined pure, a subsample of the mineral samples were further ground wet using a Pulverisette 6 planetary monomill to obtain very fine particles or zeta potential measurements. The particle size (equivalent spherical diameter) [determined using a LA-920 particle analyser (Horiba, Japan)] and measured surface areas [determined by the N_2 Brunauer–Emmett–Teller (BET) technique, using a TriStar Surface Area and Porosity Analyzer (Micromeritics, USA)] are given in Table B.18.

Table B.17 – Mineral samples used in this study

Mineral	Origin	Purchased From or Supplied By
Bastnäsite 1	Gakara Mine, Burundi	African Rare Earths (Pty.) Ltd. (South Africa)
Bastnäsite 2	Madagascar	Gregory, Bottley and Lloyd (UK)
Monazite	Yard Mine, USA	Mineralogical Research Company (USA)
Allanite	Nevada, USA	Gregory, Bottley and Lloyd (UK)
Parisite	Blackbird Mine, USA	Khyber Minerals Co (USA)
Fergusonite	Gole Quarry, Canada	David K Joyce Minerals (Canada)
$YNbO_4$	Synthetic $YNbO_4$	-
Columbite (Fe)	Mahaiza, Madagascar	Khyber Minerals Co (USA)
Zircon	Malawi	Excaibur Mineral Corp (USA)

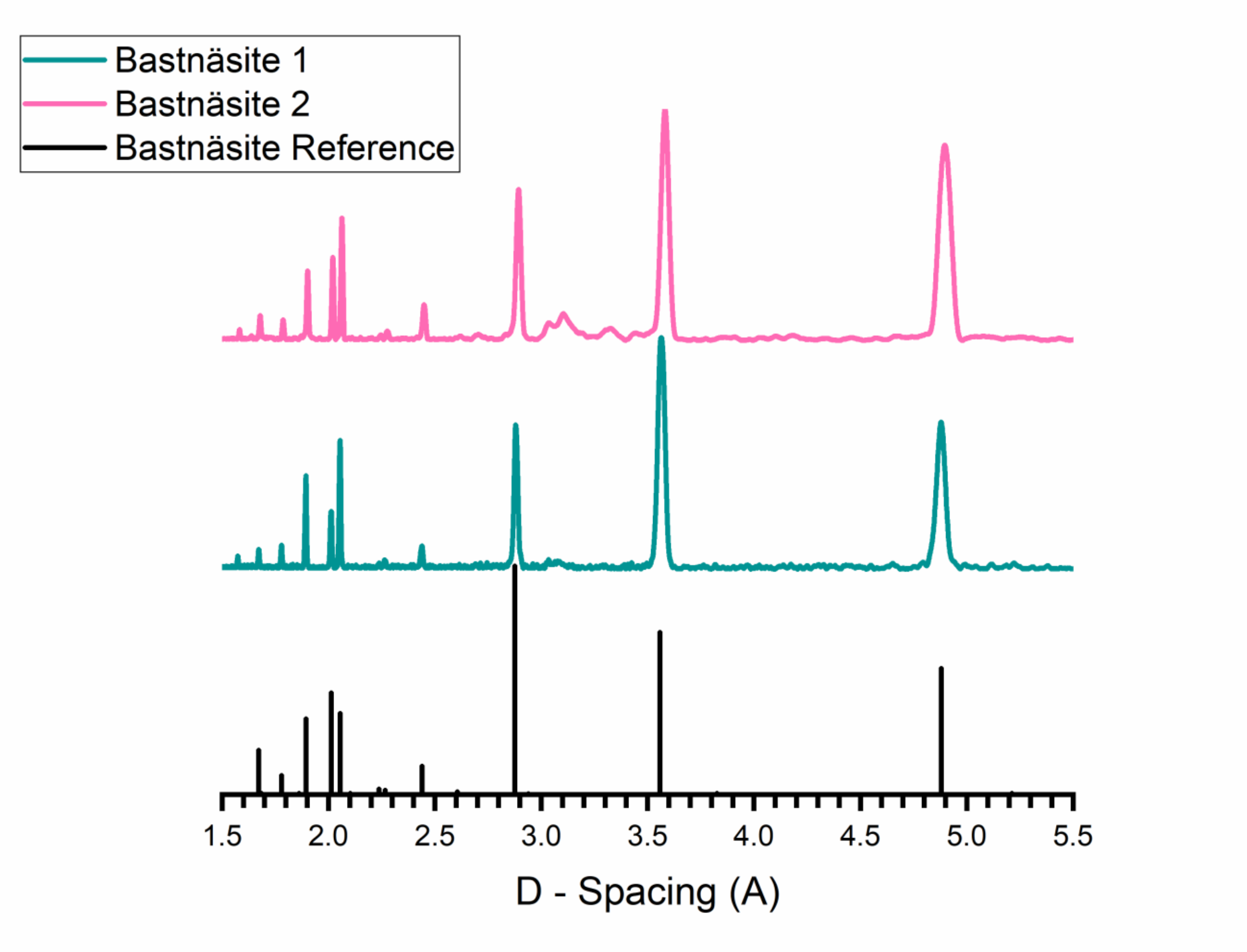

Figure B.4 – XRD pattern of the purified bastnäsite samples used in this work

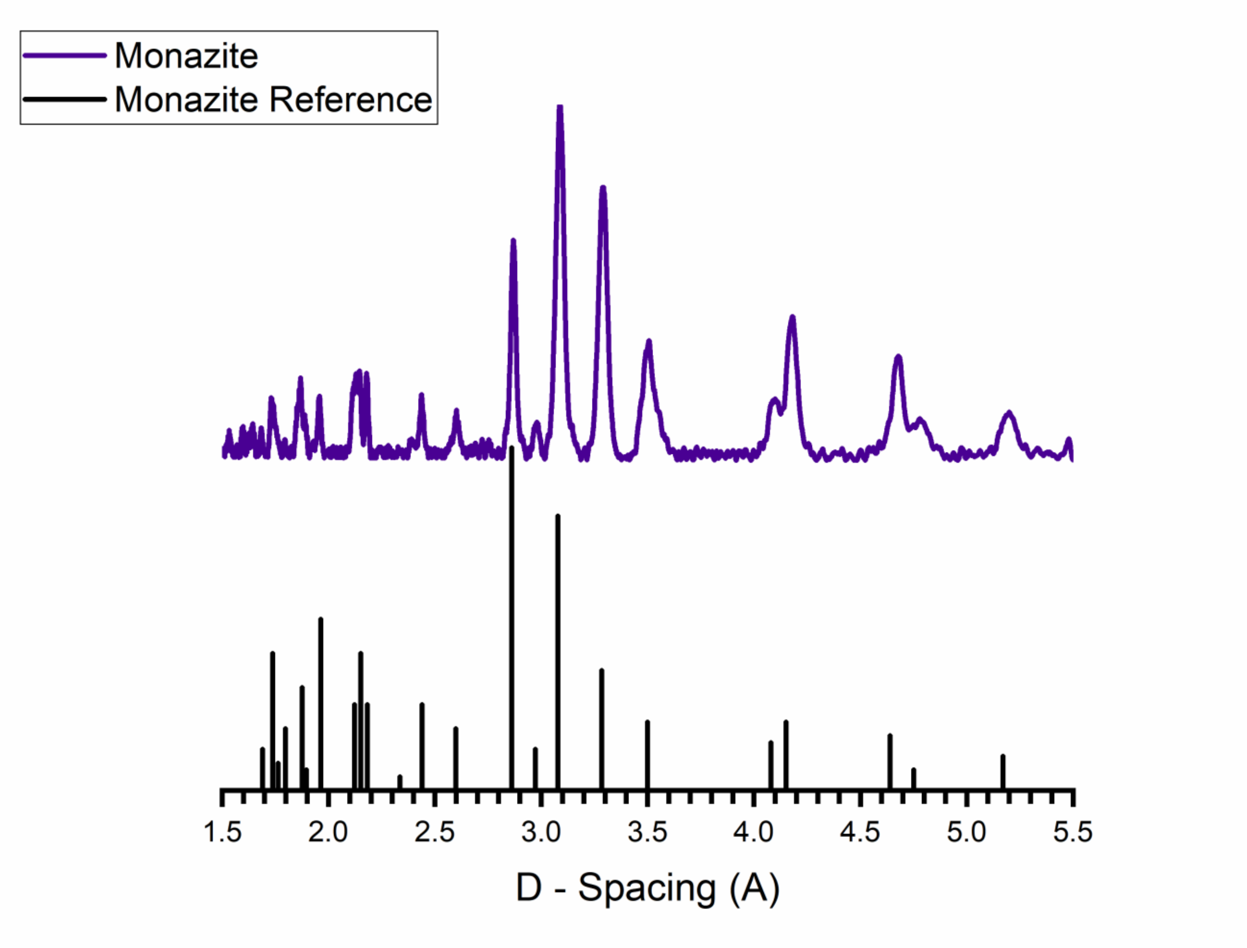

Figure B.5 – XRD pattern of the purified monazite sample used in this work

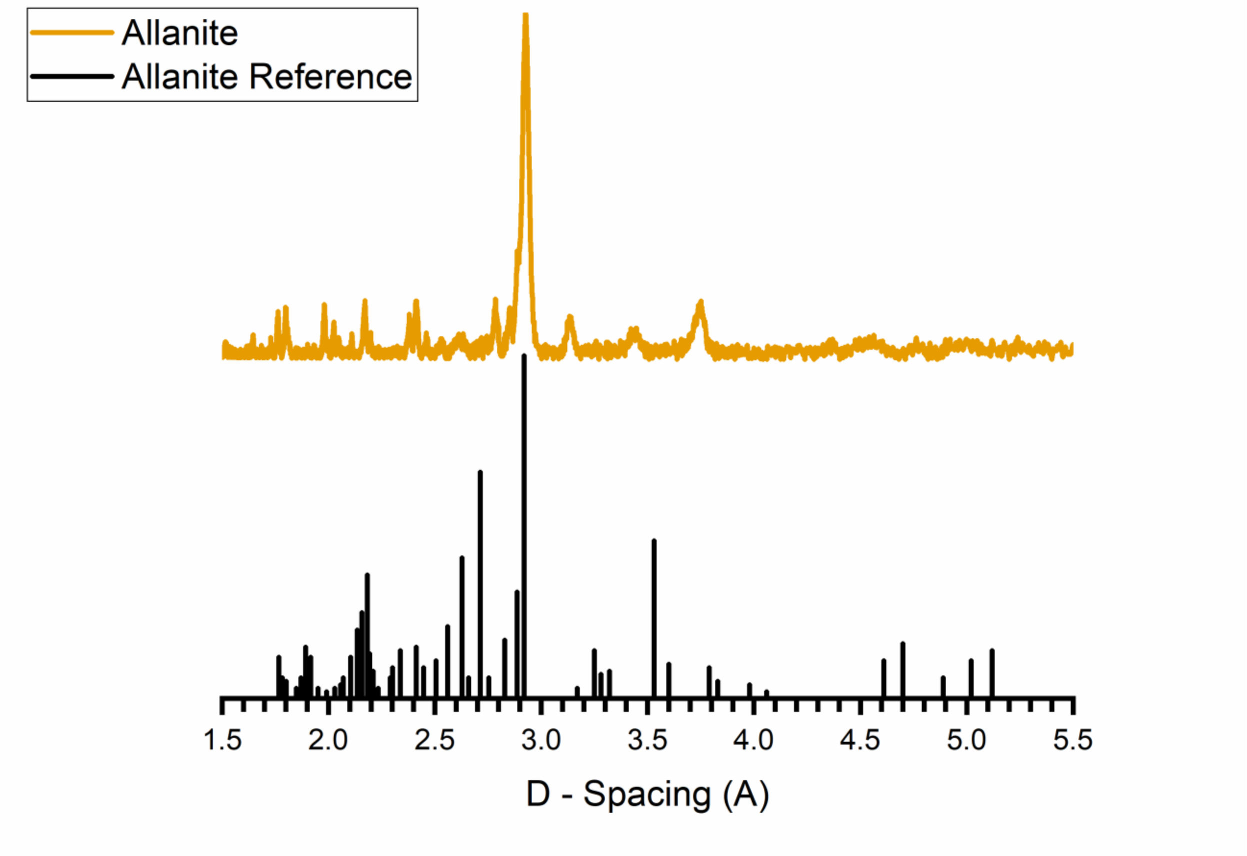

Figure B.6 – XRD pattern of the purified allanite sample used in this work

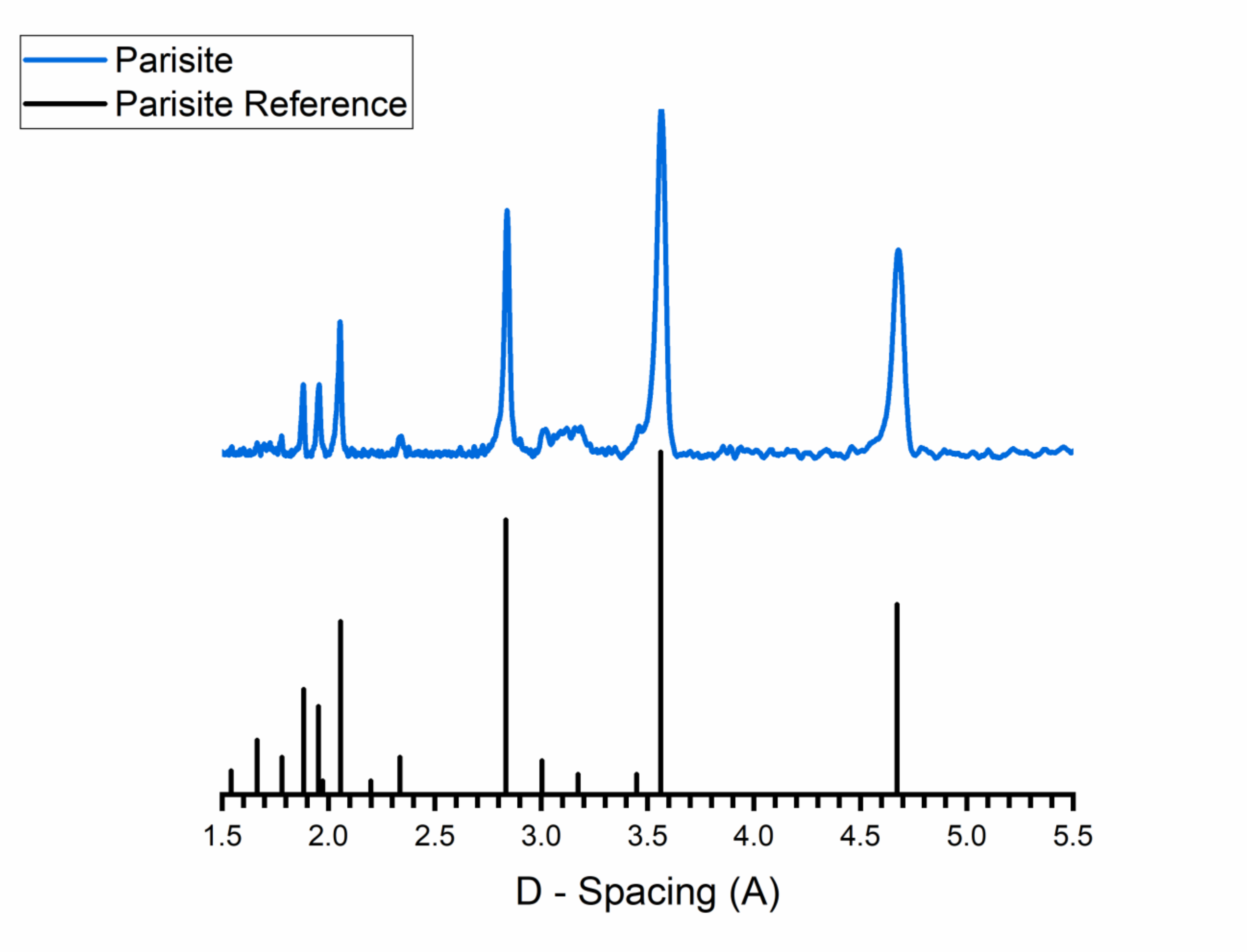

Figure B.7 – XRD pattern of the purified parisite sample used in this work

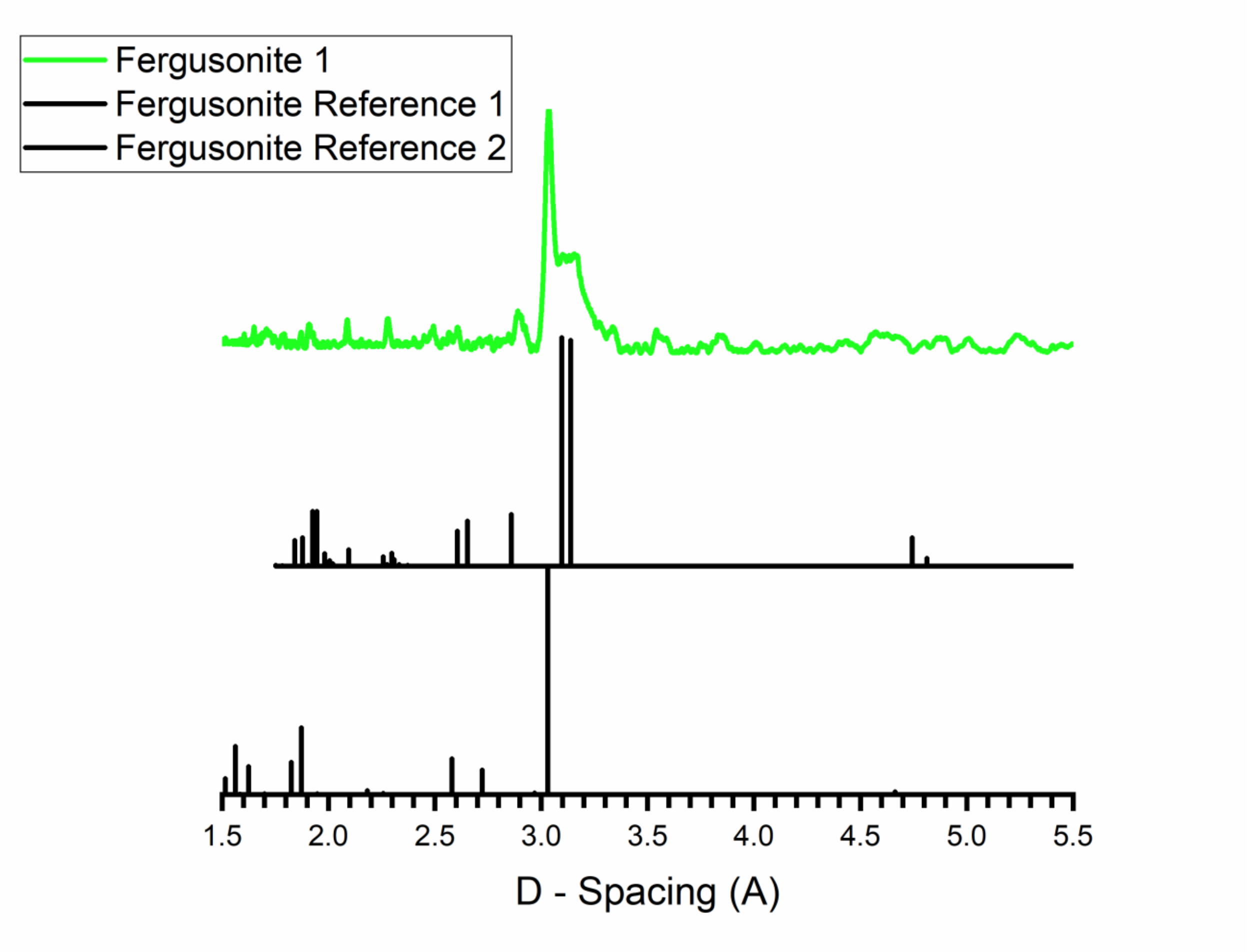

Figure B.8 – XRD pattern of the purified natural fergusonite sample used in this work

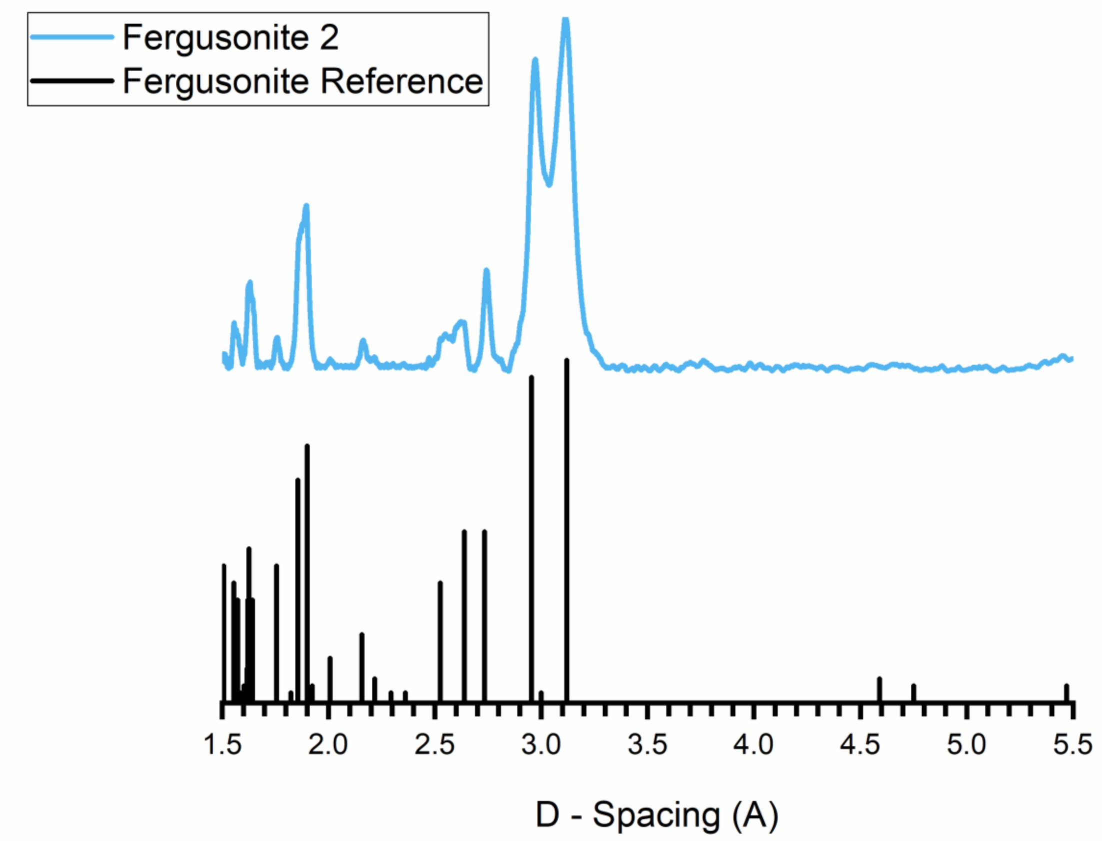

Figure B.9 – XRD pattern of the synthesized fergusonite sample used in this work

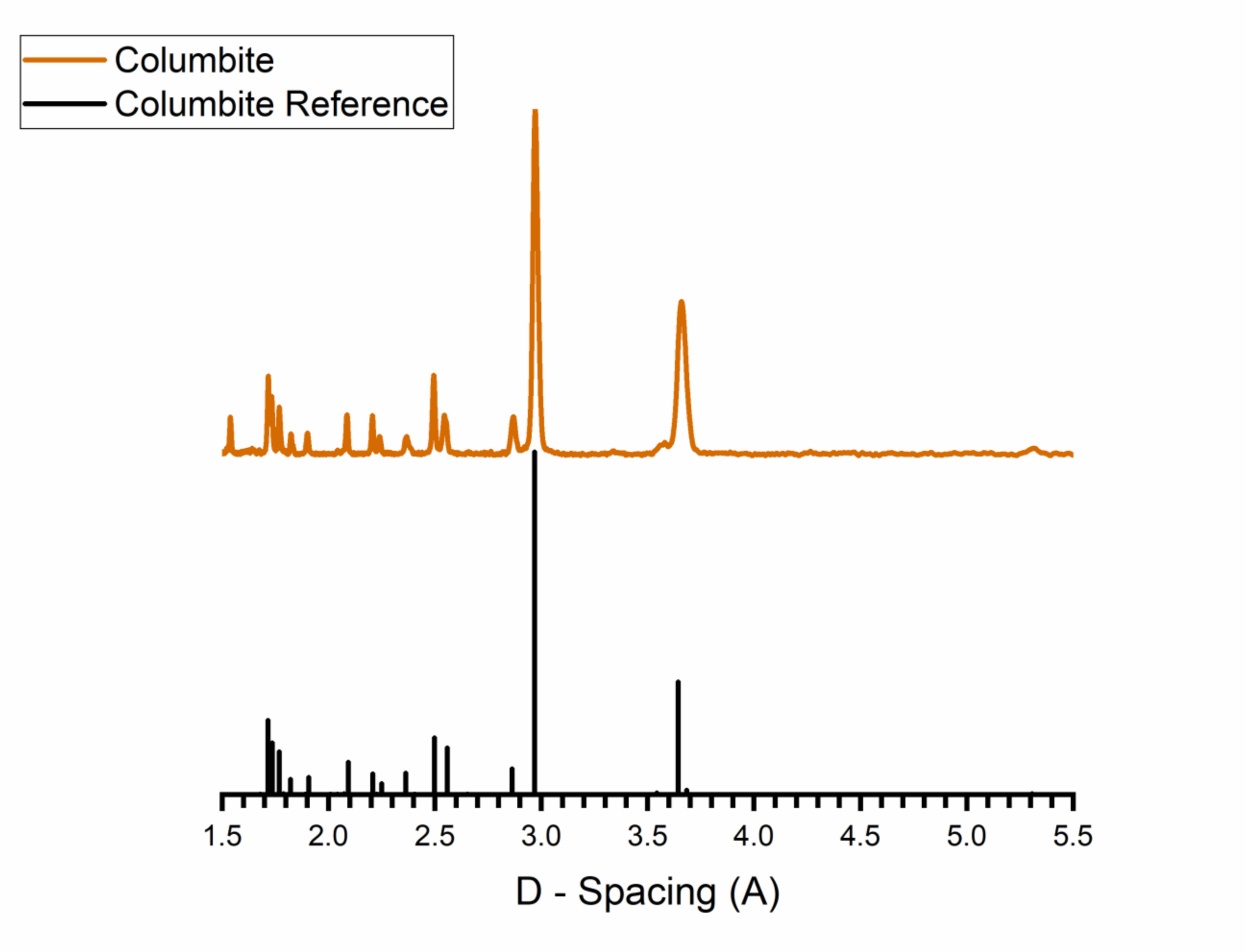

Figure B.10 – XRD pattern of the purified columbite sample used in this work

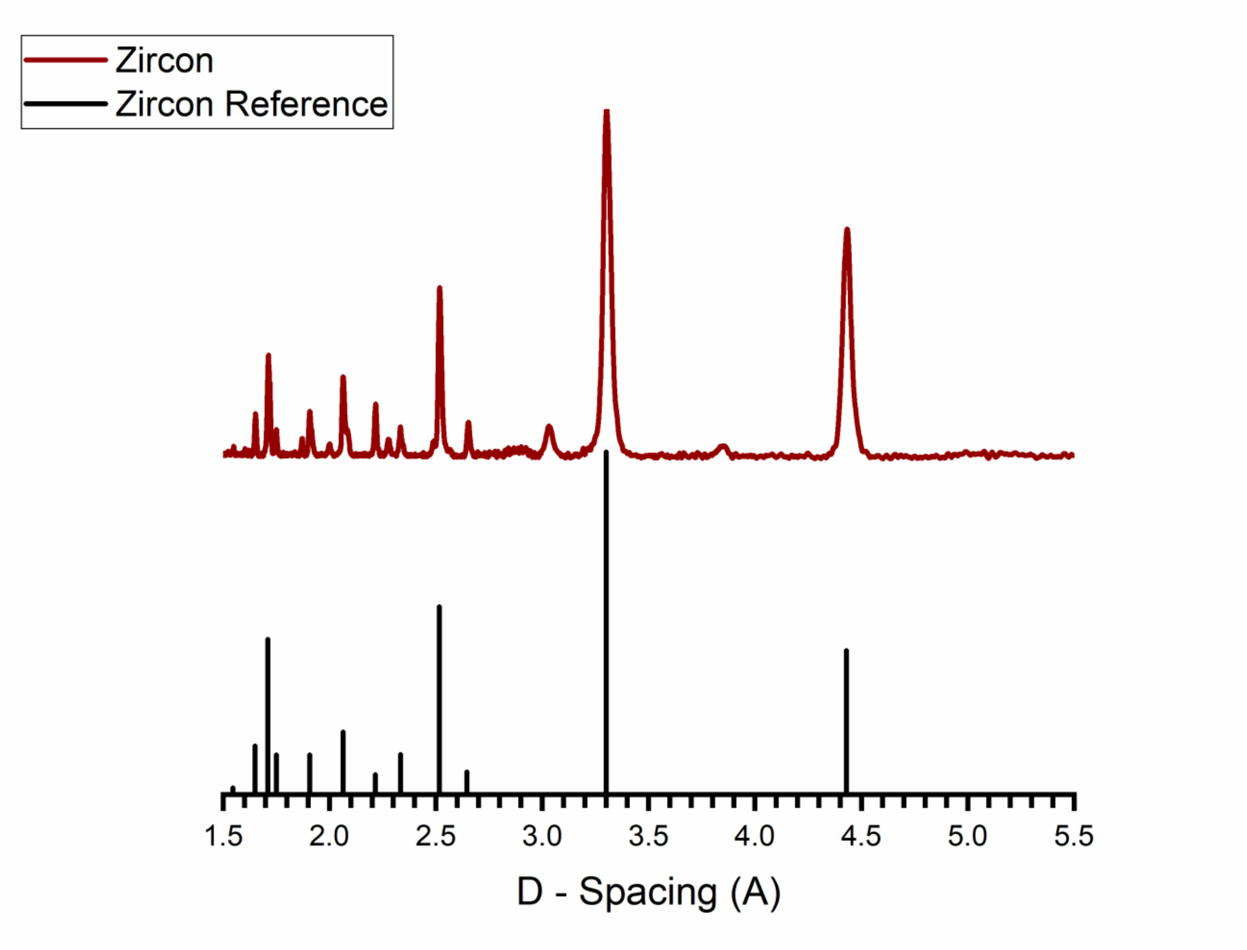

Figure B.11 – XRD pattern of the purified zircon sample used in this work

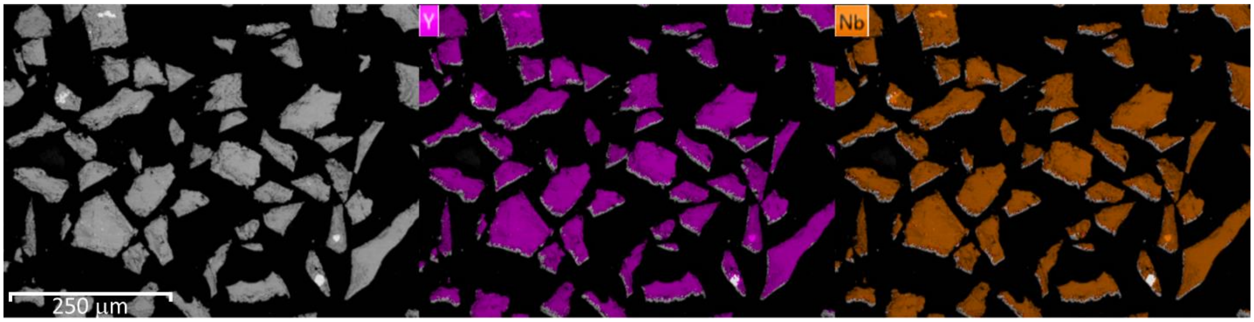

Figure B.12 – Backscattered electron image (left) and elemental phase identification (middle-yttrium, right-niobium) of the natural fergusonite sample

Table B.18 – Particle size of mineral samples used for surface chemistry investigations

Mineral	Particle Size (μm)		BET Surface Area (m^2 g^{-1})
	d_{50}	d_{80}	
Bastnäsite 1	2.0	3.6	14.35
Bastnäsite 2	1.8	3.3	11.36
Monazite	1.9	3.4	9.52
Allanite	3.2	7.1	3.84
Parisite	6.6	10.4	0.26
Fergusonite	6.8	10.2	0.66
$YNbO_4$	5.2	10.0	86.83
Columbite (Fe)	2.0	3.8	0.51
Zircon	2.0	3.5	3.40

B.2.10.2 Zeta Potential Measurements

Zeta potential measurements were conducted using a NanoBrook ZetaPlus electrophoretic analyser (Brookhaven Instruments, USA). Mineral samples were suspended in 200 mL of 10^{-3} M KCl solution at a concentration of 0.04 $\%_{wt/wt}$. The pH range investigated was from pH 3 to 10 (with measurements taken in steps of 1 pH unit), as measurements below pH 3 and above pH 10 were not possible due to the limitations of the analyser. Samples were conditioned for 30 min after collector addition (at a concentration of 40 mg/L) and for 5 min at each pH prior to taking a measurement. Fresh samples were prepared for acidic and basic zeta potential measurements to avoid zeta potential hysteresis.

B.3 An Evaluation of Hydroxamate Collectors for Malachite Flotation

Hydroxamic acid collectors are considered the most effective collectors for REM flotation (particularly for bastnäsite and monazite). However, a wide variety of different hydroxamate collectors have been studied with limited fundamental knowledge on the impact the collector's structure has on flotation. Thus, the objective of Section B.3 is to evaluate how different hydroxamate collectors effect the flotation of malachite. While malachite is not a REM, it is used in this study, as malachite is commonly floated using hydroxamate collectors, easily obtainable in large quantities and, as it is a carbonate mineral, may offer some insight into how these collectors interact with carbonate REM which may behave similarly, such as bastnäsite. The study investigated five alkyl hydroxamates of different chain length (C_1, C_2, two C_8, C_{12}) and two aromatic hydroxamates (BHA and SHA); and employed zeta potential measurements, to aid in understanding reagent adsorption, and bench scale flotation experiments, to asses the difference in flotation response between collectors. This work was reported in a manuscript published in the peer-reviewed journal *Separation and Purification Technology* (Marion, C., Jordens, A., Li, R., Rudolph, M., Waters, K.E., 2017. An Evaluation of Hydroxamate Collectors for Malachite Flotation. Separation and Purification Technology 183, 258-269) and is reproduced below.

Abstract

Copper oxide minerals, such as malachite, do not often respond well to traditional copper sulphide collectors, and require alternative flotation schemes. Hydroxamic acid collectors have been suggested as a means to directly float malachite; however, there is limited information on the effect of reagent structure on the performance of these collectors. This papnvestigated the effect of five alkyl hydroxamates and two aromatic hydroxamates on the flotation of a synthetic ore composed of pure, fully liberated, malachite and quartz. Zeta potential measurements were used to aid in understanding reagent adsorption onto the surface of the two minerals. The collectors were then evaluated using bench scale flotation results. While zeta potential measurements suggested that all the collectors investigated selectively adsorb onto the surface of malachite, only benzohydroxamic acid and C_8 alkyl hydroxamates were effective collectors in the flotation of malachite. Benzohydroxamic acid was the most selective; however, significantly lower dosages of C_8 alkyl hydroxamates were required to obtain similar malachite recoveries, with minimal increases in quartz recovery. Benzo- and octylhydroxamic acid were further examined for the flotation of fine (-38 μm) particles. For fine particle flotation experiments the effect of temperature was also investigated as a means to improve the flotation performance.

B.3.1. Introduction

The majority of copper is extracted from copper sulphide minerals, however, copper oxide minerals do account for a significant portion of copper production (Schlesinger *et al.*, 2011). There are numerous different copper oxide minerals, and in general, more than one is present in a deposit. These minerals are commonly found close to the earth's surface, as they are often the product of the weathering of copper sulphide minerals. One of the more common copper oxide minerals is malachite ($Cu_2CO_3(OH)_2$) (Bulatovic, 2010a). As with most copper oxide minerals, malachite does not respond well to traditional copper sulphide collectors, such as xanthates, and alternative flotation schemes are required (Bulatovic, 2010a). The traditional method of copper oxide flotation involves sulphidising the mineral surface prior to the addition of a copper sulphide collector (Bulatovic, 2010a). The effectiveness of sulphidisation is, however, highly dependent upon the dosage of the sulphidising agent. The high degree of dosage control required in plant situations for proper sulphidisation often leads to poor flotation performance (Laskowski and Fuerstenau, 2010; Le Normand *et al.*, 1979; Lee *et al.*, 2009). As an alternative to sulphidisation, multiple different oxhydryl collectors have been evaluated for the direct recovery of malachite, such as fatty acids (Bulatovic, 2010a; Choi *et al.*, 2016), amines (Bulatovic, 2010a), phosphonic acids (Li *et al.*, 2015), phosphinic acids (Li *et al.*, 2015) and hydroxamic acids (Bulatovic, 2010a; Le Normand, 1974; Le Normand *et al.*, 1979; Lee *et al.*, 1998; Lee *et al.*, 2009). While all these collectors have been shown to be effective at recovering malachite, they often offer poor selectivity over gangue minerals, especially relative to the selectivity of xanthates in copper sulphide flotation. Hydroxamic acids, however, have been shown to effectively and selectively recover malachite (Bulatovic, 2010a; Lee *et al.*, 1998; Lee *et al.*, 2009).

Hydroxamic acids are a group chelating collectors, capable of forming complexes with specific metal cations at the surface of minerals. The stability constants of hydroxamate-metal complexes vary depending on the metal cation. Figure B.2 (Section B.2.4.1) shows the stability constants for metal complexes with acetohydroxamic acid (AHA), salicylhydroxamic acid (SHA), and benzohydroxamic acid (BHA). The most stable complexes are formed with Fe^{3+}, Al^{3+}, Cu^{2+}, Cr^{3+} and Pb^{2+}, followed by rare earth metal cations; and the weakest complexes are formed with alkaline-earth metal cations (Fuerstenau, 2005; Khairy *et al.*, 1996; Khalil and Fazary, 2004; Sastri *et al.*, 2003). Several studies have suggested that the larger the difference in stability constant of the complexes formed with surface cations the greater the selectivity (Pavez and Peres, 1993b; Pradip and Fuerstenau, 1983). Other authors, however, believe the selectivity of hydroxamic acid collectors is more closely related to adsorption kinetics (Assis *et al.*, 1996). It has been suggested that hydroxamic acid collectors may interact with metal cations in the mineral lattice in two ways: chemisorption and surface reactions (Fuerstenau, 1983). Chemisorption involves coordinate and covalent bonding with the surface metal cation fixed in the mineral lattice. Surface reactions involve the hydrolysis of lattice cations, the formation of hydroxyl-complexes in solution, followed by re-adsorption at the mineral surface; providing sites for hydroxamic acid adsorption. It has been suggested that the kinetics of hydroxamic acid adsorption through surface reactions are much faster than those through chemisorption, and therefore the selectivity of the collector is strongly related to mineral solubility (Assis *et al.*, 1996). More soluble minerals will exhibit faster adsorption kinetics compared to less soluble ones. Another important factor to consider in hydroxamic acid flotation is bulk precipitation, which occurs when the collector reacts with dissolved metal cations in the bulk solution forming undesirable precipitates, which may consume collector or potentially adsorb onto mineral surfaces, altering the flotation response.

The use of hydroxamic acids and their salts (collectively referred to as hydroxamates throughout this paper) have been investigated in the flotation of a wide variety of minerals. Table B.19 indicates the minerals (grouped by the lattice metal for which the mineral is considered to be an economically exploitable resource) for which hydroxamate collectors have been shown to be effective, along with the structure of the hydrophobic group of the hydroxamates investigated. Although the use of hydroxamates as flotation collectors has received extensive research, there is limited information available on the effect of hydroxamate structure on flotation. Some work has been conducted investigating the effect of the hydrocarbon chain length of alkyl hydroxamates (Palmer *et al.*, 1973; Sreenivas and Padmanabhan, 2002); suggesting that an improved flotation performance can be achieved with a longer hydrocarbon chain. Others, however, have noted a reduced flotation performance with hydroxamates which have carbon chains higher than C_9 (Bulatovic, 2007a). While the vast majority of the work to date investigating the flotation of minerals with hydroxamate collectors focuses on the use of alkyl hydroxamates, Xia *et al.* (2014) compared the use of three different aromatic hydroxamates (BHA, SHA and a naphthoyl hydroxamate) in the flotation of a rare earth ore. The authors found that all three collectors were effective at recovering rare earth minerals; however, depending on the rare earth cation present in the mineral lattice each collector resulted in a different flotation response. Later a more extensive study on the same ore was performed, investigating 3 aromatic hydroxamates (BHA, SHA and tert-butyl benzo hydroxamate), a cyclic alkyl hydroxamate (cyclohexylhydroxamate) and an alkyl hydroxamate [octylhydroxamic acid (OHA)] (Hart *et al.*, 2014). It is important to note that there is currently no commercial process for manufacturing tert-butyl benzo hydroxamate; however, all other hydroxamate collectors which were investigated are manufactured commercially. Similar results were obtained to the previous study, however, in this case the authors also indicated that lower dosages of OHA were required to obtain similar recoveries to the other collectors investigated (Hart *et al.*, 2014). Similarly, Xia *et al.* (2015a) compared the use of two aromatic hydroxamates (BHA and tert-butyl benzo hydroxamate) to alkyl and cyclic alkyl hydroxamates (OHA and cyclohexylhydroxamate) in the flotation of ilmenite and wolframite. The greatest recovery of ilmenite was obtained with tert-butyl benzo hydroxamate, with recoveries decreasing according to OHA>cyclohexyl hydroxamate>BHA. While tert-butyl benzo hydroxamate was not examined for wolframite flotation, the results differed from ilmenite flotation, with cyclohexyl hydroxamate resulting in the best flotation performance (followed by OHA and then BHA). The authors concluded that while the hydroxamate structure plays a significant role on flotation, the selectivity and recovery performance of specific hydroxamate collectors varies depending on the mineral.

Table B.19 – Minerals for which hydroxamate collectors have been shown to be effective

Lattice Metal	Mineral	Mineral Type	Hydroxamate Hydrophobic Group	Reference
Rare Earth Elements	Bastnäsite	Carbonate	Alkyl	(Pavez *et al.*, 1996; Pradip and Fuerstenau, 1991)
			Aromatic	(Jordens *et al.*, 2014b; Ren *et al.*, 1997)
	Monazite	Phosphate	Alkyl	(Nduwa Mushidi, 2016; Pavez *et al.*, 1996; Pavez and Peres, 1993b, c)
Copper	Chrysocolla	Silicate	Alkyl	(Laskowski and Fuerstenau, 2010; Peterson *et al.*, 1965)
	Malachite	Carbonate	Alkyl	(Le Normand, 1974; Le Normand *et al.*, 1979)
Tin	Cassiterite	Oxide	Alkyl	(Sreenivas and Padmanabhan, 2002)
			Aromatic	(Qin *et al.*, 2011; Wu and Zhu, 2006)
Niobium	Fersmite	Oxide	Alkyl	(Ren *et al.*, 2004)
			Cyclic Alkyl	(Ren *et al.*, 2004)
	Pyrochlore	Oxide	Aromatic	(Gibson *et al.*, 2015b)
Iron	Hematite	Oxide	Alkyl	(Fuerstenau *et al.*, 1970; Han *et al.*, 1973; Raghavan and Fuerstenau, 1975)
Manganese	Hubernite	Oxide	Alkyl	(Fuerstenau, 2005)
	Pyrolusite	Oxide	Alkyl	(Natarajan and Fuerstenau, 1983)
	Rhodochrosite	Carbonate	Alkyl	(Zhou *et al.*, 2015a; Zhou *et al.*, 2015c)
	Rhodonite	Silicate	Alkyl	(Palmer *et al.*, 1973)
Titanium	Ilmenite	Oxide	Alkyl	(Nduwa Mushidi, 2016; Xia *et al.*, 2015a)
			Cyclic Alkyl	(Xia *et al.*, 2015a)
			Aromatic	(Xia *et al.*, 2015a)
	Rutile	Oxide	Alkyl	(Nduwa Mushidi, 2016; Pavez and Peres, 1993b, c; Wang *et al.*, 2014)
			Aromatic	(Marabini and Rinelli, 1983)
Tungsten	Scheelite	Oxide	Aromatic	(Yin and Wang, 2014)
	Wolframite	Oxide	Alkyl	(Hu *et al.*, 1997; Meng *et al.*, 2015; Xia *et al.*, 2015a)
			Cyclic Alkyl	(Xia *et al.*, 2015a)
			Aromatic	(Xia *et al.*, 2015a; Yang *et al.*, 2014)
Zinc	Sphalerite	Sulphide	Aromatic	(Natarajan and Nirdosh, 2006)
Zirconium	Zircon	Silicate	Alkyl	(Nduwa Mushidi, 2016; Pavez and Peres, 1993b, c)

With limited information on the effect of reagent structure on the performance of hydroxamate collectors, this paper investigates the effect of five alkyl hydroxamates and two aromatic hydroxamates on a synthetic ore made of malachite and quartz. Zeta potential measurements were used to aid in understanding reagent adsorption to the surface of malachite and quartz. The collectors were then evaluated using bench scale flotation results. Collectors showing the best results were further examined for the flotation of fine (-38 μm) particles. For fine particle flotation experiments the effect of temperature was also investigated as a means to improve the flotation performance.

B.3.2 Experimental

B.3.2.1 Materials

Malachite and quartz used for this work were purchased from AMR Mineral and Metal Inc. (Canada) and Unmin Canada Ltd. (Canada) respectively. Both samples were analysed by X-ray diffraction, and no other mineral phases were discerned.

The malachite sample was initially broken into approximately 2-3 cm pieces using a hammer and chisel. The sample was then stage pulverized to produce a -150 +38 μm and -38 μm size fractions for flotation experiments. Quartz was sieved to produce samples with the same size distributions. For zeta potential measurements, -38 μm samples of malachite and quartz were ground wet using a Pulverisette 6 planetary monomill (Fritsch, Germany) to produce very fine particle sizes (malachite $d_{50} = 3.3$ μm, $d_{80} = 7.0$ μm; quartz $d_{50} = 3.8$ μm, $d_{80} = 6.1$ μm). Particle size (equivalent spherical diameter) was determined using a LA-920 particle analyser (Horiba, Japan).

The hydroxamate collectors used in this investigation are shown in Table B.20. All collectors were prepared by dissolving the respective solids in deionized water, whereas tetradecylhydroxamic acid (THA) was dissolved in ethanol at a 1:20 mass ratio of THA:ethanol. Hydrochloric acid and sodium hydroxide, used for pH modifications in both zeta potential and flotation experiments, were purchased from Fisher Scientific. For flotation experiments F150 (obtained from Flottec, USA) was used as frother. All reagents were used as provided.

Table B.20 – Hydroxamate collectors used in zeta potential and flotation experiments

Hydroxamate	Abbreviation	Structure	Manufacturer
Benzo	BHA	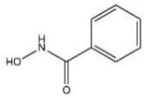	Sigma Aldrich (USA)
Salicyl	SHA	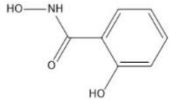	Alfa Aesar (USA)
Aceto	AHA	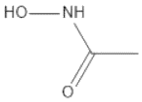	Alfa Aesar (USA)
K-Butyl	KBH	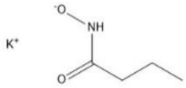	Synthesized
Octyl	OHA	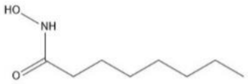	Synthesized
K-Octyl	POH	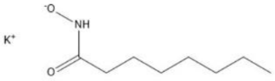	Synthesized
Tetradecyl	THA	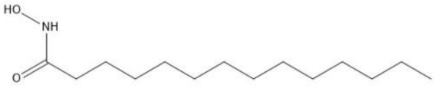	Synthesized

B.3.2.2 Synthesis of Alkyl Hydroxamate Collectors

The procedures for synthesis of alkyl hydroxamates follow the descriptions in Hauser and Renfrow (1939) for benzohydroxamic acid, replacing the ester reagent ethyl benzoate by methyl butyrate, methyl octanoate or methyl myristate for synthesis of butyl-, octyl- and tetradecyl-hydroxamates respectively. The reactions involved were discovered and described by Lossen (1872) and are therefore referred to as "Lossen reactions". All chemicals mentioned bellow are ACS reagent quality and were acquired from Sigma Aldrich. For the synthesis of POH, a solution of 46.7 g (0.67 mol) hydroxyl amine hydrochloride in 240 mL (189.6 g) methanol was prepared at 65°C and slowly cooled to 30°C. The solution was added to a solution of 56.1 g (1 mol) potassium hydroxide in 140 mL (110.6 g) methanol (cooled to 30°C). The mixture was placed in an ice bath for 5 min for precipitation of potassium chloride. Subsequently, 52.7 g (0.33 mol) of methyl octanoate was added under rigorous stirring. The mixture was quickly filtered, and the filter cake washed with methanol. The filtrate was quickly placed in an Erlenmeyer flask and shut to reduce contact with air. POH crystals begin to form in the flask and after 48 hours the crystals were filtered, washed with ethanol and dried in air. For the PBH instead of methyl octanoate, 0.33 mol (33.7 g) of methyl butyrate is used for crystallization and the methanol content is reduced by evaporation at 70°C. For potassium tetradecyl-hydroxamate 0.33 mol (80 g) of methyl myristate is used and due to strong crystallization double the amount of methanol is used. For synthesis of the hydroxamic acids (OHA and THA) 0.2 mol of hydroxamate salt were dissolved in 1.25 mol of acetic acid at elevated temperatures, until a clear solution is formed. The hydroxamic acid separates as white crystals at reduced temperatures in an ice bath. The crystals were filtered, washed with deionized water and dried. For further purification the hydroxamic acid was dissolved in 4.5 times its weight of hot ethyl acetate. The solution was filtered to remove any remaining solids, and the filtrate was cooled to room temperature. The white crystals which separate were filtered and washed with toluene and air dried.

In this way KBH, POH, OHA and THA were synthesized and qualitatively analyzed with ATR-FTIR [Tensor 27 (Bruker, Germany) equipped with the ATR module MIRacle (PIKE Technologies, USA) using a ZnSe reflection crystal]. The results are presented in Figure B.13. The signatures correspond very well to those presented in Higgins *et al.* (2006) and Hope *et al.* (2010a), and furthermore, no signatures corresponding to the educts used as reagents in the synthesis procedure are present. Specific vibrational bands can be assigned using the spectra presented in Hope *et al.* (2010a).

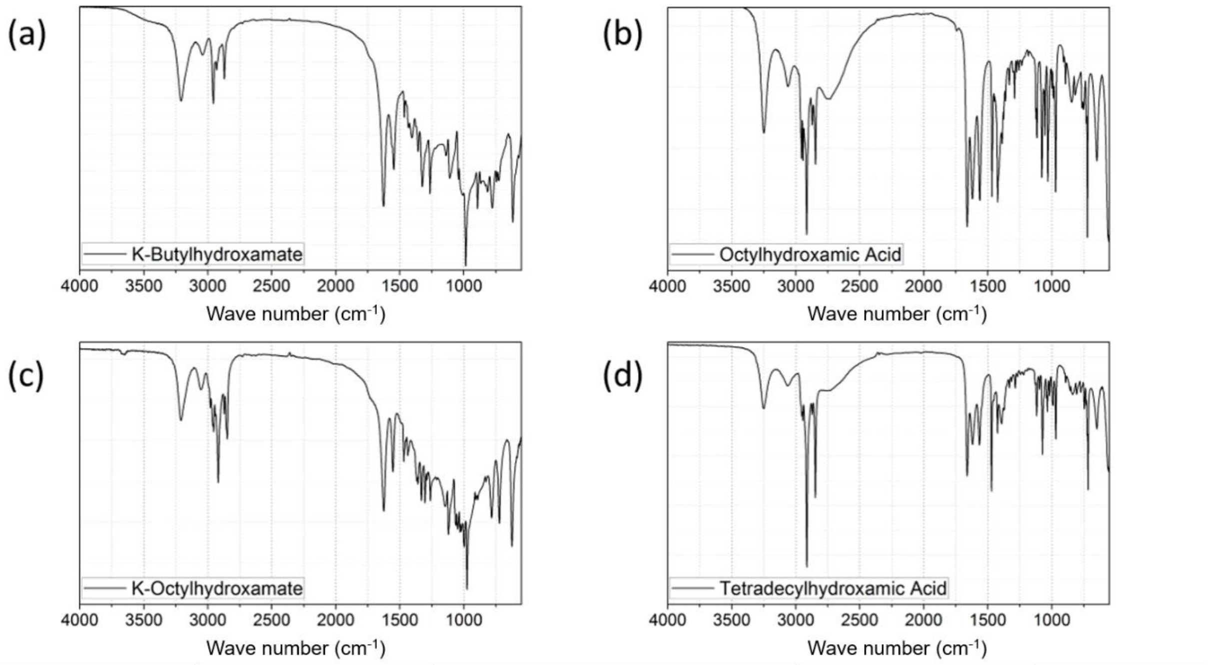

Figure B.13 – ATR-FTIR transmittance results for (a) PBH (b) OHA (c) POH (d) THA

B.3.2.3 Zeta Potential Measurements

Zeta potential measurements were conducted using a NanoBrook ZetaPlus electrophoretic analyser (Brookhaven Instruments, USA). Malachite and quartz samples were suspended in 200 mL of 10^{-3} M KCl solution at a concentration of 0.04 wt. %. The pH range investigated was from pH 4 to 10 (with measurements taken in steps of 1 pH units), as at pH values below 4 malachite was fully dissolved in solution, and measurements above pH 10 were not possible due to the limitations of the analyser. Samples were conditioned for 30 min after collector addition, and were allowed to equilibrate for 5 min at each pH prior to taking a measurement. Fresh samples were prepared for acidic and basic zeta potential measurements to avoid zeta potential hysteresis. Particle sizes, measured surface areas [determined by the N_2 Brunauer–Emmett–Teller (BET) technique, using a TriStar Surface Area and Porosity Analyzer (Micromeritics, USA)], and hydroxamate dosages are shown in Table B.21 for malachite and quartz.

Table B.21 – Hydroxamate dosages used for malachite and quartz zeta potential measurements

Mineral	Particle Size (d_{50})	BET Surface Area	Hydroxamate dosage	
	(μm)	($m^2\ g^{-1}$)	($mol\ m^{-2}$)	($mol\ ton^{-1}$)
Malachite	3.3	11.2	1.5×10^{-4}	1.7×10^{3}
Quartz	4.0	5.3	3.2×10^{-4}	1.7×10^{3}

B.3.2.4 Flotation

Flotation experiments were conducted on a synthetic malachite ore prepared by mixing 10 g malachite with 90 g quartz. All flotation tests were carried out using a 1.5 L Denver flotation cell operating at 1200 rpm with an air flow rate of 5.6 L min^{-1}. For each test, a fresh batch of ore was mixed with tap water in the flotation cell, with the water level adjusted to a set height. The ore was conditioned for 1 min following the addition of collector and pH adjustment. All flotation tests were carried out with 2 drops of F150 added to the cell. Following the conditioning step, the air was turned on and froth was collected after 0.5, 1, 2, 5 and 12 min to produce 5 concentrates. After each concentrate, the pH was readjusted to the desired value and the water level was readjusted to the set height. In all cases flotation experiments were performed in triplicate.

Initial flotation experiments were conducted on synthetic ore samples with a size distribution of -150 +38 μm (d_{50} = 115 μm, d_{80} =134 μm). BHA was used as a baseline collector to determine the best pH for flotation. The collector dosage was kept constant with the dosage used in zeta potential measurements, on a basis of moles of collector per m^2 of malachite (1.5×10^{-4} mol $m^{-2}_{malachite}$, 3.65 mol ton^{-1}_{ore}). Following this investigation, the pH was kept constant and each collector was tested. Collector concentrations were kept constant on a basis of mol ton^{-1}. Concentrates were analysed using a Frantz Isodynamic Separator (Frantz, USA) to magnetically separate malachite from quartz. At this size range, malachite can be easily separated from quartz, using a Frantz Isodynamic Separator, due to its paramagnetic properties (Rosenblum and Brownfield, 1999).

Due to the complexity of some ore bodies, requiring fine grinding to liberate valuable minerals, further investigation into the flotation of fine particles was performed using the hydroxamate collectors which showed the most promising results. Flotation experiments were conducted on -

38 μm samples (d_{50} = 18 μm, d_{80} = 30 μm), to investigate the effect of particle size on flotation performance. For fine particle flotation experiments the effect of temperature was also investigated as a means to improve the flotation performance. Heated flotation tests were conducted by placing the flotation cell in a hot water bath, heated using a HS30 hotplate (Torrey Pines Scientific, USA) equipped with PID temperature control to keep the temperature of the slurry inside the flotation cell at a constant 60 ˚C (± 5 ˚C). Water added to the cell throughout the test was added as hot tap water to avoid large fluctuations in temperature. As the particles were too fine for effective separation using the Frantz Isodynamic Separator, samples produced from fine particle flotation experiments were analysed using an AA240FS Fast Sequential Atomic Absorption Spectrometer (Varian, USA). Prior to analysis, representative 0.2 g samples were taken from concentrates and tailings. Standard sampling processes described by Gy (2012) were followed and three samples were taken from each test to limit the sampling error. Samples were digested in 15 mL hydrochloric acid and diluted 100 times. The resulting solutions were examined for copper content. An average of the three assays was used to determine the copper content. The copper concentration from each sample was then compared to the copper concentration of a pure malachite sample to determine malachite content.

B.3.3 Results and Discussion

B.3.3.1 Zeta Potential Measurements

The zeta potential results of malachite and quartz in the absence and presence of collectors are shown in Figures B.14 – B.16. The electrophoretic zeta potential data has been presented as a fitted trendline (third order polynomial), with calculated confidence intervals about the trendline. Figure B.14 displays the zeta potential trend for the two minerals without collectors. The data for quartz displays a negative trend across the pH range investigated, corresponding well to previous work (Deju and Bhappu, 1967; Fuerstenau, 1956b; Kosmulski, 2001; Li and De Bruyn, 1966). The malachite studied has an isoelectric point (IEP) at pH 7.8, which is consistent with work by Le Normand *et al.* (1979) (IEP 7.9) and Li *et al.* (2015) (IEP 8.3); however, other authors have reported an IEP much closer to pH 9 (Attia and Deason, 1989; Choi *et al.*, 2016). The shift to a higher pH may be due to insufficient conditioning prior to taking measurements. Le Normand *et al.* (1979) suggested that since dissolved CO_2 can produce potential determining ions for malachite, insufficient conditioning would not allow the suspension to reach an equilibrium with the atmospheric CO_2 resulting in the IEP to shift to a higher pH value. Another possible explanation for the differences in IEP may be due to differences in solids concentration used in each study. Mineral dissolution and the resultant differences in potential determining ion content in the bulk is likely to have a significant effect on the zeta potential trend of malachite. Other authors have shown that an increase in solids content, when measuring the zeta potential of bastnäsite (Jordens *et al.*, 2014b) and muscovite (Nosrati *et al.*, 2011), resulted in a shift in IEP to a higher pH. The maxima observed in the zeta potential trend of malachite at pH 5-6 can be explained by the fact that malachite begins to dissolve as the pH becomes more acidic. Figures B.15 and B.16 show the results for malachite and quartz in the presence of the seven different hydroxamate collectors. It can be seen from Figure B.15 that the addition of all of the collectors has a significant effect on the zeta potential of malachite, in all cases shifting the IEP to a lower pH value, suggesting adsorption to the mineral surface. The observed shift in zeta potential at $pH > 8$ (when the surface of malachite is negatively charged), demonstrates that collector adsorption is occurring through chemisorption or surface reactions rather than by physisorbing mechanisms. Figure B.16 shows that the reagents have little effect on the zeta potential of quartz, suggesting that the hydroxamate collectors are not adsorbing onto the surface of quartz and selective flotation of malachite would be possible. While there is a minor shift in zeta potential trend obtained for quartz in some cases, which may suggest collector adsorption, it is likely a result of electrical double layer compression due to the high collector concentrations added to the suspension; as previous investigations in literature have suggested there is little to no interaction of hydroxamate collectors with quartz (Hope *et al.*, 2010b; Jordens *et al.*, 2014b).

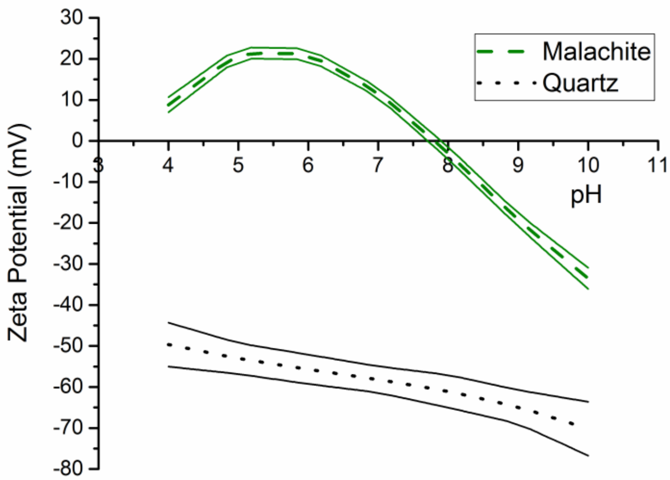

Figure B.14 – Zeta potential trend of malachite and quartz in 10^{-3} mol L^{-1} KCl (Error intervals shown are 95 % confidence intervals)

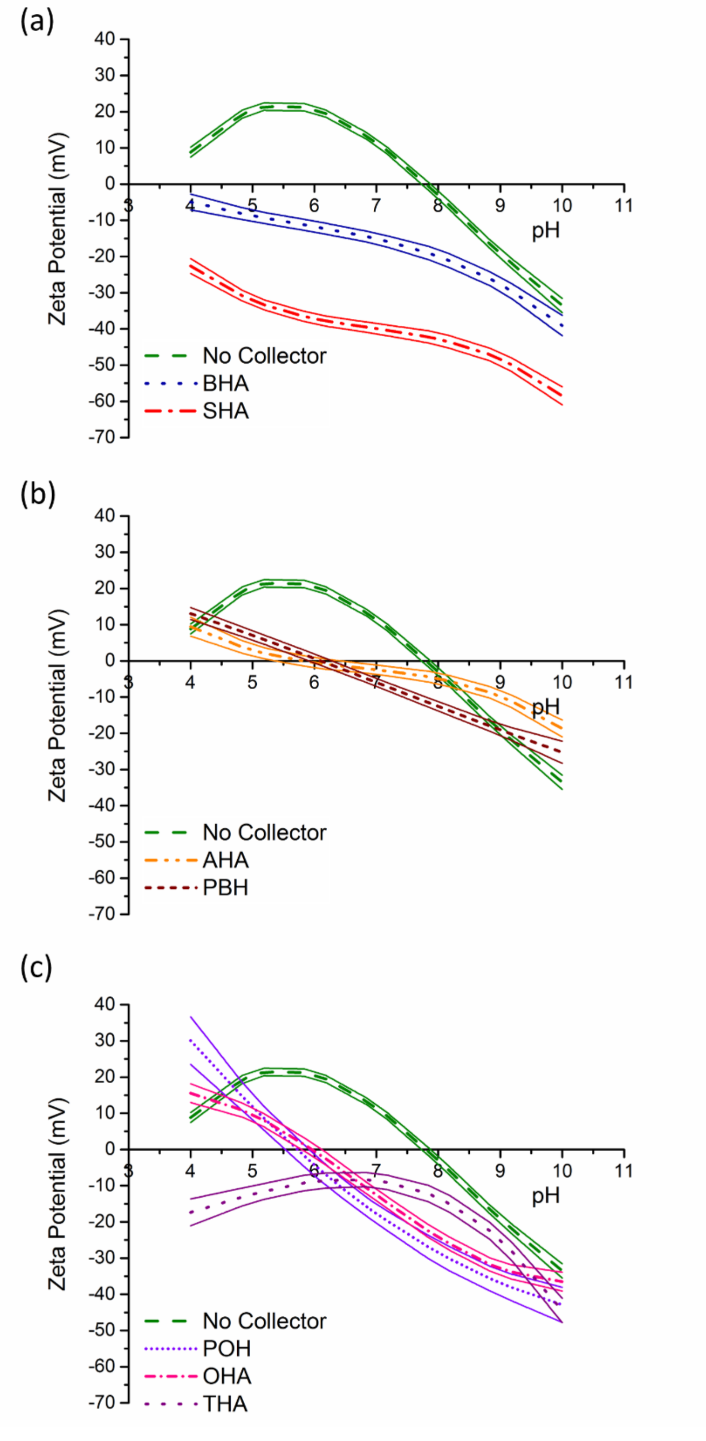

Figure B.15 – Zeta potential trend of malachite in the presence and absence of (a) aromatic, (b) short chain alkyl (C_2 and C_4) and (c) long chain alkyl (C_8 and C_{14}) hydroxamates at a concentration of 1.7×10^3 mol ton^{-1} (Error intervals shown are 95 % confidence intervals)

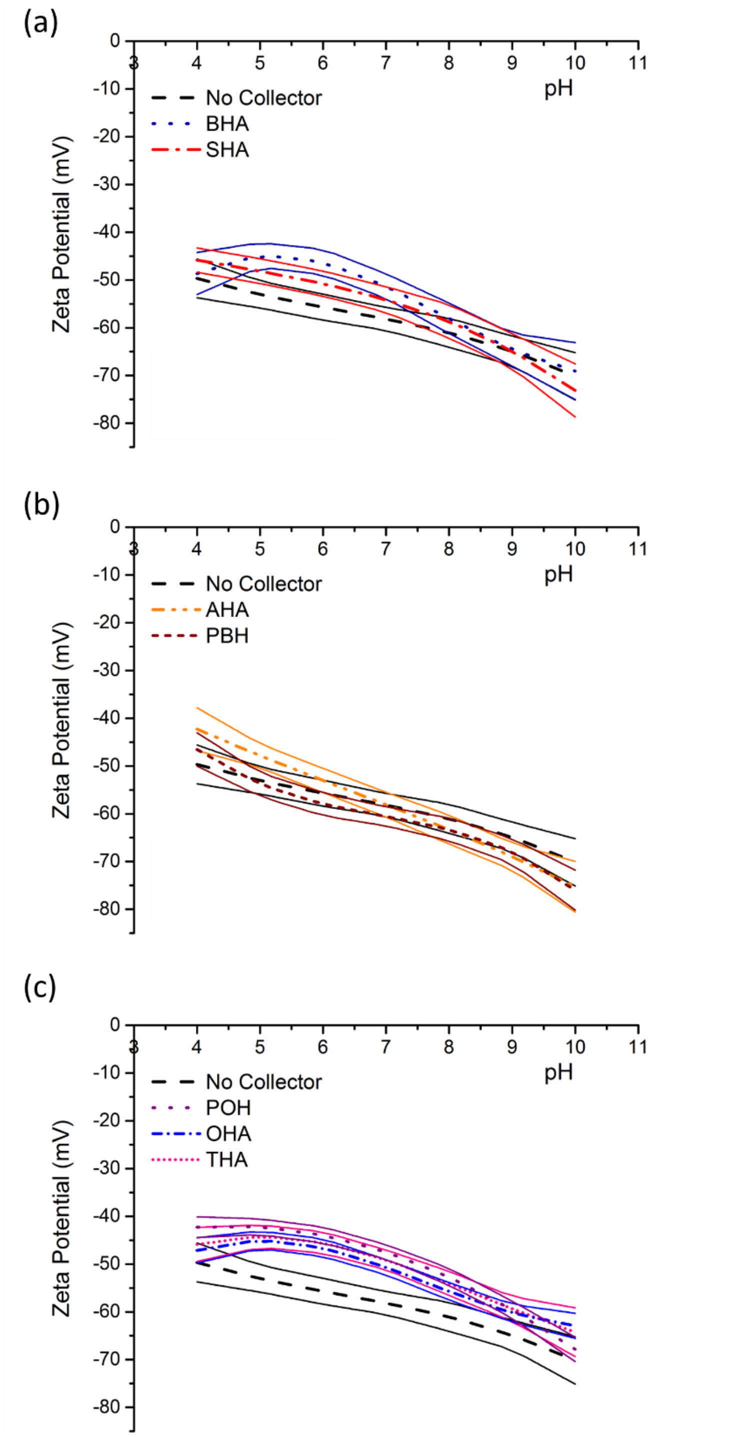

Figure B.16 – Zeta potential trend of quartz in the presence and absence of (a) aromatic, (b) short chain alkyl (C_2 and C_4) and (c) long chain alkyl (C_8 and C_{14}) hydroxamates at a concentration of 1.7×10^3 mol ton^{-1} (Error intervals shown are 95 % confidence intervals)

B.3.3.2 Froth Flotation

B.3.3.2.1 Effect of pH

In order to properly evaluate the flotation performance of the different collectors at various conditions, both the recovery and rate of recovery of malachite and quartz must be considered. To determine the effect of pH using BHA as collector, the recovery data obtained from flotation experiments at each condition were fit to a first-order rate model of the form (Arbiter *et al.*, 1985):

$$R= R_{max}(1 - e^{-kt}) \tag{B.1}$$

Where R is the recovery (%) at time t (min), R_{max} is the maximum possible flotation recovery and k is the flotation rate constant (min^{-1}). Statistical software, Stata13 (StataCorp, USA), was used to perform non-linear regressions, outputting R_{max} and k for each condition (shown in Table B.22). Recovery vs. time plots (Figure B.17) were generated by substituting R_{max} and k back into Equation B.1. Examining Figure B.17 and the k and R_{max} values obtained for each condition (detailed in Table B.22) it can be seen that the best flotation results were obtained at pH 8; with a decrease in malachite recovery and flotation rate kinetics obtained at both pH 6 and 9. An increase in quartz recovery was also observed at pH 6. For semi soluble minerals, such as malachite, it has been suggested that hydroxamate-mineral interactions occur mainly through surface reactions and bulk precipitation (Fuerstenau, 1983). Therefore, the aqueous speciation of malachite plays a crucial role in collector adsorption. Using HYDRA (Puigdomenech, 2009) and MEDUSA (Puigdomenech, 2010), dissolved species of Cu^{2+} and CO_3^{2-} were calculated based on thermodynamic data and are presented in Figure B.18 (log concentration as a function of pH). It is important to note that Figure B.17 does not directly represent malachite dissolving in water, but the dissolved Cu^{2+} and CO_3^{2-} species in equilibrium with malachite (along with other minerals having higher stabilities than malachite in very acidic to very alkaline pH conditions). From Figure B.18, it can be seen that below pH 6, Cu^{2+} is the predominant ion in solution, which is likely to result in the precipitation of cupric hydroxamate; depleting the collector species available for malachite flotation. In this case, an increase in quartz recovery was also observed, most likely due to cupric hydroxamate adsorbing/precipitating on the surface of quartz, thus causing it to float. The hydroxamate collector may also be directly adsorbing on to the surface of quartz at pH 6; which may explain the observed shift in the zeta potential of malachite when in the presence of benzohydroxamic acid at this pH (Figure B.15a, Section B.3.3.1). At pH 8, where optimum flotation conditions are observed, $CuOH^+$ and HCO_3^- are the predominate species in solution. In other mineral systems an increased concentration of metal hydroxyl species has been suggested to result in an improved flotation performance (Assis *et al.*, 1996); suggesting that $CuOH^+$ ions may have a larger effect than HCO_3^- ions on malachite flotation. As the concentration of $CuOH^+$ ions is higher at pH 8 than 9, this may explain the reduction in recovery observed at pH 9. Another explanation for the poor flotation performance at pH 9 may be due to the electrostatic repulsion of the negatively charged mineral surface (Figure B.14, Section B.3.3.1) and collector.

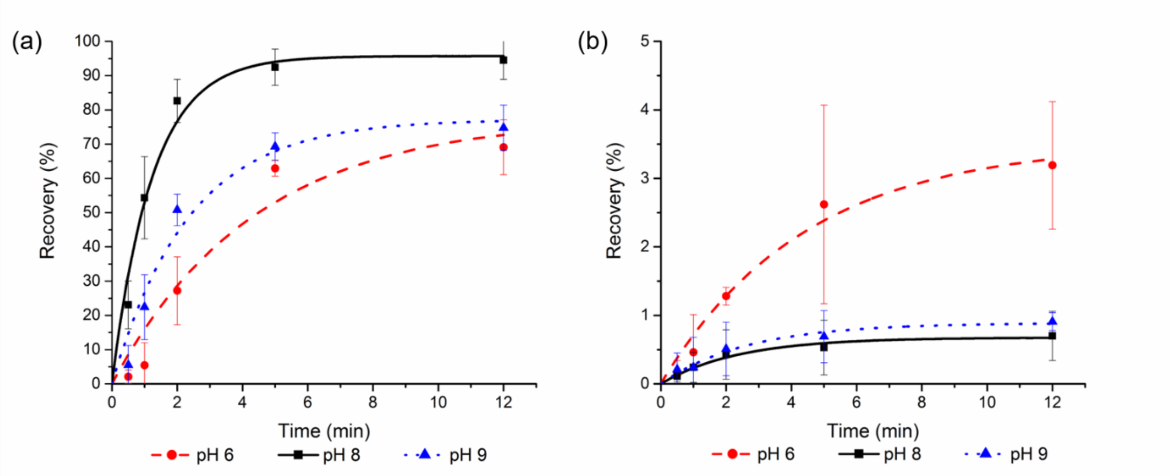

Figure B.17 – (a) Malachite and (b) quartz recovery at pH 6, 8 and 9, using BHA as collector. Data points shown are average recovery values with 95 % confidence intervals. Recovery vs. time curves were generated from the first-order flotation rate model

Table B.22 – Output of non-linear regression fitting to first-order rate equation for malachite and quartz using BHA at pH 6, 8 and 9

pH	Malachite			Quartz		
	k (min^{-1})	R_{max} (%)	R^2	k (min^{-1})	R_{max} (%)	R^2
6	0.23	77.6	0.97	0.23	3.5	0.99
8	0.81	95.7	0.99	0.42	0.7	0.87
9	0.42	77.2	0.99	0.38	0.9	0.96

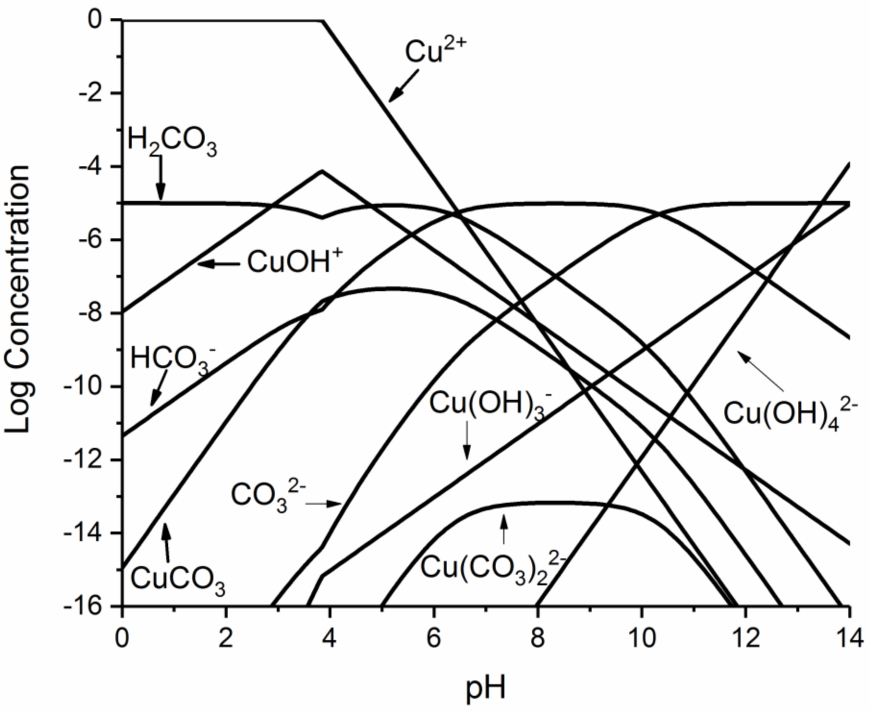

Figure B.18 – Log concentration (mol/L) of copper(II) and carbonate species, calculated in equilibrium with atmospheric CO_2 at 25 °C

B.3.3.2.2 Effect of Hydroxamate Structure

The mass recovery obtained using all seven hydroxamate collectors at pH 8 can be observed in Figure B.19. The results show that short chain (C_2 and C_4) alkyl hydroxamates and SHA resulted in very low mass recoveries. While zeta potential measurements suggest that these collectors selectively adsorb onto the surface of malachite, an increase in collector dosage is likely required for these collectors to be effective. Since OHA and POH recovered nearly all the mass at the initial concentration investigated (3.65 mol ton^{-1}), the dosage was reduced to 0.13 mol ton^{-1} to obtain mass recoveries much closer to the concentration of malachite in the flotation feed. The recovery of quartz using these two collectors may suggest that the observed shift in zeta potential (Figure B.16c, Section B.3.3.1) could be due to collector adsorption onto the mineral surface. THA was initially examined at 0.13 mol ton^{-1}, as the reduced collector dosage provided reasonably good results when using the two C_8 alkyl hydroxamate collectors. However, low mass recoveries were obtained and the collector dosage was increased to 0.21 mol ton^{-1}.

Malachite and quartz recovery data, for flotation with the different hydroxamate collectors (concentrates produced using SHA, AHA and PBH were not examined due to low mass recoveries), were fitted to the first-order rate kinetic model (Equation B.1, Section B.3.3.2.1). The k and R_{max} values obtained for each condition can be seen in Table B.23 and the recovery vs. time curves generated can be seen in Figure B.20. Comparing the results, it can be seen that flotation with BHA resulted in the greatest recovery of malachite and lowest recovery of quartz. However, similar malachite recoveries and a significant increase in flotation rate constant were observed with significantly lower dosages of OHA and POH. Both collectors, however, resulted in similar increases in quartz recovery when compared to flotation with BHA. The lower dosages required with the two C_8 alkyl hydroxamates is consistent with work by Hart *et al.* (2014), who observed a similar trend when comparing OHA to aromatic and cyclic alkyl hydroxamates for the flotation of a rare earth ore.

As a change in collector results in changes in both R_{max} and k for both minerals comparing the selectivity of BHA to the two C_8 alkyl hydroxamates becomes challenging. One way of comparing total flotation response is by using the modified rate constant introduced by Xu (1998); defined as the product of R_{max} and k:

$$K_m = R_{max} \times k \qquad (2)$$

Based on this modified rate constant, a selectivity index (or relative rate constant) between malachite and quartz can be defined as the ratio of their modified rate constants (Xu, 1998):

$$SI\left({}^{malachite}/_{quartz}\right) = \frac{K_m \; of \; malachite}{K_m \; of \; quartz} \qquad (3)$$

Modified rate constants and selectivity indices can be seen in Table B.23. The selectivity indices obtained under each condition suggest that BHA is the most selective collector, however, the drastic decrease in collector concentration required when using OHA or POH may outweigh these improvements in selectivity. The results also indicate that there is little difference in flotation performance when using the C_8 alkyl hydroxamate in its acid or salt form, suggesting that the use of hydroxamic acids vs hydroxamate salts does not affect flotation for the collectors investigated here. THA resulted in poor malachite recoveries; corresponding well to previous work, which has suggested that a reduced flotation performance is obtained when using alkyl hydroxamates with a carbon chain longer than C_9 (Bulatovic, 2007a).

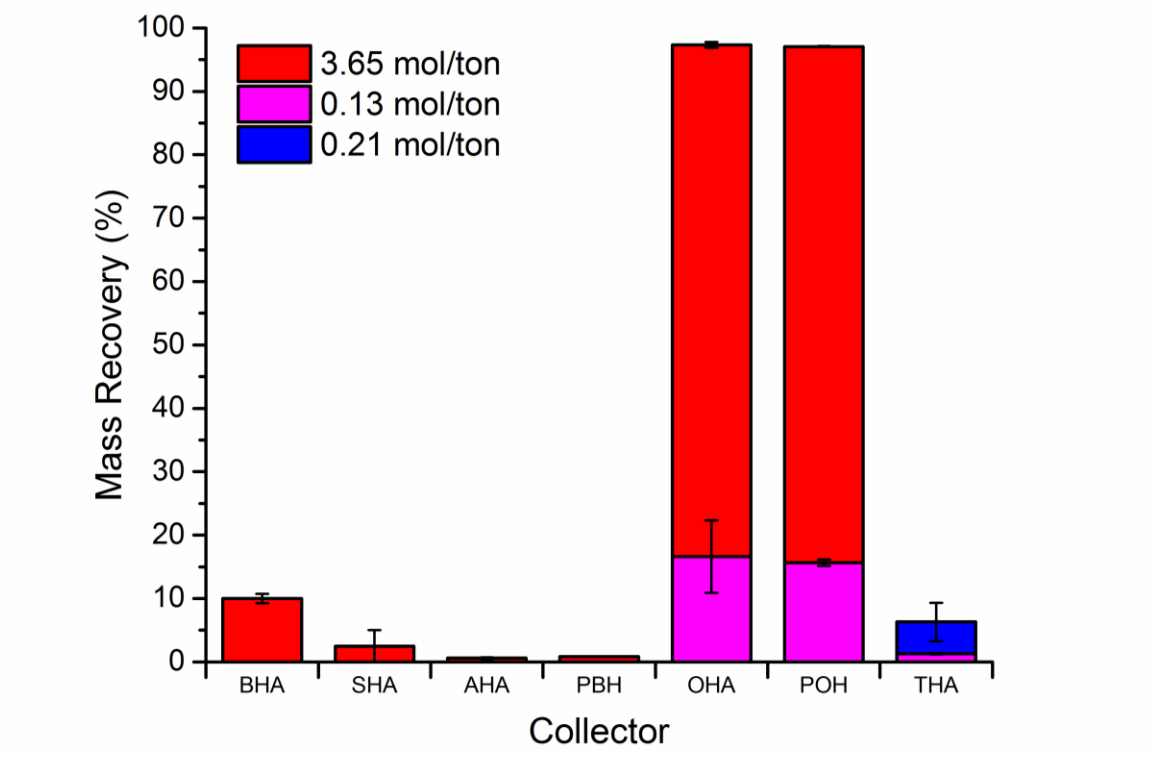

Figure B.19 – Mass recoveries obtained using the 7 different hydroxamate collectors. Error bars are 95 % confidence intervals

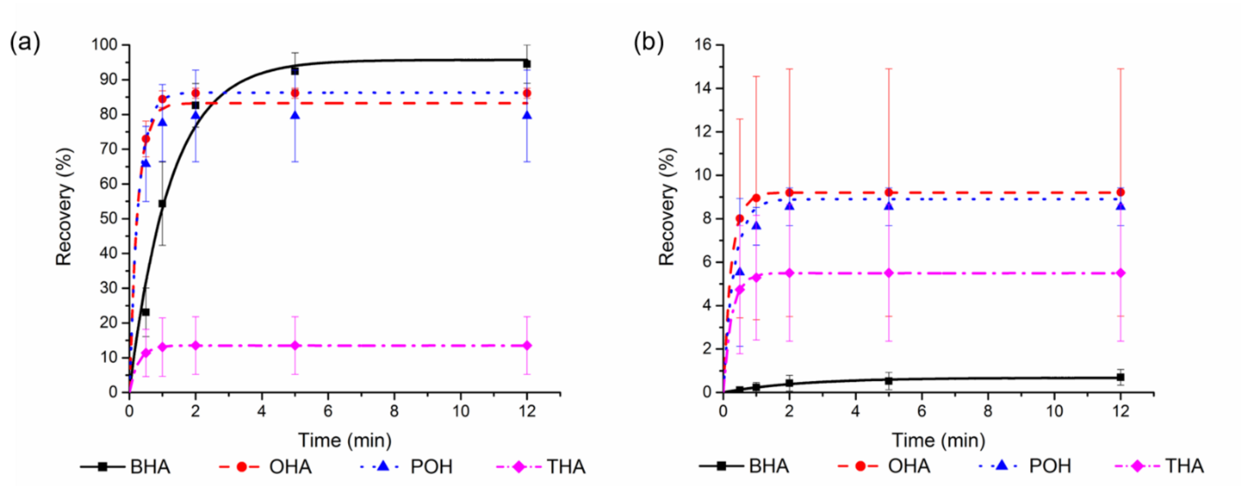

Figure B.20 – (a) Malachite and (b) quartz recovery with BHA, OHA, POH and THA at pH 8. Data points shown are average recovery values with 95 % confidence intervals. Recovery vs. time curves were generated from the first-order flotation rate model

Table B.23 – Output of non-linear regression fitting to first-order rate equation for malachite and quartz using BHA, OHA, POH, THA

	Malachite				Quartz				
Collector	**k (min^{-1})**	**R$_{max}$ (%)**	**R^2**	**K$_M$**	**k (min^{-1})**	**R$_{max}$ (%)**	**R^2**	**K$_M$**	**SI (Malachite/Quartz)**
BHA	0.81	95.7	0.99	77.5	0.42	0.7	0.87	0.3	263.7
OHA	3.98	83.3	0.99	331.5	4.07	9.2	0.89	37.4	8.9
POH	3.67	86.3	0.99	316.7	3.04	8.9	0.99	27.1	11.7
THA	3.67	13.5	0.89	49.5	3.91	5.5	0.91	21.5	2.3

B.3.3.2.3 Effect of Particle Size

The effect of particle size on flotation was examined using BHA and OHA as collectors. All other hydroxamate collectors demonstrated a poor flotation performance and therefore were not tested further. POH was not examined as the hydroxamate salt offered little difference in flotation response to OHA. The results obtained from fitting the recovery data obtained after floating the synthetic feed (sized at -38 μm) with both collectors to the first-order rate model (Equation B.1, Section B.3.3.2.1) are shown in Table B.24 and the recovery vs time plots can be seen in Figure

B.21 and B.22 for BHA and OHA respectively. The results indicate a decrease in malachite recovery and flotation kinetics when compared to coarse particle flotation tests for both collectors; as well as a significant increase in quartz recovery. It is well established that the flotation of fine particles often results in a reduction in flotation performance (Collins and Read, 1971; Flint and Howarth, 1971; Fuerstenau, 1980; Miettinen *et al.*, 2010; Reay and Ratcliff, 1973; Sivamohan, 1990; Sutherland, 1948; Trahar, 1981; Trahar and Warren, 1976; Yoon and Luttrell, 1989). This reduction in performance is likely explained by multiple different physical and chemical sub-processes such as: the increased consumption and non-selective adsorption of reagents as a result of higher surface energies and surface areas; the increased recovery by non-selective entrainment; and a decrease in flotation kinetics and recovery due to a decreased probability of collision between particles and bubbles. To improve flotation performance collector dosages could be increased and the froth properties could be altered to limit the recovery of unwanted gangue through hydraulic entrainment. It is well known that non-selective entrainment is strongly correlated to water recovery. Water recovery depends on bubble size, gas rate and frother type, and therefore by optimizing these characteristics an improvement in flotation could be observed.

It has also been suggested that flotation at elevated temperatures with hydroxamate collectors leads to a more selective and enhanced adsorption of the collector at the mineral surface; resulting in improvements in both grade and recovery (Pradip and Fuerstenau, 1985). As a means to improve the flotation response when floating fine particles, the effect of elevated temperatures on flotation was examined. The results from flotation experiments conducted at 60 ˚C are shown in Table B.24 and Figures B.21 and B.22. Significant improvements in flotation are observed with BHA. While there are no improvements in total malachite recovery, the rate of malachite recovery is significantly improved and quartz recovery has decreased. These improvements are likely a result of the increased solubility of malachite at elevated temperatures resulting in faster adsorption kinetics. Flotation using OHA at elevated temperatures was detrimental to malachite flotation. Slight reductions in both the recovery and rate of recovery of quartz were observed, however, a significant decrease in malachite recovery was also observed. While more work is required to determine why malachite flotation is reduced when using OHA, one explanation may be that the increased malachite solubility results in a more elevated concentration of Cu^{2+} ions in solution, and this coupled with the rapid reaction kinetics of OHA results in an increase of the bulk precipitation of copper-hydroxamate species reducing the concentration of collector available for malachite flotation. As the concentration of OHA (0.21 mol ton^{-1}) is significantly lower than that of BHA (3.65 mol ton^{-1}) the consumption of collector by bulk precipitation may have a much more significant impact on flotation.

Comparing the flotation rate constants obtained for the two minerals at each condition (Table B.24), in general the flotation rate constant for malachite is significantly higher than that of quartz, indicating the possibility of selectively separating malachite from quartz by exploiting differences in flotation kinetics. By plotting the cumulative recovery of quartz as a function of cumulative malachite recovery (Figure B.23), an optimal flotation time can be determined. When using BHA as collector, flotation for longer than 5 min results in limited improvements in malachite recovery and when floating fine particles significant increases in quartz recovery. At elevated temperatures flotation for 2 min is sufficient to maximize malachite recovery while limiting quartz recovery. When using OHA, flotation kinetics are much faster and the majority of the malachite is recovered after 1 min for coarse particles and 2 min for fine particles, with longer flotation times resulting in significant increases in quartz recovery. The grade and recovery of malachite are shown in Figure B.24, with the values at optimal flotation times for each condition are compared to those obtained after 12 min of flotation in Table B.25. It can be seen that significant improvements in grade, with limited reductions in recovery can be obtained by taking into account the rate of recovery of each mineral.

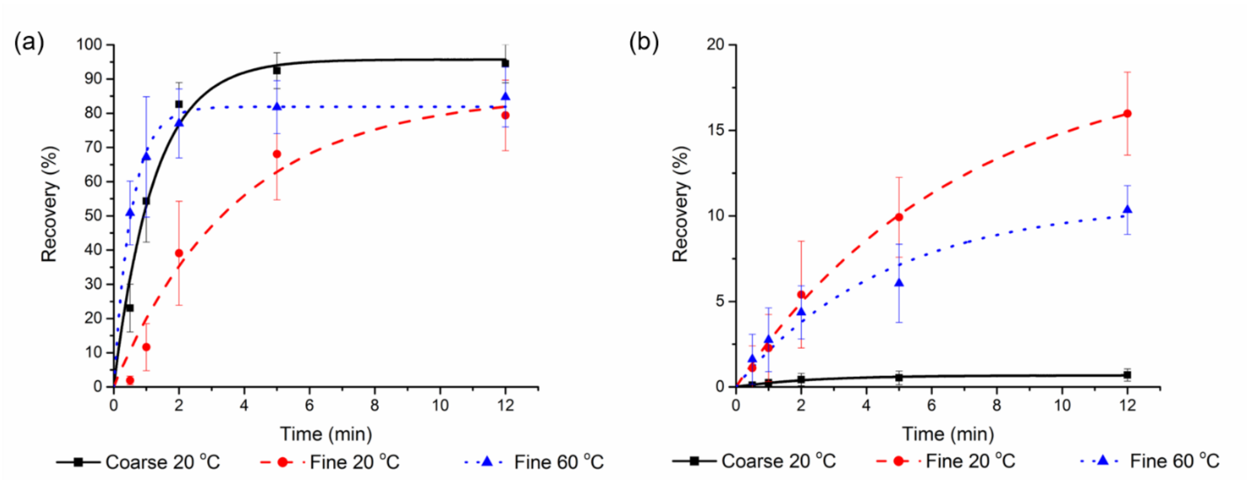

Figure B.21 – (a) Malachite and (b) quartz recovery for coarse (-150 +38 μm) and fine (-38 μm) particle flotation, using BHA (3.65 mol ton^{-1}) at 20 and 60 ˚C. Data points shown are average recovery values with 95 % confidence intervals. Recovery vs. time curves were generated from the first-order flotation rate model

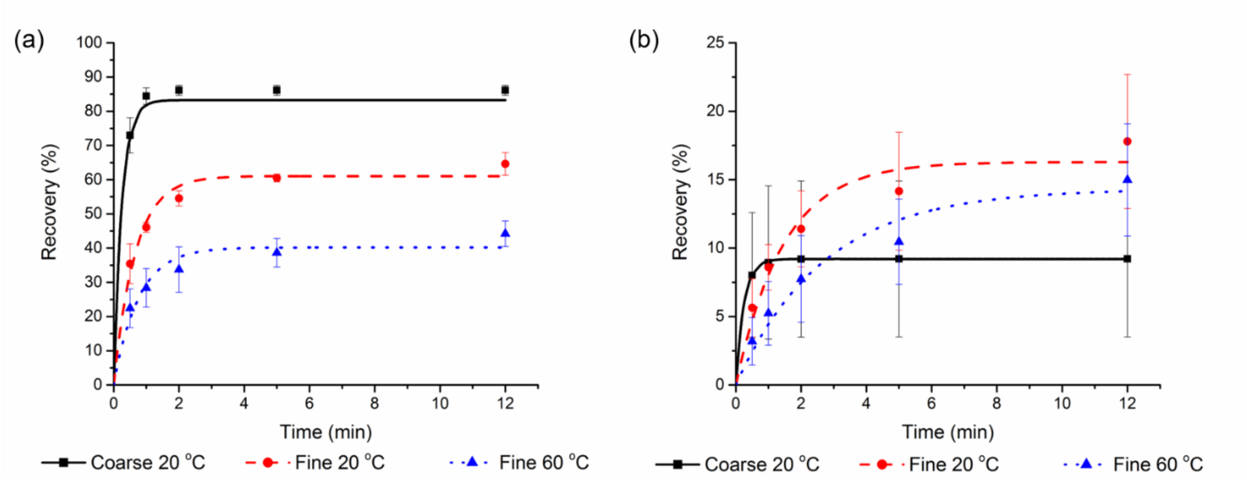

Figure B.22 – (a) Malachite and (b) quartz recovery for coarse (-150 +38 μm) and fine (-38 μm) particle flotation, using OHA (0.21 mol ton^{-1}) at 20 and 60 ˚C. Data points shown are average recovery values with 95 % confidence intervals. Recovery vs. time curves were generated from the first-order flotation rate model

Table B.24 – Output of non-linear regression fitting to first-order rate equation for coarse and fine particle flotation experiments at 20 ˚C and 60 ˚C

`Collector	Particle Size (μm)	Temperature (˚C)	Malachite				Quartz				SI (Malachite/Quartz)
			k (min^{-1})	R_{max} (%)	R^2	K_M	k (min^{-1})	R_{max} (%)	R^2	K_M	
BHA	-150 +38	20	0.81	95.7	0.99	77.5	0.42	0.7	0.87	0.3	263.7
	-38	20	0.27	85.4	0.98	23.1	0.15	19.2	0.99	2.9	8
	-38	60	1.82	81.9	0.99	149.1	0.22	10.8	0.97	2.4	62.7
OHA	-150 +38	20	3.98	83.3	0.99	331.5	4.07	9.2	0.89	37	8.9
	-38	20	1.52	61.0	0.99	92.7	0.68	16.3	0.98	11	8.4
	-38	60	1.31	40.2	0.99	52.7	0.37	14.3	0.97	5.3	10

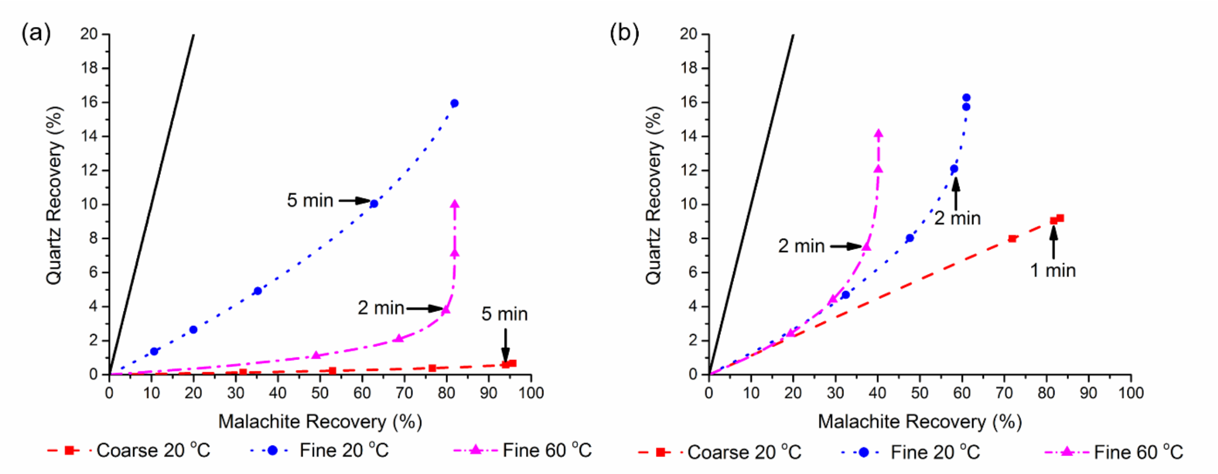

Figure B.23 – Plot of cumulative malachite recoveries as a function of cumulative quartz recoveries for coarse (-150 +38 μm) and fine (-38 μm) particle flotation, using (a) BHA and (b) OHA as collectors. Data points indicate times where flotation concentrates were taken (0.5, 1, 2, 5 and 12 min). The solid line represents an equality line (y=x) where no separation between malachite and quartz occurs

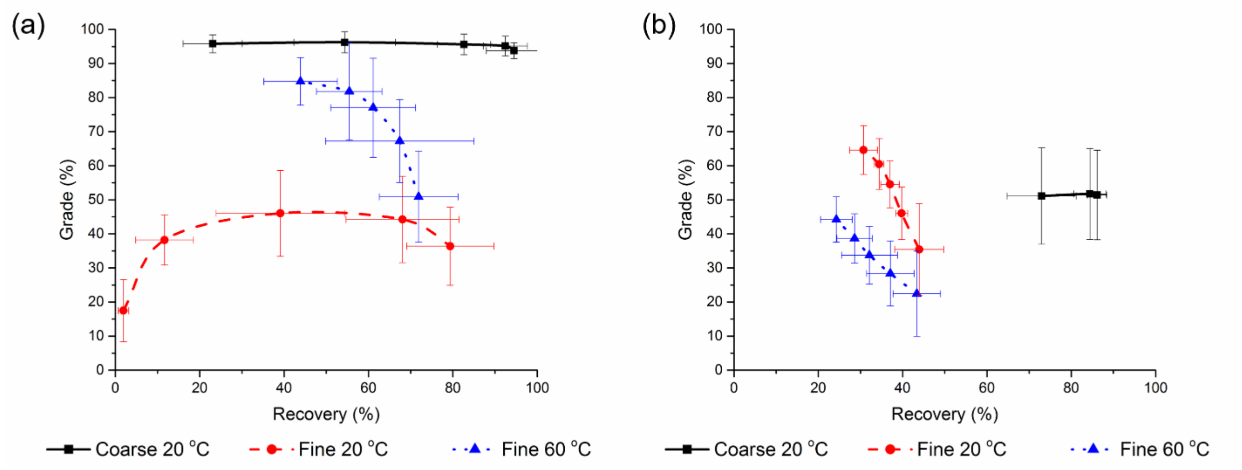

Figure B.24 – Malachite grade *vs.* recovery curve for coarse (-150 +38 µm) and fine (-38 µm) particle flotation, using (a) BHA and (b) OHA as collectors. Error bars are 95 % confidence intervals

Table B.25 – Cumulative grade and recovery of malachite at optimal flotation times and 12 minutes

			Optimal Flotation Time			**12 Minutes**	
Collector	**Particle Size (µm)**	**Temperature (˚C)**	**Time (min)**	**Grade (%)**	**Recovery (%)**	**Grade (%)**	**Recovery (%)**
BHA	-150 +38	20	5	95	94	94	96
	-38	20	5	41	63	36	82
	-38	60	2	70	80	48	82
OHA	-150 +38	20	1	50	82	50	83
	-38	20	2	34	58	29	61
	-38	60	2	35	37	24	40

B.3.4 Conclusions

This work investigated the separation of malachite from quartz using seven different hydroxamate collectors. The investigation included zeta-potential measurements to understand reagent interactions with malachite and quartz; and bench scale flotation experiments on a synthetic malachite ore to evaluate the differences in malachite recovery and selectivity obtained with each collector. The hydroxamate collectors showing the best results were further evaluated for fine particle flotation at both 20 and 60 ˚C to determine the effects of particle size and temperature on flotation. The conclusions are as follows:

1. Zeta potential measurements suggest that all seven hydroxamate collectors investigated selectively adsorb onto the surface of malachite
2. Benzo- and the two C_8 alkyl hydroxamates result in the best flotation response; with all other collectors resulting in low malachite recoveries
3. The greatest malachite selectivity can be achieved using benzo hydroxamate, however, similar malachite recoveries and significantly higher flotation kinetics were observed with much lower concentrations of the two C_8 alkyl hydroxamates
4. The use of hydroxamic acids *vs*. hydroxamate salts does not have a significant effect on flotation results
5. Significant reductions in flotation performance using both benzo- and octyl hydroxamates were observed when floating fine particles; with elevated temperatures offering significant improvements in flotation when using BHA but not OHA
6. Flotation kinetics are generally fast when using hydroxamate collectors; and the selective separation of malachite from quartz can be optimized by exploiting differences in flotation kinetics

B.3.5 Acknowledgements

The authors would like to acknowledge the Natural Sciences and Engineering Research Council of Canada (NSERC) and Avalon Rare Metals for providing funding for this work through the Discovery Grants program (RGPIN-2014-06230). C. Marion would also like to acknowledge funding from the NSERC Canada Graduate Scholarships Program and the McGill Engineering Doctoral Award and A. Jordens would like to acknowledge funding from the NSERC Alexander Graham Bell Canada Graduate 21 Scholarships Program. The authors also acknowledge the assistance of B. Miller in conducting some of the zeta potential measurements.

B.4 A Physico-Chemical Investigation into the Flotation of Rare-Earth Minerals

Section B.3 demonstrated that the structure of the hydroxamate collector plays an important role in both the selectivity and collectivity of malachite flotation. The study identified that C_8 alkyl hydrixamates (OHA and POH) and BHA were the most effective collectors of those which were studied. Section B.4 looks to expand this study to REM flotation, by examining the physico-chemical properties of various REE-bearing minerals and their interaction with POH and BHA, using zeta potential measurements and microflotation experiments. The minerals which were studied are allanite, bastnäsite, columbite, eudialyte, fergusonite, monazite, parisite, and zircon. As is evident from Section B.2, for many of these minerals there exist limited fundamental understanding of their physico-chemical properties or their flotation response to different hydroxamate collectors. As many of these minerals are present in the Nechalacho deposit, the zeta potential and microflotation results for those minerals are related to the flotation of this ore using an industrial hydroxamate collector. This chapter contains a manuscript that is to be submitted to a peer-reviewed journal and is presented below.

Abstract

Many new rare earth mineral (REM) deposits with novel mineralogy are being investigated. These deposits are often complex and contain multiple REMs for which there is limited processing knowledge. This study looked to expand the flotation knowledge base of various REMs through an improved understanding of their physico-chemical properties and interactions with hydroxamate collectors. The minerals investigated were bastnäsite, monazite, allanite, parisite, fergusonite, a synthetic $YNbO_4$ sample, columbite and zircon. The study included zeta potential and microflotation studies using benzohydroxamic acid (BHA) and K-octyl hydroxamate (POH) as collectors, which are then related to the bench scale flotation of an ore sample from the Nechalacho deposit, which contains these minerals (or in the case of parisite, a very similar mineral in synchysite). Zeta potential experiments suggest BHA adsorption to bastnäsite, monazite, parisite, fergusonite and the synthetic $YNBO_4$ sample, which correspond to the minerals which were most readily recovered by microflotation. POH adsorption was indicated for all minerals investigated, however, at the collector dosages tested only bastnäsite, monazite, parisite, allanite and fergusonite were readily recovered. Bench scale flotation of the ore produced a cumulative concentrate which recovered 77 % of the light rare-earth elements (LREE), 52 % of the heavy rare-earth elements (HREE) and 40 % of the zirconium. The respective upgrading of each being 2.8 times, 1.9 times and 1.6 times.

B.4.1 Introduction

The rare-earth elements (REE) are the fifteen elements of the lanthanoid series of the periodic table plus yttrium. These elements are typically split into two sub-groups: the light rare-earth elements (LREE), which includes lanthanum to gadolinium, and the heavy rare-earth elements (HREE), which include the remaining eight elements, terbium to lutetium, as well as yttrium. In recent years, REE have become indispensable to the development of many high-technology applications, including modern defense systems, electronic applications and green technologies. The growing economic and strategic importance of these sectors, coupled with concerns about the future supply of REE, has led to several new rare-earth mineral (REM) deposits being investigated (Hatch, 2015). These new deposits are often complex and contain multiple REMs for which there is limited processing knowledge.

To date there are more than 250 rare earth minerals that have been discovered (Jordens *et al.*, 2013). However, only three of these minerals, bastnäsite, monazite and xenotime, are commonly exploited commercially (Jordens *et al.*, 2013). REE deposits are commonly beneficiated using a combination of many mineral processing techniques, with the most important being froth flotation. Flotation is commonly applied to rare-earth ores due to its ability to process a wide range of fine particle sizes and it can be tailored to the mineralogy of a specific deposit. A summary of the use of flotation as applied to REM beneficiation and the surface chemical properties of various REM is presented here but a more detailed summary of the literature on all REM beneficiation techniques can be found in Jordens *et al.* (2013) and Zhang and Edwards (2012). For a more general discussion of mineral processing readers are referred to Wills and Finch (2016a)

Compared to other beneficiation techniques, flotation has received the most research. The research has primarily focused on bastnäsite and monazite surface characteristics and their relation to flotation response. Most of the work focused on the flotation of ore deposits has been performed on Bayan Obo (China) and Mountain Pass (USA) ores, where bastnäsite is the main REE-bearing mineral. There is also a limited amount of information with regards to the flotation of other REE deposits, such as Mount Weld (Australia) (Chan, 1992; Guy *et al.*, 2000), Kvanefjeld (Greenland) (Sorensen and Lundgaard, 1966), Nechalacho (Canada) (Jordens *et al.*, 2016a), Bear Lodge (USA) (Cui and Anderson, 2017a), as well as several Chinese deposits (Li and Yang, 2016).

The flotation of bastnäsite and monazite is typically accomplished using oxhydryl collectors, such as fatty acids or hydroxamates. While fatty acids, such as sodium oleate, have been shown to be capable collectors for REM, they are generally unselective and require large dosages of depressants and elevated temperatures (Jordens *et al.*, 2013). For these reasons, recent work is focused on using hydroxamate collectors, which are much more selective than fatty acids. There is a large body of work demonstrating the effectiveness hydroxamate collectors in both bastnäsite (Cao *et al.*, 2018a; Jordens *et al.*, 2014b; Luo and Chen, 1984; Pavez *et al.*, 1996; Ren *et al.*, 1997; Sarvaramini *et al.*, 2016; Yang *et al.*, 2017) and monazite (Abaka-Wood *et al.*, 2017; Espiritu and Waters, 2018; Luo and Chen, 1984; Nduwa-Mushidi and Anderson, 2017; Pavez *et al.*, 1996; Sarvaramini *et al.*, 2016; Zhang *et al.*, 2016; Zhang *et al.*, 2017) flotation; and they are used to process the Bayan Obo deposit (Zhang and Edwards, 2012). However, as new deposits are being developed, an understanding of the flotation response of other REM when using these collectors is required.

In flotation, the electrical double layer at the mineral-water interface governs the adsorption of flotation reagents. Zeta potential measurements can be used to characterize the electrical double layer and understand the surface characteristics of mineral particles in flotation. By measuring the zeta potential as a function of pH, it is possible to define an isoelectric point (IEP) as the pH at which the zeta potential is zero. The IEP can aid in predicting the sign of the charge on a mineral surface at a specific pH. Understanding the zeta potential of a mineral can help understand mechanisms of collector adsorption and select optimal flotation conditions to effectively separate a valuable mineral from gangue minerals. For an introduction to the concept of surface charge and zeta potentials and their application in flotation, interested readers should consult Riley (2009) and Fuerstenau and Pradip (2005)

A summary of the surface chemistry studies focused on REM is shown in Table B.2 to Table B.4. These tables contain the origin of the mineral sample and reported IEPs. Zircon is included in Table B.4, as in some REM deposits, such as the Nechalacho deposit, it is an important REE-bearing mineral (Ciuculescu et al*., 2*013; Grammatikopoulos et al., 2011). It should be noted, however, that there are no published surface chemistry studies investigating REE-bearing zircon. With the exception of bastnäsite (Table B.2) and monazite (Table B.3), which have been extensively characterized, test work investigating other REM (Table B.4) is limited. The large differences in reported IEP values, for bastnäsite (4.6 to 9.3), monazite (1.1 to 9.0), xenotime (2.3 to 7.0), fergusonite (2.7 to 6.3) and zircon (2.3 to 6.0) have been suggested to be a result of variations in potential determining ions, mineral composition and the structure of the mineral surfaces, as well as differences in the procedure and/or technique used to determine the IEP (Cheng, 2000; Jordens *et al.*, 2014b). For semi-soluble minerals, such as bastnäsite, it is likely that differences in procedure or techniques used have a larger impact than mineral origin. This is evident by the fact that bastnäsite from a single source, the Mountain Pass deposit, has a wide range of reported IEP values (Azizi *et al.*, 2016; Herrera-Urbina *et al.*, 2013; Jordens *et al.*, 2014b; Pradip *et al.*, 2015; Sarvaramini *et al.*, 2016; Smith and Shonnard, 1986; Smith and Steiner, 1980). Variations in solids concentration and conditioning time will impact mineral dissolution and therefore result in differences in the amount of potential determining ions in the bulk. This has been demonstrated by Smith and Steiner (1980), who noted that after 30 min of conditioning the IEP was at pH 5.3, whereas after 24 hours it increased to pH 7.2. Similarly, Jordens *et al.* (2014b) measured the same bastnäsite sample using both electrophoretic and electroacoustic techniques. The electroacoustic technique, which used a much greater solids concentration, measured an IEP of 8.1, compared to 6.8 measured using electrophoresis. As monazite has a low dissolution rate (Oelkers and Poitrasson, 2002), it is unlikely that variations in its IEP are due to the same mechanism as bastnäsite. However, Geneyton *et al.* (2018) tested three synthetic monazites with different REE in their lattice and have suggested that IEP variations are due to procedural differences and not substitutions of REE in the mineral lattice. The authors indicated that ions resulting from CO_2 dissociation are potential determining ions for monazite which influence its zeta potential significantly. Therefore, if the suspension has not reached an equilibrium with dissolved CO_2 from the atmosphere, variations in the IEP will exist. Although there exists a wide discrepancy of reported IEPs for bastnäsite and monazite, most work indicates their IEPs to occur between pH 6 to 8 and pH 5 to 6, respectively. This does, however, demonstrate the importance of obtaining a similarly large database of surface chemical studies for other REM.

Zeta potential measurements are generally conducted along with, and compared to, small-scale, single mineral, flotation experiments. These studies are summarized in Table B.5 – B.7, which includes the type of hydroxamate used and optimum pH for recovery. It should be noted that the optimum pH for flotation often occurs at around pH 9. At this pH, elevated concentrations of rare-earth hydroxy species are present. It has been suggested that the presence of metal hydroxy complexes provide optimal conditions for collector adsorption (Assis *et al.*, 1996). This is also roughly the pKa of hydroxamic acid collectors (Fuerstenau and Pradip, 2005; Gupta, 2013; Pradip and Fuerstenau, 1983). Fuerstenau and Pradip (2005) suggested that at the pKa of the hydroxamic acid collector, the hydroxamate anion adsorbs alongside the neutral molecule, resulting in multilayers of collector adsorption. Table B.7 further demonstrates the need to develop an improved understanding into the interaction of hydroxamate collectors with REM. While these collectors are effective for carbonate and phosphate minerals, they may not be very effective for silicate minerals such as allanite (Jordens *et al.*, 2014a).

Recently, Jordens *et al.* (2016a) investigated the use of benzohydroxamic acid for the flotation of the Nechalacho deposit. This deposit contains seven different REE-bearing minerals, namely bastnäsite (carbonate), synchesite (carbonate), fergusonite (niobate), columbite (Fe) (niobate), monazite (phosphate), allanite (silicate) and zircon (silicate), for which the authors suggested have varying flotation response dependant on mineral type. The carbonate, niobate and phosphate minerals demonstrated a greater floatability than the silicate minerals. It was suggested that this was due to mineral solubility, as proposed by (Assis *et al.*, 1996); with more soluble minerals resulting in a greater flotation performance. While this study demonstrates the impact mineral type may have on flotation, for many of these minerals there exists limited fundamental understanding of their physico-chemical properties which govern flotation.

The objective of this paper is to provide an improved understanding into the surface chemical properties of REM present in the Nechalacho ore, through zeta potential and microflotation experiments. The test work focusses on the flotation response of REM using alkyl hydroxamate [K-octyl hydroxamate (POH)] and aromatic hydroxamate [benzohydroxamic acid (BHA)] collectors. An alkyl and aromatic hydroxamate are tested as previous work has shown the structure of the hydroxamate which is employed is also likely to play an important role in flotation (Marion *et al.*, 2017). The minerals examined are bastnäsite (carbonate), parisite (carbonate), fergusonite (niobate), columbite (Fe) (niobate), monazite (phosphate), allanite (silicate) and zircon (silicate). Parisite, while not present in the Nechalacho ore, is studied here, as it, along with bastnäsite, may give insight into the physico-chemical properties of synchysite (a member of the same polysomatic series of minerals). The grain size of synchysite in ore deposits is typically very low, which makes obtaining enough pure crystals for fundamental flotation studies difficult. The findings from zeta potential and microflotation experiments are then compared to bench scale flotation experiments on Necholacho gravity tailings using an industrial hydroxamate collector.

B.4.2 Materials and Methods

B.4.2.1 Materials

The REM used in this work, their origin and the source from which they were obtained are summarized in Table B.26. The procedure for synthesis of $YNbO_4$ follows the protocol described by Hirano and Dozono (2013). The as-received natural mineral samples were stage ground dry using a Pulverisette 6 planetary monomill (Fritsch, Germany) with ceramic grinding media and sieved to produce samples in the size range of – 150 + 38 μm. Minerals which were not received pure were purified using a Mozley MKII Laboratory Separator (Mozley, UK) and/or a Frantz Isodynamic Separator (Frantz, USA). X-ray diffraction (XRD) was employed to verify the success of the purification steps. The XRD analyses were performed using a Bruker D8 Discovery X-ray Diffractomers equipped with a cobalt X-ray generating source. The resulting diffraction patterns and corresponding mineral reference files are shown in Figures B.4 -B.11. The XRD patterns for the allanite and fergusonite sample were less conclusive at determining mineral purity than the others. The allanite sample is the same sample as used by Jordens *et al.* (2014a), which was received as 65 % allanite (as determined by QEMSCAN analysis) and then concentrated using a Frantz Isodynamic Separator. Concentration steps were deemed successful and any differences in XRD patterns compared to available reference patterns were said to be due to differences in allanite composition (Jordens *et al.*, 2014a). To ensure mineral purity of fergusonite it was analyzed using a scanning electron microscope (SEM) and energy dispersive X-ray spectroscopy (EDS). The SEM used was a Hitachi SU8000 cold field emission SEM (Hitachi High-Technologies, Canada), equipped with an 80 mm^2 X-Max^N Silicon Drift EDS detector (Oxford Instruments, UK). The X-ray map of the fergusonite sample is provided in Figure B.12. From XRD and SEM analyses it can be concluded that all minerals are of relatively high purity. Once determined pure, a subsample of the – 150 + 38 μm natural mineral samples were further ground wet using a Pulverisette 6 planetary monomill to obtain very fine particles or zeta potential measurements. The particle size (equivalent spherical diameter) [determined using a LA-920 particle analyser (Horiba, Japan)] and measured surface areas [determined by the N_2 Brunauer–Emmett–Teller (BET) technique, using a TriStar Surface Area and Porosity Analyzer (Micromeritics, USA)] are given in Table B.27.

The Nechalacho ore sample used in this work was the gravity tailings produced from the gravity and magnetic separation experiments detailed in Jordens *et al.* (2016b). The gravity tailings were passed through a lab-scale model WD(20) wet drum permanent magnetic separator (Carpco Inc., USA) equipped with a rare earth (medium intensity) permanent magnet to remove magnetite gangue prior to flotation. The magnetic fraction produced was verified as predominately magnetite using XRD. The non-magnetic fraction was dried, mixed and split using a rotary splitter. The resulting fractions were riffled to produce 500 g samples for flotation. The particle size (d50) of the flotation feed was 8 μm (determined using a LA-920 particle size analyser).

BHA was purchased from Sigma Aldrich, USA and POH was synthesized at the Helmholtz Institute Freiberg for Resource Technology (Freiberg, Germany), following the descriptions of Hauser and Renfrow (1939). The exact procedure followed and analysis of the synthesized product can be found in Marion *et al.* (2017). Florrea 7510 (a commercial hydroxamic acid collector used for ore flotation) and F150 (a polypropylene glycol-based frother) were obtained from Flottec (USA). Hydrochloric acid and sodium hydroxide, used for pH modification in both zeta potential and flotation experiments, were purchased from Fisher Scientific. All reagents were used as provided.

Table B.26 – Mineral samples used in this study

Mineral	Origin	Purchased From or Supplied By
Bastnäsite 1	Gakara Mine, Burundi	African Rare Earths (Pty.) Ltd. (South Africa)
Bastnäsite 2	Madagascar	Gregory, Bottley and Lloyd (UK)
Monazite	Yard Mine, USA	Mineralogical Research Company (USA)
Allanite	Nevada, USA	Gregory, Bottley and Lloyd (UK)
Parisite	Blackbird Mine, USA	Khyber Minerals Co (USA)
Fergusonite	Gole Quarry, Canada	David K Joyce Minerals (Canada)
$YNbO_4$	Synthetic $YNbO_4$	-
Columbite (Fe)	Mahaiza, Madagascar	Khyber Minerals Co (USA)
Zircon	Malawi	Excaibur Mineral Corp (USA)

Table B.27 – Particle size of mineral samples used for surface chemistry investigations

Mineral	Particle Size (μm)		BET Surface Area (m^2 g^{-1})
	d_{50}	d_{80}	
Bastnäsite 1	2.0	3.6	14.35
Bastnäsite 2	1.8	3.3	11.36
Monazite	1.9	3.4	9.52
Allanite	3.2	7.1	3.84
Parisite	6.6	10.4	0.26
Fergusonite	6.8	10.2	0.66
$YNbO_4$	5.2	10.0	86.83
Columbite (Fe)	2.0	3.8	0.51
Zircon	2.0	3.5	3.40

B.4.2.2 Zeta Potential Measurements

Zeta potential measurements were conducted using a NanoBrook ZetaPlus electrophoretic analyser (Brookhaven Instruments, USA). Mineral samples were suspended in 200 mL of 10^{-3} M KCl solution at a concentration of 0.04 wt.%. The pH range investigated was from pH 3 to 10 (with measurements taken in steps of 1 pH unit), as measurements below pH 3 and above pH 10 were not possible due to the limitations of the analyser. Samples were conditioned for 30 min after collector addition (at a concentration of 40 mg/L) and for 5 min at each pH prior to taking a measurement. Fresh samples were prepared for acidic and basic zeta potential measurements to avoid zeta potential hysteresis. The electrophoretic zeta potential data is presented as a fitted trendline (third order polynomial), with calculated confidence intervals about the trendline.

B.4.2.3 Microflotation

Prior to microflotation, one gram of mineral sample was placed in a beaker and conditioned for 1 min in 15 mL collector solution adjusted to pH 9. Due to the minimal mass available for many of the REM investigated the entire pH range could not be tested. As most REM have been shown to respond most favourably to hydroxamates at pH 9, this was chosen as the pH for testing. During conditioning 1 drop of 10 g/L F150 (Flottec, USA) frother solution was added to the suspension. The collector concentrations used were determined by first floating Bastnäsite 1 over a range of concentrations until a relatively high recovery was achieved. This concentration, determined to be 15 kg/t for BHA and

600 g/t for POH, was then used for all other minerals investigated. After conditioning, the suspension was transferred to a modified Hallimond tube and filled to a volume of approximately 170 mL, with pH adjusted deionized water. Air was then introduced to the cell at a rate of 36 mL/min and flotation was conducted for 1 min. The floated and non-floated material were dried and weighed to calculate recovery. Microflotation testwork was not performed on the synthetic fergusonite sample due to only having a limited amount of mineral sample at a very fine particle size (Table B.27).

B.4.2.3 Ore Flotation

Flotation experiments on the Nechalacho gravity tailings were carried out in a 3 L Denver flotation cell operated at 1200 rpm with an air flow rate of 5.5 L/min. A fresh batch of ore (500 g) was added to the flotation cell where the pulp level was adjusted to a set height by adding tap water. The collector (6 kg/t) was added to the slurry and conditioned for 1 min prior to turning the air on. Froth was then collected for 2 min. After 2 min, the air was turned off and 4 kg/t of collector was added and conditioned for 1 min. The air was then turned back on and the froth was collected for another 2 min, before a final reconditioning step (4 kg/t collector addition conditioned for 1 min). Following this reconditioning step, the froth was collected for 6 min. Throughout each flotation test the cell level and pH were continuously adjusted to ensure consistent conditions. Flotation tests were performed in triplicate and reproducibility was ensured through mass pulls. Concentrates from each test were then combined and analysed using inductively coupled plasma mass spectrometry (ICP-MS). To digest the samples, a homogenous melt was formed by mixing 0.1 g of sample with sodium peroxide which was then heated. The melt was then digested in hydrochloric acid. All digestions and ICP-MS analysis in this work were conducted by SGS Canada (Lakefield, Canada).

B.4.3 Results and Discussion

B.4.3.1 Zeta Potential Measurements

B.4.3.1.1 Bastnäsite

The zeta potential results of the two bastnäsite samples in the absence and presence of BHA and POH are shown in Figures B.25 and B.26. The results indicate an IEP at pH 6.4 and 6.8 for Bastnäsite 1 and Bastnäsite 2, respectively. This corresponds well to IEP values reported in literature, which as discussed earlier (Section B.4.1) generally range between pH 6 and 8. The similarities in zeta potential trends of the two mineral samples re-iterates that mineral origin plays a much less significant role in the observed IEP variations than differences in the procedure followed or the measurement technique which is used.

The zeta potential of the two bastnäsite samples in the presence of BHA indicates adsorption, particularly from pH 4 – 10 for Bastnäsite 1 and from pH 6 – 9 for Bastnäsite 2. These results correspond well to the findings of Jordens *et al.* (2014b), who found a similar positive shift in the zeta potential of bastnäsite when in the presence of BHA. Adsorption to the bastnäsite surface can also be suggested for POH, which resulted in a similar positive shift in zeta potential from pH 6 – 10 and pH 8 – 10 for Bastnäsite 1 and Bastnäsite 2, respectively. The results for Bastnäsite 2 in the presence of POH may be indicative of electrical double layer compression (no change in IEP with a positive zeta potential shift at pH > IEP and a negative shift at pH < IEP). However, there is a great deal of work demonstrating this collector's interaction with the surface of bastnäsite (Section B.4.1), therefore, the resultant changes are assumed to be from collector adsorption. Although both collectors have been reported to show a negative shift in zeta potential (Espiritu *et al.*, 2018b; Pavez *et al.*, 1996), both this work and the work of Jordens *et al.* (2014b) used long conditioning times (30 min), allowing for a greater degree of mineral dissolution. The resultant dissolved species are likely playing a role in the positive shift in the zeta potential of bastnäsite while in the presence of the hydroxamate collectors. Jordens et al. (2014c) suggested a possible mechanism is the adsorption of positively charged REE-hydroxamate complexes, produced from the reaction of the hydroxamic acid molecule and hydrolysed REE cations in the bulk solution, to the surface of bastnäsite (Jordens *et al.*, 2014b). It is noted that the results suggest the interaction of BHA and POH with Bastnäsite 2 may be less than that of Bastnäsite 1 (less significant changes in zeta potential), which may result in different flotation responses.

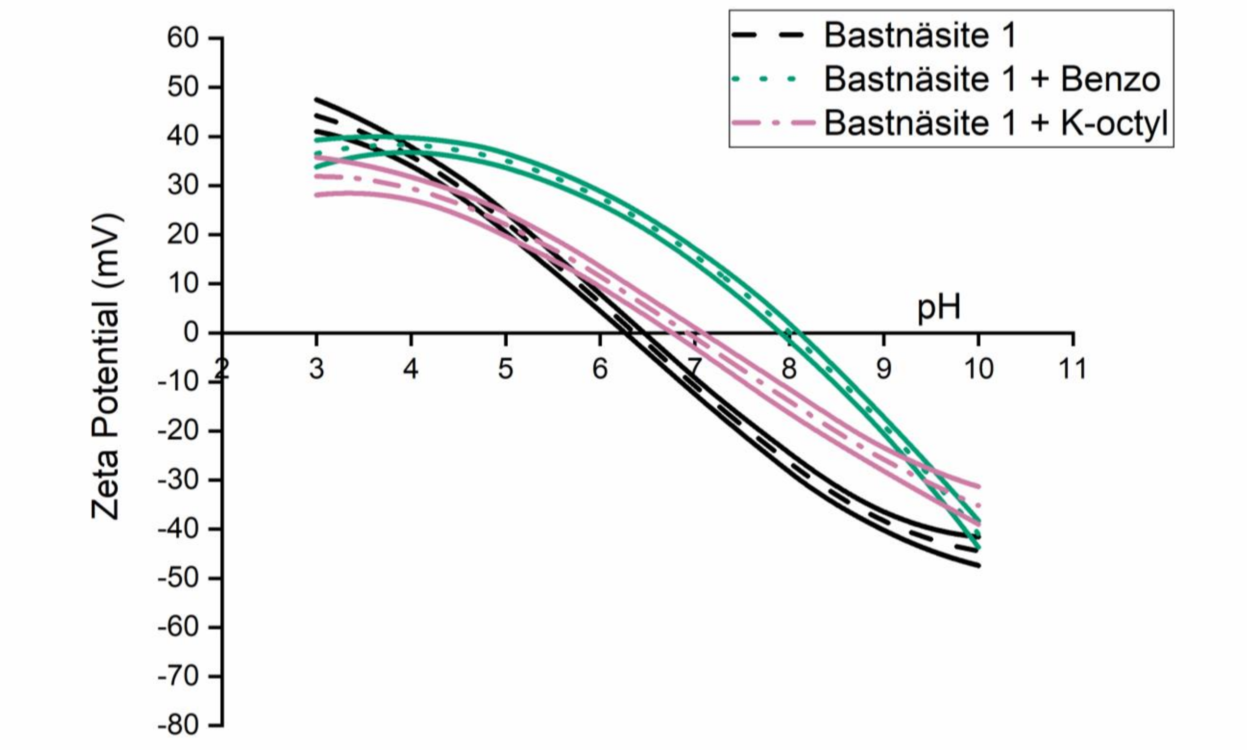

Figure B.25 – Zeta potential trend of Bastnäsite 1 in the presence and absence of benzohydroxamic acid and k-octyl hydroxamate at a concentration of 40 mg/L (Error intervals shown are 99 % confidence intervals)

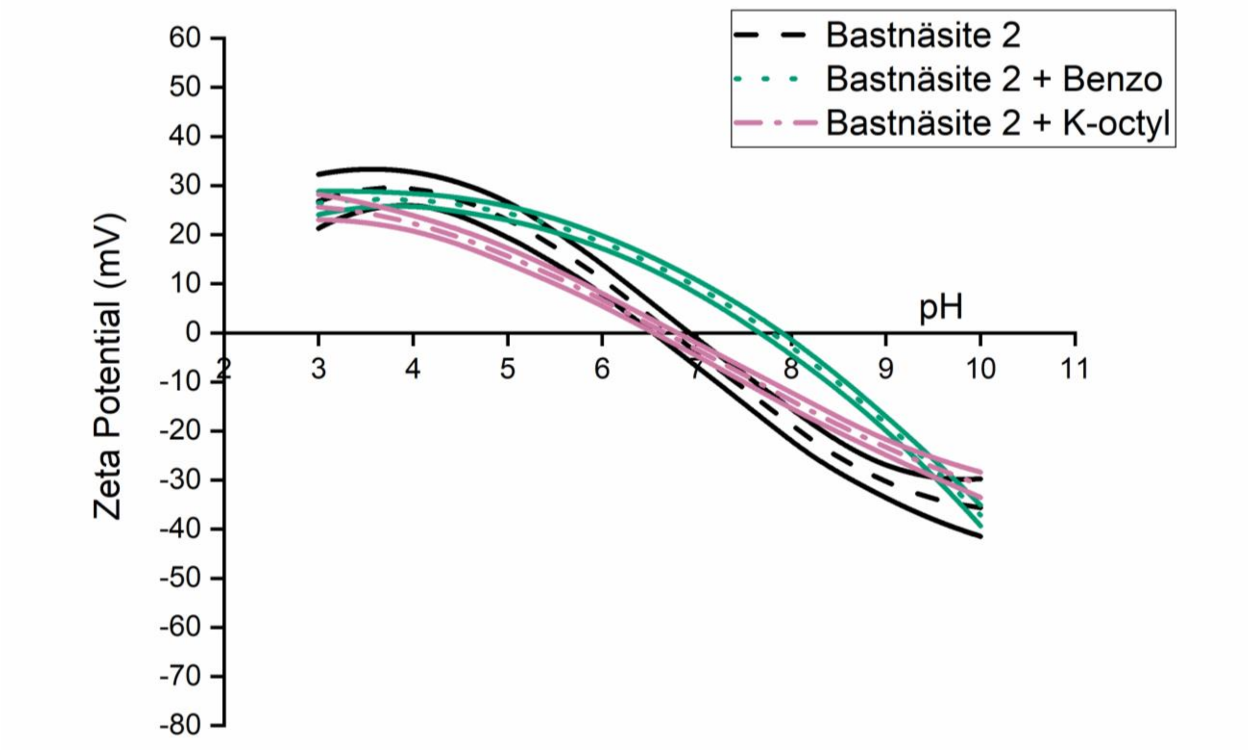

Figure B.26 – Zeta potential trend of Bastnäsite 2 in the presence and absence of benzohydroxamic acid and k-octyl hydroxamate at a concentration of 40 mg/L (Error intervals shown are 99 % confidence intervals)

B.4.3.1.2 Monazite

The zeta potential results of monazite in the absence and presence of BHA and POH is shown in Figure B.27. The results indicate an IEP at pH 5.1. This corresponds well to IEP values reported in literature, which as discussed earlier (Section B.4.1) generally range between pH 5 and 6. The results in the presence of BHA and POH indicate adsorption across the entire pH range investigated. Although these reagents have been previously shown to provide a negative shift in zeta potential following adsorption to the monazite surface (Espiritu *et al.*, 2018b; Pavez *et al.*, 1996), much like the results for bastnäsite, a positive shift in zeta potential is observed from pH 3 – 10 and pH 6 – 10 for BHA and POH, respectively. Although monazite is less soluble than bastnäsite, a similar explanation as was provided for bastnäsite (Section B.4.3.1.1) may explain the positive shift occurring after the addition of the anionic collectors.

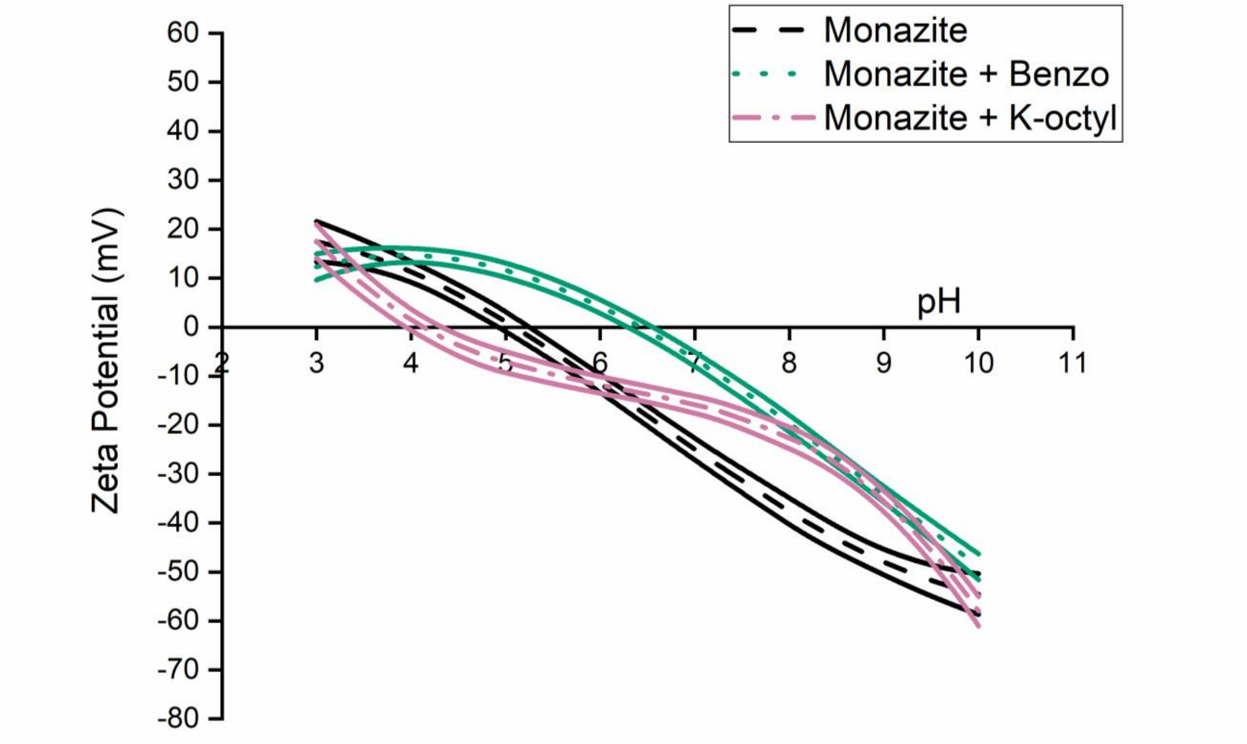

Figure B.27 – Zeta potential trend of monazite in the presence and absence of benzohydroxamic acid and k-octyl hydroxamate at a concentration of 40 mg/L (Error intervals shown are 99 % confidence intervals)

B.4.3.1.3 Allanite

The zeta potential results of allanite in the absence and presence of BHA and POH is shown in Figure B.28. The results indicate an IEP at pH 3.5, which corresponds well to value reported by Jordens *et al.* (2014a) (pH 4.0). The results in the presence of BHA also correspond well to the finding of Jordens *et al.* (2014a); indicating the collector does not adsorb to the mineral surface. The results for POH, however, suggest adsorption across the entire pH investigated. This may indicate that while the aromatic hydroxamate collector BHA is incapable of rendering the allanite surface hydrophobic (Jordens *et al.*, 2014a), using a less selective alkyl hydroxamate such as POH allanite may be recovered by flotation. The upward shift in zeta potential with the addition of the anionic POH collector is again noted. While the explanation provided for bastnäsite is possible here, the limited solubility of allanite may suggest a different mechanism.

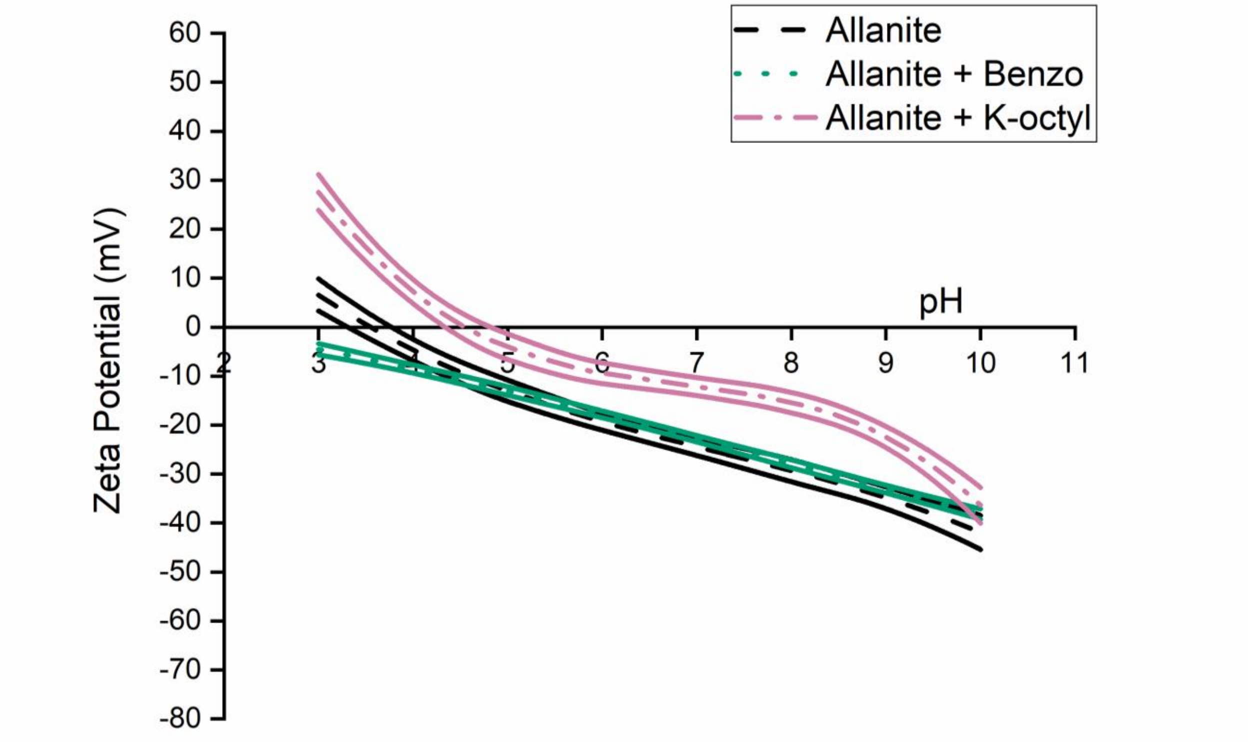

Figure B.28 – Zeta potential trend of allanite in the presence and absence of benzohydroxamic acid and k-octyl hydroxamate at a concentration of 40 mg/L (Error intervals shown are 99 % confidence intervals)

B.4.3.1.4 Parisite

The zeta potential results of parisite in the absence and presence of BHA and POH is shown in Figure B.29. The results indicate an IEP at pH 7.2, which higher than the value reported by (Owens *et al.*, 2018) of pH 5.3. Much like is observed for bastnäsite in literature, the difference is likely due to procedural differences. The measured IEP of parisite does correspond well to those measured for the bastnäsite samples tested (pH 6.4 and 6.8); which is expected due to the limited differences between the two minerals. However, it is interesting to note that while the zeta potential trends in the presence of BHA and POH suggest collector adsorption from pH 3 – 9 and pH 3 – 10, respectively, they result in a negative shift in the zeta potential. As both reagents resulted in a positive shift in the zeta potential of bastnäsite, this may suggest that the differences in crystal structure between bastnäsite and parasite may play a role in the exact mechanism of collector adsorption.

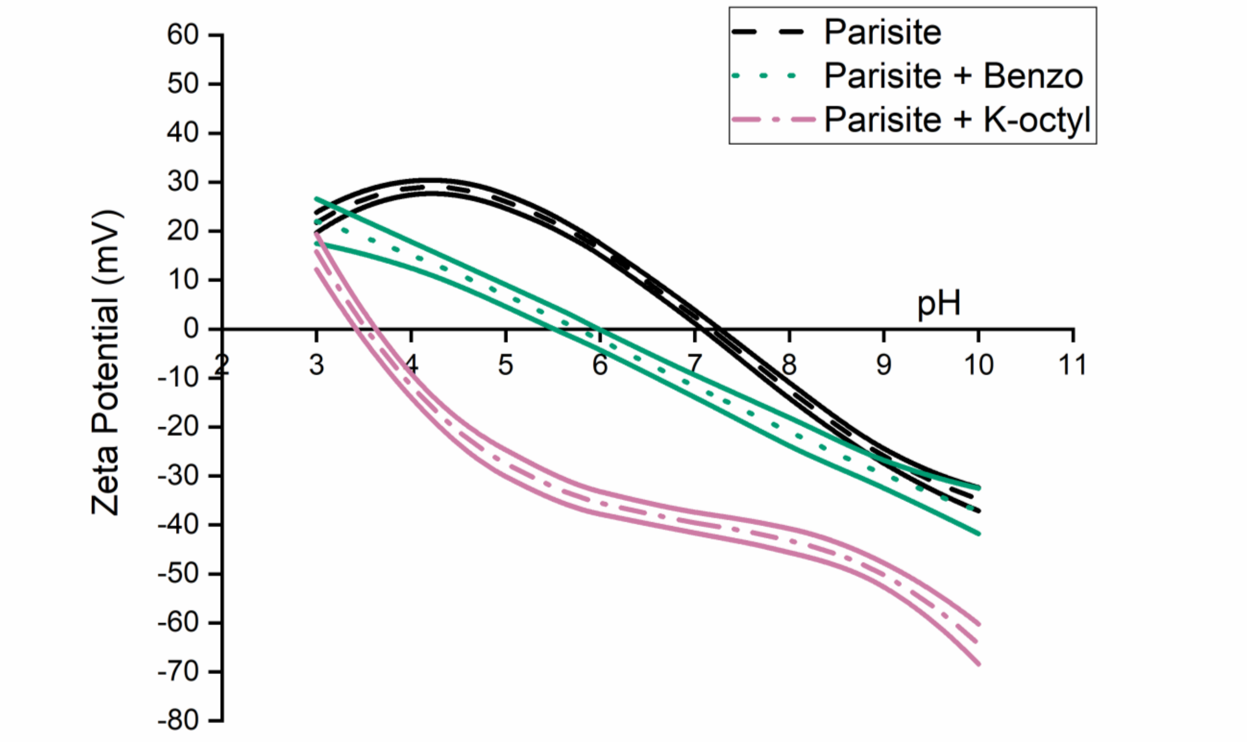

Figure B.29 – Zeta potential trend of parisite in the presence and absence of benzohydroxamic acid and k-octyl hydroxamate at a concentration of 40 mg/L (Error intervals shown are 99 % confidence intervals)

B.4.3.1.5 Fergusonite

The zeta potential results of the natural fergusonite and synthetic $YNbO_4$ in the absence and presence of BHA and POH is shown in Figure B.30 and Figure B.31, respectively. The results indicate an IEP < pH 3 for the natural sample and an IEP at pH 6.9 for the synthetic $YNbO_4$ sample. The IEP of the natural sample corresponds well to the value reported by Fawzy (2018) (IEP at pH 2.7); whereas, the IEP of the synthetic $YNbO_4$ corresponds well with the value reported by Malas *et al.* (2013) (IEP at pH 6.3). It is interesting to note that the source of the natural fergusonite sample is the same as the sample used by Malas *et al.* (2013), and a similar procedure was followed in this study. However, the fergusonite sample tested by Malas *et al.* (2013) remained embedded in a matrix of magnesium and aluminum silicate, whereas the sample used here was of high purity (Figure B.9 and B.12), which likely explains the differences in IEP. The observed differences in the IEP for synthetic $YNbO_4$ versus natural fergusonite should be noted. The synthesis of $YNbO_4$ uses reagent grade materials providing clean mineral surfaces, whereas the surface properties of the natural sample are likely affected by contamination of other minerals and lattice damage caused by radiation due to the presence of uranium and thorium. Therefore, surface chemical studies on a synthetic sample may not represent a real-world situation, which should be acknowledged by any researchers performing such studies on synthetic specimens.

Examining both the natural fergusonite and the synthetic $YNbO_4$ sample in the presence of BHA and POH suggests adsorption. The natural sample indicates a negative shift in the zeta potential from pH 7 – 10 in the presence of BHA and from pH 5 – 9 in the presence of POH. The presence of the two collectors result in very similar zeta potential trends for the synthetic sample causing a positive shift from pH 6 – 10. Although adsorption is suggested in all cases, these results suggest that the difference in structure of the two samples may impact the exact mechanism of collector adsorption.

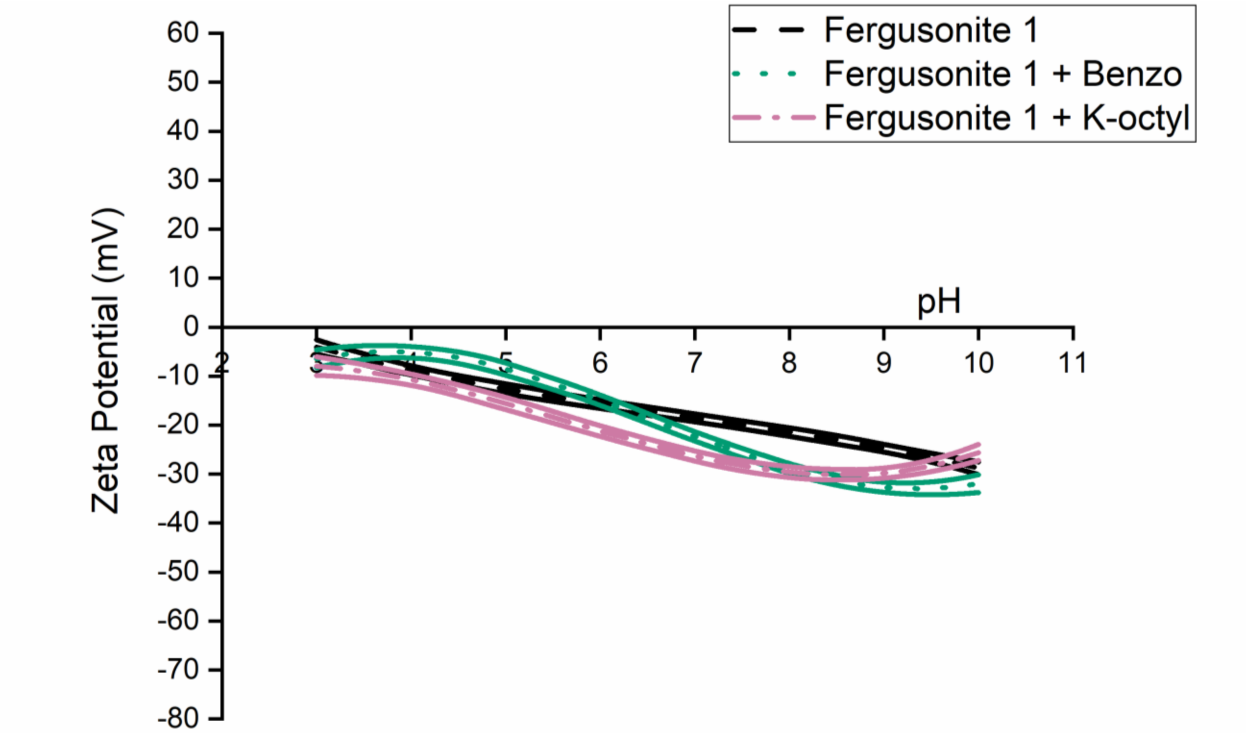

Figure B.30 – Zeta potential trend of natural fergusonite in the presence and absence of benzohydroxamic acid and k-octyl hydroxamate at a concentration of 40 mg/L (Error intervals shown are 99 % confidence intervals)

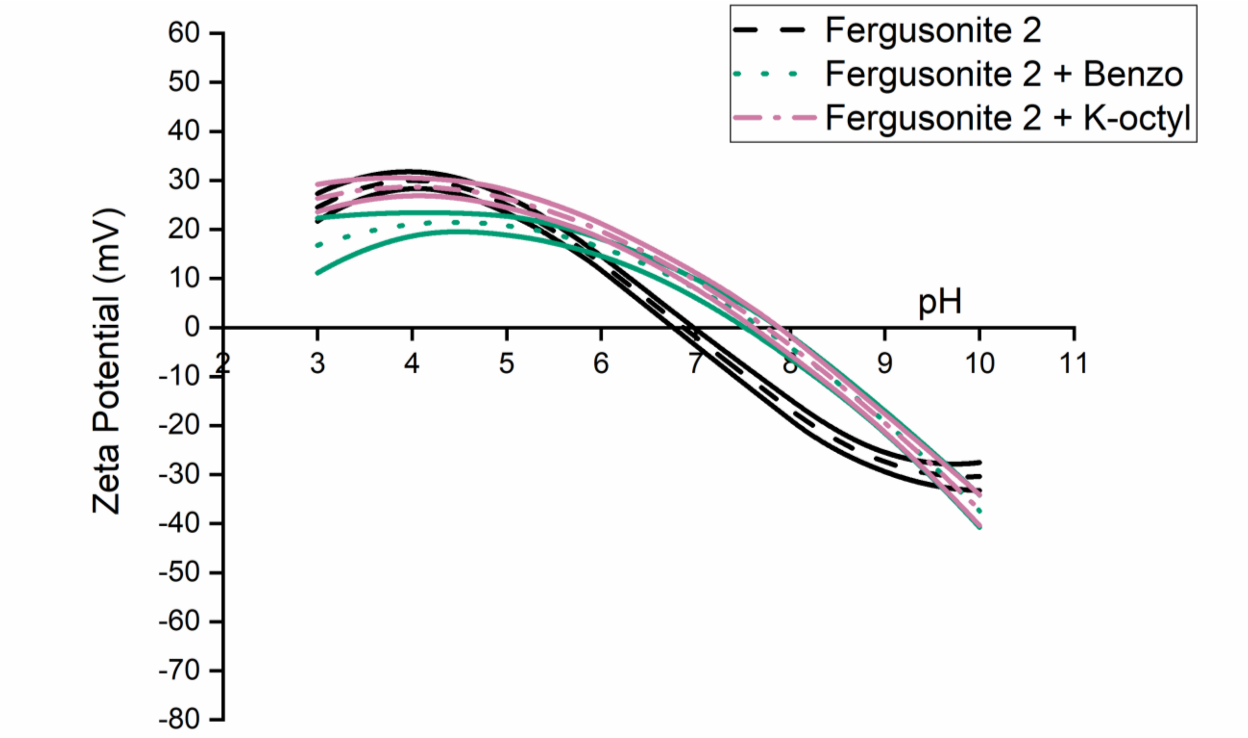

Figure B.31 – Zeta potential trend of synthetic fergusonite ($YNbO_4$) in the presence and absence of benzohydroxamic acid and k-octyl hydroxamate at a concentration of 40 mg/L (Error intervals shown are 99 % confidence intervals)

B.4.3.1.6 Columbite

The zeta potential results of columbite in the absence and presence of BHA and POH is shown in Figure B.32. The results indicate an IEP < pH 3, which is lower than the values reported by Harada *et al.* (1993) (pH 4.0 and 4.5). The observed differences in zeta potential caused by the presence of BHA are minimal and therefore inconclusive. The presence of POH causes more significant changes to the zeta potential of columbite, particularly from pH 4 – 8, which indicates adsorption. However, the much like BHA, the difference in zeta potential from pH 8 – 10 are minimal and may therefore suggest no adsorption within this pH range. This may suggest a different pH for optimal flotation conditions than those observed with other minerals, which generally occurs at pH 9.

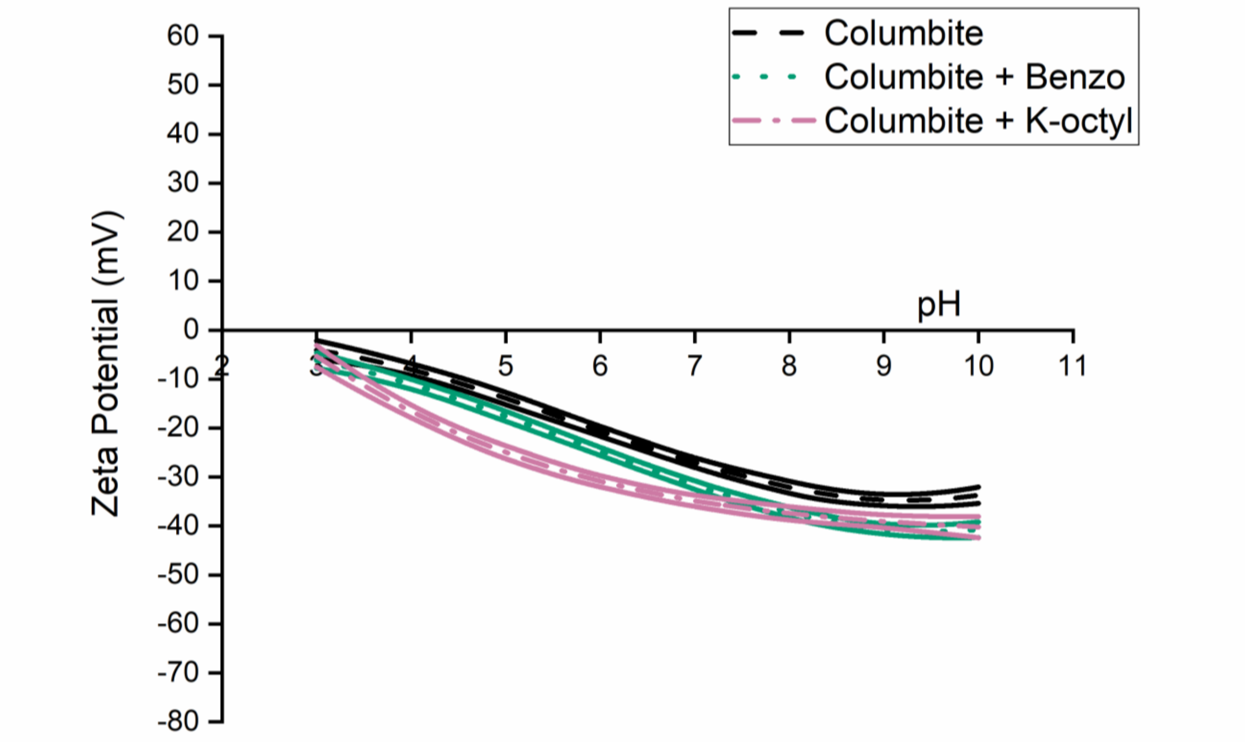

Figure B.32 – Zeta potential trend of columbite in the presence and absence of benzohydroxamic acid and k-octyl hydroxamate at a concentration of 40 mg/L (Error intervals shown are 99 % confidence intervals)

B.4.3.1.7 Zircon

The zeta potential results of zircon in the absence and presence of BHA and POH is shown in Figure B.33. The results indicate an IEP at pH 5.5, which falls within the range of 2.3 – 6.0 reported by other authors (Table B.4). Examining the zeta potential trends in the presence of the collectors suggests limited interaction of BHA and adsorption of POH across the entire pH range observed. This may suggests that successful flotation is possible using the alkyl hydroxamate, whereas it will not be successful when using the aromatic BHA collector.

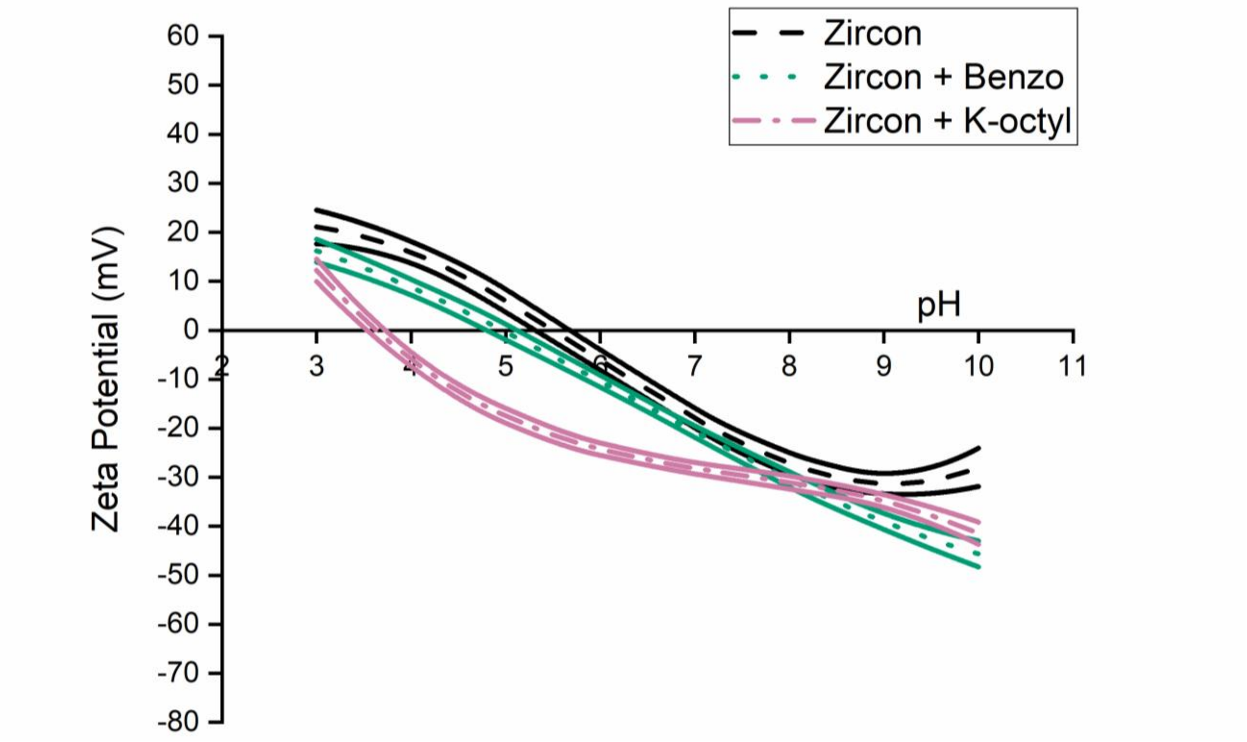

Figure B.33 – Zeta potential trend of zircon in the presence and absence of benzohydroxamic acid and k-octyl hydroxamate at a concentration of 40 mg/L (Error intervals shown are 99 % confidence intervals)

B.4.3.2 Microflotation

The results of microflotation using BHA (15 kg/t) and POH (600 g/t) at pH 9 are provided in Figures B.34 and B.35, respectively. The collector concentration for each reagent was determined by floating the Bastnäsite 1 sample with increasing dosage until a recovery of > 70 % was achieved. For BHA this dosage was determined to be 15 kg/t and for POH 600 g/t, which corresponds well to previous work that suggested much more elevated concentrations of the aromatic hydroxamic acid collector are required when compared to the C_8 alkyl hydroxamate (Hart *et al.*, 2014; Marion *et al.*, 2017). However, the BHA dosage of 15 kg/t is much greater than the 2 kg/t dosage used by Jordens *et al.* (2014b) to obtain similar bastnäsite recoveries. The main difference between that study and this one is the flotation cell used (modified Hallimond tube versus modified Partridge-Smith cell), the source of the bastnäsite samples (Gakara Mine, Burundi versus Mountain Pass, USA) and the frother concentration (1 drop 10 g/L F150 added to 170 mL suspension versus 2 drop 20 g/L F150 added to 50 mL suspension). Based on the work of Jordens *et al.* (2014b), who tested MIBC (a relatively weak frother) and F150 (a relatively strong frother) and found that the collecting ability of hydroxamate could only be achieved when using the strong frother, it is likely that the reason for requiring much higher collector dosages is due to significantly lower frother concentrations are used here. While outside the scope of this study, these findings re-iterate those from Jordens *et al.* (2014b), demonstrating that frother selection and concentration play a critical role in bastnäsite flotation when using BHA and should be investigated as hydroxamate use becomes more prevalent.

Comparing the two bastnäsite samples demonstrates significantly different responses to both collectors, particularly with POH. While this does correspond to the suggested results from zeta potential measurements (Figures B.25 and B.26) which indicated greater interaction of both collectors with Bastnäsite 1 compared to Bastnäsite 2, the exact mechanism behind this remain unknown. One possibility may be that Bastnäsite 2 has much higher surface area (3.48 g/m^2) compared to the Bastnäsite 1 sample (0.18 g/m^2). This increased surface area is likely due to the high degree of micro-fracturing of the Bastnäsite 2 sample (Figure B.36), which is not present in for Bastnäsite 1 (Figure B.37). Collector may enter these fractures, and adsorb there, depleting collector available for surfaces able to contact air bubbles, thus reducing the flotation response. While this is one hypothesis, more work is required to determine the mechanism at play here.

Monazite responds well to both BHA and POH with average recoveries of 60 % and 68 %, respectively. These results correspond well to the zeta potential results (Figure B.27) which indicate adsorption for both collectors, as well as those of other authors (Table B.6) who have demonstrated that monazite can be recovered with both collectors. Flotation recoveries and rates (visually observed during microflotation test) were lower than those for Bastnäsite 1, which corresponds well to the findings of Jordens *et al.* (2016a) who found greater recoveries and recovery rates of bastnäsite than monazite while floating the Nechalacho ore using BHA.

The flotation results for allanite in the presence of BHA indicate limited floatability (< 20 %), corresponding well to zeta potential results (Figure B.28), which indicate limited collector interaction, and the work of Jordens *et al.* (2014a) who found little to no recovery when using this collector. The flotation of allanite with POH offers a completely different response, with an average recovery of 88 %. This corresponds well to the zeta potential results (Figure B.28) which indicate collector adsorption. These findings demonstrate the importance hydroxamate structure selection when trying to float different minerals. While BHA is not a collector which can be used alone for the recovery of allanite, POH seems to be a highly effective collector for its recovery.

As expected, parisite responds favorably to both collectors, recovering 88 % when using BHA and 99 % with POH. This corresponds well to the zeta potential results (Figure B.29), which indicate adsorption in both cases. These results suggest that the minerals of the polysomatic series of fluorocarbonate minerals, which consists of bastnäsite, parisite, röntgenite and synchysite, are all likely to respond similarly to hydroxamic acid-based collectors.

Fergusonite responds to both collectors; however, relative to the recovery of Bastnäsite 1, POH is much more effective. When using BHA recoveries are much lower than those observed when floating Bastnäsite 1 (46 % versus 74 %), whereas when using POH similar recoveries were obtained (84 % vs 79 %). The lower recoveries when using BHA do not correspond to the findings of Jordens *et al.* (2016a), who found fully liberated fergusonite had a greater flotation response compared to fully liberated bastnäsite when floating the Nechalacho ore. This may suggest that the nature of the fergusonite sample plays a role in flotation or perhaps in the case of the Nechalacho ore fergusonite is being inadvertently activated causing it to float more readily.

Columbite flotation using BHA and POH is poor. To the authors knowledge, there is no published work demonstrating the response of this mineral to hydroxamates; however, these results suggest that they are not effective. This again contradicts the findings of Jordens *et al.* (2016a), who was able to recover this mineral to a high degree while floating the Nechalacho ore with BHA. Much like fergusonite, this may suggest that the two niobate minerals are easily activated or that differences between the minerals' chemistry and crystal structure from different locations may result in differences in a flotation response.

The last mineral which was tested is zircon. This mineral does not respond to either collector, with an average recovery below 10 % in both cases. These findings suggest that REM deposits such as the Nechalacho, which contain zircon as a valuable mineral may have to utilize different flotation reagents or different beneficiation techniques if it is to be recovered. It should be noted that the zircon sample used here contains approximately 0.1 % REE (measured by ICP-MS) and perhaps more REE rich zircon would respond more favorably. For example, Jordens *et al.* (2016a) found zircon could be recovered (~60 % recovery) using BHA to float the Nechalacho ore. The observed recovery could be due to elevated REE content in zircon present in the ore, or inadvertent activation from dissolved species present during ore flotation.

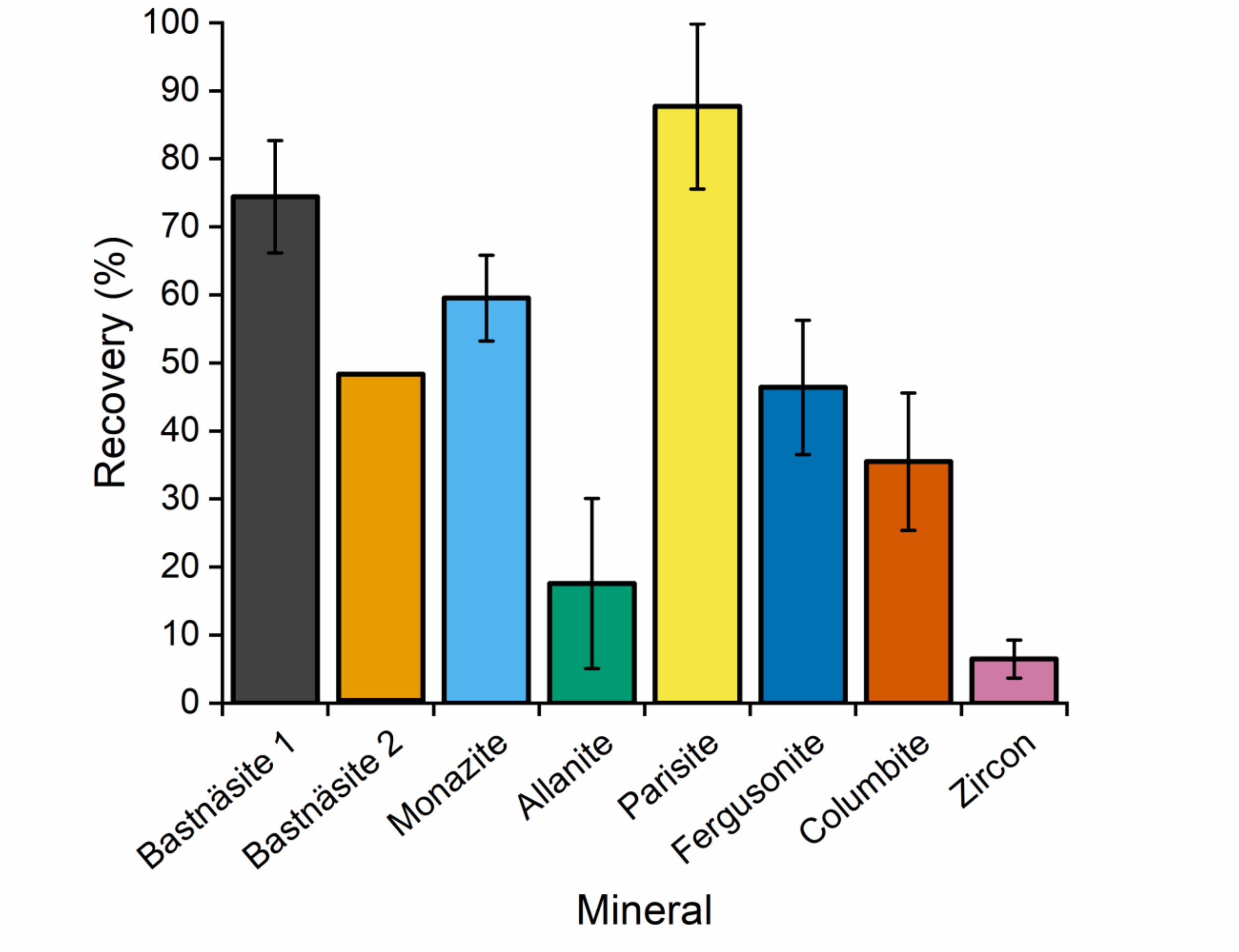

Figure B.34 – Microflotation results using benzohydroxamic acid at a concentration of 15 kg/t at pH 9 (Error intervals shown are 95 % confidence intervals)

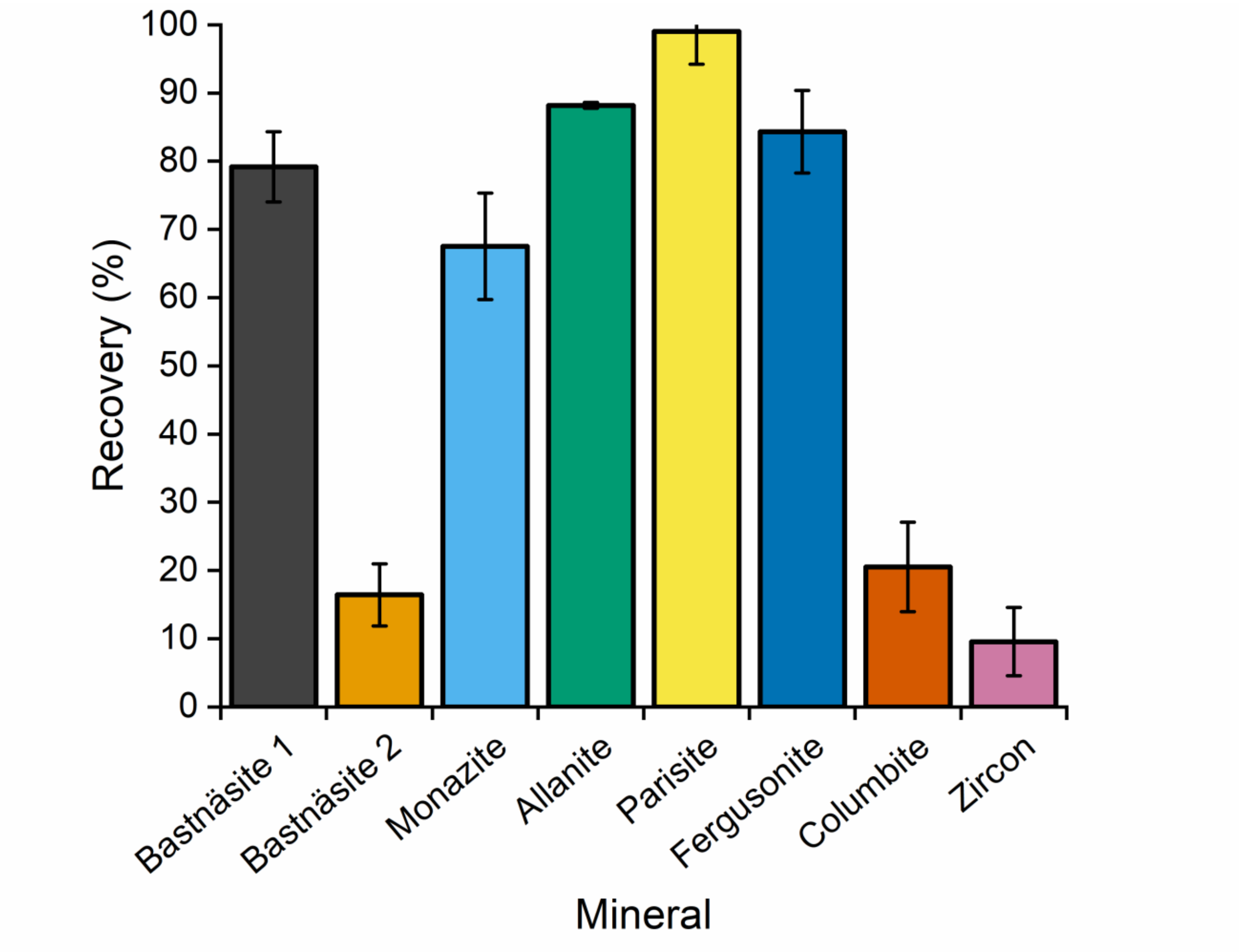

Figure B.35 – Microflotation results using benzohydroxamic acid at a concentration of 15 kg/t at pH 9 (Error intervals shown are 95 % confidence intervals)

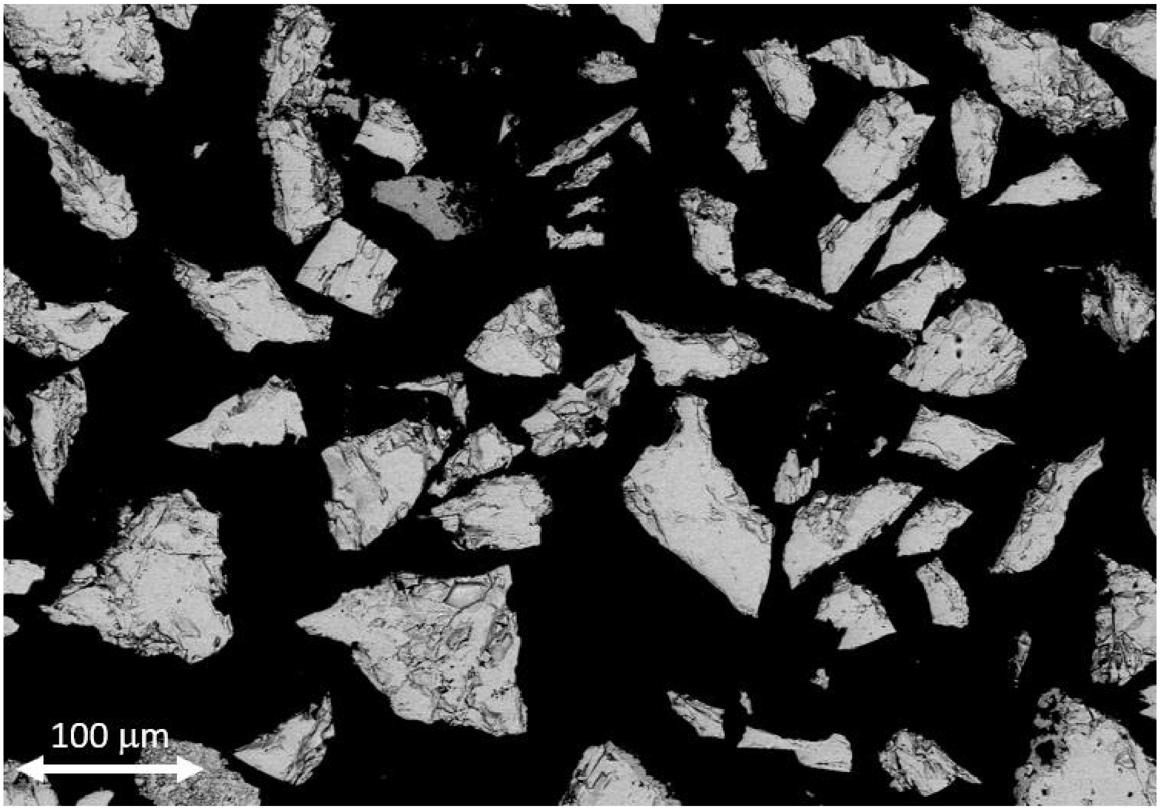

Figure B.36 – BSE image of Bastnäsite 2 sample indicating particles with a high degree of micro-fracturing

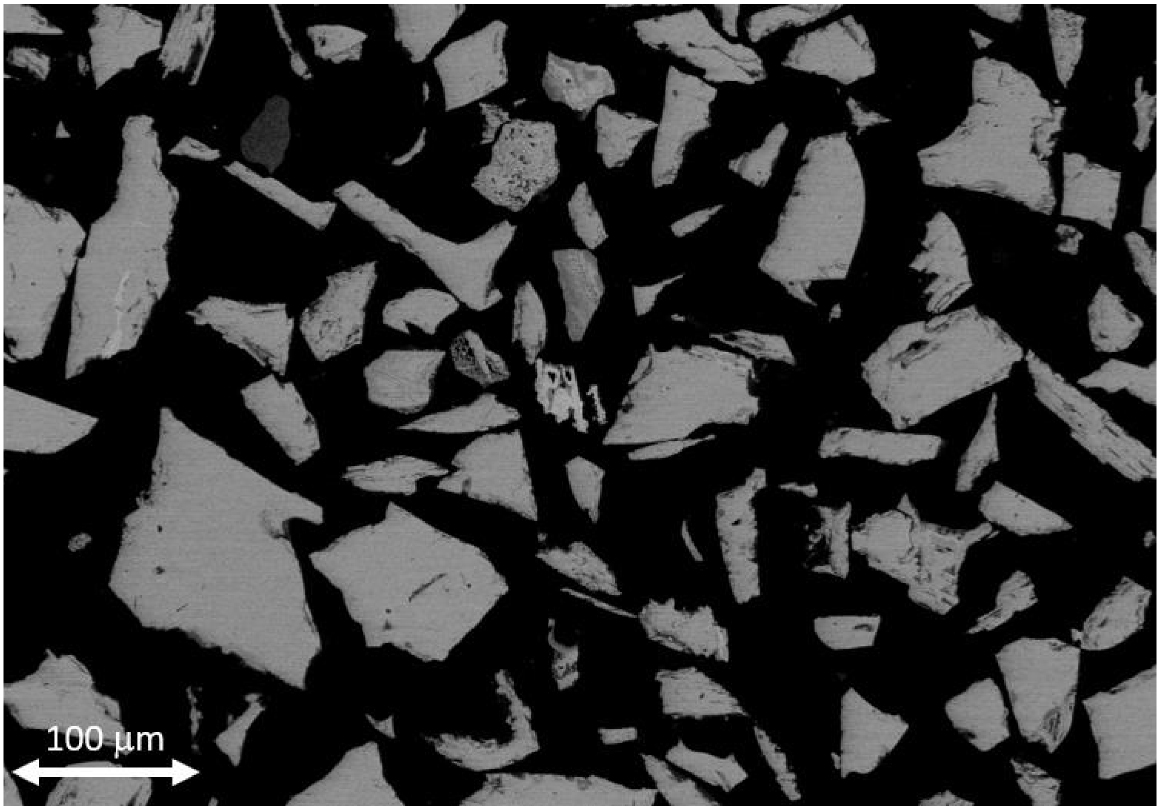

Figure B.37 – BSE image of Bastnäsite 1 sample indicating limited micro-fracturing when compared to Bastnäsite 2 (Figure B.36)

B.4.3.3 Ore Flotation

Following zeta potential and microflotaion experiments, a Nechalacho feed sample was subjected to bench scale flotation using an industrial aromatic hydroxamic acid collector (Florrea 7510). The results of this are provided in Figure B.38. Following 10 min of flotation LREE, HREE and zirconium recoveries were 77 %, 52 % and 40 % respectively, with a mass pull of 27 %. The cumulative grades of LREE, HREE and zirconium in the flotation products were 4.4 %, 0.4 % and 5.1 %, respectively; representing upgrade ratios of 2.8, 1.9 and 1.6. The product with the highest LREE grade was the first concentrate which had a grade of 7.2 % (upgrade ratio of 4.7) recovering 21 % of LREEs. The third concentrate had the highest HREE and zirconium grades, 0.43 % (upgrade ratio of 2.0) and 5.8 % (upgrade ratio of 1.7) respectively. It is expected that the results for HREE and zirconium correspond with one another as the majority of HREE present in the ore are in zircon.

These findings correspond well to those of zeta potential and microflotation experiments. In the Nechalacho deposit LREE are primarily present in the minerals bastnäsite, synchysite, allanite and monazite. With the exception of allanite, all the LREE-bearing minerals were shown to float quite readily when using either hydroxamate collector; which is represented here with high recoveries and significant upgrading. It is interesting to compare these flotation results to those of Jordens *et al.* (2016a), who floated the concentrate produced from the gravity test work (Jordens *et al.*, 2016b) of which the tailings became the feed for this work. Using BHA (addition of 5 kg/t followed by an additional 5 kg/t after 5 min of flotation), Jordens *et al.* (2016a) produced LREE grades slightly greater than 7 % after 0.5 min, approximately 6 % after 5 min of flotation, and 4.5 % following a second addition of collector and a total of 12 min. The respective cumulative recoveries at each of these points were approximately 25 %, 45 % and 75 %. These values correspond very well to the three flotation concentrates produced here. The feed used here is of much lower LREE grade (1.5 % versus 3.7 %) and the particle size was much finer (d_{80} = 8 μm versus 50 μm), suggesting that, for this deposit, LREE can be successfully processed by flotation using hydroxamate collectors regardless of feed grade or particle size.

In microflotation experiments, zircon did not respond well to either collector. However, zeta potential results did indicate POH adsorption, suggesting hydroxamic acid-based collectors can interact with zircon. This is evident by the results of bench scale flotation. After two stages of flotation (where 10 kg/t of collector had been added) zirconium recovery (13 %) remained low with minimal upgrading (1.2 times). However, after a third addition of collector (4 kg/t) and an additional 6 min of flotation 26 % of the zirconium was recovered with improved upgrading (1.7 times). While these results are not as significant as those observed for LREE, they do suggest that prolonged flotation times and elevated collector dosages are beneficial to zircon recovery; which is a shared observation of Jordens *et al.* (2016a).

From Figure B.38 (a) it can be observed that either HREE rich zircon is preferentially being recovered over zircon particles which contain no or lower proportions of REE, or there does exist some HREE recovery which is not associated with zircon. Microflotation results do suggest that fergusonite recovery is expected. The same results suggest columbite flotation to be low, however, results detailed in Jordens *et al.* (2016a) do suggest that both fergusonite and columbite are readily recovered using BHA. Therefore, in this case the elevated HREE recovery (52 %) compared to that of zirconium (40 %) is most likely due to the recovery of fergusonite and columbite.

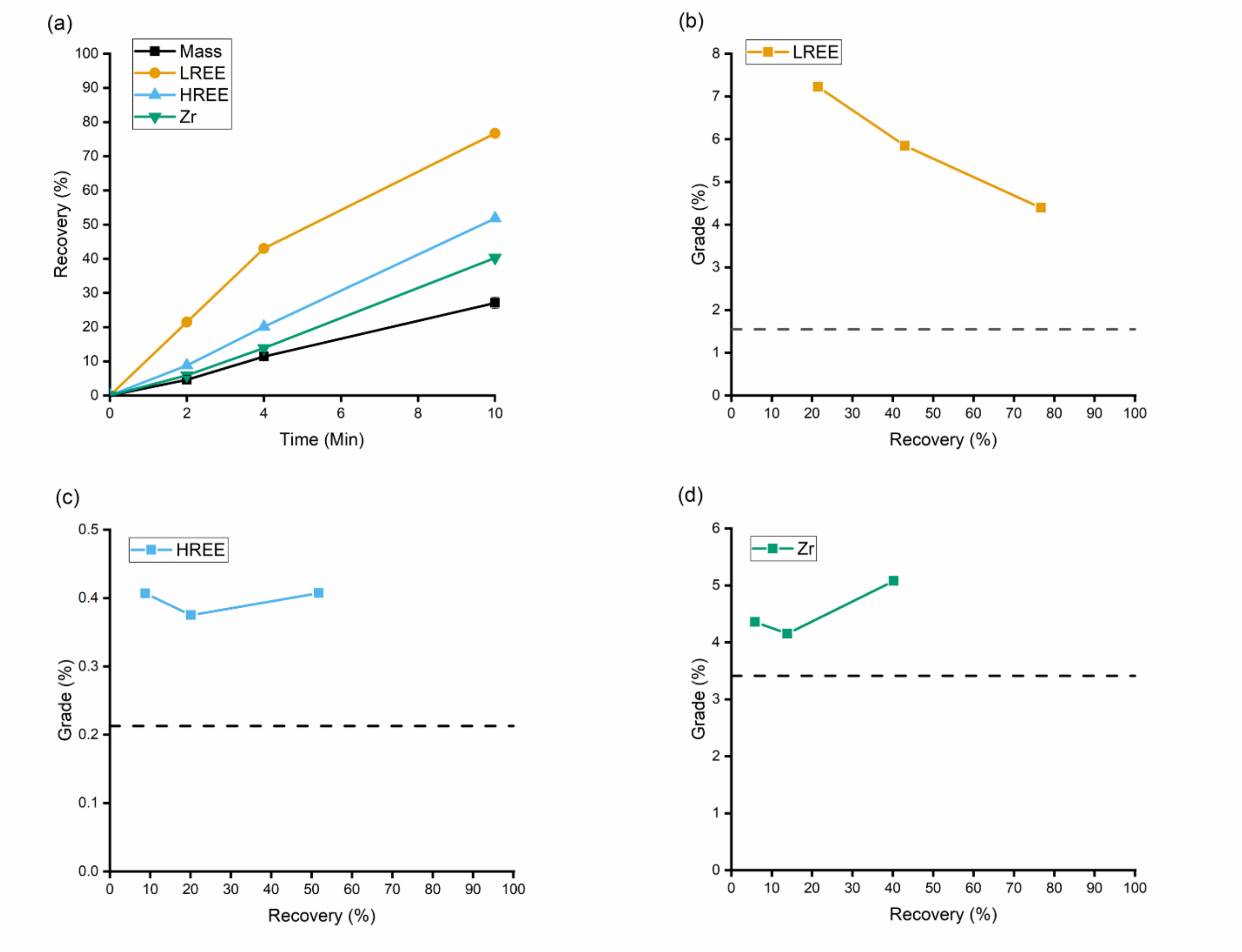

Figure B.38 – Results of Nechalacho ore flotation using Florrea 7510 as collector: (a) Recovery versus time of mass, LREE, HREE and zirconium; and grade versus recovery of (b) LREE, (c) HREE, and (d) zirconium. The dashed line represents the feed grade.

As the average particle of this feed sample is very fine (d_{50} = 8 µm), it is expected that there would be some degree of recovery due to unselective entrainment. To evaluate this, the cumulative water recovery after each flotation stage is shown in Figure B.39. Multiple authors have clearly established the correlation between non-selective fine particle entrainment and water recovery (Johnson *et al.*, 1974; Laplante *et al.*, 1989; Trahar, 1981). Trahar (1981) found that the recovery of quartz with an average particle size of 9 µm (which is similar to the average particle size of the flotation feed) was approximetely 59 % of that of the water. Using this correlation, the recovery of material via entrainment was estimated and plotted along with the water recovery and mass recovery in Figure B.39. The total estimated recovery from entrainment is 22 %, compared to a overall mass pull of 27 %. This suggests that the majority of the mass is recovered via non-selective entrainment and the recovery of valuable minerals, particularily LREM, through true flotation is highly selective. Significant improvements could potentially be realized by limiting the recovery through entrainment, which could possibly be achieved through optimized hydrodynamic conditions, the use of wash water and/or using other flotation technologies which may be better suited for fine particle flotation, such as a jameson cell.

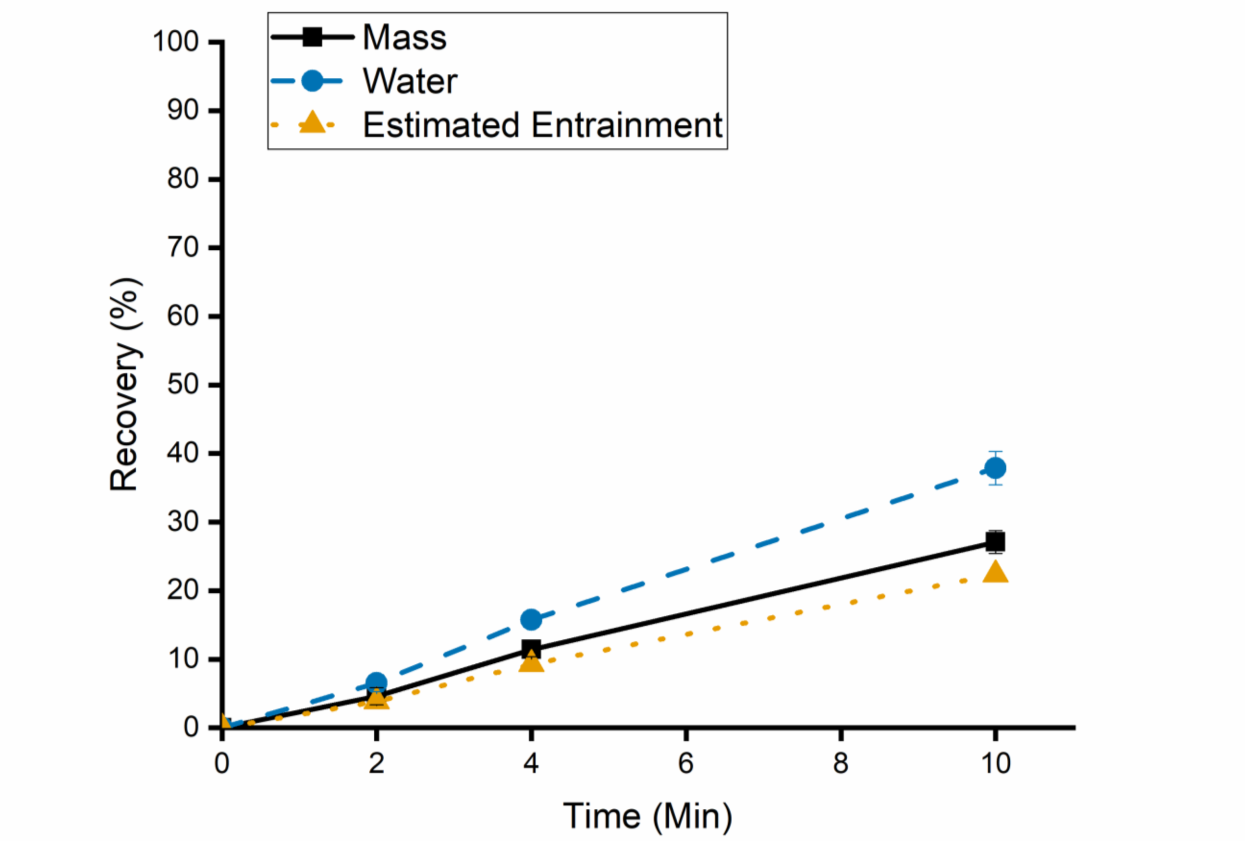

Figure B.39– Recovery of mass, water and estimated entrainment. Error bars represent 95 % confidence intervals

B.4.4 Conclusions

This work investigated the flotation of various REM using hydroxamic acid collectors. The investigation included zeta-potential measurements and microflotation experiments to understand the interaction of two different hydroxamate collectors (BHA and POH) with each REM. These results were then related to the bench scale flotation of the Nechalacho ore using an industrial hydroxamate (Florrea 7510). The conclusions are as follows:

1. The iso-electric points were determined for bastnäsite (Burundi) (6.4), bastnäsite (Madagascar) (6.8), monazite (5.1), allanite (3.5), parisite (7.2), fergusonite (< 3), synthetic $YNbO_4$ (6.9), columbite (< 3) and zircon (5.5).
2. Zeta potential measurements indicate the adsorption of BHA to the surface of bastnäsite (Burundi), bastnäsite (Madagascar), monazite, parisite, fergusonite and synthetic $YNbO_4$.
3. Zeta potential measurements indicate the adsorption of POH to all nine minerals investigated.
4. Microflotation results suggested significantly higher concentrations of BHA compared to POH are required for successful flotation; and frother selection and concentration may play a significant role.
5. Greater than 50 % mineral recoveries using 15 kg/t BHA for microflotation experiments were only observed for bastnäsite (Burundi), monazite and parisite.
6. Greater than 50 % mineral recoveries using 600 g/t POH for microflotation experiments were observed for bastnäsite (Burundi), monazite, parisite, allanite and fergusonite.
7. Bench scale flotation tests on the Nechalacho ore using Florrea 7510 was successful at concentrating LREE-bearing minerals and to a lesser extend zircon and other HREE-bearing minerals. After three stages of flotation 77 % of LREE were recovered and upgraded 2.8 times, 52 % of HREE were recovered and upgraded 1.9 times and 40 % of the zirconium was recovered and upgraded 1.6 times.
8. The best products in terms of grade for LREE was following the first stage of flotation where they were upgraded 4.7 times (recovery of 21 %). Zircon was much slower floating and was mostly recovered following the third flotation stage, where 67.5 % of the zirconium recovered reported with a grade of 5.8 % (upgrade ratio of 1.7)

B.5 References

Abaka-Wood, G.B., Addai-Mensah, J., Skinner, W., 2017. A Study of Flotation Characteristics of Monazite, Hematite, and Quartz Using Anionic Collectors. International Journal of Mineral Processing 158, 55-62.

Abeidu, A.M., 1972. The Separation of Monazite from Zircon by Flotation. Journal of the Less Common Metals 29, 113-119.

Anderson, C., 2015. Improved Understanding of Rare Earth Surface Chemistry and Its Application to Froth Flotation, Phd Thesis, Metallurgical and Materials Engineering. Colorado School of Mines, Colorado, USA.

Andrews, W.H., Collins, D.N., Hollick, C.T., 1990. The Flotation of Rare Earths - a Contribution to Industrial Hygiene, AusIMM, Rotorua, New Zealand.

Argus Media Ltd., 2015. Argus White Paper: Impact of Changes to Chinese Policy on the Rare Earths Market in 2015. Argus Media Ltd., London, UK.

Assis, S.M., Montenegro, L.C.M., Peres, A.E.C., 1996. Utilisation of Hydroxamates in Minerals Froth Flotation. Minerals Engineering 9, 103-114.

Azizi, D., Larachi, F., Latifi, M., 2016. Ionic-Liquid Collectors for Rare-Earth Minerals Flotation Case of Tetrabutylammonium Bis(2-Ethylhexyl)-Phosphate for Monazite and Bastnäsite Recovery. Colloids and Surfaces A: Physicochemical and Engineering Aspects 506, 74-86.

Azizi, D., Sarvaramini, A., Larachi, F., 2017. Liquid-Liquid Mineral Separation Via Ionic-Liquid Complexation of Monazite and Bastnäsite—an Alternate Route for Rare-Earth Mineral Beneficiation. Colloids and Surfaces A: Physicochemical and Engineering Aspects 520, 301-323.

Baba, Y., Kubota, F., Kamiya, N., Goto, M., 2011. Recent Advances in Extraction and Separation of Rare-Earth Metals Using Ionic Liquids. Journal of Chemical Engineering of Japan 44, 679-685.

Babchin, A.J., Chow, R.S., Sawatzky, R.P., 1989. Electrokinetic Measurements by Electroacoustical Methods. Advances in Colloid and Interface Science 30, 111-151.

Beer, G., Dawes, W., Brady, A.E., Bryson, M., Sehlotho, N., 2014. Development of a Metallurgical Flow Sheet for the Songwe Hill Rare Earth Project in Malawi, Conference of Metallurgists, Vancouver, Canada.

Binnemans, K., 2007. Lanthanides and Actinides in Ionic Liquids. Chemical reviews 107, 2592-2614.

Boulanger, J.-F., Bazin, C., Turgeon, K., 2019. Effect of Depressants and Temperature on Bastnaesite and Monazite Flotation Separation from a Canadian Rare Earth Element (Ree) Ore. Minerals 9, 225.

Brown, M., Eggert, R., 2018. Simulating Producer Responses to Selected Chinese Rare Earth Policies. Resources Policy 55, 31-48.

Bulatovic, S., 1988. Froth Flotation of Bastnasite, in: United States Patent Office (Ed.), pp. 1-5.

Bulatovic, S., Willett, G.C., 1991. A Monazite Beneficiation Process. World Intellectual Property Organization,, pp. 1-40.

Bulatovic, S.M., 1999. Use of Organic Polymers in the Flotation of Polymetallic Ores: A Review. Minerals Engineering 12, 341-354.

Bulatovic, S.M., 2007a. Collectors, in: Bulatovic, S.M. (Ed.), Handbook of Flotation Reagents. Elsevier, Amsterdam, pp. 5-41.

Bulatovic, S.M., 2007b. Interaction of Organic Regulating Reagents, in: Bulatovic, S.M. (Ed.), Handbook of Flotation Reagents. Elsevier, Amsterdam, pp. 185-202.

Bulatovic, S.M., 2007c. Modifying Reagents, in: Bulatovic, S.M. (Ed.), Handbook of Flotation Reagents. Elsevier, Amsterdam, pp. 53-79.

Bulatovic, S.M., 2010. Flotation of Reo Minerals, in: Bulatovic, S.M. (Ed.), Handbook of Flotation Reagents: Chemistry, Theory and Practice. Elsevier, Amsterdam, pp. 151-173.

Cao, S., Cao, Y., Liao, Y., Ma, Z., 2018a. Depression Mechanism of Strontium Ions in Bastnaesite Flotation with Salicylhydroxamic Acid as Collector. Minerals 8, 66.

Cao, Z., Cao, Y., Qu, Q., Zhang, J., Mu, Y., 2019. Separation of Bastnäsite from Fluorite Using Ethylenediamine Tetraacetic Acid as Depressant. Minerals Engineering 134, 134-141.

Cao, Z., Wang, J., Cao, Y., 2018b. Selective Depression Mechanism of Edta on Fluorite in Bastnaesite Flotation, XXIX International Mineral Processing Congress, Moscow, Russia.

Castor, S.B., 2008. Rare Earth Deposits of North America. Resource Geology 58, 337-347.

Chan, T.N., 1992. A New Beneficiation Process for Treatment of Supergene Monazite Ore, Rare Earths: Resources, Science, Technology and Applications. Minerals, Metals & Materials Society, San Diego, pp. 77-94.

Che, L., 1993. Study on Rare Earth Minerals Flotation with New Collector· H205, XVlll lnternalional Mineral Processing Congress, Sydney, Australia.

Che, L., Yu, Y., Wang, X., Zhang, F., 2003. Study Flotation of Rare Earth Minerals by New Collector Dh XXII International Mineral Processing Congress Cape Town, South Africa

Chen, X., Jin, X., Tan, J., Li, W., Chen, M., Yao, L., Yang, H., 2016. Large-Scale Synthesis of Water-Soluble Luminescent Hydroxyapatite Nanorods for Security Printing. Journal of Colloid and Interface Science 468, 300-306.

Cheng, T.-W., Holtham, P.N., Tran, T., 1993. Froth Flotation of Monazite and Xenotime. Minerals Engineering 6, 341-351.

Cheng, T.-W., Partridge, A.C., Tran, T., Wong, P.L.M., 1994. The Surface Properties and Flotation Behaviour of Xenotime. Minerals Engineering 7, 1085-1098.

Cheng, T.W., 2000. The Point of Zero Charge of Monazite and Xenotime. Minerals Engineering 13, 105-109.

Chi, R., Xu, S., Zhu, G., Xu, J., Qiu, X., 2001. Beneficiation of Rare Earth Ore in China, in: Anjier, J.L. (Ed.), Light Metals. The Minerals, Metals & Materials Society, New Orleans, USA.

Choi, H.S., Whang, K.U., 1963. Surface Properties and Floatability of Zircon. The Canadian Mining and Metallurgical Bulletin 56, 466-468.

Ciuculescu, T., Foo, B., Gowans, R., Hawton, K., Jacobs, C., Spooner, J., 2013. Technical Report Disclosing the Results of the Feasibility Study on the Nechalacho Rare Earth Elements Project. Avalon Rare Metals Inc., pp. 1-307.

Connelly, N.G., Damhus, T., Hartshorn, R.M., Hutton, A.T., 2005. International Union of Pure and Applied Chemistry: Iupac Recommendations. RCS Publishing, Cambridge, UK.

Cui, H., Anderson, C.G., 2017a. Alternative Flowsheet for Rare Earth Beneficiation of Bear Lodge Ore. Minerals Engineering 110, 166-178.

Cui, H., Anderson, C.G., 2017b. Fundamental Studies on the Surface Chemistry of Ancylite, Calcite, and Strontianite. Journal of Sustainable Metallurgy 3, 48-61.

Cui, J., Hope, G.A., Buckley, A.N., 2012. Spectroscopic Investigation of the Interaction of Hydroxamate with Bastnaesite (Cerium) and Rare Earth Oxides. Minerals Engineering 36-38, 91-99.

Deng, L., Zhao, G., Zhong, H., Wang, S., Liu, G., 2016. Investigation on the Selectivity of N-((Hydroxyamino)-Alkyl) Alkylamide Surfactants for Scheelite/Calcite Flotation Separation. Journal of Industrial and Engineering Chemistry 33, 131-141.

Deng, T., Hill, G., 2014. Flotation of Ree Bearing Minerals from Silicate and Carbonate Host Deposits, Conference of Metallurgists, Vancouver, Canada.

Department of the Interior, 2018. Final List of Critical Minerals 2018, Federal Register.

Dostal, J., 2016. Rare Metal Deposits Associated with Alkaline/Peralkaline Igneous Rocks, in: Verplanck, P.L., Hitzman, M.W. (Eds.), Rare Earth and Critical Elements in Ore Deposits. Society of Economic Geologists, p. 0.

Dudka, S., Adriano, D.C., 1997. Environmental Impacts of Metal Ore Mining and Processing: A Review. Journal of Environmental Quality 26, 590-602.

Duruibe, J.O., Ogwuegbu, M., Egwurugwu, J., 2007. Heavy Metal Pollution and Human Biotoxic Effects. International Journal of physical sciences 2, 112-118.

Espiritu, E.R.L., da Silva, G.R., Azizi, D., Larachi, F., Waters, K.E., 2018a. The Effect of Dissolved Mineral Species on Bastnäsite, Monazite and Dolomite Flotation Using Benzohydroxamate Collector. Colloids and Surfaces A: Physicochemical and Engineering Aspects 539, 319-334.

Espiritu, E.R.L., Naseri, S., Waters, K.E., 2018b. Surface Chemistry and Flotation Behavior of Dolomite, Monazite and Bastnäsite in the Presence of Benzohydroxamate, Sodium Oleate and Phosphoric Acid Ester Collectors. Colloids and Surfaces A: Physicochemical and Engineering Aspects 546, 254-265.

Espiritu, E.R.L., Waters, K.E., 2018. Flotation Studies of Monazite and Dolomite. Minerals Engineering 116, 101-106.

European Commission, 2017. Study on the Review of the List of Critical Raw Materials: Criticality Assesments. European Commission.

Fawzy, M.M., 2018. Surface Characterization and Froth Flotation of Fergusonite from Abu Dob Pegmatite Using a Combination of Anionic and Nonionic Collectors. Physicochem. Probl. Miner. Process 54, 677-687.

Fekete, J., 2014. Canada Looking to Break into 'Critical' Rare Earth Elements Mining. Ottawa Citizen Ottawa Canada.

Ferron, C.J., Bulatovic, S.M., Salter, R.S., 1991. Beneficiation of Rare Earth Oxide Minerals, in: Siribumrungsukha, B., Arrykul, S., Sanguansai, P., Pungrassami, T., Sikong, L., Kooptarnond, K. (Ed.), International Conference on Rare Earth Minerals and Minerals for Electronic Uses, Prince of Songklia University, Hat Yai, Thailand.

Filippov, L.O., Dehaine, Q., Filippova, I.V., 2016. Rare Earths (La, Ce, Nd) and Rare Metals (Sn, Nb, W) as by-Products of Kaolin Production – Part 3: Processing of Fines Using Gravity and Flotation. Minerals Engineering 95, 96-106.

Filippov, L.O., Duverger, A., Filippova, I.V., Kasaini, H., Thiry, J., 2012. Selective Flotation of Silicates and Ca-Bearing Minerals: The Role of Non-Ionic Reagent on Cationic Flotation. Minerals Engineering 36-38, 314-323.

Filippova, I.V., Filippov, L.O., Duverger, A., Severov, V.V., 2014. Synergetic Effect of a Mixture of Anionic and Nonionic Reagents: Ca Mineral Contrast Separation by Flotation at Neutral Ph. Minerals Engineering 66-68, 135-144.

Förstner, U., Wittmann, G.T., 2012. Metal Pollution in the Aquatic Environment. Springer Science & Business Media.

Fuerstenau, D.W., 1956. Measuring Zeta Potentials by Streaming Potential Techniques Mining Engineering, 834 - 835.

Fuerstenau, D.W., Pradip, 2005. Zeta Potentials in the Flotation of Oxide and Silicate Minerals. Advances in Colloid and Interface Science 114-115, 9-26.

Fuerstenau, M.C., 2005. Chelating Agents as Flotation Collectors, Innovations in natural resource processing: proceedings of the Jan D. Miller symposium. Society for Mining, Metallurgy & Exploration, Salt Lake City, USA.

Gambogi, J., 2015. Rare Earths, 2015 Minerals Yearbook. United States Geological Survey.

Gao, Y., Gao, Z., Sun, W., Yin, Z., Wang, J., Hu, Y., 2018. Adsorption of a Novel Reagent Scheme on Scheelite and Calcite Causing an Effective Flotation Separation. Journal of Colloid and Interface Science 512, 39-46.

Geneyton, A., Filippov, L.O., Menad, N.E., 2018. Influence of Monazite Chemistry and Carbon Dioxide on Zeta Potential and Fatty Acid Collector Adsorption, XXIX International Mineral Processing Congress, Moscow, Russia.

Gibson, C.E., Kelebek, S., Aghamirian, M., 2015. Niobium Oxide Mineral Flotation: A Review of Relevant Literature and the Current State of Industrial Operations. International Journal of Mineral Processing 137, 82-97.

Goode, J.R., Payne, R., Gao, F., Brown, J., 2014. The Recovery of Rare Earths, Uranium and Pyrite from Pele Mountain's Proposed Eco Ridge Mine Project, Conference of Metallurgists, Vancouver, Canada.

Goodenough, K.M., Wall, F., Merriman, D., 2018. The Rare Earth Elements: Demand, Global Resources, and Challenges for Resourcing Future Generations. Natural Resources Research 27, 201-216.

Grammatikopoulos, T., Mercer, W., Gunnning, C., Prout, S., 2011. Quantitative Characterization of the Ree Minerals by Qemscan from the Nechalacho Heavy Rare Earth Deposit, Thor Lake Project, Nwt, Canada, 43rd Annual Meeting of the Canadian Mineral Processors, Ottawa, Canada.

Greenwood, R., 2003. Review of the Measurement of Zeta Potentials in Concentrated Aqueous Suspensions Using Electroacoustics. Advances in Colloid and Interface Science 106, 55-81.

Greenwood, R., Lapčíková, B., Surýnek, M., Waters, K., Lapčík, L., 2007. The Zeta Potential of Kaolin Suspensions Measured by Electrophoresis and Electroacoustics. Chemical Papers 61, 83-92.

Gül, A., 2004. Flotation Behaviours of Microlite and Zircon. Minerals Engineering 17, 561-563.

Gupta, S.P., 2013. Hydroxamic Acids: A Unique Family of Chemicals with Multiple Biological Activities. Springer.

Guy, P.J., Bruckard, W.J., Vaisey, M.J., 2000. Beneficiation of Mt Weld Rare Earth Oxides by Gravity Concentration, Flotation and Magnetic Separation, Seventh Mill Operators' Conference. The Australasian Institute of Mining and Metallurgy, Kalgoorlie, Australia.

Hadley, T., Catovic, E., 2014. Beneficiation and Extraction of Ree from Northern Minerals' Browns Range Heavy Rare Earth Project, Conference of Metallurgists, Vancouver, Canada.

Harada, T., Owada, S., Takiuchi, T., Kurita, M., 1993. A Flotation Study for Effective Separation of the Heavy Mineral Sands, XVIII International Mineral Processing Congress, p. 10.

Harbi, H.M., Eldougdoug, A.A., El-Shahawi, M.S., 2011. Mineral Processing and Extraction of Rare Earth Elements from the Wadi Khamal Nelsonite Ore, Northwestern Saudi Arabia. Arabian Journal of Geosciences 4, 353-363.

Harrison, R.M., Laxen, D., 1981. Lead Pollution, Causes and Control. Springer.

Hart, B., Dimov, S., Xia, L., 2014. Ree Bearing Mineral Recovery: A Microflotation and Surface Chemistry Study Using Hydroxamate Collectors and Citric Acid, International Mineral Processing Congress Santiago, Chile.

Hedrick, J.B., Sinha, S.P., Kosynkin, V.D., 1997. Loparite, a Rare-Earth Ore (Ce, Na, Sr, Ca)(Ti, Nb, Ta, Fe+3)O3. Journal of Alloys and Compounds 250, 467-470.

Herrera-Urbina, R., Pradip, Fuerstenau, D., 2013. Electrophoretic Mobility and Computations of Solid-Aqueous Solution Equilibria for the Bastnaesite-H 2 O System. Mining, Metallurgy & Exploration 30, 18-23.

Hirano, M., Dozono, H., 2013. Direct Formation and Luminescence Properties of Yttrium Niobate Ynbo4 Nanocrystals Via Hydrothermal Method. Journal of the American Ceramic Society 96, 3389-3393.

Hope, G.A., Woods, R., Parker, G.K., Buckley, A.N., McLean, J., 2010. A Vibrational Spectroscopy and Xps Investigation of the Interaction of Hydroxamate Reagents on Copper Oxide Minerals. Minerals Engineering 23, 952-959.

Houot, R., 1982. Beneficiation of Phosphatic Ores through Flotation: Review of Industrial Applications and Potential Developments. International Journal of Mineral Processing 9, 353-384.

Houot, R., Cuif, J.P., Mottot, Y., Samama, J.C., 1991. Recovery of Rare Earth Minerals with Emphasis on Flotation Process, in: Siribumrungsukha, B., Arrykul, S., Sanguansai, P., Pungrassami, T., Sikong, L., Kooptarnond, K. (Ed.), International Conference on Rare Earth Minerals and Minerals for Electronic Uses, Hat Yai, Thailand, pp. 301-324.

Hunter, R.J., 1998. Recent Developments in the Electroacoustic Characterisation of Colloidal Suspensions and Emulsions. Colloids and Surfaces A: Physicochemical and Engineering Aspects 141, 37-66.

Hyung, S.C., Ki, U.W., 1963. Mechanism of Collector Adsorption on Monazite. Journal of the Korean Chemical Society 7, 91-95.

Jeong, C., Cho, H., 2014. Concentration of Rare Earth Elements by Flotation of Ree Ores from Mushgai, Khudag Area, Mongolia, XXVII International Mineral Processing Congress, Chile.

Johnson, P.R., 1999. A Comparison of Streaming and Microelectrophoresis Methods for Obtaining the Z Potential of Granular Porous Media Surfaces. Journal of Colloid and Interface Science 209, 264-267.

Jordens, A., Cheng, Y.P., Waters, K.E., 2013. A Review of the Beneficiation of Rare Earth Element Bearing Minerals. Minerals Engineering 41, 97-114.

Jordens, A., Marion, C., Grammatikopoulos, T., Hart, B., Waters, K.E., 2016a. Beneficiation of the Nechalacho Rare Earth Deposit: Flotation Response Using Benzohydroxamic Acid. Minerals Engineering 99, 158-169.

Jordens, A., Marion, C., Kuzmina, O., Waters, K.E., 2014a. Physicochemical Aspects of Allanite Flotation. Journal of Rare Earths 32, 476-486.

Jordens, A., Marion, C., Kuzmina, O., Waters, K.E., 2014b. Surface Chemistry Considerations in the Flotation of Bastnäsite. Minerals Engineering 66–68, 119-129.

Jordens, A., McCarthy, S., Waters, K.E., 2014c. The Effect of Activating Ions on the Adsorption of a Benzohydroxamic Acid Collector onto a Rare Earth Silicate, Conference of Metallurgists, Vancouver, Canada.

Jordens, A., Zhiyong, Y., Cappuccitti, F., 2016b. The Application of Florrea 8920, a New Hydroxamate-Based Flotaiton Collector for the Flotation of Rare Earth Minerals, XXVIII International Mineral Processing Congress Proceedings, Quebec, Canada.

Khairy, E.M., Shoukry, M.M., Khalil, M.M., Mohamed, M.M., 1996. Metal Complexes of Salicylhydroxamic Acid: Equilibrium Studies and Synthesis. Transition Metal Chemistry 21, 176-180.

Khalil, M.M., Fazary, E.A., 2004. Potentiometric Studies on Binary and Ternary Complexes of Di- and Trivalent Metal Ions Involving Some Hydroxamic Acids, Amino Acids, and Nucleic Acid Components. Monatshefte für Chemie / Chemical Monthly 135, 1455-1474.

Kim, J.A., Dodbiba, G., Fujita, T., Fujii, N., 2010. Characteristics Analysis of a Bastnaesite Rare Earth Mineral for Recovery of Cerium, XXV International Mineral Processing Congress, Brisbane, Australia, pp. 2927-2932.

Kingsnorth, D.J., 2010. Rare Earths: Facing New Challenges in the New Decade, Presentation at the SME Annual Meeting, Phoenix, USA.

Klein, B., Altun, N.E., Colebrook, M., Pawlik, M., 2012. Electroacoustic Measurements of Mixed Quartz and Iron Oxide Mineral Systems. International Journal of Mineral Processing 110-111, 12-17.

Kosmulski, M., 2002. The Ph-Dependent Surface Charging and the Points of Zero Charge. Journal of Colloid and Interface Science 253, 77-87.

Kosmulski, M., 2004. Ph-Dependent Surface Charging and Points of Zero Charge Ii. Update. Journal of Colloid and Interface Science 275, 214-224.

Kosmulski, M., 2006. Ph-Dependent Surface Charging and Points of Zero Charge: Iii. Update. Journal of Colloid and Interface Science 298, 730-741.

Kosmulski, M., 2009. Ph-Dependent Surface Charging and Points of Zero Charge. Iv. Update and New Approach. Journal of Colloid and Interface Science 337, 439-448.

Kosmulski, M., 2011. The Ph-Dependent Surface Charging and Points of Zero Charge: V. Update. Journal of Colloid and Interface Science 353, 1-15.

Kosmulski, M., 2014. The Ph Dependent Surface Charging and Points of Zero Charge. Vi. Update. Journal of Colloid and Interface Science 426, 209-212.

Kosmulski, M., 2018. The Ph Dependent Surface Charging and Points of Zero Charge. Vii. Update. Advances in Colloid and Interface Science 251, 115-138.

Kosmulski, M., 2020. The Ph Dependent Surface Charging and Points of Zero Charge. Viii. Update. Advances in Colloid and Interface Science 275, 102064.

Krishnamurthy, N., Gupta, C., 2016. Extractive Metallurgy of Rare Earths. CRC Press, Boca Raton.

Li, F., Wang, J., Zeng, X., 1988. A Process on the Recovery of Re Minerals with a Chelating Collector, in: Bautista, R.G., Wong, M.M. (Eds.), Rare Earths, Extraction, Preparation and Applications. The Minerals, Metals and Materials Society, Warrendale, USA, pp. 71-79.

Li, M., Gao, K., Zhang, D., Duan, H., Ma, L., Huang, L., 2018. The Influence of Temperature on Rare Earth Flotation with Naphthyl Hydroxamic Acid. Journal of Rare Earths 36, 99-107.

Li, R., 2018. An Investigation into Using Ionic Liquids for Rare Earth Mineral Flotation, Meng Thesis, Department of Mining and Materials Engineering. McGill University, Montreal, Canada.

Liu, W., McDonald, L.W., Wang, X., Miller, J.D., 2018. Bastnaesite Flotation Chemistry Issues Associated with Alkyl Phosphate Collectors. Minerals Engineering 127, 286-295.

Liu, W., Wang, X., Wang, Z., Miller, J.D., 2016. Flotation Chemistry Features in Bastnaesite Flotation with Potassium Lauryl Phosphate. Minerals Engineering 85, 17-22.

Lu, Y., Drelich, J., Miller, J.D., 1998. Oleate Adsorption at an Apatite Surface Studied by Ex-Situ Ftir Internal Reflection Spectroscopy. Journal of Colloid and Interface Science 202, 462-476.

Luo, J., Chen, X., 1984. Research into the Recovery of High-Grade Rare-Earth Concentrate from Baotou Complex Iron Ores, China. Mineral Processing and Extractive Metallurgy, 663-675.

Malas, K.W., Jordens, A., Mirnezami, M., Chu, P., Gauvin, R., Waters, K.E., 2013. Surface Characterisation of Fergusonite. Canadian Metallurgical Quarterly 52, 278-284.

Mao, M., Fornasiero, D., Ralston, J., Smart, R.S.C., Sobieraj, S., 1994. Electrochemistry of the Zircon—Water Interface. Colloids and Surfaces A: Physicochemical and Engineering Aspects 85, 37-49.

Marion, C., Li, R., Williams, H., Hundt, D., Waters, K.E., 2019. A Physico-Chemical Investigation into the Separation of Zircon and Quartz by Flotation, IMPC 2018 - 29th International Mineral Processing Congress, pp. 4062-4072.

Marlow, B.J., Fairhurst, D., Pendse, H., 1988. Colloid Vibration Potential and the Electrokinetic Characterization of Concentrated Colloids. Langmuir 4, 611-626.

McEwen, R., Hansen, G.W., Lee, G.F., 1976. Single-Stage Flotation of Alkali Feldspars, Ilmenite, Rutile, Garnet, and Monazite, with Mixed Cationic/Anionic Collectors. Transactions of the Society of Mining Engineers 260, 97-100.

Miller, N.P., Berg, J.C., 1991. A Comparison of Electroacoustic and Microelectrophoretic Zeta Potential Data for Titania in the Absence and Presence of a Poly (Vinyl Alcohol) Adlayer. Colloids and Surfaces 59, 119-128.

Morrice, E., Wong, M.M., 1982. Flotation of Rare Earths from Bastnasite Ore United States Department of the Interior Bureau of Mines.

Nadeau, O., Cayer, A., Pelletier, M., Stevenson, R., Jébrak, M., 2015. The Paleoproterozoic Montviel Carbonatite-Hosted Ree–Nb Deposit, Abitibi, Canada: Geology, Mineralogy, Geochemistry and Genesis. Ore Geology Reviews 67, 314-335.

Nagaraj, D., 2018. The Chemistry and Application of Chelating or Complexing Agents in Minerals Separations, Reagents in Mineral Technology. Routledge, pp. 273-350.

Nduwa-Mushidi, J., Anderson, C.G., 2017. Surface Chemistry and Flotation Behaviors of Monazite–Apatite–Ilmenite–Quartz–Rutile–Zircon with Octanohydroxamic Acid. Journal of Sustainable Metallurgy 3, 62-72.

Neale, S., 1946. The Electrical Double Layer, the Electrokinetic Potential, and the Streaming Current. Transactions of the Faraday Society 42, 473-478.

Negeri, T., Boisclair, M., 2016. Flotation-Magnetic Separation Hybrid Process for Concentration of Rare Earth Minerals Contained in a Carbonatite Ore, XXVIII International Mineral Processing Congress Proceedings, Quebec, Canada.

O'Brien, R., 1990. The Electroacoustic Equations for a Colloidal Suspension. Journal of Fluid Mechanics 212, 81-93.

O'Brien, R.W., 1995. The Dynamic Mobility of a Porous Particle. Journal of Colloid and Interface Science 171, 495-504.

O'Brien, R.W., Midmore, B.R., Lamb, A., Hunter, R.J., 1990. Electroacoustic Studies of Moderately Concentrated Colloidal Suspensions. Faraday Discussions of the Chemical Society 90, 301-312.

Oelkers, E.H., Poitrasson, F., 2002. An Experimental Study of the Dissolution Stoichiometry and Rates of a Natural Monazite as a Function of Temperature from 50 to 230 °C and Ph from 1.5 to 10. Chemical Geology 191, 73-87.

Owens, C.L., Nash, G.R., Hadler, K., Fitzpatrick, R.S., Anderson, C.G., Wall, F., 2018. Zeta Potentials of the Rare Earth Element Fluorcarbonate Minerals Focusing on Bastnäsite and Parisite. Advances in Colloid and Interface Science 256, 152-162.

Owens, C.L., Nash, G.R., Hadler, K., Fitzpatrick, R.S., Anderson, C.G., Wall, F., 2019. Apatite Enrichment by Rare Earth Elements: A Review of the Effects of Surface Properties. Advances in Colloid and Interface Science 265, 14-28.

Oyediran, Y., Cheung, L., Roux, N., Gilders, R., 2014. Northern Quebec's Strange Lake Rare Earth Elements (Ree) Deposit Rougher Flotation Study, Conference of Metallurgists Vancouver, Canada.

Ozeren, M.S., Hutchinson, H., 1990. The Selective Flotation of Xenotime from Heavy Minerals, AusIMM, Rotorua, New Zealand.

Palmer, B.R., Gutierrez, B.G., Fuerstenau, M.C., 1973. Mechanisms Involved in the Flotation of Oxides and Silicates with Anionic Collectors Part I. Transactions of the Metallurgical Society of AIME 258, 257-260.

Parks, G.A., 1965. The Isoelectric Points of Solid Oxides, Solid Hydroxides, and Aqueous Hydroxo Complex Systems. Chemical Reviews 65, 177-198.

Pavez, O., Brandao, P.R.G., Peres, A.E.C., 1996. Adsorption of Oleate and Octyl-Hydroxamate on to Rare-Earths Minerals. Minerals Engineering 9, 357-366.

Pavez, O., Peres, A., 1993a. Flotation of Monazite-Zircon-Rutile with Sodium Oleate and Hydroxamates, XVIII International Mineral Processing Congress, Sydney, pp. 1007-1012.

Pavez, O., Peres, A.E.C., 1993b. Effect of Sodium Metasilicate and Sodium Sulphide on the Floatability of Monazite-Zircon-Rutile with Oleate and Hydroxamates. Minerals Engineering 6, 69-78.

Pavez, O., Peres, A.E.C., 1994. Technical Note Bench Scale Flotation of a Brazilian Monazite Ore. Minerals Engineering 7, 1561-1564.

Pearse, M.J., 2005. An Overview of the Use of Chemical Reagents in Mineral Processing. Minerals Engineering 18, 139-149.

Peng, H., Luo, W., Wu, D., Bie, X., Shao, H., Jiao, W., Liu, Y., 2017. Study on the Effect of Fe3+ on Zircon Flotation Separation from Cassiterite Using Sodium Oleate as Collector. Minerals 7, 108.

Pereira, C.A., Peres, A.E.C., 1997. Flotation Concentration of a Xenotime Pre-Concentrate. Minerals Engineering 10, 1291-1295.

Pol'kin, S.I., Ilie, P., Solnyshkin, V.I., Zakharov, A.E., 1967. Selective Desorption of Sodium Oleate from Pyrochlore, Zircon and Monazite by Sodium Sulfide, in: Plaksin, I.N. (Ed.), Flotation Properties of Rare Metal Minerals. Primary Sources, New York, USA, pp. 46-56.

Pope, M.I., Sutton, D.I., 1973. The Correlation between Froth Flotation Response and Collector Adsorption from Aqueous Solution. Part I. Titanium Dioxide and Ferric Oxide Conditioned in Oleate Solutions. Powder Technology 7, 271-279.

Pradip, 1981. The Surface Properties and Flotation of Rare-Earth Minerals. PhD Thesis, Department of Materials Science and Mineral Engineering. University of California, Berkeley, Berkeley, USA.

Pradip, Fuerstenau, D.W., 1983. The Adsorption of Hydroxamate on Semi-Soluble Minerals. Part I: Adsorption on Barite, Calcite and Bastnaesite. Colloids and Surfaces 8, 103-119.

Pradip, Fuerstenau, D.W., 1985. Adsorption of Hydroxamate Collectors on Semisoluble Minerals Part Ii: Effect of Temperature on Adsorption. Colloids and Surfaces 15, 137-146.

Pradip, Fuerstenau, D.W., 1991. The Role of Inorganic and Organic Reagents in the Flotation Separation of Rare-Earth Ores. International Journal of Mineral Processing 32, 1-22.

Pradip, Li, C.C.H., Fuerstenau, D.W., 2015. Surface Chemical Characterization of Bastnaesite through Electrokinetics. KONA Powder and Particle Journal, 1-8.

Rao, S.R., 2013. Surface Chemistry of Froth Flotation: Volume 1: Fundamentals. Springer Science & Business Media.

Ren, J., Lu, S., Song, S., Niu, J., 1997. A New Collector for Rare Earth Mineral Flotation. Minerals Engineering 10, 1395-1404.

Ren, J., Song, S., Lopez-Valdivieso, A., Lu, S., 2000. Selective Flotation of Bastnaesite from Monazite in Rare Earth Concentrates Using Potassium Alum as Depressant. International Journal of Mineral Processing 59, 237-245.

Ren, J., Wang, W., Luo, J., Zhou, G., Tang, F., 2003. Progress of Flotation Reagents of Rare Earth Minerals in China. Journal of Rare Earths 21, 1-8.

Riley, J., 2009. Charge in Colloidal Systems, Colloid Science: Principles, Methods and Applications. Blackwell Publishing, Oxford, pp. 14-35.

Sanematsu, K., Watanabe, Y., 2016. Characteristics and Genesis of Ion Adsorption-Type Rare Earth Element Deposits, in: Verplanck, P.L., Hitzman, M.W. (Eds.), Rare Earth and Critical Elements in Ore Deposits. Society of Economic Geologists.

Sarvaramini, A., Azizi, D., Larachi, F., 2016. Hydroxamic Acid Interactions with Solvated Cerium Hydroxides in the Flotation of Monazite and Bastnäsite—Experiments and Dft Study. Applied Surface Science 387, 986-995.

Sastri, V.R., Perumareddi, J., Rao, V.R., Rayudu, G., Bünzli, J.-C., 2003. Modern Aspects of Rare Earths and Their Complexes. Elsevier Amsterdam.

Satur, J.V., Calabia, B.P., Hoshino, M., Morita, S., Seo, Y., Kon, Y., Takagi, T., Watanabe, Y., Mutele, L., Foya, S., 2016. Flotation of Rare Earth Minerals from Silicate–Hematite Ore Using Tall Oil Fatty Acid Collector. Minerals Engineering 89, 52-62.

Sengupta, D., Gosen, B.S.V., 2016. Placer-Type Rare Earth Element Deposits in: Verplanck, P.L., Hitzman, M.W. (Eds.), Rare Earth and Critical Elements in Ore Deposits. Society of Economic Geologists.

Smith, R., Shonnard, D., 1986. Electrokinetic Study of the Role of Modifying Agents in Flotation of Salt-Type Minerals. AIChE journal 32, 865-868.

Smith, R., Steiner, S., 1980. Autoactivation in Anionic Flotation of Bastnaesite, Solids Separation Processes, Institute of Chemical Engineers Symposium Series, pp. 1-12.

Sorensen, E., Lundgaard, T., 1966. Selective Flotation of Steenstrupine and Monazite from Kvanefjeld Lujavrite – Report for the Danish Atomic Energy Commission. Danish Atomic Energy Commission, Roskilde.

Sreenivas, T., Padmanabhan, N.P.H., 2002. Surface Chemistry and Flotation of Cassiterite with Alkyl Hydroxamates. Colloids and Surfaces A: Physicochemical and Engineering Aspects 205, 47-59.

Stark, T., Silin, I., Wotruba, H., 2017. Mineral Processing of Eudialyte Ore from Norra Kärr. Journal of Sustainable Metallurgy 3, 32-38.

Sun, X., Ji, Y., Chen, J., Ma, J., 2009. Solvent Impregnated Resin Prepared Using Task-Specific Ionic Liquids for Rare Earth Separation. Journal of Rare Earths 27, 932-936.

Sun, X., Luo, H., Dai, S., 2012. Solvent Extraction of Rare-Earth Ions Based on Functionalized Ionic Liquids. Talanta 90, 132-137.

Sun, X., Waters, K.E., 2014. Development of Industrial Extractants into Functional Ionic Liquids for Environmentally Friendly Rare Earth Separation. ACS Sustainable Chemistry & Engineering 2, 1910-1917.

Verplanck, P.L., Mariano, A.N., Mariano, A., Jr., 2016. Rare Earth Element Ore Geology of Carbonatites, in: Verplanck, P.L., Hitzman, M.W. (Eds.), Rare Earth and Critical Elements in Ore Deposits. Society of Economic Geologists.

Wang, C.H., Qiu, X.Y., Hu, Z., Li, H.W., Wang, T., Zou, J.J., 2012. Study on Improved Beneficiation Technology for Rare Earth Ores, XXVI International Mineral Processing Congress, New Deli, India.

Wen Qi, G., 1993. Use of the Qem∗Sem Analysis in Flotation Testwork on a Phosphate Ore Containing Monazite. International Journal of Mineral Processing 37, 89-108.

Wills, B.A., Finch, J.A., 2016. Chapter 12 - Froth Flotation, in: Wills, B.A., Finch, J.A. (Eds.), Wills' Mineral Processing Technology (Eighth Edition). Butterworth-Heinemann, Boston, pp. 265-380.

Xia, L., Hart, B., Chelgani, S., Douglas, K., 2014. Hydroxamate Collectors for Rare Earth Mineral Flotation, 53rd Annual Conference of Metallurgists Vancouver, Canada.

Xia, L., Hart, B., Loshusan, B., 2015. A Tof-Sims Analysis of the Effect of Lead Nitrate on Rare Earth Flotation. Minerals Engineering 70, 119-129.

Yang, X., Satur, J.V., Sanematsu, K., Laukkanen, J., Saastamoinen, T., 2015. Beneficiation Studies of a Complex Ree Ore. Minerals Engineering 71, 55-64.

Yang, Z., Wu, W., Bian, X., 2017. Synthesis of 3-Hydroxy-2-Naphthyl Hydroxamic Acid Collector: Flotation Performance and Adsorption Mechanism on Bastnaesite. Journal of the Southern African Institute of Mining and Metallurgy 117, 593-598.

Yu, B., Oyediran, Y.O., Robart, M., 2016a. Flotation Development Testwork on Ree Samples from the Strange Lake Alkalic Complex, XXVIII International Mineral Processing Congress Proceedings Quebec, Canada.

Yu, J., Ge, Y., Hou, J., 2016b. Behavior and Mechanism of Collophane and Dolomite Separation Using Alkyl Hydroxamic Acid as a Flotation Collector. Physicochemical Problems of Mineral Processing 52.

Zakharov, A.E., Ilie, P., POLKIN, S.I., Solnyshkin, V.I., 1967. Reaction of Sodium Sulfide with Pyrochlore, Zircon, and Monazite in Flotation with Sodium Oleate, in: Plaksin, I.N. (Ed.), Flotation Properties of Rare Metal Minerals. Primary Sources, New York, USA, pp. 71-82.

Zepf, V., 2013. Rare Earth Elements: A New Approach to the Nexus of Supply, Demand and Use: Exemplified Along the Use of Neodymium in Permanent Magnets. Springer Berlin Heidelberg.

Zepf, V., 2016. Chapter 1 - an Overview of the Usefulness and Strategic Value of Rare Earth Metals, in: Borges De Lima, I., Leal Filho, W. (Eds.), Rare Earths Industry. Elsevier, Boston, pp. 3-17.

Zhang, J., Edwards, C., 2012. A Review of Rare Earth Mineral Processing Technology, 44th Annual Meeting of The Canadian Mineral Processors, Ottawa, Canada.

Zhang, W., Honaker, R., 2017. A Fundamental Study of Octanohydroxamic Acid Adsorption on Monazite Surfaces. International Journal of Mineral Processing 164, 26-36.

Zhang, W., Honaker, R., Groppo, J., 2016. Fundamental Study of the Monazite-Calcite Flotation Separation, XXVIII International Mineral Processing Congress, Québec, Canada.

Zhang, W., Honaker, R.Q., 2018. Flotation of Monazite in the Presence of Calcite Part Ii: Enhanced Separation Performance Using Sodium Silicate and Edta. Minerals Engineering 127, 318-328.

Zhang, W., Honaker, R.Q., Groppo, J.G., 2017. Flotation of Monazite in the Presence of Calcite Part I: Calcium Ion Effects on the Adsorption of Hydroxamic Acid. Minerals Engineering 100, 40-48.

Zhang, X., Du, H., Wang, X., Miller, J., 2013. Surface Chemistry Considerations in the Flotation of Rare-Earth and Other Semisoluble Salt Minerals. Mining, Metallurgy & Exploration 30, 24-37.

Zhang, Y., Anderson, C., 2017a. A Comparison of Sodium Silicate and Ammonium Lignosulfonate Effects on Xenotime and Selected Gangue Mineral Microflotation. Minerals Engineering 100, 1-8.

Zhang, Y., Anderson, C., 2017b. Surface Chemistry and Microflotation of Xenotime and Selected Gangue Minerals Using Octanohydroxamic Acid as the Collector. Journal of Sustainable Metallurgy 3, 39-47.

Zhou, F., Wang, L., Xu, Z., Liu, Q., Chi, R., 2014. Interaction of Reactive Oily Bubble in Flotation of Bastnaesite. Journal of Rare Earths 32, 772-778.

Zhou, F., Wang, L., Xu, Z., Liu, Q., Chi, R., 2015. Reactive Oily Bubble Technology for Flotation of Apatite, Dolomite and Quartz. International Journal of Mineral Processing 134, 74-81.